MONASH UNIVERSITY
THESIS ACCEPTED IN SATISFACTION OF THE
REQUIREMENTS FOR THE DEGREE OF
DOCTOR OF PHILOSOPHY
ON.....[redacted]...............
Sec. ~~Ph~~.D. and Scholarships Committee

PhD Thesis Title: **Thin-Walled Tubular Connections under Fatigue Loading**

Author: **Fidelis Rutendo MASHIRI**

ERRATA

p 7, last sentence: "cyclic in-plane bending" for "cyclic in-plane"
p 19, section 2.2.5, 8th line: "extent" for "extend"
p 28, section 2.4.1, 5th line: insert comma after "itself"
p 38, section 2.4.7, 2nd line: "welded nodal joints" for "welded, nodal joints"
p 70, para 2, 1st line: "extent" for "extend"
p 70, para 2, 2nd line: "extent" for "extend"
p 134, para 4, 1st line: "connection series names" for "series names"
p 139, section 5.2.2, 6th line: add comma after "load cell exciter"
p 140, section 5.3, 2nd line: add comma after "1.6mm"
p 147, para 2, 5th line: "finishing" for "finishings"
p 160, para 2, 2nd line: "polymide-backed gauges" for "student gauges"
p 167, para 3, 2nd line: "connection series names" for "series names"
p 195, para 1, 10th line: space between "B," and "C"
p 195, para 3, 2nd line: "leg length" for "led length"
p 233, section 7.7, 10th line: "result" for "results"
p 243, para 2, 7th line: space between "tubes." and "which"
p 243, para 2, 7th line: comma for full stop after "tubes"
p 243, para 2, 8th line: full stop for semi-colon
p 260, para 1, 2nd line: "Two sets" for "Two set"
p 264, para 2, 11th line: "positioning of strain gauges is" for "positioning of strain gauges are"
p 321, section 11.8, 7th line: space between "scatter" and "band"

THIN-WALLED TUBULAR CONNECTIONS UNDER FATIGUE LOADING

A Thesis

By

Fidelis Rutendo Mashiri

BSc. Eng (Hons.), M.E. (Hons).

A Thesis Submitted for the
Degree of Doctor of Philosophy in the
Department of Civil Engineering,
MONASH UNIVERSITY

AUSTRALIA

March 2001

ABSTRACT

The main aim of this research is to determine fatigue design rules for welded tube-to-plate and tube-to-tube T-joints made up of thin-walled cold-formed square hollow sections where the tube wall thicknesses are less than 4mm.

The factors influencing fatigue life of welded joints have been reviewed to understand potential key parameters in the fatigue behaviour of welded thin-walled joints. Design rules for welded tube-to-plate T-joints in Australian, European and Canadian standards have been reviewed to highlight the gaps that exist in the fatigue design of tube-to-plate T-joints under cyclic in-plane bending. Design Rules for welded tube-to-tube T-joints in American, British, European, IIW and CIDECT standards have also been reviewed to show the lack of design S-N curves for welded thin-walled tubular connections with wall thicknesses less than 4mm.

One of the factors likely to greatly influence the fatigue life of welded thin-walled joints is the weld defects, particularly undercut at the weld toes. The suitability of using the gas-metal arc welding (MIG) and the gas-tungsten arc welding (TIG) methods in joining thin-walled ($t<4mm$) joints with particular emphasis on compliance of weld toe undercut dimensions to Australian welding standards is verified. A further study on the effects of weld profile and weld toe undercut dimensions on both thin-walled and thick-walled cruciform joints using the boundary element method is carried out to develop an understanding of the key parameters influencing fatigue life in thin-walled joints.

The aim of this research program is to define the behaviour of welded thin-walled tube-to-plate and tube-to-tube T-joints in the high-cycle fatigue region. The level of loading required to produce a high-cycle fatigue response in tube-to-plate and tube-to-tube T-joints made up of thin-walled square hollow sections is determined from moment versus angle-of-inclination graphs obtained from static tests.

An extensive fatigue testing program is carried out using a multiple fatigue test rig to obtain S-N data of thin-walled tube-to-plate and tube-to-tube T-joints under cyclic in-plane bending load and to document the failure modes in these connections. Tests are also carried out to determine experimental stress concentration factors. The experimental stress concentration factors are used to convert nominal stress ranges to hot spot stress ranges.

From the resulting experimental S-N data, design S-N curves for welded tube-to-plate T-joints made up of thin-walled (t<4mm) tubes are determined using the least squares method for both the classification method and the hot spot stress method. A comparison is carried out between the design S-N curves obtained from experimental data of welded thin-walled tube-to-plate T-joints with the design rules from Australian, European, and Canadian standards.

Design S-N curves are also determined for welded tube-to-tube T-joints made up of thin-walled (t<4mm) tubes from the resulting experimental S-N data in the hot spot stress method, using the least squares method. A comparison is carried out between the design S-N curves obtained from experimental data of welded thin-walled tube-to-tube T-joints with the design rules from IIW, CIDECT, American, European and British standards.

New design S-N curves for welded thin-walled tube-to-plate and tube-to-tube T-joints made up from cold-formed square hollow sections of tube wall thicknesses less than 4mm are proposed.

PREFACE

This thesis is submitted to Monash University, Melbourne, Australia, for the degree of Doctor of Philosophy. The work described in this thesis was carried out by the candidate in the Department of Civil Engineering, Clayton Campus, at Monash University during the period 1997 to 2001 under the supervision of Dr. Xiao-Ling Zhao and Professor Paul Grundy.

This thesis, except with the committee's approval contains no material that has been accepted for the award of any other degree or diploma in any university or other institution. I affirm that to the best of my knowledge, the thesis contains no material previously published or written by another person, except where due reference is made in the text of the thesis.

Ten supporting papers that are based on the work presented in this thesis have been written with Dr. Xiao-Ling Zhao and Professor Paul Grundy. They are:

Conference Papers

1) Mashiri F.R, Zhao. X.L., Grundy P. 1997, "Crack Propagation Analysis of Welded Thin-Walled Cruciform Joint using the Boundary Element Method", Materials Research Forum '97 Conference Proceedings, Institute of Metals and Materials Australasia Ltd (IMMA), Melbourne, Australia, pp. 109-112

2) Mashiri F.R, Zhao. X.L., Grundy P. 1998, "Effects of Weld Profile on the Fatigue Life of Thin-walled Cruciform Joint", *Tubular Structures VIII*, Proceedings of the 8th International Symposium on Tubular Structures, ISTS8, Editors: Choo Y.S. and van Der Vegte G.J., 26-28 August 1998, pp. 331-340

3) Mashiri F.R, Zhao. X.L., Grundy P. 1998, "Effects of Weld Undercut on the Fatigue Life of Welded Connections in Thin-Walled Structures", *Structural Intergrity and Fracture,* Proceedings, Australian Fracture Group Inc., 21-22 September 1998, pp. 81-91

4) Mashiri F.R, Zhao. X.L., Grundy P. 1999, "3D BEM Analysis of Thin-walled Tube-to-tube T-joints under Fatigue Loading", Paper U-072, The Second Australasian Congress on Applied Mechanics (ACAM99),CD-ROM, 10-12 February 1999, Canberra, Australia

5) Mashiri F.R, Zhao. X.L., Grundy P. 1999, "Fatigue Strength of Thin-Walled Tube-to-Tube T-joints under In-Plane Bending", *Advances in Steel Structures* Vol. II, Proceedings of The Second International Conference on Advances in Steel Structures, ICASS99, Editors Chan S.L. and Teng G.J., Elsevier Science Ltd, Hong Kong, 15-17 December 1999, pp. 983-990

6) Mashiri F.R, Zhao. X.L., Grundy P. 2000, "Fatigue Design of Welded Very Thin-walled Tube-to-Plate Joints using the Classification Method", *Structural Failure and Plasticity*, Proceedings of The 7th International Symposium on Structural Failure and Plasticity, IMPLAST2000, Editors: Zhao X.L. and Grzebieta R.H., Melbourne, Australia, 4-6 October 2000, pp. 735-740

7) Mashiri F.R, Zhao. X.L., Grundy P. 2001, "Fatigue behaviour of thin-walled tube-to-tube T-joints under in-plane bending" *Tubular Structures IX*, Proceedings of The 9th International Symposium on Tubular Structures, ISTS9, Editors: Puthli R. and Herion S., 3-5 April 2001 ***(Accepted for Publication)***

Journal Papers

8) Mashiri F.R, Zhao. X.L., Grundy P. 2000, "Crack Propagation Analysis of Welded Thin-Walled Joints using Boundary Element Method" *Computational Mechanics*, Vol. 26, No. 2, Springer-Verlag 2000, pp. 157-165

9) Mashiri F.R, Zhao. X.L., Grundy P. 2001, "Effect of weld profile and undercut on fatigue crack propagation life of thin-walled cruciform joint" *Thin-Walled Structures*, Vol. 39, Issue 3, March 2001, Elsevier Science Ltd, pp. 261-285

10) Mashiri F.R, Zhao. X.L., Grundy P. 2001, "Fatigue Tests and Design of Thin Cold-Formed SHS-to-Plate T-Joints under In-Plane Bending" *Journal of Structural Engineering*, ASCE ***(Under Review)***

[redacted]

FIDELIS RUTENDO MASHIRI

March 2001

ACKNOWLEDGEMENTS

I am sincerely grateful to my supervisors Dr. Xiao-Ling Zhao and Professor Paul Grundy for their expert advice and invaluable support during my candidature at Monash University. To Dr. Xiao-Ling Zhao, thank you for trusting me to take up this candidature even when I was thousands of miles away in Chile, South America.

I would also like to thank Professor Takeshi Mori of Hosei University, Japan for his help in the use of the silicon imprint technique used for measuring weld profile and undercut dimensions in this research and for his comments in many other aspects related to this research.

Thanks are given to Prof. Jaap Wardenier, Dr. Arnoldus Martinus van Wingerde in The Netherlands, Prof. Ram Puthli in Germany and Prof. Jeffrey Packer in Canada for their encouragement and comments.

I am also grateful to the sponsors of this project; the Australian Research Council (ARC) for providing a Large Grant and to the International Committee for the Development and Study of Tubular Structures (CIDECT) for a providing CIDECT fund.

Thanks to BHP Steel-Structural and Pipeline Products, now OneSteel (Australia) and Voest Alpine (Austria) for supplying cold-formed SHS tubes. I am also indebted to Mr. Hayden Dagg for providing all the literature relating to the BHP steel and to Mr. Suppan Werner for providing technical details of the European steel used in this project.

Thanks also to Mr. Roger Doulis and Mr. Roy Goswell, Mr. Max Graham and Mr. Graham Rundle of Monash University, Civil Engineering Laboratories for their support in building the control systems and accessories used in the multiple fatigue rig testing. To Mr. Roy Goswell, my sincere gratitude for your selfless dedication in helping with all the modifications of and additions to the test rigs. I am also grateful to Mr. Roger Doulis for his help and expertise in programming the PLC. Lots of thanks to Mr. Jeff Doddrell and Mr. Len Doddrell and Mr Peter Dunbar for their help in setting up and many other tasks around the strong floor.

I am also grateful to the Department of Materials Engineering staff, Dr. Chris Davies, Dr. Simon Ringer, Mr Hugh Venables, Mr. Long Kim Goh, Mr. Renjii Pan and Mr. Irek Kozicki for their assistance with the hardness tests, macro-cross section examination tests, measurement of silicon imprint samples and the use of microscopes.

I will also like to thank my friends and colleagues for their support and encouragement during my research as well as the laughs we had together, Mr. Masood Alikhail, Mr. Dishan Candappa, Mr Deric Ong and Mr. Kiew Kwong. I will always cherish the wonderful times we had together.

I am also grateful to my Mom, Mai Rutendo; my Dad, Baba Rutendo; my brothers, Tawanda, Farai and Simbisai and my sisters, Fadzai, Chiedza and Vongai for their encouragement and giving me hope during my research.

To my wife, Soledad and to my daughter, Micaela, thank you for your love and patience and for always being there for me.

FIDELIS RUTENDO MASHIRI

TABLE OF CONTENTS

NOTATION

The following symbols are used in the thesis. The interpretation of a symbol will be evident from the context if more than one meaning is assigned to the symbol.

LATIN LETTERS

A	Area of cross section, or
	Intercept of S-N curve when *log N* is the dependent variable, or
	Current
a	Crack length (mm), or
	Intercept of S-N curve when *log S* is the dependent variable
A_0	Cross-sectional area of the chord member
Al	Aluminium
API	American Petroleum Institute
ARC	Australian Research Council
AS	Australian Standard
AWS	American Welding Society
B	Width of cross section, or
	Slope of S-N curve when *log N* is the dependent variable
b	Section width of member, or
	Slope of S-N curve when *log S* is the dependent variable
b_0	External width of hollow section chord member
b_1	External width of hollow section brace member (90^0 to the plane of the truss)
b_e	Effective width of bracing member
BEASY	Boundary Element Analysis System Software
BEM	Boundary element analysis
BSI	British Standards Institute
C	Crack growth rate coefficient, or
	Carbon
c	Value to minimize the scatter in the N (number of cyles)

	direction
CE	Carbon equivalence
CEN	Committee for European Standardization
CHS	Circular hollow section
CIDECT	International Committee for the Development and Study of Tubular Structures
COV	Coefficient of variation
Cr	Chromium
Cu	Copper
D	Depth of cross section
d	Depth of undercut, or Mean diagonal of indentation of diamond indenter
$d_{1,2}$	Diagonals of indentation of diamond indenter
da	Crack length increment
DEn	Department of Energy
dN	Number of cycles to cause crack length increment, da
DnV	Det noske Veritas
E	Young's Modulus
EC	Eurocode
f	Crack opening function
F	Axial force, or Force
f(n)	Function to allow the reduction in connection moment capacity in the presence of large compression chord forces.
F_e	Correction factor for crack shape
FEM	Finite element analysis
F_g	Correction factor for stress gradient
F_h	Correction factor for eccentricity of crack against central axis of plate
f_k	Buckling stress according to steelwork specification, using a column slenderness ratio KL/r
F_s	Correction factor for surface crack
F_t	Correction factor for finite thickness and width of plate

f_u	Ultimate tensile strength
f_y	Yield stress
f_{y0}	Yield stress of chord member
f_{y1}	Yield stress of the brace member
G.F.	Gauge factor
h	Section height of member
h_1	External depth (in plane of truss) of hollow section brace member
HAZ	Heat affected zone
h_0	External depth of hollow section chord member
HSSNR	Hot spot strain range
HV	Vickers hardness
IIW	International Institute of Welding
JSSC	Japanese Society of Steel Construction
K	Effective length factor
K_c	Critical stress intensity factor ($N.mm^{-3/2}$)
K_{eff}	Effective stress intensity factor
K_{eff}^{max}	Maximum effective stress intensity factor
K_{eff}^{min}	Minimum effective stress intensity factor
K_I	Stress intensity factor for mode I ($N.mm^{-3/2}$)
K_{Ic}	Fracture toughness under plane strain conditions
K_{II}	Stress intensity factor for mode II ($N.mm^{-3/2}$)
$K_{III}^{P'}$	Stress intensity factor for mode III at point P' on the crack front
$K_{II}^{P'}$	Stress intensity factor for mode II at point P' on the crack front
$K_I^{P'}$	Stress intensity factor for mode I at point P' on the crack front
K_{max}	Maximum stress intensity factor ($N.mm^{-3/2}$)
K_{min}	Maximum stress intensity factor ($N.mm^{-3/2}$)
K_{op}	Opening stress intensity factor below which the crack is closed
K_t	Stress concentration factor
L	Length of member, or Length of attachment
l_1	Throat thickness of weld at an angle of 22.5° to the horizontal

l_2	Throat thickness of weld at an angle of 67.5^0 to the horizontal
M	Bending moment
m	Exponent in Paris equation, material constant
M_0	Bending moment in the chord member
M_1	Bending moment in the brace member
MCM1	Multi-Channel Monitors
$M_{elastic.max}$	Maximum elastic moment below which the moment-deflection curve is linear
MF	Multiplication factor in modified Paris Equation
MIG	Gas-Metal Arc Welding
M_{ip}	Static strength of joint for in-plane bending
$M_{ip}*$	Connection resistance for in-plane bending, expressed as a bending moment in bracing member.
Mn	Manganese
Mo	Molibdinum
M_s	Nominal section moment capacity
M_{static}	Nominal static strength of joint for in-plane bending
N	Number of cycles
n	Exponent
N_0	Axial force applied to the chord member
N_1	Number of cycles corresponding to a 15% change in strain measured "near" the crack initiation point
N_2	Number of cycles corresponding to the first "visible" crack
N_3	Number of cycles corresponding to through-thickness crack
N_4	Number of cycles corresponding to the end of the test or the complete loss of failure
N_B	Fatigue life for a reference plate thickness, t_B
N_c	Through-thickness fatigue life
N_f	Number of cycles to failure
Ni	Nickel
P	Point load, or Phosphorus
p	Exponent in modified Paris equation (NASGRO equation)

PLC	Programmable Logic Controller
P_{max}	Point load corresponding to $M_{elastic,max}$, maximum elastic moment
PWHT	Post weld heat treatment
q	Exponent in modified Paris equation (NASGRO equation)
R	Stress ratio, or Outside radius of the chord
r	Radius of gyration, or Outside radius of the brace
r_0	Length of the initial crack extension
S	Stress range, or Sulphur, or Strain energy density factor
S_0	Elastic modulus of the chord member
SAA	Standards Association of Australia
S_B	Fatigue strength for a reference plate thickness, t_B
SCF	Stress concentration factor
SCF_{a0}	Stress concentration factor due to nominal axial stress in the chord
SCF_{a1}	Stress concentration factor due to nominal axial stress in the brace
$SCF_{axial\text{-}force\text{-}in\text{-}brace}$	SCF for load condition "axial force in brace"
$SCF_{axial\text{-}force\text{-}in\text{-}chord}$	SCF for load condition "axial force in chord"
$SCF_{axial\text{-}force\text{-}in\text{-}COV\text{-}brace}$	SCF for load condition "axial force in carry-over brace"
$SCF_{axial\text{-}force\text{-}in\text{-}REF\text{-}brace}$	SCF for load condition "axial force in reference brace"
SCF_{chord}	Maximum stress concentration factor in the chord
$SCF_{ipb\text{-}in\text{-}brace}$	SCF for load condition "in-plane-bending in brace"
$SCF_{ipb\text{-}in\text{-}chord}$	SCF for load condition "in-plane-bending in chord "
$SCF_{ipb\text{-}in\text{-}REF\text{-}brace}$	SCF for load condition "in-plane-bending in reference brace"
SCF_l	Stress concentration factor determined by the linear extrapolation method
SCF_{m0}	Stress concentration factor due to nominal in-plane bending stress in the chord

SCF_{ml}	Stress concentration factor due to nominal in-plane bending stress in the brace
$SCF_{opb\text{-}in\text{-}brace}$	SCF for load condition "out-of-plane-bending in brace"
$SCF_{opb\text{-}in\text{-}COV\text{-}brace}$	SCF for load condition "out-of-plane-bending in carry-over brace"
$SCF_{opb\text{-}in\text{-}REF\text{-}brace}$	SCF for load condition "out-of-plane-bending in reference brace"
SCF_q	Stress concentration factor determined by the quadratic extrapolation method
SCF_{tot}	Total stress concentration factor, obtained by dividing total hot spot stress concentration factor by the nominal stress in the brace, influence of induced bending in the chord is not taken into account (S_{hs}/σ_{ml})
S_{eq}	Equivalent stress range for variable stress amplitude loading
S_{hs}	Total hot spot stress at any hot spot location
SHS	Square Hollow Section
S_i	Stress range "i" in variable stress amplitude loading
Si	Silicon
S_{max}	Maximum applied stress
S_{min}	Minimum strain energy density factor
SP	Structural Purpose
S_r	Nominal stress range (MPa)
SR	Ratio of maximum applied stress to flow stress
$S_{r,axial\text{-}force\text{-}in\text{-}brace}$	Nominal stress range due to axial force in brace
$S_{r,axial\text{-}force\text{-}in\text{-}chord}$	Nominal stress range due to axial force in chord
$S_{r,axial\text{-}force\text{-}in\text{-}COV\text{-}brace}$	Nominal stress range due to axial force in carry-over brace
$S_{r,axial\text{-}force\text{-}in\text{-}REF\text{-}brace}$	Nominal stress range due to axial force in reference brace
$S_{r,ipb\text{-}in\text{-}brace}$	Nominal stress range due to in-plane-bending in brace
$S_{r,ipb\text{-}in\text{-}chord}$	Nominal stress range due to in-plane-bending in chord
$S_{r,ipb\text{-}in\text{-}REF\text{-}brace}$	Nominal stress range due to in-plane-bending in reference brace
$S_{r,opb\text{-}in\text{-}brace}$	Nominal stress range due to out-of-plane-bending in brace
$S_{r,opb\text{-}in\text{-}COV\text{-}brace}$	Nominal stress range due to out-of-plane-bending in carry-over

	brace
$S_{r,opb\text{-}in\text{-}REF\text{-}brace}$	Nominal stress range due to out-of-plane-bending in reference brace
$S_{r,t}$	Nominal stress range of the thickness t, under consideration
$S_{r,hs}$	Total hot spot stress range at any hot spot location, usually defined by lines A to E
$S_{r,hs,25}$	Stress range for a reference thickness of 25mm
$S_{r,hs,t}$	Hot spot stress range of the section of thickness, t in the joint under consideration,
$S_{r,hs32}$	Hot spot stress range of the T-curve, which relates to a reference thickness of 32mm
S_{rhs}	Hot-spot stress range (MPa)
$S_{rhs,16}$	Hot spot stress range for a reference thickness of 16mm
S_{ri}	Nominal stress range at 2 million cycles for welded construction with i depth of undercut
$S_{r\text{-}nom}$	Nominal stress range (MPa)
$S_{r\text{-}nom,2mil}$	Nominal stress range for mean S-N curve corresponding to 2 million cycles of failure
S_{ro}	Nominal stress range at 2 million cycles for welded construction with "zero" depth of undercut
t	Wall thickness of member, or Thickness of cross section, or Wall thickness of the brace
T	Wall thickness of the chord, or Plate thickness
t_0	Thickness of hollow section chord member
t_1	Thickness of hollow section brace member
t_B	Reference plate thickness
T_{cr}	Wall thickness of cracked member
TIG	Gas-Tungsten Arc Welding
t_t	Throat thickness of weld at an angle of 45° to the horizontal
t_w	Weld leg length
t_{wh}	Weld leg length in the chord

t_{wv}	Weld led length in the chord
u_b^P	Projection of $\mathbf{u}^P$ on the coordinate direction b of the local crack front coordinate system
u_n^P	Projection of $\mathbf{u}^P$ on the coordinate direction n of the local crack front coordinate system
$\mathbf{u}^P$	Displacement at point **P**
u_t^P	Projection of $\mathbf{u}^P$ on the coordinate direction t of the local crack front coordinate system
V	Vanadium, or
	Voltage
W	Plate width
x	Variable
Y	Stress intensity correction factor
y	Variable
Z	Elastic section modulus
Z_0	Elastic section modulus of the chord
Z_1	Elastic section modulus of the brace
Z_1	Plastic section modulus of the brace member
Z_e	Effective section modulus

GREEK LETTERS

α	Relative chord length ($2l_0/b_0$), or
	Plain stress/strain constraint factor
β	Brace width to chord width ratio
Δa	Incremental size at crack front point
Δa_{max}	Incremental size at the crack front point corresponding to $\max\{S_{min}\}$
ΔK	Stress intensity factor range ($N.mm^{-3/2}$)
ΔK_{eff}	Effective stress intensity factor range
ΔK_{th}	Threshold stress intensity factor range ($N.mm^{-3/2}$)
δV	Change in reading in microvolts

$\Delta\sigma$	Nominal stress range (MPa)
ε	Mean true strain measured by an active gauge
ε_x	Strain perpendicular to the weld toe
ε_y	Strain parallel to the weld toe
ε_z	Strain normal to the x-y plane
2γ	Chord width to chord thickness ratio
Φ	Weld toe angle
μ	Shear modulus of elasticity or Mean
υ	Poisson's ratio
θ	Angle between *r* and *n* in crack front coordinate system
θ_1	Included angle between bracing member and the chord
σ	Stress, or Standard deviation
$\hat{\sigma}_{\log N}$	Standard deviation of the normal distribution for *log N*
$\hat{\sigma}_{\log S}$	Standard deviation of the normal distribution for *log S*
σ_o	Flow stress
σ_{UTS}	Uniaxial ultimate tensile strength of material
σ_{ys}	Uniaxial yield stress of material
σ_{a0}	Nominal axial stress in the chord
σ_{a1}	Nominal axial stress in the brace
σ_{hs}	Hot Spot Stress
σ_{m0}	Nominal in-plane bending stress in the chord
σ_{m1}	Nominal in-plane bending stress in the brace
σ_{nom}	Beam theory nominal stress
$\sigma_{nom.exp}$	Experimental nominal stress, obtained from strain gauge measurements
$\sigma_{r.a0}$	Nominal axial stress range in the chord
$\sigma_{r.a1}$	Nominal axial stress range in the brace
$\sigma_{r.m0}$	Nominal in-plane bending stress range in the chord

$\sigma_{r,mI}$	Nominal in-plane bending stress range in the brace
σ_{tot}	Total hot spot stress at any hot spot location
σ_x	Stress perpendicular to the weld toe
τ	Brace wall thickness to chord wall thickness ratio

Chapter 1
INTRODUCTION

1.1 BACKGROUND

There has been an increase in the use of cold-formed sections in the building industry (Walker 1975; Yu 1991; Hancock 1994; Packer and Henderson 1997; Zhao and Mahendran 1998). Cold-formed tubular sections are hollow sections formed and shaped at ambient temperature from a single strip of steel, the seam being continuously welded by electric resistance welding. All the tubular sections manufactured in Australia are now cold-formed. Approximately one million tonnes of steel are used each year in Australia, of which 125,000 tonnes are cold-formed open sections such as purlins and girts and 400,000 tonnes are tubular members. In Australia, the total quantity of cold-formed products now exceeds the total quantity of hot-rolled products (Hancock 1999). The cold-formed sections are relatively thin, ranging from 12.7 mm to 1.6 mm, when compared with hot-rolled sections, ranging from 12.7 mm to 90 mm, used in offshore structures. The use of cold-formed sections means that, there has been a trend towards using thin-walled tubular sections in the construction industry. Thin-walled hollow sections result in lighter structural connections that are cheaper but at the same time providing enough static strength (Zhao and Hancock 1998).

Thin-walled structural hollow sections offer a good ratio between weight and resistance of longitudinal and lateral forces from all directions. Compared to open sections, hollow structural sections also have a large torsional resistance that prevents lateral buckling. They also have a better cross-sectional area to exposed area compared to open sections resulting in cheaper protection against corrosion and better fire-resistance. Aesthetically their shape and joints appeal to architects (Wardenier 1982; Wardenier 1999).

Cold-formed tubular members are used more often in modern steel construction such as the new Olympic Aquatic Centre at Homebush bay in Sydney, which has a steel structural roof consisting of mainly tubular members, and the Melbourne Central where about 13 kilometres of tubular sections are used (Zhao *et al*, 1996). Building structures are mainly subjected to static loads.

A significant amount of research has been undertaken in Australia to determine the static behaviour of these sections (Key *et al* 1998; Zhao and Hancock 1992, 1995a, 1998; Zhao *et al* 1995; Wilkinson and Hancock 1998c) and welded connections (Zhao and Hancock 1991, 1995b, 1995c, 1996; Wilkinson and Hancock 1998a, 1998b, 1998d, 2000a, 2000b; Zhao *et al* 1999c).

Tubular sections are suitable for construction of steel communication towers (Dean & Bennett, 1994), truss bridges (BHP, 1995), crane booms, lighting poles and highway sign supports (Packer and Henderson 1997). These types of constructions are under fatigue loading.

Thin-walled tubular sections (t<4mm) are increasingly being used in the road transportation industry and agricultural industry for applications such as lighting poles, traffic sign supports, truck trailers, swing-ploughs, haymakers and linkage graders. The support systems and undercarriages in these applications are subjected to fatigue loading and some failures have been observed.

Although a lot of research has been done on fatigue of welded tubular structures (Verheul & Noordhoek 1987; van Wingerde 1992, van Wingerde *et al* 1996a,1997b,1997c), only to name a few, little has been done on the fatigue of thin-walled sections below 4mm (Wardenier 1982; Puthli *et al* 1989, van Wingerde *et al* 1996b).

A review of current fatigue design guidelines such as EC3 (1992), Department of Energy Guidelines (1990), AS4100-1998 (SAA 1998a), IIW (2000) and CIDECT Design Guide No. 8 (Zhao *et al* 1999a) show that existing fatigue design rules apply only to welded tubular joints with thicknesses greater than or equal to 4mm.

Failure of welded connections under fatigue loading is a result of the stress concentrations resulting from the overall joint and weld geometry. In the hot-spot stress method, which aims to include the effects of the overall joint geometry on the stress distribution and hence on the fatigue behaviour of the joint, the S_{rhs}-N_f curve shows that fatigue strength improves as the thickness of member which fails becomes thinner (van Wingerde *et al* 1997b) However, this may not be the case when the thickness of the member which fails becomes significantly small, the depth of undercut, for example becomes a considerable percentage of the thickness. Fatigue life may reduce significantly for sections with a thickness less than 4mm due to the effect of weld defects (Puthli *et al* 1989, Mashiri *et al* 1997, 1998b). Weld defects occur in the form of undercuts at the weld toe. Therefore, there is a need to determine fatigue design rules for welded tubular joints with thicknesses less than 4mm.

This investigation is a research project on fatigue of welded joints in thin-walled tubes (t<4mm) currently running at Monash University, Australia (Zhao *et al* 1998). The project is sponsored by the Australian Research Council (ARC), International Committee for the Development and Study of Tubular Structures (CIDECT) and BHP Structural and Pipeline Products (now OneSteel). In this research, the fatigue behaviour of T-joints made of thin-walled square hollow sections (SHS) is investigated. The T-joints are subjected to cyclic in-plane bending load. The wall thicknesses of the sections are below 4mm. Three wall thicknesses of square hollow sections (SHS) were chosen, that is 1.6mm, 2mm and 3mm. The T-joints are divided into two types as shown in Figure 1-1, the tube-to-plate connections and the tube-to-tube connections. This is because a review of the design rules for welded tube-to-plate T-joints in Australian (SAA 1998a), European (EC3 1992) and Canadian (CSA 1989) standards shows that there are no guidelines in these current standards for the fatigue design of these joints. Design rules for welded tube-to-tube T-joints in American (API 1991, AWS 1998), British (DEn 1990), European (EC3 1992), IIW (2000) and CIDECT (Zhao *et al* 1999a) fatigue design standards have also been reviewed and show the lack of design S-N curves for welded thin-walled tubular connections with wall thicknesses less than 4mm. A series of tests will be performed for each connection type with the parameter range shown in Table 1-1. Constant stress-amplitude fatigue loading will be applied.

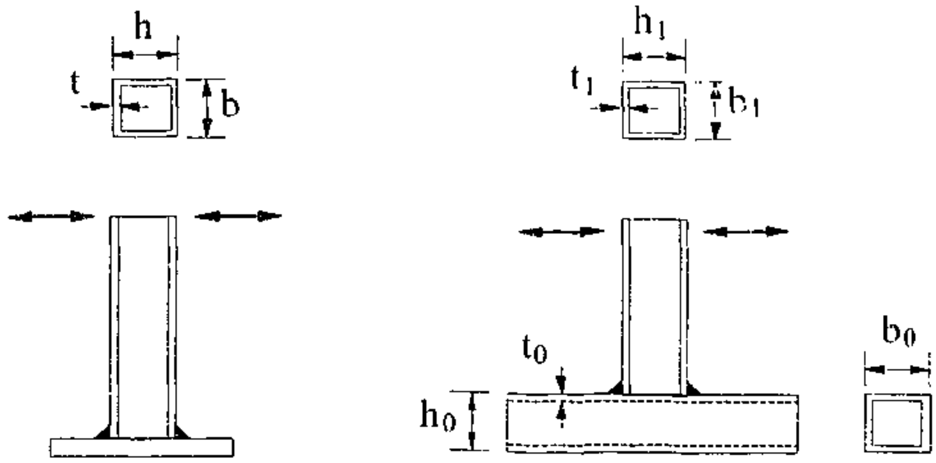

(a) Tube-to-Plate Connection *(b) Tube-to-Tube Connection*

Figure 1-1: Types of T-joints

The connections in this investigation are made up of cold-formed square hollow sections (SHS). The following grades of tubes are used in this investigation;

(a) Grade C350LO, non-galvanised cold-formed tubes manufactured by One Steel, Australia

(b) Grade C450LO, DuraGal "in-line" galvanised tubes also manufactured by One Steel, Australia and

(c) Grade S355JOH, manufactured by Voest Alpine, Krems, Austria

Table 1-1: Parameter Range of T-joints

Steel Type	**Type of Joint**	**2γ** $\left(=\frac{h_o}{t_o}\right)$	**β** $\left(=\frac{b_1}{b_o}\right)$	**τ** $(=\frac{t_1}{t_o})$	**R**
C350LO	Tube-to-Plate	-	-	0.3; 0.16	0.1; 0.5
	Tube-to-Tube	33; 25	0.35; 0.5; 0.67	1.0; 0.5	0.1
C450LO DuraGal	Tube-to-Plate	-	-	0.3; 0.2	0.1
	Tube-to-Tube	33, 25	0.35; 0.5; 0.67	1.0; 0.5	0.1
S355JOH	Tube-to-Plate	-	-	0.3; 0.2	0.1
	Tube-to-Tube	33; 23	0.3; 0.5; 0.57; 0.6; 0.71	0.7; 1.0	0.1

1.2 OBJECTIVES OF THESIS

The proposed research aims to investigate the fundamental fatigue mechanism for welded tube-to-plate and tube-to-tube T-joints made up of thin-walled square hollow sections where the tube wall thicknesses are less than 4mm. The effect of welding profiles and welding defects especially undercut on thin-walled joints will be addressed. Thickness effect as it relates to welded thin-walled connections will also be discussed. The key parameters influencing fatigue life in welded thin-walled joints will be identified. Accurate and reliable fatigue rules for welded thin-walled tube-to-plate and tube-to-tube T-joints used in onshore structures will be established.

The following are specific objectives relating to fatigue behaviour of welded joints, which are covered in this thesis in order to understand and address the issues relating to the fatigue behaviour of welded thin-walled tubular joints:

(a) To study the factors influencing fatigue life of welded joints, methods used for fatigue design and design rules for welded joints in existing fatigue design guidelines.

(b) To verify the suitability of the gas-metal arc welding (MIG) and the gas-tungsten arc welding (TIG) methods in joining thin-walled ($t<4$mm) joints with particular emphasis on compliance of weld toe undercut dimensions to Australian welding standards.

(c) To determine the level of loading required to produce a high-cycle fatigue response in tube-to-plate and tube-to-tube T-joints made up of thin-walled square hollow sections.

(d) To obtain experimentally, S-N data of thin-walled tube-to-plate T-joints under cyclic in-plane bending and to document the failure modes in these connections.

(e) To obtain experimentally, S-N data of thin-walled tube-to-tube T-joints under cyclic in-plane bending and to document the failure modes in these connections.

(f) To verify the effects of weld profile and weld toe undercut dimensions on both thin-walled and thick-walled cruciform joints using the boundary element method in order to develop an understanding of the key parameters influencing fatigue life in thin-walled joints.

(g) To determine design S-N curves for welded tube-to-plate T-joints made up of thin-walled (t<4mm) tubes, under cyclic in-plane bending and to compare them with existing design S-N curves for tube-to-plate joints.

(h) To determine design S-N curves for welded tube-to-tube T-joints made up of thin-walled (t<4mm) tubes, under cyclic in-plane bending and to compare them with existing design S-N curves for tube-to-tube joints.

(i) To propose new design S-N curves for welded thin-walled tube-to-plate and tube-to-tube T-joints made up from square hollow sections of tube wall thicknesses less than 4mm.

(j) To identify areas of future research in fatigue behaviour and design of welded thin-walled joints

1.3 SCOPE OF THESIS

The following tasks have been carried out in each chapter of the thesis to address the objectives of this research as follows:

Chapter 2: Literature Review

- Discuss the factors affecting fatigue of welded connections such as weld shape, weld toe and weld root conditions. The effects of residual stress and stress ratio on fatigue life are also discussed.
- Review the methods used for fatigue assessment of welded tubular joints such as the classification, hot spot stress, punching shear, failure criterion, static strength and fracture mechanics methods.
- Review the design rules for tubular welded connections from different guidelines such as the Department of Energy (1990), API (1991), DnV (1981), EC3 (1992), AWS (1998), CIDECT Design Guide No. 8 (Zhao *et al* 1999a) and IIW (2000).
- Review the fracture mechanics theories which can be used for estimating fatigue crack propagation life as given in different guidelines such as BSI (1991), JSSC (1995) and Computational Mechanics BEASY Ltd (1998).
- Discuss the thickness effect in both welded plated joints and welded tubular joints.

- Review the static strength of welded tubular T-joints made up of square hollow sections in order to determine the levels of stress applicable for a high cycle fatigue response.

Chapter 3: Welding Procedure and Welding Defects

- Determine the welding procedures of welded thin-walled tubular joints made from square hollow sections (SHS) of wall thicknesses below 4mm, using the gas-metal arc welding (MIG) and gas-tungsten arc welding (TIG) methods.
- Check the compliance of the MIG and TIG welding procedures to Australian welding standards in relation to macro-cross section examination and hardness tests.
- Determine the weld profiles in thin-walled joints and to compare their sizes to minimum recommended sizes in the standards.
- Verify the occurrence of weld toe undercuts and to determine the magnitude of their depth, width and radius as well as to check the compliance of the measured depth of undercut with Australian welding standards.
- Check the occurrence of surface cracks on the welded interface of thin-walled joints using the magnetic particle testing methods.

Chapter 4: Material Properties and Static Tests

- Use tensile coupon tests to verify the steel grades of different steels used in this investigation.
- Determine moment versus angle-of-inclination and moment versus deflection curves of tube-to-plate and tube-to-tube T-joints.
- Deduce the elastic region of static response of the tube-to-plate and tube-to-tube T-joints from the moment versus angle-of-inclination graphs, and use the loads corresponding to the elastic region of static response to obtain a high-cycle fatigue response.

Chapter 5: Fatigue Tests and Experimental SCF of Tube-to-Plate T-joints

- Obtain S-N data for thin-walled ($t<4mm$) tube-to-plate T-joints under cyclic in-plane.

- Observe the modes of fatigue failure of tube-to-plate T-joints under cyclic in-plane bending.
- Verify the effect of galvanising, steel grade, stress ratio and tube-wall thickness on fatigue life of tube-to-plate T-joints.
- Determine the magnitude of stress concentration factors (SCFs) in tube-to-plate T-joints experimentally using strain gauges.

Chapter 6: Fatigue Tests and Experimental SCF of Tube-to-Tube T-joints

- Obtain S-N data for thin-walled (t<4mm) tube-to-tube T-joints under cyclic in-plane bending.
- Observe the modes of fatigue failure of tube-to-tube T-joints under cyclic in-plane bending.
- Determine the magnitude of stress concentration factors (SCFs) in tube-to-tube T-joints experimentally through strain gauges measurements.
- Compare the magnitude of stress concentration factors (SCFs) determined experimentally to the SCFs determined using existing parametric equations.
- Determine the influence of induced axial load in the chord due to applied in-plane bending load in the brace on SCFs as well as to check the influence of induced bending moment in the chord due to the applied in-plane bending load in the brace on SCFs.

Chapter 7: Effect of Weld Profile and Weld Undercut on Fatigue Crack Propagation Life of Thin-Walled Cruciform Joints

Improve the understanding of the effects of weld profiles and weld undercut on welded thin-walled welded joints using simpler joints, that is non-load carrying cruciform joints and employing the boundary element method for analysis to determine fatigue crack propagation life, as follows:

- Determine the effect of weld profiles measured from the MIG and TIG welded connections on fatigue crack propagation life of welded thin-walled cruciform joints using the boundary element method.

- Evaluate the effect of undercut depth, undercut width and undercut radius on fatigue crack propagation life of thin-walled cruciform joints using the boundary element method.
- Compare the effects of undercut depth, width and radius on fatigue crack propagation life of thin-walled and thick-walled cruciform joints.

Chapter 8: Design Rules for Tube-to-Plate T-joints

- Determine design curves from S-N fatigue data for thin-walled tube-to-plate T-joints using the least-squares method for both the classification approach and the hot spot stress approach.
- Determine design curves using the least-squares method for the cases when either *log N* or *log S* is the dependent variable.
- Determine design curves for the natural slope of the S-N data and when the slope of the S-N curve is fixed to a predetermined value from the standards.
- Compare the design S-N curves of the tube-to-plate T-joints with tube of wall thicknesses less than 4mm to the existing design S-N curves for tube-to-plate joints in the current standards.

Chapter 9: Design Rules for Tube-to-Tube T-joints

- Determine design curves from $S_{r,hs}$-N fatigue data for thin-walled tube-to-tube T-joints using the least-squares method for the hot spot stress approach.
- Determine design curves using the least-squares method for the cases when either *log N* or *log S* is the dependent variable.
- Determine design curves for the natural slope of the S-N data and when the slope of the S-N curve is fixed to a predetermined value from the standards.
- Compare the design S-N curves of the tube-to-tube T-joints with tubes of wall thicknesses less than 4mm to the existing design S-N curves for tube-to-tube joints in current guidelines.

Chapter 10: 3D Crack Propagation Analysis of Tube-to-Plate T-Joint using Boundary Element Method

- Determine the stress concentration factors (SCFs) of a tube-to-plate T-joint using the boundary element method.
- Compare the SCFs for the tube-to-plate T-joint obtained numerically from the boundary element method with those determined experimentally from strain gauge measurements.
- Estimate the fatigue crack propagation life of a tube-to-plate T-joint using the boundary element method.
- Compare the S-N curve for the determined from the 3D crack growth analysis with the S-N curve derived from experimental S-N data of tube-to-plate T-joints.

Chapter 11: Conclusions

- Conclusions arrived at in the different Chapters of the thesis are highlighted.
- Recommendations for the fatigue design of welded thin-walled (t<4mm) tube-to-plate and tube-to-tube T-joints under in-plane bending given.
- Future research areas in the fatigue behaviour and design of welded thin-walled joints are identified.

Chapter 2
LITERATURE REVIEW

Fatigue is the process by which a crack can form and then grow under repeated or fluctuating loading. When the crack is permitted to propagate to a critical size, damage due to sudden collapse, excessive deflection or leakage of a container can occur. The loading required to produce fatigue cracking may be much less than the load corresponding to the allowable static design stress. Any variation in the loading experienced by a member should be considered as potential fatigue loading, no matter how small or infrequent (Maddox 1991; Marshall 1992).

Fatigue loading may occur as a result of the following:

(i) Variations in live load applied during the service life of the structure,
(ii) Pressure changes,
(iii) Vibrations,
(iv) Temperature fluctuations,
(v) Wave forces, and
(vi) Wind forces.

Welded structures under fatigue loading include;

(i) Road transport and agricultural industry equipment such as road and agricultural trailers, swing ploughs, graders and haymakers,
(ii) Bridges,
(iii) Cranes,
(iv) Excavators,
(v) Ships,
(vi) Vehicles,
(vii) Masts,
(viii) Recreation structures such as giant wheels in amusement parks,
(ix) Offshore Structures, and
(x) Pipelines.

Fatigue cracking can and generally does arise under allowable applied stresses. Fatigue cracks initiate when the applied stress is less than the ultimate strength of the component, because of stress concentrations. Stress concentrations are caused by all discontinuities in a stressed member. At these locations, the level of stress is raised above the average stress in that region.

2.1 FACTORS AFFECTING FATIGUE OF WELDED CONNECTIONS

2.1.1 Stress Concentration caused by Weld Shape

A weld bead made across a piece of plate could produce a change of shape and if loaded perpendicular to the axis of the weld would produce a stress concentration. The stress concentration occurs at the toe of the weld. The toe of the weld is the junction of the plate surface and the weld metal. The magnitude of stress concentration at the toe of the weld depends on the transition between the plate and the weld metal. A smooth transition results in a lower stress concentration compared to an abrupt change. A fillet weld produces a higher stress concentration compared to a butt weld. A weld does not necessarily need to be load carrying to introduce a stress concentration. Therefore, all welded attachments are stress concentration areas, and potential fatigue crack sites.

When loaded parallel to the weld, stress concentrations are caused by weld ripples and lumps due to stop-starts (Maddox 1991).

2.1.2 Welds Toe Conditions

Undercutting of the plate surface often occurs at the toes of the welds. The weld may also adopt an abrupt convex profile. Very small crack-like discontinuities termed "intrusions" exist at the weld toe and they are a product of conditions during welding which, arise in most of the arc welding processes. All these conditions in welded connections result in stress concentrations. The difference between welded and unwelded details is that in welded constructions the number of stress cycles needed to initiate a fatigue crack is therefore greatly reduced, while for unwelded details fatigue crack initiations may occupy a significant portion of the total fatigue life (Maddox 1991).

2.1.3 Weld Root Condition

Partial penetration welded joints, contain the weld root which cause local stress concentration. The crack can initiate at the root and can propagate across the weld throat (Maddox 1991).

2.1.4 Residual Stress

Welding operations produce "locked-in" stresses whose existence is independent of external loading. The locked-in stresses are balanced within the body of the material, producing a system of tensile and compressive stresses in equilibrium. Residual stresses arise as a result of the weld heating and cooling cycle. The natural expansion and contraction of material close to the heat source is inhibited by the restraining effect of adjacent material at a lower temperature. During the cooling stage, the longitudinal shrinkage of the weld metal is resisted. The weld metal therefore has to accommodate its unnatural length by plastic strain. When cold the weld metal is subjected to longitudinal tensile stress. Stresses of yield point magnitude will exist. The existence of residual stresses of yield stress magnitude implies that stress cycles which are partially or even wholly compressive would be expected to be damaging, from the fatigue point of view, as cycles with the same stress range which are wholly tensile (Gurney 1977b). If the residual stress is at yield in tension, there will be little effect of the externally applied stress ratio since the local stress ratio (stress ratio at the weld toes) will be positive (Harrison 1981). Longitudinal as well as transverse residual stresses occur and in both cases tensile stresses are balanced by compressive stresses. The fact that tensile residual stresses having values equal to the yield stress of the weld metal, means that if an external tensile stress is applied yielding of the joint happens on the onset of loading (Maddox 1991).

Gurney (1977b) reported on fatigue tests which were carried out under pulsating tension (R=0) loading on as-welded and stress relieved specimens of both transverse and longitudinal non-load carrying fillet welds in plated joints to determine the influence of residual stress. For the as-welded joints, spot heating on parts of the welds which forms the hot spot region was performed to induce tensile residual stresses. The stress relieved specimens tended to give a longer life than the as-welded specimens and there was a distinct indication of a higher fatigue limit. Fatigue failure also occurred under fully compressive (R = 0), partly compressive (R = -2) and alternating (R = -1) loading in the as-welded condition. Cracking initiated in the region of the heated spot (tensile residual stress) and propagated along the weld toe as in tensile fatigue tests. In the stress relieved condition, compressive loading is more or less non-damaging, and this shows that the presence of residual stresses transforms compressive stresses into being damaging.

Shi *et al* (1990) investigated the effects of welding residual stresses on the fatigue crack growth rate and its relation with the position of the crack and its orientation with respect to the weld line. Crack growth behaviour was also examined in a "cross-bond type specimen" where the crack front was composed of both the weld metal region and the parent metal region. Crack growth in the cross-bond specimen may represent the complex situation in the real welded joints. For a crack growing within the weld or at the toes of the weld in butt-welded plate joints, crack closure is controlled by both transverse and longitudinal residual stresses and is gradually weakened with increasing fatigue crack length due to partial welding residual stress relief and its redistribution. Fatigue crack growth rate is strongly dependent on the residual stresses due to welding.

Finch and Burdekin (1992) used the ABAQUS finite element techniques to evaluate interactions between applied and typical residual stress distributions in various geometries of welded joints. The overall objective of their work was to develop a method of quantifying welding residual stress effects in the defect assessment of tubular joints in offshore structures. Analyses were conducted on central defects in flat plate butt welds under the effects of the longitudinal residual stresses, weld root defects in multi-run butt welded plates under the effects of the transverse residual stresses and weld toe and weld root defects in T-butt welds between a pipe and a circular plate. It was concluded that tensile residual stress at the weld toe reduces the fracture strength of the welded structure with weld-toe defects. The compressive residual stress at the weld root has the beneficial effect of closing the defect under conditions of residual stress and a small tensile load. Compressive residual stress always reduces the applied stress intensity factor and hence increases the fracture strength and decreases the crack growth rate if cyclic loading is applied.

Finch (1992) investigated the interactions between applied and residual stresses for different crack sizes and load levels in T-tubular joints. Weld toe through-thickness and half-elliptical surface defects in T-tubular joints were analysed. The studies on T-tubular joints represented one of the first attempts to investigate the effects of residual stresses in complex welded structures.

(i) In the through-thickness defects, the contribution of residual stresses to the J-integral values is generally positive along the outer (top) half of the crack front and negative along the inner (bottom) half of the crack front. This is due to the nature of the residual stress distribution (large tensile at the outer surface and compressive at the middle section of the chord thickness). Due to the large stress concentration factor at the outer surface of the tubular joint saddle position, the external load is the dominant factor and the effects of residual stresses are very small, despite the fact that they are as high as the material yield stress at the outer surface.

(ii) In surface defects, the contribution of residual stresses to J-integral is generally positive at all positions along the crack front for crack depths up to $a/T = 0.6$, and becomes negligible at the deepest position of the crack depth, $a/T = 0.8$. This is due to the nature of the residual stress distribution (large tensile at the outer surface and compressive at the middle section of the chord thickness).

Some of the methods for improving fatigue strength of welded joints depend on their efficacy on replacing the tensile residual stresses at the point of crack initiation by compressive stresses. Some of the methods which are used to overcome the detrimental effect of residual stresses are peening methods (hammer, needle, shot, ultrasonic), overloading methods (initial overloading, local compression) and thermal methods (thermal stress relief, spot heating, Gunnert's method) (Smith and Hirt 1985; Haagensen 1989). The effect of repair or reinforcement of fatigue life can also be found in Puthli *et al* (1992), Mang and Bucak (1996) and Romeijn *et al* (1993).

2.1.5 Undercut

Undercut can be defined as a surface depression along the interface between weld and parent metal, caused by missing material. During the welding process, erosion of the base material beside the weld interface can occur, followed by subsequent solidification of the weld metal, without the depression becoming filled (Petershagen 1985). Undercuts can be formed in fully mechanised welding of long fillet welds in the horizontal position with high heat input. The weld metal on the vertical plate sags before it can solidify to give the required weld shape. In manual arc-welding, an injudicious guidance of the electrode can result in a deficiency of weld metal at the weld interface at the time when the weld surface is solidifying.

Allowable limits for undercuts relate to the depth of the notch, to their length, as well as to the separation between adjacent undercuts. Allowable limits also depend on the direction of main stress, whether it is perpendicular or parallel to the axis of the weld. The AWS regulations state that undercut shall be no more than 0.25mm deep when its direction is transverse to primary tensile stress in the part that is undercut, nor more than 1mm for all other situations for tubular structures (AWS 1998).

AS1554.1-1995 (SAA 1995a) states that for continuous-undercut and structural purpose (SP) welds the maximum allowable undercut depth should be $t/20$ but not greater than 1mm. For intermittent-undercut and structural purpose (SP) welds the maximum allowable undercut depth should be $t/10$ but not greater than 1.5mm. AS1554.1-1995 also states that undercut less than 0.5mm in depth should be disregarded.

These recommendations, especially the absolute maximum depth of undercut values of 1mm for continuous-undercut and 1.5mm for intermittent-undercut, are unreasonable limits when considering thin-walled structures of thicknesses less than 4mm, for example tubes of 1.6mm, 2mm and 3mm tested in this project. This is because these values are based on thicker walled specimens.

The shape of weld toe undercut can be fully determined using the imprint technique (Miki *et al* 1990) where silicone rubber is generally used. The impression can be cut up at places of interest and the measurements of the undercuts carried out with the help of a microscope. The parameters used to define the undercut are depth (d), width (δ), and the radius (ρ) as shown in Figure 2-1.

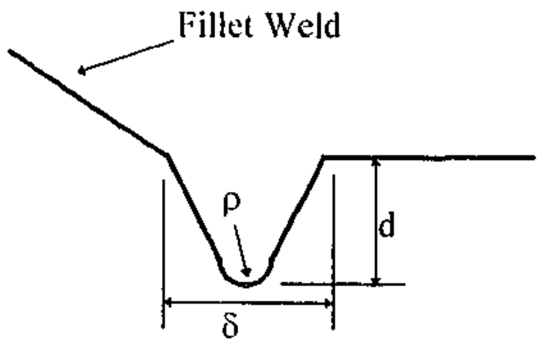

Figure 2-1: Dimensions of Undercut

The influence of undercuts on the fatigue strength depends on their shape. Undercuts can exhibit crack-like flaws at the base of the notch. This is normally the case for welded joints (Smith and Hirt 1983).

2.1.6 Stress Ratio

The stress ratio, R, is defined as the ratio of the minimum stress to the maximum stress in a cycle of stress. Each stress cycle contributes to the initiation and growth of fatigue cracks. Generally it is the tensile stresses which produce fatigue damage, so that a stress variation of a given stress range which is partly compressive will be less damaging than one which is wholly tensile, and consequently the fatigue life will be greater. The damaging effect of a fully tensile cyclic stress range tends to increase as the mean stress or stress ratio increases. For a given stress range, a cyclic stress ratio of +0.5 will therefore be more damaging than one with a stress ratio of zero and will result in a shorter fatigue life.

These basic principles do not always adequately predict the fatigue behaviour of welded joints, in the as-welded condition since they contain residual stresses (Maddox 1991).

2.2 METHODS USED FOR FATIGUE ASSESSMENT OF WELDED TUBULAR JOINTS

There are several methods for fatigue strength assessment of welded tubular joints (Wardenier 1982; van Wingerde 1992; Zhao *et al* 1999a). These include the classification method, hot spot stress method, punching shear method, failure criterion method, static strength method and the fracture mechanics method.

2.2.1 Classification Method

The classification method is based on nominal stress determined from the beam theory, where $\sigma_{nom} = F/A + M/Z$. Joints with similar behaviour are grouped together. The class of the group is related to the stress range at 2 million cycles. Joints with a large range of stress are grouped together, and the joint with the lowest fatigue strength determines the class of the group. This method was adopted by AS4100-1998 (SAA 1998a), Eurocode 3 (EC3 1992), Japanese Society of Steel Construction (JSSC 1995), American Institute of Steel Construction (AISC 1993) and the Canadian Standards Association (CSA 1989).

The application of the classification method is limited for tubular joint types to attachments and lattice girders. For lattice girders, detail categories are only available for uniplanar K- and N-joints, but parameters are very limited (Zhao *et al* 1999a). A large variation in fatigue behaviour may occur for joints within the same category, which may result in a considerable variation in fatigue life (van Wingerde 1997c).

2.2.2 Hot Spot Stress Method

The hot spot stress range instead of the nominal stress range is used in this method. The hot spot stress can be defined as the "structural stress" which is the stress at weld toe including only structural stress concentration but not including local stress concentration due to the weld bead (Nihei *et al* 1997). The fatigue of the joint in this method is related to the maximum (hot spot) geometrical stress occurring in the joint. This is the location where the cracks usually initiate. For square hollow section welded connections, the stresses/strains tend to be highest at the corners of the brace on the brace-chord interface. In the hot spot stress method all the joints are related to the same S_{rhs}-N_f curves by the stress concentration factor. The stress concentration factors for different joints are normally given by parametric formulae. Care should be taken when using parametric formulae for estimating stress concentration factors because they are valid only in certain domains or parametric ranges (Soh and Soh 1990; Zhao *et al* 1999a). This method has been adopted in the recommendations of the International Institute of Welding Subcommission XV-E (IIW 2000) and CIDECT Design Guide No. 8 (Zhao *et al* 1999a).

More information about the hot spot stress method is given in section 2.3.

2.2.3 Punching Shear Method

The punching shear method is similar to the classification method except that the punching shear stress is used. It is adopted by the American Petroleum Institute (API 1991) and the American Welding Institute (AWS 1998). This method involves a check of the nominal punching shear stress range in the chord and nominal stress range in the bracings (Wardenier 1982). Checking the punching shear stress range in the chord separately from the stress range in the bracings is essential in that it takes the important influence of wall thickness ratio between chord and bracings into account. The curves used are lower bound S-N curves from a certain range of validity (Marshall 1992).

2.2.4 Failure Criterion Method

This method provides diagrams showing the nominal stress ranges or maximum stresses at 2 million cycles in relation with joint geometry and loading parameters. The critical member in a joint can be determined using these diagrams. This method is only applicable to certain types of joints with limited validity range (Mang and Bucak 1982). The stress concentration factors are indirectly taken into account by giving an allowable nominal stress range at 2 million cycles. The nominal stress or stress range is given in diagrams for a stress ratio, $R = -1$, as a function of the joint parameters. The S-N curve is then described by the stress range at 2 million cycles, a slope for the S-N curve and an influence function for the stress ratio. The influence of secondary bending stress is not taken into account resulting in diagrams depended on the test set-up (Wardenier 1982).

2.2.5 Static Strength Method

The method relates the static strength behaviour to the fatigue behaviour of a joint. Within certain parameter ranges, a reasonable relationship can be obtained. The method may be used only as a preliminary design tool before extensive finite element analysis for stress concentration factors has been carried out (Kurobane 1989; Niemi 1995). In this method the fatigue strength of hollow section joints is given in relation to the static strength. This is because the static strength depends on the geometrical parameters that influence the hot spot stress. The static strength is therefore related to the geometrical stress concentration factor and to some extend to the strain gradient which also influence the fatigue strength. This method is suitable for giving an indication of the behaviour under low cycle fatigue (Wardenier 1982). There are a few theoretical objections against this approach. For example, fatigue behaviour is a weakest link driven mechanism (i.e. a strong joint will still have a low fatigue life if there is one point of weakness), whereas the static behaviour is more dependent on the total strength and allows stress redistribution (van Wingerde *et al* 1997a)

2.2.6 Fracture Mechanics Method

The fracture mechanics method can be used to estimate the fatigue crack propagation life of a structural component with crack-like defects. The crack initiation phase can be determined using the local strain approach (Sedlacek *et al* 1992).

The prime characterisation and prediction parameter is the stress intensity factor. The Paris equation is normally used for this purpose. It relates the rate of crack growth per cycle of stress (*da/dn*) to the stress intensity factor range.

This method has the advantage of being able to take into account effects related to fabrication such as the weld profile (flat, convex, concave) and the local condition of the weld toe such as weld toe radius and undercut (Mashiri *et al* 1997, 1998a, 1998b, 2000b).

One of the main problems of using this approach for the design of tubular joints is that the crack propagation is complicated. Sometimes small cracks develop at several locations along the perimeter of the joint and then coalesce. In other types of joints the crack starts from one point and then grows along the perimeter, extending into the member (Wardenier 1982).

The fracture mechanics method has been mainly applied to welded simple joints (Gurney 1979a; Bell *et al* 1989; Swamidas *et al* 1989; Maddox 1991; Sedlacek *et al* 1992, Nguyen and Wahab 1995; Mori *et al* 1997; Mashiri *et al* 1998a, 1998b). This method demands higher computing capacity and more sophisticated software in order to predict fatigue life of welded tubular joints (Sedlacek *et al* 1998; Mashiri *et al* 1999a, 2000b).

More information about the fracture mechanics method is given in section 2.5.

2.3 HOT-SPOT STRESS FATIGUE ANALYSIS

Hot spot stress is the maximum geometrical stress occurring in the joint where the cracks are usually initiated (van Wingerde 1992). In Nihei *et al* (1997), hot spot stress is defined as "structural stress" which is the stress at weld toe including only structural stress concentration but not including local stress concentration due to the weld bead. The geometrical hot spot stress method does not cover the condition of the weld toe for instance the toe radius and the influence of weld toe improvement techniques, see Figure 2-2. The local stress concentrations due to weld geometry and irregularities at the weld toe are difficult to determine since they are dependent on fabrication and are therefore not taken into account in the hot spot stress method. Extrapolation is therefore carried out outside this region. The stress (strain) concentration factor is then determined as a ratio of the hot spot stress (strain) at the joint to the nominal stress (strain) in the member due to a basic member load which causes this hot spot stress (strain).

The stresses and strains close to the joint are not uniformly distributed because of the variation in stiffness around the joint. In rectangular hollow sections, the stresses tend to be highest near the corners of the brace. The advantage of the hot spot stress method (Zhao *et al* 1999a; IIW 2000) is that:

(i) it takes the uneven stress distribution around the perimeter of the joint into account directly,

(ii) different types of circular hollow section (CHS) and rectangular hollow section (RHS) joints can be analysed using the same S_{rhs}-N_f curves The S_{rhs}-N_f curves used for the different tubular joints depend on the thickness of the failed member,

(iii) joints with different welding profiles and weld toe conditions can be analysed using the same set of S_{rhs}-N_f curves, since the hot spot stress range excludes the effects of fabrication such as the configuration of the weld (flat, convex, concave) and the local condition of the weld toe (radius of weld toe, undercut),

(iv) the hot spot stress S_{rhs}-N_f curves are determined from S-N data which cover a wide range of parameters, and

(v) although the hot spot stress method does not take into account the actual peak stress at the toe of the weld on the "hot spot", it provides a consistent definition of stress and hence a more consistent fatigue life assessment.

Hot spot stresses can be obtained through finite element analysis, boundary element analysis or experimentally through the use of strain gauges.

The determination of the hot spot stresses using linear or quadratic extrapolation methods is given in section 2.3.1. More details about the determination of hot spot stresses from the finite element (FE) method, the boundary element (BE) method or experimentally is given in section 2.3.2.

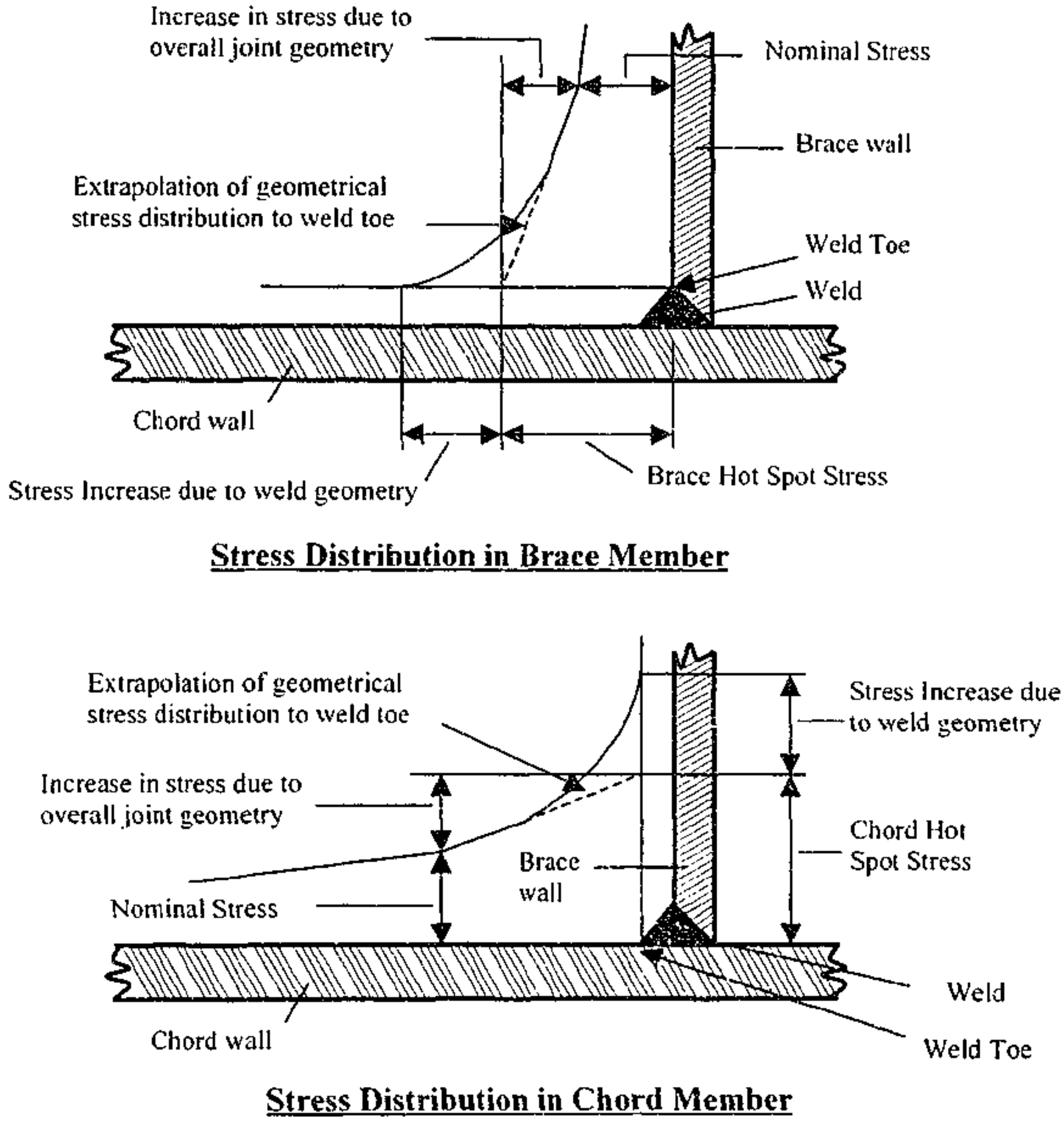

Figure 2-2: Hot Spot Definition in Nodal Joints (IIW 2000)

2.3.1 Determination of Hot Spot Stress

The definition of hot spot stress is still under debate. The existence of different definitions of hot spot stress makes the comparison between various research results such as parametric formula and design recommendations difficult. There are several methods, which are used to evaluate hot spot stress (Nihei *et al* 1997; van Wingerde 1992):

(i) 1-point representative method, where the hot spot stress is defined as the stress at a specified point distant from the weld toe,

(ii) 2-point extrapolation method which involves linear extrapolation using two points at specified distances from the weld toe, and

(iii) quadratic extrapolation.

Nihei *et al* (1997), proposed a value of hot spot stress such that the hot spot stress is equal to the stress at a distance 0.3 times the thickness of the plate from the toe of the weld (Nihei *et al* 1997). With this method hot spot stresses are obtained relatively easier compared to the 2-point extrapolation method. The one point representative method has been found to be applicable for practical use in T-plated joints that are fillet welded. In order to determine the hot spot stress in rectangular or square hollow section (RHS/SHS) joints and circular hollow section (CHS) joints, the extrapolation region must be defined. Details of the extrapolation region for rectangular or square hollow section (RHS/SHS) joints and circular hollow section (CHS) joints and the extrapolation distances are given by van Wingerde (1992), Marshall (1992) and Romeijn (1994).

(a) Rectangular/Square Hollow Section (RHS/SHS) Joints

To perform linear or quadratic extrapolation, curve fitting is first performed by hand or numerically through all available data points to determine points that are subsequently used for extrapolation using either method (van Wingerde 1992). In linear extrapolation the first point is at a distance $0.4t$ or a minimum of 4mm from the toe of the weld (Gurney 1979a; van Delft 1981). The second point is a distance $0.6t$ further away from the first point. While the first point is at the same distance as in linear extrapolation, the second point in quadratic extrapolation is at a distance of $1.0t$ further away from the first. All data points between the first and second points of extrapolation are used in quadratic extrapolation. These extrapolation distances have been adopted in current standards for design of hollow section joints (Zhao *et al* 1999a; IIW 2000). Connections made of rectangular sections produce geometric strain which are strongly non-linear making the determination of SNCF using quadratic extrapolation more realistic (van Wingerde 1992).

(b) Circular Hollow Section (CHS) Joints

Distances for use in linear extrapolation in circular hollow section nodal joints have also been proposed by different researchers (Snedden 1981; Dijkstra and de Back 1980; Gibstein 1981), as shown in Table 2-1 (Marshall 1992). The distance from where the extrapolation to the toe should be carried out is important. A value of $0.2\sqrt{(rt)}$, where r and t are the radius and thickness of the brace, was originally used by Working Group III of the ECSC for the closest point to the weld toe for extrapolation. However the influence of r on the position of extrapolation has since become doubtful (van Wingerde 1992). As a result a value of $0.4t$ has since been adopted, with a minimum value of 4mm (Gurney 1979a; van Delft 1981). The location of the second point which has been adopted in current standards for hollow section design (Zhao *et al* 1999a; IIW 2000), is that given in Table 2-1 from the references by Gurney (1979a) and van Delft (1981). The second point is however less critical since for circular hollow section joints the stress distribution in the extrapolation region is nearly linear (van Wingerde 1992).

Table 2-1: Distances for linear extrapolation in circular hollow section nodal joints

Source/Reference	**Distance of first point of extrapolation from weld toe for brace and chord**	**Distance of second point of extrapolation from weld toe for brace**	**Distance of second point of extrapolation from weld toe for chord**
Dijkstra and de Back (1980)	$0.2\sqrt{r \cdot t}$ but not less than 4mm	$0.65\sqrt{r \cdot t}$	$0.65\sqrt{R \cdot T}$
Snedden (1981)	$0.2\sqrt{r \cdot t}$ but not less than 4mm	$0.65\sqrt{r \cdot t}$	$0.4\sqrt[4]{r \cdot t \cdot R \cdot T}$
Gurney (1979a), van Delft (1981)	$0.4t$	$0.65\sqrt{r \cdot t}$	$0.4\sqrt[4]{r \cdot t \cdot R \cdot T}$
Gibstein (1981)	Branch: $0.25t$ Chord: $0.25t$	–	–

Notes: r is the outside radius of the brace, R is the outside radius of the chord, t is the wall thickness of the brace, and T is the wall thickness of the chord.

The hot spot stresses and stress concentration factors are normally based on strains. This is because strains are easier to measure compared to stresses. Strains are measured using individual strain gauges, whereas strain gauge rosettes are required for the determination of stresses.

Resulting $S_{rh.s}$-N_f from the strain concentration factors (SNCF) often show the stresses exceeding the yield or even the ultimate stress. This is because in low cycle fatigue the strains exceed the yield strains. In order to determine high cycle fatigue $S_{rh.s}$-N_f data, fatigue tests are carried out for the stress ranges where the load-displacement response is linear or elastic. Therefore the design $S_{rh.s}$-N_f curves are determined from the $S_{rh.s}$-N_f data determined from the stress ranges where the load-displacement response is linear or elastic. To make the design curves complete they are then extrapolated into region of low cycle fatigue where the strains exceed the yield strains.

From numerical analysis both stress and strain concentration factors can be determined. The ratio of stress to strain concentration factors has been found to be between 0.6 and 1.4 (van Wingerde 1992).

Principal stress and stress perpendicular to the toe of the weld is often used in determining the hot spot stress concentration factors. The IIW, DEn and EC3 definitions all use principal stresses. (van Wingerde *et al* 1992). However the IIW states that these stresses are usually perpendicular to the toe in simple connections. The AWS and API use hot spot stresses perpendicular to the weld toe. Principal stresses can be tens of percent higher than stress perpendicular to the toe of the weld. Closer to the weld toe the stresses are diverted perpendicular to the weld by the stiffening influence of weld and attached wall. Therefore the ratio of principal stress to stress perpendicular to the weld toe decreases at locations closer to the weld toe (Marshall 1992; van Wingerde 1992; Zhao *et al* 1999a). The use of stresses (strains) perpendicular to the weld toe is recommended in CIDECT Design Guide No. 8 (Zhao *et al* 1999a).

2.3.2 Stress Concentration Factors

The stress concentration factor (SCF) is the ratio between the hot spot stress at the joint and the nominal stress in the member due to a basic member load which causes this hot spot stress (IIW 2000).

The determination of hot spot stresses that are used in the calculation of stress concentration factors can be obtained experimentally or through numerical methods such as the finite element or the boundary element methods. The nominal stresses are determined through the use of the simple beam theory.

In the experimental approach the strains are determined through the use of strain gauges. Strain gauge rosettes are used to determine principal strains. Simple strain gauges are used to determine the strains perpendicular to the weld toe. CIDECT Design Guide No. 8 recommends the use of stresses perpendicular to the toe of the weld for determining hot spot stresses in the calculation of stress concentration factors (Zhao *et al* 1999a). The strain gauges are located at lines perpendicular to the toe of the weld for determining normal or principal strains. Two strain gauges are used for determining strains required for linear extrapolation. Three or more strain gauges are used for determining strains for quadratic extrapolation. The positioning of strain gauges is determined as described in section 2.3.1. For joints made up of rectangular/square hollow sections, the quadratic extrapolation method is required because of the strong non-linear strain distribution observed within the extrapolation region (van Wingerde 1992; Mashiri *et al* 2000c). For joints made up of circular hollow sections, the linear extrapolation method can be used since the gradient is nearly linear (Romeijn 1994). One of the difficulties in the determination of hot spot stresses using strain gauges, is the size of the distance making up the extrapolation region in thin-walled structures with thicknesses less than 4mm. For a square hollow section tube of 4mm thickness for example, the extrapolation region is 4mm. Since at least three points are required for quadratic extrapolation, it implies that a strip strain gauge having at least three individual gauges is required to measure the strain distribution within the distance of 4mm. This makes strain gauging difficult and at the same time it becomes hard to find strain gauges of this size. Numerical analysis can be a better way to determine strain distributions within the extrapolation regions in thin-walled joints with thicknesses less than 4mm.

Hot spot stresses can also be determined using numerical methods such as the finite element method or the boundary element method. In finite element analysis, different researchers have used different packages such as DIANA (van Wingerde 1992), MARC (Heemskerk 2000), ABAQUS (Morgan and Lee 1998; Chang and Dover 1999), PAFEC (Connolly *et al* 1990; Hellier *et al* 1990a,b) and ANSYS. In this research a boundary element analysis system software (BEASY) is used (Mashiri *et al* 1999a, 2000b). In numerical analysis a convergence test should be carried out to ensure that any further refinement of the element mesh does not result in a substantial change of stress in the modeled joint, especially the extrapolation region. Different researchers have used different element types. The element type has to be a compromise between accuracy and the CPU-time required for analysis. The CPU-time required depends on the complexity of the model (2D or 3D), number of elements, number of degrees of freedom, software version and hardware. In the finite element method different researchers have used different element types for modeling nodal joints;

(i) 20 noded solid elements for part of the members near the weld including the weld and 8 noded thick shell elements for the part of the joint away from the weld toe and the weld (van Wingerde 1992),

(ii) 20 noded solid elements for the whole joint, that is the weld area and the chord and brace members (Heemskerk 2000),

(iii) 8 noded thin shell elements for the whole joint (Morgan and Lee 1998a,b,c; Chang and Dover 1999), and

(iv) 8 noded semi-Loof thin shell elements for the whole joint (Connolly *et al* 1990; Hellier *et al* 1990a,b).

It is generally agreed that using solid elements to model the weld area is recommended (van Wingerde 1992; Romeijn 1994; Heemskerk 2000). Solid elements produce more accurate results but require larger CPU-time for analysis. However with the continuous development of hardware and software the problem associated with high CPU-times should become less important with time.

Stress concentration factors are usually expressed in terms of parametric equations. These parametric equations are normally derived from results of stress concentration factors determined within a certain parameter range. The parametric equations are formulated for use by design engineers.

A lot of research effort has been made to derive parametric equations for fatigue strength assessment of tubular Y- and T-joints in circular hollow sections (Kuang *et al* 1977; Efthymiou and Durkin 1985; Wordsworth and Smedley 1978; UEG 1985; Smedley and Fisher 1991; Hellier *et al* 1990a,b; Connolly *et al* 1990; Chang and Dover 1999).

Parametric equations for predicting stress concentration factors at the hot spots in square or rectangular hollow section T-joints have been determined by van Wingerde (1992) and Soh and Soh (1990). The equations derived by van Wingerde (1992) have been adopted in the IIW Fatigue Design Procedure (IIW 2000) and the CIDECT Design Guide No. 8 (Zhao *et al* 1999a). Details of the parametric equations from van Wingerde (1992) and Soh and Soh (1990) are given in Appendix F.

2. 4 FATIGUE DESIGN GUIDELINES

2.4.1 UK Department of Energy (1990)

The hot spot stress method is used for the design of nodal joints. The hot spot stress is defined as the greatest value of stress around the brace/chord intersection of the extrapolation to the weld toe of the geometrical stress distribution near the weld toe. The hot spot stress incorporates the effects of overall joint geometry (i.e. the relative size of brace and chord) but omits the stress concentration influence of the weld itself which results in a local stress distribution. The hot spot stress is lower than the peak stress but provides a consistent definition of stress range for the design S-N curve.

The guideline recommends the determination of hot spot stress from physical model studies, finite element analysis or by the use of semi-empirical parametric formulae. In thin-shell finite element analysis, calculations do not allow for the effect of weld geometry and hence the hot spot stress at the weld toe can be estimated from the value obtained directly at the brace/chord interface. Parametric equations should be used with caution in view of their inherent limitations, they are valid for specific parameter ranges.

Linear extrapolation is used for T- and X-joints, and non-linear extrapolation is recommended for Y- and K-joints.

The design curves are based on the mean-minus-two-standard-deviation curves for the relevant data. Their use results in structures with a finite probability of failure. An additional factor on life should be considered for cases of inadequate structural redundancy. This factor depends on:
(i) the accessibility of the joint,
(ii) the proposed degree of inspection and
(iii) consequences of failure.

All tubular joints are assumed to be in class T, for full penetration welded nodal joints. The stress range to be used is the hot spot stress range at the weld toe. The T curve has slopes of 1:3 between 10^4 and 10^7 cycles, and 1:5 between 10^7 and 10^8 cycles. The reference hot spot stress range at 2 million cycles for the T-curve is 90N/mm^2, Figure 2-3. For partial penetration welds where weld throat failure is a possibility, fatigue should be assessed using the W curve, and the shear stress estimated at the weld root. Other types of joints including tube-to-plate, may fall in one of eight classes, B, C, D, E, F, F2, G or W.

The T curve is a basic S-N curve which relates to a thickness of 32mm. The correction on the hot spot stress range is of the form:

$$S_{r.hs.t} = S_{r.hs.32}\left(\frac{32}{t}\right)^{1/4} \qquad \textbf{(2.1)}$$

where $S_{r.hs.t}$ is the hot spot stress range of the joint under consideration, $S_{r.hs.32}$ is the hot spot stress range of the joint using the T-curve, which relates to a thickness of 32mm and t is the actual thickness of the member under consideration A value of t=22mm should be used when the actual thickness is less than 22mm.

An improvement in fatigue strength of at least 30%, equivalent to a factor of 2.2 on life, can be obtained by controlled local machining or grinding of the weld toe. A smooth concave profile should be produced at the weld toe with the depth of the depression penetrating into the plate surface at least 0.5mm below the bottom of any visible undercut. Machining or grinding should not exceed 2mm or 5% of the plate thickness.

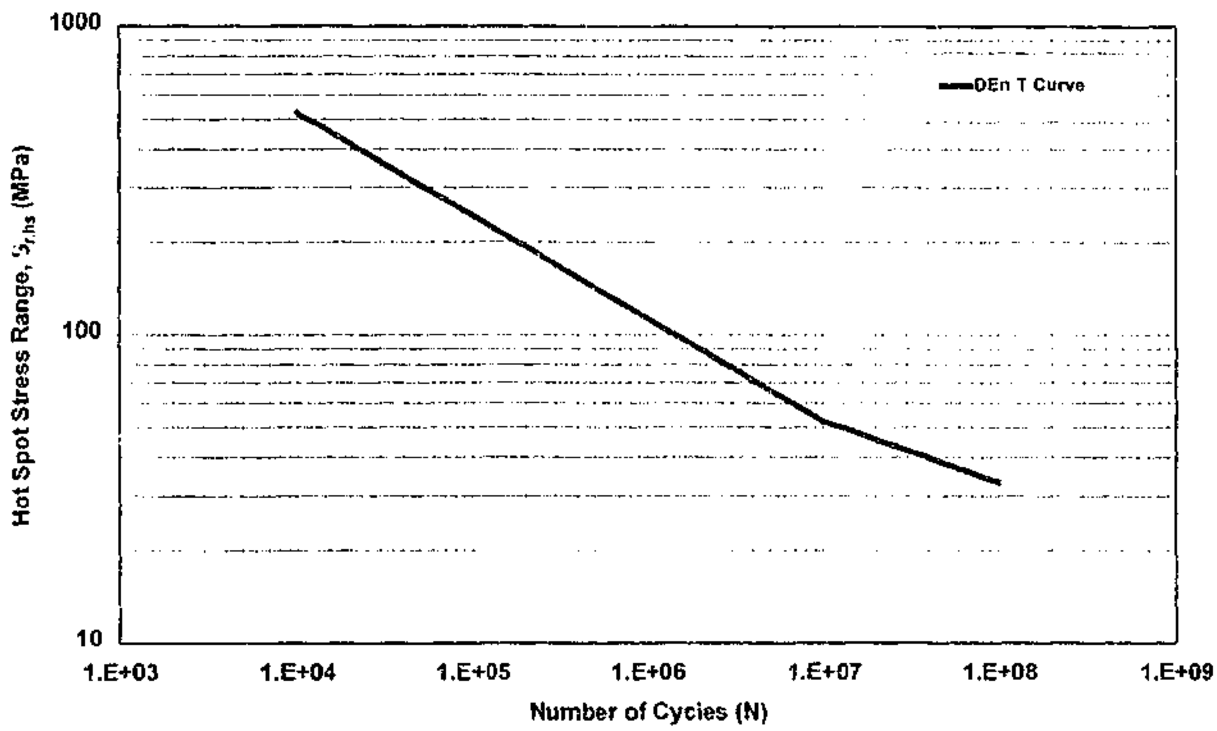

Figure 2-3: Department of Energy (1990), T Curve- Basic design S-N curve for nodal joints

2.4.2 American Petroleum Institute (API 1991)

The hot spot stress method is used for determining fatigue strength of tubular joints. The hot spot stress is defined as the stress in the immediate vicinity of a structural discontinuity.

Curve X is applied to connections with welds which merge smoothly with the adjoining base metal. The X curve has a slope of 1:4.38 between 10^4 and $2x10^8$ cycles. The hot spot cyclic stress range at 2 million cycles for the X curve is 100MPa. Curve X' is applied to those connections whose welds do not merge smoothly with the adjoining base metal. The X' curve has a slope of 1:3.74 between 10^4 and $2x10^8$ cycles. The hot spot cyclic stress range at 2 million cycles for the X' curve is 79MPa. Both the X and X' curves have a fatigue limit at $2x10^8$ cycles, see Figure 2-4.

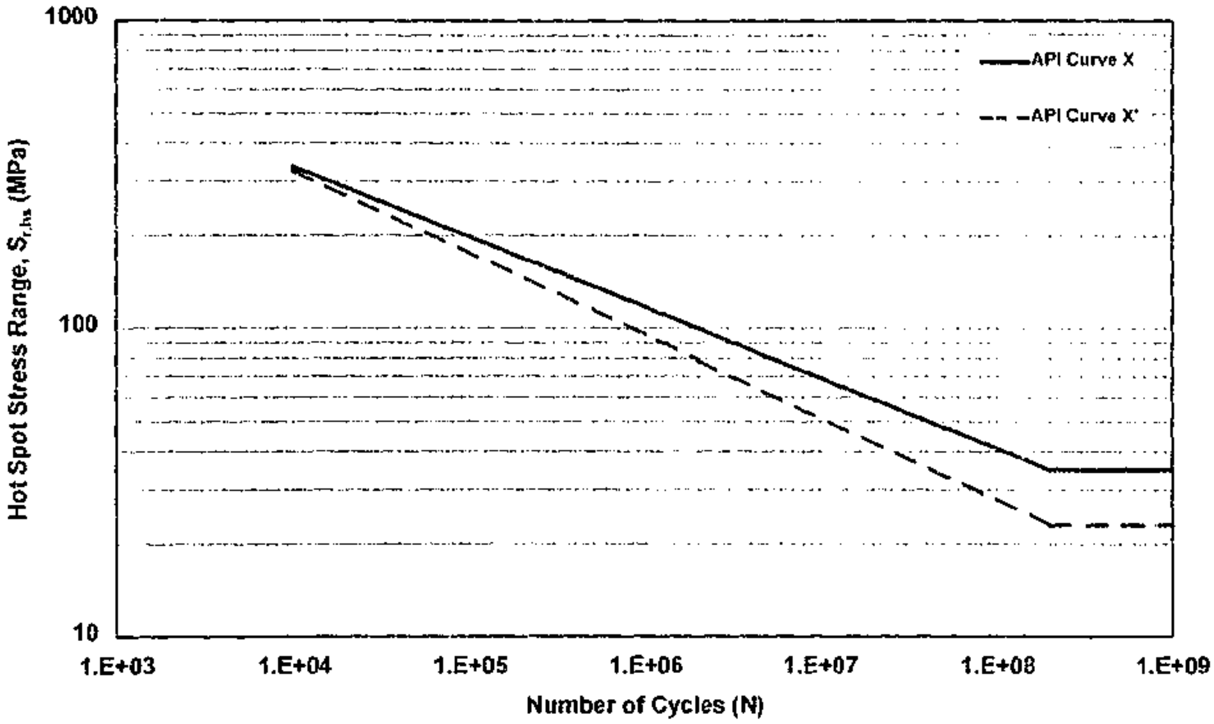

Figure 2-4: API (1991), X and X' Curves

2.4.3 Det Noske Veritas (1981)

The hot spot stress method is used in the determination of allowable number of cycles from the X curve. The hot spot stress is defined as the nominal brace stress multiplied by an appropriate stress concentration factor. (SCF). The stress concentration factor is normally not to be taken as less than 2.5 for simple joints and 5.0 for overlapping joints. Stress concentration factors (SCF) may be obtained from relevant tests or analyses. Different stress components may be associated with different stress concentration factors. Different locations of hot spots for different stress components may be taken into account if relevant documentation on their locations is available. Stress concentration due to the construction geometry, but excluding that for the weld itself shall be accounted for.

The X curve consists of a slope of 1:4.1 between 10^4 and $2x10^8$ cycles. The fatigue limit occurs at 200 million cycles. The stress range at the fatigue limit is 34MPa as shown in Figure 2-5. The hot spot cyclic stress range at 2 million cycles for the X curve is 104MPa.

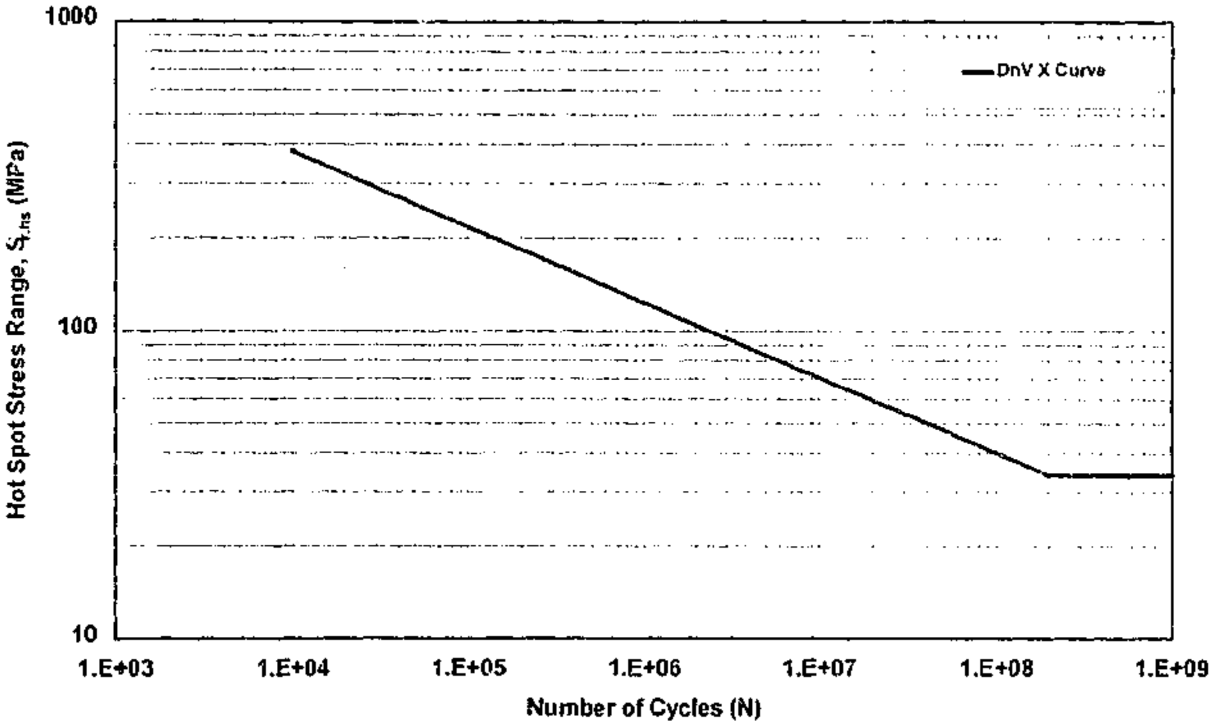

Figure 2-5: DnV (1981), X Curve

2.4.4 Eurocode 3 (1992)

Fatigue assessment in Eurocode 3 is done using both the hot spot stress method and the classification method. The hot spot stress (or geometric stress) is defined as the maximum principal stress in the parent material adjacent to the weld toe, which takes into account stress concentration effects due to the overall geometry of a particular constructional detail, but excludes the local stress concentration effects due to weld geometry and discontinuities in the weld and the adjacent parent material. In fatigue assessments based on geometric stress ranges the maximum value of geometric stress range can be determined by investigating various locations at the weld around the welded joint or stress concentration area. The stress concentration factors used to determine the geometric stress may be obtained from parametric formulae within their domains of validity, finite element analysis or an experimental model.

Partial safety factors are given for fatigue loading and fatigue strength. They depend (like in those given by the Det Norske Veritas (1981), Department of Energy (1990) and AWS (1998) on the:

(i) ease of access for inspection or repair.

(ii) likely frequency of inspection and maintenance, and

(iii) consequences of failure.

The value of the stress range corresponding to a value of 2 million cycles is calculated for a 75% confidence interval of 95% probability of survival for *log N*, taking into account the standard deviation and the sample size. The number of data points (not lower than 10) shall be used in the statistical analysis.

Hollow section joints details for lattice girders have a single slope of 1:5 from 10^4 to 10^8 cycles. The type of joints covered are K- and N- joints. These are analysed using the classification method. The stresses applied to the members are axial. Effects of secondary bending moments may be taken into account by multiplying the stress ranges due to axial member forces by appropriate coefficients for circular or square hollow sections.

Fatigue assessment of all the constructional details not included in the classes of EC3 and all hollow section members and tubular joints with wall thicknesses greater than 12.5mm are carried out using the procedure based on geometric (hot spot) stress range.

Fatigue assessments based on geometric stress ranges is based on the curves with double slopes of 1:3 between 10^4 and $5x10^6$ cycles and 1:5 between $5x10^6$ and 10^8 cycles as shown in Figure 2-6. The following curves corresponding to the following values of stress range at 2 million cycles (detail category) are used:

(i) 90 for full penetration butt welds, when both the weld profile and permitted weld defects acceptance criteria are satisfied,

(ii) 71 for full penetration butt welds, when only the permitted weld defects acceptance criterion is satisfied, and

(iii) 36 for load carrying partial penetration butt welds and fillet welds.

Variation of fatigue strength with thickness shall be taken into account for material thicknesses greater than 25mm by reducing the fatigue strength using;

$$S_{r.hs.t} = S_{r.hs.25}\left(\frac{25}{t}\right)^{1/4} \qquad \text{for } t>25\text{mm} \qquad \textbf{(2.2)}$$

For material thicknesses less than 25mm the fatigue strength is taken as that for a thickness of 25mm.

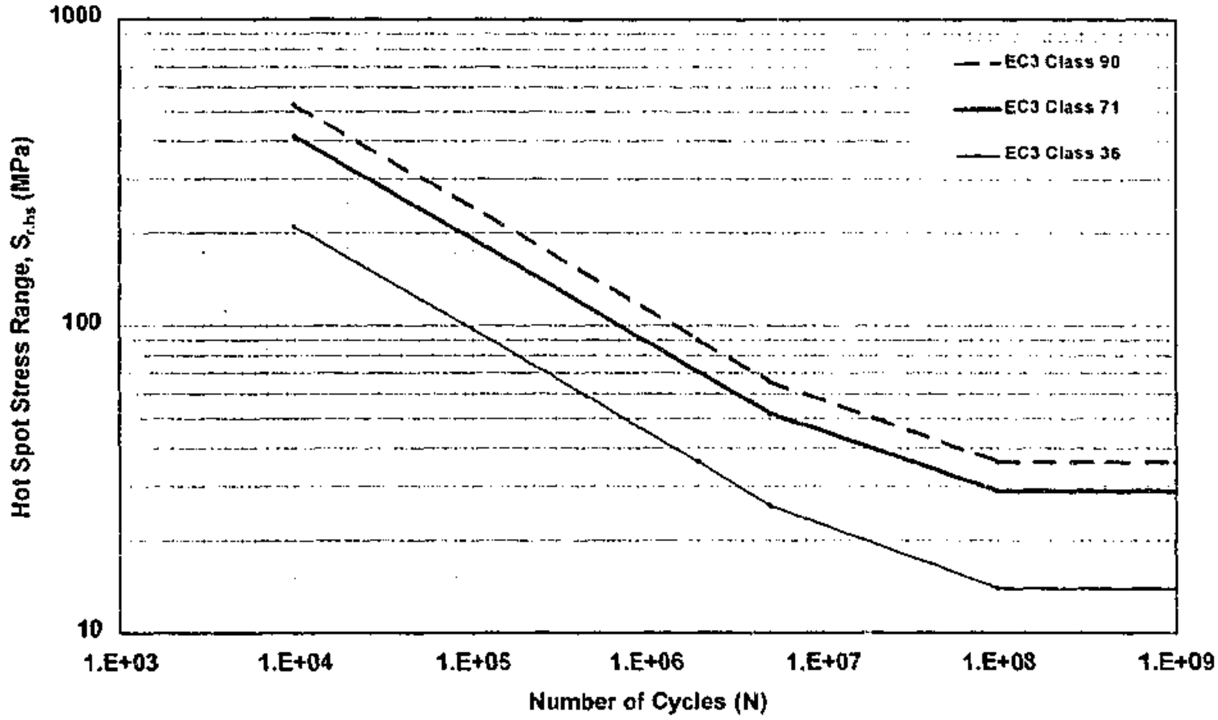

Figure 2-6: EC3 (1992), Class 36, Class 71 and Class 90 S-N Curves

2.4.5 Structural Welding Code (AWS 1998)

Hot-spot strain is defined as the cyclic total range of strain, which would be measured at the point of highest stress concentration in a welded connection. When measuring hot-spot strain, the strain gauge should be sufficiently small to avoid averaging high and low strains in the regions of steep gradients.

The stress categories given by the Structural Welding Code is for circular hollow sections. Stress category X_2 is for intersecting members at simple T-, Y- and K-connections as well as any connection whose adequacy is determined by testing an accurately scaled model or theoretical analysis. The greatest total range of hot spot stress/strain on the outside surface of intersecting members at the toe of the weld joining them can be determined in model or prototype connections or calculated with the best available theory.

For those connections whose profile has been improved the stress category X_1 can be used. Some of the methods recommended for profile improvement include a capping layer applied so that the as-welded surface merges smoothly with the adjoining base metal, grinding and peening to produce local plastic deformation which smooths the transition between weld and base metal. After grinding it is preferable to have final grinding marks transverse to the toe of the weld, thereby preventing stress concentrations perpendicular to the toe of the weld.

Like the X and X' curves from the API (1991), the X_1 and X_2 curves from AWS (1998), have hot spot cyclic stress ranges of 100MPa and 79MPa respectively, see Figure 2-4.

2.4.6 CIDECT Design Guide No. 8 (Zhao *et al* 1999a)

The aim of the CIDECT Design Guide No. 8 is to provide design recommendations for welded CHS and RHS joints under fatigue loading. The types of CHS joints covered are T/Y, X, K(gap), XX and KK(gap). The type of RHS joints covered are T/X, K(gap), K(overlap) and KK(gap). The fatigue life of welded joints depends upon the joint type, joint loading and structural detailing of the joint.

The classification method used in Eurocode 3 (EC3 1992) for the fatigue design of lattice girders and attachments is summarized in the CIDECT Design Guide No. 8. For lattice girders, detail categories are only available for uniplanar K- and N-joints, but parameters are very limited. For lattice girder joints, the thickness ratio (t_0/t_1) has a great effect on the detail category. The fatigue strength curves for attachments and lattice girders are in terms of the nominal stress range.

The fatigue design of welded joints made up of circular hollow sections and rectangular or square hollow sections in CIDECT Design Guide No. 8, is carried out using the hot spot stress method (see section 2.3 for more details about the hot spot stress method). In the hot spot stress method, the design procedure involves the determination of the following:

(i) axial forces and bending moments in the chord and braces using a structural analysis method,

(ii) nominal stress ranges using the simple beam theory,

(iii) stress concentration factors using parametric equations or graphs,

(iv) hot spot stress ranges as defined by the equations 2.3 to 2.6 for the chord and brace member, and

(v) the permissible number of load cycles for a given hot spot stress range at a specific joint location from the fatigue strength curves shown in Figure 2-7.

The methods of structural analysis and ways of determining the nominal stress ranges are detailed in CIDECT Design Guide No. 8. The stress concentration factors for the tubular joints are determined using simplified parametric formulae (such as those shown in Appendix F for RHS) or graphs. The stress concentration factors (SCFs) are calculated for different locations of interest at the hot spots of a given joint. Parametric formulae are given for both CHS joints and RHS joints. Hot spot stress range values in the chord and brace member can be determined in order to estimate the fatigue life in both the chord and brace members.

The hot spot stress range at:

(a) any location in the *chord member* for all joints except CHS XX-joints is given by,

$$S_{rhs} = SCF_{axial-force-in-brace} \cdot S_{r,axial-force-in-brace} + SCF_{iph-in-brace} \cdot S_{r,iph-in-brace} + SCF_{oph-in-brace} \cdot S_{r,oph-in-brace} + SCF_{axial-force-in-chord} \cdot S_{r,axial-force-in-chord} + SCF_{iph-in-chord} \cdot S_{r,iph-in-chord} \quad \textbf{(2.3)}$$

(b) any location in the *chord member* for CHS XX-joints is given by,

$$S_{rhs} = SCF_{axial-force-in-REF-brace} \cdot S_{r,axial-force-in-REF-brace} + SCF_{iph-in-REF-brace} \cdot S_{r,iph-in-REF-brace} + SCF_{oph-in-REF-brace} \cdot S_{r,oph-in-REF-brace} + SCF_{axial-force-in-chord} \cdot S_{r,axial-force-in-chord} + SCF_{axial-force-in-COV-brace} \cdot S_{r,axial-force-in-COV-brace} + SCF_{oph-in-COV-brace} \cdot S_{r,oph-in-COV-brace} \quad \textbf{(2.4)}$$

(c) any location in the *brace member* for all joints except CHS XX-joints is given by,

$$S_{rhs} = SCF_{axial-force-in-brace} \cdot S_{r,axial-force-in-brace} + SCF_{iph-in-brace} \cdot S_{r,iph-in-brace} + SCF_{oph-in-brace} \cdot S_{r,oph-in-brace} \quad \textbf{(2.5)}$$

(d) any location in the *brace member* for CHS XX-joints is given by,

$$S_{rhs} = SCF_{axial-force-in-REF-brace} \cdot S_{r,axial-force-in-REF-brace} + SCF_{iph-in-REF-brace} \cdot S_{r,iph-in-REF-brace} + SCF_{oph-in-REF-brace} \cdot S_{r,oph-in-REF-brace} + SCF_{axial-force-in-COV-brace} \cdot S_{r,axial-force-in-COV-brace} + SCF_{oph-in-COV-brace} \cdot S_{r,oph-in-COV-brace} \quad \textbf{(2.6)}$$

For multi-planar joints, the load in one brace plane may affect the hot spot stress range in another brace plane. This is called the carry-over effect.

The fatigue strength curves used in CIDECT Design Guide No. 8 have a thickness correction factor and are given in terms of the hot spot stress range. The basic S_{rhs}-N_f curve for hollow section joints is that for a wall thickness of 16mm. Thickness correction factors are introduced for joints with wall thicknesses other than 16mm. Based on the analysis in the data sets for square and circular hollow sections, the DEn T' curve equivalent to a class of 114 in EC3, is recommended as the reference S_{rhs}-N_f line for 16mm wall joints between circular and square members. The S_{rhs}-N_f curve used in design is that corresponding to the thickness of the member under consideration. The equations for determining the S_{rhs}-N_f curves for CHS joints and RHS joints are shown in Table 2-2. The resultant S_{rhs}-N_f curves from the equations in Table 2-2 are given in Figure 2-7. The equations in Table 2-2 are valid for the following thicknesses only; (a) in CHS joints, $4mm \le t \le 50mm$ and (b) RHS joints, $4mm \le t \le 16mm$.

Table 2-2: Equations for S_{rhs}-N_f curves for CHS joints ($4mm \le t \le 50mm$) and RHS joints ($4mm \le t \le 16mm$)

For $10^3 < N_f < 5 \cdot 10^6$	$\log(S_{rhs}) = \frac{1}{3}\left(12.476 - \log(N_f)\right) + 0.06 \cdot \log(N_f) \cdot \log\left(\frac{16}{t}\right)$ or $\log(N_f) = \dfrac{12.476 - 3 \cdot \log(N_f)}{1 - 0.18 \cdot \log\left(\frac{16}{t}\right)}$
For $5 \cdot 10^6 < N_f < 10^8$ (for variable amplitude only)	$\log(S_{rhs}) = \frac{1}{5}\left(16.327 - \log(N_f)\right) + 0.402 \cdot \log\left(\frac{16}{t}\right)$ or $\log(N_f) = 16.327 - 5 \cdot \log(S_{rhs}) + 2.01 \cdot \log\left(\frac{16}{t}\right)$

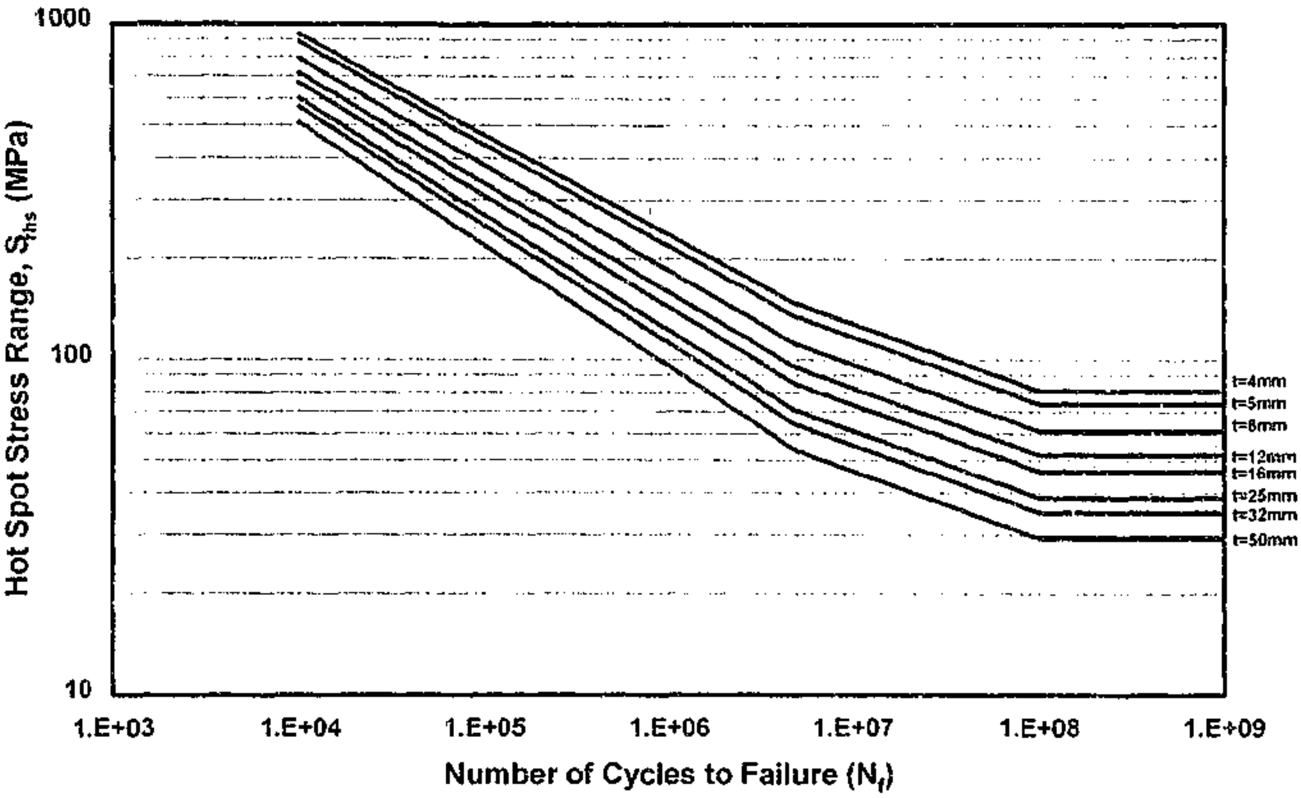

Figure 2-7: Fatigue strength curves for CHS joints ($4mm \le t \le 50mm$) and RHS joints ($4mm \le t \le 16mm$) according to the hot spot stress method

2.4.7 IIW Fatigue Design Procedure (IIW 2000)

The recommendations in the IIW Fatigue Design Procedure deal with the design and analysis of unstiffened, welded, nodal joints in braced structures composed of hollow sections of circular or square shape under fatigue loading. The design rules and procedures in IIW Fatigue Design Procedure are similar to those in CIDECT Design Guide No. 8 for the design of CHS and RHS joints using the hot spot stress method. The equations and graphs for S_{rhs}-N_f curves given in section 2.4.6 for CHS and RHS joints are identical to those used in the IIW Fatigue Design Procedure (IIW 2000).

2.5 FRACTURE MECHANICS

Fracture mechanics based fatigue assessment is a powerful, yet often under-utilised methodology. One of the key advantages of the fracture mechanics approach to fatigue over the conventional S-N approach is the ability to examine analytically the effect of geometric and loading variables on the fatigue performance of a structure (Grover 1989). For welded joints, it is often assumed that there is no initiation period due to the presence of weld defects. Small fatigue cracks actually initiate at an early stage of fatigue in the welded joints, where crack-like defects or high stress concentrations exist. These reduce the initiation stage of the fatigue and make it relatively less important than the propagation stage (Yamada & Kainuma 1996). The small crack-like discontinuities, termed intrusions, exist at the weld toe. They are a product of conditions during welding which, arise with most of the arc processes (Maddox 1991). It is necessary to understand the parameters affecting crack propagation.

In order to accurately predict fatigue of welded structures it has been determined that the following factors have to be considered in modifying Paris' equation (Yamada & Kainuma 1996):

(i) The fatigue crack growth rate gradually deviates from Paris' equation, $da/dN = C \cdot \Delta K^n$ when ΔK decreases. The fatigue crack does not propagate when ΔK is less than the threshold stress intensity factor range, ΔK_{th}.

(ii) Fatigue crack growth rates and ΔK_{th} are largely influenced by the stress ratio, residual stresses and crack closure. Crack closure occurs when plastic elongation, which develops near the crack tip, remains at the crack surface after crack propagation, and closes the crack during the unloading stage.

Different expressions and parameters, for crack propagation rate have been used by different researchers (JSSC 1995; BSI 1991; Computational Mechanics BEASY Ltd 1998).

2.5.1 Fatigue Crack Propagation Life Estimation Recommended by the Japanese Society of Steel Construction (JSSC 1995)

The fatigue crack propagation rate:

$$\frac{da}{dN} = C \cdot \left(\Delta K^n - \Delta K_{th}^n\right) \qquad \text{when } \Delta K \geq \Delta K_{th} \qquad \textbf{(2.7)}$$

$$\frac{da}{dN} = 0 \qquad \text{when } \Delta K \leq \Delta K_{th} \qquad \textbf{(2.8)}$$

$$\Delta K = F_g . F_e . F_s . F_t . F_h . \Delta\sigma . \sqrt{(\pi a)} \qquad \textbf{(2.9)}$$

The following values are recommended for determining mean fatigue strength. For values of da/dN in m/cycle,

$C = 1.5x10^{-11}$

$n = 2.75$

$\Delta K_{th} = 2.9\, MPa\sqrt{m}$.

The values of C, n and ΔK_{th} have been determined through the analysis of data which were obtained by fatigue crack propagation tests simulating high tensile residual stress conditions.

2.5.2 Fatigue Crack Propagation Life Estimation according to PD 6493: 1991, British Standards Institution (BSI 1991).

The overall relationship between da/dN and ΔK is normally observed to be a sigmoidal curve with three distinct regions, in $log\ da/dN$ versus $log\ \Delta K$ plot, see Figure 2-8. There is a central linear portion, region two, whose rate of crack propagation is given by:

$$\frac{da}{dN} = C \cdot \Delta K^n \qquad \text{when } \Delta K \geq \Delta K_{th} \tag{2.10}$$

In region one, the crack growth rate goes asymptotically to zero as ΔK approaches a threshold value, ΔK_{th}. This means that for stress intensity factor ranges below ΔK_{th} there is no crack growth, that is there is a fatigue limit:

$$\frac{da}{dN} = 0 \qquad \text{when } \Delta K \leq \Delta K_{th} \tag{2.11}$$

The threshold effect is believed to be caused by a number of different processes which lead to crack blocking for small stress intensity factor ranges. In welded offshore structures, the early stages of fatigue crack growth are most likely to occur in region one and two. During the transition from region two to region three, the crack growth rate accelerates dramatically as K_{max} approaches K_{Ic}, the fracture toughness under plain strain conditions (Monahan 1999).

ΔK is a function of stress range, structural geometry and crack size:

$$\Delta K = Y.(\Delta\sigma).\sqrt{(\pi a)} \tag{2.12}$$

where Y is the stress intensity correction factor.

For ferritic steels with yield or 0.2% proof strength below 600N/mm^2 operating in air or other non-aggressive environments at temperatures up to 100°C and for values of *da/dN* in mm/cycle,

$C = 3x10^{-13}$

$n = 3$

$\Delta K_{th} = 63\,MPa\sqrt{mm}$.

For situations in which crack growth near the threshold is particularly significant the rate of crack propagation:

$$\frac{da}{dN} = C \cdot \Delta K_{eff}^{n} \tag{2.13}$$

where

$$\Delta K_{eff} = \Delta K \quad \text{for } \Delta K \geq \frac{\Delta K_{th}}{R} \text{ and } R \text{ is positive} \tag{2.14}$$

$$\Delta K_{eff} = \frac{\Delta K - \Delta K_{th}}{1 - R} \text{ for } \Delta K \leq \frac{\Delta K_{th}}{R} \text{ and any value of } R. \tag{2.15}$$

The values of material constants C and n will usually be different from those in the equation representing the central linear potion of the sigmoidal curve.

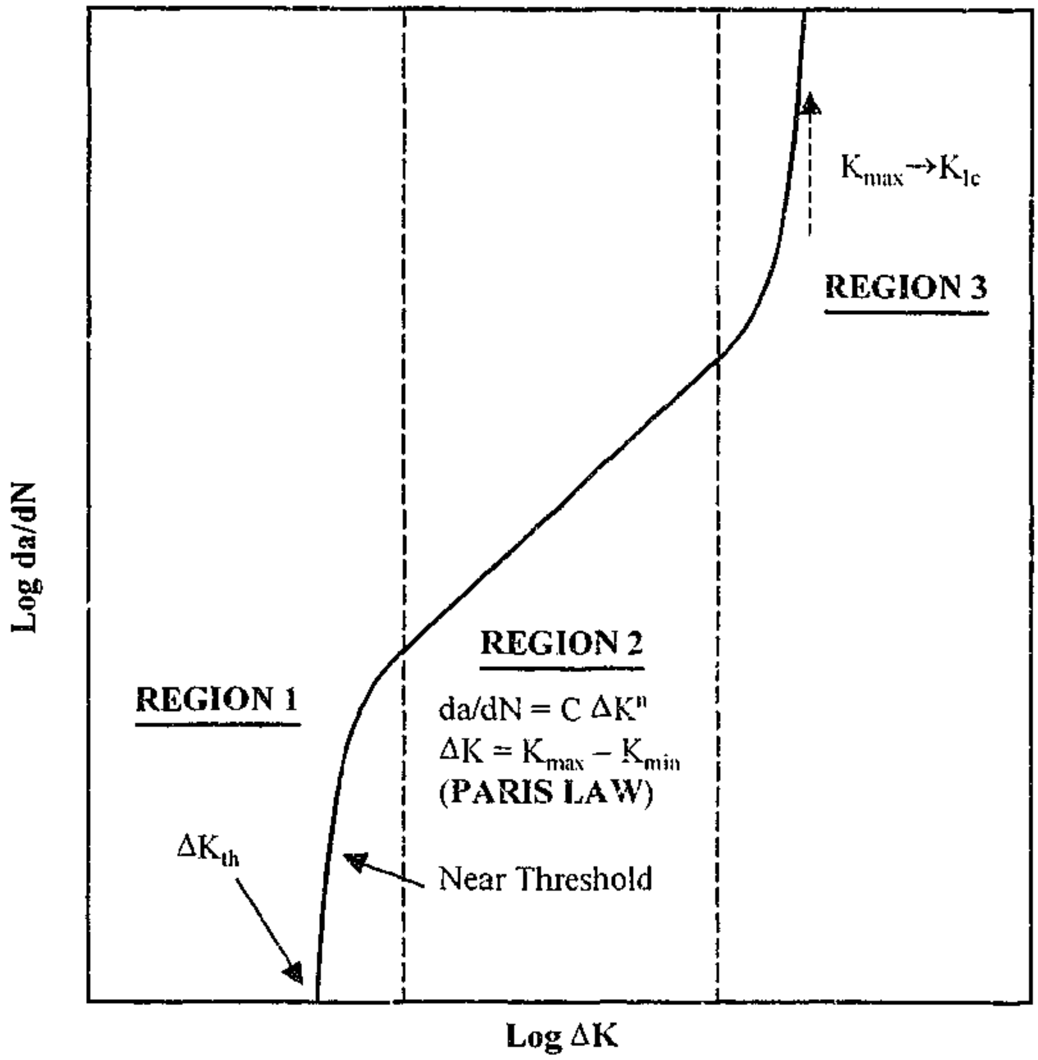

Figure 2-8: Typical crack growth rate data for fatigue tests conducted in air (Monahan 1999)

2.5.3 Fatigue Propagation Life Estimation used in BEASY (Computational Mechanics BEASY Ltd 1998)

The boundary element analysis system software (BEASY) uses the NASGRO (Forman *et al* 1993) equation for predicting fatigue life:

$$\frac{da}{dN} = \frac{C \cdot (1-f)^n \cdot \Delta K^n \cdot \left(1 - \frac{\Delta K_{th}}{\Delta K}\right)^p}{(1-R)^n \cdot \left(1 - \frac{\Delta K}{(1-R)K_c}\right)^q} \quad \textbf{(2.16)}$$

$$\Delta K = K_{max} - K_{min} = K_{max}(1-R) \quad \textbf{(2.17)}$$

$$R = \frac{K_{min}}{K_{max}} \tag{2.18}$$

The crack only grows when ΔK is greater than ΔK_{th}. For a 2D model which is subjected to mode I and mode II loading:

$$K_{max} = \sqrt{K_I^2 + 2K_{II}^2} \tag{2.19}$$

For a 3D mixed-mode problem, where the model is subjected to mode I (opening), mode II (shearing) and mode III (tearing) the stress intensity factor, K_{max} is replaced by,

$$K_{max} = K_{eff} = \sqrt{\left(K_I + |K_{III}|\right)^2 + 2K_{II}^2} \tag{2.20}$$

where a is the crack depth (mm), ΔK is the stress intensity factor range (N·mm$^{-3/2}$), ΔK_{th} is the threshold stress intensity factor range (N·mm$^{-3/2}$), f is the crack opening function . K_c is the critical stress intensity factor (N·mm$^{-3/2}$), K_{max} is the maximum stress intensity factor (N·mm$^{-3/2}$), K_{eff} is the effective stress intensity factor, K_{min} is the minimum stress intensity factor (N·mm$^{-3/2}$), K_I is the stress intensity factor for mode I (N·mm$^{-3/2}$), K_{II} is the stress intensity factor for mode II (N·mm$^{-3/2}$), K_{III} is the stress intensity factor for mode III (N·mm$^{-3/2}$), C is the crack growth rate coefficient, n,q,p are the exponents and N is the number of cycles for fatigue crack propagation life.

The program takes into account fatigue crack closure analysis for 2D models only, for calculating the effect of the stress ratio on crack growth rate under constant amplitude fatigue loading (Computational Mechanics BEASY Ltd 1998). Experiments and analyses on metallic materials have shown that fatigue cracks, under constant and variable amplitude loading, remain closed during part of the load cycle (Newman Jr 1984).

In considering the effect of crack closure, the crack opening function, f, for plasticity induced crack closure defined by Newman Jr (1984) is given by;

$$f = \frac{K_{op}}{K_{max}} = \max\left\{R;\, A_0 + A_1 \cdot R + A_2 \cdot R^2 + A_3 \cdot R^3\right\} \text{ for } 0 \le R < 1 \tag{2.21}$$

where,

$$A_0 = \left(0.825 - 0.34\alpha + 0.05\alpha^2\right)\left[\cos\left(\frac{\pi}{2}\right)SR\right]^{\frac{1}{\alpha}} \tag{2.22}$$

$$A_1 = (0.415 - 0.071\alpha)SR \tag{2.23}$$

$$A_2 = 1 - A_0 - A_1 - A_3 \tag{2.24}$$

$$A_3 = 2A_0 + A_1 - 1 \text{, and} \tag{2.25}$$

$$SR = \frac{S_{max}}{\sigma_0} \tag{2.26}$$

where α is the plain stress/strain constraint factor from the BEASY database file, S_{max} is the maximum applied stress, σ_o is the flow stress, taken to be the average between uniaxial yield stress and uniaxial ultimate tensile strength of the material, i.e $((\sigma_{ys} + \sigma_{UTS})/2)$, K_{op} is the opening stress intensity factor below which the crack is closed, and K_{eff} is the effective stress intensity factor.

2.5.4 Comparison of the different equations used for estimating fatigue propagation life

The equations used for estimating the fatigue propagation life are based on the Paris equation. The Paris equation is suitable for predicting the rate of crack growth on the linear part of the *log da/dN* versus *log ΔK* plot, which is a sigmoidal curve. Different fatigue propagation equations have adopted different multiplication factors *(MF)* to try to simulate the sigmoidal curve, so that the equation for crack propagation becomes:

$$\frac{da}{dN} = (MF) \cdot C \cdot \Delta K^n . \tag{2.27}$$

This helps to predict the fatigue life more accurately when the value of ΔK is close to ΔK_{th}.

PD 6493: BSI (1991) adopts the Paris equation and therefore a multiplication factor *(MF)* of unity, (see PD 6493 curve in Figure 2-9).

The Japanese Society of Steel Construction's equation has a multiplication factor:

$$MF = \left(1 - \frac{\Delta K_{th}^n}{\Delta K^n}\right). \tag{2.28}$$

The factor increases from values slightly greater than zero when ΔK is slightly greater than ΔK_{th} to values close to one when ΔK becomes large compared to ΔK_{th}, (see JSSC curve in Figure 2-9).

The multiplication factors for the NASGRO equations are:

(i) for 2D modelling, taking into account the effect of crack closure,

$$MF = \frac{(1-f)^n \left(1 - \frac{\Delta K_{th}}{\Delta K}\right)^p}{(1-R)^n \left(1 - \frac{\Delta K}{(1-R)K_c}\right)^q} = F(\Delta K, p, q) \text{ and} \quad \textbf{(2.29)}$$

(ii) for 3D modelling, assuming that the effect of crack closure is negligible, that is when $f=R$,

$$MF = \frac{\left(1 - \frac{\Delta K_{th}}{\Delta K}\right)^p}{\left(1 - \frac{\Delta K}{(1-R)K_c}\right)^q} = F(\Delta K, p, q) \quad \textbf{(2.30)}$$

The NASGRO equation from BEASY (Computational Mechanics BEASY Ltd 1998) tries to simulate the sigmoidal curve for values of ΔK slightly greater than ΔK_{th}. A value of p and q of 0.5 is adopted in BEASY and used in this research. When ΔK is significantly greater than ΔK_{th} the multiplication factor increases almost parabolically. This shows that this equation gives conservative values of N for ΔK values significantly greater than ΔK_{th}. The MF-ΔK line for a value of p and q of 0.5 is shown in Figure 2-9, (see NASGRO 0.5 curve). It can be noted that as the value of p and q in the multiplier for the NASGRO equation approaches zero, the NASGRO equation approaches the Paris equation. This is demonstrated by the MF-ΔK line when a value of p and q of 0.2 is adopted, (see NASGRO 0.2 curve, Figure 2-9) and when a value of p and q of 0.1 is adopted, (see NASGRO 0.1 curve, Figure 2-9). A value of p and q of 0.5 is used in this research because this is the value given for ASTM Specification Grade Steel (Computational Mechanics BEASY Ltd 1998) that has a grades close to that of the steel being investigated in this project, (Mashiri *et al* 1997; 2000b).

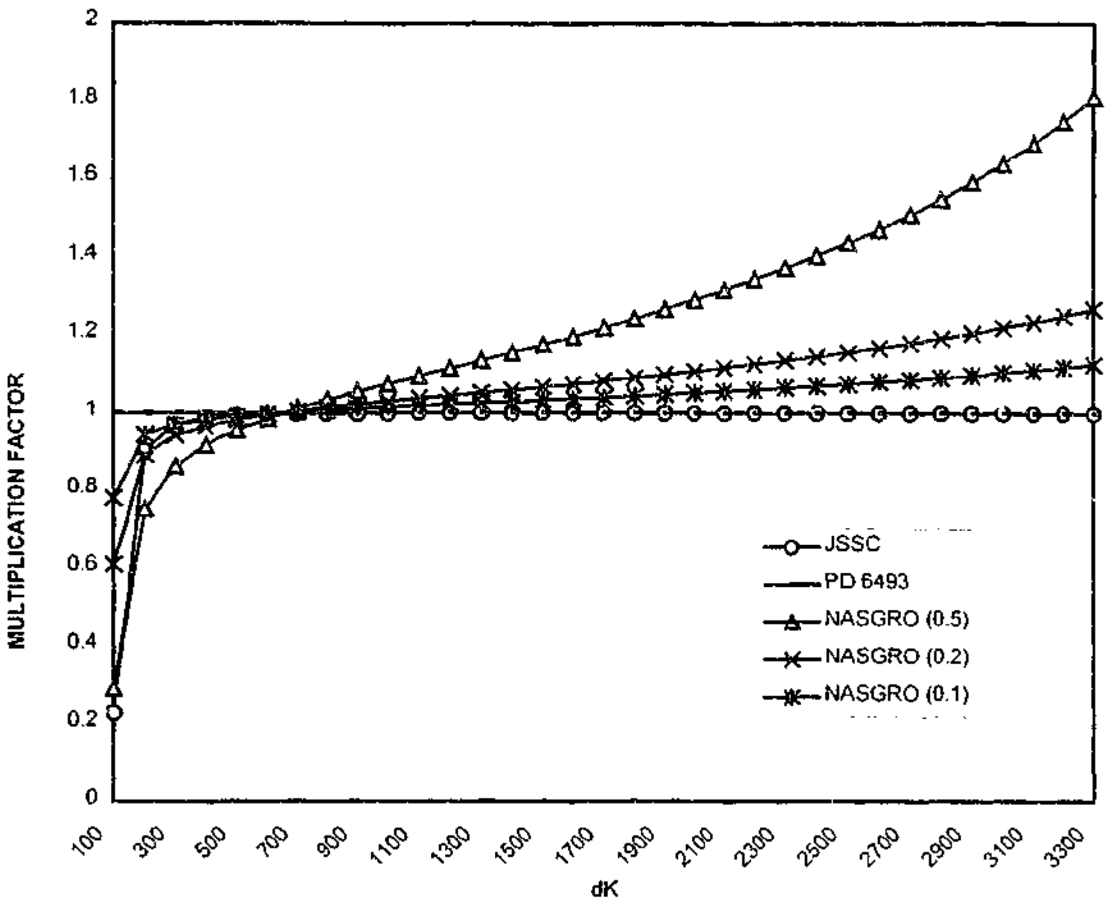

Figure 2-9: Comparison of fatigue crack propagation equations

2.6 THICKNESS EFFECT

The thickness effect is the phenomenon in fatigue of welded connections where the fatigue strength decreases as the thickness of the joint where fatigue cracks initiate and propagate to final fracture or failure increases.

The thickness effect can be demonstrated using both fracture mechanics theory and experimental work. The thickness correction factor was first introduced in a fatigue design guideline in 1984. in the revised version of the UK Department of Energy Guidance Notes (Gurney 1989). A lot earlier than the introduction of the thickness effect on fatigue of welded connections. Phillips and Heywood (1951) demonstrated the size dependence of fatigue strength of unwelded specimens. However it had long been known that plate thickness was likely to be a relevant variable for fatigue strength under bending stresses. because the stress gradient through the thinner specimen would be steeper and therefore less damaging than that in thicker specimens. In 1977 however, with the use of fracture mechanics theory, it became apparent that the fatigue strength of welded joints could be affected by plate thickness even when they were subjected to axial loading (Gurney 1977a). It was pointed out on the basis of fracture mechanics analysis and experimental evidence, that the effect of plate thickness on fatigue strength could be significant (Gurney 1979b). Using S-N data for plate welds and for tubular joints, covering the range of plate thicknesses up to 50mm Gurney (1981), proposed an empirical thickness correction for fatigue strength;

$$S = S_B \left(t_B / t\right)^{0.25} \tag{2.31}$$

where S_B is the fatigue strength for a reference plate thickness, t_B. Since the number of cyles, N, is related to the stress range, S, by $N \cdot S^3 = const.$, the corresponding thickness correction for fatigue life is;

$$N = N_B \left(t_B / t\right)^{0.75} \tag{2.32}$$

where N_B is the fatigue life for a reference plate thickness t_B. Welded plate specimens tested in seawater show a more pronounced thickness effect (de Back *et al* 1989) which can be given by;

$$N = N_B \left(t_B / t\right)^{1.1}. \tag{2.33}$$

These relationships between fatigue strength and thickness of member under failure were obtained by plotting the relative fatigue strength normalised to a thickness of 32mm versus the thickness of different plate and tubular joints, Figure 2-10 (Gurney 1989). The thickness correction was first included in 1984 in the UK Department of Energy Guidance Notes for offshore structures. The reference plate thickness for plate joints was taken as 22mm, for tubular joints the reference thickness was taken as 32mm. For thicknesses less than the reference thickness, the fatigue strength is taken as equal to the strength of the reference thickness. Other than the Department of Energy (1990) guidelines, thickness corrections have also been included in EC3 (1992) and the Australian Standard, AS4100-1998 (SAA 1998a). The thickness correction factors are provided which can be used to predict the fatigue strength of wall thicknesses other than the reference thickness.

The thickness effect is also taken into account in current fatigue design guidelines for circular and rectangular hollow section joints such as IIW (2000) and the CIDECT Design guide (Zhao *et al* 1999a). In these design guidelines the thickness effect has been incorporated into the hot spot stress S-N curves resulting in higher fatigue life for thinner walled tubular members under fatigue loading.

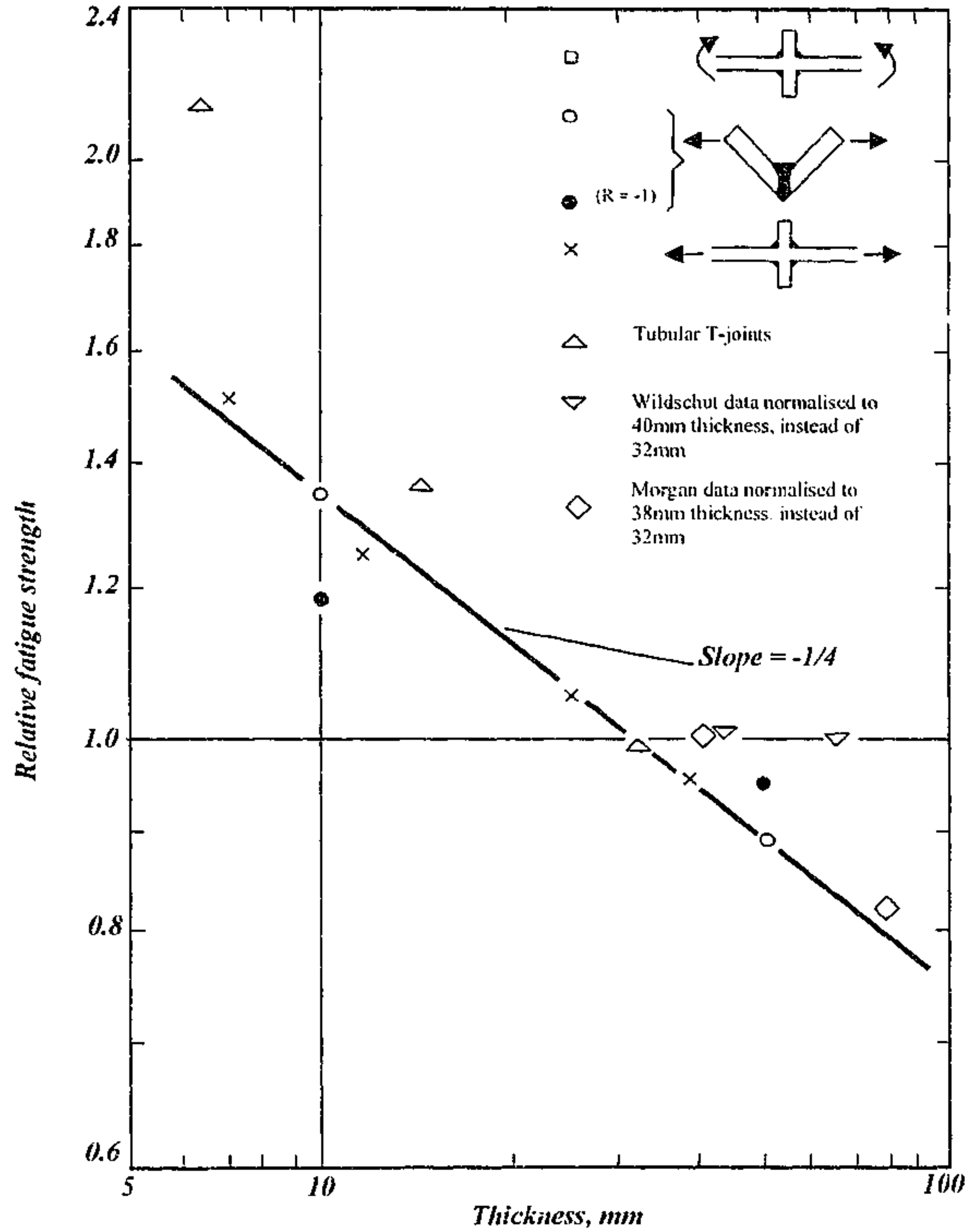

Figure 2-10: Influence of plate thickness on fatigue strength, normalised to a thickness of 32mm. All tests at R=0 except where stated. (Gurney 1989)

The thickness effect can be explained using the following models or interpretations;

(a) Statistical size effect: Thickness effect or size effect in fatigue may be interpreted using the so-called statistical effect which stems from the fact that fatigue is a weakest link process, nucleating at the location where stresses, geometry, defects and material properties combine to form optimum conditions for fatigue crack initiation and growth. Increasing the size of a specimen will statistically produce locations that are more vulnerable to fatigue failures (Berge 1989). Örjasaeter *et al* (1987) termed the statistical effect, the volume effect, and interpreted it as a correlation between the volume of highly stressed material and fatigue strength. Fatigue tests of welded joints are influenced by the initiation and growth of small ellipsoidal cracks from the weld toe. The length of the weld toe from which the cracks initiate is therefore an influencing factor for fatigue strength since a larger length results in more likelihood of initiation and failure of the welded joint (Overbeeke and Wildschut 1987). For welded joints, size effect is a function of weld length in the hot spot region. For plate specimens, for example, with transverse welds there is a size effect linked to the width dimension (Berge and Webster 1987).

(b) Fracture mechanics model: This model can be used for explaining the thickness effect in welded joints where fatigue cracks initiate from the weld toes. The following assumptions are adopted in this model (Berge 1985; Berge and Webster 1987); (i) Welded joints of the same type in various plate thicknesses are geometrically similar. This is typical of load-carrying welded joints, (ii) Initial conditions of fatigue crack growth are independent of plate thickness. Therefore the initial cracks in welds of different thicknesses are the same, see Figure 2-11. Therefore the stress distribution across the load-carrying plates in the crack growth plane are geometrically similar, leading to a steeper stress gradient in the thinner joint, according to assumption (i). Using assumption (ii), the initial crack in the thinner plate will experience a smaller stress than the initial crack of the same length in the thicker plate. This results in a smaller initial crack growth in the thinner joint (Berge 1989, de Back *et al* 1989).

(c) Technological size effect: Technological size effects are the results of differences in production parameters. For example, due to differences in rolling reduction ratios, the mechanical properties diminish with increasing plate thickness. This effect can be neglected if mechanical properties are essentially the same for different thicknesses. Technological size effect can be considered to occur as a result of varying residual stresses caused by welding in different plate thicknesses. Technological size effect can also be understood in terms of geometrical size effect, which originates from incomplete scaling. When all dimensions are scaled up or down equally, the material properties such as grain size, flaw dimensions and mechanical properties do not change (Overbeeke and Wildschut 1987).

(d) Crack propagation rates obtained using fracture mechanics theory show that in thicker plates, the crack propagates faster, which results in a shorter fatigue life (Gurney 1979b). The calculated influence of thickness effect using fracture mechanics models show a less pronounced thickness effect, maybe due to the fact that no initiation period is taken into account. The dependency of thickness effect on fatigue life and the tendency that the slopes of the S-N lines are different for several wall thicknesses indicates that the initiation period cannot be neglected (de Back *et al* 1989)

(e) The toe of the weld has nearly always the same radius due to the welding process and can hardly be influenced just by a good welding procedure. Assuming that both the radius and local angle of the weld toe will be independent of plate thickness, the relative radius (r/T), will decrease with increasing plate thickness. Therefore notches at the weld toe in large joints are relatively sharper compared to those in thinner joints. This results in a higher strain concentration factor for thicker plates and results in shorter initiation and propagation periods (de Back *et al* 1989).

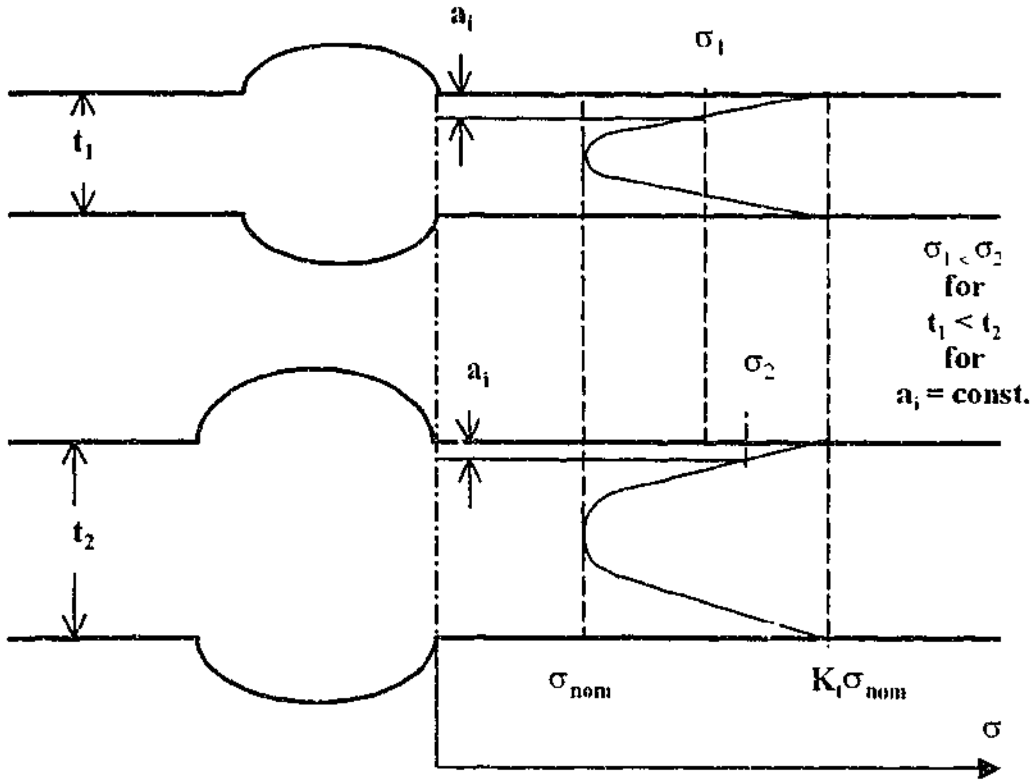

Figure 2-11: Model for describing the effect of thickness in fatigue failures initiating from the weld toe (Berge and Webster 1987).

2.6.1 Plate T-joints; Constant Amplitude in Air

A significant amount of work has been carried out to show the influence of thickness effect on fatigue strength of welded connections in plate T-joints under constant amplitude loading in air (Mohaupt *et al* 1987; Vosikovsky *et al* 1989; Booth 1987; Berge *et al* 1987; Overbeeke and Wildschut 1987; Örjasaeter *et al* 1987).

Mahaupt *et al* (1987) and Vosikovsky *et al* (1989) carried out fatigue tests on T-plate joints (Figure 2-12) under 3 point bending in the as welded condition in air at a stress ratio of 0.05, to determine the influence of thickness on fatigue life. The T-joints had equal plate thicknesses for both the main plate and the transverse welded plate. Loading was via the upstand. The joints were made up of plates of thicknesses 16, 26, 52, 78 and 103mm. There was a reduction in initiation life as well as a reduction in crack propagation life with increasing plate thickness, resulting in an overall reduction in total life. Crack initiation occurred as multi-nucleation of cracks along the weld toe. This resulted in the growth of several semi-elliptical cracks. Final coalescence of the semi-elliptical cracks resulted in a straight fronted crack (Mohaupt *et al* 1987). Initiation life, propagation life and total life were all found to show the influence of thickness effect. Crack initiation life was defined as the number of cycles at which a crack of about 0.5mm depth was detected using the AC or DC Potential Drop technique with the use of probes. Endurance or total life of the specimen was the number of cycles when the crack depth was one half of the plate thickness. These results showed that parallel lines did not provide the best fit for the data, and the data was better described by a set of lines with decreasing negative slope. This decreasing slope results in a stronger thickness effect at low stress ranges.

Booth (1987) carried out fatigue tests of T-plate joints under four point bending (Figure 2-13) in the as welded condition under constant amplitude loading, at a stress ratio of zero (Booth 1987). The joints were made up of plates with thicknesses of 25, 38, 50, 75 and 100mm and joined by welds of 60° flank angle. Failure was defined when the machine could no longer apply the required load due to an increase in specimen compliance. This generally corresponded to a fatigue crack penetrating approximately 50% of the plate thickness. Multiple crack initiation occurred along the weld toe and the individual small fatigue cracks coalesced to form a single crack approximately 3 to 5mm deep across the full specimen width. This crack then advanced approximately uniformly through the plate thickness. A clear influence of plate thickness on fatigue life was observed. Post weld heat treated joints also showed a significant decrease in fatigue strength, similar to the as welded joints, as the plate thickness in the joints increased. A similar thickness effect was observed for toe ground joints. However weld toe grinding resulted in a significant increase in fatigue performance compared to the as-welded joints. The S-N curve was rotated in an anti-clockwise direction, such that the benefit of grinding increased as stress range decreased. Considerable scatter due to variations in the quality of grinding was observed. It should be noted that simple fracture mechanics cannot be used to describe toe ground joints because of the increase in initiation life associated with them, making initiation life a significant portion of total life.

Berge *et al* (1987) carried out fatigue tests on T-plate joints under a cantilever loading system (Figure 2-14) in the as welded condition under constant amplitude loading. The joints were made up of plates of thicknesses 20, 100 and 150mm which were joined by welds with throat angles in the range of 30°-35°. Thickness effect was observed. Crack initiation was detected visually by applying the soap water method. The soap water method is very sensitive and enabled fatigue crack lengths of the order of 1-3mm to be detected (Berge *et al* 1987). Both initiation and total fatigue life showed significant thickness effect.

Overbeeke and Wildschut (1987) performed fatigue tests on T-shaped specimens with a full penetration K-weld under pure bending in air in the post weld heat treated condition. The joints were made up of plates of thicknesses 16, 25, 40 and 70mm. The specimens were regarded as broken when the cracks had grown to half-way the plate thickness at the sides of the specimens. In the stress relieved condition the effect of specimen size was described by,

$$S = S_B (t_B/t)^{0.15}. \quad \textbf{(2.34)}$$

Örjasaeter *et al* (1987) peformed endurance tests on plate T-joints in air at a stress ratio of 0.1. The plates making up the joints were made up of low carbon micro-alloyed steel. The joints were made up of plates of thicknesses 30, 70, 100, 130 and 160mm. Tests were carried out on as-welded joints as well as post weld heat treated plate T-joints under cantilever bending, Figure 2-14. Tests were also carried out under 3 point bending, with the load applied just under the welded upstand as shown in Figure 2-15. The thickness effect was clearly apparent in all tests.

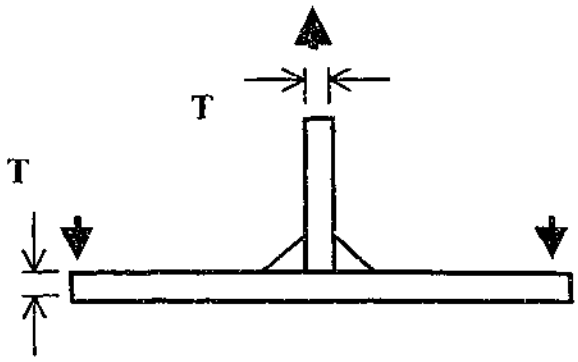

Figure 2-12: Plate T-joints under cyclic 3-point bending load, load applied through welded upstand (Vosikovsky et al 1989; Mohaupt et al 1987)

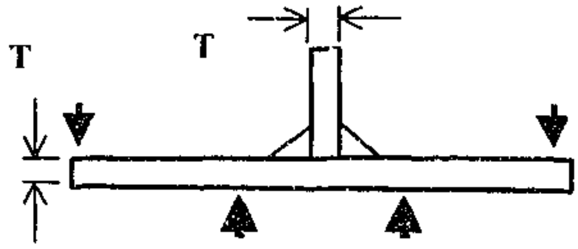

Figure 2-13: Plate T-joints under four point bending (Booth 1987)

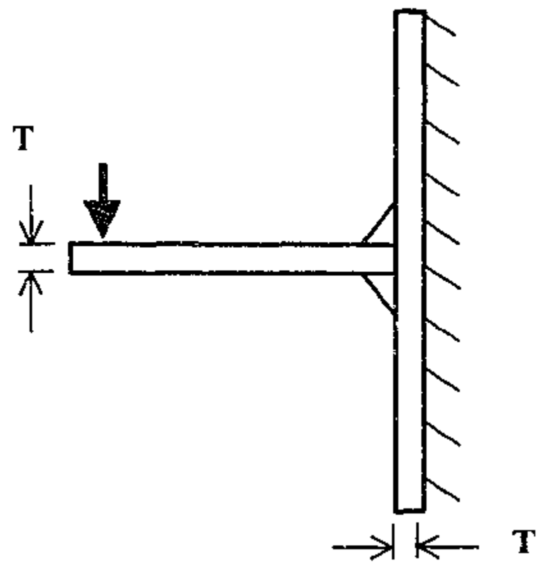

Figure 2-14: Plate T-joints under cantilever loading system (Berge et al 1987; Örjasaeter et al 1987)

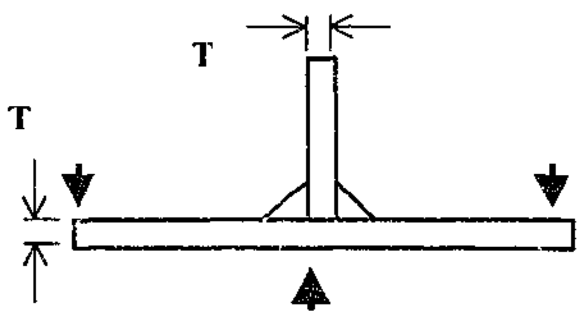

Figure 2-15: Plate T-joints under cyclic 3-point bending load, load applied directly below the welded upstand (Orjasaeter et al 1987)

2.6.2 Plate T-joints; Variable Amplitude in Air

Vosikovsky *et al* (1989) performed fatigue tests of plate T-joints shown in Figure 2-12, under variable amplitude loading in air. When the results for variable amplitude loading are expressed in terms of an equivalent stress range, there is good agreement with results from constant amplitude tests for both initiation and total life. This demontrates that the thickness effect is not changed by random loading. The equivalent stress range, S_{eq} is:

$$S_{eq} = \sqrt[m]{\frac{\sum S_i^m}{N}} \qquad \textbf{(2.35)}$$

where m is the exponent in the Paris equation, and has a common value of 3.

2.6.3 Plate T-joints; Constant Amplitude in Seawater

Mahaupt *et al* (1987) and Vosikovsky *et al* (1989) carried out tests on plate T-joints shown in Figure 2-12, at constant amplitude in seawater (Mohaupt *et al* 1987; Vosikovsky *et al* 1989). The tests included unprotected, optimum cathodically protected and overprotected joints for thicknesses ranging from 16mm to 103mm. Statistical comparison of data obtained in air with that obtained in seawater with or without cathodic protection, showed that the seawater environment reduces fatigue life by a factor of 2.5 to 3. The beneficial effects of cathodic protection are too small to be recognised in fatigue design codes (Mohaupt *et al* 1987). Thickness effect is not altered by corrosive environments. The average portion of life spent in crack initiation was similar to that measured in air. However there were far more initiation sites than in the in-air tests and an almost straight fronted crack formed when the maximum crack depth was 5mm for tests in sythetic seawater with free corrosion, optimum cathodic protection or cathodic overprotection. This implies that there is a stronger affect of the seawater environment on fatigue crack propagation life.

Overbeeke and Wildschut (1987) performed fatigue tests on T-shaped specimens with a full penetration K-weld under pure bending in seawater in the as-welded joints of similar shape but different weld geometry. The joints were made up of plates of thicknesses 16 and 40mm. A weld throat angle of 45° instead of 60° increased the indurance by 36% for the as welded geometry. Weld throat angle did hardly influence the endurance when the weld toe was dressed by grinding. However grinding improved the endurance by a factor of 2 to 2.3. Different seawater temperatures of 5°C and 20°C had no influence on the endurance. Thickness effect was evident in all cases.

2.6.4 Plate T-joints; Attachment Thickness and Weld Profile; Constant Amplitude in Air

Vosikovsky *et al* (1989) carried out fatigue tests on plate T-joints to show the influence of attachment thickness and improved weld profile on fatigue under constant amplitude loading. Figure 2-16 illustrate the specimens tested (Vosikovsky *et al* 1989). A relationship of the fatigue strengths for the different joints is given in Table 2-3. Ratios of fatigue initiation life, fatigue propagation life and fatigue total life for the different joints is given to illustrate the effects which both attachment thickness and weld profile have on fatigue life. N_I/N_{II} demonstrates the thickness effect. When both the attachment and the base plate were doubled, without any change in overall weld profile or toe radius fatigue life decreased. The penalty for thickness effects in the Department of Energy Guidelines is based on comparisons of this type. N_{III}/N_{II} shows the advantage to be gained by using thinner attachments, without any change in the flat 45° profile. The use of an attachment plate which is thinner than the main plate can improve the fatigue life available and mitigate the relative loss in life caused by using thicker main plates (Hilton and Webster 1989; Vosikovsky *et al* 1989). If the 45° flat weld profile and associated toe radius are replaced by the AWS concave profile, case IV, there is a further improvement in fatigue strength as shown by the ratio N_{IV}/N_{III}.

Noordhoek *et al* (1987) performed fatigue tests on plate T-joints under four point bending in the as welded condition in air with constant amplitude loading at a stress ratio of 0.1. The plate T-joints had transverse attachments as well as longitudinal attachments. The scale effect for a specimen with a transverse attachment includes two thickness effects. One thickness effect is caused by the variation in thickness of the main plate while the other is caused by the variation of the thickness of the attachment. The thickness effect of the main plate seems to increase with an increase in thickness of the attachment. On the other hand the thickness effect of the attachment seems to increase with an increase in the thickness of the main plate. Fatigue strength decreases for a thicker main plate as well as for a thicker attachment, Figure 2-17. Thickness effect was also observed for the plates with a longitudinal attachment, due to different thicknesses of the main plate for a constant thickness of a longitudinal attachment, Figure 2-18. This is despite the fact that for the longitudinal attachment, the main stress direction is parallel to the attachment. In the case of a longitudinal attachment the crack initiation occurs at a very early stage, less than 1% of total life, but in the cracked stage, there is a long crack propagation life.

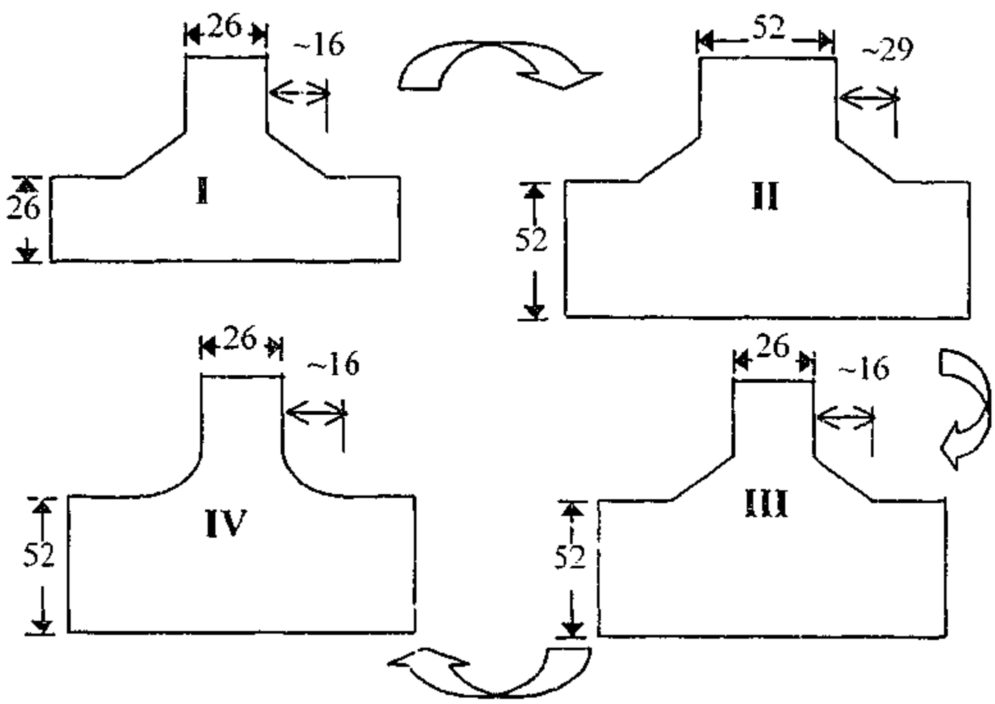

Figure 2-16: Schematic representation of joints geometries used to evaluate the effects of attachment thickness and improved weld profile (Vosikovsky et al 1989)

Table 2-3: Life ratios for S=100MPa (Vosikovsky et al 1989)

	N_I/N_{II}	N_{III}/N_{II}	N_{IV}/N_{III}	N_{IV}/N_{II}
Total life	3.3	1.5	2.0	3.0
Initiation life	3.6	2.0	2.3	4.7
Propagation life	3.2	1.4	1.7	2.3

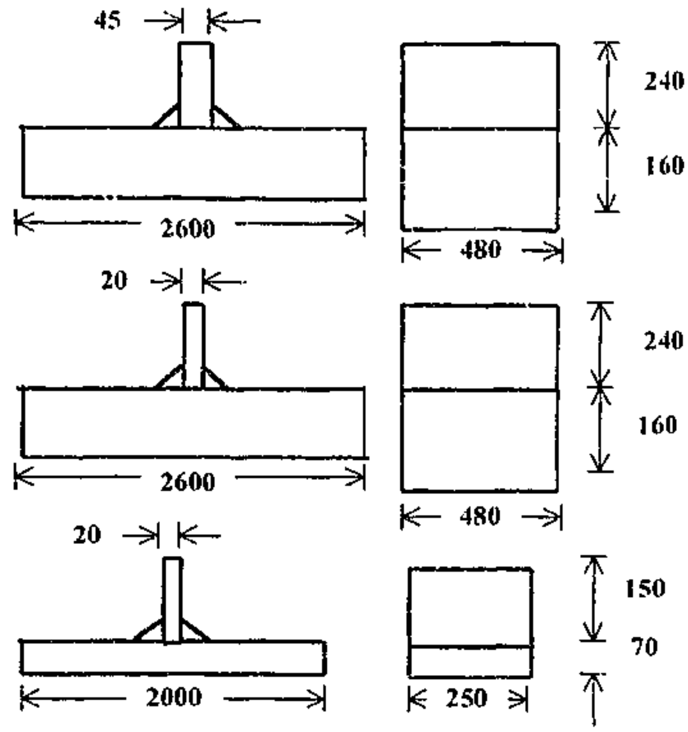

Figure 2-17: Plate T-joints with transverse attachments (Noordhoek et al 1987)

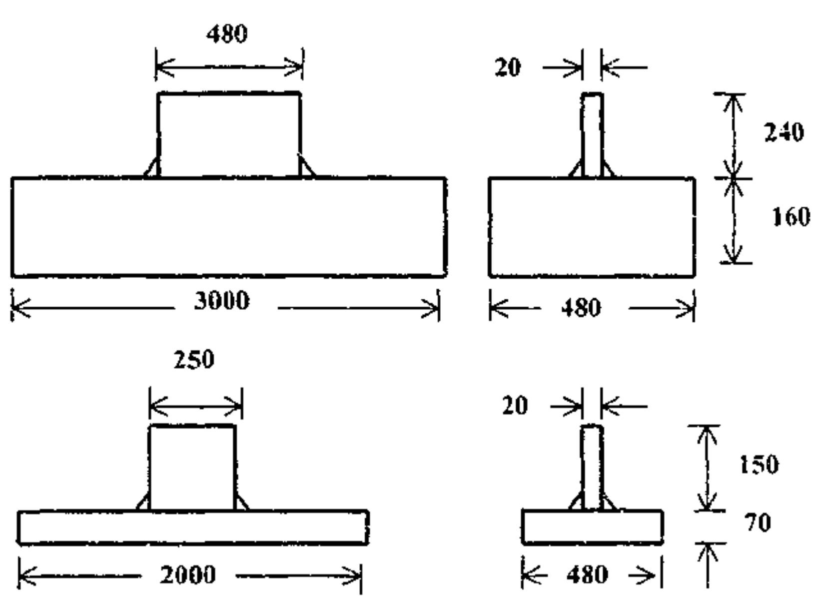

Figure 2-18: Plate T-joints with longitudinal attachments (Noordhoek et al 1987)

2.6.5 Plates with Longitudinal Edge Attachments

Tests for plates with longitudinal attachments were carried out for different widths of 40, 80 and 200mm. These joints were stress-relieved and were carried out at a stress ratio of zero under tensile cyclic loading. The joint shown in Figure 2-19 has a distinct similarity to a joint with transverse non-load-carrying fillet welds. The plate width, *W*, is the equivalence of the plate thickness in transverse fillet welded joints. For these joints fatigue strength decreases with an increase in plate width, *W*. Cracks propagate across the width, *W* (Gurney 1989).

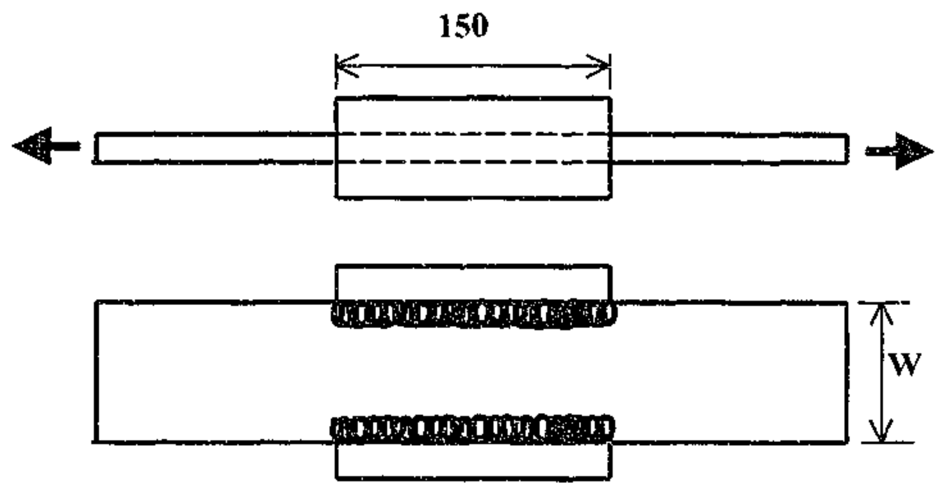

Figure 2-19: Plates with longitudinal edge attachments

2.6.6 Plate Girders

Large scale plate girders with plate thicknesses 20, 40 and 60mm were tested under four point bending. A significant effect of plate thickness was found. Compared to the data obtained with the 20mm plate thickness models, the plate girder models with 40 and 60mm plate thicknesses showed a reduction in fatigue life by a factor of 2.0 and 1.9 respectively. A fracture mechanics model was used and it accurately predicted the effect of plate thickness on fatigue life. The fracture mechanics model included the effects of local weld geometry and crack ellipticity (Eide and Berge 1987).

The following conclusions can be made for thickness effect in welded plate joints (Berge 1989; Viskovsky *et al* 1989);

1. When S-N data is obtained from plate specimens with welds transverse to the principal stress direction, the thickness effect appears to be essentially the same for a wide range of weld geometries and loading systems.
2. The thickness effect is essentially unaffected by and superimposed on any effects of post weld heat treatment (PWHT), variable amplitude load history and seawater environment .
3. A smooth weld toe transition will in general lead to an improved fatigue strength, but the thickness effect appears to be the same, regardless of weld geometry.

2.6.7 Thickness Effect in Tubular Joints

The scale effect is recognised in most design guidelines such as IIW (2000), Department of Energy (1990), EC3 (1992), AWS (1998) and AS4100 (SAA 1998a), usually resulting in a higher S-N curve for smaller wall thicknesses. The major factor which determines thickness effect is the wall thickness of the failed member (van Wingerde *et al* 1997b). In tubular joints the direction of the weld toe is transverse to the direction of stress, so that it is expected that the critical dimension is the wall thickness of the tube (Gurney 1989).

Some of the studies which have been undertaken on thickness effect in tubular joints are summarised below. These analyses used a large number of data from different sources to arrive at conclusions which showed that the thickness effect in tubular joints depends on the thickness of member in the connection which fails under fatigue. Connections in which thicker members failed under fatigue were found to have reduced fatigue strength compared to connections in which the failed member was relatively thinner (van Delft *et al* 1985, van Wingerde *et al* 1997b).

Fatigue test data of about 200 welded large size tubular joints was analysed by van Delft *et al* (1985), using multiple linear regression analysis. The analysis included S-N data from T-, Y-, X-, K- and KT- joints which were tested under axial, in-plane bending and out-of-plane bending loads. The effect of specimen size, loading mode, joint type and environment were studied. The scale effect was found to be the dominating factor on fatigue strength and by taking the scale effect into account the scatter of the S-N data could be reduced considerably. The S-N data was plotted on a log-log scale for Hot Spot

Strain Range (HSSNR) and number of cycles to crack through fatigue life. A considerable scatter was observed with a factor of about 100 on life, based on plus and minus two times the standard deviation. This scatter showed a trend that the thinner walled joints have a better fatigue life for a given hot spot strain range (HSSNR) compared to thicker walled joints. It was observed from this data that runouts for thinner walled joints occur at higher hot spot strain ranges compared to the runouts in thicker walled joints which occur at lower hot spot strain ranges. This is an indication that the fatigue limit for thinner walled joints is much higher than the fatigue limit in thicker walled joints. A multiple linear regression analysis which takes into account interaction, that is, that the influence of a variable is affected by the value of another was used. The multiple linear regression analysis took into account that the influence of the thickness of the failed member on fatigue behaviour is also dependent on the crack through fatigue life. The relation between the hot spot strain range (HSSNR), number of cycles to crack through (N_c) and the wall thickness of the cracked member (T_{cr}) from the regression analysis was found to be,

$$\log HSSNR = 4.53 - 0.175 \cdot \log N_c + 0.075 \cdot \log N_c \cdot \log T_{cr}. \qquad \textbf{(2.36)}$$

From Equation 2.36, the relationship between the $HSSNR$ and N_c for various tube wall thicknesses T_{cr} was plotted as shown in Figure 2-20. The S-N curves are plotted from their intersection point at 1 cycle onwards, but are not valid at such high strain range levels. The S-N curves show that the slope is dependent on the wall thickness. The thickness effect seems to be dependent on fatigue life or strain range levels (van Delft *et al* 1985). This is in agreement with the analysis of the results in the low cycle fatigue range, where no thickness effect was found (van der Vergte 1988). The shallower slope of the S-N lines for small scale tubular joints with wall thicknesses ranging from 4-16mm was also reported by Wardenier (1982). Based on this statistical analysis of European fatigue data, van Delft *et al* (1985) found a thickness effect of $t^{-0.075\log N}$ for tubular joints between circular members, whereas van Wingerde (1992) established a factor of $t^{-0.110\log N}$ for tubular joints between square members with thicknesses ranging from 4-16mm.

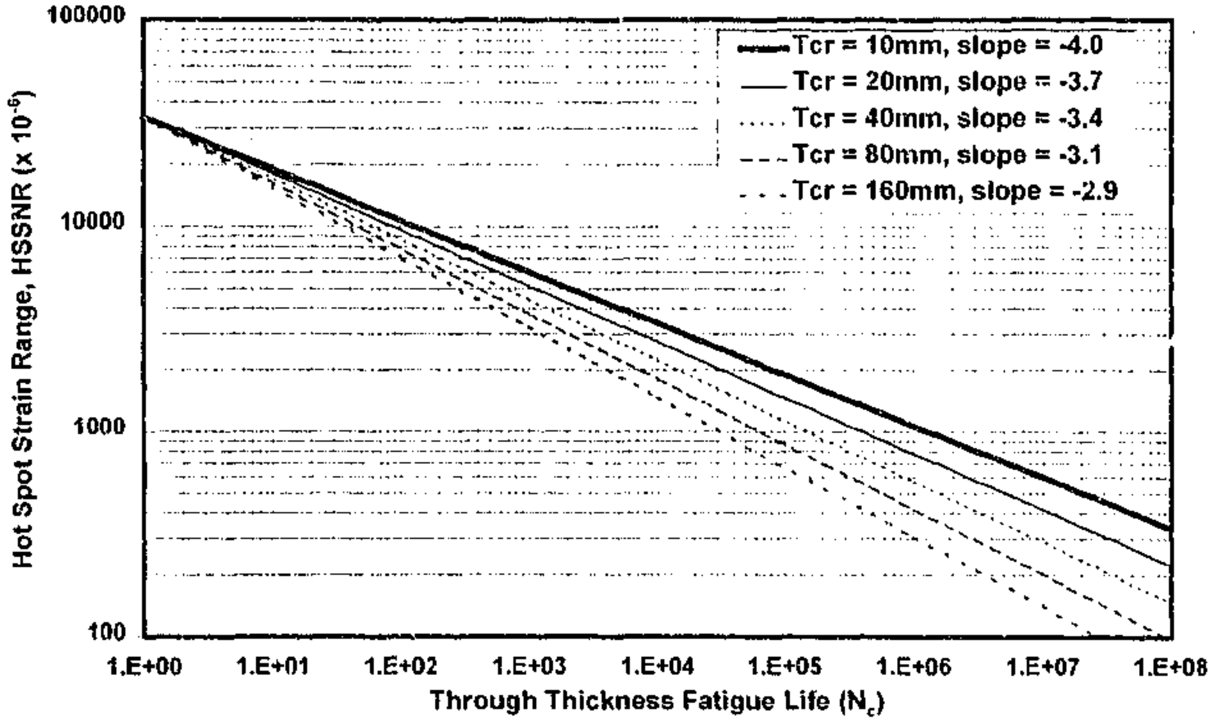

Figure 2-20: S-N curves for different thicknesses according to Equation 2.36 (van Delft et al 1985)

van Wingerde *et al* (1997b) studied the thickness effect of connections made from both circular and square hollow sections screened from a large database of S-N data from different research institutions. The analysis grouped together joints of different types such as T-, Y-, X- and K-joints. These different types of joints had also been tested under different loading conditions such as axial, in-plane bending and out-of-plane bending. The S-N data included only the specimens which had been tested in air. Specimens whose mode of failure corresponded to complete loss of failure only were used. In some of the data, the number of cycles corresponding to complete loss of strength was determined from the ratio of the number of cycles to complete loss of strength to number of cycles to through thickness cracking determined empirically from data of circular hollow sections. The avarage ratio between number of cycles to complete loss of strength to number of cycles to through thickness cracking was 1.49, with some specimens having a ratio as high as 3. The hot spot stress range was defined as the extrapolated value of stress to the weld toe. Similar to the analysis done by van Delft *et al* (1985), the plot of S-N data showed that the thickness of the cracked member was the most dominant factor influencing fatigue behaviour. Two methods were used to determine the thickness effect of the screened data. The first method involved determining a correction factor of the form.

$$S_{rhs,t} = S_{rhs,16} \cdot \left(\frac{16}{t}\right)^{c}, \tag{2.37}$$

for a 16mm reference thickness. A value of c was obtained by minimising the scatter in the N direction. However this method gives S-N curves which are parallel to each other for all cycle ranges, which is a clear limitation of this method. This is because the thickness effect has been found to be less pronounced for the low cycle (van der Vergte 1988, van Delft *et al* 1985). The second method stems from the work done by van Delft *et al* (1985), using multiple regression analysis. van Delft *et al* (1985) obtained the S-N lines for other thicknesses by rotating the reference line around its intersection with N = 1 cycle. This resulted in a thickness correction of the form,

$$S_{rhs,t} = S_{rhs,16} \cdot \left(\frac{16}{t}\right)^{c \cdot \log N}. \tag{2.38}$$

This thickness correction results in S-N curves of different slopes, and shows that the thickness effect is greatest at lower stress ranges. From the resulting screened data van Wingerde *et al* (1997b) showed by analysing S-N data points of joints from circular hollow sections (173 data points) and from square hollow sections (65 data points) seperately that they could both be represented by a thickness correction of the form,

$$S_{rhs,t} = S_{rhs,16} \cdot \left(\frac{16}{t}\right)^{-0.06 \cdot \log N}. \tag{2.39}$$

In both analysis the EC3 class 114 line was used as the reference curve for a thickness of 16mm. By including the thickness correction into the S-N equation of the reference thickness, the following equations relating hot spot stress range (S_{rhs}) and number of cycles to failure (N_f) were obtained:

$$\log S_{rhs} = \frac{1}{3}\left(12.476 - \log N_f\right) + 0.06 \log N_f \cdot \log\left(\frac{16}{t}\right), \tag{2.40}$$

$$\text{for } 10^3 < N_f < 5 \cdot 10^6 \text{ and}$$

$$\log S_{rhs} = \frac{1}{5}\left(16.327 - \log N_f\right) + 0.402 \log N_f \cdot \log\left(\frac{16}{t}\right), \tag{2.41}$$

$$\text{for } 5 \cdot 10^6 < N_f < 10^8.$$

Equation 2.40 is for constant amplitude loading while equation 2.41 is valid for variable amplitude only. A representation of the resultant S-N curves from these equations is shown in Figure 2-21. These equations have been adopted in the fatigue design recommendations for circular and rectangular tubular welded connections, where the valididty range for CHS joints is $4mm \le t \le 50mm$ and the valididty range for RHS joints is $4mm \le t \le 16mm$ (IIW 2000; Zhao *et al* 1999a).

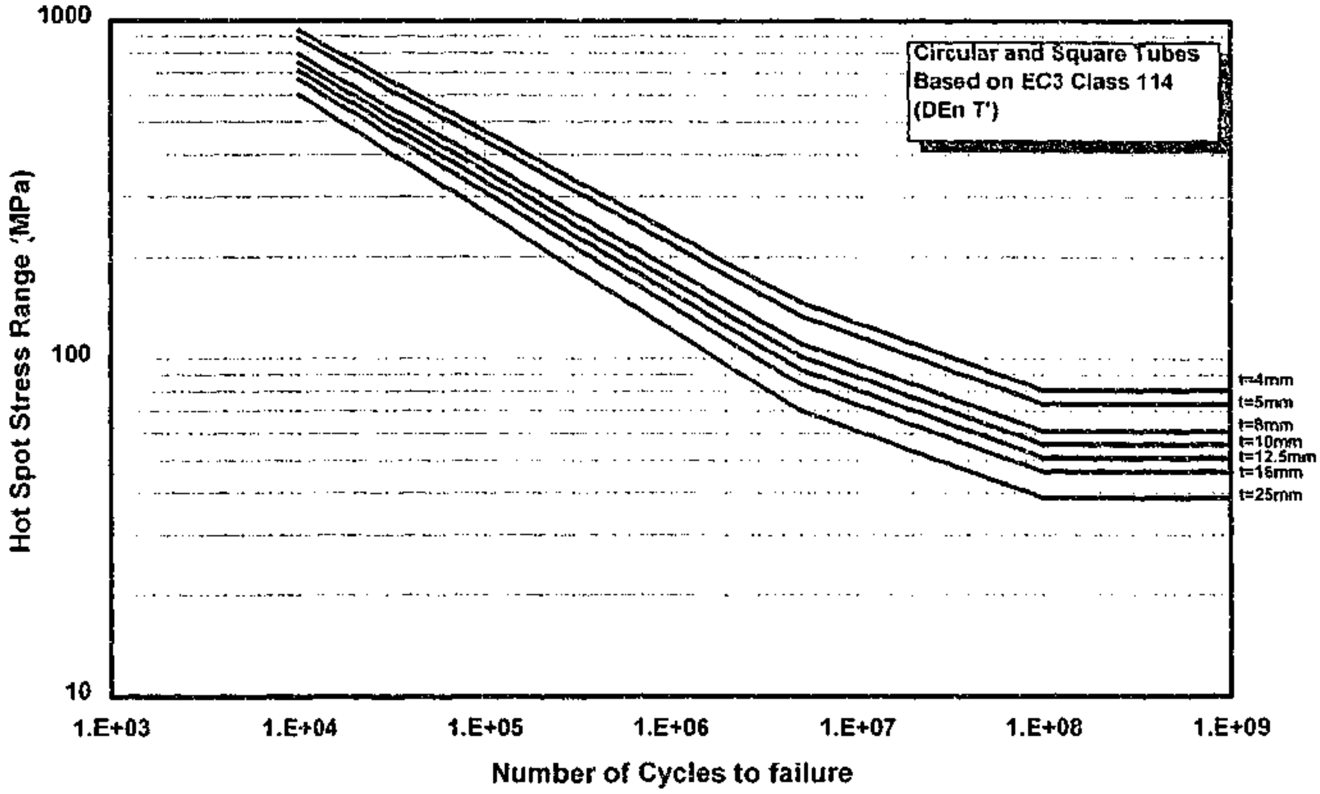

Figure 2-21: Recommended S_{rhs}-N_f lines for tubular joints (circular and square tubes) (van Wingerde et al 1997b)

2.7 STATIC STRENGTH OF VIERENDEEL CONNECTIONS

Vierendeel trusses are made up of chord and brace members connected to each other at right angles, Figure 2-22. The method of transfer of forces between the brace and chord members is mainly through bending, although axial and shear force transfer occur but to a lesser extent. They differ from triangulated Warren and Pratt trusses where the chord and brace members are loaded predominantly by axial forces (Packer *et al* 1992).

The tests in this research involve Vierendeel connections, which are T-joints under in-plane bending. Fatigue damage is caused by cyclic loading conditions under service. The fatigue loading applied to these connections is therefore dependent on the static strength of the connections.

The strength and flexural rigidity of an unstiffened connection decreases as the chord slenderness ratio b_o/t_o increases and the branch to chord width ratio b_1/b_o (or β) decreases. Connections with β=1.0 and a low b_o/t_o value approach full rigidity. All other unstiffened connections are classified as semi-rigid. The semi-rigid connections can be stiffened to achieve full rigidity through the use of bracing plate stiffeners, chord plate stiffeners, haunch stiffeners or truncated pyramid stiffeners (Packer *et al* 1992).

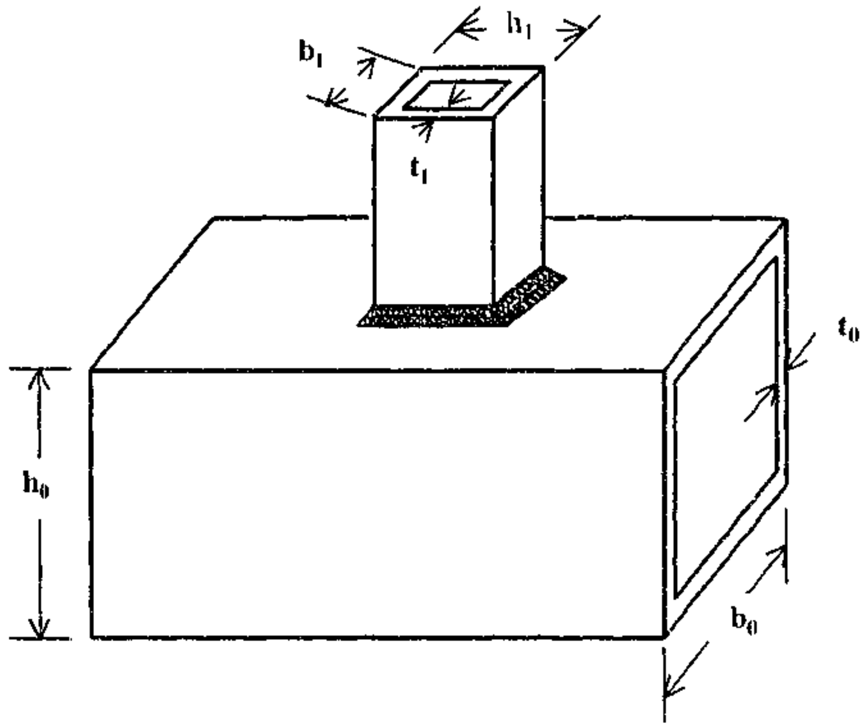

Figure 2-22: Vierendeel Connection

The unstiffened Vierendeel connections have five possible modes of failure when subjected to in-plane bending as follows (see Figure 2-23) (Packer *et al* 1992; Packer & Henderson 1997);

(a) Chord face yielding

(b) Cracking in chord

(c) Cracking in brace member

(d) Crippling of the chord side walls, and

(e) Chord shear failure

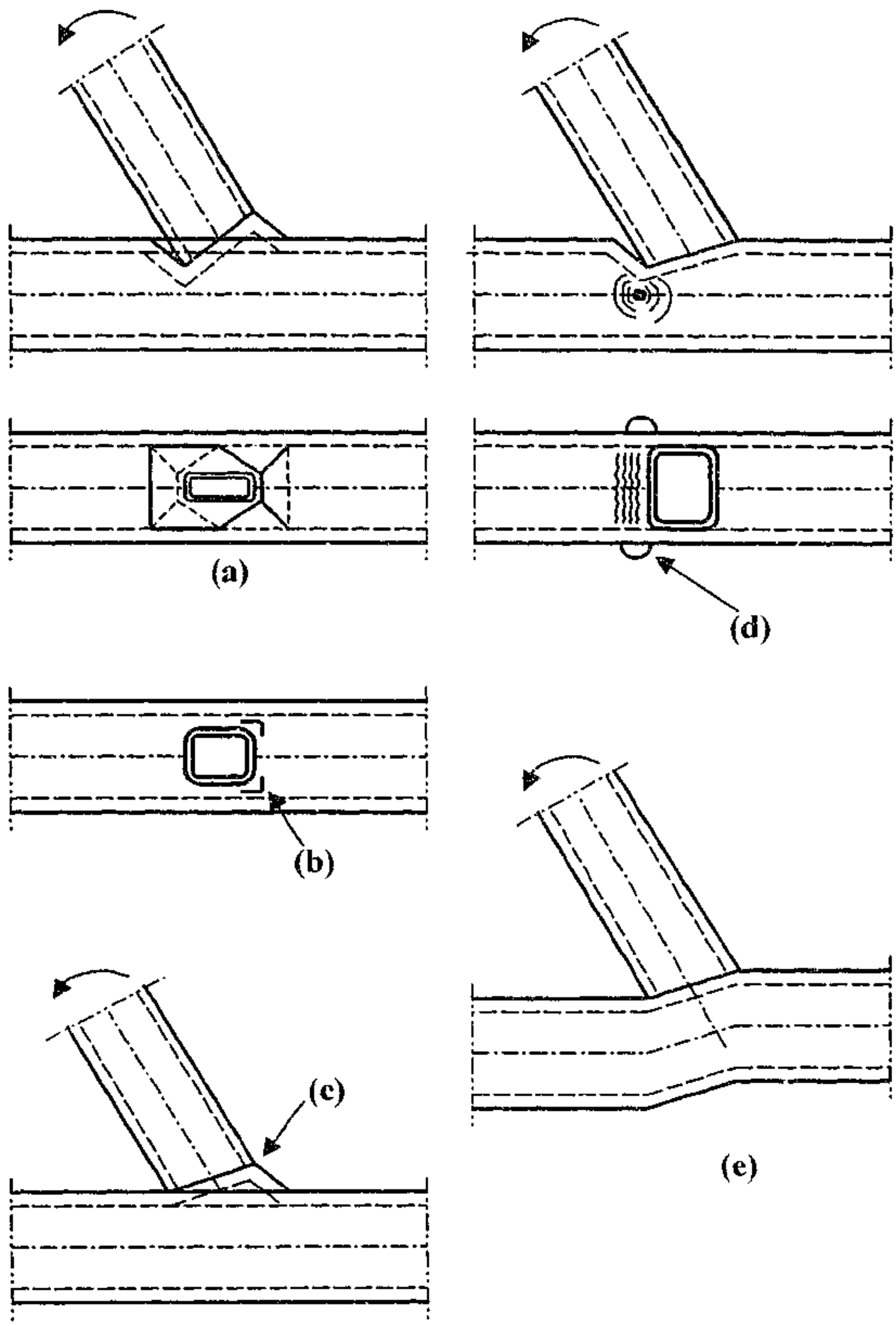

Figure 2-23: Modes of Failure (Packer et al 1992)

The moment capacities of vierendeel connections for different failure modes are summarized below:

(a) Chord face yielding (Failure Mode (a))

For low to moderate β values, and when the influence of membrane effects and strain hardening are neglected, the moment capacity is determined by the yield line model, see Figure 2-24.

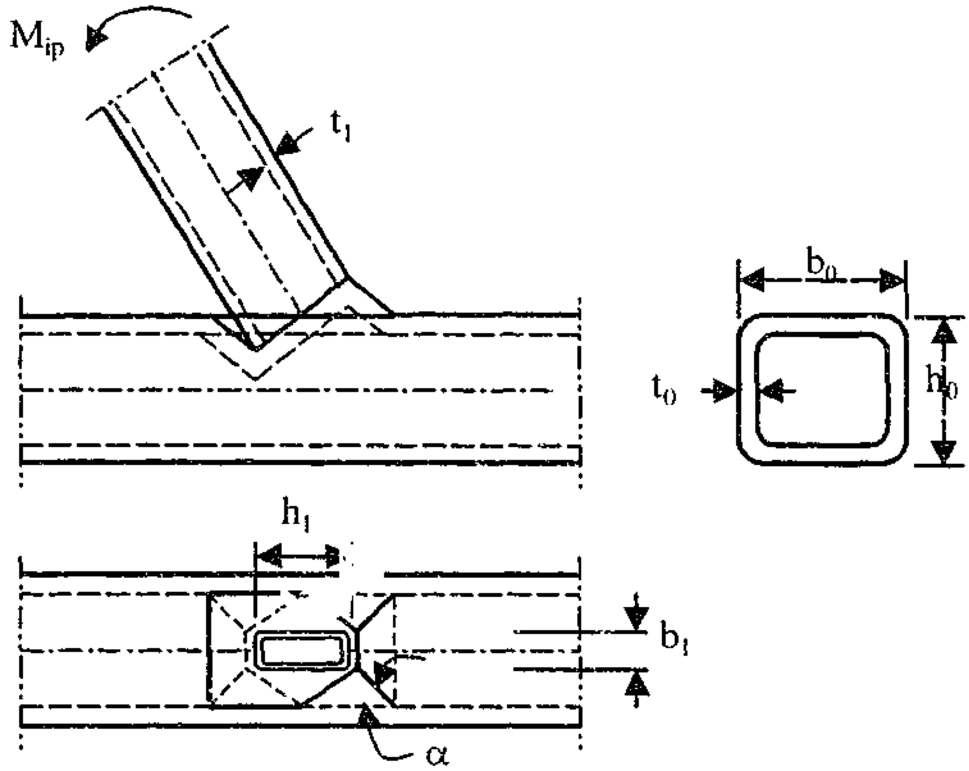

Figure 2-24: Yield Line Model

$$M_{ip}^{*} = 0.5 f_{y0} t_0^2 b_0 \left\{ 1 + \frac{4h_1/b_0}{\sin\theta_1 \sqrt{1-\beta}} + \frac{2(h_1/b_0)^2}{\sin^2\theta_1 (1-\beta)} \right\} f(n) \text{ for } \beta \le 0.85 \quad \textbf{(2.42)}$$

where M_{ip}* is the connection resistance for in-plane bending, expressed as a bending moment in the bracing member, f_{yo} is the yield stress of the chord member, t_o is the thickness of hollow section chord member, b_o is the external width of the hollow section chord member, h_l is the external depth (in plane of truss) of the hollow section brace member, θ_l is the included angle between bracing member and the chord, and β is the width ratio between the bracing member and the chord.

$f(n)$ is a function to allow the reduction in connection moment capacity in the presence of large compression chord forces.

$$f(n) = 1.3 + \left(\frac{0.4}{\beta}\right)n \text{ but } f(n) \leq 1.0 \tag{2.43}$$

where $$n = \frac{N_0}{A_0 f_{y0}} + \frac{M_0}{S_0 f_{y0}} \tag{2.44}$$

where S_0 is the elastic modulus of the chord member, A_0 is the cross-sectional area of the chord member, M_0 is the bending moment in the chord member, and N_0 is the axial force applied to the chord member.

For tension chords $f(n) = 1$.

For a value θ_1 of 90°, the moment capacity equation becomes

$$M_{ip}^{*} = f_{y0} t_0^2 h_1 \left\{ \frac{1}{2h_1/b_0} + \frac{2}{\sqrt{1-\beta}} + \frac{(h_1/b_0)}{(1-\beta)} \right\} \text{ for } \beta \leq 0.85 \tag{2.45}$$

(b) Cracking in brace member (Failure Mode (c))

The effective width approach is used to relate the reduced capacity of the bracing member (considered to be the same on the tension and compression flanges of the bracing member) to the applied bracing moment as follows:

$$M_{ip}^{*} = f_{y1} \left\{ Z_1 - \left(1 - \frac{b_e}{b_1}\right) b_1 t_1 \left(h_1 - t_1\right) \right\} \text{ for } 0.85 < \beta \leq 1.0 \tag{2.46}$$

where f_{y1} is the yield stress of the brace member, Z_1 is the plastic section modulus of the brace member, b_e is the effective width of the bracing member, b_1 is the external width of hollow section brace member (90° to the plane of the truss), and t_1 is the thickness of hollow section brace member.

The effective width of the bracing member, b_e is:

$$b_e = \frac{10}{b_0/t_0} \cdot \frac{f_{y0} t_0}{f_{y1} t_1} \cdot b_1 \text{ but } b_e \leq b_1 \tag{2.47}$$

(c) Crippling of the chord side walls (Failure Mode (d))

A chord side wall bearing or buckling capacity can conservatively be given by:

$$M_{ip}^{*} = 0.5 f_k t_0 \left(h_1 + 5t_0\right)^2 \tag{2.48}$$

where f_k is the buckling stress according to the steelwork specification, using a column slenderness ratio KL/r, K is the effective length factor, L is the length of member, and r is the is radius of gyration.

(c) Cracking in the chord (Failure Mode (b)) and Chord shear failure (Failure Mode (e))

Cracking in the chord or chord punching shear has not actually been observed in any tests, and chord shear is strictly a member failure so analytical solutions for modes (b) and (e) have not been considered by Packer *et al* (1992) and Packer and Henderson (1997).

Chapter 3

WELDING PROCEDURE AND WELD DEFECTS

3.1 INTRODUCTION

Chapter 3 details the welding procedure qualification for the tube-to-tube and tube-to-plate T-joints tested in this project. The tube-to-tube T-joints are made from square hollow sections with brace wall thicknesses ranging from 1.6mm to 3.0mm, while all the chord wall thicknesses are 3mm. In tube-to-plate T-joints the square hollow sections which are used as braces have wall thicknesses ranging from 1.6mm to 3.0mm, which are welded to a 10mm thick plate. The welding procedures are qualified for three steel grades; C350LO, C450LO and S355JOH. The weldability of steels depends on the carbon equivalent determined from the steel chemical composition. Two welding methods were used, the gas-metal arc welding method (MIG) and the tungsten-arc weld method (TIG). These two welding methods produced two different weld profiles.

Macro-cross section examination was undertaken to determine weld shape, the extend of penetration and soundness of the welded joints. The extend of penetration is important as it ensures that the joint will be able to withstand stresses due to applied loads and efficiently transfer load from one part of the joint to another without yielding of the joint. Adequate penetration of the weld into the parent metal at the root of the weld also prevents the creation of severe stress concentrations at the root. These stress concentrations can become sites for crack initiation especially for joints subjected to fatigue loading.

Hardness tests were performed to ensure that there was no problem associated with heat-affected zone (HAZ) cracking and that the joints were not susceptible to plastic deformation in the parent metal heat-affected zone as a result of large differences in strength between the parent and weld metal.

Fatigue cracks in welded connections initiate from high stress concentration sites. In tubular joints the stress concentration sites occur at the toes of the weld. Other than the geometrical configuration of the joint, the weld shape and the undercut are features of the welded joints, which influence the stresses at the weld toes. The silicon imprint technique was used to determine the weld profile and weld undercut dimensions. The weld undercut in particular may have a significant influence on fatigue of thin-walled welded connections with wall thicknesses less than 4mm. This is because the undercut depth reduces a significant portion of the wall thickness where crack propagation occurs while at the same time augmenting stress concentration at the weld toe where fatigue cracks initiate.

Magnetic particle testing of the joints before fatigue or static testing was performed as a check for surface cracks. This ensured that there were no inherent cracks in the joints before fatigue testing and hence no potential of premature fatigue failure.

3.2 WELDING PROCEDURE QUALIFICATION

3.2.1 Welding Procedure

The welding procedure is determined for the tube-to-plate T-joint shown in Figure 3-1 and the tube-to-tube T-joint shown in Figure 3-2. The connections are made up of cold-formed square hollow sections (SHS) of grades C350LO, DuraGal C450LO and S355JOH. Grades C350LO and DuraGal C450LO are manufactured by BHP Steel, Australia and conform to AS1163-1991 (SAA 1991a). Grade S355JOH is manufactured by Voest Alpine, Krems, Austria and conforms to EN10219.2-1997 (CEN 1997). Tables 3-1 and 3-2 show the chemical composition and the mechanical properties of the steel hollow sections respectively.

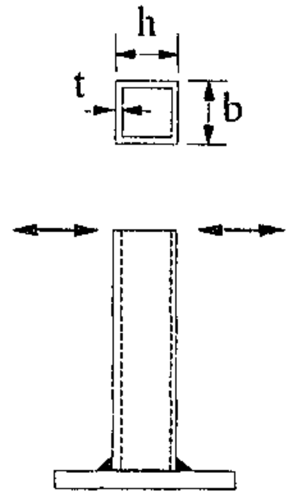

Figure 3-1: Fillet welded (tube-to-plate) T-joint

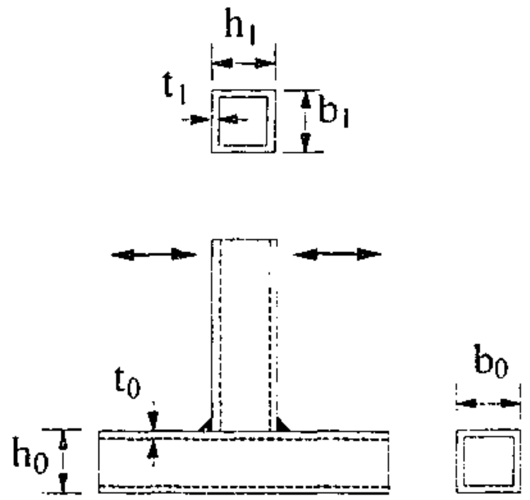

Figure 3-2: Fillet welded (tube-to-tube) T-joint

For truss connections using hollow sections, which are subjected to fatigue loading, the throat thickness of a fillet weld shall not be less than the wall thickness of the hollow section which it connects (EC3 1992; AS4100-1998 (SAA 1998a)). Therefore, for the tube-to-tube T-joints the weld throat thickness must be greater than or equal to the thickest tube wall in the joint. For the tube-to-plate T-joints the weld throat thickness was made so that its size was equal to or greater than the tube wall welded to the plate. The minimum size of weld recommended for the tube-to-plate T-joints was therefore of throat thickness size 1.6mm, 2.0mm and 3.0mm, which corresponded to the 1.6mm, 2.0mm and 3.0mm tube wall thicknesses tested as tube-to-plate joints. The minimum size of the weld recommended for the tube-to-tube T-joints has a throat thickness of

3mm since in all the tube-to-tube T-joints the larger wall thickness was always 3mm, corresponding to the chord wall thickness. Category SP (structural purpose) welds are used, complying to both AS1554.1-1995 (SAA 1995a) and AS1554.5-1995 (SAA 1995b).

Table 3-1: Chemical Properties of Grades C350LO, C450LO DuraGal and S355JOH Square Hollow Sections (SHS)

Grade	**Chemical Composition, % max**						
	C	Si	Mn	P	S	Al	CE
C350LO	0.20	0.05	1.60	0.040	0.030	0.10	0.39
C450LO	0.20	0.35	1.60	0.040	0.030	0.10	0.39
S355JOH	0.13-0.15	0.18-0.23	1.30-1.50	ca. 0.01	ca. 0.005	0.03-0.05	max. 0.41

Table 3-2: Mechanical Properties of Grades C350LO, C450LO DuraGal and S355JOH Square Hollow Sections (SHS)

Grade and Mechanical Properties			
Grade	**Minimum Yield Stress (MPa)**	**Minimum Tensile Strength (MPa)**	**Minimum elongation, %**
C350LO	350	430	16
C450LO	450	500	14
S355JOH	355	490	20

The carbon equivalent given in Table 3-1 is calculated from the steel chemical composition of each steel grade as follows:

$$CE = C + \frac{Mn}{6} + \frac{Cr + Mo + V}{5} + \frac{Ni + Cu}{15} \tag{3.1}$$

The carbon equivalent calculated using the above equation determines the weldability of the steel. For steels with a carbon equivalent value less than 0.40, such as grade C350LO and grade C450LO DuraGal, any electrode type or welding process can satisfactorily be used for welding. For steels with a carbon equivalent value between 0.40 and 0.45, such as grade S355JOH, hydrogen controlled electrodes or semi-automatic processes are recommended, but rutile or other electrodes may be used (WTIA 1996).

All the welding should start and stop in the middle of the flat part of the branch member in connections made up of square or rectangular hollow sections. Starting and stopping weld runs at corners of the brace member on the tube-to-tube or tube-to-plate interface, is detrimental to connections subjected to fatigue loading since this is where the maximum stresses occur. Weld starts and stops introduce irregularities, which cause stress concentrations (van Wingerde 1992; Packer and Henderson 1997).

The welding procedure sheets for the gas metal-arc (MIG) and gas tungsten-arc (TIG) welding methods used for grades C350LO, DuraGal C450LO and S355JOH square hollow section (SHS) connections are shown in Tables 3-3 to 3-8.

Table 3-3: Welding Procedure Sheet for MIG Welding, Grade C350LO Steel SHS

Reference Specification	AS1554.1-1995; AS1554.5-1995
Welding Machine	Miller Dimension 400
Joint Type and Preparation	F1, Table 4.4(C) of AS1554.1-1995, AS1554.5-1995
Position	Multiple Position-5F, ANSI/AWS D1.1-1998
Material	AS1163-1991: C350LO
Thickness Range Qualified	1.6-3.0mm tubes welded to 3.0mm tube 1.6-3.0mm tubes welded to 10mm plate
Process	Gas metal-arc welding (MIG)
Description	Single Pass Fillet Weld
Weld run	One
Current (A)	138
Voltage (V)	24
Welding Speed (mm/min)	320
Heat Input (kJ/mm)	0.621
Electrode Trade Name	AustMIG ES6
Designer's Requirement	W50X (AS2717.1; AWS 5.18)
Electrode Size (mm)	0.8
Weld Metal Yield Stress (MPa)	480
Weld Metal Tensile Strength (MPa)	580
Gas Trade Name	M1 Air Liquide
Gas Classification	Argon-CO_2, 82% Argon; 18%CO_2
Gas Flow Rate (L/min)	15
Welder	Paul Calcinai, Crossline Engineering Pty Ltd, Melbourne, Australia

Table 3-4: Welding Procedure Sheet for TIG Welding, Grade C350LO Steel SHS

Reference Specification	AS1554.1-1995; AS1554.5-1995
Welding Machine	Miller Syncrowave
Joint Type and Preparation	F1, Table 4.4(C) of AS1554.1-1995, AS1554.5-1995
Position	Multiple Position-5F, ANSI/AWS D1.1-1998
Material	AS1163-1991: C350LO
Thickness Range Qualified	1.6-3.0mm tubes welded to 3.0mm tube 1.6-3.0mm tubes welded to 10mm plate
Process	Gas tungsten-arc welding (TIG)
Description	Single Pass Fillet Weld
Weld run	One
Current (A)	150
Voltage (V)	14
Welding Speed (mm/min)	90
Heat Input (kJ/mm)	1.4
Electrode Trade Name	Comeweld Super Steel ER70S-2
Designer's Requirement	W502 (AS1167.2; AWS 5.18)
Electrode Size (mm)	2.4
Weld Metal Yield Stress (MPa)	425
Weld Metal Tensile Strength (MPa)	520
Gas Trade Name	Argon
Gas Classification	Welding Grade 99.99%
Gas Flow Rate (L/min)	8
Welder	Paul Calcinai, Crossline Engineering Pty Ltd, Melbourne, Australia

Table 3-5: Welding Procedure Sheet for MIG Welding, Grade C450LO DuraGal Steel SHS

Reference Specification	AS1554.1-1995; AS1554.5-1995
Welding Machine	Miller Dimension 400
Joint Type and Preparation	F1, Table 4.4(C) of AS1554.1-1995, AS1554.5-1995
Position	Multiple Position-5F, ANSI/AWS D1.1-1998
Material	AS1163-1991: DuraGal C450LO
Thickness Range Qualified	1.6-3.0mm tubes welded to 3.0mm tube 1.6-3.0mm tubes welded to 10mm plate
Process	Gas metal-arc welding (MIG)
Description	Single Pass Fillet Weld
Weld run	One
Current (A)	134
Voltage (V)	23
Welding Speed (mm/min)	320
Heat Input (kJ/mm)	0.58
Electrode Trade Name	AustMIG ES6
Designer's Requirement	W50X (AS2717.1; AWS 5.18)
Electrode Size (mm)	0.8
Weld Metal Yield Stress (MPa)	480
Weld Metal Tensile Strength (MPa)	580
Gas Trade Name	M1 Air Liquide
Gas Classification	Argon-CO_2, 82% Argon; 18%CO_2
Gas Flow Rate (L/min)	15
Welder	Paul Calcinai, Crossline Engineering Pty Ltd, Melbourne, Australia

Table 3-6: Welding Procedure Sheet for TIG Welding, Grade DuraGal C450LO Steel SHS

Reference Specification	AS1554.1-1995; AS1554.5-1995
Welding Machine	Miller Syncrowave
Joint Type and Preparation	F1, Table 4.4(C) of AS1554.1-1995, AS1554.5-1995
Position	Multiple Position-5F, ANSI/AWS D1.1-1998
Material	AS1163-1991: DuraGal C450LO
Thickness Range Qualified	1.6-3.0mm tubes welded to 3.0mm tube 1.6-3.0mm tubes welded to 10mm plate
Process	Gas tungsten-arc welding (TIG)
Description	Single Pass Fillet Weld
Weld run	One
Current (A)	130
Voltage (V)	14
Welding Speed (mm/min)	85
Heat Input (kJ/mm)	1.28
Electrode Trade Name	Comeweld Super Steel ER70S-2
Designer's Requirement	W502 (AS1167.2; AWS 5.18)
Electrode Size (mm)	2.4
Weld Metal Yield Stress (MPa)	425
Weld Metal Tensile Strength (MPa)	520
Gas Trade Name	Argon
Gas Classification	Welding Grade 99.99%
Gas Flow Rate (L/min)	8
Welder	Paul Calcinai, Crossline Engineering Pty Ltd, Melbourne, [illegible]ralia

Table 3-7: Welding Procedure Sheet for MIG Welding, Grade S355JOH Steel SHS

Reference Specification	AS1554.1-1995; AS1554.5-1995
Welding Machine	Miller Dimension 400
Joint Type and Preparation	F1, Table 4.4(C) of AS1554.1-1995, AS1554.5-1995
Position	Multiple Position-5F, ANSI/AWS D1.1-1998
Material	EN10219.2-1997: S355JOH
Thickness Range Qualified	1.6-3.0mm tubes welded to 3.0mm tube 1.6-3.0mm tubes welded to 10mm plate
Process	Gas metal-arc welding (MIG)
Description	Single Pass Fillet Weld
Weld run	One
Current (A)	130
Voltage (V)	24
Welding Speed (mm/min)	310
Heat Input (kJ/mm)	0.6
Electrode Trade Name	AustMIG ES6
Designer's Requirement	W50X (AS2717.1; AWS 5.18)
Electrode Size (mm)	0.8
Weld Metal Yield Stress (MPa)	480
Weld Metal Tensile Strength (MPa)	580
Gas Trade Name	M1 Air Liquide
Gas Classification	Argon-CO_2, 82% Argon; 18%CO_2
Gas Flow Rate (L/min)	15
Welder	Paul Calcinai, Crossline Engineering Pty Ltd, Melbourne, Australia

Table 3-8: Welding Procedure Sheet for TIG Welding, Grade S355JOH Steel SHS

Reference Specification	AS1554.1-1995; AS1554.5-1995
Welding Machine	Miller Syncrowave
Joint Type and Preparation	F1, Table 4.4(C) of AS1554.1-1995, AS1554.5-1995
Position	Multiple Position-5F, ANSI/AWS D1.1-1998
Material	EN10219.2-1997: S355JOH
Thickness Range Qualified	1.6-3.0mm tubes welded to 3.0mm tube 1.6-3.0mm tubes welded to 10mm plate
Process	Gas tungsten-arc welding (TIG)
Description	Single Pass Fillet Weld
Weld run	One
Current (A)	130
Voltage (V)	14
Welding Speed (mm/min)	85
Heat Input (kJ/mm)	1.28
Electrode Trade Name	Comeweld Super Steel ER70S-2
Designer's Requirement	W502 (AS1167.2; AWS 5.18)
Electrode Size (mm)	2.4
Weld Metal Yield Stress (MPa)	425
Weld Metal Tensile Strength (MPa)	520
Gas Trade Name	Argon
Gas Classification	Welding Grade 99.99%
Gas Flow Rate (L/min)	8
Welder	Paul Calcinai, Crossline Engineering Pty Ltd. Melbourne, Australia

3.2.2 Cross-Section Examination

The macro cross-section examination tests were carried out in accordance with the Australian Standard AS2205.5.1-1988: Macro Test-Cross-section Examination (SAA 1988a), which forms part of the Australian Standard 2205-1988: Methods of Destructive Testing of Welds in Metal.

The test from Method 5.1 of AS 2205-1988 reveals the weld shape, the extent of penetration and the soundness of the welded joint. Test pieces were examined for both the MIG and TIG welding methods, for grades C350LO, C450LO and S355JOH square hollow section (SHS) welded connections. For each connection that was examined under Method 5.1 of AS2205-1988, one specimen was taken from the corner while the other was taken from the flat position at the welded interface, see Figure 3-4(a) in Section 3.2.3.

The thickness of the test piece for macro-cross section examination is recommended to be approximately 10mm (SAA 1988a). The prepared macro-cross examination samples were also used for hardness traverse tests. The surface of the test piece was prepared for etching. The smooth filed surface was abraded on successively finer grades of waterproof silicon carbide paper, with the following sequence, 100grit, P240, P600 and finally by P1200. The specimen was carefully abraded against each grade of paper using a unilinear motion and applying moderate pressure until all surface indications from the previous treatment were removed.

Abrasive paper was lubricated with water before and during abrasion. The specimen was washed after each grade of abrasive paper to remove the abrasive. The direction of abrasion with the next finer grade of abrasive paper was at right angles to the marks made by the previous paper.

After the above preparation the test piece was etched. Etching was carried out by immersion in the etchant until a good definition of structure was obtained. The etchant used was nitric acid in alcohol (2 percent nital). This is prepared by adding 2mL of nitric acid to 98mL of alcohol (ethanol or methylated spirit).

After etching the test piece was washed thoroughly with water and then rinsed in ethanol. It was then quickly dried with a hot air blast. To preserve it permanently, it was coated with a thin clear lacquer.

The macro-section was examined for soundness and the etched surface revealed satisfactory penetration and fusion and freedom from weld defects.

For each of the different grade steels, C350LO, C450LO DuraGal and S355JOH, connections of either tube-to-plate or tube-to-tube or both were welded and macro-sections examined. The tube-to-tube and tube-to-plate T-joints that were made up for the macro-cross section examination are listed in Table 3-9. These connections were joined through the use of both the MIG and TIG welding methods.

Table 3-9: Connections of tube-to-tube and tube-to-plate T-joints for macro-cross section examination and hardness tests for both MIG and TIG welding methods

	Welding Method	**Steel Grade**	**Connection**	**Brace**	**Chord/ Plate Thickness**	β	τ	2γ
TUBE-TO-TUBE T-JOINTS	MIG	C350LO	S3S1	50x50x3	100x100x3	0.5	1.0	33.3
		C450LO	D3D1	50x50x3	100x100x3	0.5	1.0	33.3
			D3D2	50x50x1.6	100x100x3	0.5	0.5	33.3
		S355JOH	V3V1	50x50x3	100x100x3	0.5	1.0	33.3
	TIG	C350LO	S3S1	50x50x3	100x100x3	0.5	1.0	33.3
		C450LO	D3D1	50x50x3	100x100x3	0.5	1.0	33.3
			D3D2	50x50x1.6	100x100x3	0.5	0.5	33.3
		S355JOH	V3V1	50x50x3	100x100x3	0.5	1.0	33.3
TUBE-TO-PLATE T-JOINTS	MIG	C450LO	D7P	40x40x2	10mm Plate	-	-	-
			D1P	50x50x3	10mm Plate	-	-	-
		S355JOH	V1P	50x50x3	10mm Plate	-	-	-
	TIG	C450LO	D7P	40x40x2	10mm Plate	-	-	-
			D1P	50x50x3	10mm Plate	-	-	-
		S355JOH	V1P	50x50x3	10mm Plate	-	-	-

The macrographs from Grade C350LO, Grade C450LO DuraGal and Grade S355JOH SHS welded connections are shown in Appendix A. The macrographs for Grade C350LO steel are shown in Figures A1 to A4. The macrographs for Grade C450LO DuraGal steel are shown in Figures A5 to A20 and those for Grade S355JOH steel in Figures A21 to A28. From each welded connection that has been analysed, macrographs were taken from the corner and the flat position of the brace member on the tube-tube or tube-plate welded interface. Two typical macrographs are shown in Figure 3-3.

Some of the macrographs for Grade C450LO DuraGal steel welded sections revealed small root inclusions, see Figures A12 and A13. As the zinc coating vaporises during welding, it might be entrapped in the weld metal, forming these inclusions. Other features that have been observed are the necking and distortion that occurs in the 1.6mm welded tubes as shown Figure A7 and A13 respectively. Zhao and Hancock (1993) observed a similar phenomenon. This problem may result in blow-holes. The thinner welded tubes, 1.6mm and 2mm, also showed significant penetration almost similar to complete penetration butt welds, Figures A7, A8 and A18. This results in a very small or insignificant root gap.

(a)

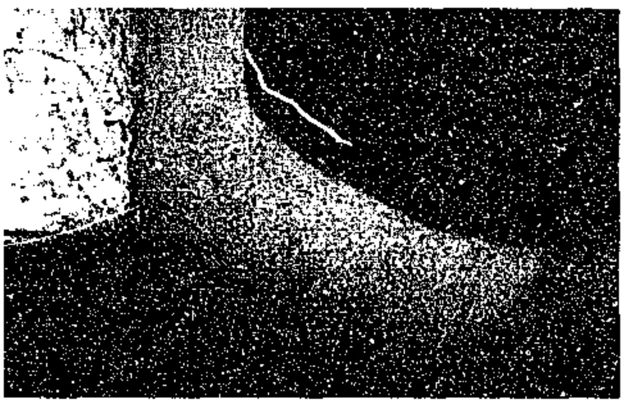

(b)

Figure 3-3: Typical Macrographs, (a) Grade DuraGal C450LO SHS. 50x50x3SHS-100x100x3SHS, Corner Position, MIG (b) Grade DuraGal C450LO Steel; 50x50x3SHS-Plate; Corner Position, TIG

3.2.3 Hardness Tests

The test is intended to measure the hardness of the weld metal, heat-affected zone (HAZ) and the parent metal on the prescribed traverses located in the regions of expected maximum and minimum hardness (SAA 1988b).

The hardness was measured by means of the Vickers Hardness Test. Several measurement locations in the weld metal, heat-affected zone and the parent metal were identified in the microstructure level. A nominal force of 49N (HV5) was used. The distance between centres of adjacent HV5 indentations was about 0.5mm. Measurement of hardness consisted of pressing the diamond indenter into the surface of the test piece under force and measuring the diagonals d_1 and d_2 of the indentation and then determining the mean value, d. The indenter is a right pyramid with square base whose angle between opposite faces is 136°. Vickers Hardness is given by,

$$HV = \frac{2F\sin\frac{136}{2}}{9.806 * 65d^2} \tag{3.2}$$

$$HV \approx 0.1891\frac{F}{d^2} \tag{3.3}$$

where HV is the Vickers Hardness, F is the force in N, and d is the mean diagonal of indentation in mm.

The results of Vickers Hardness Tests for TIG and MIG welding for grade C350LO steel are shown in Tables 3-10 and 3-11 respectively. The welding procedure can be qualified by testing according to Section 4.10 of AS1554.1-1991. Hardness tests, according to AS1817.1 (SAA 1991b), containing consumables not qualified shall show that the weld metal hardness does not exceed the parent metal hardness by more than 100HV10. Hardness tests, according to AS 2205.6.1 (SAA 1988b), shall reveal that the hardness of the heat-affected zone shall be not more than 350HV10. The results in Tables 3-10 and 3-11 show that these conditions are satisfied.

Table 3-10: Vickers Hardness results for TIG welded joint sample, Grade C350LO Steel

Metal	**d_1 (mm)**	**d_2 (mm)**	**d (mm)**	**Hardness (HV 5)**
Parent	0.227	0.248	0.238	166
Parent	0.256	0.273	0.265	133
Parent	0.257	0.262	0.260	138
Parent	**Mean**	-	-	**146**
HAZ	0.237	0.242	0.240	162
HAZ	0.232	0.271	0.252	150
HAZ	**Mean**	-	-	**156**
Weld	0.220	0.228	0.224	185
Weld	0.202	0.218	0.210	211
Weld	0.198	0.212	0.205	220
Weld	**Mean**	-	-	**205**

Table 3-11: Vickers Hardness Results for MIG Welded Joint Sample, Grade C350LO Steel

Metal	**d_1 (mm)**	**d_2 (mm)**	**d (mm)**	**Hardness (HV 5)**
Parent	0.252	0.245	0.249	150
Parent	0.241	0.245	0.243	157
Parent	0.246	0.249	0.248	152
Parent	0.240	0.243	0.242	159
Parent	**Mean**	-	-	**155**
HAZ	0.227	0.248	0.238	166
HAZ	0.238	0.241	0.240	162
HAZ	**Mean**	-	-	**164**
Weld	0.224	0.225	0.225	184
Weld	0.222	0.220	0.221	190
Weld	**Mean**	-	-	**187**

Detailed hardness traverse tests were carried out on Grade C450LO DuraGal and S355JOH SHS welded connections. These connections were also welded using two different methods, MIG and TIG. Some of the connection series in these grades of steel were chosen for the hardness traverse tests. Figure 3-4(b) shows the direction of traverses 1 and 2 in each sample that was analysed. Samples for hardness tests were obtained from the flat and at the corner of a square hollow section at the welded interface, Figure 3-4(a).

Hardness values were measured in the weld metal, heat-affected zone and the parent metal, and then plotted to show their compliance with the Australian Standards. The hardness traverse plots for different connection series are shown in Appendix B. From each welded connection that has been analysed, the hardness tests were performed on the macrographs in Appendix A. The hardness traverse plots for Grade C450LO DuraGal SHS welded connections are shown in Figures B1 to B8. Figures B9 to B12 show the hardness traverse plots for Grade S355JOH SHS welded connections. A typical hardness traverse plot is shown in Figure 3-5.

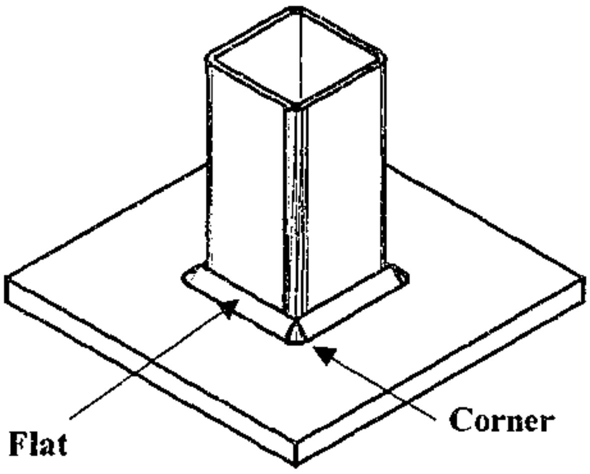

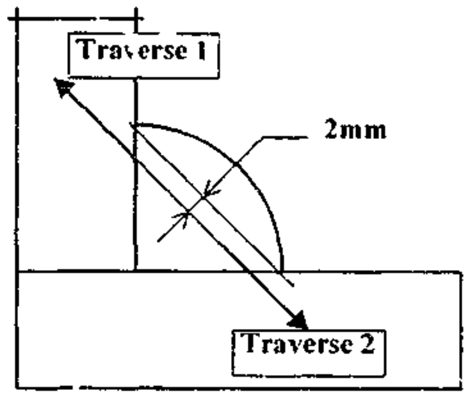

(a) *(b)*

Figure 3-4: (a) Side and Corner of SHS at welded interface (b) Hardness Traverse Locations

Figures 3-6 and 3-8 show that the maximum hardness value of the heat-affected zone in each sample tested is less than 350HV10, for C450LO steel and S355JOH steel respectively. When the hardness value of the heat-affected zone is less than 350HV10, there is little danger of HAZ cracking. The value of 350HV10 is conservative and many of the materials currently used are capable of sustaining a higher value without cracking (WTIA 1998).

Figures 3-7 and 3-9 show that the difference in the hardness value between the weld metal and the parent metal is less than 100HV10, for C450LO steel and S355JOH steel respectively. This test is intended to ensure that the strength of the weld metal does not greatly exceed the strength of the parent material, in order that, when plastic deformation occurs, it is not concentrated in the parent metal heat-affected zone (HAZ) (WTIA 1998).

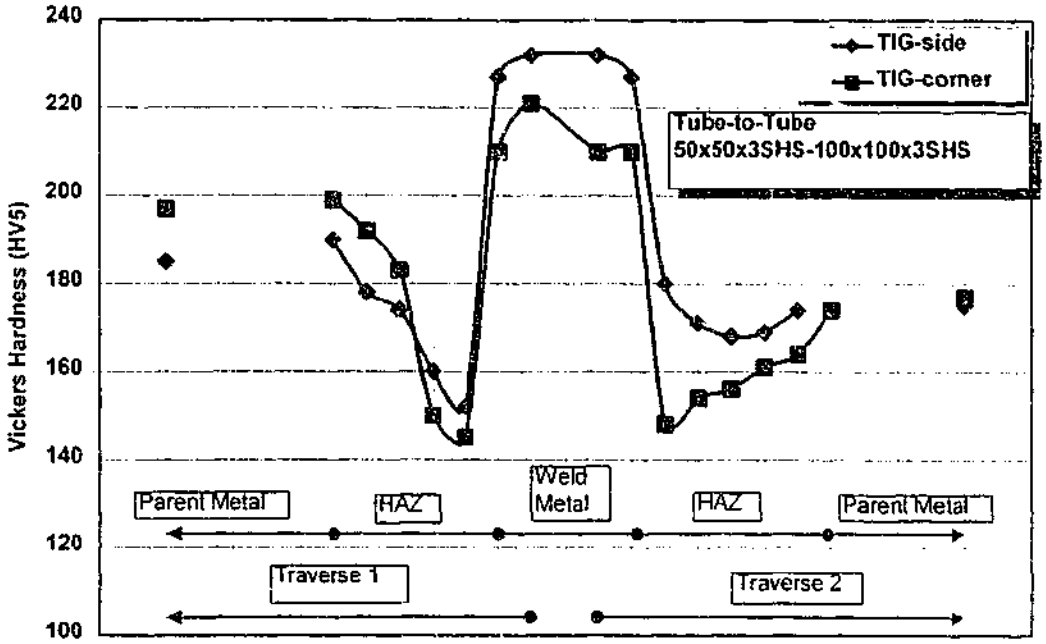

Figure 3-5: Typical hardness traverse plot

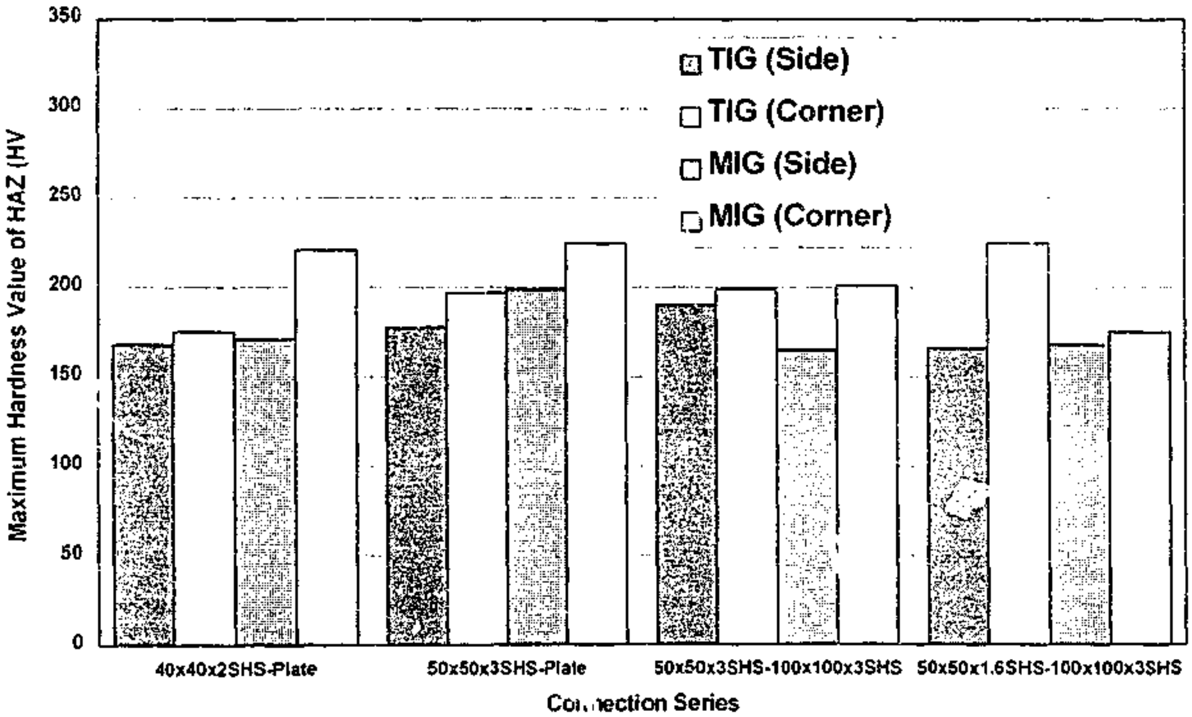

Figure 3-6: Hardness Test – Maximum Hardness Values of the heat-affected zone (HAZ), compliance to AS2205.6.1, DuraGal C450LO

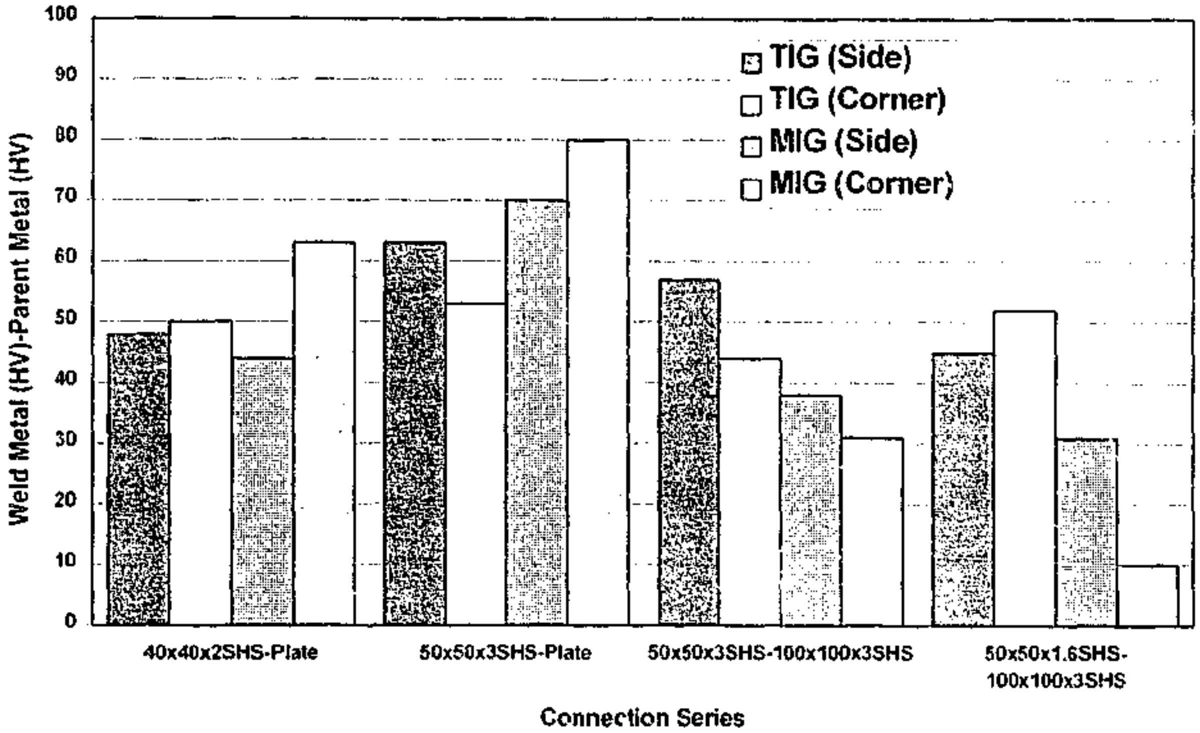

Figure 3-7: Hardness Comparison Test – Difference in Hardness Values between Weld Metal and Parent Metal, DuraGal C450LO

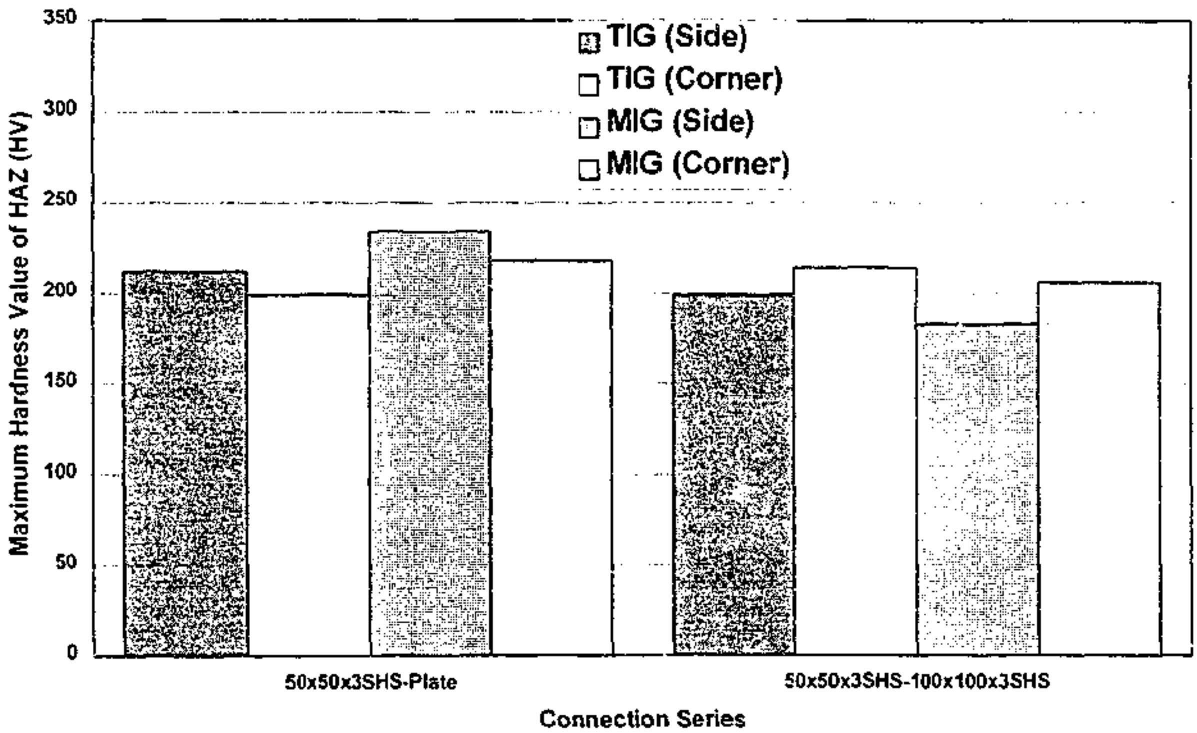

Figure 3-8: Hardness Test – Maximum Hardness Values of the heat-affected zone (HAZ), compliance to AS2205.6.1, S355JOH

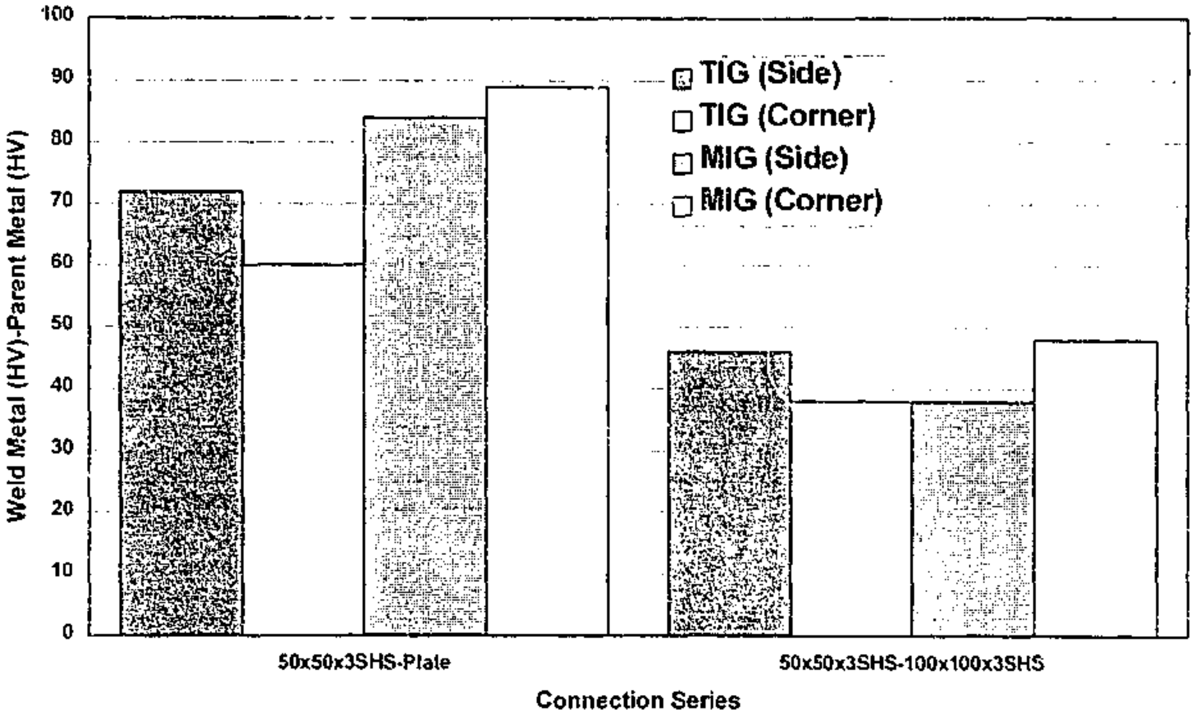

Figure 3-9: Hardness Comparison Test – Difference in Hardness Values between Weld Metal and Parent Metal, S355JOH

3.3 WELD PROFILE AND UNDERCUT MEASUREMENT

The silicon imprint technique was used to determine the weld shape (convex or concave), the weld toe radius, the weld flank angle and the shape of the undercut. The shape of the undercut is idealised as shown in Figure 3-10. The weld profile parameters measured are those shown in Figure 3-11. Oil for removing rust (KURE CRC 5-56) was sprayed on the weld and cleaning done using a wire brush and a cloth. The impression material (vinyl polysiloxane impression material) was prepared through mixing equal parts of exafine putty type base and exafine putty type catalyst. The mixed material was placed on the weld so that it covered the welded interface and was pushed firmly so that a negative of the weld profile was obtained. After the material had hardened it was then removed and cut into test pieces of approximately 1 mm in thickness. The required profile of the weld was measured using a Nikon Profile Projector, Model V-16.

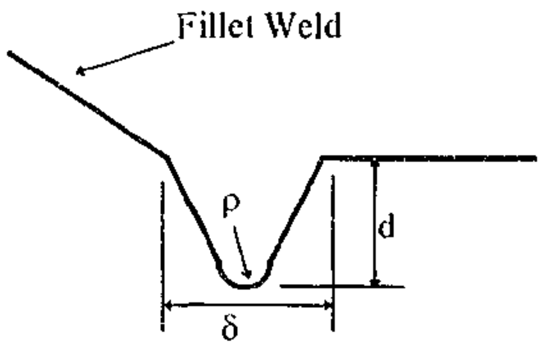

Figure 3-10: Dimensions of undercut

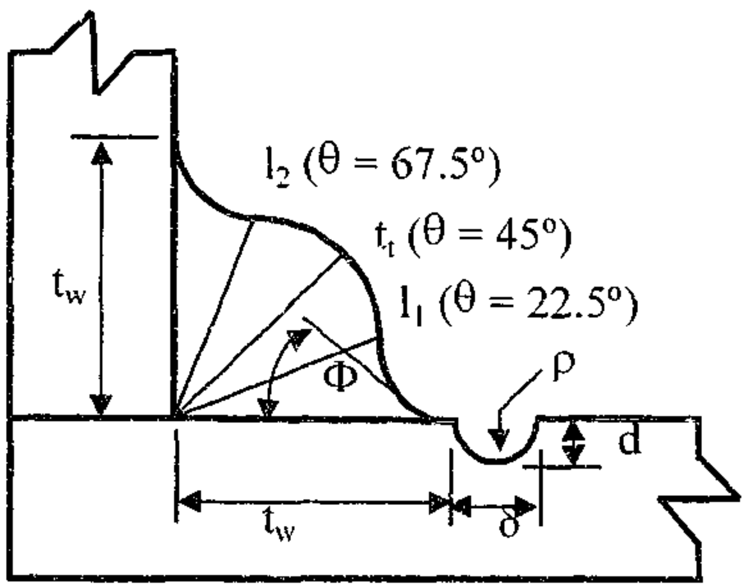

Figure 3-11: Weld Profile Parameters for a Fillet-welded Joint (Note that although the undercut has been shown on one of the toes of the weld, in practice it can occur in either of the weld toes)

For each of the different grades of steel, C350LO, C450LO and S355JOH, different connections were made from which silicon imprint samples were obtained. For each steel grade, connections were joined using both the MIG and TIG welding methods. A list of the connections which were manufactured for determination of weld profile and weld undercut measurements for each welding method and steel grade is shown in Tables 3-12 to 3-14. The number of silicon imprint samples for each connection and the total samples for each welding method are also shown in Table 3-12 to 3-14 for the different steel grades.

Table 3-12: Connections and silicon imprint samples for weld profile and undercut measurements for C350LO steel for both MIG and TIG welding methods

Welding Method	Connection	Brace	Chord/ Plate Thickness	β	τ	2γ	No. of Silicon imprint samples
MIG	S1PMIG1	50x50x3SHS	10mm Plate	-	-	-	10
	S1PMIG2	50x50x3SHS	10mm Plate	-	-	-	8
	S1PMIG3	50x50x3SHS	10mm Plate	-	-	-	8
	S2PMIG1	50x50x1.6SHS	10mm Plate	-	-	-	10
	S2PMIG2	50x50x1.6SHS	10mm Plate	-	-	-	8
	S2PMIG3	50x50x1.6SHS	10mm Plate	-	-	-	8
	S3S1MIG1	100x100x3SHS	50x50x3SHS	0.5	1.0	33.3	10
	S3S1MIG2	100x100x3SHS	50x50x3SHS	0.5	1.0	33.3	8
	S3S1MIG3	100x100x3SHS	50x50x3SHS	0.5	1.0	33.3	8
	S3S2MIG1	100x100x3SHS	50x50x1.6SHS	0.5	0.5	33.3	10
	S3S2MIG2	100x100x3SHS	50x50x1.6SHS	0.5	0.5	33.3	8
	S3S2MIG3	100x100x3SHS	50x50x1.6SHS	0.5	0.5	33.3	8
	TOTAL SILICON IMPRINT SAMPLES						104
TIG	S1PTIG1	50x50x3SHS	10mm Plate	-	-	-	10
	S1PTIG2	50x50x3SHS	10mm Plate	-	-	-	8
	S1PTIG3	50x50x3SHS	10mm Plate	-	-	-	8
	S2PTIG1	50x50x1.6SHS	10mm Plate	-	-	-	10
	S2PTIG2	50x50x1.6SHS	10mm Plate	-	-	-	8
	S2PTIG3	50x50x1.6SHS	10mm Plate	-	-	-	8
	S3S1TIG1	100x100x3SHS	50x50x3SHS	0.5	1.0	33.3	10
	S3S1TIG2	100x100x3SHS	50x50x3SHS	0.5	1.0	33.3	8
	S3S1TIG3	100x100x3SHS	50x50x3SHS	0.5	1.0	33.3	8
	S3S2TIG1	100x100x3SHS	50x50x1.6SHS	0.5	0.5	33.3	10
	S3S2TIG2	100x100x3SHS	50x50x1.6SHS	0.5	0.5	33.3	8
	S3S2TIG3	100x100x3SHS	50x50x1.6SHS	0.5	0.5	33.3	8
	TOTAL SILICON IMPRINT SAMPLES						104

Table 3-13: Connections and silicon imprint samples for weld profile and undercut measurements for C450LO DuraGal steel for both MIG and TIG welding methods

Welding Method	Connection	Brace	Chord/ Plate Thickness	β	τ	2γ	No. of Silicon imprint samples
MIG	D1PMIG1	50x50x3SHS	10mm Plate	-	-	-	16
	D1PMIG2	50x50x3SHS	10mm Plate	-	-	-	16
	D7PMIG1	40x40x2SHS	10mm Plate	-	-	-	16
	D7PMIG2	40x40x2SHS	10mm Plate	-	-	-	16
	D3D1MIG1	100x100x3SHS	50x50x3SHS	0.5	1.0	33.3	16
	D3D1MIG2	100x100x3SHS	50x50x3SHS	0.5	1.0	33.3	16
	D3D2MIG1	100x100x3SHS	50x50x1.6SHS	0.5	0.5	33.3	16
	D3D2MIG2	100x100x3SHS	50x50x1.6SHS	0.5	0.5	33.3	16
	TOTAL SILICON IMPRINT SAMPLES						128
TIG	D1PTIG1	50x50x3SHS	10mm Plate	-	-	-	16
	D1PTIG2	50x50x3SHS	10mm Plate	-	-	-	16
	D7PTIG1	40x40x2SHS	10mm Plate	-	-	-	16
	D7PTIG2	40x40x2SHS	10mm Plate	-	-	-	16
	D3D1TIG1	100x100x3SHS	50x50x3SHS	0.5	1.0	33.3	16
	D3D1TIG2	100x100x3SHS	50x50x3SHS	0.5	1.0	33.3	16
	D3D2TIG1	100x100x3SHS	50x50x1.6SHS	0.5	0.5	33.3	16
	D3D2TIG2	100x100x3SHS	50x50x1.6SHS	0.5	0.5	33.3	16
	TOTAL SILICON IMPRINT SAMPLES						128

Table 3-14: Connections and silicon imprint samples for weld profile and undercut measurements for S355JOH steel for both MIG and TIG welding methods

Welding Method	Connection	Brace	Chord/ Plate Thickness	β	τ	2γ	No. of Silicon imprint samples
MIG	V1PMIG1	50x50x3SHS	10mm Plate	-	-	-	16
	V1PMIG2	50x50x3SHS	10mm Plate	-	-	-	16
	V2PMIG1	40x40x2SHS	10mm Plate	-	-	-	16
	V2PMIG2	40x40x2SHS	10mm Plate	-	-	-	16
	V3V1MIG1	100x100x3SHS	50x50x3SHS	0.5	1.0	33.3	16
	V3V1MIG2	100x100x3SHS	50x50x3SHS	0.5	1.0	33.3	16
	V3D4MIG1	100x100x3SHS	30x30x2SHS	0.3	0.7	33.3	16
	V3V4MIG2	100x100x3SHS	30x30x2SHS	0.3	0.7	33.3	16
	TOTAL SILICON IMPRINT SAMPLES						128
TIG	V1PTIG1	50x50x3SHS	10mm Plate	-	-	-	16
	V1PTIG2	50x50x3SHS	10mm Plate	-	-	-	16
	V2PTIG1	40x40x2SHS	10mm Plate	-	-	-	16
	V2PTIG2	40x40x2SHS	10mm Plate	-	-	-	16
	V3V1TIG1	100x100x3SHS	50x50x3SHS	0.5	1.0	33.3	16
	V3V1TIG2	100x100x3SHS	50x50x3SHS	0.5	1.0	33.3	16
	V3D4TIG1	100x100x3SHS	30x30x2SHS	0.3	0.7	33.3	16
	V3V4TIG2	100x100x3SHS	30x30x2SHS	0.3	0.7	33.3	16
	TOTAL SILICON IMPRINT SAMPLES						128

104 silicon imprint test pieces from each of the MIG and TIG welding methods were prepared and measured, for Grade C350 steel connections. 128 silicon imprint test pieces from each of the MIG and TIG welding methods were prepared and measured, for both Grades C450 DuraGal and S355JOH steel connections. The test pieces were prepared from the test joints shown in Figure 3-12. Figure 3-13(a) shows the resulting silicon rubber with the weld shape. Weld ripples can clearly be seen on the silicon rubber. The resulting silicon imprint samples are shown in Figure 3-13(b) and 3-13(c) for the MIG and TIG weld profiles respectively. These samples are negatives of the typical profiles shown in Figures 3-3(a) and 3-3(b) for MIG and TIG weld profiles respectively. The vertical and horizontal sides of the silicon imprint samples, Figures 3-13(b) and 3-13(c), represent the vertical and horizontal walls of the welded tubes or plates. The shape of the weld can be seen towards the ends of the flats of the imprint sample where the extended vertical and horizontal sides of the imprint meet to form a right angle.

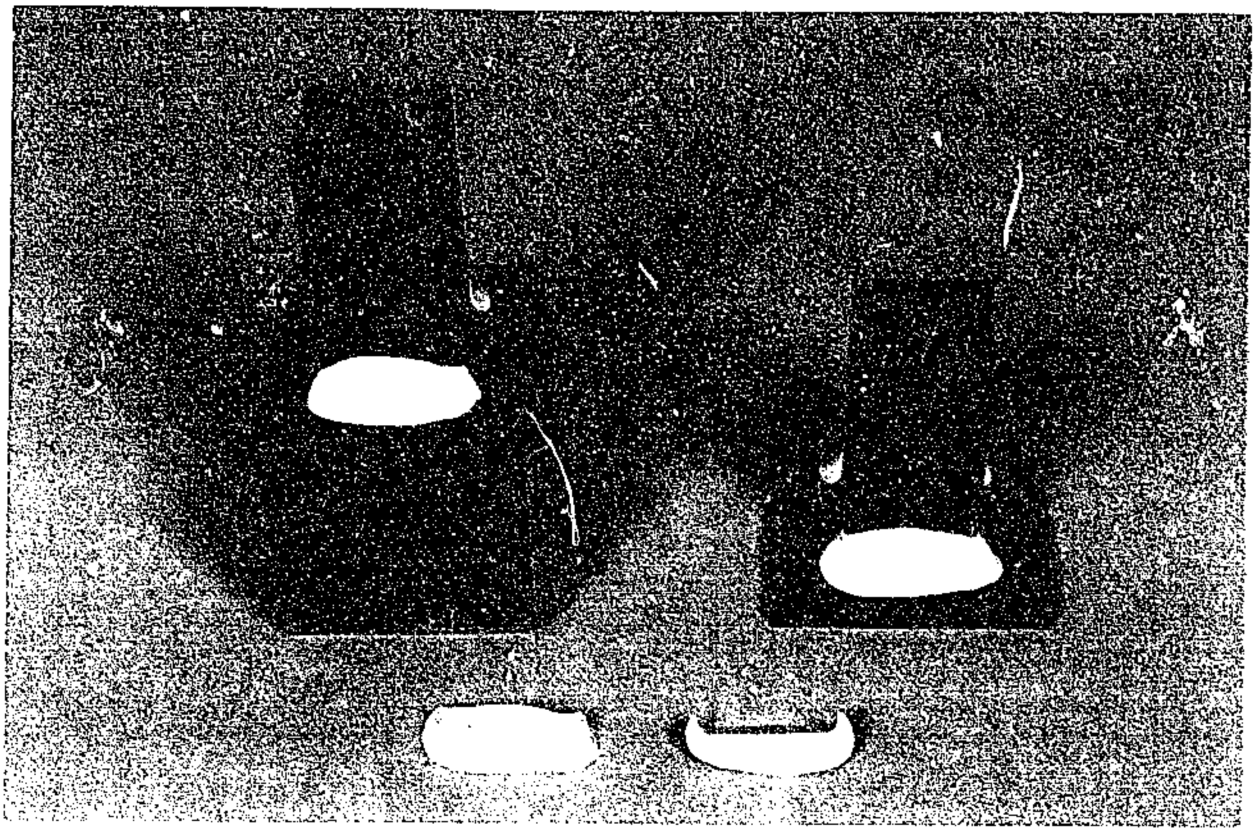

Figure 3-12: Welded connection specimens with silicon rubber

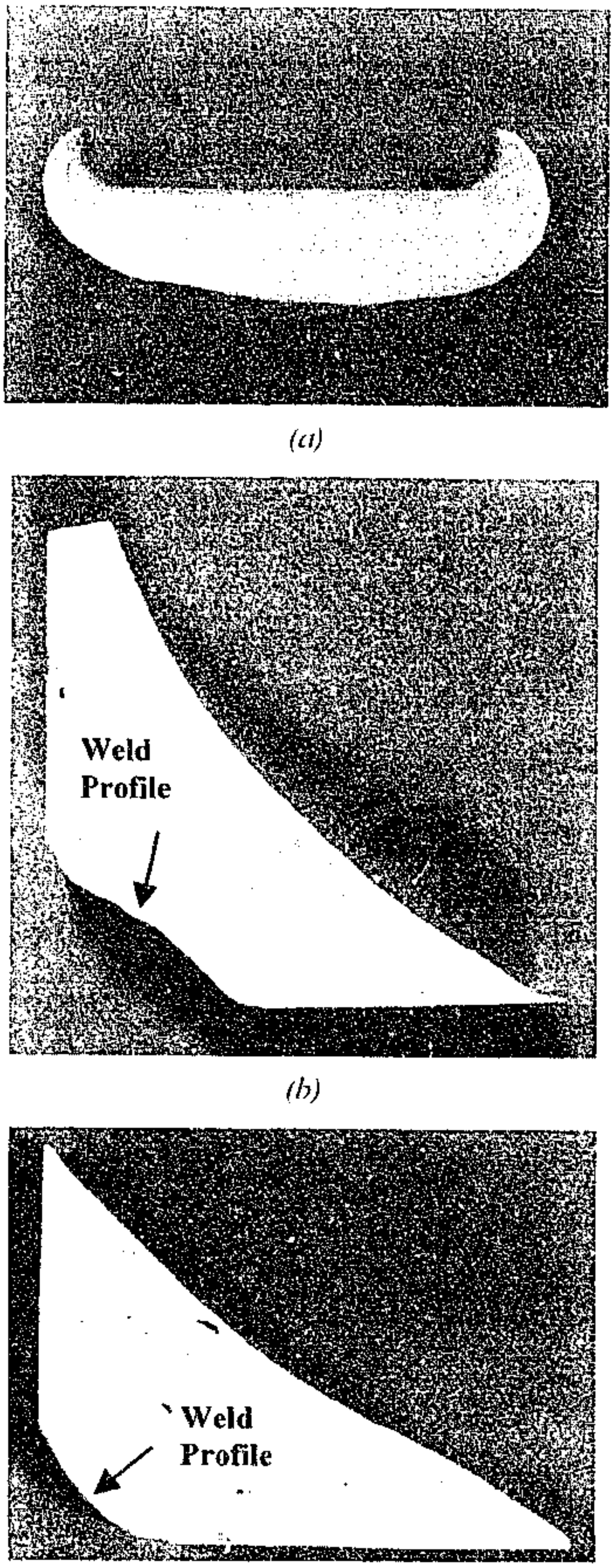

(a)

(b)

(c)

Figure 3-13: (a) Silicon rubber showing weld profile and weld ripples (b) MIG Silicon Imprint sample (c) TIG Silicon Imprint sample

The statistical results of the weld profiles from the MIG welds and the TIG welds are shown in Tables 3-15 and 3-16 respectively, for Grade C350LO steel, Grade C450 DuraGal steel and S355JOH steel. The resultant weld shapes, from the mean values of measurements, from the two welding methods are shown schematically in Figure 3-14 and 3-15, for grades C350LO steel, C450 DuraGal steel and S355JOH steel. These weld profiles are comparable to the actual profiles shown in Appendix A, for the two welding methods.

The weld profiles obtained from the MIG welded connections are convex-like, while the weld profiles from the TIG welded connections are concave-like. The MIG weld profiles are characterised by larger throat thicknesses and smaller toe radii, compared to the TIG weld profiles, which have smaller throat thicknesses and larger toe radii.

EC3 (1992) and AS 4100-1998 (SAA 1998a) recommend that the throat thickness of a fillet weld shall not be less than the wall thickness of the hollow section which it connects. In tube-to-plate T-joints the throat thickness should therefore range from 1.6mm to 3mm since this is the range of thicknesses that were tested. For the tube-to-tube T-joints the throat thicknesses should be equal to 3mm since the chord wall thickness used was always equal to 3mm. Table 3-15 shows that the mean values of throat thickness are always greater than 3mm for MIG welded profiles. Maximum values of throat thickness obtained are much greater than 3mm. This shows that the welds are oversized in most of the MIG welded connections. For the TIG welded connections however, the welds are generally undersized.

The results of the weld profiles obtained from C350LO steel connections have been used to in a numerical study on 2-dimensional cruciform joints, to determine the effect of weld profiles on fatigue crack propagation life. The study is carried out on non-load carrying cruciform joints with plate thicknesses of 3mm. Details of this study are given in Chapter 7.

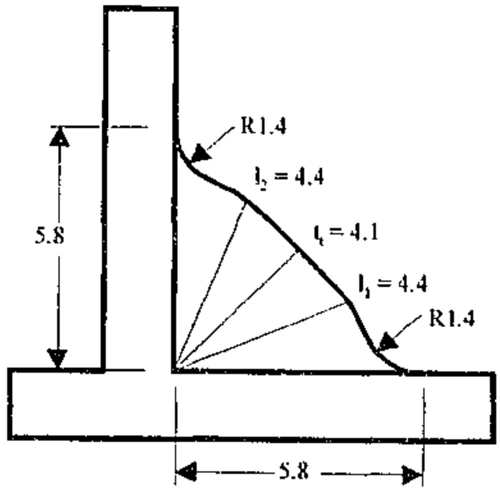

(a) C350LO

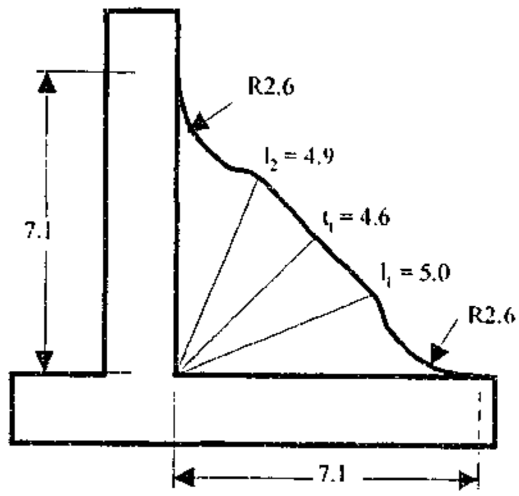

(b) C450LO

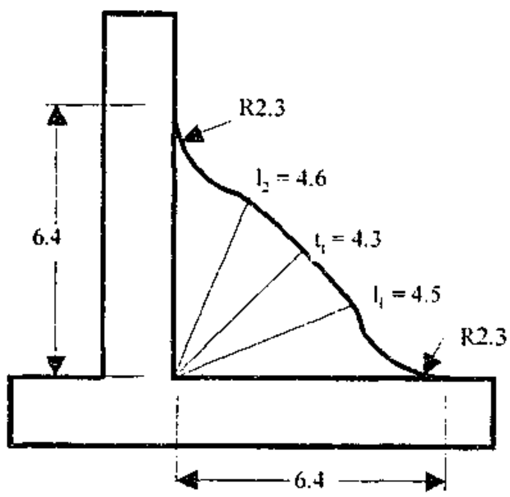

(c) S355JOH

Figure 3-14: MIG Weld Profiles from mean values

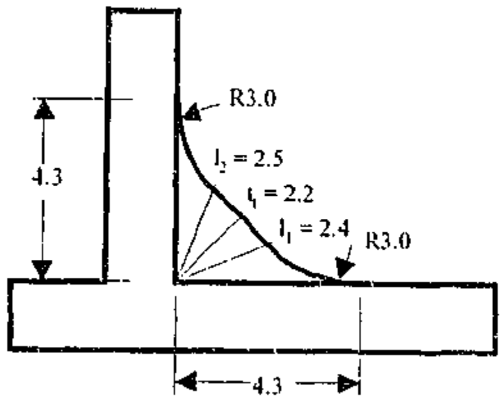

(a) C350LO

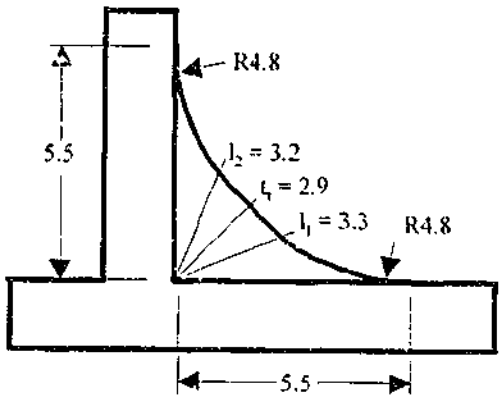

(b) C450LO

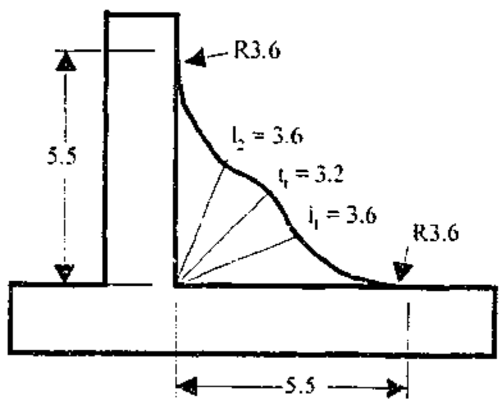

(c) S355JOH

Figure 3-15: TIG Weld Profiles from mean values

The statistical results for the undercut measurements from the MIG and TIG welding profiles are also shown in Tables 3-17 and 3-18 respectively. For Grade C350LO SHS connections, undercut was found in 5 out of the 104 silicon imprint samples that were prepared and measured for the MIG welding method. Out of the 104 silicon imprint samples that were prepared and measured for the TIG welding method, 14 were found to contain undercut, for the grade C350LO SHS connections. The dimensions of the undercuts from grade C350LO SHS connections, found for the two welding methods are shown in Tables 3-19 and 3-20, see Figure 3-10.

For Grade C450LO DuraGal SHS connections, undercut was also found in 5 out of the 128 silicon imprint samples that were prepared and measured for the MIG welding method. Out of the 128 silicon imprint samples that were prepared and measured for the TIG welding method, 21 were found to contain undercut, for the Grade C450LO DuraGal SHS connections. The dimensions of the undercuts from grade C450LO DuraGal SHS connections, found for the two welding methods are shown in Tables 3-21 and 3-22.

For Grade S355JOH SHS connections, undercut was found in 4 silicon imprint samples out of the 128 that were prepared and measured for the MIG welding method. Out of the 128 silicon imprint samples that were prepared and measured for the TIG welding method, 23 were found to contain undercut, for the Grade S355JOH SHS connections. The dimensions of the undercuts from the grade S355JOH SHS connections, found for the MIG and TIG welding methods are shown in Tables 3-23 to 3-24.

In all cases most the undercut was found to occur at the corners of the welded square hollow sections. Figure 3-16(a) shows undercut on the vertical wall of a TIG welded tubular joint. Figure 3-16(b) is the close up revealing the depth, width and radius of the undercut.

More occurrences of undercut were found in the silicon imprint samples from the TIG welded profiles compared to the MIG welded profiles. A possible explanation of this might be slightly higher heating than required, occurring during welding due to slightly unfavourable combination of voltage and current, in the TIG welded connections. Despite the more occurrences of undercut in the TIG welded profiles the mean values of undercut depth were similar to those for the MIG welded profiles. For the MIG welded profiles the mean values of undercut depth found were 0.12mm, 0.10mm and 0.14mm for the C350LO, C450LO and S355JOH SHS connections respectively, see Table 3-17. For the TIG welded profiles the mean values of undercut depth found were 0.16mm, 0.16mm and 0.14mm for the C350LO, C450LO and S355JOH SHS connections respectively, see Table 3-18. According to AS1554.1-1995 (SAA 1995a), the maximum permissible depth of undercut depends on wall thickness. The maximum permissible depth for intermittent undercut must be equal to *t/10* but not exceeding 1.5mm. This means that the mean values of undercut depth in both the TIG and MIG welded connections, satisfy the allowable limits in AS1554.1-1995 for the 1.6mm to 3mm thick tubes.

The maximum values of undercut depth found in the MIG welded profiles, were 0.16mm, 0.11mm and 0.20mm for grade C350LO, C450LO and S33JOH steel connections respectively, see Table 3-17, Section 3.3. The smallest tubes from which the MIG welded connections were prepared for grade C350LO, C450LO and S355JOH SHS had thicknesses of 1.6mm, 1.6mm and 2.0mm respectively, see Tables 3-12 to 3-14. This shows that for the MIG welded connections the maximum depth of undercut also satisfies AS1554.1-1995. This however is not the case for the TIG welded connections where the maximum values of undercut depth found in the TIG welded profiles were 0.30mm, 0.32mm and 0.18mm for grade C350LO, C450LO and S33JOH steel connections respectively, see Table 3-18. The smallest tubes from which the TIG welded connections were prepared for grade C350LO, C450LO and S355JOH SHS also had thicknesses of 1.6mm, 1.6mm and 2.0mm respectively, see Tables 3-12 to 3-14. Although the mean values of undercut depth for the TIG welded connections satisfy AS1554.1-1995, the maximum depth of undercut obtained for these connections do not satisfy AS1554.1-1995.

The MIG welding method was therefore chosen as the method of joining the connections that were fatigue tested in this investigation. This was because in addition to less occurrences of undercut in MIG welded connections (Tables 3-19 to 3-24), the weld undercut depth values found in the MIG welded samples also satisfied the maximum allowable undercut depth in AS1554.1-1995 (SAA 1995a). The MIG welding method is also a more commonly used welding method compared to the TIG welding method. However, with the right combination of voltage and current the high occurrences and larger depths of undercut found in the TIG welded samples may be corrected. The occurrence of undercut in welded connections, might be responsible for the reduction in fatigue strength associated with thinner welded tubular joints with wall thicknesses less than 4mm as has been reported by Puthli *et al* (1989) and Mashiri *et al* (2000c).

The results of the weld toe undercut obtained from C350LO steel connections have been used to in a numerical study on 2-dimensional cruciform joints, to determine the effect of weld toe undercut on fatigue crack propagation life. The study is carried out on non-load carrying cruciform joints with plate thicknesses of 3mm. Details of this study are given in Chapter 7.

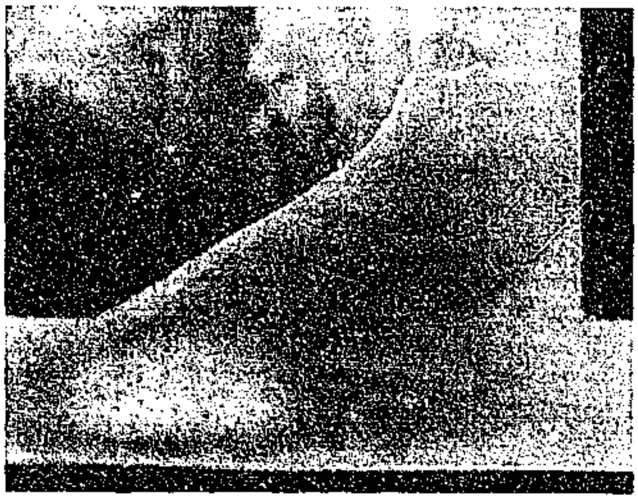

(a)

(b)

Figure 3-16: (a) Undercut on vertical wall at weld toe (b) Close up of undercut showing depth, width and radius of undercut

Table 3-15: Statistical Data of MIG weld profile results; Grade C350LO, Grade C450LO DuraGal and S355JOH

	Steel Grade	t_w (mm)	l_1 (mm)	t_t (mm)	l_2 (mm)	Toe Radius (mm)	Toe Angle (°)
Max	**C350LO**	8.7	5.7	5.3	6.7	3.0	79
	DuraGal	11.6	7.3	7.1	7.1	6.60	86
	S355JOH	8.4	6.0	5.6	6.1	5.08	60
Min	**C350LO**	3.5	3.1	3.1	2.7	0.3	20
	DuraGal	3.7	2.9	2.9	3.1	0.51	11
	S355JOH	4.5	3.2	3.0	3.3	0.51	18
Mean	**C350LO**	5.8	4.4	4.1	4.4	1.4	46.3
	DuraGal	7.1	5.0	4.6	4.9	2.57	24
	S355JOH	6.4	4.5	4.3	4.6	2.34	32
Coefficient of Variation (COV)	**C350LO**	0.14	0.14	0.12	0.14	0.43	0.23
	DuraGal	0.19	0.19	0.19	0.18	0.50	0.31
	S355JOH	0.13	0.13	0.13	0.12	0.41	0.25

Table 3-16: Statistical Data of TIG weld profile results; Grade C350LO, Grade C450LO DuraGal and S355JOH

	Steel Grade	t_w (mm)	l_1 (mm)	t_t (mm)	l_2 (mm)	Toe Radius (mm)	Toe Angle (°)
Max	**C350LO**	6.8	4.3	3.2	3.8	5.8	58
	DuraGal	7.6	5.0	4.0	4.4	7.62	38
	S355JOH	8.1	5.1	4.8	5.0	7.62	51
Min	**C350LO**	1.7	1.6	1.6	1.6	1.0	11
	DuraGal	3.0	2.2	2.0	2.1	1.52	10
	S355JOH	3.1	2.4	2.2	2.6	0.51	15
Mean	**C350LO**	4.3	2.4	2.2	2.5	3.0	29.4
	DuraGal	5.5	3.3	2.9	3.2	4.77	24
	S355JOH	5.5	3.6	3.2	3.6	3.61	29
Coefficient of Variation (COV)	**C350LO**	0.16	0.17	0.14	0.16	0.40	0.30
	DuraGal	0.15	0.15	0.15	0.15	0.29	0.24
	S355JOH	0.15	0.15	0.16	0.15	0.49	0.23

Table 3-17: Statistical Data of MIG Undercut results; Grade C350LO, Grade C450LO DuraGal and S355JOH

	Steel Grade	d (mm)	δ (mm)	ρ (mm)
Max	**C350LO**	0.16	0.97	0.76
	DuraGal	0.11	1.16	0.76
	S355JOH	0.20	1.71	1.52
Min	**C350LO**	0.06	0.47	0.25
	DuraGal	0.08	0.74	0.51
	S355JOH	0.06	0.33	0.25
Mean	**C350LO**	0.12	0.79	0.40
	DuraGal	0.10	0.97	0.56
	S355JOH	0.14	1.01	0.76
Coefficient of Variation (COV)	**C350LO**	0.32	0.25	0.57
	DuraGal	0.12	0.19	0.20
	S355JOH	0.43	0.73	0.82

Table 3-18: Statistical Data of TIG Undercut results; Grade C350LO, Grade DuraGal C450LO and S355JOH

	Steel Grade	d (mm)	δ (mm)	ρ (mm)
Max	**C350LO**	0.30	2.50	3.81
	DuraGal	0.32	2.53	2.03
	S355JOH	0.18	1.52	1.02
Min	**C350LO**	0.06	0.50	0.25
	DuraGal	0.07	0.05	0.25
	S355JOH	0.07	0.43	0.25
Mean	**C350LO**	0.16	1.44	1.46
	DuraGal	0.16	1.18	0.95
	S355JOH	0.11	0.93	0.57
Coefficient of Variation (COV)	**C350LO**	0.43	0.41	0.91
	DuraGal	0.42	0.52	0.68
	S355JOH	0.18	0.17	0.55

Table 3-19: Dimensions of undercut from MIG welds, Grade C350LO

No.	Depth, d (mm)	Width, δ (mm)	Radius, ρ (mm)
1	0.06	0.77	0.76
2	0.13	0.82	0.51
3	0.16	0.97	0.25
4	0.12	0.47	0.25
5	0.15	0.92	0.25

Table 3-20: Dimensions of undercut from TIG welds, Grade C350LO

No.	Depth, d (mm)	Width, δ (mm)	Radius, ρ (mm)
1	0.18	2.50	3.56
2	0.19	1.56	0.51
3	0.10	1.20	1.52
4	0.19	1.94	0.76
5	0.15	1.49	2.03
6	0.21	1.87	1.27
7	0.06	0.66	0.25
8	0.07	0.50	0.25
9	0.13	1.31	0.51
10	0.12	1.27	1.12
11	0.20	2.00	3.81
12	0.30	1.30	0.51
13	0.20	2.00	3.81
14	0.08	0.60	0.51

Table 3-21: Dimensions of undercut from MIG welds, Grade C450LO DuraGal

No.	Depth, d (mm)	Width, δ (mm)	Radius, ρ (mm)
1	0.08	0.82	0.51
2	0.10	1.16	0.51
3	0.11	1.14	0.51
4	0.11	0.74	0.51
5	0.10	1.01	0.76

Table 3-22: Dimensions of undercut from TIG welds, Grade C450LO DuraGal

No.	Depth, d (mm)	Width, δ (mm)	Radius, ρ (mm)
1	0.07	0.57	0.51
2	0.08	1.20	1.02
3	0.17	1.19	0.76
4	0.20	1.90	2.03
5	0.13	0.40	0.25
6	0.08	0.05	0.51
7	0.14	1.17	1.52
8	0.17	0.66	0.25
9	0.12	1.00	0.76
10	0.25	1.30	0.76
11	0.20	1.99	2.03
12	0.11	1.00	1.02
13	0.27	2.00	2.03
14	0.13	1.18	2.03
15	0.32	2.53	1.52
16	0.22	1.70	0.51
17	0.15	1.48	0.51
18	0.15	1.32	0.51
19	0.10	0.50	0.25
20	0.10	0.56	0.25
21	0.14	1.14	1.02

Table 3-23: Dimensions of undercut from MIG welds, Grade S355JOH

No.	Depth, d (mm)	Width, δ (mm)	Radius, ρ (mm)
1	0.06	0.33	0.25
2	0.13	1.71	1.02
3	0.20	0.42	0.25
4	0.15	1.56	1.52

Table 3-24: Dimensions of undercut from TIG welds, Grade S355JOH

No.	Depth, d (mm)	Width, δ (mm)	Radius, ρ (mm)
1	0.07	1.07	1.02
2	0.11	1.15	1.02
3	0.10	0.74	0.25
4	0.14	1.05	0.51
5	0.14	0.99	0.25
6	0.14	1.04	0.51
7	0.08	0.87	1.02
8	0.09	0.90	0.51
9	0.18	1.52	0.76
10	0.07	1.21	0.25
11	0.10	0.84	0.51
12	0.09	0.71	0.51
13	0.07	0.43	0.25
14	0.08	0.61	0.25
15	0.11	0.62	0.51
16	0.13	1.04	1.02
17	0.07	0.55	0.25
18	0.08	1.24	1.02
19	0.17	1.20	0.51
20	0.10	0.74	0.51
21	0.08	0.71	1.02
22	0.10	1.01	0.51
23	0.17	1.09	0.25

3.4 MAGNETIC PARTICLE TESTING

Prior to the fatigue and static testing of the welded connection specimens, the quality of the welds were checked according to Section 6 of AS1554.1-1995. The magnetic particle method of inspection was used for checking the welded connections in their as welded condition.

The magnetic particle method is a non-destructive testing method complying with AS1171-1998 (SAA 1998b). Magnetic particle testing is suitable for all types of ferromagnetic products and components with surface discontinuities.

A Weston electromagnetic bridge was used to induce adequate magnetic flux in the welded joint, Figure 3-17. For this method to be effective, the path of the magnetic field must be substantially at right angles to the principal axis of any discontinuities. It is recommended that the examination be done in at least two directions at right angles to each other.

The magnetic ink which was used is the Ezy Check E8.50 fluorescent magnetic fluid. The room where the inspection was made was darkened. Inspection was carried out under Novalite UV270 Black light.

The areas under examination, which included the surface of the weld, the weld toes and heat-affected zone were cleaned of any foreign matter, which would interfere with the interpretation of the results, such as scale, dirt, grease and paint.

Discontinuities, when present in the examined area, are indicated by a fluorescent indication when using fluorescent magnetic ink.

This test satisfied Table 6.2 of AS1554.1-1995, which gives the maximum permissible levels of imperfections allowed in fillet welds when the visual, magnetic particle and liquid penetrant methods of inspection are used to examine the weld zone. No cracks are allowed when the former non-destructive methods of inspection are used.

Hundred percent of the fillet welds which were going to be subjected to maximum principal stresses under cyclic bending were examined, and no surface defects were detected. Only one incident of a blow-hole was observed in a tube-to-plate joint with a 50x50x1.6mm SHS, Figure 3-18.

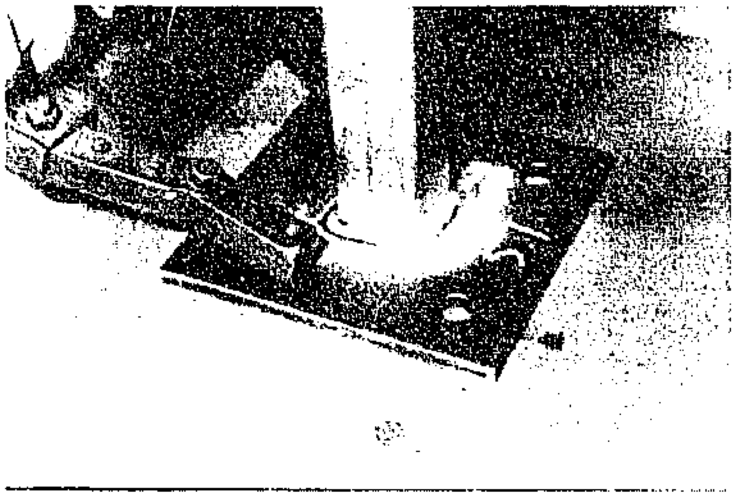

Figure 3-17: Magnetic Particle Testing showing Weston electromagnetic bridge and welded connection

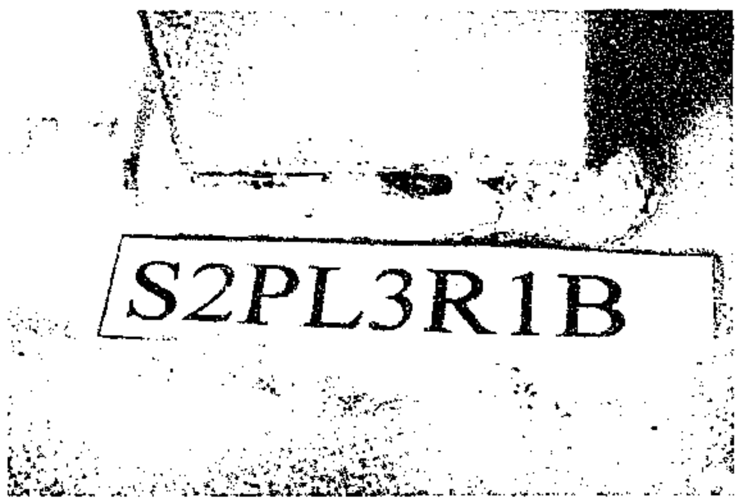

Figure 3-18: Blow-hole on tube-to-plate connection with 50x50x1.6SHS

3.5 SUMMARY

The welding procedures for the three different steel grades, C350LO, C450LO and S355JOH have been described. Measurements of weld profiles and weld toe undercuts have been performed and detailed. The welding procedures and weld defects relate to welded tubular joints with thicknesses less than 4mm.

The following are observations, conclusions and discussions relating to the weld procedures, weld profiles and weld defects;

(a) The steel grades for which the welding procedures were determined, that is C350LO, C450LO and S355JOH were all welded using the same electrodes for either the MIG or TIG welding method. This is because the weldability of steel depends on its carbon equivalence as determined by its chemical composition. GradesC350LO and C450LO both have a carbon equivalence of 0.39 while S355JOH steel has a maximum carbon equivalence of 0.41. The carbon equivalence for each of these different grade steels is therefore similar. This implies that they have the same weldability and can therefore be welded using the same electrode for a given welding method.

(b) The macro sections were prepared, etched and examined for soundness. The etched surface revealed satisfactory penetration and fusion and freedom from significant weld defects. Some of the macro sections especially those involving the 1.6mm tubes revealed a significant amount of penetration identical to that in full penetration welds. Some of the connections made from galvanised sections revealed small root inclusions. These small root inclusions might be a result of entrapped zinc coating, which vaporises during welding of the galvanised sections.

(c) All the hardness tests showed that the hardness value in the heat-affected zone was less than 350HV10. This showed that there is little danger of heat-affected zone cracking. The difference in values between the weld metal and the parent metal hardnesses was found to be less than 100HV10 in all cases. This demonstrated that the strength of the weld metal does not greatly exceed the strength of the parent metal. This reduces the possibility of plastic deformation being concentrated to the parent metal heat-affected zone when deformation of the joint occurs.

(d) The weld profiles measured showed that the MIG weld profiles had a convex-like profile. The TIG weld profiles had a concave-like weld profile. The weld toe radii found in the MIG weld profiles, were smaller compared to those found in the TIG weld profiles. Larger toe radii occur in the TIG weld profiles as a result of a smoother merge between the concave-like profile of the TIG weld and the adjoining tube walls or plates. In MIG weld profiles the smaller toe radius is a result of the more abrupt merge between the convex-like profile of the MIG weld and the adjoining plates or tube walls.

(e) More occurrences of undercut were found in silicon imprint samples from the TIG welded connections, compared to those from the MIG welded connections. A possible explanation of this might be slightly higher heating occurring during welding due to slightly unfavourable combination of voltage and current, in the TIG welded connections. Despite the more occurrences of undercut in the TIG welded profiles the mean values of undercut depth were similar to those for the MIG welded profiles, and satisfied the maximum permissible depth of undercut in AS1554.1-1995. According to AS1554.1-1995 (SAA 1995a), the maximum permissible depth of undercut depends on wall thickness. The maximum permissible depth for intermittent undercut must be equal to *t/10* but not exceeding 1.5mm. The maximum values of undercut depth found in the MIG welded profiles also satisfied the maximum permissible depth of undercut recommended by AS1554.1-1995, see Table 3-17. This however is not the case for the TIG welded connections where some of the maximum values of undercut depth found were greater than the maximum permissible depth of undercut recommended by AS1554.1-1995, see Table 3-18. Although the mean values of undercut depth for the TIG welded connections satisfy AS1554.1-1995, the maximum depth of undercut obtained for these connections do not satisfy AS1554.1-1995. The MIG welding method was therefore chosen as the method of joining the connections that were fatigue tested in this investigation. This was because in addition to less occurrences of undercut in MIG welded connections (Tables 3-19 to 3-24), the weld undercut depth values found in the MIG welded samples also satisfied the maximum allowable undercut depth in AS1554.1-1995 (SAA 1995a). The MIG welding method is also a more commonly used welding method compared to the TIG welding method. However, with the right combination of voltage and current the high occurrences and larger depths of undercut found in the TIG welded samples may be corrected. The occurrence of undercut in welded connections might be responsible for the reduction in fatigue strength associated with thinner welded tubular joints with wall thicknesses less than 4mm as has been reported by Puthli *et al* (1989) and Mashiri *et al* (2000c).

(f) Magnetic particle testing was performed on hundred percent of the fillet welds which were going to be subjected to the maximum principal stresses under cyclic or static bending loads. Therefore the whole length of weld, adjoining the plate and the tube in the tube-to-plate T-joints were magnetic particle tested. For the tube-to-tube T-joints, hundred percent of the weld adjoining the brace to the chord were also magnetic particle tested. No inherent surface cracks were found in all but one of the joints. This joint, a tube-to-plate T-joint with a tube wall thickness of 1.6mm was found to have a blow-hole. Although there was only one occurrence of a blow-hole in all the welded joints tested, it is recommended that the 100% visual scanning of the structural purpose (SP) joints recommended in AS1554.1-1995 be strictly adhered to for thin-walled tubular joints with tube wall thicknesses less than 4mm.

Chapter 4

MATERIAL PROPERTIES AND STATIC TESTS

4.1 INTRODUCTION

The characteristics of cold-formed steel stress-strain curves are detailed in Chapter 4. These characteristics are a result of cold forming. A rounded stress-strain curve is obtained for cold-formed steel compared to the typical stress-strain graphs with clear yielding plateaus for hot-rolled or mild steel. The stress-strain graphs of cold-formed steel are characterised by reduced ductility and higher yield stress and ultimate tensile strengths.

Tensile coupon tests are carried out for grade C350LO, C450LO and S355JOH SHS to determine the mechanical properties of the tubes used in the fatigue tests. Grade C350LO and C450LO conform to Australian Standard AS1163-1991 (SAA 1991a), while grade S355JOH conforms to EN10219.2-1997 (CEN 1997). All the tubes are cold formed. At least two tensile coupons are tested for each tube with the tensile coupons being derived from the faces opposite or adjacent to the seam weld. The mechanical properties are important in estimating the static strength of the tube-to-tube and tube-to-plate T-joints under investigation. Static strength of both the tube-to-tube and tube-to-plate T-joints depends on the yield stress of the tubes forming the joints and their sectional properties. Fatigue loading on the other hand is a function of the static strength, since fatigue damage is caused by repeated load during service.

Static tests are also performed to determine the static strength of both the tube-to-tube and the tube-to-plate T-joints. Static tests for grade C350LO only were carried out. The static responses of grade C450LO and S355JOH steels and there relation to fatigue loading were deduced from the static tests results of grade C350LO since static strength depends on yield stress and sectional properties of the tube members in the connection. The static strength of the other different grade steels can be estimated since connections of similar flexural rigidity to those of grade C35LO were under investigation for grade

C450LO and S355JOH steels. Moment-deflection and moment-angle of inclination graphs were obtained from the tests. The maximum elastic moment below which the connection has a linear response was determined from the moment-deflection and moment-angle of inclination graphs. The loads corresponding to the maximum elastic moment of a connection and below were then used in the fatigue tests to obtain high cycle fatigue response.

The importance of static tests is that they define the linear part of the load-deformation curves where high cycle fatigue occurs and the magnitude of these linear relationships for connections of different flexural rigidity.

4.2 TENSILE COUPON TESTS

4.2.1. General

The mechanical properties of steel sections are affected by cold work of forming which takes place mainly in the regions of bends, especially in square and rectangular hollow sections. In these regions, the material ultimate tensile strength and yield stresses are enhanced with a commensurate reduction in material ductility. AS1163-1991 (SAA 1991a) however requires that coupons for tensile tests be taken only from the flats of the rectangular or square sections. This requirement results in mechanical properties which do not take into account significant cold work of forming which takes place at the corners of rectangular or square hollow sections.

For cold-formed square or rectangular sections, the flat faces will also have undergone cold work as a result of forming the section into a circular tube and then reworking it into a rectangle or square. It is very difficult to compute theoretically the enhancement of yield strength in the flats and the measured yield strength of the steel after forming is used in design. The distribution of ultimate strength and yield strength measured in a cold-formed square hollow section indicates that the properties are reasonably uniform across the flats except at the weld location (Hancock 1994), see Figure 4-1.

The non-uniformity of cold work over the cross-section of the member causes the material to be non-homogeneous with respect to yield strength, initial stresses and durability (Lind, 1974).

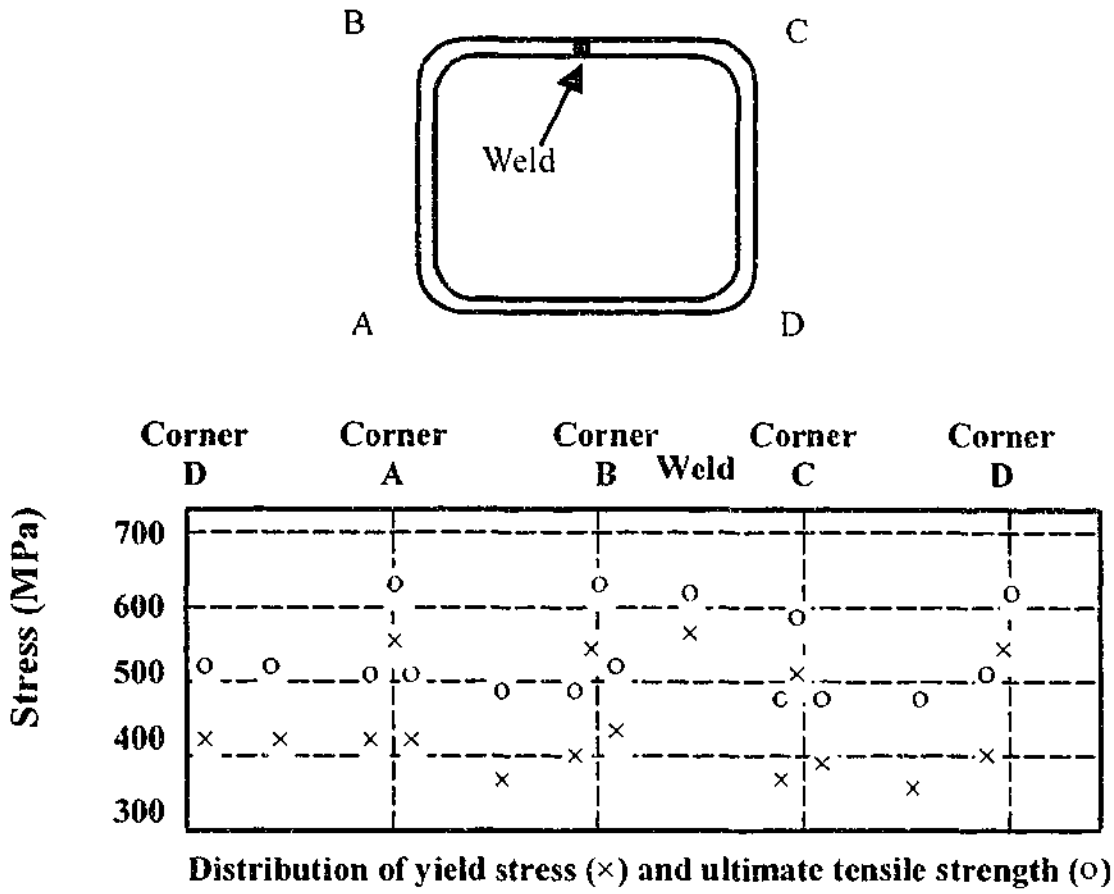

Figure 4-1: Tensile Property Distribution in a Cold-Formed Hollow Section (Grade C350 to AS1163) (Hancock 1994)

There are factors in cold-formed materials, which reduce their ability to resist rapid fracture:

(i) Reduced ductility, which reduces the energy absorbed in plastically deforming and fracturing at the tip of a crack and hence its fracture toughness. Fracture toughness relates to the amount of plastic work, which is needed in crack extension. Crack extension relates to the elastic energy released from the loaded body as the volume in the vicinity of the crack surfaces elastically relaxes.

(ii) The increased residual stresses in cold-formed sections, produced by the forming processes, which increases the energy release as the crack propagates.

As a result of cold work of forming, the area under the stress-strain curve decreases. This is significant because the area under the stress-strain curve represents the amount of energy required to fracture the steel. Therefore the amount of energy required for fracture decreases when a steel is cold worked (Louthan 1992).

4.2.2 Mechanical Properties

4.2.2.1 Grade C350LO Steel

The mechanical properties for grade C350LO steel were determined through the testing of tensile coupons using a Baldwin machine at a load range of 20kN. A 50mm gauge extensometer was used for measuring the strains. A straining rate of 4% per millimetre range of 0.0008strain/min was used. The procedure of testing was such that enough strain was measured to allow the determination of 0.2% proof strain. After a strain of about 0.008, the extensometer was disabled, but the load reading maintained in order to determine the peak load from which the tensile strength is calculated. The extensometer was disabled to avoid its damage at final fracture of the tensile coupon.

For each tensile coupon test, the load applied and the corresponding strain at each load were recorded. The load applied was converted to applied stress using the original cross sectional area of the gauge. A plot of stress versus the strain was then used to determine the 0.2% proof stress of each coupon. By plotting a line parallel to the straight part of the stress-strain curve from a strain value of 0.002, and extending it until it meets the stress-strain curve, the yield stress was determined as the value of stress at the intersection of the two curves, Figure 4-2. The yield stress is the 0.2% proof stress. All the C350LO tensile coupons exhibited stress-strain curves with no yield plateau.

The ultimate tensile strength can be read from the stress-strain curve as the maximum stress from the graph recorded from the tensile test. Alternatively it can be calculated from the peak load reading which is obtained from the Baldwin machine. The Baldwin machine retains in memory the peak load reached during testing. The ultimate tensile strength can be obtained as the ratio of the peak load during testing to the original area of the gauge. Prior to testing of each coupon a gauge length was marked on each tensile coupon. After final fracture the tensile coupon is reassembled and with the fractured surface touching in a match, the length corresponding to the marks of the original gauge is measured. The percentage elongation of the coupon can thus be determined from the values of the final and original gauge lengths.

Three samples were obtained per section size for Grade C350LO steel. The samples correspond to each side of the square hollow section (SHS) except the side with the seam weld. Samples *Aa* and *Ab* were obtained from the faces adjacent to the face with the seam weld. Sample *O* is from the face opposite the seam weld, see Figure 4-3.

The measured thickness, width and corresponding cross sectional area for each coupon are given in Table 4-1 for Grades C350LO steel. The cross sectional area determined from the measured original thickness and width of each coupon are used in determining the stresses at different applied loads and ultimate tensile strength from the peak load.

The original gauge length, final gauge length and the corresponding percentage elongation for each coupon are given in Table 4-2 for Grade C350LO steel.

The yield stress and ultimate tensile strength for each coupon are given in Tables 4-3 for Grades C350LO steel. The mean values of yield stress, ultimate tensile strength and percentage elongation, are summarised in Table 4-10 for grade C350LO steel. All the mean values of mechanical properties obtained through measurement are greater than the minimum values specified in AS1163-1991 (SAA 1991a).

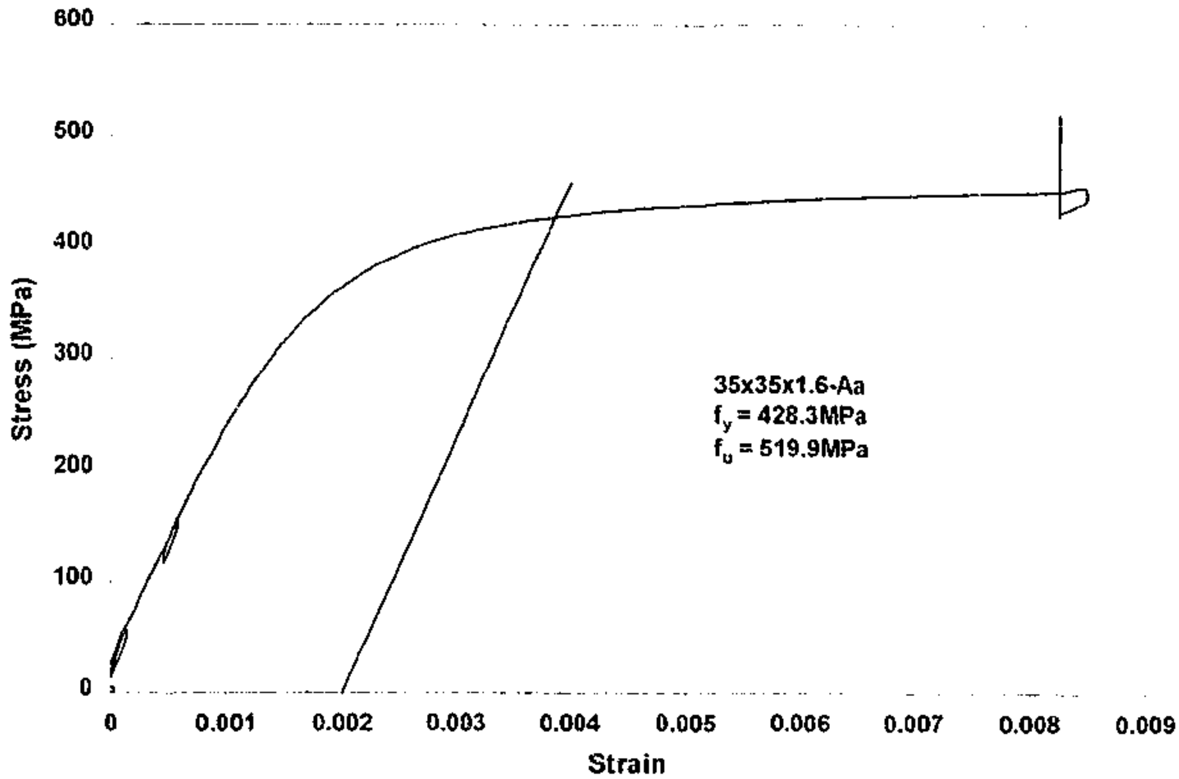

Figure 4-2: Stress-Strain Curve of a C350LO Steel Manufactured to AS1163-1991, used for fatigue tests.

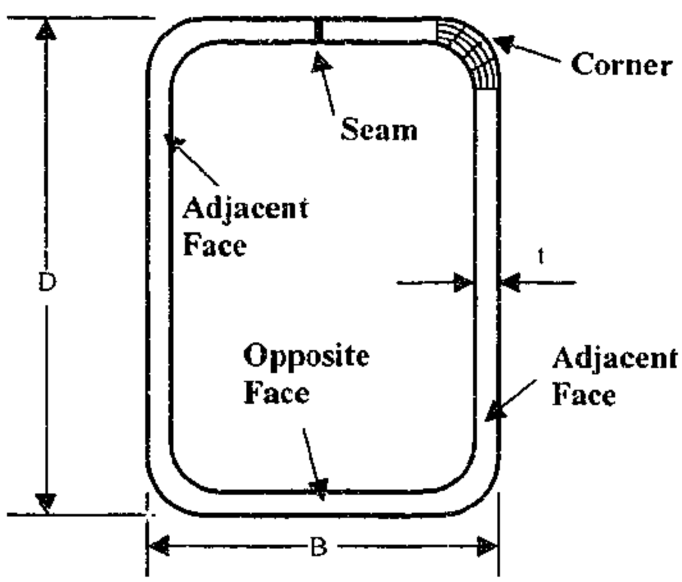

Figure 4-3: Section Nomenclature (Zhao and Hancock 1993)

Table 4-1: Measured thickness and width and corresponding sectional area for Grade C350LO tensile coupons

Section	Tensile Coupon sample	Peak Load (kN)	Thickness (mm)	Width (mm)	Area (mm^2)
100x100x3SHS	S3-Aa	17.82	2.80	11.63	32.56
	S3-Ab	18.51	2.86	11.95	34.18
	S3-O	20.08	2.95	12.11	35.72
75x75x3SHS	S6-Aa	18.39	2.88	11.76	33.87
	S6-Ab	18.40	2.88	11.84	35.34
	S6-O	18.96	2.89	12.23	34.10
50x50x3SHS	S1-Aa	19.45	2.93	11.87	34.78
	S1-Ab	19.02	2.92	11.70	34.39
	S1-O	18.50	2.88	11.94	34.16
50x50x1.6SHS	S2-Aa	9.30	1.58	11.78	18.61
	S2-Ab	9.36	1.58	11.93	18.85
	S2-O	9.25	1.58	11.85	18.72
35x35x3SHS	S4-Aa	20.24	2.94	12.08	35.51
	S4-Ab	19.96	2.93	11.84	35.07
	S4-O	18.91	2.91	12.03	34.19
35x35x1.6SHS	S5-Aa	9.38	1.52	11.99	18.22
	S5-Ab	9.51	1.49	11.84	17.64
	S5-O	9.33	1.48	12.03	17.80

Table 4-2: Original gauge length, final gauge length and percentage elongation for Grade C350LO tensile coupons

Section	Tensile Coupon sample	Original Gauge Length (mm)	Final Gauge Length (mm)	Percentage Elongation (%)
100x100x3SHS	S3-Aa	50	63.0	26
	S3-Ab	50	63.5	27
	S3-O	50	63.0	26
75x75x3SHS	S6-Aa	50	63.0	26
	S6-Ab	50	63.0	26
	S6-O	50	64.0	28
50x50x3SHS	S1-Aa	50	58.0	16
	S1-Ab	50	59.0	18
	S1-O	50	61.0	22
50x50x1.6SHS	S2-Aa	50	63.5	27
	S2-Ab	50	62.5	25
	S2-O	50	61.5	23
35x35x3SHS	S4-Aa	50	61.0	22
	S4-Ab	50	60.0	20
	S4-O	50	60.5	21
35x35x1.6SHS	S5-Aa	50	61.5	23
	S5-Ab	50	61.5	23
	S5-O	50	61.0	22
MEAN				23
COV				0.141

Table 4-3: Yield Stress and Ultimate Tensile Strength for Grade C350LO tensile coupons

Section	Tensile Coupon sample	Yield Stress, f_y (MPa)	Ultimate Tensile Strength, f_u (MPa)
100x100x3SHS	S3-Aa	428.0	547.3
	S3-Ab	398.5	541.5
	S3-O	470.9	562.2
75x75x3SHS	S6-Aa	397.7	543.0
	S6-Ab	395.2	539.5
	S6-O	392.2	543.0
50x50x3SHS	S1-Aa	488.2	559.2
	S1-Ab	485.4	556.8
	S1-O	469.4	537.9
50x50x1.6SHS	S2-Aa	396.3	499.7
	S2-Ab	401.0	496.6
	S2-O	405.8	494.1
35x35x3SHS	S4-Aa	478.9	570.0
	S4-Ab	496.4	569.1
	S4-O	476.5	553.1
35x35x1.6SHS	S5-Aa	428.3	514.8
	S5-Ab	427.9	539.1
	S5-O	422.4	524.2
MEAN		436.6	538.4
COV		0.088	0.044

4.2.2.2 Grade C450LO Steel

A similar procedure for determining stress-strain graphs to that used for grade C350LO (section 4.2.2.1) was used for grade C450LO steel coupons. Two samples were obtained per section for Grade C450LO steel. The samples are *Aa* from one of the adjacent faces and *O* from the opposite face.

The measured thickness, width and corresponding cross sectional area for each coupon are given in Table 4-4 for Grade C450LO steel. The cross sectional area determined from the measured original thickness and width of each coupon are used in determining the stresses at different applied loads and ultimate tensile strength from the peak load.

The original gauge length, final gauge length and the corresponding percentage elongation for each coupon are given in Table 4-5 for Grade C450LO steel.

Like the C350LO steel coupons, all the C450LO tensile coupons exhibited stress-strain curves with no yield plateaus. The stress is therefore determined as the 0.2% proof stress.

The yield stress and ultimate tensile strength for each coupon are given in Table 4-6 for Grades C450LO steel.

The mean values of yield stress, ultimate tensile strength and percentage elongation, are summarised in Table 4-10 for grade C450LO steel. All the mean values of mechanical properties obtained through the measurements are greater than the minimum values specified in AS1163-1991 (SAA 1991a).

Table 4-4: Measured thickness and width and corresponding sectional area for Grade C450LO tensile coupons

Section	Tensile Coupon sample	Peak Load (kN)	Thickness (mm)	Width (mm)	Area (mm^2)
100x100x3SHS	D3-Aa	19.83	2.84	12.56	35.67
	D3-O	20.79	2.90	12.62	36.60
75x75x3SHS	D6-Aa	19.31	2.80	12.54	35.11
	D6-O	20.55	2.76	12.72	35.11
50x50x3SHS	D1-Aa	20.97	2.86	12.50	35.75
	D1-O	21.76	2.92	12.80	37.38
50x50x1.6SHS	D2-Aa	10.79	1.54	12.38	19.07
	D2-O	11.24	1.58	12.60	19.91
40x40x2SHS	D7-Aa	12.98	1.72	12.40	21.33
	D7-O	13.32	1.88	12.56	23.61
35x35x3SHS	D4-Aa	22.37	3.04	12.48	37.94
	D4-O	20.89	2.84	12.68	36.01
35x35x1.6SHS	D5-Aa	10.85	1.56	12.52	19.53
	D5-O	11.56	1.46	12.70	18.54

Table 4-5: Original gauge length, final gauge length and percentage elongation for Grade C450LO tensile coupons

Section	Tensile Coupon sample	Original Gauge Length (mm)	Final Gauge Length (mm)	Percentage Elongation (%)
100x100x3SHS	D3-Aa	50	62.63	25
	D3-O	50	60.75	21
75x75x3SHS	D6-Aa	50	62.70	25
	D6-O	50	59.33	19
50x50x3SHS	D1-Aa	50	60.93	22
	D1-O	50	67.55	15
50x50x1.6SHS	D2-Aa	50	61.82	24
	D2-O	50	59.08	18
40x40x2SHS	D7-Aa	50	60.75	21
	D7-O	50	59.73	19
35x35x3SHS	D4-Aa	50	58.81	18
	D4-O	50	60.01	20
35x35x1.6SHS	D5-Aa	50	58.79	17
	D5-O	50	57.22	14
MEAN				19
COV				0.172

Table 4-6: Yield Stress, Ultimate Tensile Strength and Young's Modulus for Grade C450LO tensile coupons

Section	Tensile Coupon sample	Yield Stress, f_y (MPa)	Ultimate Tensile Strength, f_u (MPa)
100x100x3SHS	D3-Aa	422.8	525.4
	D3-O	474.1	550.8
75x75x3SHS	D6-Aa	408.6	511.7
	D6-O	499.7	554.6
50x50x3SHS	D1-Aa	501.8	555.7
	D1-O	516.9	576.7
50x50x1.6SHS	D2-Aa	437.6	517.8
	D2-O	476.6	540.1
40x40x2SHS	D7-Aa	458.4	524.8
	D7-O	500.9	538.2
35x35x3SHS	D4-Aa	577.1	592.7
	D4-O	513.6	553.0
35x35x1.6SHS	D5-Aa	454.8	521.0
	D5-O	517.9	554.6
MEAN		482.9	544.1
COV		0.092	0.043

4.2.2.3 Grade S355JOH Steel

A similar procedure for determining stress-strain curves to that used for grade C350LO (section 4.2.2.1) was used for grade S355JOH steel. Two samples were obtained per section for Grade S355JOH steel. The samples are *Aa* from one of the adjacent faces and *O* from the opposite face.

The measured thickness, width and corresponding cross sectional area for each coupon are given in Table 4-7 for Grades S355JOH steel. The cross sectional area determined from the measured original thickness and width of each coupon are used in determining the stresses at different applied loads and ultimate tensile strength from the peak stress. The original gauge length, final gauge length and the corresponding percentage elongation for each coupon are given in Table 4-8 for Grades S355JOH steel.

Like the stress-strain curves in grades C350LO and C450LO steel, all the S355JOH tensile coupons exhibited stress-strain curves with no yield plateaus. The yield stress was therefore defined as the 0.2% proof stress.

The yield stress and ultimate tensile strength for each coupon are given in Table 4-9 for Grade S355JOH steel.

The mean values of yield stress, ultimate tensile strength and percentage elongation, are summarised in Table 4-10 for grade S355JOH steel. All the mean values of mechanical properties obtained through the measurements are greater than the minimum values specified in EN10219.2-1997 (CEN 1997).

Table 4-7: Measured thickness and width and corresponding sectional area for Grade S355JOH tensile coupons

Section	Tensile Coupon sample	Peak Load (kN)	Thickness (mm)	Width (mm)	Area (mm^2)
100x100x3SHS	V3-Aa	17.17	2.80	13.00	36.40
	V3-O	17.44	2.66	12.00	31.92
70x70x3SHS	V6-Aa	18.44	2.81	12.96	36.42
	V6-O	18.35	2.70	11.96	32.29
60x60x3SHS	V5-Aa	18.40	2.76	12.06	33.29
	V5-O	18.91	2.78	12.18	33.86
50x50x3SHS	V1-Aa	18.34	2.80	13.00	36.40
	V1-O	18.44	2.76	12.10	33.40
40x40x2SHS	V2-Aa	13.36	1.84	12.20	22.45
	V2-O	13.43	1.90	12.10	22.99
30x30x2SHS	V4-Aa	12.54	1.78	11.80	21.00
	V4-O	12.63	1.94	12.00	23.28

Table 4-8: Original gauge length, final gauge length and percentage elongation for Grade S355JOH tensile coupons

Section	Tensile Coupon sample	Original Gauge Length (mm)	Final Gauge Length (mm)	Percentage Elongation (%)
100x100x3SHS	V3-Aa	50	64.18	28
	V3-O	50	63.66	27
70x70x3SHS	V6-Aa	75	94.00	25
	V6-O	50	62.72	25
60x60x3SHS	V5-Aa	50	63.54	27
	V5-O	50	62.79	26
50x50x3SHS	V1-Aa	50	67.85	36
	V1-O	50	67.14	34
40x40x2SHS	V2-Aa	50	66.04	32
	V2-O	50	66.49	33
30x30x2SHS	V4-Aa	50	69.30	38
	V4-O	50	67.26	34
MEAN				30
COV				0.151

Table 4-9: Yield Stress, Ultimate Tensile Strength and Young's Modulus for Grade S355JOH tensile coupons

Section	Tensile Coupon sample	Yield Stress, f_y (MPa)	Ultimate Tensile Strength, f_u (MPa)
100x100x3SHS	V3-Aa	360	471
	V3-O	381	479
70x70x3SHS	V6-Aa	386	501
	V6-O	331	486
60x60x3SHS	V5-Aa	379	487
	V5-O	415	501
50x50x3SHS	V1-Aa	403.9	503.3
	V1-O	390.7	505.8
40x40x2SHS	V2-Aa	396.5	513.4
	V2-O	389.5	515.7
30x30x2SHS	V4-Aa	400.8	489.2
	V4-O	423.6	492.8
MEAN		388.1	495.4
COV		0.063	0.027

Table 4-10: Measured Mean and Recommended Minimum Values of Yield Stress, Ultimate Tensile Strength and Percentage Elongation for Grade C350LO, C450LO and S355JOH steels

Section	Yield Stress, f_y (MPa)		Ultimate Tensile Strength, f_u (MPa)		Percentage Elongation (%)	
	Mean	Min.	Mean	Min.	Mean	Min.
C350LO	436.6	350	538.4	430	23	16
C450LO	482.9	450	544.1	500	19	14
S355JOH	388.1	355	495.4	490	30	20

4.3 STATIC TESTS

Fatigue loading should not exceed the service loading allowable in a structure. The service load which a structure can support is a function its static strength. Static tests were carried out to determine the load corresponding to the linear portion of the moment-deflection curves. From the linear part of the moment-deflection curves, the maximum elastic moment, ($M_{elastic,max}$) which can be applied as fatigue loading was determined. The load corresponding to the maximum moment on the linear moment-deflection curves was also used to determine the sizes of the cylinders used in the fatigue rigs for cycling. The loads under which the welded connections behave elastically are applied in high cycle fatigue tests. These loads are a fraction of the design static strength of the welded connections.

The nominal static strength (M_{static}) of the tube-to-plate T-joints can be calculated from the nominal section moment capacity (M_s) as given in AS4100-1998 (SAA 1998a):

$$M_{static} = M_s = f_y Z_e \tag{4.1}$$

where f_y is the yield stress for the tube used in design and Z_e is the effective section modulus.

For tube-to-tube connections the static strength (M_{static}) for in-plane bending is given by Packer *et al* (1992), for different modes of failure. Chord face yielding has been observed as the mode of failure for the tube-to-tube T-joints tested in this investigation. All the tube-to-tube T-joints tested have a β value less than 0.7.

For low to moderate β values, and when the influence of membrane effects and strain hardening are neglected, the moment capacity (M_{ip}) is determined by the yield line mechanism shown in Figure 4-5 (Packer *et al* 1992).

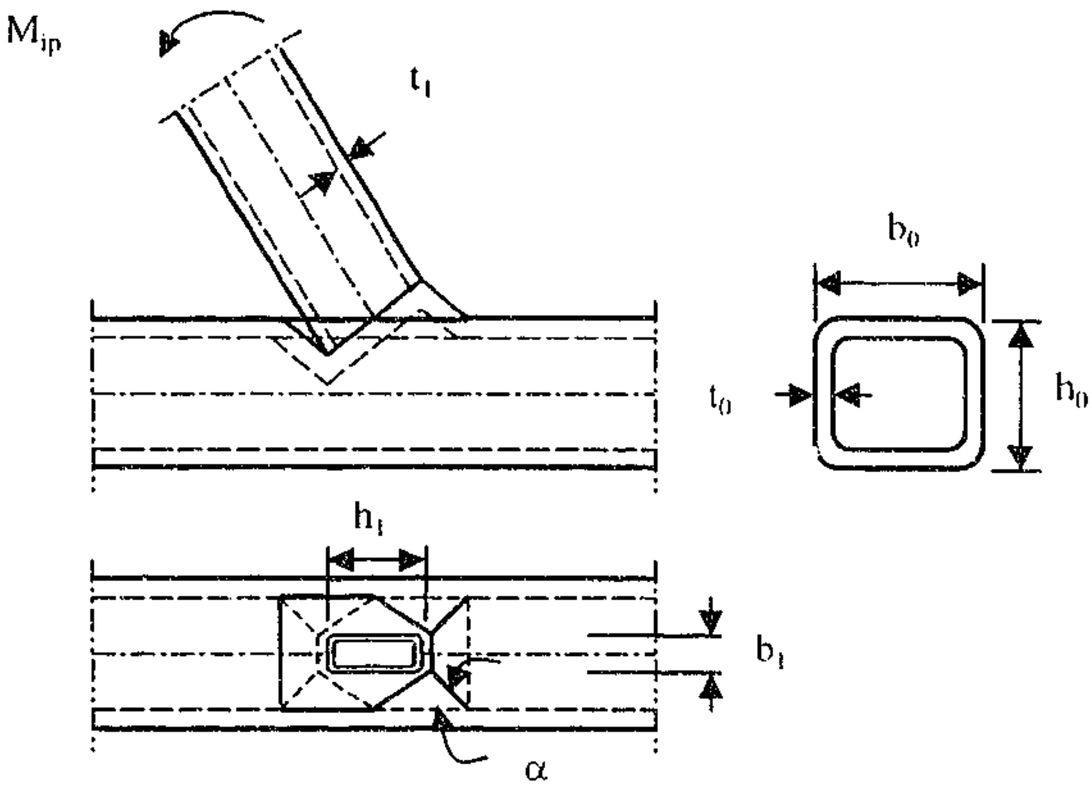

Figure 4-5: Yield Line Mechanism

$$M_{static} = M_{ip} = 0.5 f_{y0} t_0^2 b_0 \left\{ 1 + \frac{4h_1/b_0}{\sin\theta_1 \sqrt{1-\beta}} + \frac{2(h_1/b_0)^2}{\sin^2\theta_1(1-\beta)} \right\} f(n) \text{ for } \beta \le 0.85 \qquad \textbf{(4.2)}$$

where M_{ip} is the static strength for in-plane bending, expressed as a bending moment in bracing member, f_{yo} is the yield stress of chord member, t_o is the thickness of hollow section chord member, b_o is the external width of hollow section chord member, h_l is the external depth (in plane of truss) of hollow section brace member, θ_l is the included angle between bracing member and the chord, and β is the width ratio between bracing member and the chord.

f(n) is a function to allow the reduction in connection moment capacity in the presence of large compression chord forces.

$$f(n) = 1.3 + \left(\frac{0.4}{\beta}\right) n \quad \text{but } f(n) \le 1.0 \qquad \textbf{(4.3)}$$

$$\text{where} \quad n = \frac{N_0}{A_0 f_{y0}} + \frac{M_0}{S_0 f_{y0}} \tag{4.4}$$

where S_o is the elastic modulus of the chord member, A_o is the cross-sectional area of the chord member, M_o is the bending moment in the chord member, and N_o is the axial force applied to the chord member.

For the tube-to-tube connections tested in this investigation $M_o/S_o f_{yo} = 0$ and $N_o/A_o f_{yo}$ is very close to zero.

Therefore a value of $f(n) = 1$ is adopted.

For a value θ_1 of 90°, the moment capacity equation becomes

$$M_{static} = M_{ip} = f_{y0} t_0^2 h_1 \left\{ \frac{1}{2h_1/b_0} + \frac{2}{\sqrt{1-\beta}} + \frac{(h_1/b_0)}{(1-\beta)} \right\} \text{ for } \beta \leq 0.85 \tag{4.5}$$

The set-ups of the static tests for the tube-to-plate and tube-to-tube T-joints are shown in Figures 4-6 and 4-7 respectively. The set-up was made to simulate the same loading and support conditions that were to be applied during the fatigue tests. The tests were performed in a 500kN capacity Baldwin Universal testing machine.

Inclinometers were set to monitor the change in angle with application of load. One inclinometer was set on the base of the angle plate to act as a reference and the other was set on the specimen to monitor the change in angle as the load was applied. The deflection at the point of application of load was recorded during the static test.

Moment-deflection and moment-angle of inclination graphs obtained for tube-to-plate and tube-to-tube T-joints made from square hollow sections are shown in Figures C1 to C14, Appendix C. The maximum elastic moment below which the connection behaves elastically is determined from the linear portion of the moment-deflection or the moment angle of inclination graphs shown in Appendix C, for each connection tested. The curves show both loading and unloading of the connections.

Failure of the tube-to-plate T-joints occurs due to deflection of the brace resulting in yielding at the corners of the tube on the tube-plate welded interface. In the tube-to-tube T-joints chord face yielding occurs, Figure 4-8.

Figure 4-9 shows moment-angle of inclination curves for a tube-to-plate joint and tube-to-tube joints. It also shows that both the strength and flexural rigidity of an unstiffened vierendeel connection decrease as the chord slenderness ratio (b_0/t_0) increases, and as the bracing to chord width ratio (b_1/b_0 or β) decreases (Packer *et al* 1992).

A summary of the design moment capacity of the connections and the maximum elastic moment below which the connections behave elastically, $M_{elastic.max}$, are given in Table 4-11. The Department of Energy (1990) guidelines state in Section 21.2.3 that the calculated tensile stress in a member under fatigue loading operating conditions should not exceed 60 per cent of the yield stress. The values in Table 4-11 show that this is the case for most of the tested connections.

Table 4-11: Design moment capacity and Maximum elastic moment of connections

Connection	** P_{max} Applied (kN)	**Measured Maximum elastic moment, $M_{elastic.max}$ (kNm)**	* **Calculated Design Static Strength, M_{static} (kNm)**	$\frac{M_{elastic.max}}{M_{static}}$
50x50x3SHS-Plate	7.10	2.30	4.20	0.55
50x50x1.6SHS-Plate	3.40	1.10	2.10	0.52
50x50x3SHS-100x100x3SHS	0.99	0.32	0.76	0.42
35x35x3SHS-100x100x3SHS	0.40	0.10	0.49	0.20
35x35x1.6SHS-100x100x3SHS	0.48	0.12	0.49	0.24
50x50x3SHS-75x75x3SHS	1.85	0.60	0.98	0.61
50x50x1.6SHS-75x75x3SHS	1.36	0.44	0.98	0.45

* f_y = 350MPa for 35x35x1.6SHS, 50x50x1.6SHS, 75x75x3SHS and 100x100x3SHS
f_y = 450MPa for 35x35x3SHS and 50x50x3SHS
** P_{max} is calculated from $M_{elastic.max}$ for a lever-arm of $5b_1$+74mm

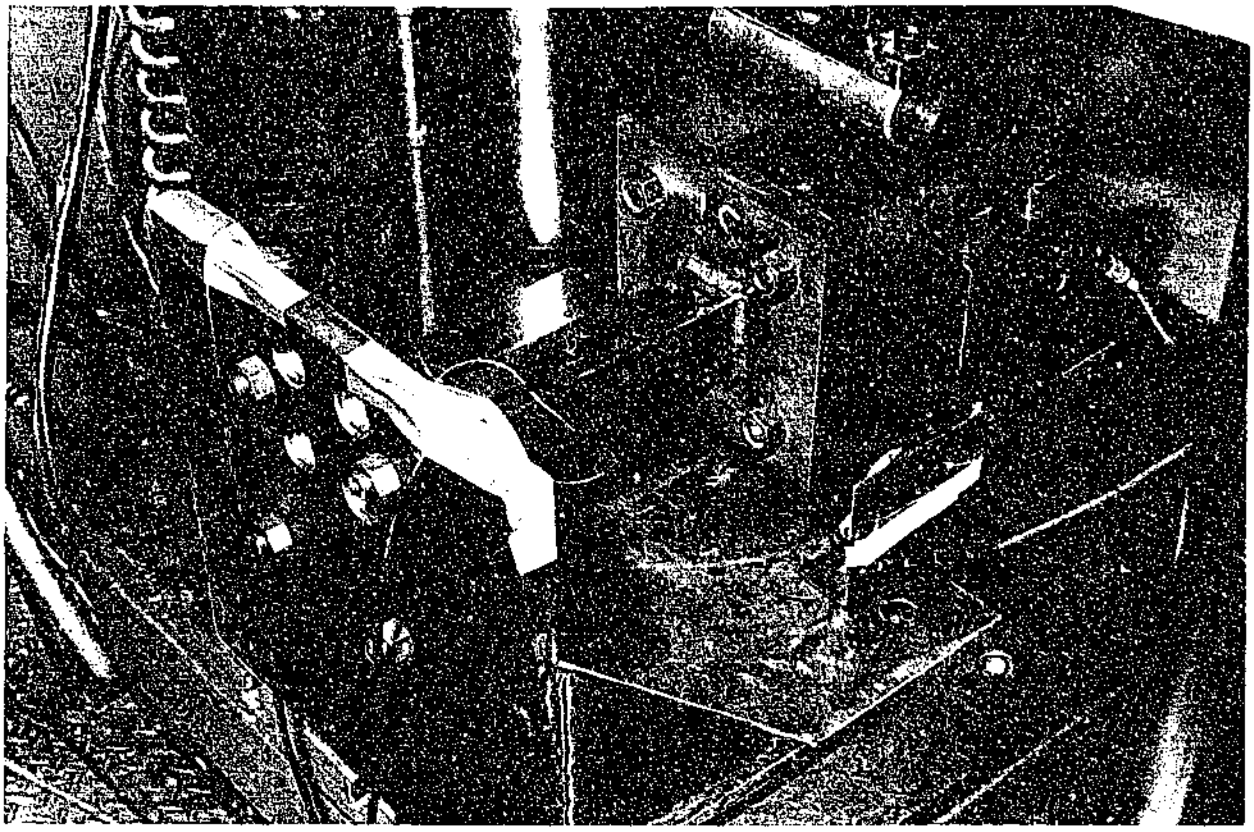

(a)

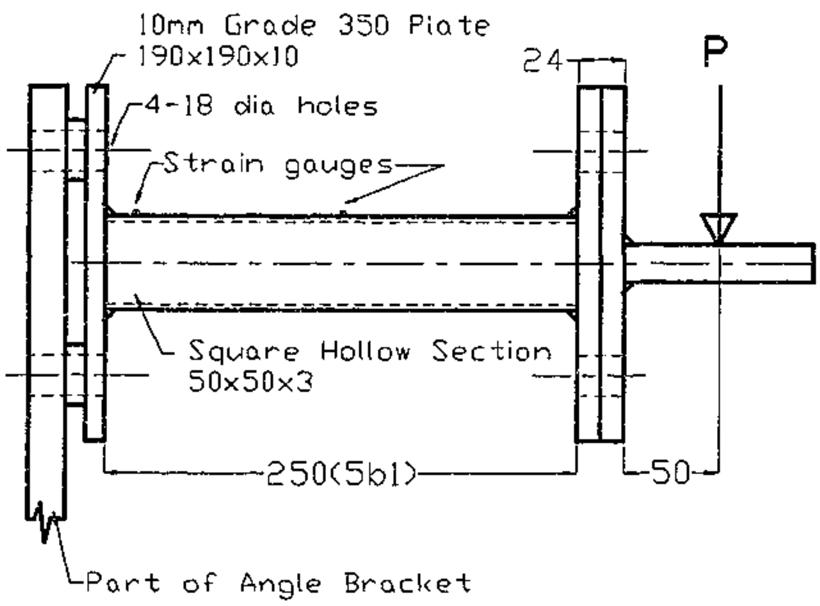

(b)

Figure 4-6: (a) Setup of tube-to-plate static test; (b) Schematic diagram of a tube-to-plate T-joint under static test

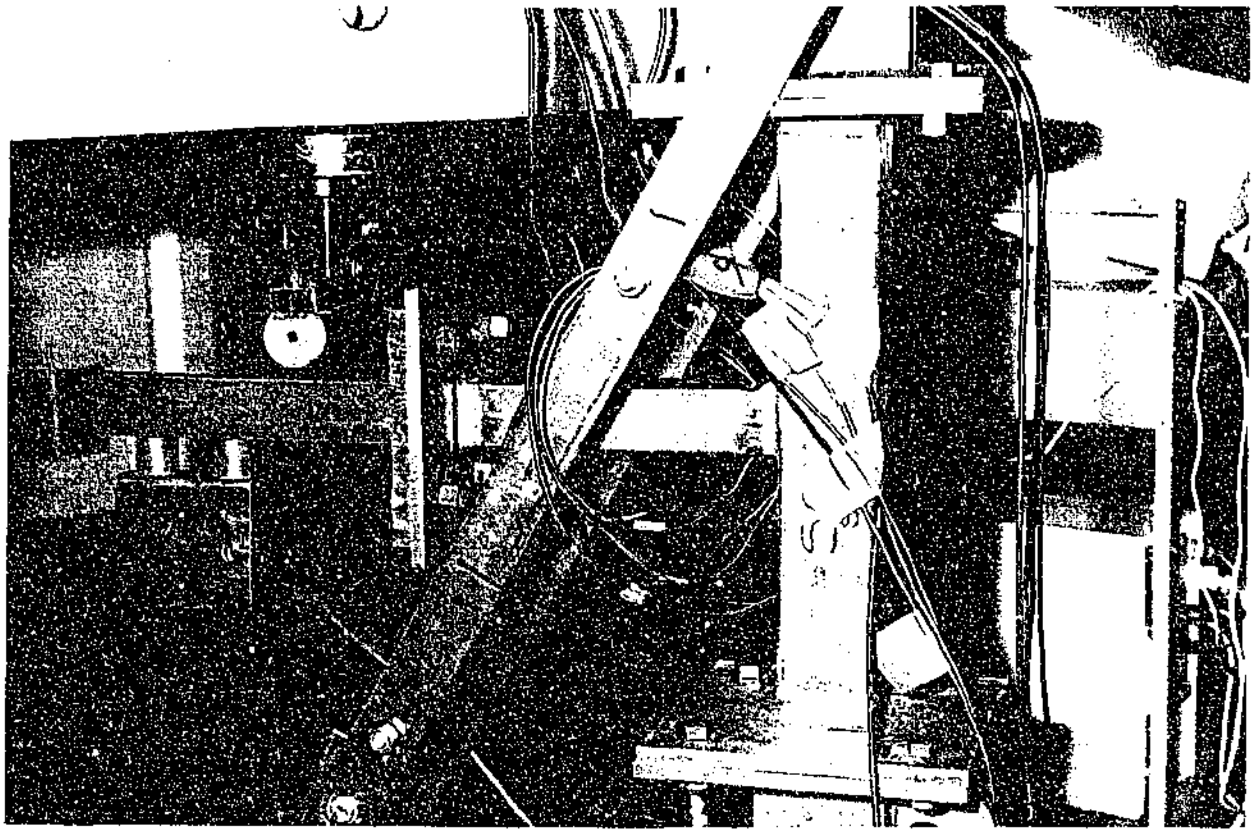

(a)

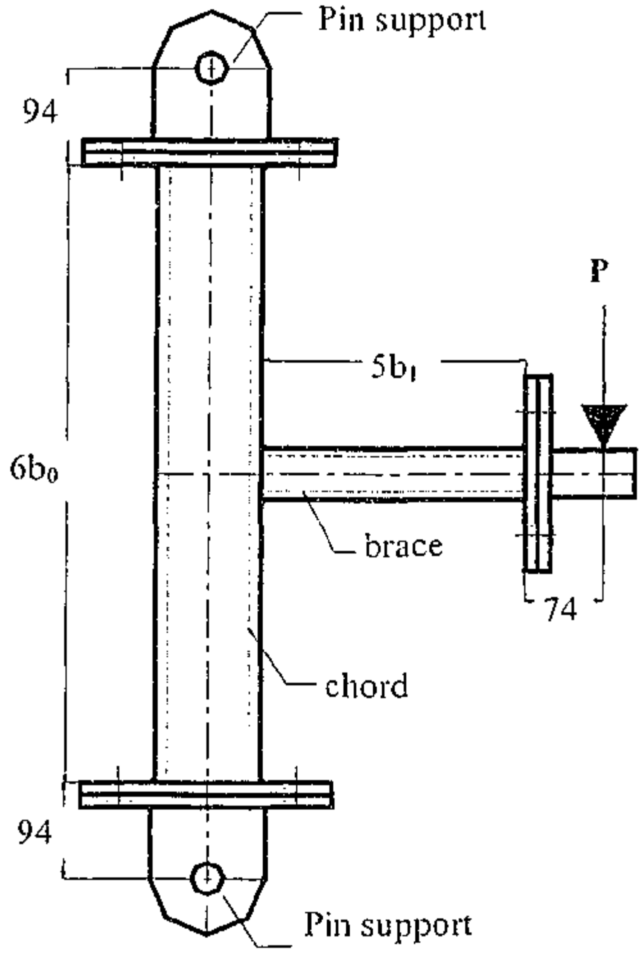

(b)

Figure 4-7: (a) Setup of static test and (b) Schematic diagram of tube-to-tube static test

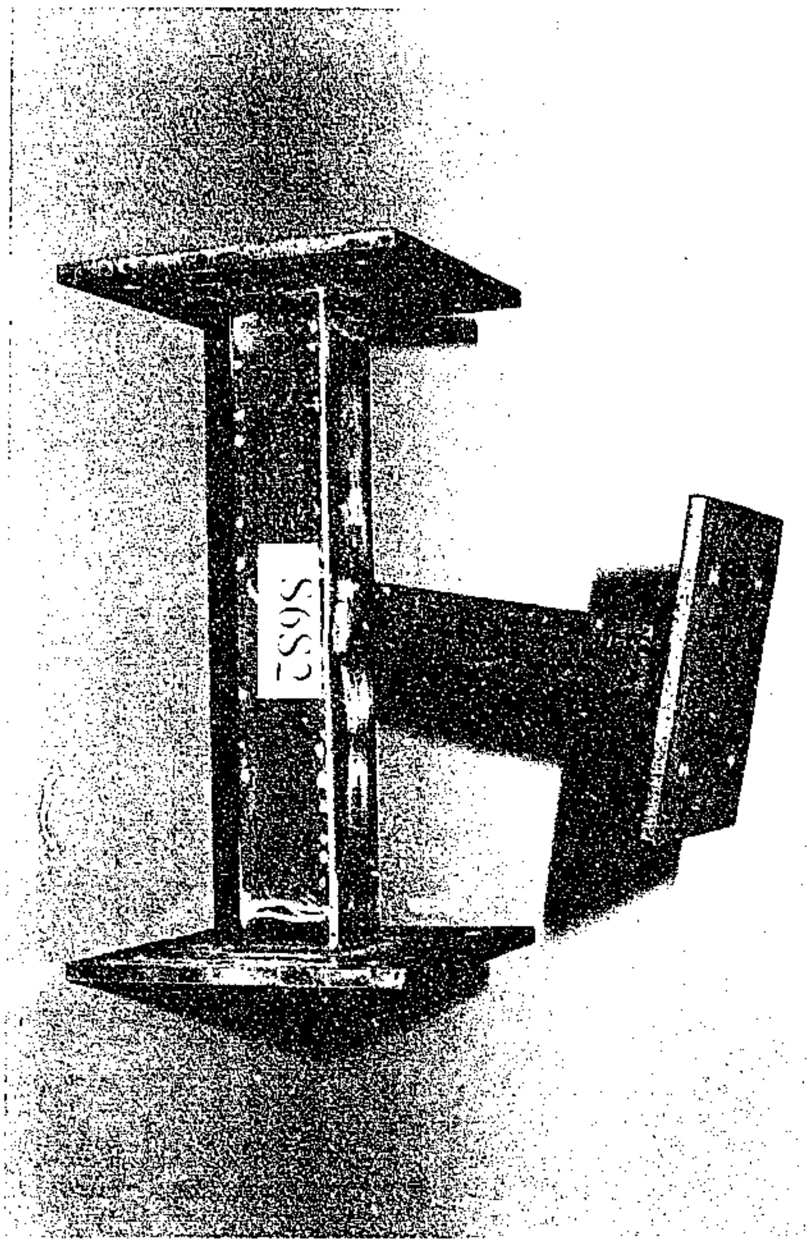

Figure 4-8: Failure mode of tube-to-tube T-joints

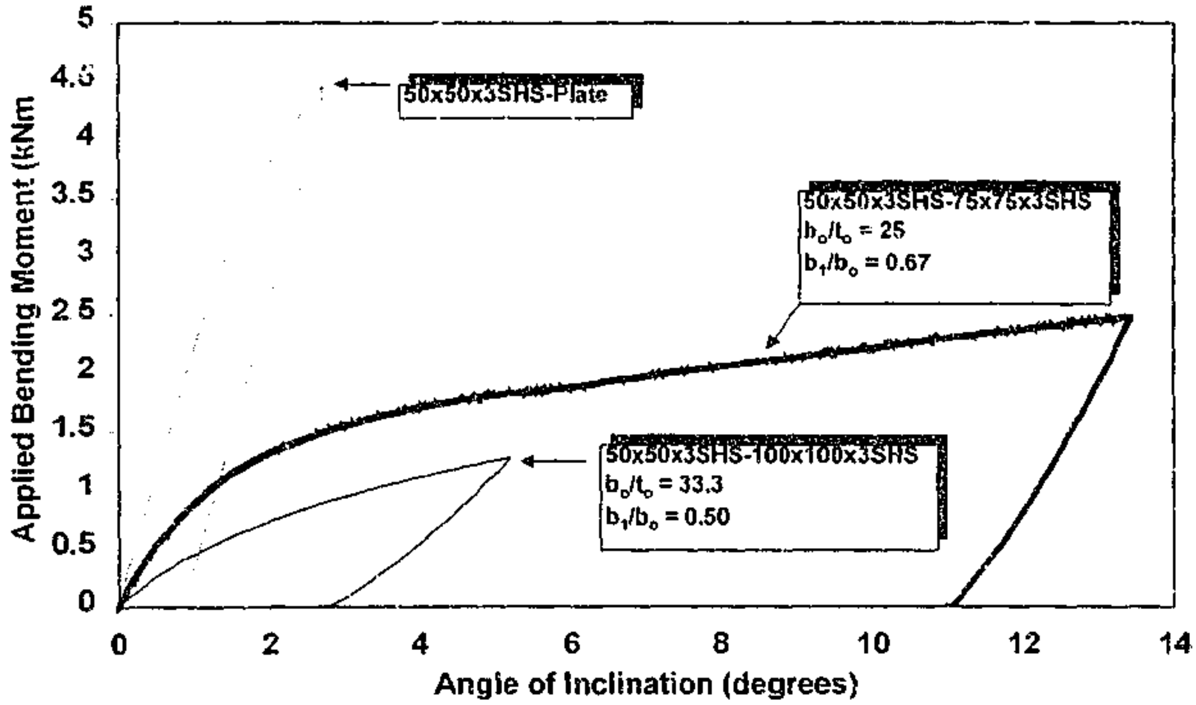

Figure 4-9: Moment-angle of inclination graphs for tube-to-plate and tube-to-tube T joints

4.4 SUMMARY

(a) The characteristics of stress-strain curves for cold-formed sections are given in existing literature (Hancock 1994). Cold form of working results in an increase in both the yield stress and ultimate tensile strength but in reduced ductility. Cold form of working has been demonstrated by Hancock (1994), through the testing of tensile coupons from the corners and the flats of a cold-formed square hollow section, resulting in the distribution of yield stress and ultimate tensile strength in rectangular or square hollow sections being given. The yield stress and ultimate tensile strength at the corners is significantly higher than that at the flats of the square or rectangular hollow section due to increased cold work of forming at the corners. Although there is a significant difference in the mechanical properties between the flats and the corners of the square or rectangular hollow sections, AS1163-1991 defines the yield stress and ultimate tensile strength of the section as that obtained from the flat face.

(b) In this investigation, more than one tensile coupon specimen was tested for determining the mechanical properties of each section, with coupons being obtained from the faces adjacent and opposite to the seam weld. The mean yield stresses and ultimate tensile strength from the tensile coupon tests for each steel grade, were found to be greater than the minimum yield and tensile strength specified by the Australian Standard AS1163-1991 for grades C350LO and C450LO steels and EN 10219-2: 1997 for S355JOH steel. The nature of the stress-strain graphs for the cold-formed steels tested is that the yield stresses have to be defined as the 0.2% proof stress. This is because the stress-strain graphs of these cold-formed steels do not exhibit a yield plateau, as is the case for mild steel and hot rolled steel.

(c) Moment-deflection and moment-angle of inclination graphs showed that part of these graphs is a linear response between load and deformation. Both the moment-deflection and moment-angle of inclination graphs gave similar values of maximum elastic moment for each connection tested. Moment-angle of inclination graphs showed that both the strength and flexural rigidity of an unstiffened vierendeel connection decrease as the chord slenderness ratio (b_0/t_0) increases and as the bracing to chord width ratio (b_1/b_0 *or* β) decreases (Packer *et al* 1992).

(d) Failure of the tube-to-plate T-joints was due yielding at the corners of the brace tube at the tube-plate welded interface. Maximum stress concentration factors have subsequently been found to occur at the corners of the brace tube at the tube-plate welded interface. Fatigue crack initiation has also been observed to start at the corners of the brace tube at the tube-plate welded interface during fatigue tests of tube-to-plate T-joints.

(e) Failure of tube-to-tube T-joints was due to chord face yielding. This is consistent with observations from other researchers where the β value of the connection is less than 0.85 (Packer *et al* 1992; Packer and Henderson 1997). The tube-to-tube T-joints tested in this investigation all had β value less than 0.7. Most of the fatigue cracks in subsequent fatigue tests were found to initiate in the chord where yielding was observed during static testing. Similarly maximum SCF also occur in the chord for tube-to-tube T-joints under in-plane bending (IIW 2000).

(f) The ratio of maximum elastic moment, $M_{elastic,max}$ to static strength, M_{static}, was found to be always less than 0.6. This is in agreement with the Department of Energy (1990) guidelines, which states that the calculated tensile stress in a member under fatigue loading conditions should not exceed 60% of the yield stress.

Chapter 5

FATIGUE TESTS AND EXPERIMENTAL STRESS CONCENTRATION FACTORS OF TUBE-TO-PLATE T-JOINTS

5.1 INTRODUCTION

The fatigue rig testing system used in the fatigue testing of tube-to-plate T-joints under in-plane bending is described in Chapter 5. This includes the support system, the measuring system and the loading system of the fatigue test rig.

Fatigue tests are carried out on tube-to-plate T-joints made from square hollow sections welded to a 10mm plate, under in-plane bending. The square hollow sections are of three different steel grades, C350LO, C450LO and S355JOH. Grades C350LO and S355JOH tubes are non-galvanised cold-formed steel tubes. Grade C450LO tubes, are in-line galvanised steel tubes.

The tube-to-plate T-joints are made up of square hollow section tubes of wall thicknesses below 4mm. A typical connection detail of a tube-to-plate T-joint made from a 50x50x3SHS tube is shown in Figure 5-1. The length of the specimens is chosen so that the measured strains are not affected by end conditions. The measurements have to be taken at about *2b* to *2.5b* from the end conditions (van Wingerde, 1992). Since nominal strains were to be measured in the brace to determine the applied forces, the brace was chosen to be a length $5b_1$ or greater. This means that strain gauges located at mid height of the brace would not be affected by the end plate conditions.

Table 5-1 shows the details of the series names, square hollow section sizes, stress ratio, and the corresponding joint parameters, for the different steel grades tested.

The mode of failure for the tube-to-plate T-joints made from tubes of wall thicknesses less than 4mm and fillet welded to a 10mm plate is described.

The fatigue test results are given in terms of the classification method. In the classification method the nominal stress range applied and the corresponding number of cycles are used to define the S-N curve.

Tests on the tube-to-plate T-joints under in-plane bending have been carried out for in-line galvanised steel known as DuraGal and for non-galvanised steels as well. The effect of in-line galvanising on steel under fatigue loading will be discussed.

The effect of steel grade on fatigue strength will also be demonstrated. Tubes of steel grades S355JOH, C350LO and C450LO have been tested for the tube-to-plate T-joints under in-plane bending. This allows the effect of steel grade on the fatigue strength of welded tube-to-plate T-joints to be investigated.

The effect of stress ratio on fatigue strength will also be analysed. Two different stress ratios of 0.1 and 0.5 have been used during the testing of the specimens made from 3mm thick tubes.

The effect of tube wall thickness on fatigue life will also be examined. Tubes of three different thicknesses have been fatigue tested. The tubes have 3mm, 2mm and 1.6mm thicknesses. This analysis of S-N data from the 3mm, 2mm and 1.6mm tubes will show the trend of fatigue strength with thickness. The trend of fatigue strength of the tubes with wall thicknesses less than 4mm will be compared with the existing trend of fatigue strength for tubular joints with thicknesses greater than 4mm. This analysis of S-N data for tube-to-plate T-joints with thicknesses less than 4mm may help confirm the loss of fatigue strength in thinner walled joints with thicknesses less than 4mm. The loss of strength in thinner walled joints is associated with the greater impact of weld defects such as undercuts on thin-walled welded joints as reported by Puthli *et al* 1989 and Mashiri *et al* 1997, 1998b.

Experimental stress concentration factors have also been determined for tube-to-plate T-joints. Strip strain gauges have been used to obtain the stress distributions perpendicular to the weld toe. The stress distributions have been used to determine the stress concentration factors at hot spot locations A and E. The hot spot stress location occurs at the corner of the brace on the brace-plate welded interface.

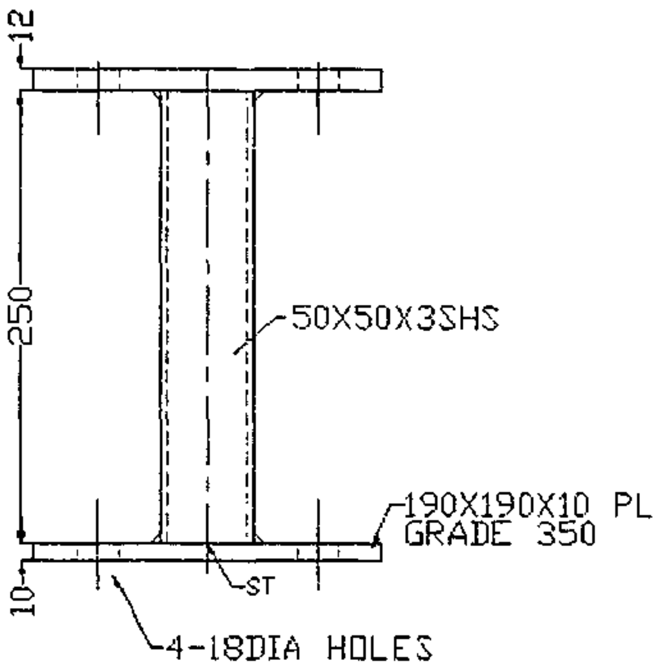

Figure 5-1: Tube-to-plate joint; Brace size 50x50x3 SHS, Plate size 190x190x10 PL

Table 5-1: Tube-to-plate T-joints tested for the three different steel grades

Steel/ Description	Connection Series	Plate Thickness (mm)	Brace Member	τ	R
C350LO Non-galvanised	S1P	10	50x50x3 SHS	0.3	0.1; 0.5
	S2P	10	50x50x1.6 SHS	0.16	0.1
C450LO Galvanised	D1P	10	50x50x3 SHS	0.3	0.1; 0.5
	D7P	10	40X40X2 SHS	0.2	0.1
S355JOH Non-galvanised	V1P	10	50x50x3 SHS	0.3	0.1; 0.5
	V2P	10	40X40X2 SHS	0.2	0.1

5.2 FATIGUE RIG TESTING SYSTEM

The fatigue rig testing system, used for testing the tube-to-plate T-joints, is shown in Figure 5-2. Six identical rigs were built to speed up the testing program. A schematic diagram of the test rig set up is shown in Figures 5-3. The test rig can be used for testing both the tube-to-plate and the tube-to-tube T-joints.

5.2.1 Support System

The tube-to-plate T-joints are mounted onto the rig with spacers. This is to avoid a contact problem and allow free bending of the plate between the bolt supports. This simplifies the modelling involved in the numerical analysis of this joint. Plumber blocks are used at the test specimen and the air-cylinder ends. The plumber blocks have self-aligning bearings which enhance point load application and also allow self-adjustment of the system as deformation occurs in the fatigue sample due to propagating cracks. A clevis is connected to each plumber block with pins. The plumber blocks are also less susceptible to local deformation with impact loading as cycling occurs, as is likely to happen when a thick plate is used for transferring load through a clevis-joint system. Robust framing has been used in the rig to avoid cracking of the supporting system and to minimise alignment problems due to deformation of the rig. Complete penetration butt welds have been used on the interface of the beam-column interface where maximum bending stresses occur during cycling. Butt welds have been shown to make welded constructions that are more fatigue resistant compared to fillet welded constructions (Maddox 1991).

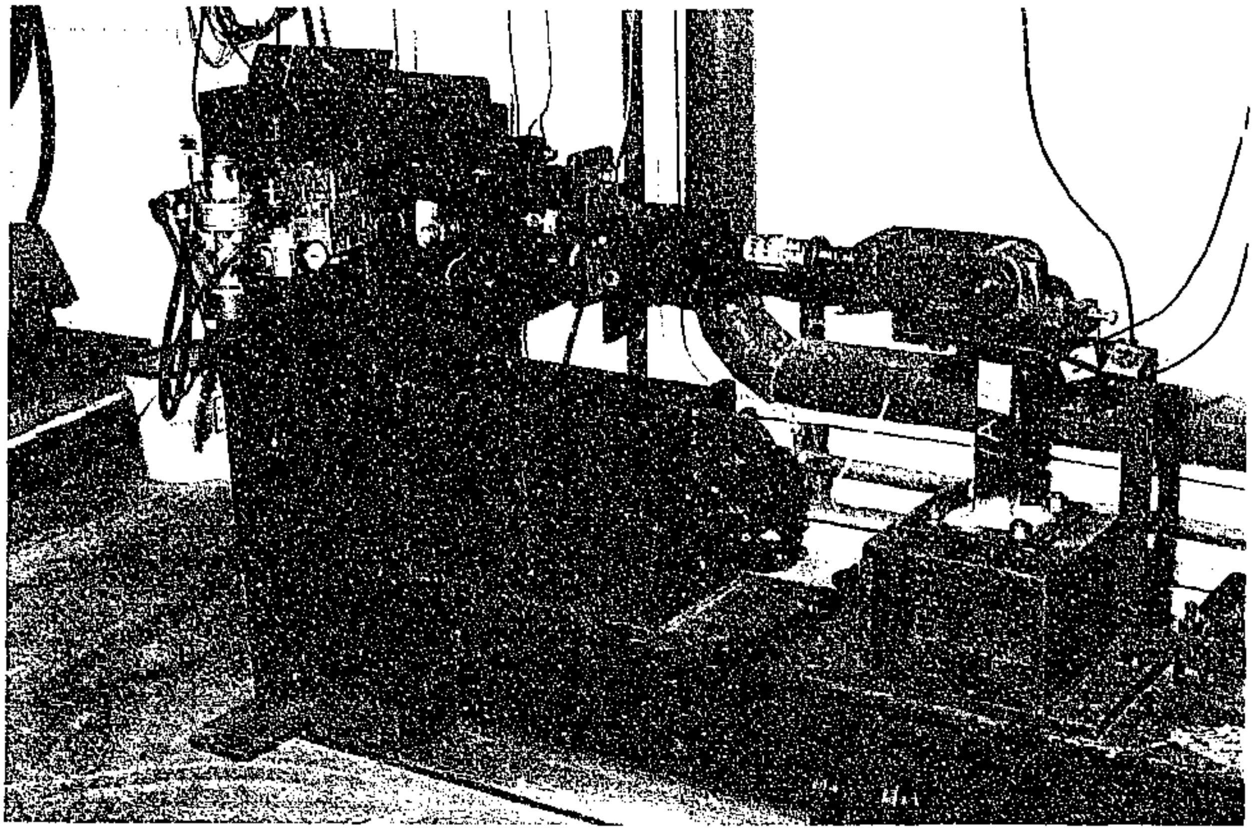

Figure 5-2: Test set-up for tube-to-plate specimen under cyclic bending load

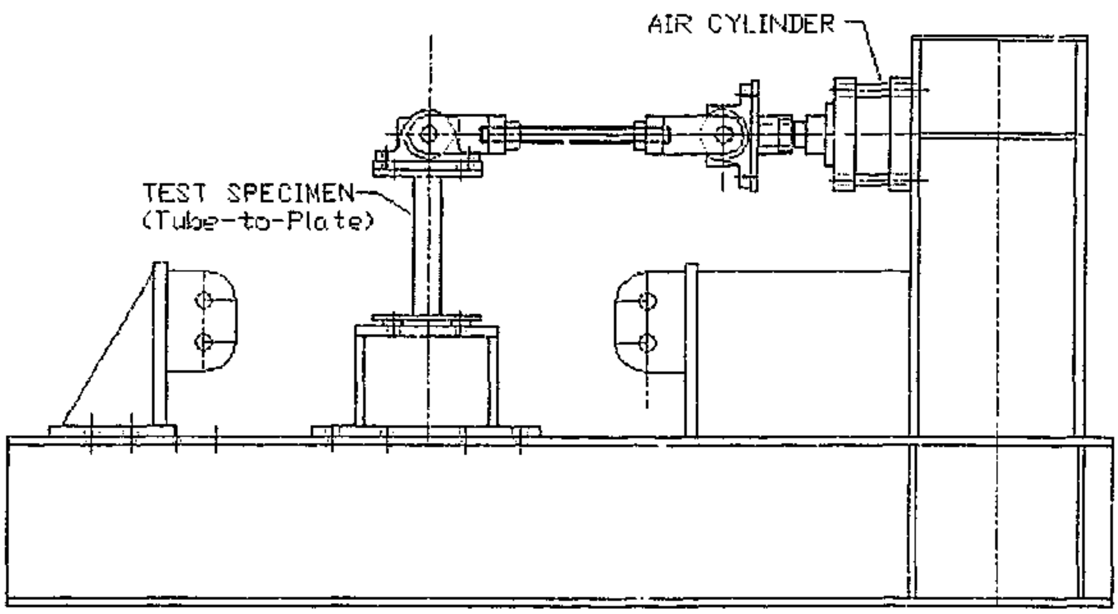

Figure 5-3: Schematic diagram of Test Rig for the testing of Tube-to-Plate joints

5.2.2 Loading System

Air cylinders are used to apply constant amplitude cyclic loading at a frequency of about 1Hz. Control valves are used to determine and maintain the loads corresponding to the minimum and maximum stresses during cycling. A load cell is used to determine the magnitude of loads required during cycling. Prior to fatigue tests, the load cells have been calibrated with the aid of a load cell exciter and the calibration factor determined. The calibrated load cell and load cell exciter are then used in the fatigue rig testing system to determine applied loads. This gives the system the flexibility to allow application of different nominal stress ranges to different test specimens.

5.2.3 Measuring System

The maximum and minimum loads were measured using the calibrated load cell and load cell exciter. These were the values of loads that were used to determine the nominal stress range using simple beam theory. Two strain gauges were placed at mid-height of the brace to determine applied stresses and, hence, nominal stress ranges. Extrapolation of the strains at mid-height to determine strains at the tube-plate interface allows the stresses applied using the load cell to be confirmed independently. This helps to check the accuracy of the load cell system.

Cycle counting is done through a Programmable Logic Controller (PLC) that monitors and controls the opening and closing in the pressure control valves and, hence, the number of cycles as the fatigue test progresses.

When sudden collapse of the sample occurs, the test is automatically stopped through a break detector connected to the PLC. The welded connection's deflection during sudden collapse causes it to touch and trigger the break detector switch. A signal is transmitted to the PLC causing it to stop the cyclic loading. The break detector system avoids continuous cycling after sudden collapse and hence protects the air cylinder system from damage.

5.3 FATIGUE TEST RESULTS

Tube-to-plate T-joints were tested for three different thicknesses. Square hollow section tubes of thicknesses 3mm, 2mm and 1.6mm were used to make the test specimens. For each tube wall thickness, the welded joint specimens were tested at 3 or more different stress levels. Replication was also employed, allowing more than one specimen to be tested at any given nominal stress range, for most of the stress ranges considered. This improves the reliability of the results by defining a scatter band for the S-N data. Specimens were also made up from three different steels as follows; (a) C350LO, non-galvanised steel, (b) C450LO, galvanised steel, known as DuraGal and (c) S355JOH, non-galvanised steel.

5.3.1 Mechanical Properties

The specified mechanical properties of the steel tested in this program are given in Table 5-2. The details of the measured yield stresses, measured ultimate tensile strengths and elongation from tensile coupon tests for the three steel grades are given in Section 4.2 of Chapter 4.

Table 5-2: Mechanical Properties of Square-Hollow Sections used

Steel Type	Origin	Minimum Yield Stress (MPa)	Minimum Ultimate Tensile Strength (MPa)	Minimum Elongation, %
C450LO, galvanised (DuraGal)	Australia	450	500	14
C350LO, non-galvanised	Australia	350	430	16
S355JOH, non-galvanised	Europe	355	490-680	20

5.3.2 Failure Mode

Cracks initiated on the weld toe at the corner of the brace on the brace-plate interface and were noticed as surface cracks. The surface cracks grew in length from the corners toward the middle of the brace width as shown in Figure 5-4.

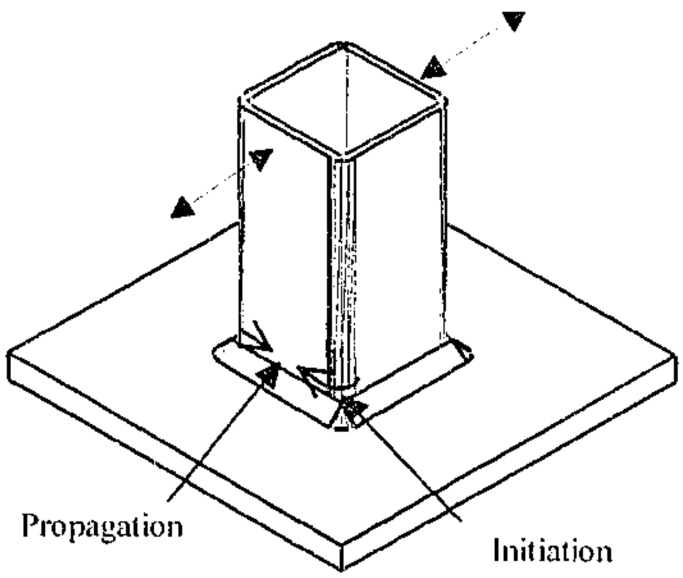

Figure 5-4: Tube-to-plate T-joint showing growth of surface cracks.

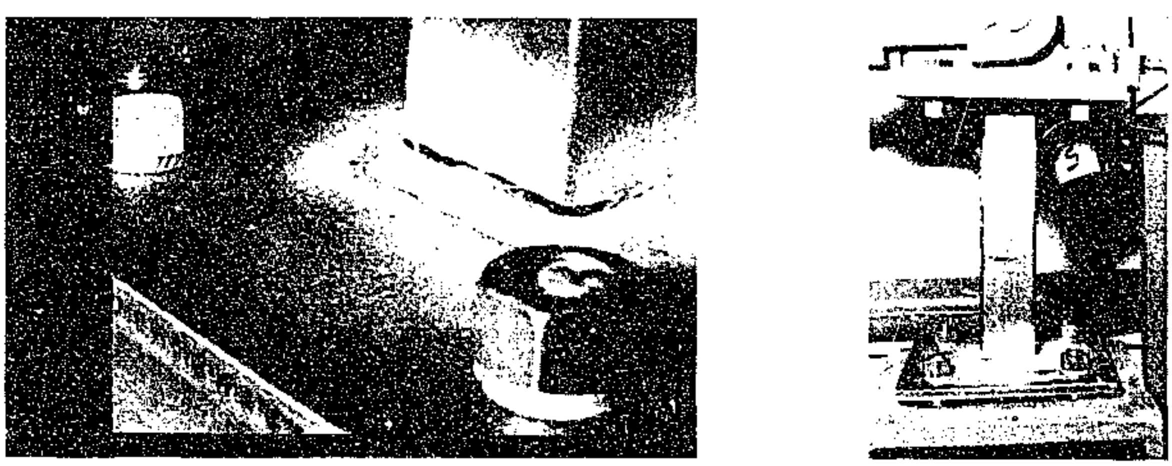

(a) **(b)**

Figure 5-5: (a) Failure mode of Tube-to-plate connection; (b) Test Specimen

As cycle loading continued the cracks propagated into through-thickness cracks along the entire length of the brace width. This resulted in separation of the brace from the plate along the entire length of the brace width. Failure was defined as a through thickness crack along the entire width of the brace, Figure 5-5. The through-thickness crack occurred on the weld toe in the brace on the side under tension. This failure mode is similar to the one adopted by van Wingerde (1992) for nodal T-joints, where failure was defined as a crack extending over a length of the brace width, for failure in the brace.

5.3.3 Fatigue Test Data

Fatigue test results for the 3mm, 2mm and 1.6mm tubes are shown in Tables 5-3, 5-4 and 5-5 respectively. The tube-to-plate T-joints made up of 3mm square hollow section tubes were tested at two different stress ratios of 0.5 and 0.1. The rest of the tests were carried out at a stress ratio of 0.1. Fatigue tests were carried out for specimens with and without in-line galvanising. For each group of tests, the specimens were tested at three or more stress nominal stress ranges to allow the determination of the slope of the S-N curves resulting from this fatigue data.

Table 5-3: Fatigue data of tube-to-plate T-joints under in-plane bending, t=3mm

Connection Name	**Tube Size (DxBxt) (mm)**	**Nominal Stress Range, $S_{r\text{-}nom}$ (MPa)**	**Stress Ratio**	**Fatigue Life, N (Cycles)**	**Weld Leg Lengths (mm)**		**Steel Grade/ Description**
					t_{wv}	t_{wh}	
S1PL1R1A	50x50x3	141.4	0.5	144472	5.3	7.1	C350LO, Non-galvanised
S1PL1R1B	50x50x3	141.4	0.5	164737	4.9	7.0	C350LO, Non-galvanised
S1PL2R1A	50x50x3	96.4	0.5	659561	4.4	6.8	C350LO, Non-galvanised
S1PL2R1B	50x50x3	96.4	0.5	372127	4.8	4.7	C350LO, Non-galvanised
S1PL3R1A	50x50x3	47.8	0.5	6106079	5.8	6.8	C350LO, Non-galvanised
S1PL3R1B	50x50x3	72.3	0.5	3454479	5.4	5.5	C350LO, Non-galvanised
S1PL1R2A	50x50x3	260.4	0.1	19005	4.7	6.6	C350LO, Non-galvanised
S1PL1R2B	50x50x3	260.4	0.1	11160	4.2	5.9	C350LO, Non-galvanised
S1PL2R2A	50x50x3	192.9	0.1	172406	5.7	5.8	C350LO, Non-galvanised
S1PL2R2B	50x50x3	130.8	0.1	713660	5.1	6.8	C350LO, Non-galvanised
S1PL3R2A	50x50x3	144.7	0.1	620076	5.1	6.2	C350LO, Non-galvanised
S1PL3R2B	50x50x3	144.7	0.1	287465	3.9	5.4	C350LO, Non-galvanised
D1PL1R2A	50x50x3	144.7	0.1	1467994	5.9	6.7	C450LO, Galvanised
D1PL2R2A	50x50x3	192.9	0.1	162443	4.6	7.3	C450LO, Galvanised
D1PL3R2A	50x50x3	260.4	0.1	30073	6.3	6.6	C450LO, Galvanised
D1PL3R2B	50x50x3	260.4	0.1	16743	5.7	6.8	C450LO, Galvanised
D1PL1R1A	50x50x3	72.3	0.5	1895574	6.4	7.2	C450LO, Galvanised
D1PL2R1A	50x50x3	96.5	0.5	372781	6.2	6.3	C450LO, Galvanised
D1PL3R1A	50x50x3	144.7	0.5	188422	5.6	6.5	C450LO, Galvanised
V1PL1R2A	50x50x3	144.7	0.1	362463	6.1	7.1	S355JOH, Non-galvanised
V1PL2R2A	50x50x3	155.9	0.1	231547	5.4	7.5	S355JOH, Non-galvanised
V1PL3R2A	50x50x3	260.4	0.1	119420	6.2	6.9	S355JOH, Non-galvanised
V1PL1R1A	50x50x3	72.3	0.5	2071985	5.8	7.7	S355JOH, Non-galvanised
V1PL2R1A	50x50x3	96.4	0.5	354539	6.1	7.1	S355JOH, Non-galvanised
V1PL3R1A	50x50x3	144.7	0.5	158652	5.9	6.0	S355JOH, Non-galvanised

Table 5-4: Fatigue data of tube-to-plate T-joints under in-plane bending, t=2mm

Connection Name	Tube Size (DxBxt) (mm)	Nominal Stress Range, $S_{r\text{-}nom}$ (MPa)	Stress Ratio	Fatigue Life, N (Cycles)	Weld Leg Lengths (mm)		Steel Grade/ Description
					t_{wv}	t_{wh}	
D7PL1A	40x40x2	257.1	0.1	25466	5.5	6.3	C450LO, Galvanised
D7PL1B	40x40x2	257.1	0.1	25960	5.9	4.9	C450LO, Galvanised
D7PL2A	40x40x2	190.4	0.1	416682	5.8	5.5	C450LO, Galvanised
D7PL2B	40x40x2	190.4	0.1	184785	5.2	6.9	C450LO, Galvanised
D7PL3A	40x40x2	108.7	0.1	613926	5.4	6.0	C450LO, Galvanised
D7PL3B	40x40x2	108.3	0.1	195414	5.2	6.1	C450LO, Galvanised
D7PL3C	40x40x2	105.4	0.1	496711	4.6	5.5	C450LO, Galvanised
V2PL1A	40x40x2	257.1	0.1	33316	5.1	5.3	S355JOH, Non-galvanised
V2PL1B	40x40x2	257.1	0.1	32671	5.2	5.1	S355JOH, Non-galvanised
V2PL2A	40x40x2	190.4	0.1	248767	5.7	6.2	S355JOH, Non-galvanised
V2PL2B	40x40x2	190.4	0.1	208325	6.1	6.7	S355JOH, Non-galvanised
V2PL3A	40x40x2	108.7	0.1	286896	4.9	6.2	S355JOH, Non-galvanised
V2PL3B	40x40x2	108.2	0.1	376389	5.9	6.3	S355JOH, Non-galvanised

Table 5-5: Fatigue data of tube-to-plate T-joints under in-plane bending, t=1.6mm

Connection Name	Tube Size (DxBxt) (mm)	Nominal Stress Range, $S_{r\text{-}nom}$ (MPa)	Stress Ratio	Fatigue Life, N (Cycles)	Weld Leg Lengths (mm)		Steel Grade/ Description
					t_{wv}	t_{wh}	
S2PL1R2A	50x50x1.6	202.6	0.1	57098	4.5	4.8	C350LO, Non-galvanised
S2PL1R2B	50x50x1.6	202.6	0.1	77270	5.6	6.2	C350LO, Non-galvanised
S2PL2R2A	50x50x1.6	162.0	0.1	79755	4.5	7.7	C350LO, Non-galvanised
S2PL2R2B	50x50x1.6	162.0	0.1	99806	4.4	6.3	C350LO, Non-galvanised
S2PL3R2A	50x50x1.6	105.9	0.1	398331	5.8	7.7	C350LO, Non-galvanised
S2PL3R2B	50x50x1.6	81.0	0.1	11962622	5.8	7.1	C350LO, Non-galvanised (RUNOUT)
S2PL3R2C	50x50x1.6	105.9	0.1	273091	3.8	7.4	C350, Non-galvanised
D2PL1R2A	50x50x1.6	211.8	0.1	51856	4.4	6.9	C450LO, Galvanised
D2PL1R2B	50x50x1.6	211.8	0.1	62528	4.9	7.7	C450LO, Galvanised
D2PL2R2A	50x50x1.6	162.0	0.1	88902	4.5	7.5	C450LO, Galvanised

Figure 5-6 shows an S-N data plot of the tube-to-plate T-joints tested in this investigation and shown in Tables 5-3 to 5-5. The S-N data plots show that the tested tube-to-plate t-joints with thicknesses less than 4mm have a fatigue life greater than that given by the existing S-N curves for these joints. The following specimens were tested; (a) 25 specimens made from 3mm thick tubes, (b) 13 specimens made from 2mm thick tubes and (c) 10 specimens made from 1.6mm thick tubes. Of all the specimens one run-out was obtained. The run-out was from a specimen made from grade C350LO steel tube and with a thickness of 1.6mm.

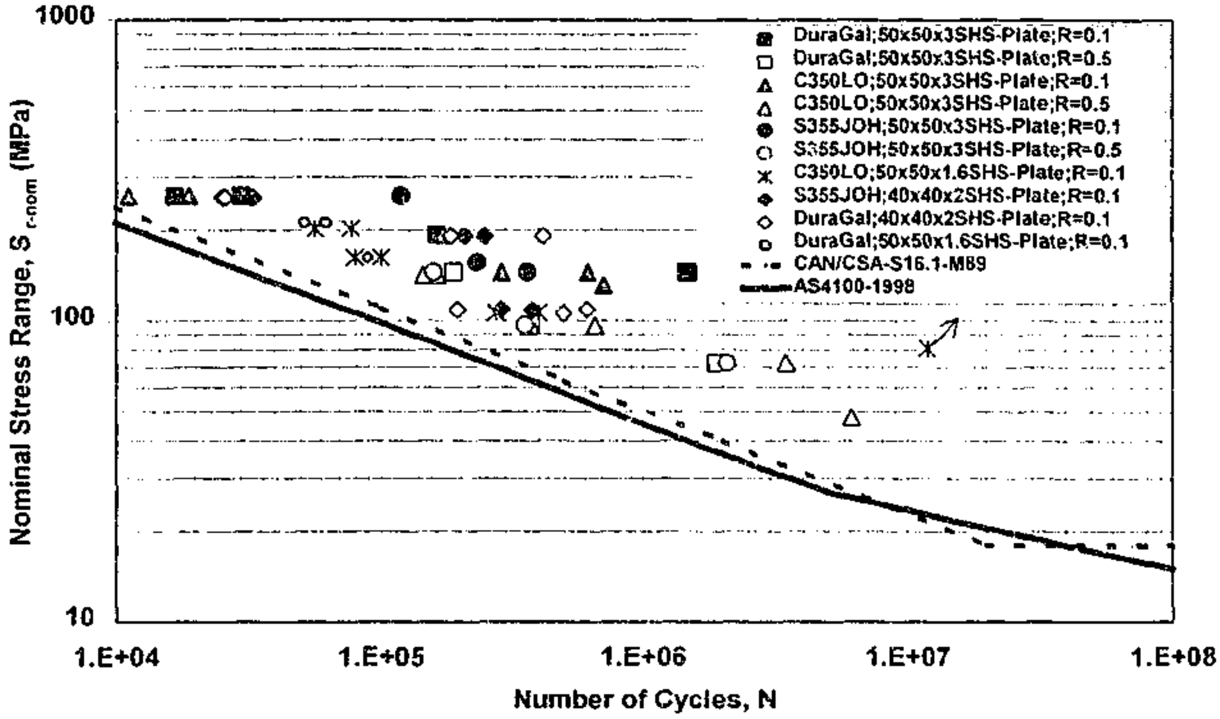

Figure 5-6: S-N data plots of tube-to-plate T-joints tested in this investigation

5.4 EFFECTS OF STEEL GRADE, GALVANIZING, STRESS RATIO AND WALL THICKNESS ON FATIGUE LIFE

5.4.1 Effect of Steel Grade

The effect of steel grade on fatigue life can be determined by comparing S-N data plots for specimens with the same thickness, stress ratio, surface finishing but different steel grades. In all the cases for the tube-to-plate joints tested, failure occurred in the brace member. The brace member thickness or tube thickness is therefore always the critical thickness in the tube-to-plate T-joints.

S-N data for specimens made up of the 3mm thick non-galvanised square hollow sections (SHS) tested at a given stress ratio can be compared to determine the influence of steel grade on fatigue life. Figure 5-7 shows the S-N data plots from the specimens made from 3mm thick non-galvanised SHS tested at a stress ratio of 0.1. Figure 5-8 shows the S-N data plots from the specimens made from 3mm thick non-galvanised SHS tested at a stress ratio of 0.5.

The S-N data plots in both Figures 5-7 and 5-8 show that there is no noticeable trend in the distribution of number of cycles at a given stress relating to steel grade. Fatigue tests on axially loaded end to end connections made from square hollow sections, with steel grades Fe 360, Fe 510, St E 47 and St E 70 also showed no influence of steel grade on fatigue life. This was valid for fillet welded sections with thicknesses of 4mm, 6.5mm and 8mm (Noordhoek *et al* 1980).

Steel grade does not have an influence on fatigue life because the greater portion of fatigue life in welded connections is spent in the fatigue crack propagation stage. This is because welded structures have inherent crack-like defects that are a result of arc welding processes (Maddox 1991). The fatigue life of welded structures is therefore depended on the fatigue crack growth coefficient, C, in the Paris equation. For ferritic steels with a yield or 0.2% proof stress below 600MPa operating in air or other non-aggressive environments at temperatures up to 100°C and for values of crack growth rate da/dN in mm/cycle, the value of the crack growth coeffient, C, can be assumed to be equal to 3×10^{-3} according to PD6493: 1991 (BSI 1991). Adopting the same crack growth coefficient for different strength grade steels means that the rate at which the cracks grow in different steel grades is about the same.

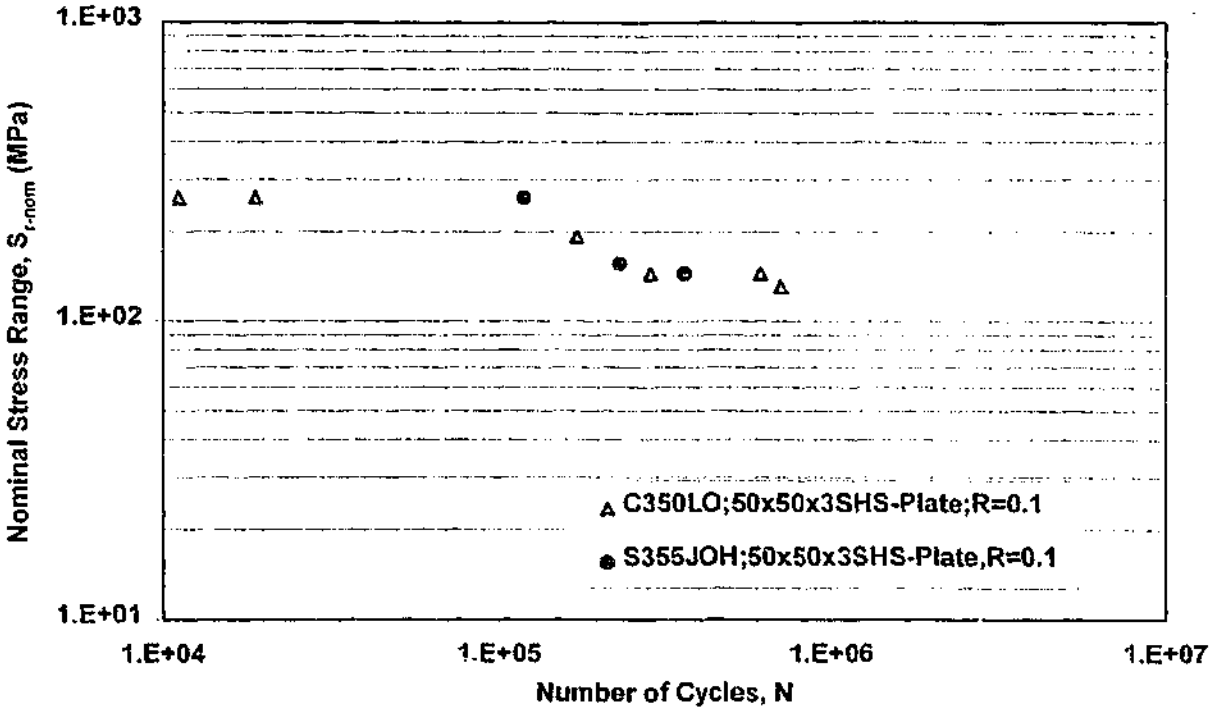

Figure 5-7: Plot of S-N data for 3mm thick tubes, at R=0.1 to show effect of stress grade

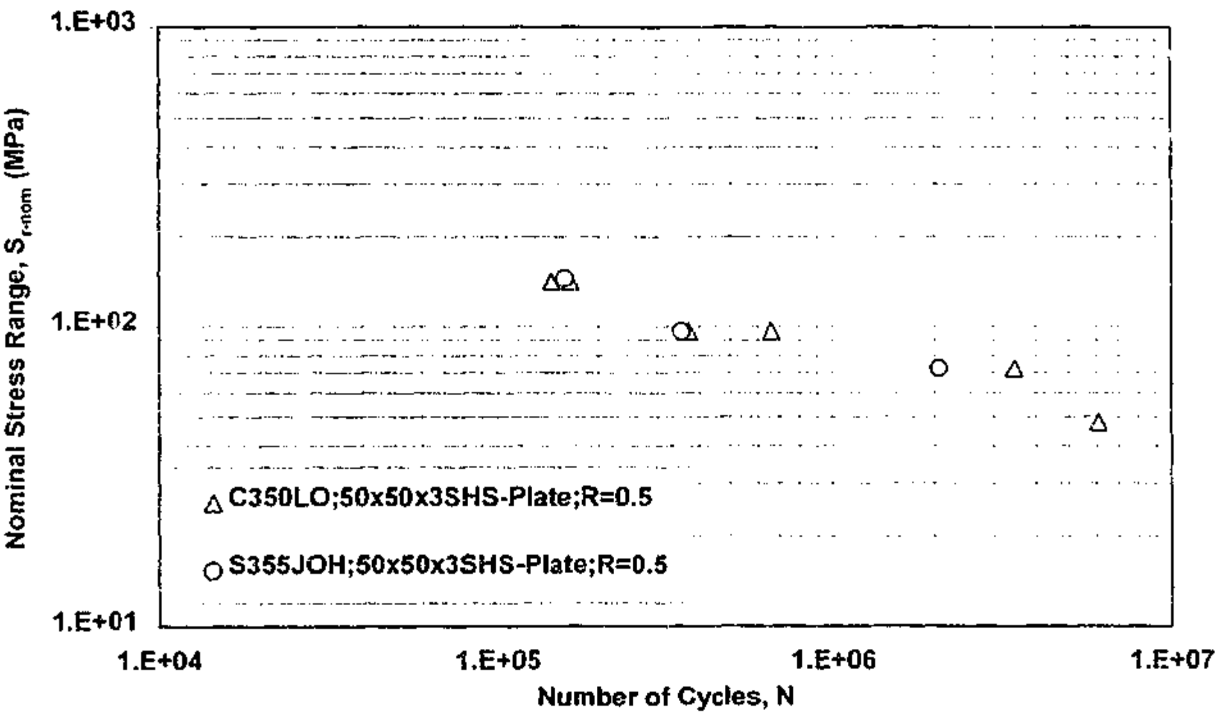

Figure 5-8: Plot of S-N data for 3mm thick tubes, at R=0.5 to show effect of stress grade

5.4.2 Effect of Galvanizing on Fatigue Strength

All the tubes used to make the specimens for fatigue test are cold-formed. However Grade C450LO steel, also known as DuraGal is produced using an "in-line" galvanizing process. In making DuraGal, the square hollow sections are coated on the exterior surface by in-line hot-dip galvanizing with a minimum average coating of 100g/m^2 of zinc and are further protected with a passivation coating. The other steel sections from grades C350LO and S355JOH are non-galvanized. The galvanized tubes are welded in their natural state without removing the galvanizing. Compared to black steel a 0.5volt to 1volt increase in voltage, is enough to maintain a given arc length while welding galvanized steel if the speed is kept constant (Tubemakers of Australia 1994).

Fatigue tests for the 3mm thick square hollow sections have been carried out on both the non-galvanized and galvanized cold-formed welded connections. In order to be able to determine the effect of in-line galvanizing on fatigue strength of these joints, S-N data is plotted for specimens with the same stress ratio and thickness, but different surface finishings. Stress grade has been shown not to affect fatigue strength of welded connections (Noordhoek *et al* 1980) and also in the previous Section, 5.4.1. As such S-N data of galvanized square hollow section connections are compared to data of all non-galvanized square hollow section connections with the same thickness and stress ratio. These plots are shown in Figure 5-9 for the connections made from 3mm thick tubes of steel grade DuraGal C450LO, C350LO and S355JOH, tested at a stress ratio of 0.1 and in Figure 5-10 for the connections made from 3mm thick tubes tested at a stress ratio of 0.5. Figure 5-11 also shows the S-N data plots for the connections made from 2mm thick tubes of grade C450LO and S355JOH tested at a stress ratio of 0.1.

It can be deduced that there is no visible trend of the effect of in-line galvanizing on the tube-to-plate welded connections although small root inclusions have been observed in galvanized steel connection macrographs. As the zinc coating vaporizes during welding it might be entrapped in the weld metal forming these inclusions. Fatigue cracks in the tube-to-plate T-joints were observed to initiate at the corner of the brace, on the toe of the weld at the brace-plate interface. This is the point of maximum principle stress in the connection. As such the inclusions which may occur at the root of the weld are likely to have no significant influence on fatigue strength of the galvanized tube-to-plate T-joints.

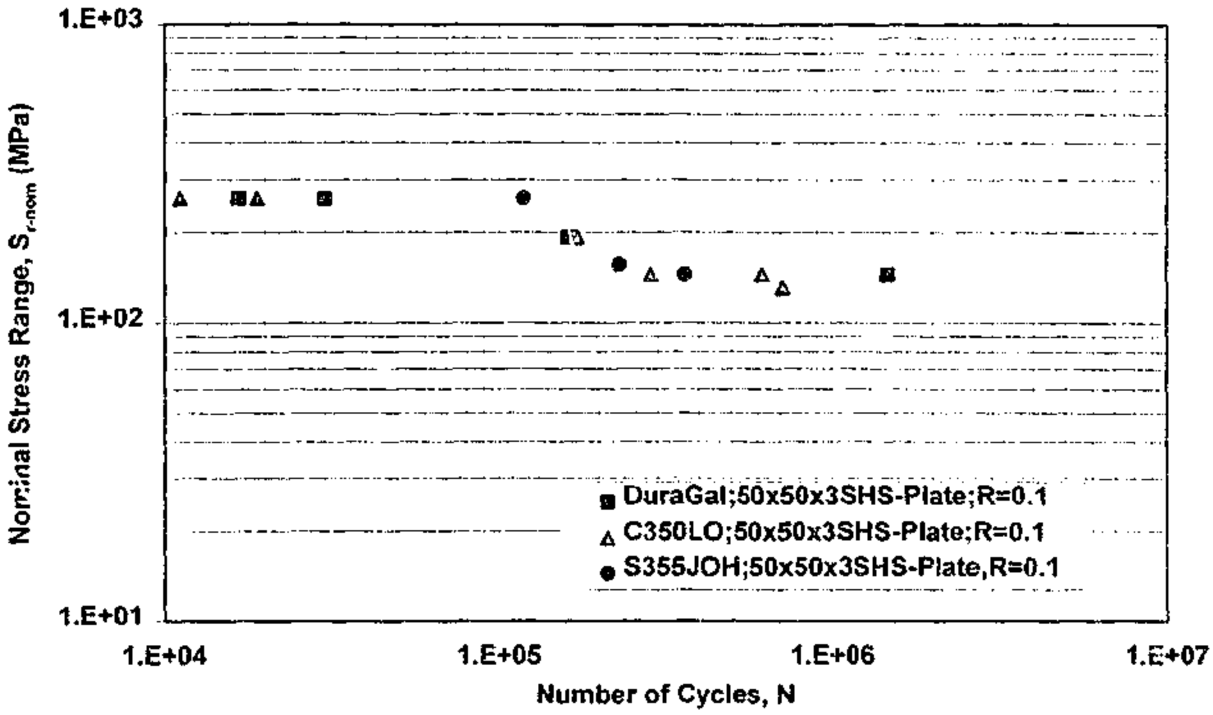

Figure 5-9: Plot of S-N data for 3mm thick tubes at R=0.1 to show effect of galvanizing

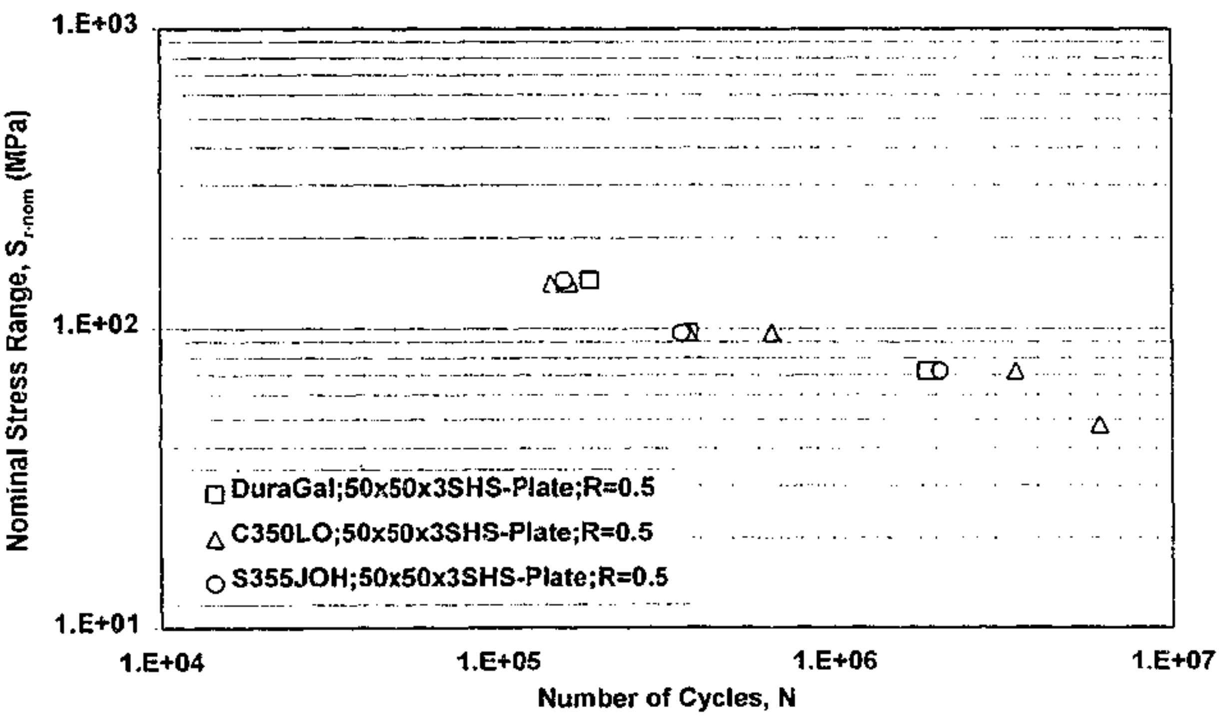

Figure 5-10: Plot of S-N data for 3mm thick tubes at R=0.5 to show effect of galvanizing

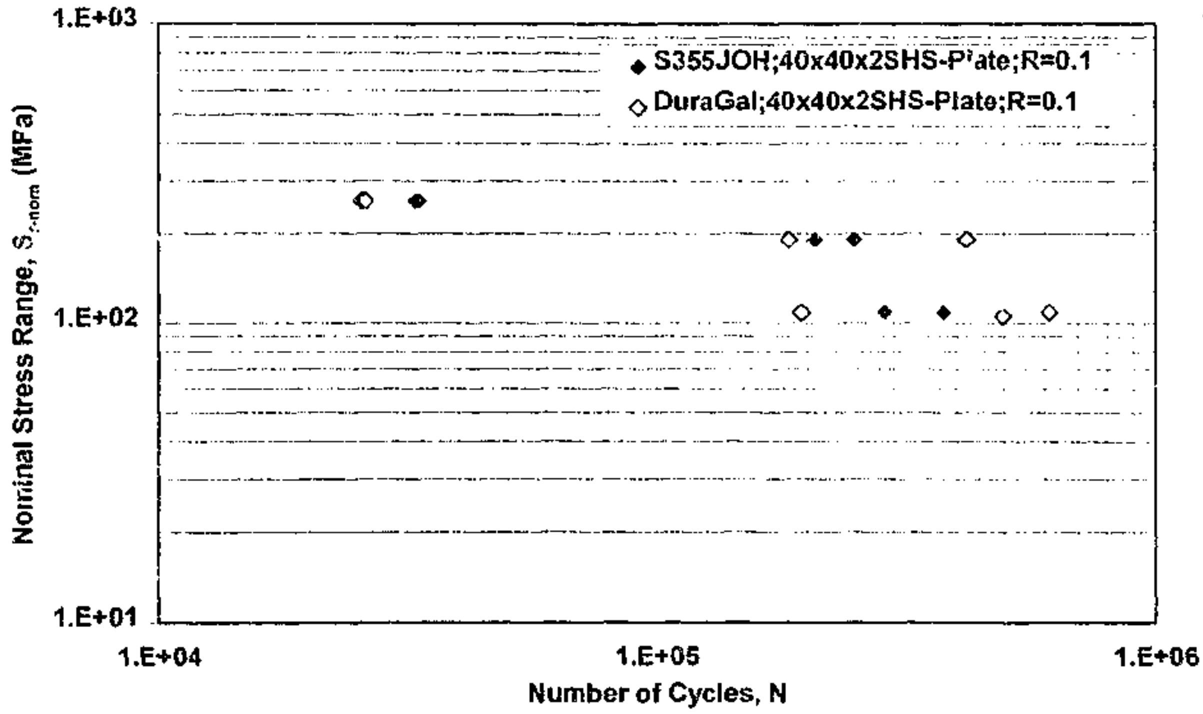

Figure 5-11: Plot of S-N data for 2mm thick tubes at R=0.1 to show effect of galvanizing

5.4.3 Effect of Stress Ratio

The tube-to-plate T-joints, made from 3mm thick square hollow section tubes were tested at two different stress ratios of 0.1 and 0.5. This was done to determine the influence of stress ratio on fatigue strength of these connections.

The influence of stress ratio is obtained as a general trend by the use of mean S-N curves through fatigue data for the different stress ratios. Figure 5-12 shows a plot of fatigue data for the two different stress ratios. The data for the two stress ratios has been analyzed using the least-squares method to determine the mean S-N curve for each stress ratio. Both the parameters A and B in the linear model $log\ N = A + B \cdot logS$ were determined from least-squares, producing curves of different slopes. These S-N curves take the natural slope of the available data. Figure 5-12 shows that there is a difference in fatigue life between the two stress ratios, with the life at the stress ratio of 0.1 being longer than that at a stress ratio of 0.5. The difference in fatigue life also tends to increase as the stress range decreases.

Figure 5-13 also shows a plot of fatigue data for the two different stress ratios. The data, in Figure 5-13 has been analyzed using the least-squares method to determine the mean

S-N curve for each stress ratio, with the inverse of the slope B fixed to –3. The inverse of the slope is normally adopted as –3 in design standards such as the Canadian Standard, CAN/CSA-S16.1-M89 (CSA 1989). Figure 5-13 also shows that there is a difference in fatigue life between the two stress ratios.

Figures 5-12 and 5-13 demonstrate the fact that the damaging effect of a fully tensile cyclic stress range tends to increase as the mean stress or stress ratio increases (Maddox 1991).

Traditionally the effect of stress ratio on fatigue life of welded connections is negligible and is not a factor considered in design S-N curves. This is because there exists tensile residual stresses of yield stress magnitude in welded connections. The application of external forces in welded connections means that cycling starts at stresses up to yield stress magnitude irrespective of the load applied. The influence of stress ratio realized in the tested thin-walled connections especially at lower stresses, shown by Figures 5-12 and 5-13, might be due to the fact that the residual stress distribution in these specimens is such that the tensile residual stresses at the weld toes where the cracks initiate, are not as high as the yield stress value. Further work needs to be carried out on the distribution of residual stresses in tube-to-plate T-joints made up of thin-walled tubes before a definitive conclusion can be reached.

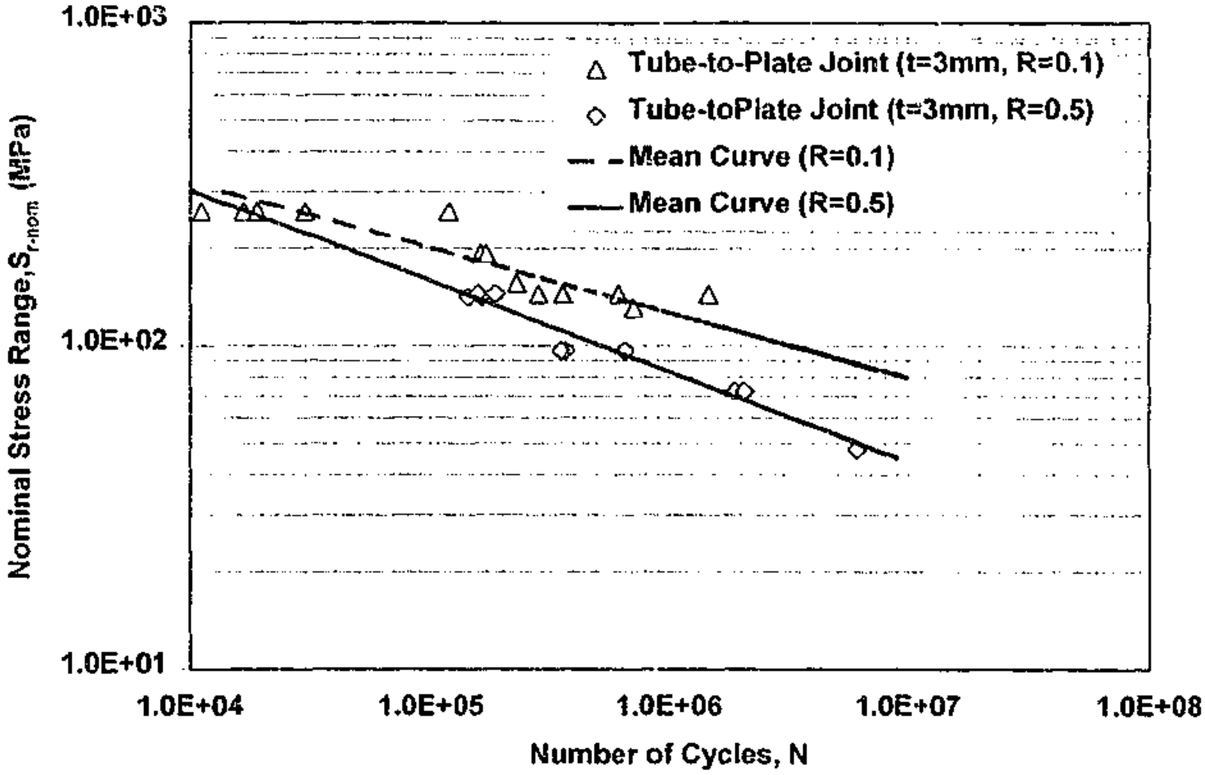

Figure 5-12: Effect of stress ratio, mean S-N curves at natural slope

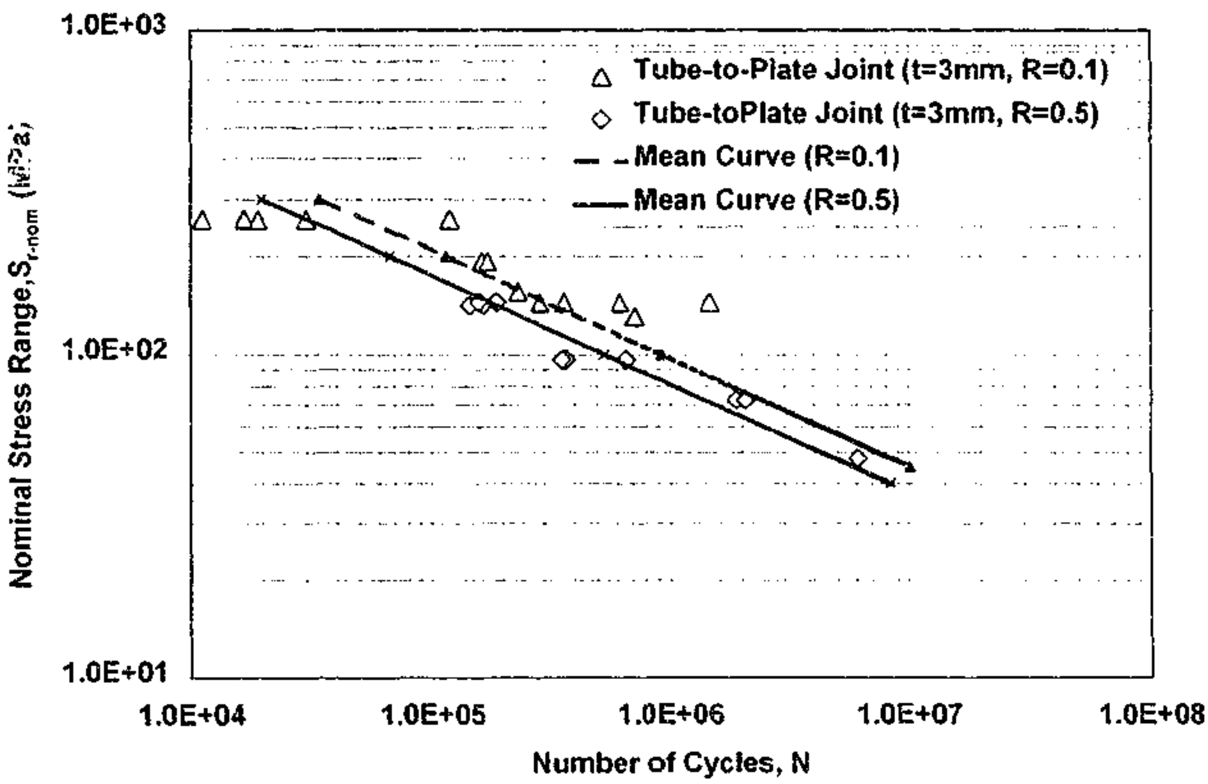

Figure 5-13: Effect of stress ratio, mean S-N curves with inverse of slope = -3

5.4.4 Effect of Tube Wall Thickness

A plot of the S-N data for the 3mm, 2mm and 1.6mm tube-to-plate T-joints is shown in Figure 5-14. Because it has been shown that there is an influence on fatigue strength caused by stress ratio, results corresponding to a stress ratio of 0.1 only are discussed here. Using a deterministic approach it can be concluded that for lower nominal stress ranges the lower bound of the scatter is determined by the thinner sections of 2mm and 1.6mm. This may be a result of defects such as undercut. In those connections where these defects occur, they may have a greater influence on fatigue strength on the thinner sections of 2mm and 1.6mm compared to the 3mm thick sections.

Other researchers have found an increase in fatigue strength as the wall thickness of the tubes failing under fatigue decreases (van Wingerde *et al* 1996a, 1997b,c). This thickness effect has resulted in design rules in some current design guides such as the CIDECT Design Guide (Zhao *et al* 1999a) and IIW Fatigue Design Procedure (IIW 2000), to introduce S-N curves which show an increase in fatigue strength as the wall thickness of the failed member decreases. There is experimental evidence to support this phenomenon for wall thicknesses of 4mm and greater (van Wingerde 1992).

In Figure 5-14, the increase in fatigue life, which is normally observed as the tube wall thickness decreases, is not realized. Instead, the smaller wall thickness tubes have produced fatigue data defining the lower bound of the scatter, especially at lower nominal stress ranges.

Fatigue tests of axially loaded end-to-end connections, reported by Noodhoek *et al* (1980), also showed that fatigue life was slightly better for the thicker sections. There is difficulty associated with welding smaller wall thickness sections.

A plot of mean regression S-N curves, Figure 5-15, shows that the nominal stress range at 2 million cycles decreases with reduced tube wall thickness of the member under failure. Figure 5-15 shows the mean S-N curves with the natural slope of the data, that is both A and B in the relationship $\log N = A + B \cdot \log S$ are determined.

Figure 5-16 shows a plot of the 3mm and 1.6mm thick tube results only. It can be seen that without the results for the 2mm thick tubes, it is clear that there is a reduction in fatigue life for the thinner tube wall specimens. The results for the 2mm thick tubes have a significant amount of scatter, probably as a result of specimens with very small weld toe undercut defects to those with weld toe undercut defects of significant size. However the mean S-N curve for the 2mm thick tubes still falls between that for the 3mm and 1.6mm thick tubes, despite the noticeable scatter associated with these results.

The mean S-N curves for the 3mm and 1.6mm thick tubes as shown with a natural slope, Figure 5-16, tend to converge at higher stress levels. This is in agreement with the analysis of the results in the low cycle fatigue range where no thickness effect was found (van Delft *et al* 1985; van der Vegte 1988; de Back *et al* 1989)

Figure 5-17 shows the mean S-N curves for the 3mm, 2mm and 1.6mm thick tubes, where the S-N curves have been designated an inverse of the slope, B of −3, as is normally the case for design S-N curves in some design guidelines (SAA 1998a). Even with the inverse of the slope of the curves fixed at −3 the mean S-N curves still show reduced fatigue life for the thinner tube wall thicknesses.

The reduced fatigue life of welded thin-walled specimens can be attributed to the greater negative impact of weld toe undercut on fatigue propagation life as reported in Mashiri *et al* (1998b, 2000b) and detailed in Chapter 7.

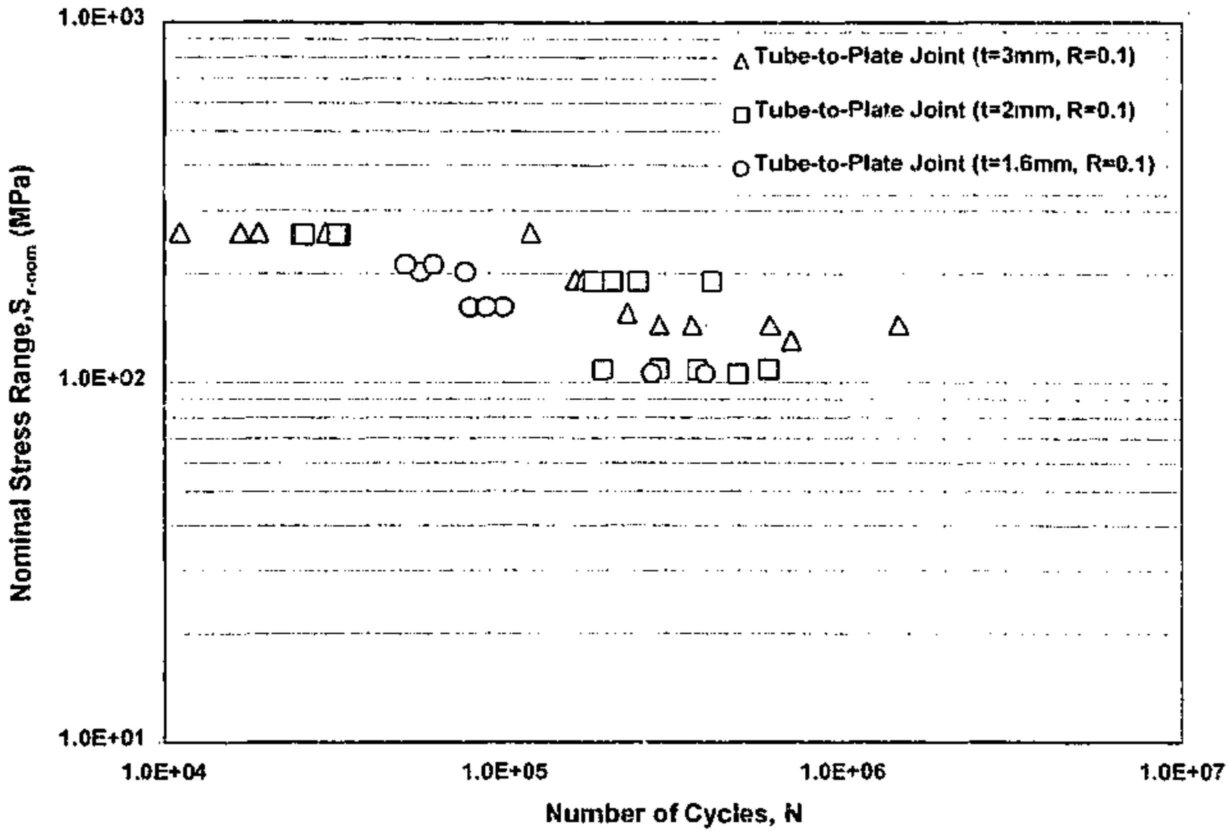

Figure 5-14: Plot of S-N data to show the effect of tube wall thickness on fatigue

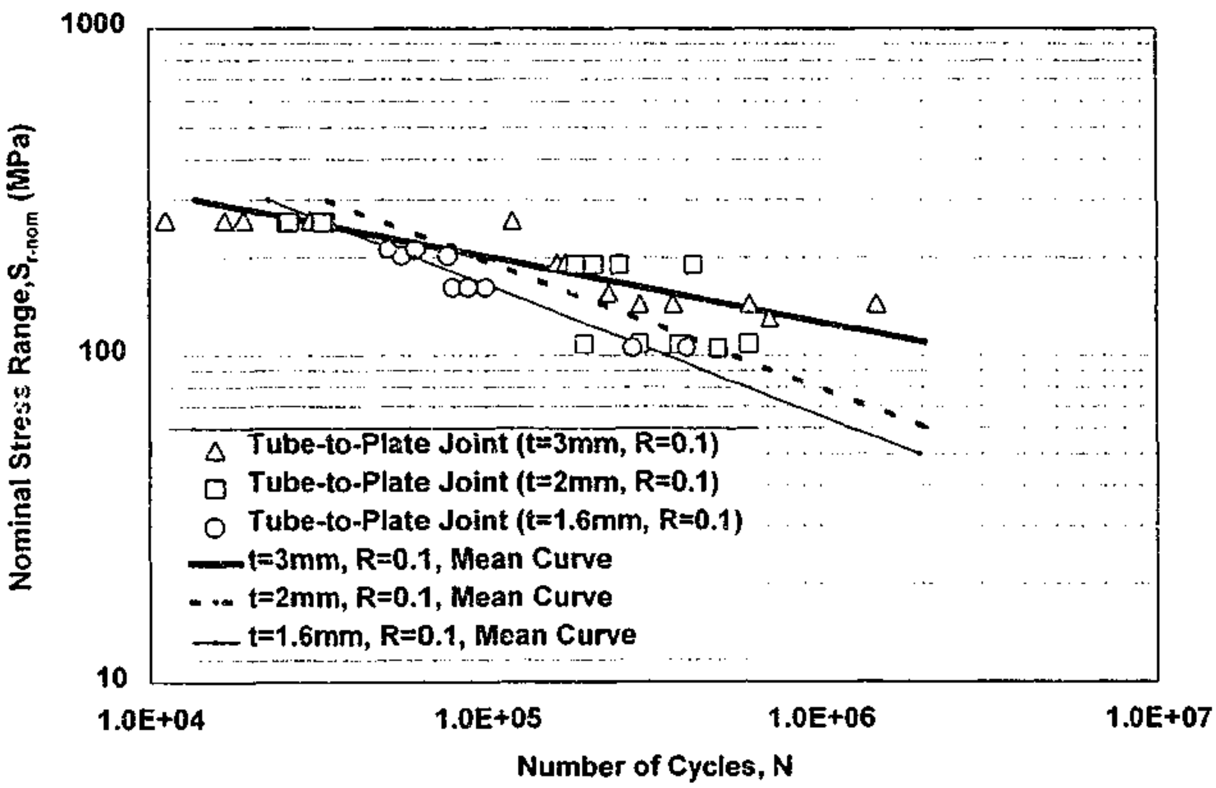

Figure 5-15: Effect of tube wall thickness on fatigue: Mean S-N curves with natural slope

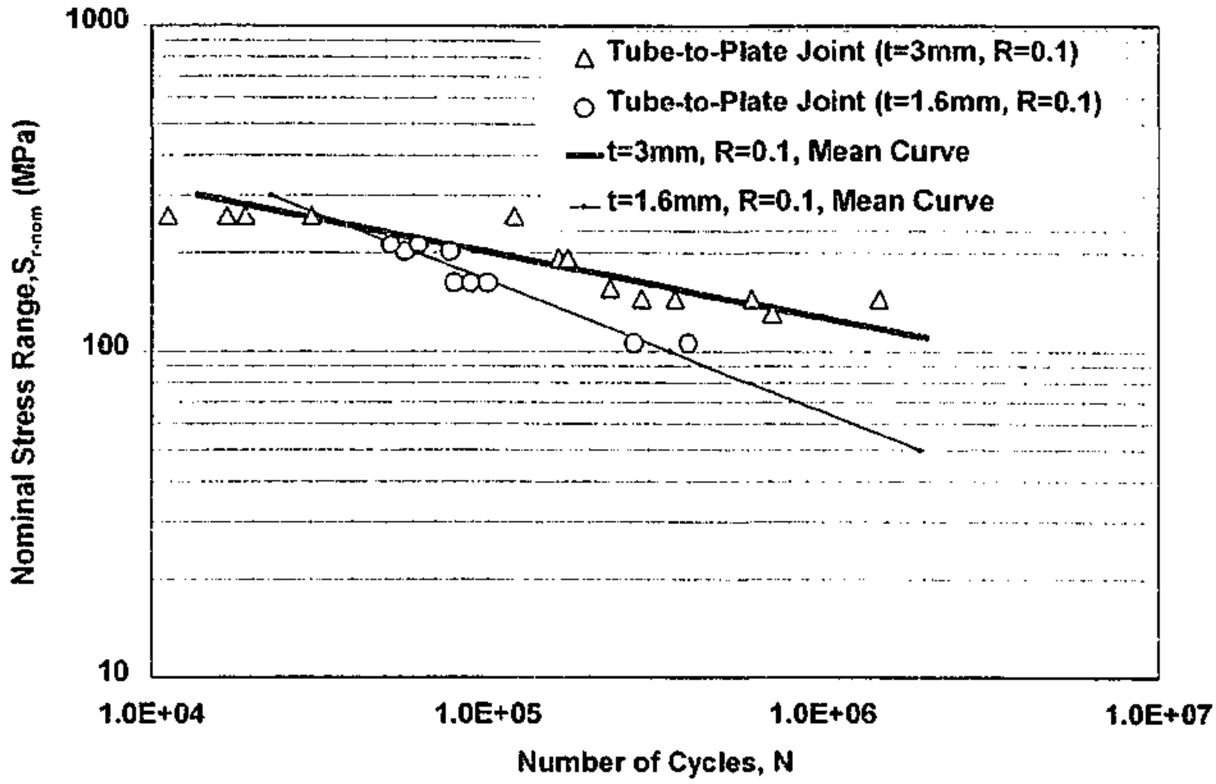

Figure 5-16: Effect of tube wall thickness on fatigue; mean S-N curves for 3mm & 1.6mm tubes

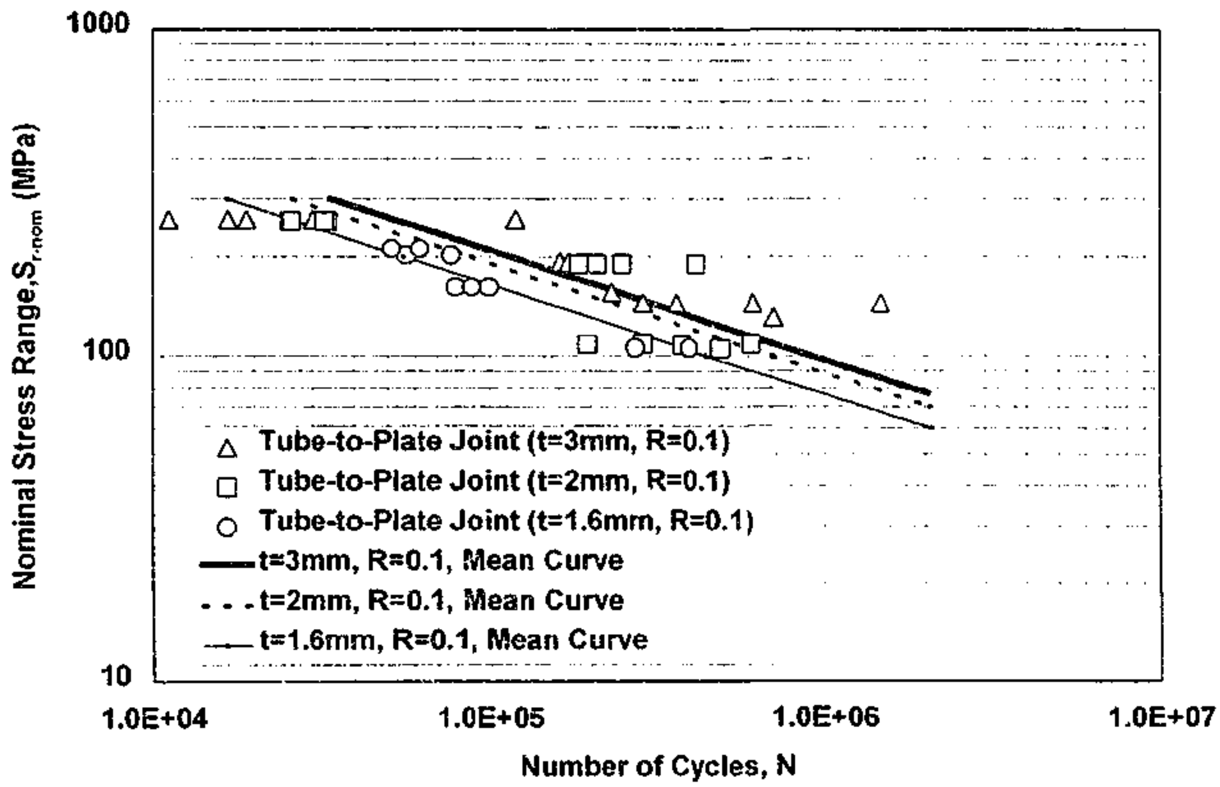

Figure 5-17: Effect of tube wall thickness on fatigue; Mean S-N curves with slope = -3

Table 5-6 shows the nominal stress range at 2 million cycles for the mean S-N curves, for each tube wall thickness. The values of nominal stress range at 2 million cycles for the two cases, where the natural slope of the S-N data for each thickness has been adopted and where the inverse of the slope of the mean S-N curves has been forced to a value of –3, are given. There is a reduction in the nominal stress range at 2 million cycles with decrease in tube wall thickness.

A plot of the nominal stress range at 2 million cycles for the mean S-N curves versus tube wall thickness confirms the fall in fatigue strength with reduction in tube wall thickness for tubes with thicknesses below 4mm, see Figure 5-18. The two cases are given by the following relationships:

(i) B=3, $S_{r-nom.2mil.mean} = 52.707t^{0.3623}$ **(5.1)**

(ii) B determined, $S_{r-nom.2mil.mean} = 25.994t^{1.2976}$ **(5.2)**

where $S_{r-nom.2mil.mean}$ is the nominal stress range at 2million cycles for mean S-N curve for a given tube wall thickness, t.

The thickness correction factor in current design standards, AS4100-1998 (SAA 1998a) and the Department of Energy (1990) are:

$$S_{r.t} = S_{r.25}\left(\frac{25}{t}\right)^{1/4} \text{ and} \tag{5.3}$$

$$S_{r.hs.t} = S_{r.hs.32}\left(\frac{32}{t}\right)^{1/4} \tag{5.4}$$

repectively. Equations 5-3 and 5-4 give a relationship between fatigue strength and thickness of the form;

$$S \propto t^{-0.25}, \tag{5.5}$$

for larger wall thicknesses. This thickness correction shows that the stress range is inversely proportional to the thickness raised to the power of one quarter. This relationship shows that the fatigue strength of a specimen decreases with an increase in thickness of the failed member.

The relationships shown in equations 5.1 and 5.2, for thicknesses less than 4mm give a relationship between fatigue strength and thickness of the form;

$$S \propto t^{m}, \tag{5.6}$$

where the value m is positive. This shows that fatigue strength in specimens of thicknesses less than 4mm decrease with a decrease in thickness of the failed member.

Table 5-6: Nominal stress range at 2 million cycles for mean S-N curves and different tube wall thicknessess below 4mm

Tube wall thickness, *t*	Nominal stress range at 2 million cycles for mean S-N curve (MPa)	
	Natural slope of S-N data, i.e *B* determined (From Figure 5-15)	**Slope of S-N data fixed at *B*=-3** (From Figure 5-17)
3.0mm	110.2	77.3
2.0mm	60.6	70.7
1.6mm	49.5	60.8

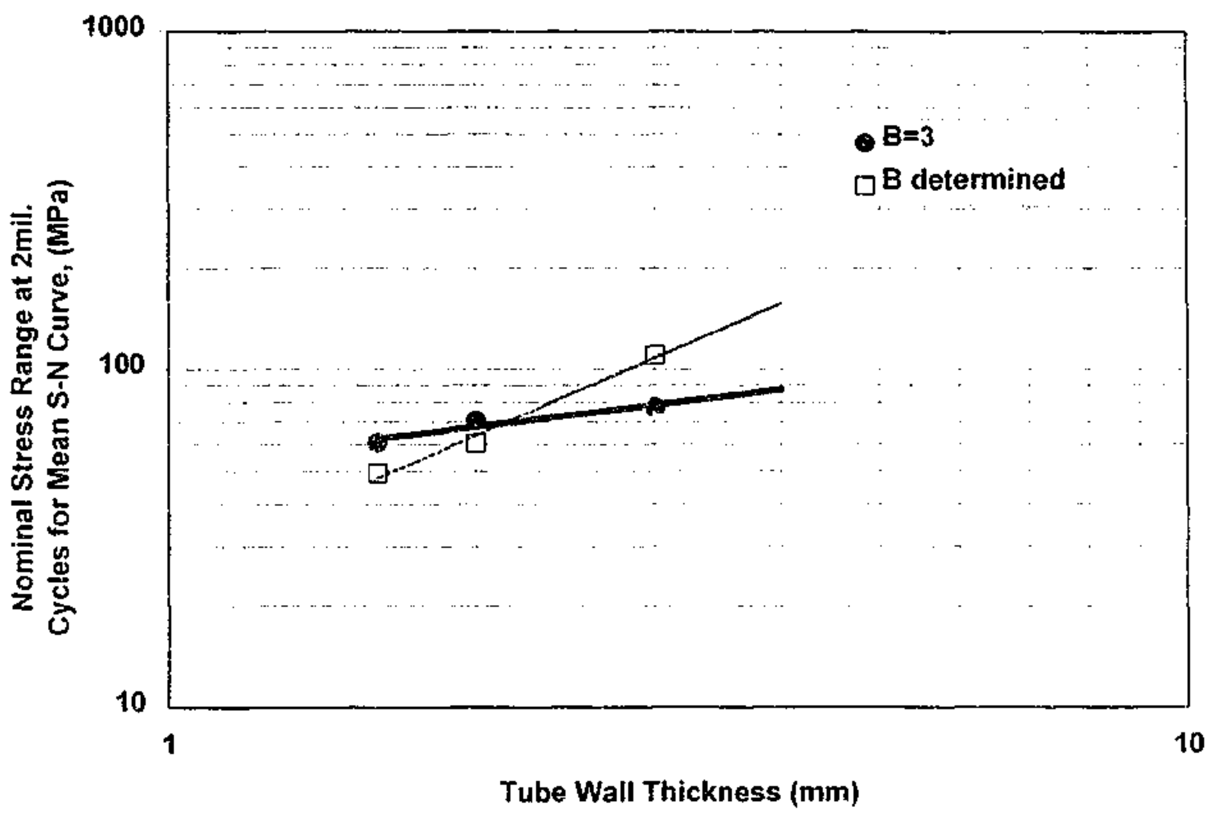

Figure 5-18: Plot of nominal stress range at 2 million cycles for mean S-N curves versus tube wall thickness

5.5 EXPERIMENTAL DETERMINATION OF STRESS CONCENTRATION FACTORS

The hot spot stresses in tube-to-plate T-joints were determined experimentally. This is done with the use of strain gauges. In order to know the hot spot location, the position of maximum principal stress in the join should be determined. This can be done using numerical methods. In this research models of the tube-to-plate joints were analysed (Mashiri *et al* 2000b). Both the numerical analysis and fatigue tests of the connections showed that the initiation point for fatigue cracks was at the weld toe in the brace, on the corner of the brace, at the brace-plate interface. No cracks initiated or propagated in the plates. The position of the initiation cracks was consistent with the region where hot spot stresses normally occur in rectangular or square hollow sections nodal joints (Zhao *et al* 1999a).

Extrapolation for hot spot stresses in tube-to-plate T-joints made of square hollow section tubes of wall thicknesses less than 4mm is made difficult by the small distances involved. Distances required in extrapolation for hot spot stresses for these joints, in the brace, where the cracks initiated and propagated, are shown in Table 5-7. The distances are calculated using the recommendations given by van Wingerde (1992). Table 5-7 shows the distances required in both linear and quadratic extrapolation, for the sizes of tubes used in this investigation. Since the strain gauge positions do not coincide with the second point required for extrapolation, the stress at the second point of extrapolation is determined from the trend of the curve fitted through all the measured values. For quadratic extrapolation, where the thickness of the tube is such that the second point falls in between the first two gauge positions like in the 1.6mm thick tubes, the three points that were used for extrapolation were; the first point corresponding to the first gauge position, the point determined from the curve fit at $0.6t$ away from the first point and the point determined from the curve fit at $1.0t$ away from the first point. Extrapolation for hot spot stresses is carried out along predefined lines A to E shown in Figure 5-19.

The stress concentration factors (SCFs) in this work are based on stress perpendicular to the toe of the weld. Strains perpendicular to the toe of the weld can be measured by simple strain gauges instead of strain gauge rosettes (Romeyn *et al* 1992, van Wingerde *et al* 1992). The use of stresses or strains perpendicular to the weld toe is recommended by the CIDECT Design Guide No. 8 (Zhao *et al* 1999a), AWS (1998) and API (1991) fatigue design guidelines.

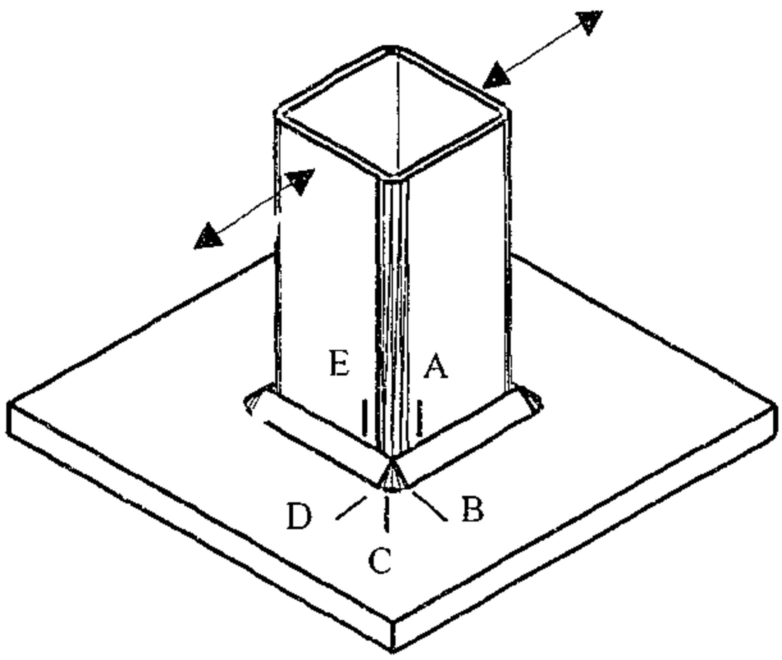

Figure 5-19: Lines A to E, along which extrapolation for hot spot stresses is recommended, for Tube-to-plate T-joints

Table 5-7: Distances required for extrapolation in determining hot spot stresses for tube-to-plate T-joints in the brace for t<4mm

Connection	Distances for Extrapolation in Brace			
	Linear Extrapolation (2 points)		Quadratic Extrapolation (3 or more points, other points are between 1st point and 2nd point)	
	1st point (0.4t_1, but not less than 4mm from weld toe)	**2nd Point** (0.6t_1 further away from 1st Point)	**1st point** (0.4t_1, but not less than 4mm from weld toe)	**2nd Point** (1.0t_1 further away from 1st Point)
S1PL2R2B (50x50x3SHS-Plate)	4mm	1.8mm	4mm	3mm
S2PL3R2A (50x50x1.6SHS-Plate)	4mm	0.96mm	4mm	1.6mm
D7PL2B (40x40x2SHS-Plate)	4mm	1.2mm	4mm	2mm

Detailed drawings of the positions of strip gauges which were used to capture the stress gradient perpendicular to the toe of the weld along lines A and E in the brace are shown in, Figures D1 to D3, Appendix D. The strip gauges used are Showa Measuring Instruments, foil strain gauges, R51-FA-1-120-11. These gauges have a base length and width of 11mm and 4mm respectively. The grid length and width, for each of the 5 individual gauges making the strips, are 1.0mm and 0.5mm respectively. The distance between the centre lines of consecutive individual gauges in the strip is 1.75mm.

All other strain gauge positions shown in Figures D1 to D3 were strain gauged using Micro-Measurements Division, CEA-Series Student gauges, CEA-06-240UZ-120.

5.5.1 Conversion of Strains to Stresses

The strains measured using the strip gauges can be converted to stresses using Hooke's Law (van Wingerde 1992):

$$\sigma_x = \frac{E}{1-\nu^2}\left(\varepsilon_x + \nu\left(\varepsilon_y + \varepsilon_z\right)\right) \qquad \textbf{(5.7)}$$

If x is the direction perpendicular to the weld and assuming that strains in the other direction are small,

$$\sigma_x = \frac{E}{1-\nu^2}\left(\varepsilon_x\right) \qquad \textbf{(5.8)}$$

If the poisson's ratio is taken as equal to 0.3,

$$\sigma_x = \frac{E}{1-\nu^2}\left(\varepsilon_x\right) = \frac{E}{0.91}\left(\varepsilon_x\right) = 1.1E\varepsilon_x \qquad \textbf{(5.9)}$$

This is also the relationship which was found to exist between strain concentration factors and stress concentration factors (Hertogs *et al* 1989). In tests on multiplanar joints made of circular hollow sections, Romeyn *et al* (1992) found the ratio of SCF to SNCF to have values between 1.0 and 1.4.

5.5.2 Nominal Stresses from Strain Gauge Measurements

Strain gauges were installed in the brace to determine the nominal stresses at the brace-plate interface due to applied loads. This allowed independent confirmation of the stresses determined from applied loads using the calibrated load cell and load cell exciter. Three student gauges were installed at the tension side and one on the compression side of the brace. The gauges were positioned so that they could measure nominal stresses as determined from simple theory.

Using the St Venant's principle the strain gauges were placed at a distance b_1 from the brace-plate interface. At a distance of the width (b_1) of the member away from the support or load application, the stress is almost uniform as a result of the reduction in stress concentrations caused by the end conditions.

The plot of the stresses on the tension side of the brace derived from the strain gauges is shown in Figures E1, E4 and E7, Appendix E, for the 50x50x3SHS-Plate, 50x50x1.6SHS-Plate and 40x40x2SHS-Plate connections respectively. For each connection strains were measured at four different load levels. The load levels were taken to be below the maximum elastic moment. The maximum elastic moment is the moment below which the joint behaves elastically as determined from moment-deflection graphs (Mashiri *et al* 1999b, 1999c).

Table 5-8 shows the predicted values of nominal stress at the brace-plate interface using the simple beam theory and the results obtained from strain gauge measurements for comparison. The nominal stresses from both methods of estimation have a percentage difference of less than 8% in all cases. A plot of the simple beam theory nominal stress and experimental nominal stress, shows a linear trend close to the 45^0 line between the stresses determined using the two different methods, Figure 5-20. A high correlation coefficient of 0.99 exists between the beam theory and experimental nominal stresses, showing that the nominal stresses applied using the fatigue rig testing system can be determined using simple beam theory.

Table 5-8: Comparison of stresses from strain gauge measurements and beam theory

Connection	Load (kN)	Beam Theory Nominal Stress σ_{nom} (MPa)	Experimental Nominal Stress $\sigma_{nom,exp}$ (MPa)	% Difference
S1PL2R2B (50x50x3SHS-Plate)	2.5	104	98	-5.8
	3.5	146	147	0.7
	4.6	191	193	1.0
	5.0	208	208	0
S2PL3R2B (50x50x1.6SHS-Plate)	1.5	104	111	6.7
	2.0	138	148	7.2
	2.5	173	185	6.9
	3.0	208	224	7.7
D7PL2B (40x40x2SHS-Plate)	1.5	140	149	6.4
	2.0	187	198	5.9
	2.5	233	247	6.0
	3.0	280	300	7.1

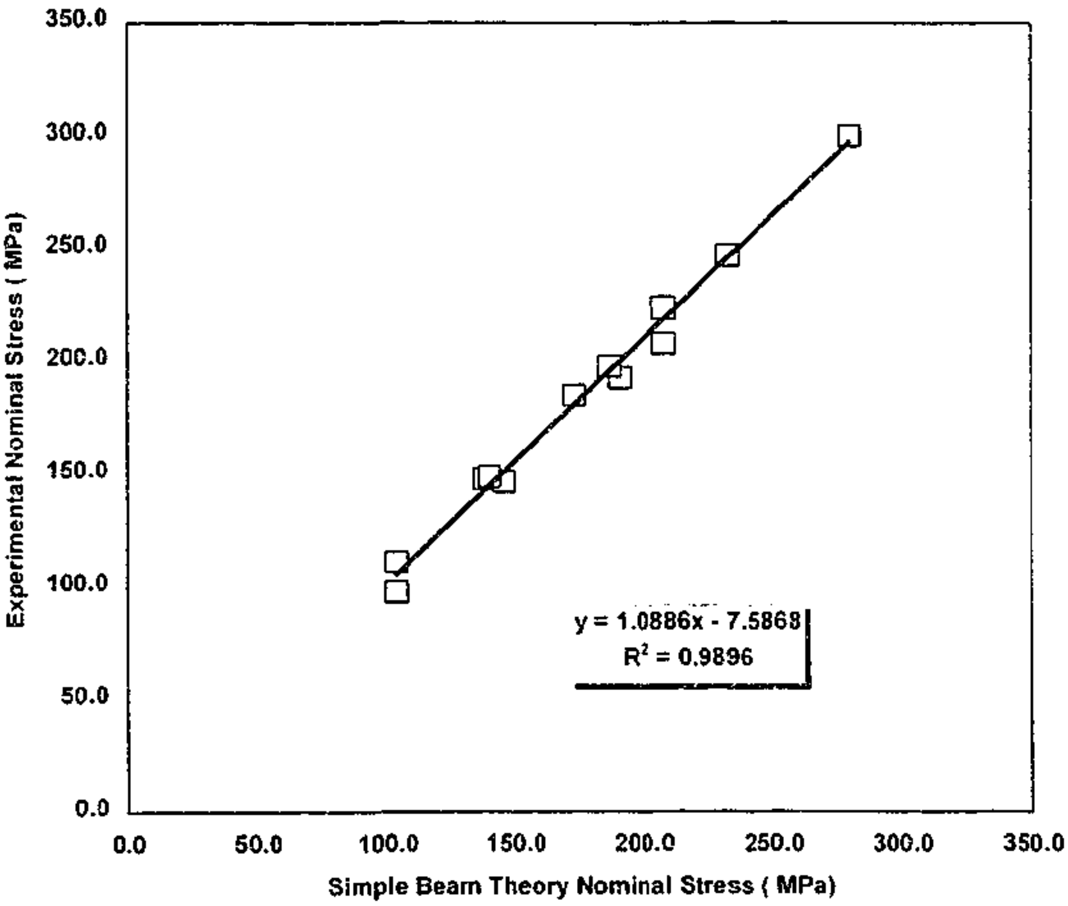

Figure 5-20: Plot of simple beam theory nominal stress versus experimental nominal stress

5.5.3 Hot Spot Stresses from Strain Gauge Measurements

The hot spot stresses for each of the tube-to-plate T-joints were determined at four different load levels. The loads applied to each connection were below the maximum elastic moment for the joints. The maximum elastic moment for each joint is the maximum moment below which the connection behaves elastically under load as determined from the moment-deflection and moment-angle of inclination graphs obtained from static tests (Mashiri *et al* 1999b, 1999c).

Figures E2, E3, E5, E6, E8 and E9, Appendix E, show the graphs for the tube-to-plate connections for lines A and E. These are the lines where the cracks initiated and hence the positions of the hot spots. The graphs of the stress distributions show parallel curves for each of the different load levels. This confirms the elastic behaviour of the joints under the different load levels.

For each load level the hot spot stresses were determined using both the linear and quadratic extrapolation methods. The linear extrapolation method produces the straight lines and the quadratic extrapolation produces the curved lines in the Figures in Appendix E. The distances used for extrapolation are those shown in Table 5-7, as determined by guidelines (van Wingerde 1992; IIW 2000; Zhao *et al* 1999a)

A summary of the hot spot stresses and the resultant SCF are shown in Table 5-9 for each connection at different load levels. The stress concentration factors for line E are higher than those for line A. This is expected, as the normal stress on a cross section under bending decreases towards the neutral axis. The stress concentration factors determined by the quadratic extrapolation method are slightly higher than those determined by the linear extrapolation method. The ratios of the stress concentration factors determined by the quadratic extrapolation method, (SCF_q) to the stress concentration factors determined by the linear extrapolation method (SCF_l) range from 1.04 to 1.18. The stress distribution for the tube-to-plate T-joints are not as highly non-linear as the stress distribution at hot spots obtained for tube-to-tube T-joints as reported in Chapter 6. This generally results in smaller SCF for the tube-to-plate T-joints compared to the SCF for the tube-to-tube T-joints.

Table 5-9: Determination of SCF, Lines A and E, Tube-to-plate T-joints

Connection	Position	Load (kN)	Nominal Stress, σ_{nom} (MPa)	Linear Extrapolation			Quadratic Extrapolation			$\frac{SCF_q}{SCF_l}$
				σ_{hs} (MPa)	SCF	SCF_l Average	σ_{hs} (MPa)	SCF	SCF_q Average	
S1PL2R2B (50x50x3 SHS-Plate)	Line E	2.5	104	172.84	1.7	1.625	191.82	1.8	1.775	1.09
		3.5	146	228.95	1.6		249.11	1.7		
		4.6	191	309.56	1.6		342.88	1.8		
		5.0	208	336.15	1.6		381.74	1.8		
	Line A	2.5	104	109.52	1.1	1.1	136.40	1.3	1.3	1.18
		3.5	146	155.95	1.1		182.56	1.3		
		4.6	191	209.88	1.1		257.67	1.3		
		5.0	208	227.97	1.1		274.40	1.3		
S2PL3R2A (50x50x1.6 SHS-Plate)	Line E	1.5	104	149	1.4	1.475	162	1.6	1.575	1.07
		2.0	138	203	1.5		219	1.6		
		2.5	173	259	1.5		272	1.6		
		3.0	208	308	1.5		320	1.5		
	Line A	1.5	104	121	1.2	1.2	134	1.3	1.25	1.04
		2.0	138	161	1.2		170	1.2		
		2.5	173	200	1.2		211	1.2		
		3.0	208	245	1.2		262	1.3		
D7PL2B (40x40x2 SHS-Plate)	Line E	1.5	140	203.67	1.5	1.425	228.43	1.6	1.6	1.12
		2.0	187	258.67	1.4		292.29	1.6		
		2.5	233	321.33	1.4		374.86	1.6		
		3.0	280	391.33	1.4		461.43	1.6		
	Line A	1.5	140	135.80	0.97	0.965	144.54	1.03	1.025	1.06
		2.0	187	178.25	0.95		194.40	1.04		
		2.5	233	222.57	0.96		236.71	1.02		
		3.0	280	273.08	0.98		283.75	1.01		

NOTES:

1. Linear Extrapolation for 50x50x3SHS-Plate: t_1 = 3mm, two points (i) 0.4 t_1 but not less than 4mm = 4mm (ii) 0.6t_1 further away from fist point = 1.8mm.
2. Quadratic Extrapolation for 50x50x3SHS-Plate: t_1 = 3mm, two or more points (i) 0.4 t_1 but not less than 4mm = 4mm (ii) 1.0t_1 further away from fist point = 3mm (iii) all points between points (i) and (ii).
3. Linear Extrapolation for 40x40x2SHS-Plate: t_1 = 2mm, two points (i) 0.4 t_1 but not less than 4mm = 4mm (ii) 0.6t_1 further away from fist point = 1.2mm.
4. Quadratic Extrapolation for 40x40x2SHS-Plate: t_1 = 2mm, two or more points (i) 0.4 t_1 but not less than 4mm = 4mm (ii) 1.0t_1 further away from fist point = 2mm (iii) all points between points (i) and (ii).
5. Linear Extrapolation for 50x50x1.6SHS-Plate: t_1 = 1.6mm, two points (i) 0.4 t_1 but not less than 4mm = 4mm (ii) 0.6t_1 further away from fist point = 0.96mm.
6. Quadratic Extrapolation for 50x50x1.6SHS-Plate: t_1 = 1.6mm, two or more points (i) 0.4 t_1 but not less than 4mm = 4mm (ii) 1.0t_1 further away from fist point = 1.6mm (iii) all points between points (i) and (ii).

5.6 SUMMARY

Tube-to-plate T-joints made up of square hollow section tubes welded to a plate were fatigue tested under in-plane bending. The following observations were made;

(a) Fatigue failure of the tube-to-plate T-joints made up of tubes of wall thicknesses less than 4mm occurs through the initiation and propagation of cracks at the toe in the brace on the corner of the brace-plate interface. The cracks initiate at both corners on the tension side of the brace, on the weld toe and propagate to form a through thickness crack along the whole length of the brace width. This leads to the separation of the brace from the plate along the weld toe in the brace and subsequently results in failure.

(b) In-line galvanizing of cold-formed tubes does not have any noticeable influence on fatigue life. Small root inclusions have been observed in macrographs from galvanised steel welded connections. However, these small root inclusions, seem not to have any impact on fatigue life since the cracks initiate from the toe of the weld and not from the root of the weld. Cracks initiate from the toe of the weld due to higher stresses at these regions.

(c) Stress grade does not influence fatigue life of the T-joints. This is because fatigue of welded connections mainly depends on the propagation of micro-cracks that are inherent in welded connections. The micro-cracks are a product of the arc welding processes (Maddox 1991). Crack propagation depends on the crack growth rate coefficient of the material through which the crack grows. Ferritic steels with a yield or 0.2% proof strength below $600N/mm^2$ operating in air all have a crack growth rate coefficient of about $3x10^{-13}$ (BSI 1991)

(d) Stress ratio has shown an influence on fatigue strength of the connections. Tests carried out using a stress ratio of 0.5 shows reduced fatigue life of the connections especially at lower nominal stress ranges, compared to those tested at a stress ratio of 0.1. The damaging effect of a fully-tensile cyclic stress range tends to increase as the mean stress or stress ratio increases (Maddox 1991).

(e) It has been demonstrated that for thinner walled tube-to-plate T-joints fatigue strength decreases with a decrease in tube wall thickness of the failed member. This is contrary to the classical fracture mechanics theory where fatigue strength is proportional to $t^{-1/4}$. This classical theory has led to the thickness correction factors in current design standards (SAA 1998a; Department of Energy 1990; EC3 1992).

For the tube-to-plate T-joints tested (t<4mm), fatigue strength has been found to be proportional to $t^{0.36}$ when the natural slopes of the S-N data was used. However fatigue strength was found to be proportional to $t^{1.3}$ if the inverse of the slope of S-N data was forced to a value of –3. There is a possibility that the effect of weld defects such as undercut may have a greater influence on fatigue strength of thinner connections, causing them to have reduced fatigue life. A detailed numerical study of the effects of weld toe undercut on welded thin-walled cruciform joints has been carried out and reported in Chapter 7. The study in Chapter 7 confirms that the reduced fatigue life of welded thin-walled specimens can be attributed to the greater negative impact of weld toe undercut on fatigue propagation life.

(f) The highest stress concentration factors were found to be located along the lines A and E on the corner of the brace on the brace-plate welded interface. These high stress concentrations on the brace toe have been manifested by initiation of fatigue cracks at these locations. Values of stress concentration factors ranging from 0.965 to 1.625 were obtained using linear extrapolation. Values of stress concentration factors ranging from 1.025 to 1.775 were obtained using quadratic extrapolation. The ratios of the stress concentration factors determined by the quadratic extrapolation method to the stress concentration factors determined by the linear extrapolation method ranged from 1.04 to 1.18. This shows that the stress distribution for tube-to-plate T-joints is not highly non-linear.

Chapter 6

FATIGUE TESTS AND EXPERIMENTAL STRESS CONCENTRATION FACTORS OF TUBE-TO-TUBE T-JOINTS

6.1 INTRODUCTION

Fatigue tests of tube-to-tube T-joints made up of square hollow sections of thicknesses less than 4mm were carried out using a multiple fatigue test rig. The joints were subjected to cyclic in-plane bending through load applied to the brace member.

Typical connection details of the tube-to-tube T-joints are shown in Figure 6-1. The length of the specimens is chosen so that the measured strains are not affected by end conditions. The measurements have to be taken at about $2b$ to $2.5b$ from the end conditions (van Wingerde, 1992). Since nominal strains were to be measured in the brace to determine the applied forces, the brace was chosen to be a length of about $5b_1$ or greater. This means that strain gauges located at mid height of the brace would not be affected by either the end plate conditions or the tube-to-tube interface conditions. The chord length was chosen to be $2.5b_o$ from the brace-chord interface. The total length of chord was chosen to be $6b_o$, allowing a value b_o for the connection of the brace to the chord. The chord member ends are pin-connected to reduce the effect of end conditions on the tube-to-tube interface, where the fatigue cracks initiate.

The square hollow sections are of three different steel grades, C350LO, C450LO and S355JOH. Table 6-1 shows the details of the series names, square hollow section sizes, stress ratio and the corresponding joint parameters for the different steel grades tested.

The modes of failure for the tube-to-tube T-joints from tubes of wall thicknesses less than 4mm under in-plane bending are described. Failure in the connections has been found to occur due to cracks developing in the brace or the chord and sometimes in both the brace and the chord.

S-N data for the tube-to-tube T-joints is given in terms of the nominal stress range. The measured leg lengths along the brace (t_{wv}) and along the chord, (t_{wh}) are given for each tested specimen. The chord and brace sizes as well as the mode of failure and steel grades are also given for each specimen tested.

Experimental stress concentration factors were determined in one connection for each connection series tested. The stresses due to the loads applied were confirmed by determining the nominal stresses through strain gauge measurements. Hot spot stresses were obtained through the use of strip strain gauges. Experimental stress concentration factors were determined from the hot spot stresses using both the linear and the quadratic method of extrapolation. The experimental stress concentration factors were compared to the values of the stress concentration factors from existing parametric equations. The influence of the induced axial load and bending moment in the chord due to applied bending in the brace, on the measured stress concentration factors, will be determined using the trend of SCFs from existing parametric equations.

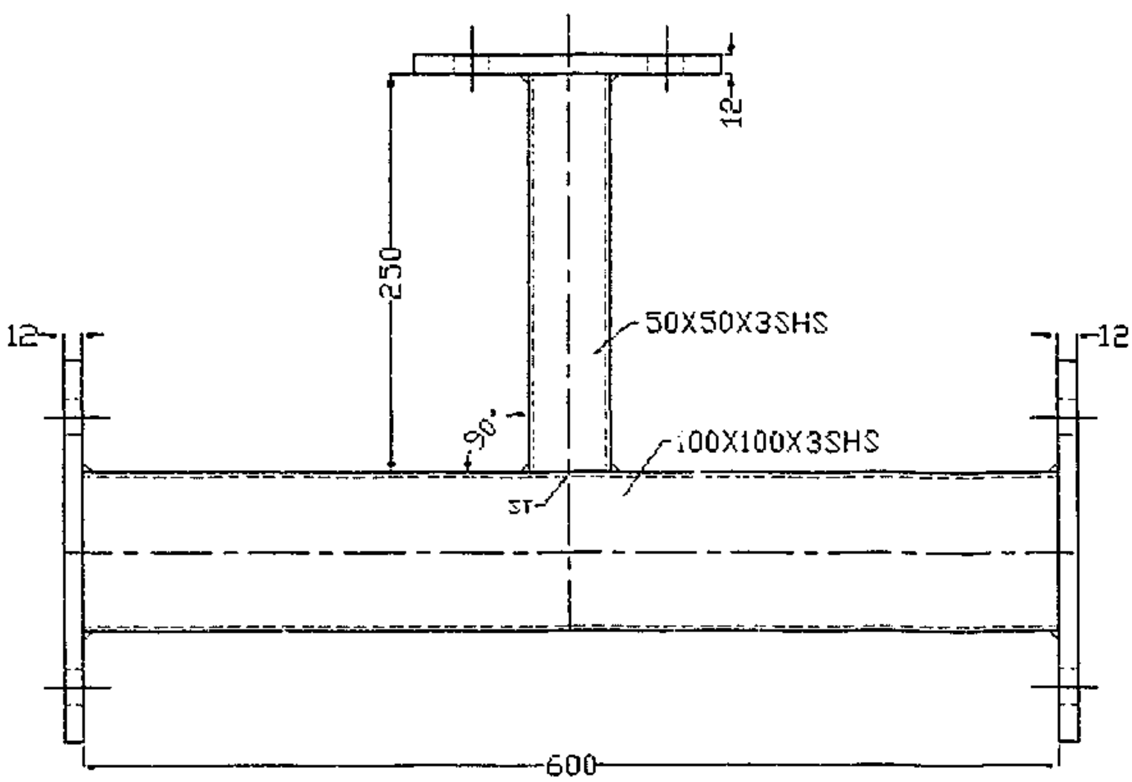

Figure 6-1: Tube-to-tube joint; brace size 50x50x3 SHS, Chord size 100x100x3 SHS

Table 6-1: Tube-to-tube T-joints tested for the three different steel grades

Steel/ Description	Connection Series	Plate/ Chord Member	Brace Member	2γ	β	τ	R
C350LO Non-galvanised	S3S5	100x100x3 SHS	35x35x1.6 SHS	33	0.35	0.5	0.1
	S3S2	100x100x3 SHS	50x50x1.6 SHS	33	0.50	0.5	0.1
	S6S2	75x75x3 SHS	50x50x1.6 SHS	25	0.67	0.5	0.1
S355JOH Non-galvanised	V3V4	100x100x3 SHS	30x30x2 SHS	33	0.30	0.7	0.1
	V3V5	100x100x3 SHS	60x60x3 SHS	33	0.60	1.0	0.1
	V3V1	100x100x3 SHS	50x50x3 SHS	33	0.50	1.0	0.1
	V6V2	70x70x3 SHS	40x40x2 SHS	23	0.57	0.7	0.1
	V6V1	70x70x3 SHS	50x50x3 SHS	23	0.71	1.0	0.1
C450LO Galvanised	D3D4	100x100x3 SHS	35x35x3 SHS	33	0.35	1.0	0.1
	D3D5	100x100x3 SHS	35x35x1.6 SHS	33	0.35	0.5	0.1
	D3D1	100x100x3 SHS	50x50x3 SHS	33	0.50	1.0	0.1
	D3D2	100x100x3 SHS	50x50x1.6 SHS	33	0.50	0.5	0.1
	D6D1	75x75x3 SHS	50x50x3 SHS	25	0.67	1.0	0.1
	D6D2	75x75x3 SHS	50x50x1.6 SHS	25	0.67	0.5	0.1

6.2 TEST-SETUP FOR FATIGUE TESTS

Tube-to-tube T-joints made up of square hollow sections were tested using the multiple fatigue rig shown in Figure 6-2. A schematic diagram showing the test set-up of the tube-to-tube T-joint for fatigue testing is shown in Figure 6-3. The support system, loading system and measuring system of the multiple fatigue rig testing system are the same as those described in Section 5.2 of Chapter 5.

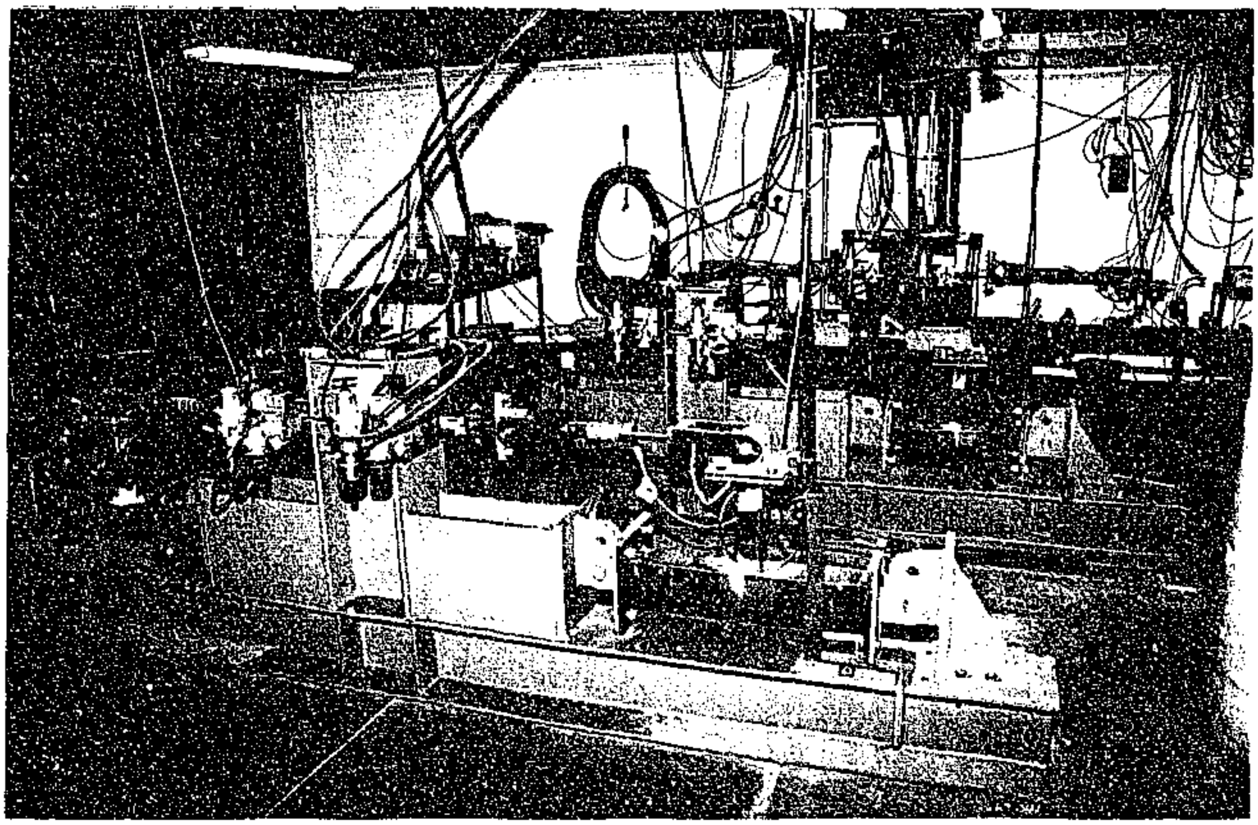

Figure 6-2: Multiple Fatigue Testing Rig

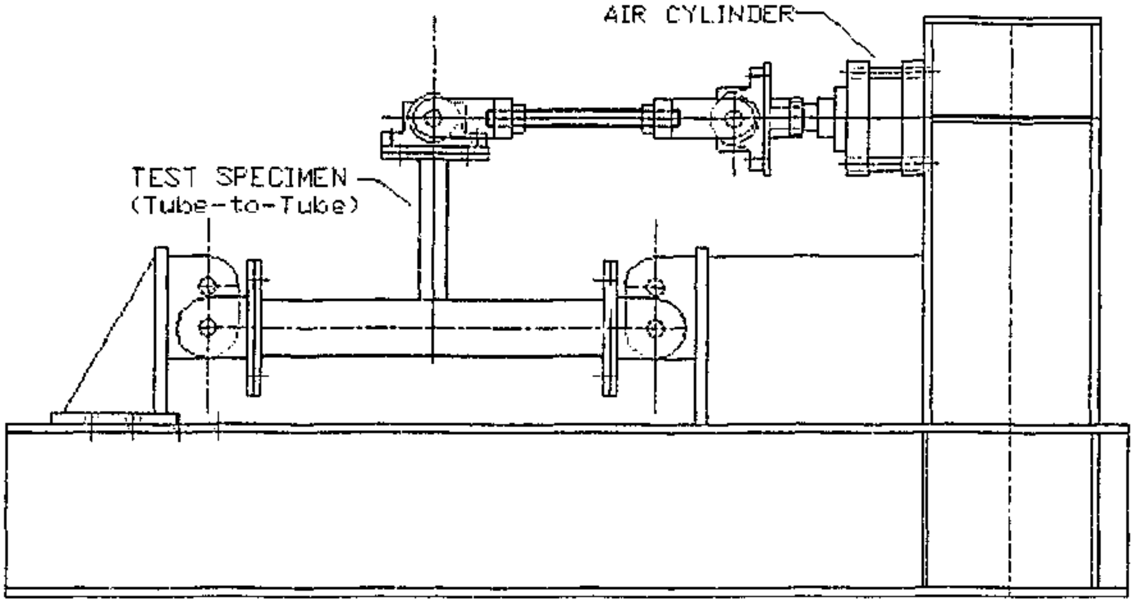

Figure 6-3: Schematic diagram of Test Rig for the testing of Tube-to-Tube T-joints

6.3 FAILURE MODES

6.3.1 Background

Different researchers have used different modes of failure during the testing of tubular nodal joints (Noordhoek *et al* 1980; Verheul and Noordhoek 1987; van Wingerde 1992).

Noodhoek *et al* (1980) reported the fatigue tests of axially loaded end to end connections and K- and N- joints made from square hollow sections. Failure was considered as complete fracture or the development of a crack of a certain length. The crack initiation stage of fatigue failure, was determined by the first sign of a crack, which could be visually detected. Failure was considered to be complete fracture or the situation in which due to extensive cracking, deformation occurred, which was too large to permit the continuation of the test.

Verhuel and Noordhoek (1987) discussed the failure of T-joints under axial loading applied to the brace member. The T-joints were made of rectangular hollow sections. Tests were stopped when the crack length had extended a length equal to the side length of the brace parallel to the chord axis. Generally the cracks started at the corners either in the brace or in the chord and grew together parallel to the chord axis. In principle three types of failure occurred, in the weld, in the brace and in the chord. Failure in the weld occurred as a result of cracks starting at the root of the weld and propagating through the weld metal. Failure in the weld was probably caused by inadequate penetration resulting in an insufficient throat thickness of the weld. High notch stresses at the root then resulted in initiation and propagation of cracks from the root of the weld. Brace failure was caused by cracks developing in the brace, while chord failure was caused by cracks developing in the chord. In both the chord and brace failures cracks initiated at the corners of the brace-chord interface on the weld toes and developed along the weld toes parallel to the chord longitudinal axis. Brace as well as chord failures resulted in a separation between the chord and the brace along the weld toe in either the brace or the chord.

van Wingerde (1992) pointed out that fatigue life is generally specified as the number of cycles (N) of stress or strain of a specified character that a given joint sustains, before a failure of a specified nature occurs. In the IIW recommendations a crack through the wall, for example, is considered as failure. In the European Offshore Programme, four modes of failure are considered as follows:

(i) N1 corresponding to a 15% change in strain measured "near" the crack initiation point,

(ii) N2 corresponding to the first "visible" crack,

(iii) N3 corresponding to a through thickness crack and

(iv) N4 corresponding to the end of the test or the complete loss of strength.

However in his work on T- and X-joints made up of square hollow sections under axial loading and bending, van Wingerde (1992) defined fatigue failure as a crack extending over a length of the brace width for failure in the brace or the brace width plus twice the projected length of the weld in the chord face for failure in the chord.

6.3.2 Failure Modes in Tube-to-tube T-joints

Different modes of failure have been observed during the fatigue testing of tube-to-tube T-joints. These failures occurred due to the initiation and propagation of cracks resulting in the separation of the brace from the chord along the weld toe in either the chord or the brace. In this investigation, the definition of failure by van Wingerde (1992) was adopted. van Wingerde (1992) defined fatigue failure as a crack extending over a length of the brace width for failure in the brace or the brace width plus twice the projected length of the weld in the chord face for failure in the chord. Most cracks initiated at the weld toe in the chord on the brace-chord interface. All the cracks initiated along the weld toe, at the corner of the brace-chord interface defined by the hot spot locations, lines A, B, C , D and E, in the chord, see Figure 6-12 in Section 6.5.1.

6.3.2.1 Chord-Tension-Side Failure

This mode of failure occurred in the majority of the T-joints with low to moderate β values of 0.30, 0.35, 0.50 and 0.60.

The cracks initiated at the weld toe in the chord at the corners of the brace-chord interface, and then propagated towards the middle of the brace width eventually resulting in failure as shown in Figure 6-4. The definition of failure adopted by van Wingerde (1992) was used, where failure was defined as a crack extending over a length of the brace width plus twice the projected length of the weld in the chord face for failure in the chord. In these welded thin-walled tube-to-tube T-joints, it was noted that when a crack length equal to that defined by van Wingerde (1992) occurred, separation of the brace from the chord along the weld toes in the chord was observed. The separation of the brace from the chord along the weld toes in the chord can be described as a through-thickness crack along the whole length of the brace width in the chord. This failure can therefore also be described as the length of a through-thickness crack extending along the whole length of the brace width in the chord resulting in the separation of the brace from the chord (Mashiri *et al* 2001).

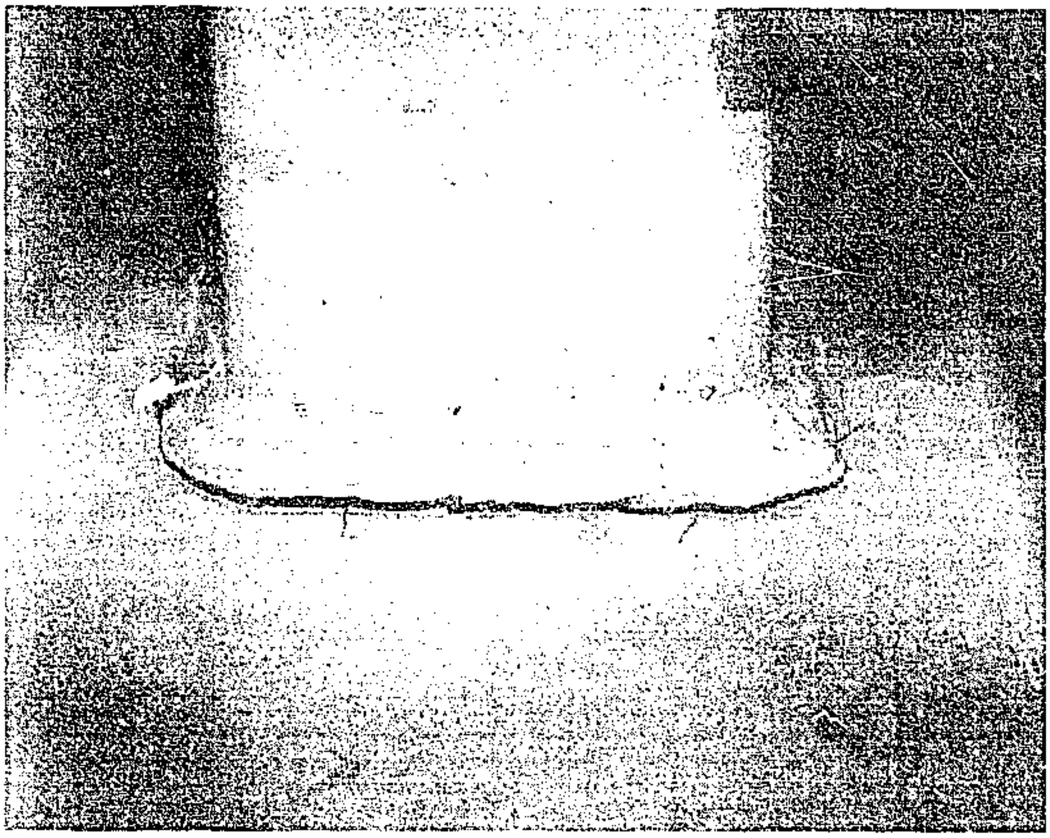

Figure 6-4: Chord-Tension-Side Failure

6.3.2.2 Chord-and-Brace-Tension-Side Failure

This mode of failure was observed in some of the connections with moderate to high β values of 0.57, 0.67 and 0.71, which are among the largest values of β for connections tested in this program. The different crack patterns obtained are shown in Figures 6-5 to 6-7. In all of these connections the cracks initiated at the weld toe in the chord, at the corner of the brace-chord interface. Later on, the cracks also initiated at the weld toe in the brace, at the corner of the brace-chord interface. This may have been due to stress redistribution resulting in higher notch stresses at the weld toes in the brace. The cracks then propagated in both the brace and the chord. Failure in these connections was deemed to occur when the sum of the crack lengths in both the brace and the chord, equaled the brace width plus twice the projected length of the weld in the chord.

In specimen D6D1L1B, the crack in the brace propagated into the weld and joined the crack at the weld toe in the chord, Figure 6-5.

In specimen D6D2L1A, Figure 6-6, the cracks initiated at one corner at the weld toe in the chord and propagated towards the middle of the brace width. At a later stage cracks developed at the other corner at the weld toe in the brace. Both cracks then simultaneously grew towards the middle of the brace until the specified length for failure was reached.

For test D6D2L2A, Figure 6-7, the cracks initiated at one corner at the weld toe in the chord but the propagation of these cracks in the chord almost stalled as they grew away from the weld toe. Subsequently the cracks initiated at the other corner at weld toe in the brace and propagated towards the corner where cracks first initiated.

Figure 6-5: Chord-and-Brace-Tension-Side Failure, D6D1L1B

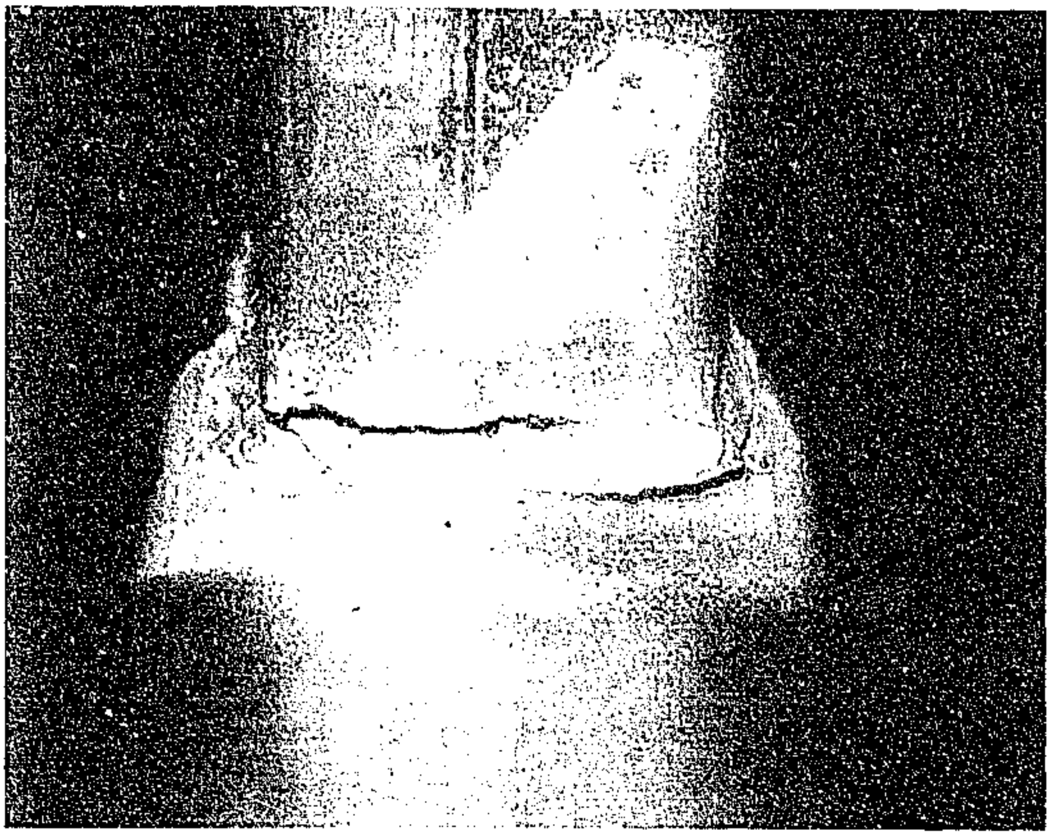

Figure 6-6: Chord-and-Brace-Tension-Side Failure. D6D2L1A

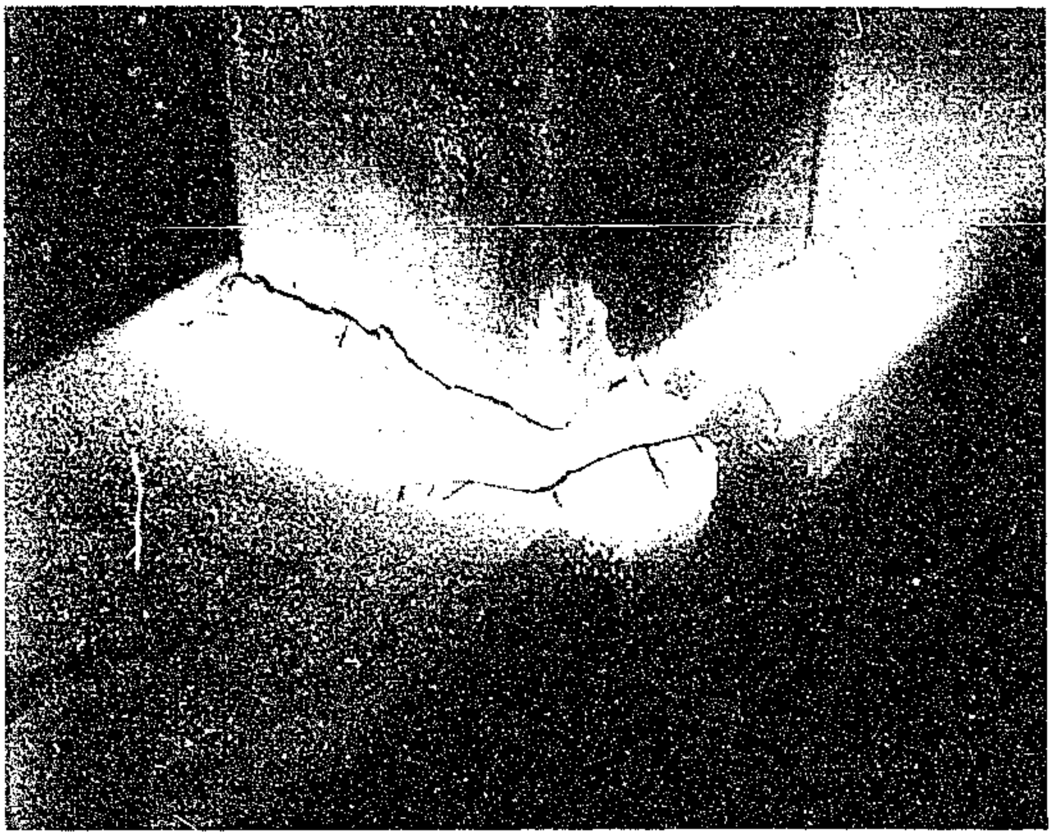

Figure 6-7: Chord-and-Brace-Tension-Side Failure, D6D2L2A

6.3.2.3 Brace-Tension-Side Failure

This mode of failure developed in connection S6S2L1A, Figure 6-8. The highest SCF according to the parametric equations (Soh and Soh 1990; van Wingerde 1992) occurs in the chord for this connection. However, in specimen S6S2L1A, cracks actually initiated and propagated in the brace. Similar failures have been observed by de Back *et al* (1989). de Back *et al* (1989) noted that when the measured weld leg length on the brace is smaller than that in the chord this results in a more acute notch at the weld toe in the brace, while the larger weld leg length in the chord results in a smoother transition of the weld shape into the chord. The notch of higher acuity at the weld toe in the brace can result in cracks initiating in the brace, although the measured stress concentration factor in the brace is smaller than that in the chord (de Back *et al* 1989). The initiation of cracks in the brace may also be due to undercuts augmenting the high notch stresses at the weld toe in the brace, especially in the 1.6mm thick brace in the connection S6S2L1A. Failure was defined as a crack extending over a length of the brace width. This mode of failure was similar to that observed in tube-to-plate T-joints, see section 5.3.2 of Chapter 5. In tube-to-plate T-joints however, failure in the brace was expected as lines A to E gave the highest SCF.

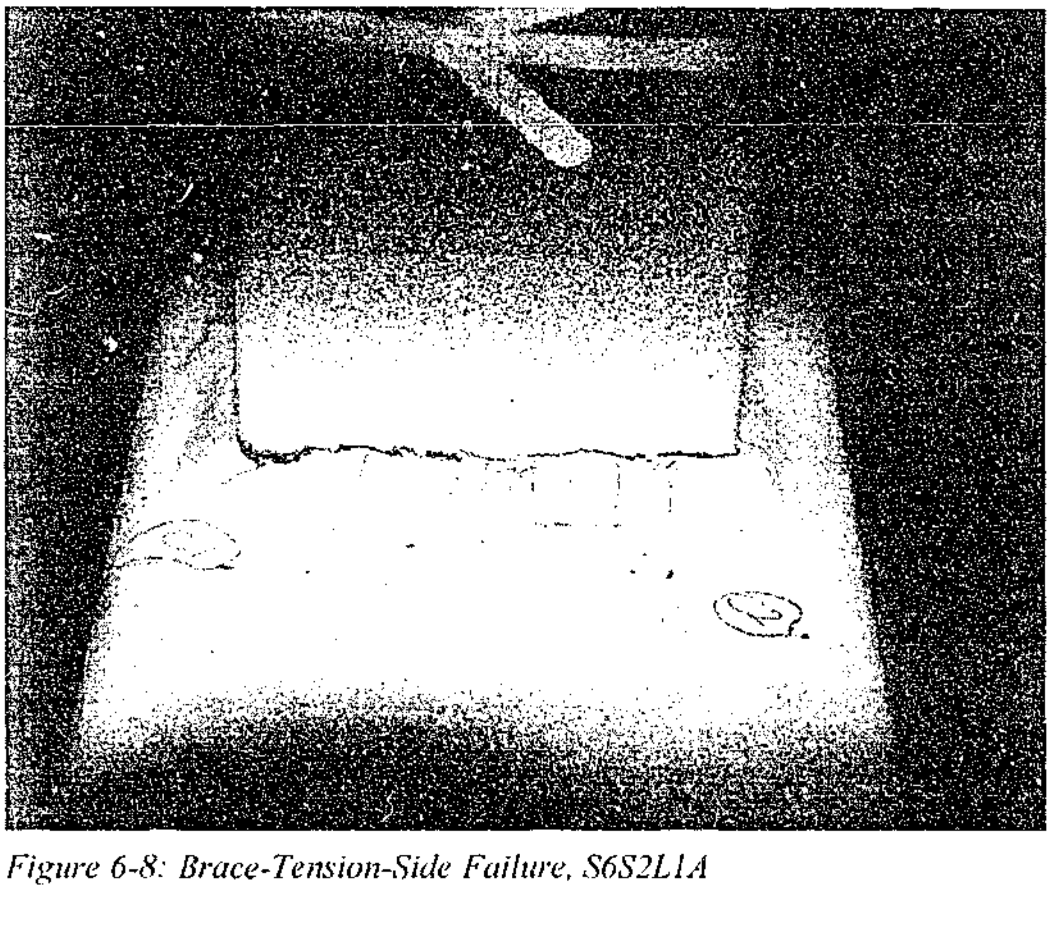

Figure 6-8: Brace-Tension-Side Failure, S6S2L1A

6.3.2.4 Chord-Compression-Side Failure

In one connection, D3D2L2A, cracks initiated on the compression side in the chord, on weld toe at the corner of the brace-chord interface. Although the cracks started at the weld toe around one corner of the brace-chord interface, they propagated away from the weld toe into the chord parent metal, Figure 6-9. The test was stopped after 10,969,239 cycles. This was because very small surface crack growth could be detected, suggesting that the cracks had developed into regions of high compressive stress resulting in crack arrest. This is likely to happen since the crack is actually propagating in the compression side of the brace-chord interface. Test specimen D3D2L2A was therefore classified as a runout.

Initiation of the crack on the compression side can be due to high tensile residual stresses resulting from welding. The tensile residual stresses may be equal to yield value (Maddox 1991). If weld defects, such as undercuts exist at the weld toes these are likely to cause high notch stresses, resulting in crack initiation when cyclic loading is applied. Although the load is actually supposed to be compressive in this region, the net stress on the compression side due to tensile residual stresses, notch stresses caused by undercut and compressive stresses from loading might be tensile. This net tensile stress may result in fatigue cracks initiating on the compression side.

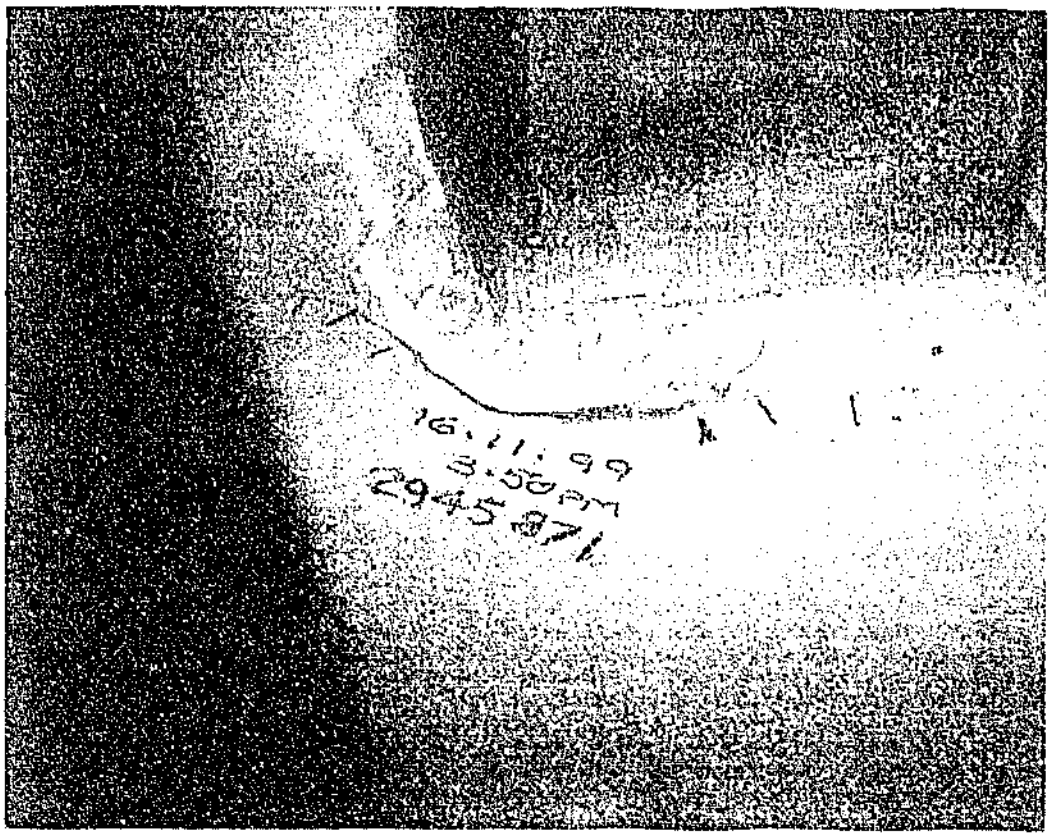

Figure 6-9: Chord-Compression-Side Failure, D3D2L2A

6.4 FATIGUE TEST RESULTS

The S-N data obtained from the fatigue tests of tube-to-tube T-joints is shown in Table 6-2, 6-3 and 6-4 for grade C450LO, S355JOH and C350LO respectively. All tests were carried out at a stress ratio of 0.1. The following tube-to-tube T-joints made up of square hollow sections of thicknesses less than 4mm were tested under cyclic in-plane bending load:

(a) 27 connections made from grade C450LO DuraGal steel tubes,

(b) 23 connections made from grade S355JOH steel tubes, and

(c) 9 connections made from grade C350LO steel tubes.

Tables 6-2 to 6-4 give the nominal stress range ($S_{r\text{-}nom}$), number of cycles (N), weld leg length along the brace (t_{wv}), weld leg length along the chord (t_{wh}), steel grading and the failure mode. A plot of the S-N data in terms of nominal stress ranges is shown in Figure 6-10.

Table 6-2: S-N data for Tube-to-Tube T-joints in terms of nominal stress range (Grade C450LO)

Connection Name	Chord SHS DxBxt (mm)	Brace SHS DxBxt (mm)	Nominal Stress Range, $S_{r\text{-}nom}$ (MPa)	Fatigue Life, N (Cycles)	Weld Leg Lengths (mm)		Mode of Failure	Steel Grade/ Description
					t_{wc}	t_{wb}		
D3D1L1A	100x100x3	50x50x3	37.1	16302	6.5	6.4	Chord Tension Side	C450LO, Galvanised
D3D1L1B	100x100x3	50x50x3	37.1	30360	5.5	7.3	Chord Tension Side	C450LO, Galvanised
D3D1L2A	100x100x3	50x50x3	15.0	786679	5.8	7.5	Chord Tension Side	C450LO, Galvanised
D3D1L2B	100x100x3	50x50x3	15.0	471200	5.6	8.6	Chord Tension Side	C450LO, Galvanised
D3D1L3A	100x100x3	50x50x3	20.0	175744	5.7	5.2	Chord Tension Side	C450LO, Galvanised
D3D1L3B	100x100x3	50x50x3	29.9	19937	4.3	6.5	Chord Tension Side	C450LO, Galvanised
D3D2L1A	100x100x3	50x50x1.6	43.6	133625	5.1	5.7	Chord Tension Side	C450LO, Galvanised
D3D2L2A	100x100x3	50x50x1.6	24.9	10969239	6.0	7.7	Chord Compression Side	C450LO, Galvanised (RUNOUT)
D3D2L3A	100x100x3	50x50x1.6	49.8	52829	4.4	7.0	Chord Tension Side	C450LO, Galvanised
D6D1L1A	75x75x3	50x50x3	44.9	170766	6.9	8.9	Chord Tension Side	C450LO, Galvanised
D6D1L1B	75x75x3	50x50x3	44.9	145444	5.1	5.8	Chord & Brace Tension Side	C450LO, Galvanised
D6D1L2A	75x75x3	50x50x3	18.7	2453350	5.0	7.0	Chord Tension Side	C450LO, Galvanised
D6D1L2B	75x75x3	50x50x3	18.7	6642981	3.8	6.8	Chord Tension Side	C450LO, Galvanised
D6D1L3B	75x75x3	50x50x3	29.9	324153	5.4	6.4	Chord & Brace Tension Side	C450LO, Galvanised
D6D1L3A	75x75x3	50x50x3	40.2	254276	6.7	7.8	Chord Tension Side	C450LO, Galvanised
D6D2L1A	75x75x3	50x50x1.6	74.8	89294	6.5	5.8	Chord & Brace Tension Side	C450LO, Galvanised
D6D2L2A	75x75x3	50x50x1.6	31.2	2885483	5.0	6.8	Chord & Brace Tension Side	C450LO, Galvanised
D6D2L3A	75x75x3	50x50x1.6	62.3	152682	5.0	5.6	Chord Tension Side	C450LO, Galvanised
D3D4L1A	100x100x3	35x35x3	26.4	288292	4.2	6.2	Chord Tension Side	C450LO, Galvanised
D3D4L1B	100x100x3	35x35x3	26.4	328247	5.0	5.8	Chord Tension Side	C450LO, Galvanised
D3D4L2A	100x100x3	35x35x3	19.0	589163	4.5	5.1	Chord Tension Side	C450LO, Galvanised
D3D4L2B	100x100x3	35x35x3	19.8	340417	4.1	7.0	Chord Tension Side	C450LO, Galvanised
D3D4L3B	100x100x3	35x35x3	13.2	3925476	3.4	6.9	Chord Tension Side	C450LO, Galvanised
D3D4L3A	100x100x3	35x35x3	19.8	799808	4.2	6.2	Chord Tension Side	C450LO, Galvanised
D3D5L1A	100x100x3	35x35x1.6	41.5	264239	3.5	6.3	Chord Tension Side	C450LO, Galvanised
D3D5L2A	100x100x3	35x35x1.6	31.1	754797	4.5	6.0	Chord Tension Side	C450LO, Galvanised
D3D5L3A	100x100x3	35x35x1.6	31.1	2959837	5.5	6.7	Chord Tension Side	C450LO, Galvanised

Table 6-3: S-N data for Tube-to-Tube T-joints in terms of nominal stress range (Grade S355JOH)

Connection Name	Chord SHS DxBxt (mm)	Brace SHS DxBxt (mm)	Nominal Stress Range, $S_{r\text{-}nom}$ (MPa)	Fatigue Life, N (Cycles)	Weld Leg Lengths (mm)		Mode of Failure	Steel Grade/ Description
					t_{wc}	t_{wb}		
V3V5L1A	100x100x3	60x60x3	29.9	124028	6.4	7.2	Chord Tension Side	S355JOH, Non-galvanised
V3V5L1B	100x100x3	60x60x3	24.5	86947	4.5	6.5	Chord Tension Side	S355JOH, Non-galvanised
V3V5L2A	100x100x3	60x60x3	12.5	5846429	5.2	7.8	Chord Tension Side	S355JOH, Non-galvanised
V3V5L2B	100x100x3	60x60x3	19.9	155368	5.0	7.2	Chord Tension Side	S355JOH, Non-galvanised
V3V5L3A	100x100x3	60x60x3	19.9	147376	6.0	7.0	Chord Tension Side	S355JOH, Non-galvanised
V3V5L3B	100x100x3	60x60x3	12.5	7536844	5.4	5.9	Chord Tension Side	S355JOH, Non-galvanised
V3V1L1A	100x100x3	50x50x3	33.7	29183	4.4	6.0	Chord Tension Side	S355JOH, Non-galvanised
V3V1L2B	100x100x3	50x50x3	33.7	22069	3.4	7.9	Chord Tension Side	S355JOH, Non-galvanised
V3V1L3A	100x100x3	50x50x3	22.5	60055	5.4	6.5	Chord Tension Side	S355JOH, Non-galvanised
V3V1L3B	100x100x3	50x50x3	15.0	2093716	5.0	6.1	Chord Tension Side	S355JOH, Non-galvanised
V6V2L1A	70x70x3	40x40x2	67.2	45365	3.2	7.0	Chord Tension Side	S355JOH, Non-galvanised
V6V2L2A	70x70x3	40x40x2	33.6	1453800	4.1	6.5	Chord & Brace Tension Side	S355JOH, Non-galvanised
V6V2L2B	70x70x3	40x40x2	58.8	105456	4.7	7.1	Chord Tension Side	S355JOH, Non-galvanised
V6V2L3B	70x70x3	40x40x2	33.6	1095618	5.2	6.4	Chord Tension Side	S355JOH, Non-galvanised
V6V2L3A	70x70x3	40x40x2	50.4	168446	4.7	6.6	Chord & Brace Tension Side	S355JOH, Non-galvanised
V6V1L1A	70x70x3	50x50x3	44.9	513067	6.2	6.6	Chord Tension Side	S355JOH, Non-galvanised
V6V1L2B	70x70x3	50x50x3	44.9	560477	4.1	6.6	Chord & Brace Tension Side	S355JOH, Non-galvanised
V6V1L3A	70x70x3	50x50x3	48.6	825878	4.9	5.8	Chord & Brace Tension Side	S355JOH, Non-galvanised
V6V1L3B	70x70x3	50x50x3	25.0	9423530	5.5	6.7	Chord & Brace Tension Side	S355JOH, Non-galvanised
V3V4L1A	100x100x3	30x30x2	37.1	162405	4.6	6.4	Chord Tension Side	S355JOH, Non-galvanised
V3V4L2A	100x100x3	30x30x2	37.1	229799	5.1	6.8	Chord Tension Side	S355JOH, Non-galvanised
V3V4L2B	100x100x3	30x30x2	43.3	303680	4.0	6.1	Chord Tension Side	S355JOH, Non-galvanised
V3V4L3A	100x100x3	30x30x2	31.0	979654	4.1	5.4	Chord Tension Side	S355JOH, Non-galvanised

Table 6-4: S-N data for Tube-to-Tube T-joints in terms of nominal stress range (Grade C350LO)

Connection Name	Chord SHS DxBxt (mm)	Brace SHS DxBxt (mm)	Nominal Stress Range, $S_{r\text{-}nom}$ (MPa)	Fatigue Life, N (Cycles)	Weld Leg Lengths (mm)		Mode of Failure	Steel Grade/ Description
					t_{wc}	t_{wb}		
S3S2L1A	100x100x3	50x50x1.6	43.6	121207	4.3	7.6	Chord Tension Side	C350LO, Non-galvanised
S3S2L2A	100x100x3	50x50x1.6	34.3	269341	4.7	6.5	Chord Tension Side	C350LO, Non-galvanised
S3S2L3A	100x100x3	50x50x1.6	24.9	3009445	4.3	6.5	Chord Tension Side	C350LO, Non-galvanised
S6S2L1A	75x75x3	50x50x1.6	74.8	43770	4.7	6.6	Brace Tension Side	C350LO, Non-galvanised
S6S2L2A	75x75x3	50x50x1.6	31.2	1641907	4.8	6.1	Chord & Brace Tension Side	C350LO, Non-galvanised
S6S2L3A	75x75x3	50x50x1.6	49.8	177201	5.2	6.1	Chord & Brace Tension Side	C350LO, Non-galvanised
S3S5L1A	100x100x3	35x3x1.6	54.0	886078	5.5	7.3	Chord Tension Side	C350LO, Non-galvanised
S3S5L2A	100x100x3	35x3x1.6	40.5	886921	5.0	6.1	Chord Tension Side	C350LO, Non-galvanised
S3S5L3A	100x100x3	35x3x1.6	27.0	1371529	5.1	5.5	Chord Tension Side	C350LO, Non-galvanised

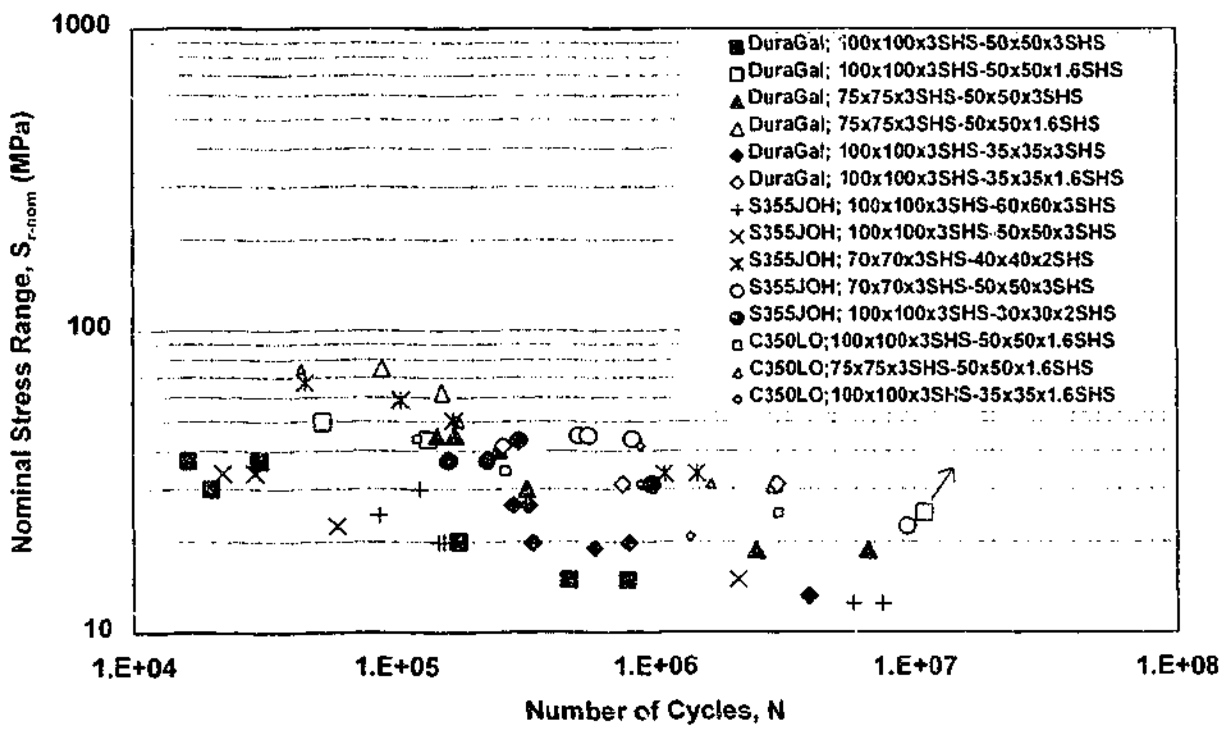

Figure 6-10: Plot of S-N data for tube-to-tube T-joints in terms of the nominal stress range

6.5 EXPERIMENTAL SCF OF TUBE-TO-TUBE T-JOINTS

6.5.1 Experimental Determination

The setup used in the determination of stress concentration factors for tube-to-tube T-joints is shown in Figure 6-11. The load was applied using the air cylinder and the load level detected using the calibrated load cell and load cell exciter.

The strains are measured using a series of Multi-Channel Monitors (MCM1). The multi-channel monitors record the change in strain in microvolts. The MCM1 has a fixed gauge factor setting of 2.00, and the actual strain measurement indicated by the display is as follows:

$$\varepsilon = 2 * \delta V / G.F. \qquad (\mu\varepsilon)$$

Where ε is the mean true strain measured by an active gauge,
δV is the change in reading in microvolts, and
G.F. is the gauge factor of the strain gauge(s).

The Micro Measurements Division, CEA-Series Student gauges, CEA-06-240UZ-120, used in this investigation have a gauge factor (G.F.) of 2.055. These gauges were used to obtain strains used in monitoring the overall behaviour of the joint. The Showa Measuring Instrument foil strain gauges, R51-FA-1-120-11, with a gauge factor of 2.05, were also used. The foil gauges consist of 5 strain-sensitive grids mounted on a common backing. These were used at some of the hot spot locations A to E for each connection. The grids are at 1.75mm centres and allow the distribution of stress within the extrapolation region to be measured.

For each connection, strains were measured at four different load levels. The loads were taken to be below the maximum elastic moment of the connection. The maximum elastic moment is the moment below which the joint behaves elastically as determined from moment-deflection graphs. For those connections where experimental static tests have not been undertaken, similar ratios of maximum elastic moment to static strength for in-plane bending, to the tested connections were used. These ratios were observed to depend on the brace width to chord width ratio, β. The ratio, maximum elastic moment to static strength for in-plane bending increases with an increase in β values.

For each connection series strains for the determination of SCF were measured at different load levels, in one of the connections in the series. This allowed the determination of SCF for each series with the same non-dimensional parameters, β, 2γ and τ The diagrams showing the positions of strain gauges are given in Figures D4 to D13, Appendix D, for each of the connections in which SCF were determined. The lines A to E along which the SCF were determined are shown in Figure 6-12. Ten different tube-to-tube connection series have been analyzed in this research program. The following connections were strip strain gauged along lines B, C and D, allowing linear and quadratic extrapolations of these positions;

(i) D3D1L3A ,	β= 0.50,	2γ=33.33,	τ=1.00
(ii) D3D2L3A ,	β= 0.50,	2γ =33.33,	τ=0.53
(iii) D3D4L3A,	β= 0.35,	2γ=33.33,	τ=1.00
(iv) D3D5L3A,	β= 0.35,	2γ =33.33,	τ=0.53
(v) D6D1L3A ,	β= 0.67,	2γ =25.00,	τ=1.00
(vi) D6D2L3A,	β= 0.67,	2γ =25.00,	τ=0.53

These measurements for stress concentration factors covered the connection series made from both grade C350LO and C450LO and also connection series V3V1 made from grade S355JOH.

The following connections were strip strain gauged, along lines C, D and E, allowing linear and quadratic extrapolations at these positions;

(i) V3V5L3A ,	β= 0.60,	2γ =33.33,	τ=1.00
(ii) V3V4L3A ,	β= 0.30,	2γ =33.33,	τ=0.67
(iii) V6V1L3A,	β= 0.71,	2γ =23.33,	τ=1.00
(iv) V6V2L3A,	β= 0.57,	2γ =23.33,	τ=0.67

These measurements for stress concentration factors covered the connection series made from grade S355JOH.

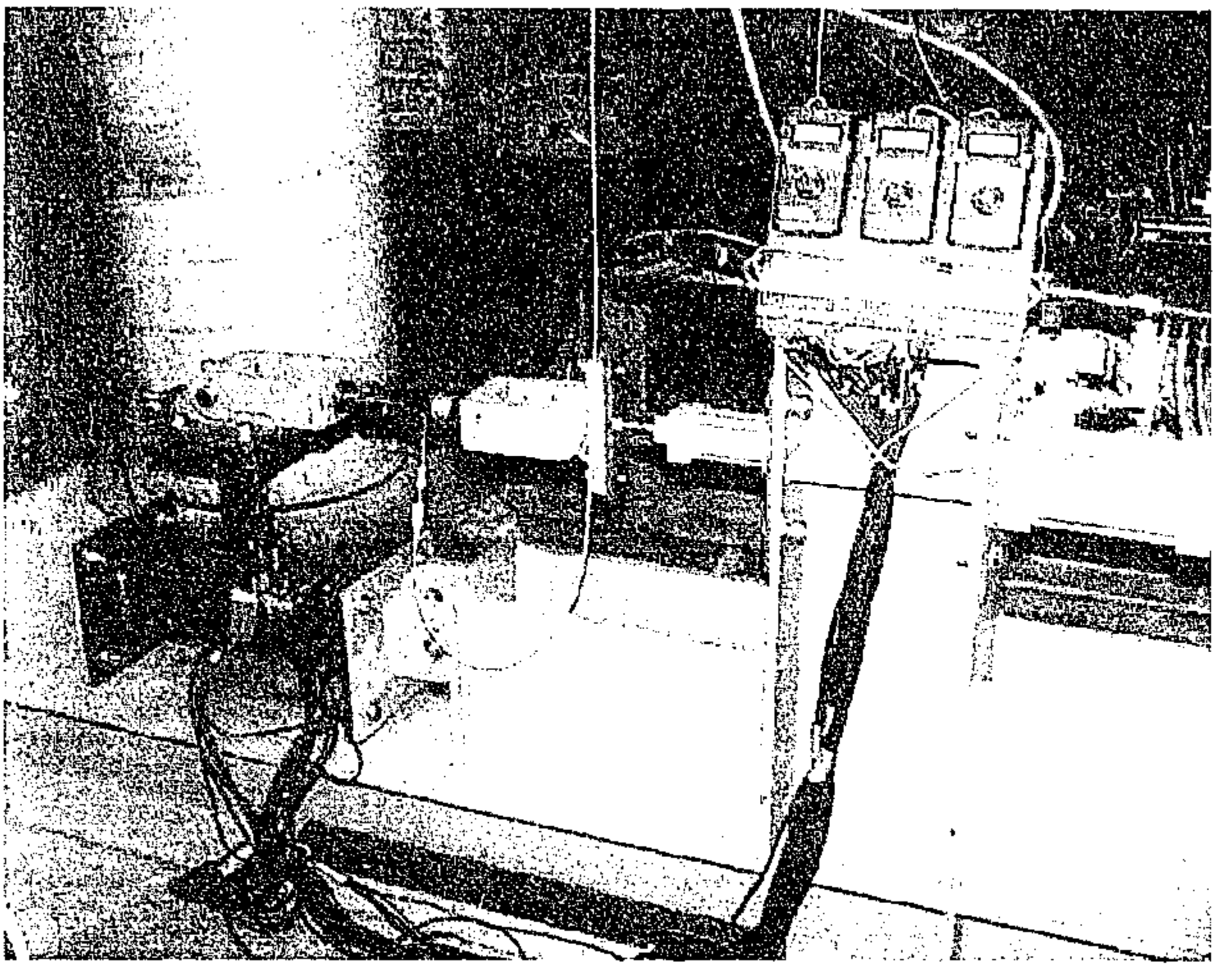

Figure 6-11: Setup for determination of SCF

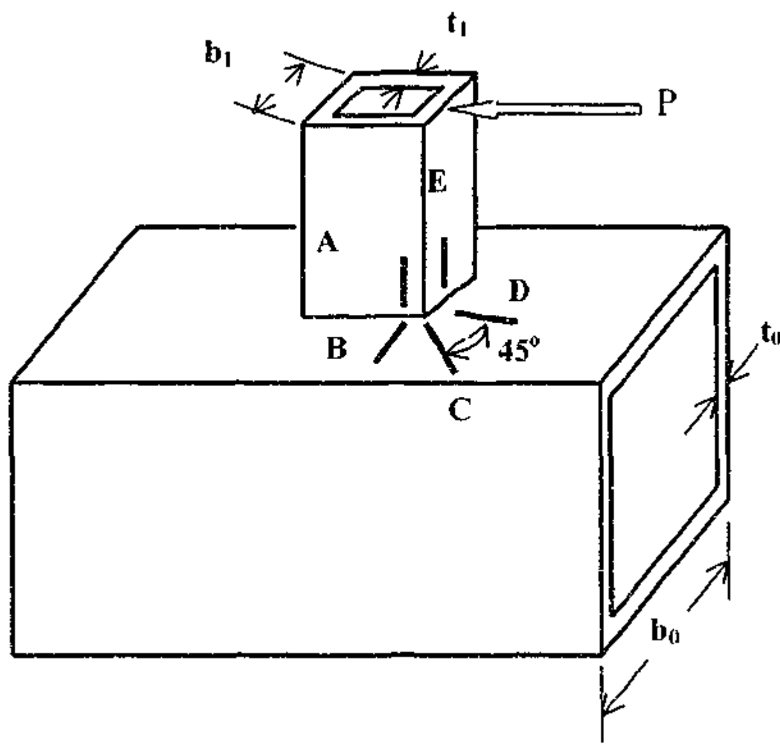

Figure 6-12: Lines A to E. Tube-to-tube T-joints

6.5.2 Nominal Stresses from Strain Gauge Measurements

Traditionally nominal stress ranges used in the S-N curves of welded connections are determined using the simple beam theory. However researchers do not always provide experimental evidence to this effect. In order to justify the use of nominal stress ranges from in this project, a comparison of the simple beam theory nominal stresses and the experimental nominal stresses was undertaken.

For each load level used in determining SCF, the strains in the brace were used to estimate the nominal stresses at the brace chord interface Three strain gauges in the brace were used for this estimation. The strain gauges close to the brace-plate interface and the brace-chord interface are placed at a distance *b*, from these interfaces. The other gauge is at mid height of the brace. The determination of nominal stresses from the strain serves to check the accuracy of load application system, which consists of an air cylinder, calibrated load-cell and load-cell exciter, and ensures that the required loads are applied. The nominal stresses for the different connections are shown in Figures E10, E14, E18, E22, E26, E30, E34, E38, E42 and E46, Appendix E. The nominal stresses at the brace-chord interface are tabulated for both the beam theory and the experimental nominal stresses determination in Table 6-5. The absolute value of percentage difference between the beam theory and the experimental nominal stresses, vary between 0.68% and 20.00%, with an average of 4.59%. The higher percentage errors occur at lower applied stresses because although the absolute differences between the beam theory and the experimental nominal stresses are small they result in large relative differences. A similar trend in percentage differences was obtained by Heemskerk (2000), in his comparison of stress concentration factors obtained from finite element analysis to those derived from parametric equations. A graph of experimental versus beam theory nominal stresses is shown in Figure 6-13. Figure 6-13 shows a linear trend line very close to the 45^0 line between the experimental and the beam theory nominal stresses. A high correlation, coefficient of 0.99 exists between the experimental and the beam theory nominal stresses.

The beam theory nominal stresses can therefore be used in determining the nominal stress ranges applied to these connections during cyclic loading. This also shows that the load application system used in this research program is reliable.

Table 6-5: Comparison of stresses from strain gauge measurements and beam theory

Connection Name	Load (kN)	Beam Theory Nominal Stress σ_{nom} (MPa)	Experimental Nominal Stress $\sigma_{nom,exp}$ (MPa)	% Difference
D3D1L3A	0.2	8.3	8.9	7.23
	0.4	16.6	16.2	-2.41
	0.6	24.96	24.3	-2.64
	0.8	33.3	33.8	1.50
D3D2L3A	0.2	13.8	12.7	-7.97
	0.4	27.7	25.7	-7.22
	0.6	41.5	39.9	-3.86
	0.8	55.4	54.6	-1.44
D3D4L3A	0.1	7.3	7.5	2.74
	0.2	14.6	14.5	-0.68
	0.3	21.9	21.6	-1.37
D3D5L3A	0.1	11.5	10.6	-7.83
	0.2	23.0	22.0	-4.35
	0.3	34.5	33.9	-1.74
D6D1L3A	0.25	10.4	10.1	-2.88
	0.5	20.8	21.3	2.40
	0.75	31.2	32.1	2.88
	1.00	41.6	43.9	5.53
D6D2L3A	0.25	17.3	17.5	1.16
	0.5	34.6	35.1	1.45
	0.75	51.9	53.3	2.70
	1.00	69.2	71.5	3.32
V3V5L3A	0.2	5.5	4.4	-20.00
	0.4	11.1	11.3	1.80
	0.6	16.6	16.8	1.20
	0.8	22.1	23.6	6.79
V3V4L3A	0.1	13.8	12.0	-13.04
	0.15	20.6	19.9	-3.40
	0.2	27.5	26.8	-2.55
	0.25	34.4	32.8	-4.65
V6V1L3A	0.15	6.2	7.2	16.13
	0.3	12.5	14.0	12.00
	0.45	18.7	18.1	-3.21
	0.6	25.0	25.0	0.00
V6V2L3A	0.15	14.0	13.1	-6.43
	0.3	28.0	31.0	10.71
	0.45	42.0	43.1	2.62
	0.6	56.0	57.3	2.32

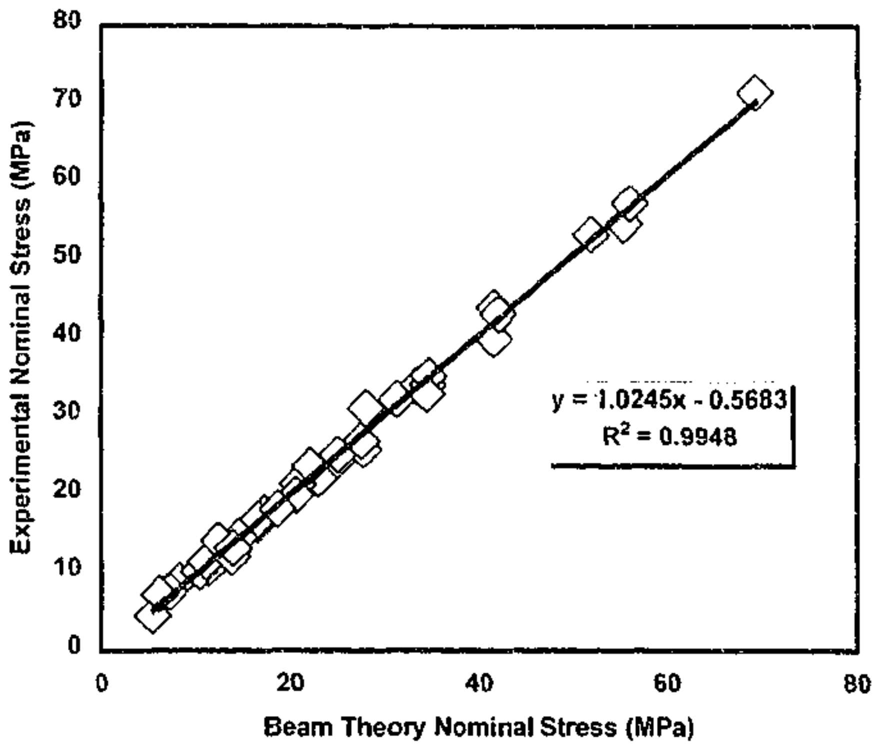

Figure 6-13: Beam Theory Nominal Stress versus Experimental Nominal Stress

6.5.? Hot Spot Stresses from Strain Gauge Measurements

The hot spot stresses for each connection series (same β, 2γ, τ) of the tube-to-tube T-joints were determined at different load levels.

Figures E10 to E49, Appendix E, show the graphs of the stress distributions along specified lines for the different connections. The strains obtained from the strain gauge measurements were converted to stresses using the relationship $\sigma = 1.1E\varepsilon$ for stresses and strains in a direction perpendicular to the weld toe as reported by van Wingerde (1992). The location around line A to E in the connection is the hot spot. This is the position where fatigue cracks initiate.

The graphs of the stress distributions along lines A to E show an increase in stresses with load increment. The stress concentration factors were determined from those load levels that gave stress distributions that were proportional to the load levels. This results in SCF that are approximately the same for the different load levels. Some higher load levels gave significantly different SCF from those at other load levels for a given line and were discarded in the determination of SCF. This was because some higher loads resulted in inelastic responses of stress distribution along some of the lines A to E. For some of the connections such as D3D2L3A, D3D4L3A and D3D5L3A, it was noted that for some of the hot spot locations, the stress distributions increased significantly, denoting inelastic behaviour. The stresses in connection D3D5L3A, for example, remained elastic for line B for all load levels under consideration. On the other hand the stresses in lines C and D gave inelastic responses of stress distribution at the same loads as those for line B. This shows that inelastic behaviour at hot spot locations can be localized to specific lines. Fatigue cracks are therefore more likely to initiate along the weld toe positions between Lines C and D in connection D3D5L3A.

Linear and quadratic extrapolation methods were used in the determination of hot spot stresses for each load level for each specified line where strain gauges were installed. Extrapolation distances recommended by guidelines (IIW 2000, Zhao *et al* 1999a) were used and are shown in the footnotes of Table 6-6. The hot spot stresses and the resultant SCF are shown in Table 6-6 for each of the connections at different load levels, for both the linear and quadratic extrapolation methods.

In most cases the SCF was highest for line C. One connection, V3V4L3A had the highest SCF along line D. Both line C and D are located in the chord. This is consistent with the chord-tension side cracks, Figure 6-4, which was the mode of failure in the majority of the tube-to-tube T-joints tested under in-plane bending.

The stress concentration factors determined by the quadratic method of extrapolation are higher than those determined by the linear extrapolation method. The ratios of the stress concentration factors determined by the quadratic extrapolation method (SCF_q) to the stress concentration factors determined by the linear extrapolation method (SCF_l) vary from 1.07 to 2.01, Table 6-6. This shows that the stress distribution of the tube-to-tube T-joints are highly non-linear compared to those of tube-to-plate T-joints where the ratios ranging from 1.04 to 1.18 were determined, see Section 5.5.3 of Chapter 5. This strong non-linearity in stress distributions along specified lines A to E has been reported by van Wingerde (1992). As such, the quadratic method of extrapolation is the recommended method of extrapolation for nodal joints made up of square or rectangular hollow sections (IIW 2000).

Table 6-6: Determination of SCF, Tube-to-tube T-joints

Connection	Position	Load (kN)	Nominal Stress, σ_{nom} (MPa)	Linear Extrapolation			Quadratic Extrapolation			$\frac{SCF_q}{SCF_l}$
				σ_{hs} (MPa)	SCF	SCF_l Average	σ_{hs} (MPa)	SCF	SCF_q Average	
D3D1L3A (100x100x3 -50x50x3)	Line B	0.2	8.3	67.7	8.2	8.2	77.998	9.4	9.275	1.13
		0.4	16.6	130.9	7.9		145.96	8.8		
		0.6	24.96	203.6	8.2		224.5	9.0		
		0.8	33.3	281.9	8.5		329.7	9.9		
	Line C	0.2	8.3	86.13	10.4	10.175	103.47	12.5	11.95	1.17
		0.4	16.6	161.93	9.8		186.72	11.2		
		0.6	24.96	253.15	10.1		298.72	12.0		
		0.8	33.3	324.99	10.4		403.7	12.1		
	Line D	0.2	8.3	56.5	6.8	6.675	62.6	7.5	7.825	1.17
		0.4	16.6	104.8	6.3		123.4	7.4		
		0.6	24.96	164.3	6.6		199.3	7.98		
		0.8	33.3	234.2	7.0		279.7	8.4		
D3D2L3A (100x100x3 -50x50x1.6)	Line B	0.2	13.8	65.2	4.7	4.9	73.5	5.3	5.55	1.13
		0.4	27.7	141.4	5.1		159.5	5.8		
	Line C	0.2	13.8	84.0	6.1	5.3	89.9	6.5	7.125	1.34
		0.4	27.7	178.2	6.4		199.4	7.2		
		0.6	41.5	231.6	5.6		327.5	7.9		
		0.8	55.4	175.8	3.2		381.9	6.9		
	Line D	0.2	13.8	62.4	4.5	4.5	69.8	5.1	5.1	1.13
D3D4L3A (100x100x3 -35x35x3)	Line B	0.1	7.3	28.1	3.8	4.0	33.2	4.5	4.633	1.16
		0.2	14.6	58.1	4.0		65.5	4.5		
		0.3	21.9	92.9	4.2		106.3	4.9		
	Line C	0.1	7.3	64.8	9.0	9.75	87.7	12.0	12.7	1.30
		0.2	14.6	153.7	10.5		195.98	13.4		
	Line D	0.1	7.3	47.1	6.5	6.5	54.9	7.7	7.7	1.18
D3D5L3A (100x100x3 -35x35x1.6)	Line B	0.1	11.5	37.4	3.3	3.4	40.5	3.5	3.7	1.09
		0.2	23.0	76.4	3.3		81.2	3.5		
		0.3	34.5	122.7	3.6		142.3	4.1		
	Line C	0.1	11.5	56.4	4.9	4.9	66.3	5.8	5.85	1.19
		0.2	23.0	113.4	4.9		135.4	5.9		
	Line D	0.1	11.5	52.3	4.5	4.5	66.4	5.8	5.8	1.29

Table 6-6 cont: Determination of SCF, Tube-to-tube T-joints

Connection	Position	Load (kN)	Nominal Stress, σ_{nom} (MPa)	Linear Extrapolation σ_{hs} (MPa)	Linear Extrapolation SCF	Linear Extrapolation SCF_l Average	Quadratic Extrapolation σ_{hs} (MPa)	Quadratic Extrapolation SCF	Quadratic Extrapolation SCF_q Average	$\frac{SCF_q}{SCF_l}$
D6D1L3A (75x75x3-50x50x3)	Line B	0.25	10.4	24.1	2.3	2.6	32.3	3.1	3.15	1.21
		0.5	20.8	54.6	2.6		60.98	2.9		
		0.75	31.2	86.8	2.8		102.6	3.3		
		1.0	41.6	116.4	2.7		139.3	3.3		
	Line C	0.25	10.4	71.2	6.8	7.275	84.3	8.1	8.375	1.15
		0.5	20.8	154.9	7.4		184.7	8.9		
		0.75	31.2	233.95	7.5		269.96	8.7		
		1.0	41.6	306.9	7.4		325.8	7.8		
	Line D	0.25	10.4	33.6	3.2	3.575	38.2	3.6	4.175	1.17
		0.5	20.8	72.7	3.5		82.0	3.9		
		0.75	31.2	113.9	3.6		130.8	4.2		
		1.0	41.6	167.5	4.0		207.8	5.0		
D6D2L3A (75x75x3-50x50x1.6)	Line B	0.25	17.3	27.8	1.6	1.725	37.5	2.2	2.475	1.44
		0.5	34.6	59.9	1.7		83.6	2.4		
		0.75	51.9	91.2	1.8		131.2	2.5		
		1.0	69.2	122.6	1.8		193.6	2.8		
	Line C	0.25	17.3	94.8	5.5	5.6	138.3	8.0	8.25	1.47
		0.5	34.6	192.9	5.6		285.9	8.2		
		0.75	51.9	291.7	5.6		422.95	8.1		
		1.0	69.2	393.95	5.7		602.6	8.7		
	Line D	0.25	17.3	22.2	1.3	1.45	24.0	1.4	1.55	1.07
		0.5	34.6	50.4	1.5		54.3	1.6		
		0.75	51.9	77.4	1.5		81.3	1.6		
		1.0	69.2	105.5	1.5		108.6	1.6		
V3V5L3A (100x100x3 -60x60x3)	Line C	0.2	5.5	57.7	10.5	11.1	63.1	11.5	11.6	1.04
		0.4	11.1	128.8	11.6		133.5	12.0		
		0.6	16.6	186.4	11.2		192.5	11.6		
		0.8	22.1	247.4	11.1		250.2	11.3		
	Line D	0.2	5.5	32.9	6.0	6.15	40.8	7.4	7.3	1.19
		0.4	11.1	68.9	6.2		77.3	7.0		
		0.6	16.6	101.2	6.1		112.2	6.8		
		0.8	22.1	139.1	6.3		176.2	8.0		
	Line E	0.2	5.5	13.4	2.4	2.55	26.3	4.8	5.125	2.01
		0.4	11.1	31.1	2.8		68.0	6.1		
		0.6	16.6	41.3	2.5		80.8	4.9		
		0.8	22.1	55.6	2.5		103.9	4.7		
V3V4L3A (100x100x3 -30x30x2)	Line C	0.1	13.8	48.1	3.5	4.025	54.6	3.9	4.4	1.09
		0.15	20.6	83.6	4.1		89.6	4.3		
		0.2	27.5	117.3	4.3		130.2	4.7		
		0.25	34.4	143.6	4.2		162.8	4.7		
	Line D	0.1	13.8	48.6	3.5	4.175	56.7	4.1	5.075	1.22
		0.15	20.6	82.8	4.0		90.3	4.3		
		0.2	27.5	125.0	4.5		154.5	5.6		
		0.25	34.4	163.2	4.7		215.0	6.3		
	Line E	0.1	13.8	18.4	1.3	1.525	22.6	1.6	1.775	1.16
		0.15	20.6	32.1	1.6		37.7	1.8		
		0.2	27.5	45.1	1.6		50.9	1.9		
		0.25	34.4	53.9	1.6		60.7	1.8		

Table 6-6 cont: Determination of SCF, Tube-to-tube T-joints

Connection	Position	Load (kN)	Nominal Stress, σ_{nom} (MPa)	Linear Extrapolation			Quadratic Extrapolation			$\frac{SCF_q}{SCF_l}$
				σ_{hs} (MPa)	SCF	SCF_l Average	σ_{hs} (MPa)	SCF	SCF_q Average	
V6V1L3A (70x70x3-50x50x3)	Line C	0.15	6.2	13.7	2.2	2.125	21.0	3.4	3.325	1.56
		0.3	12.5	25.9	2.1		39.3	3.1		
		0.45	18.7	38.4	2.1		57.8	3.1		
		0.6	25.0	53.6	2.1		91.4	3.7		
	Line D	0.15	6.2	18.98	3.1	2.45	38.2	6.2	3.425	1.40
		0.3	12.5	28.2	2.3		32.5	2.6		
		0.45	18.7	41.2	2.2		48.1	2.6		
		0.6	25.0	54.6	2.2		56.7	2.3		
	Line E	0.15	6.2	8.0	1.1	1.325	10.2	1.6	1.75	1.32
		0.3	12.5	17.0	1.4		22.8	1.8		
		0.45	18.7	26.0	1.4		32.3	1.7		
		0.6	25.0	35.0	1.4		48.6	1.9		
V6V2L3A (70x70x3-40x40x2)	Line C	0.15	14.0	53.4	3.8	4.025	72.8	5.2	5.475	1.36
		0.3	28.0	122.3	4.4		162.7	5.8		
		0.45	42.0	171.3	4.1		226.7	5.4		
		0.6	56.0	229.4	4.1		307.1	5.5		
	Line D	0.15	14.0	34.9	2.5	2.775	46.3	3.3	3.55	1.28
		0.3	28.0	82.8	3.0		106.5	3.8		
		0.45	42.0	116.9	2.8		151.1	3.6		
		0.6	56.0	154.7	2.8		197.9	3.5		
	Line E	0.15	14.0	22.4	1.6	1.775	34.3	2.5	2.425	1.37
		0.3	28.0	52.6	1.9		68.5	2.4		
		0.45	42.0	74.6	1.8		100.9	2.4		
		0.6	56.0	100.5	1.8		135.9	2.4		

1. Linear Extrapolation in 3mm thick tubes: t = 3mm, two points (i) 0.4 t but not less than 4mm = 4mm (ii) 0.6t further away from fist point = 1.8mm.
2. Quadratic Extrapolation in 3mm thick tubes: t = 3mm, two or more points (i) 0.4 t but not less than 4mm = 4mm (ii) 1.0t further away from fist point = 3mm (iii) all points between points (i) and (ii).
3. Linear Extrapolation in 2mm thick tubes: t = 2mm, two points (i) 0.4 t but not less than 4mm = 4mm (ii) 0.6t further away from fist point = 1.2mm.
4. Quadratic Extrapolation in 2mm thick tubes: t = 2mm, two or more points (i) 0.4 t but not less than 4mm = 4mm (ii) 1.0t further away from fist point = 2mm (iii) all points between points (i) and (ii).
5. Linear Extrapolation in 1.6mm thick tubes: t = 1.6mm, two points (i) 0.4 t but not less than 4mm = 4mm (ii) 0.6t further away from fist point = 0.96mm.
6. Quadratic Extrapolation in 1.6mm thick tubes: t = 1.6mm, two or more points (i) 0.4 t but not less than 4mm = 4mm (ii) 1.0t further away from fist point = 1.6mm (iii) all points between points (i) and (ii).

6.5.4 Experimental Stress Concentration Factors

A summary of the SCF for the different connections, which have been obtained through the measurement of strains, is shown in Table 6-7.

Table 6-7: Comparison of Experimental SCF with SCF from parametric equations

Series Name	Non-dimensional Joint Parameters				Soh & Soh 1990		IIW SCF Values				Experimental SCF (Average Quadratic)			
	β	2γ	τ	α	Chord	Brace	Line A/E	Line B	Line C	Line D	Line E	Line B	Line C	Line D
D3D1L3A	0.50	33	1.00	12.00	17.1	12.1	-	-	-	-	-	9.3	12.0	7.8
D3D2 L3A	0.50	33	0.53	12.00	8.4	7.6	-	-	-	-	-	5.6	7.1	5.1
D3D4 L3A	0.35	33	1.00	12.00	-	-	-	-	-	-	-	4.6	12.7	7.7
D3D5 L3A	0.35	33	0.53	12.00	-	-	-	-	-	-	-	3.7	5.9	5.8
D6D1 L3A	0.67	25	1.00	12.00	16.3	11.8	11.8	14.7	19.0	9.4	-	3.2	8.4	4.2
D6D2 L3A	0.67	25	0.53	12.00	8.0	7.4	11.8	9.2	11.8	5.9	-	2.5	8.3	1.6
V3V5 L3A	0.60	33	1.00	12.00	21.2	14.2	-	-	-	-	5.1	-	11.6	7.3
V3V4 L3A	0.30	33	0.67	12.00	-	-	-	-	-	-	1.8	-	4.4	5.1
V6V1 L3A	0.71	23	1.00	12.86	16.1	11.8	11.1	12.3	15.1	7.8	1.8	-	3.3	3.4
V6V2 L3A	0.57	23	0.67	12.86	7.8	7.2	9.5	8.9	12.2	6.9	2.4	-	5.5	3.6

6.5.4.1 Effect of τ on SCF

The connection series tested show that τ has an influence on the SCF for the hot spot locations in the chord where strain measurements were carried out. For given values of β and 2γ, SCF increases with τ. For two connections with the same β and 2γ values the nominal stress in the connection with a larger τ value is smaller since this connection has a larger wall thickness and elastic section modulus. For a given load under bending, the connection with a larger τ value therefore has a smaller nominal stress, $\sigma = M/Z$. It can be seen from Table 6-6 that the same load on two connections with the same β and 2γ values produces hot spot stresses which are almost the same. As such the ratio of hot spot stress to nominal stress is higher for the connection with a larger τ value. For example a SCF for line C for the connections D3D1L3A and D3D2L3A of 12.0 and 7.1 respectively have been determined.

Similar trends are shown in SCF determined from parametric equations especially for SCF for the hot spot locations in the chord (Soh and Soh 1990, IIW 2000, van Wingerde 1992). The stress concentration factors for hot spot locations in the brace, lines A and E, are assumed to be the equal for two connections with the same β and 2γ values, when τ is between 0.5 and 1.0 (IIW 2000).

6.5.4.2 Effect of β on SCF

To determine the influence of β on SCF, the SCF for specimens with the same values of τ and 2γ are compared. The connections D3D5L3A and D3D2L3A for example have the same values of τ and 2γ of 0.53 and 33, but different β values of 0.35 and 0.5 respectively. The SCF along lines B and C for connection with the larger β value of 0.5 are higher compared to that of the connection with the smaller β value of 0.35. For connections D6D1L3A and V6V1L3A with values of τ and 2γ that are almost the same, there is a decrease in SCF in lines C and D as β increases from 0.67 to 0.71. This is consistent with the trend shown in graphs of SCF versus β value for given τ and 2γ values given in guidelines (IIW 2000). The IIW guideline shows that for T-joints made from rectangular hollow sections under in-plane bending, the SCF increases with an increase in β up to a certain value before decreasing again, for β values between 0.35 and 1.00, for given τ and 2γ values. It should be noted however that the connections D3D5L3A and D3D2L3A tested in this program, have 2γ values which lie outside the validity range of $12.5 \leq 2\gamma \leq 25$ given in (IIW 2000).

The connections, D3D4L3A, D3D1L3A and V3V5L3A, also have the same values of τ and 2γ of 1.00 and 33.33, but different β values of 0.35 and 0.5 and 0.6. When the SCF determined from quadratic extrapolation are compared SCF of almost the same value (12.7, 12.0 and 11.6) are obtained as the β value increases (0.35, 0.50 and 0.60). The SCF determined from the linear extrapolation method however, show a slight increase magnitude (9.75, 10.175 and 11.1) with an increase in β value (0.35, 0.50 and 0.60). The connections D3D4L3A, D3D1L3A and V3V5L3A tested in this program, also have 2γ values which lie outside the validity range of $12.5 \leq 2\gamma \leq 25$ given in (IIW 2000).

Future work needs to be performed to determine the trend of SCF with β in these connections.

The trend of SCF with β for stress concentration factors obtained experimentally, shows the dependents of SCF on the non-linearity of the strains obtained within the extrapolation region, especially for the SCF obtained using the quadratic extrapolation methods. The differences in non-linearity of strains obtained in the extrapolation region for the different connections and even lines A to E within the same connection can be seen in Table 6-6 as a ratio SCF_q/SCF_l. The different weld lengths in each connection result in different regions of extrapolation from the brace-chord interface, giving stress distributions, with different non-linearities.

6.5.4.3 Comparison of Experimental SCF with SCF from Parametric Equations

The parametric equations from the IIW (2000) Fatigue Design Procedure, given in Appendix F, have parametric bounds which covers 4 out of the 10 connections tested for SCF. Table 6-7 shows the SCF values determined from the IIW parametric equations, where the joints have non-dimensional parameters within the validity range. Four connections with a value of 2γ less than 25 fall within the validity range. The experimental SCF are significantly lower than the SCF determined from the parametric equations.

The parametric equations by Soh and Soh (1990), given in Appendix F, have a validity range that covers 7 out of the 10 connections in which SCF were determined. Out of the 7 connections, 4 have experimental SCF comparable to the SCF estimated by Soh and Soh's parametric equations. The other 3 out of the 7 connections, have experimental stress concentration factors which are significantly smaller than the SCF determined by parametric equations from Soh and Soh (1990).

The SCF obtained in the connections D6D1L3A, V3V5L3A and V6V1L3A are significantly smaller compared to the SCF determined from the parametric equations. These connections have large β values of 0.67, 0.6 and 0.71 for D6D1L3A, V3V5L3A and V6V1L3A respectively. The weld leg lengths measured for these connections along the chord are 6.8mm, 7.2mm and 5.5mm for D6D1L3A, V3V5L3A and V6V1L3A respectively. These leg lengths are greater than the 4.2mm leg lengths which are required to give a weld with a throat thickness of 3mm recommended in AS4100-1998 (SAA 1998a), for nodal joints under fatigue loading. The oversized welds in connections of large β values push the positions of lines B, C and D, in the chord further away from the brace-chord interface. As the distance increases away from the brace-chord interface the stresses perpendicular to the weld toe decrease resulting in smaller SCF. Another fact is that the lines B, C and D in these connections become located in the corners of the chord, making positioning of the strain gauges difficult. The stress distribution in the corners of the chord is more complex than the stress distribution on the flats of the chord where the lines B,C and D are located in connections of low β values. This is likely to cause a considerable difference in the stresses measured perpendicular to the weld toe.

Another observation is that negative strains have been measured along lines B and C in some of the connections with large β values (D6D1L3A, Line B, Figure E27; V6V1L3A, Line C, Figure E43, Appendix E). This shows that close to and in the corner regions of the chord where the lines B and C are located for some of the joints with large β values, the section is in compression. Oversized welds move the hot spot location into or towards the compression region, resulting in smaller hot spot stresses and hence smaller SCF.

Maddox *et al* (1995) have showed that for a tubular joint geometry and loading considered, increasing the led length moves the weld toe into a lower stress region. Consequently, fatigue strength is increased with an increase in weld leg length on the chord side. Maddox *et al* (1995) also derived a correlation of the weld length on the chord side, t_{wh}, with experimental hot spot stress concentration factors for a joint with parameters β= 0.6, γ= 9.14 and τ= 0.76, as follows:

$$SCF_{chord} = 2.92 - 0.035t_{wh} \quad \textbf{(6.1)}$$

Maddox *et al* (1995) obtained a correlation coefficient of 0.63, suggesting that the variation in weld leg length alone was not sufficient to explain the variation in SCF, although this was an indication that oversized welds result in a reduction in SCF.

Measurement of weld profiles carried out in this investigation and reported in Mashiri *et al* (1999c, 2000c) has shown that the welds obtained for these thin-walled tube-to-tube with thicknesses less than 4mm are oversized.

Future work also needs to be undertaken to check if the restriction of the first point of extrapolation to not less than 4mm from the weld toe does not actually remove the measurement of stress from the region of steep gradient for thin-walled joints less than 4mm.

6.5.4.4 Influence of induced bending and axial force in chord on calculated SCF

The stress concentration factors determined in Table 6-6 and summarized in Table 6-7 are total stress concentration factors, SCF_{tot}. The total stress concentration factors are calculated by dividing the hot spot stress at a predetermined line, A to E, by the bending stress in the brace due to applied point load as follows;

$$SCF_{tot} = \frac{S_{hs}}{\sigma_{m1}} \tag{6.2}$$

where S_{hs} is the hot spot stress at a predetermined line (A to E), and σ_{ml} is the nominal stress due to bending in the brace.

The total stress concentration factors are a result of the effect of bending moment in the brace and the induced bending and axial stresses in the chord.

The tube-to-tube T-joints tested in this project were set up as shown in Figure 6-14.

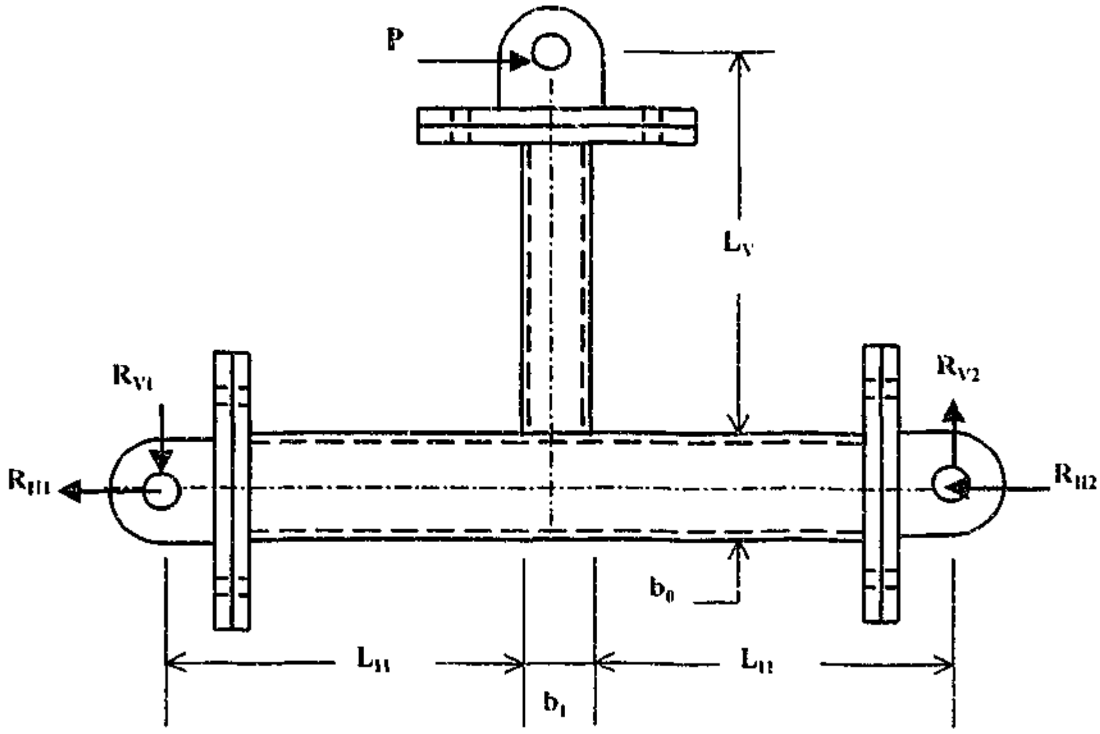

Figure 6-14: Setup of tube-to-tube T-joints

The reactions on the pins in the chord are;

$$R_{H1} = R_{H2} = P/2 \tag{6.3}$$

$$R_{V1} = -R_{V2} = P(L_V + b_0/2)/(2L_H + b_1) \tag{6.4}$$

The maximum moment in the brace at the brace-chord interface is;

$$M_1 = P \cdot L_V \tag{6.5}$$

The maximum moment in the chord at the brace-chord interface is;

$$M_0 = R_{v1} \cdot L_H = \frac{P \cdot L_H (L_V + b_0/2)}{2L_H + b_1} \tag{6.6}$$

The total hot spot stress range at any hot spot location is;

$$S_{r,hs} = \sigma_{r,a1} \cdot SCF_{a1} + \sigma_{r,m1} \cdot SCF_{m1} + \sigma_{r,a0} \cdot SCF_{a0} + \sigma_{r,m0} \cdot SCF_{m0} \tag{6.7}$$

where, SCF_{a0} is the stress concentration factor due to nominal axial stress in the chord, SCF_{a1} is the stress concentration factor due to nominal axial stress in the brace, SCF_{m0} is the stress concentration factor due to nominal in-plane bending stress in the chord, SCF_{m1} is the stress concentration factor due to nominal in-plane bending stress in the brace, $S_{r.hs}$ is the total hot spot stress range at any hot spot location usually defined by lines A to E, $\sigma_{r.a0}$ is the nominal axial stress range in the chord, $\sigma_{r.a1}$ is the nominal axial stress range in the brace, $\sigma_{r.m0}$ is the nominal in-plane bending stress range in the chord, and $\sigma_{r.m1}$ is the nominal in-plane bending stress range in the brace.

For the case shown in Figure 6-14;

$$S_{r.hs} = \sigma_{r.m1} \cdot SCF_{m1} + \sigma_{r.a0} \cdot SCF_{a0} + \sigma_{r.m0} \cdot SCF_{m0} \tag{6.8}$$

This equation can be expressed in terms of hot spot stress (instead of hot spot stress range) as follows;

$$S_{hs} = \sigma_{m1} \cdot SCF_{m1} + \sigma_{a0} \cdot SCF_{a0} + \sigma_{m0} \cdot SCF_{m0} \tag{6.9}$$

The total stress concentration factors in Tables 6-6 and 6-7 are calculated in terms of nominal stress due to bending in the brace;

$$\sigma_{m1} = \frac{M_1}{Z_1} = \frac{P \cdot L_V}{Z_1}. \tag{6.10}$$

In order to determine the component of SCF due to induced bending and axial force in the chord the terms σ_{a0} and σ_{m0} should be expressed in terms of σ_{m1}.

The nominal stress due to induced bending moment in the chord:

$$\sigma_{m0} = \frac{P \cdot L_H (L_V + b_0/2)}{Z_0(2L_H + b_1)} = \frac{\left[\left(\frac{PL_V}{Z_1}\right)L_H + \left(\frac{PL_V}{Z_1}\right) \cdot \frac{b_0 L_H}{2L_V}\right] \cdot Z_1}{Z_0(2L_H + b_1)} = \frac{\left[\sigma_{m1} \cdot L_H + \sigma_{m1} \cdot \frac{b_0 L_H}{2L_V}\right] \cdot Z_1}{Z_0(2L_H + b_1)} \tag{6.11}$$

The nominal stress due to induced axial force in the chord;

$$\sigma_{a0} = \frac{P}{2A_0} = \left(\frac{PL_r}{Z_1}\right)\cdot\frac{Z_1}{2L_r\cdot A_0} = \sigma_{m1}\cdot\frac{Z_1}{2L_r\cdot A_0} \tag{6.12}$$

Therefore;

$$S_{hs} = \sigma_{m1}\cdot SCF_{m1} + \sigma_{m0}\cdot SCF_{m0} + \sigma_{a0}\cdot SCF_{a0} \tag{6.13}$$

$$S_{hs} = \sigma_{m1}\cdot SCF_{m1} + \frac{\left[\sigma_{m1}\cdot L_H + \sigma_{m1}\cdot\frac{b_0 L_H}{2L_r}\right]\cdot Z_1}{Z_0\left(2L_H + b_1\right)}\cdot SCF_{m0} + \sigma_{m1}\cdot\frac{Z_1}{2L_r\cdot A_0}\cdot SCF_{a0} \tag{6.14}$$

The stress concentration factor due to axial force in the chord, SCF_{a0}, is equal to the stress concentration factor due to bending in the chord, SCF_{m0} (IIW 2000).

Therefore;

$$\frac{S_{hs}}{\sigma_{m1}} = SCF_{tot} = SCF_{m1} + \left[\frac{\left(2L_r\cdot L_H + L_H b_0\right)}{\left(2L_H + b_1\right)}\cdot\frac{Z_1}{2Z_0 L_r} + \frac{Z_1}{2L_r\cdot A_0}\right]\cdot SCF_{m0} \tag{6.15}$$

Equation 6.15 can be written as:

$$\frac{S_{hs}}{\sigma_{m1}} = SCF_{tot} = SCF_{m1} + [\lambda]\cdot SCF_{m0} \tag{6.16}$$

where $\lambda = \left[\frac{\left(2L_r\cdot L_H + L_H b_0\right)}{\left(2L_H + b_1\right)}\cdot\frac{Z_1}{2Z_0 L_r} + \frac{Z_1}{2L_r\cdot A_0}\right]$ **(6.17)**

The multiplier of SCF_{mo} in equation 6.16, λ is given in Table 6-8 for the different connection series tested in this research program. The values of the multiplier, λ are very small and less than 1.0.

The current design guideline (IIW 2000) gives parametric equations for SCF_{m0}. The values of SCF_{m0} plotted graphically in IIW (2000), are much smaller compared to SCF_{ml} for a given T- or X-joint especially for larger 2γ values which are characteristic of thin-walled sections.

The axial force or bending moment in the chord also causes negligible stress concentration in the brace and the values of SCF_{m0} in the brace lines A and E are taken as zero. The effect of induced loading in the chord also causes negligible stress concentration in the chord along line B, and the value of SCF_{m0} in the chord along line B can be taken as zero (IIW 2000).

Equation 6.16 can be rewritten as:

$$\frac{SCF_{tot}}{SCF_{m1}} = 1 + [\lambda] \cdot \frac{SCF_{m0}}{SCF_{m1}} \qquad \textbf{(6.18)}$$

Since previous researchers have shown that the influence of bending moment and axial force in the chord causes a negligible effect on SCF along lines A, B and E. Therefore,

$$SCF_{m0} = 0 \qquad \text{for lines A, B and E} \qquad \textbf{(6.19)}$$

$$SCF_{tot} = SCF_{m1} \qquad \text{for lines A, B and E} \qquad \textbf{(6.20)}$$

Bending moment and axial force on the chord however cause stress concentrations along lines C and D. The stress concentration factors (SCFs) due to bending moment or axial force on the chord are identical and are given as parametric equations in IIW (2000) and reported in Appendix F.

Using the existing parametric equations from IIW (2000) the ratio SCF_{m0}/SCF_{m1}, in equation 6.18 can be determined and hence the ratio SCF_{tot}/SCF_{m1}.

Table 6-9 shows the ratios SCF_{m0}/SCF_{m1} and SCF_{tot}/SCF_{m1} for the tube-to-tube T-joints under investigation. Using the existing parametric equations the ratio SCF_{m0}/SCF_{m1} for the connections under investigation are all less than 0.3. The multiplier λ, also has values less than 0.3 for all the connections tested. The resulting ratios SCF_{tot}/SCF_{m1} are all approximately equal to 1.0 with the largest ratio being 1.07. The results in Table 6-9 show that the effect of induced bending and induced axial forces in the chord has very little influence on the total stress concentration factor, SCF_{tot} of the connections under investigation. Therefore the induced bending moment and axial force in the chord has very little effect on the measured stress concentration factors reported in Table 6-7.

Table 6-8: Multiplier of SCF_{mo} in determination of SCF_{m1}

Connection	L_v (mm)	L_H (mm)	b_0 (mm)	b_1 (mm)	Z_1 (mm^3)	Z_0 (mm^3)	A_0 (mm^2)	Multiplier λ
D3D1L3A	324	369	100	50	7790	35400	1140	0.1295
D3D2L3A	324	369	100	50	4680	35400	1140	0.0778
D3D4L3A	249	376.5	100	35	3400	35400	1140	0.0611
D3D5L3A	249	376.5	100	35	2160	35400	1140	0.0388
D6D1L3A	324	294	75	50	7790	19100	841	0.2240
D6D2L3A	324	294	75	50	4680	19100	841	0.1346
V3V5L3A	324	364	100	60	11710	35410	1141	0.1922
V3V4L3A	249	379	100	30	1810	35410	1141	0.0327
V6V1L3A	324	294	70	50	7790	16440	781	0.2573
V6V2L3A	324	299	70	40	3470	16440	781	0.1165

Table 6-9: Ratios SCF_{m0}/SCF_{m1} and SCF_{tot}/SCF_{m1} for the tube-to-tube T-joints

Series Name	SCF_{m0}/SCF_{m1}				SCF_{tot}/SCF_{m1}			
	LineA&E	LineB	LineC	LineD	LineA&E	LineB	LineC	LineD
D3D1	0.00	0.00	0.04	0.11	1.00	1.00	1.00	1.01
D3D2	0.00	0.00	0.05	0.16	1.00	1.00	1.00	1.01
D3D4	0.00	0.00	0.07	0.11	1.00	1.00	1.00	1.01
D3D5	0.00	0.00	0.10	0.16	1.00	1.00	1.00	1.01
D6D1	0.00	0.00	0.07	0.23	1.00	1.00	1.01	1.05
D6D2	0.00	0.00	0.09	0.31	1.00	1.00	1.01	1.04
V3V5	0.00	0.00	0.03	0.13	1.00	1.00	1.01	1.03
V3V4	0.00	0.00	0.13	0.16	1.00	1.00	1.00	1.01
V6V1	0.00	0.00	0.08	0.28	1.00	1.00	1.02	1.07
V6V2	0.00	0.00	0.09	0.26	1.00	1.00	1.01	1.03

The ratios SCF_{m0}/SCF_{m1} and SCF_{tot}/SCF_{m1} in Table 6.9 can be used to determine the values of SCF_{m1} and SCF_{m0} from the measured value of SCF_{tot} in Table 6-7. The values of SCF_{tot} and the corresponding values of SCF_{m1} and SCF_{m0} for the different specimens at different hot spot locations are given in Table 6-10. The values of SCF_{m1} and SCF_{m0} are then used in determining the total hot spot stress range at different hot spot locations for each joint using Equation 6.8.

The S-N data for the tube-to-tube T-joints tested in this investigation are given in terms of the hot spot stress range in Tables 6-11, 6-12 and 6-13 for the C450LO, S355JOH and C350LO tubes respectively. The total hot spot stress ranges have been determined according to both equations 6.2 and 6.8 for comparison. The total hot spot stress ranges are given for the hot spot location that gave the maximum value of total hot spot stress range. All the connections series tested had a maximum value of total hot spot stress range along line C except for the connection series V6V1 and V3V4 which had a maximum value of total hot spot stress range along line D.

A comparison of the total hot spot stress ranges obtained using equation 6.8 to those determined using equation 6.2 is shown graphically in Figure 6-15. There is a high correlation between the total hot spot stress ranges obtained from Equations 6.2 and 6.8. Figure 6-15 therefore, confirms the fact that the influence of induced bending moment and induced axial force in the chord on SCFs is negligible for tube-to-tube T-joints made up of thin-walled square hollow sections, in the setup used in this investigation .

Table 6-10: Values of SCF_{tot} and the corresponding values of SCF_{m1} and SCF_{m0} for the different specimens

Name	SCF_{tot}				SCF_{m1}				SCF_{m0} or SCF_{a0}			
	LineE	LineB	LineC	LineD	LineE	LineB	LineC	LineD	LineE	LineB	LineC	LineD
D3D1	-	9.30	12.00	7.80	-	9.30	11.94	7.69	0.00	0.00	0.44	0.87
D3D2	-	5.60	7.10	5.10	-	5.60	7.07	5.04	0.00	0.00	0.37	0.78
D3D4	-	4.60	12.70	7.70	-	4.60	12.65	7.65	0.00	0.00	0.89	0.87
D3D5	-	3.70	5.90	5.80	-	3.70	5.88	5.76	0.00	0.00	0.59	0.90
D6D1	-	3.20	8.40	4.20	-	3.20	8.28	4.00	0.00	0.00	0.54	0.91
D6D2	-	2.50	8.30	1.60	-	2.50	8.20	1.54	0.00	0.00	0.76	0.48
V3V5	5.10	-	11.60	7.30	5.10	-	11.53	7.12	0.00	0.00	0.39	0.93
V3V4	1.80	-	4.40	5.10	1.80	-	4.38	5.07	0.00	0.00	0.56	0.82
V6V1	1.80	-	3.30	3.40	1.80	-	3.23	3.17	0.00	0.00	0.27	0.88
V6V2	2.40	-	5.50	3.60	2.40	-	5.45	3.49	0.00	0.00	0.47	0.92

Table 6-11: S-N data for tube-to-tube T-joints in terms of hot spot stress range (Grade C450LO)

Connection Name	Fatigue Life, N (cycles)	P_{max} (N)	R	$\sigma_{r,m1}$ (MPa)	$\sigma_{r,a0}$ (MPa)	$\sigma_{r,m0}$ (MPa)	SCF_{m1}	SCF_{a0} or SCF_{m0}	$S_{r,hs}$ (Eqn. 6.8) (MPa)	$S_{r,hs}$ (Eqn. 6.2) (MPa)
D3D1L1A	16302	990	0.1	37.06	0.39	4.08	11.94	0.44	444.55	442.85
D3D1L1B	30360	990	0.1	37.06	0.39	4.08	11.94	0.44	444.55	442.85
D3D1L2A	786679	400	0.1	14.97	0.16	1.65	11.94	0.44	179.62	178.93
D3D1L3A	471200	400	0.1	14.97	0.16	1.65	11.94	0.44	179.62	178.93
D3D1L3B	175744	533	0.1	19.95	0.21	2.20	11.94	0.44	239.34	238.57
D3D1L3B	19937	800	0.1	29.95	0.32	3.29	11.94	0.44	359.24	357.86
D3D2L1A	133625	700	0.1	43.62	0.28	2.88	7.07	0.37	309.58	310.76
D3D2L2A	10969239	400	0.1	24.92	0.16	1.65	7.07	0.37	176.90	177.58
D3D2L3A	52829	800	0.1	49.85	0.32	3.29	7.07	0.37	353.81	355.15
D6D1L1A	170766	1200	0.1	44.92	0.64	9.16	8.28	0.54	377.18	376.20
D6D1L1B	145444	1200	0.1	44.92	0.64	9.16	8.28	0.54	377.18	376.20
D6D1L2A	2453350	500	0.1	18.72	0.27	3.82	8.28	0.54	157.16	156.75
D6D1L2B	6642981	500	0.1	18.72	0.27	3.82	8.28	0.54	157.16	156.75
D6D1L3B	324153	800	0.1	29.95	0.43	6.11	8.28	0.54	251.45	250.80
D6D1L3A	254276	1075	0.1	40.24	0.58	8.21	8.28	0.54	337.89	337.01
D6D2L1A	89294	1200	0.1	74.77	0.64	9.16	8.20	0.76	620.39	616.85
D6D2L2A	2885483	500	0.1	31.15	0.27	3.82	8.20	0.76	258.49	257.02
D6D2L3A	152682	1000	0.1	62.31	0.54	7.63	8.20	0.76	516.99	514.04
D3D4L1A	288292	400	0.1	26.36	0.16	1.27	12.65	0.89	334.66	334.83
D3D4L1B	328247	400	0.1	26.36	0.16	1.27	12.65	0.89	334.66	334.83
D3D4L2A	589163	288	0.1	19.01	0.11	0.91	12.65	0.89	241.29	241.41
D3D4L2B	340417	300	0.1	19.77	0.12	0.95	12.65	0.89	251.00	251.12
D3D4L3B	3925476	200	0.1	13.18	0.08	0.63	12.65	0.89	167.33	167.42
D3D4L3A	799808	300	0.1	19.77	0.12	0.95	12.65	0.89	251.00	251.12
D3D5L1A	264239	400	0.1	41.50	0.16	1.27	5.88	0.59	244.74	242.78
D3D5L2A	754797	300	0.1	31.13	0.12	0.95	5.88	0.59	183.56	182.08
D3D5L3A	2959837	300	0.1	31.13	0.12	0.95	5.88	0.59	183.56	182.08

Table 6-12: S-N data for tube-to-tube T-joints in terms of hot spot stress range (Grade S355JOH)

Connection Name	Fatigue Life, N (cycles)	P_{max} (N)	R	$\sigma_{r,m1}$ (MPa)	$\sigma_{r,a0}$ (MPa)	$\sigma_{r,m0}$ (MPa)	SCF_{m1}	SCF_{a0} or SCF_{m0}	$S_{r,hs}$ (Eqn. 6.8) (MPa)	$S_{r,hs}$ (Eqn. 6.2) (MPa)
V3V5L1A	124028	1200	0.1	29.88	0.47	4.94	11.53	0.39	346.51	346.63
V3V5L1B	86947	985	0.1	24.53	0.39	4.06	11.53	0.39	284.42	284.53
V3V5L2A	5846429	500	0.1	12.45	0.20	2.06	11.53	0.39	144.38	144.43
V3V5L2B	155368	800	0.1	19.92	0.32	3.29	11.53	0.39	231.00	231.09
V3V5L3A	147376	800	0.1	19.92	0.32	3.29	11.53	0.39	231.00	231.09
V3V5L3B	7536844	500	0.1	12.45	0.20	2.06	11.53	0.39	144.38	144.43
V3V1L1A	29183	900	0.1	33.69	0.36	3.71	11.94	0.44	404.04	402.59
V3V1L2B	22069	900	0.1	33.69	0.36	3.71	11.94	0.44	404.04	402.59
V3V1L3A	60055	600	0.1	22.46	0.24	2.47	11.94	0.44	269.36	268.39
V3V1L3B	2093716	400	0.1	14.97	0.16	1.65	11.94	0.44	179.57	178.93
V6V2L1A	45365	800	0.1	67.23	0.46	7.11	5.45	0.47	369.64	368.07
V6V2L2A	1453800	400	0.1	33.61	0.23	3.56	5.45	0.47	184.82	184.04
V6V2L2B	105456	700	0.1	58.82	0.40	6.22	5.45	0.47	323.43	322.06
V6V2L3B	1095618	400	0.1	33.61	0.23	3.56	5.45	0.47	184.82	184.04
V6V2L3A	168446	600	0.1	50.42	0.35	5.33	5.45	0.47	277.23	276.05
V6V1L1A	513067	1200	0.1	44.92	0.69	10.67	3.17*	0.88*	152.55	149.36
V6V1L2B	560477	1200	0.1	44.92	0.69	10.67	3.17*	0.88*	152.55	149.36
V6V1L3B	9423530	600	0.1	22.46	0.35	5.33	3.17*	0.88*	76.28	74.68
V6V1L3A	825878	1169	0.1	43.76	0.67	10.39	3.17*	0.88*	148.61	145.50
V3V4L1A	162405	300	0.1	37.14	0.12	0.95	5.07*	0.82*	189.31	188.50
V3V4L2A	229799	300	0.1	37.14	0.12	0.95	5.07*	0.82*	189.31	188.50
V3V4L2B	303680	350	0.1	43.33	0.14	1.11	5.07*	0.82*	220.86	219.92
V3V4L3A	979654	250	0.1	30.95	0.10	0.79	5.07*	0.82*	157.76	157.09

* Most of the SCF giving the highest total hot spot stress range occurred along line C except in the connection series V3V4 and V6V1 where the highest total hot spot stress range occurred along line D

Table 6-13: S-N data for tube-to-tube T-joints in terms of hot spot stress range (Grade C350LO)

Connection Name	Fatigue Life, N (cycles)	P_{max} (N)	R	$\sigma_{r.m1}$ (MPa)	$\sigma_{r.a0}$ (MPa)	$\sigma_{r.m0}$ (MPa)	SCF_{m1}	SCF_{a0} or SCF_{m0}	$S_{r.hs}$ (Eqn. 6.8) (MPa)	$S_{r.hs}$ (Eqn. 6.2) (MPa)
S3S2L1A	121207	700	0.1	43.62	0.28	2.88	7.07	0.37	309.58	310.76
S3S2L2A	269341	550	0.1	34.27	0.22	2.27	7.07	0.37	243.24	244.17
S3S2L3A	3009445	400	0.1	24.92	0.16	1.65	7.07	0.37	176.90	177.58
S6S2L1A	43770	1200	0.1	74.77	0.64	9.16	8.20	0.76	620.39	616.85
S6S2L2A	1641907	500	0.1	31.15	0.27	3.82	8.20	0.76	258.49	257.02
S6S2L3A	177201	800	0.1	49.85	0.43	6.11	8.20	0.76	413.59	411.23
S3S5L1A	886078	400	0.1	41.50	0.16	1.27	5.88	0.59	244.74	242.78
S3S5L2A	886921	300	0.1	31.13	0.12	0.95	5.88	0.59	183.56	182.08
S3S5L3A	1371529	200	0.1	20.75	0.08	0.63	5.88	0.59	122.37	121.39

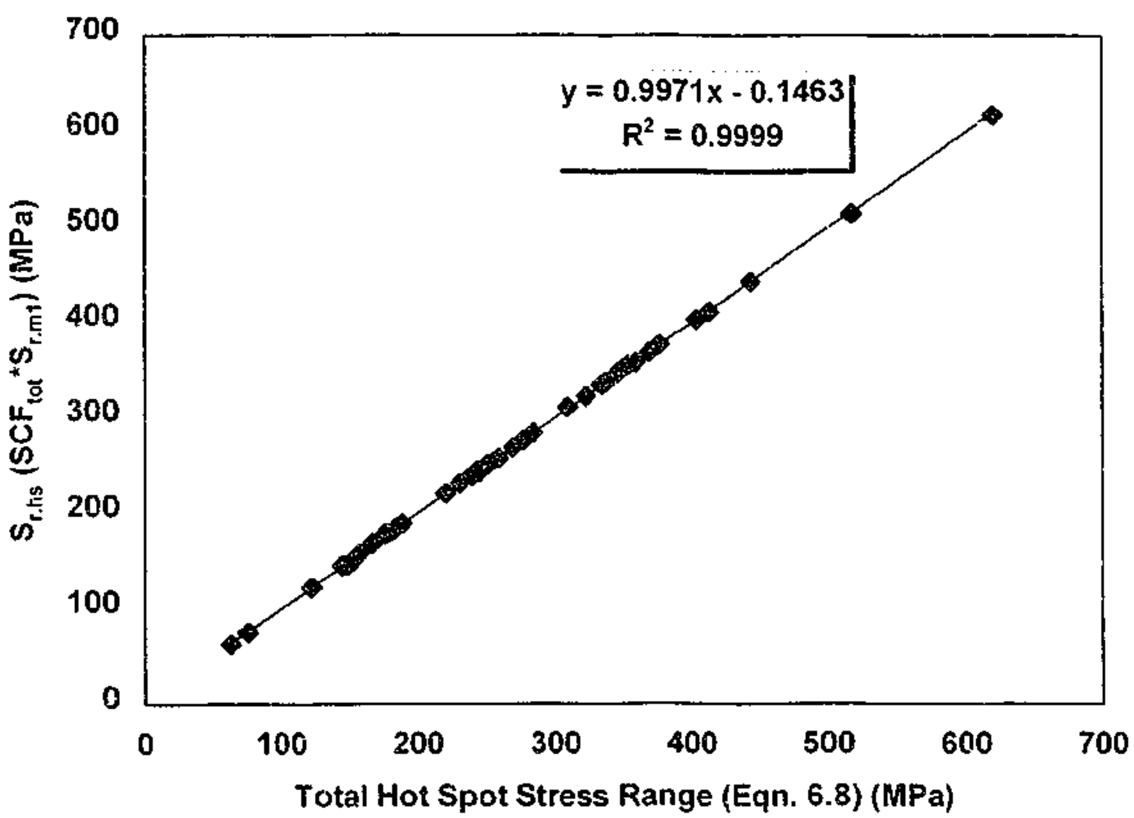

Figure 6-15: Comparison of Hot Spot Stress Range with and without influence of induced actions in chord

6.6 SUMMARY

The following observations, discussions and conclusions are related to the fatigue tests and experimental stress concentration factors carried out and determined for tube-to-tube T-joints made up of thin-walled square hollow sections.

(a) Different modes of failure were observed during the fatigue testing of tube-to-tube T-joints under in plane bending. The different modes of failure are summarised in Table 6-14.

(b) The nominal stresses determined from the strain gauge measurements were compared to the values determined using the simple beam theory. The absolute value of percentage difference between the beam theory and the experimental nominal stresses varied between 0.68% to 20%, with an average absolute difference of 4.59%. A high correlation of 0.99 exists between the experimental and the beam theory nominal stresses.

(c) Hot spot stresses were used to determine the experimental stress concentration factors using both the linear and quadratic extrapolation methods. The stress concentration factors determined for different load levels were found to be reasonably close to each other when the load applied was below the maximum elastic moment of the connection for most of the joints tested. In some few cases however a non-linear response was observed in the distribution of the stress near the weld toe at higher applied loads. In the cases where a non-linear response was observed the stress concentration factors at these higher loads were discarded. The non-linear response might be a result of higher notch stresses in some of the nodal joints causing a non-linear response between load and strain close to the toe of the weld although the moment applied was below the maximum elastic moment of the connection.

(d) The stress concentration factors determined by the quadratic method of extrapolation are higher than those determined by the linear extrapolation method. The ratios of the stress concentration factors determined by the quadratic extrapolation method (SCF_q) to the stress concentration factors determined by the linear extrapolation method (SCF_l) vary from 1.07 to 2.01, Table 6-6. This shows that the stress distribution of the tube-to-tube T-joints are highly non-linear compared to those of tube-to-plate T-joints (see section 5.5.3) where the ratios ranging from 1.04 to 1.18 were determined.

(e) The experimental stress concentration factors were found to be considerably lower than the stress concentration factors from the existing parametric equations by van Wingerde (1992) and Soh and Soh (1990). The lower stress concentration factors are attributed to the oversized welds associated with thin-walled joints. Maddox *et al* (1995) showed that for a tubular joint geometry and loading considered, increasing the leg length moves the weld toe into a lower stress region. The leg length of the welds measured showed that the welds in the tube-to-tube T-joints tested in this investigation are oversized (Tables 6-2 to 6-4). This is more so for the leg length in the chord. The oversized welds in the chord may be associated with gravity causing the molten welds to slump along the chord face during welding. Future work also needs to be undertaken to check if the restriction of the first point of extrapolation to not less than 4mm from the weld toe does not actually remove the measurement of stress from the region of steep gradient for thin-walled joints less than 4mm.

(f) It has been demonstrated that the influence of induced bending moment and induced axial force in the chord on stress concentration factors (SCFs) is negligible for tube-to-tube T-joints under in-plane bending load made up of thin-walled square hollow sections of thicknesses less than 4mm. for the test setup used in this investigation.

Table 6-14: Modes of failure

Mode of Failure	**Compression/ Tension Side**	**Crack Location**	**Comment**
Chord-Tension-Side Failure	Tension	Chord	Majority of test specimens with β values of 0.30, 0.35, 0.50 and 0.60, Higher SCF in chord, Figure 6-4
Chord-and-Brace-Tension-Side Failure	Tension	Chord and Brace	Some of the test specimens with β values of 0.57, 0.67 and 0.71, stress redistribution resulting in higher stresses in the brace, Figures 6-5 to 6-7
Brace-Tension-Side Failure	Tension	Brace	One Specimen with a β value of 0.67 and τ value of 0.53, Smaller leg length on brace resulting in higher notch stresses, Figure 6-8
Chord-Compression-Side Failure	Compression	Chord	One Specimen with a β value of 0.5, Tensile residual stresses, undercuts, larger than usual micro-cracks, Figure 6-9

Chapter 7

EFFECTS OF WELD PROFILE AND UNDERCUT ON FATIGUE CRACK PROPAGATION LIFE OF THIN-WALLED CRUCIFORM JOINTS

7.1 INTRODUCTION

Chapter 7 details the numerical analyses carried out to determine the influence of weld profile and weld toe undercut on fatigue crack propagation life of 2 dimensional cruciform joints. The cruciform joint models were made up of thin-walled plates of 3mm thicknesses. The dimensions of undercut and weld profiles used in these analyses are those reported in Chapter 3, and measured from welded connections made from grade C350LO steel. The cruciform joints analysed are under cyclic tensile loading.

There has been an increased use of thin-walled tubular sections with thicknesses less than 4mm in the construction of undercarriages and support systems of agricultural and road equipment. The structural systems such as trailers, haymakers, graders and swing-ploughs are subjected to fatigue loading under service. Fatigue failures may occur in these structures. Although a lot of research has been done on fatigue of welded tubular connections (Wardenier 1982; Marshall 1992; van Wingerde 1992; van Wingerde *et al* 1996a; Packer and Henderson 1997; IIW 2000), little has been done on the fatigue of thin-walled tubular sections below 4mm thickness. The latest CIDECT (International Committee for the Development and Study of Tubular Structures) Design Guide for welded tubular joints under fatigue loading covers steel hollow sections only with a thickness of 4mm and above (Zhao *et al* 1999a). The weld profiles and weld undercut may affect the fatigue crack propagation life of welded joints especially for thin-walled sections.

Few fatigue tests of joints with thicknesses less than 4mm have been reported (Puthli *et al* 1989; Mashiri *et al* 1999b, 2000a). In tests on K-joints with gap made up of tubular sections (Puthli *et al* 1989) it has been observed that for thicknesses less than 4mm, the trend of increase in fatigue life with decrease in wall thickness of the failed member is no longer true. In tests on tube-to-plate T-joints (Mashiri *et al* 1999b, 2000a), the fatigue life of joints with 1.6mm thick tubes was found to be less than that of joints with 3mm tubes. It is believed that in thinner walled structures, the weld toe undercuts may have a more negative impact on fatigue life resulting in lower fatigue life than expected from the traditional trend of thickness effect. It is important therefore to study the influence of weld defects and weld geometry on fatigue crack propagation life for thin-walled sections.

Measurement of weld profiles and weld undercut using the silicon imprint technique (Miki *et al* 1990) is reported in Chapter 3 for welded tubular T-joints with thicknesses less than 4mm. The ranges of undercut depth, width and radius from Grade C350LO connections which were used in these 2 dimensional analyses are summarised in Table 7-1.

Table 7-1: Ranges of undercut depth, width and radius

Parameter of Undercut	Range (mm)
Depth (mm)	0.08-0.3
Width (mm)	0.5-2.5
Radius (mm)	0.25-3.81

Two-dimensional cruciform joints with thickness of 3mm were analysed using the Boundary Element Analysis System Software (BEASY) which uses fracture mechanics theory to carry out crack propagation analysis. The measured weld profiles and undercut were utilised in the analysis to demonstrate their effects on fatigue crack propagation life.

The results of the present study were also compared with those of a similar study on 20mm thick cruciform joints (Miki *et al* 1990). It seems that the weld undercut has a more severe influence on fatigue crack propagation life for thin-walled sections.

7.2 WELD PROFILES AND WELD UNDERCUT

7.2.1 Material properties and welding procedure

In order to obtain the weld profiles and undercuts which are likely to occur in "real" thin-walled joints, tubular T-joints have been manufactured using the gas-metal arc (MIG) and gas-tungsten arc (TIG) welding methods, to produce fillet welds. The tubes used were of 3mm and 1.6mm thicknesses. They were used to make both tube-to-plate and tube-to-tube T-joints. The measurements give details of weld profiles and weld undercuts likely to occur during the welding of thin-walled connections. The tubes are of grade C350LO and have a yield stress and ultimate tensile strength of 350MPa and 430MPa respectively. The MIG welds are done using the electrode AustMIG ES6, which gives welds of yield stress and tensile strength of 480MPa and 580MPa respectively. The TIG welding method involved use of the Comeweld Super Steel ER70S-2 electrode giving welds with a yield stress of 425MPa and a weld metal tensile strength of 520MPa. The MIG and TIG welds satisfied the qualification requirements for macro-cross section examination to check the soundness of the weld. Hardness tests to check the magnitude and hence comparative hardness values of the parent metal, heat-affected zone and weld metal, stipulated in the Australian Standards, AS1554.1-1995 (SAA 1995a) and AS 1554.5-1995 (SAA 1995b), were also conducted. Detailed information on weld procedure qualification is given in Chapter 3.

7.2.2 Undercut

Undercut can be defined as a surface depression along the interface between weld and parent metal, caused by weld procedure and resulting in missing material. During the welding process, erosion of the base material beside the weld interface can occur, followed by subsequent solidification of the weld metal, without the depression becoming filled (Petershagen 1985). Undercuts can be formed in fully mechanised welding of long fillet welds in the horizontal position with high heat input. The weld metal on the vertical plate sags before it can solidify to give the required weld shape. In manual arc-welding, an injudicious guidance of the electrode can result in a deficiency of weld metal at the weld interface at the time when the weld surface is solidifying.

Allowable limits for undercuts relate to the depth of the notch, to their length, as well as to the separation between adjacent undercuts. AS1554.1-1995 (SAA 1995a) gives a maximum permissible depth of undercut depending on wall thickness. The maximum permissible depth for intermittent undercut must be equal to *t/10* but not exceeding 1.5mm. For the 3mm thick joints analysed in this chapter the maximum permissible depth of undercut is therefore 0.3mm. The influence of undercuts on the fatigue strength depends on their shape. Undercuts can exhibit crack-like flaws at the base of the notch. This is normally the case for welded joints (Smith and Hirt 1983)

The parameters which were used to define the undercut were the depth (d), width (δ), and the radius (ρ) as shown in Figure 7-1. The shape of weld toe undercut, defined by these parameters, were determined using the imprint technique (Miki *et al* 1990), where silicone rubber was used. A more detailed description of the silicon imprint technique is given in Section 3.3 of Chapter 3.

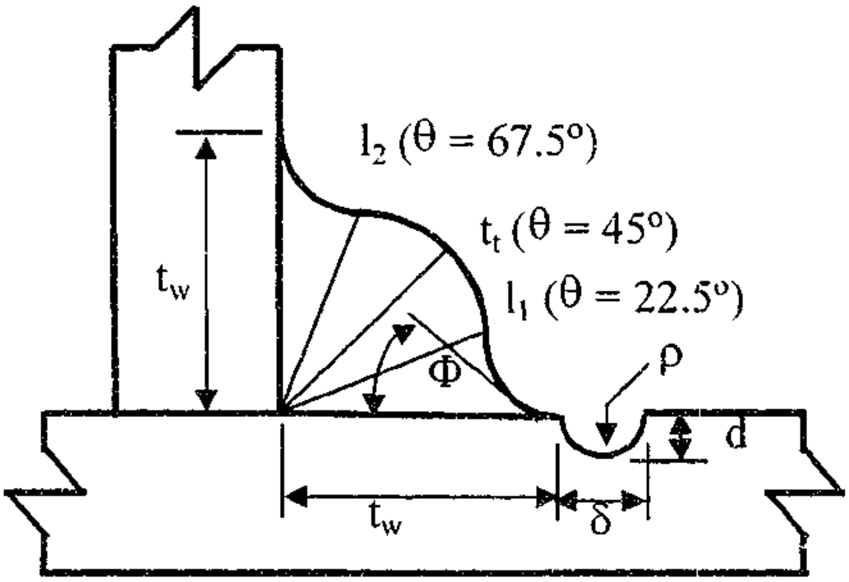

Figure 7-1: Parameters defining Weld Profile and Undercut for a Fillet-welded Joint

7.2.3 Weld profile

The parameters which were used to define the weld profiles were the leg length (t_w), throat thicknesses (t_t, l_1, l_2), weld toe radius and weld toe angle (Φ) as shown in Figure 7-1. Note that although the undercut in Figure 7-1 has been shown on one of the weld toes, in practice it can occur on either of the weld toes.

Typical weld profiles from the MIG and TIG welded connections are shown in Figure 7-2. Details of the measurement of weld profiles using the silicon imprint technique are given in Section 3.3 of Chapter 3.

The profiles adopted in the modelling shown in Figures 7-5a and 7-5b match the typical profiles obtained from the MIG and TIG welding methods as shown in Figures 7-2a and 7-2b respectively.

The silicon imprint technique allows the measurement of the sectional dimensions of the weld profile and weld toe undercut only, from the silicon rubber slices obtained. The measurements carried out only give the sectional dimensions of the weld profile and weld toe undercut but do not give an estimate of the length of the undercut or change in profile with length. The 2-dimensional cruciform models analysed in this chapter only require the section dimensions of the undercut and hence assume that the weld toe undercut is continuous along the weld toe in the cruciform joint. The assumption that weld toe undercut is continuous along the weld toe in the 2-dimensional cruciform joint models results in a conservative value of fatigue crack propagation life being computed. Compared to real life crack propagation life where semi-elliptical cracks initiate at different locations and then coalesce to form a single crack (Booth 1987), the 2-dimensional models assume a straight crack front and a continuous undercut along the weld toe.

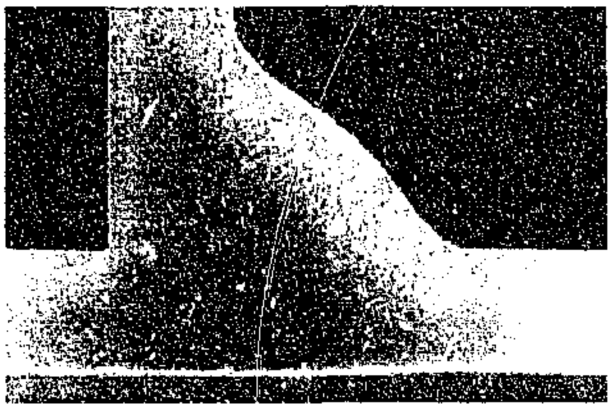

(a) MIG welded profile

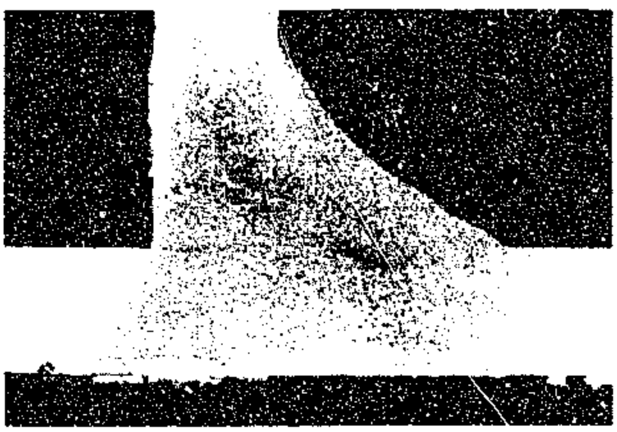

(b) TIG welded profile

Figure 7-2: Typical profiles from MIG and TIG welded joints

7.3 CRACK PROPAGATION

7.3.1 General

Fracture mechanics based fatigue assessment is a powerful, yet often under-utilised methodology. One of the key advantages of the fracture mechanics approach to fatigue over the conventional S-N approach is the ability to examine analytically the effect of geometric and loading variables on the fatigue performance of a structure (Grover 1989). For welded joints, it is often assumed that there is no initiation period due to the presence of weld defects. Small fatigue cracks actually initiate at an early stage of fatigue in the welded joints, where crack-like defects or high stress concentrations exist. These reduce the initiation stage of the fatigue and make it relatively less important than the propagation stage (Yamada & Kainuma 1996; Zhao *et al* 1999b). The small crack-like discontinuities, termed intrusions, exist at the weld toe. They are a product of conditions during welding which arise with most of the arc processes (Maddox 1991).

7.3.2 Fatigue propagation life estimation using BEASY (Computational Mechanics BEASY Ltd 1998).

The simulation of general mixed-mode crack growth using numerical techniques requires the capability of predicting the direction and amount of each crack growth for each given load increment as well as the robustness to update the numerical model to account for the changing crack geometry (Mi & Aliabadi 1994). BEASY possesses these characteristics. The solution of the general crack problem is not possible with the direct application of the boundary element method in a single region analysis. This is because of the coincidence of crack surfaces which gives rise to a singular system of algebraic equations (Portela & Aliabadi 1992). This drawback has led to the development of alternative formulations such as the dual boundary element method. BEASY uses dual elements for 2D crack growth analysis. The dual boundary element method incorporates two independent boundary integral equations; the displacement equation applied at the collocation point on one of the crack surfaces and the traction equation applied on the other surface (Trevelyan 1994). The crack growth direction and stress intensity factor equivalent are computed by the minimum strain energy density criterion proposed by Sih and Cha (1974). The J-integral technique is used to compute the stress intensity factors.

The boundary element analysis system software (BEASY) uses the NASGRO equation (7.1), which is a modified form of the Paris equation:

$$\frac{da}{dN} = \frac{C \cdot (1-f)^n \cdot \Delta K^n \cdot \left(1 - \frac{\Delta K_{th}}{\Delta K}\right)^p}{(1-R)^n \cdot \left(1 - \frac{\Delta K}{(1-R)K_c}\right)^q} \tag{7.1}$$

Details of the NASGRO equation (7.1) are given in Section 2.5.3 of Chapter 2.

Since in 2-dimensional models the cracks are represented by line elements, a straight crack front is assumed, as compared to the semi-elliptical crack front which is normally assumed in 3-dimensional models and confirmed by some occurrences of beach-marks in real structures. The effect of residual stresses was not taken into account. This is because residual stresses have little effect on stress range and hence stress intensity factor range (van Delft 1981). Fatigue crack propagation life depends on stress intensity factor range as shown in equation (7.1). The modified Paris equation used in the BEASY program calculates fatigue crack propagation life. In order to estimate crack propagation life, there should be an initial crack in the 2D models. It can be assumed that there are crack-like defects in welded structures which make the initiation period relatively less important. The S-N curves produced from this analysis are therefore of stress range versus fatigue crack propagation life. Fatigue crack propagation life is determined automatically for the 2-dimensional models through integration of the modified Paris equation between an initial crack depth of 0.1mmm to a final crack depth, which put the crack front at 40% of the thickness of the plate. There is no significant increase in fatigue crack propagation life in 2-dimensional cruciform joint models after this stage (Mori *et al* 1997). The use of the initial crack depth of 0.1mm is explained in section 7.4.2.

The following crack propagation iterations are performed automatically by BEASY;

(i) a boundary element analysis of the cracked structure,

(ii) computation of stress intensity factors for each crack tip,

(iii) computation of the direction of crack-extension increment for each crack tip, in the direction of maximum principal stress or in the direction of minimum strain energy density,

(iv) extension of the crack by one element in the direction of maximum principal stress or in the direction of minimum strain energy density, and

(v) repeating step (ii) to (v) until the crack extension is such that the crack tip is located at 40% of the plate thickness.

After step (iv), the number of cycles for fatigue crack propagation life for each crack growth increment is determined. The sum of the *dN* values for all the crack growth increments correspond to the fatigue crack propagation life for the modelled joint.

7.4 BOUNDARY ELEMENT ANALYSES

7.4.1 Elements

The fatigue propagation analyses were carried out using the Boundary Element Analysis System Software (BEASY). Two-dimensional models were used in these analyses as shown in Figure 7-5. In boundary element analysis, elements must be placed on all external boundaries and on any interface surfaces or lines between sub-regions of the model. Elements were therefore placed to define the welded plates and the welds and at the same time used to define the different weld profiles and undercuts. For 2D models, boundary elements are lines. More elements or nodes were placed in the part of the model around the toe of the weld and weld toe undercut from which the crack was propagated. This is the stress concentration region because of the crack, the weld and the undercut. Every element has nodes, where the problem variables are calculated. Elements can be constant (1 node), linear (2 nodes) or quadratic (3 nodes). All line elements also have three mesh points, which are geometric points to define the position and curvature of the line element. In this analysis quadratic elements were used. Quadratic elements produce the most accurate results (Computational Mechanics BEASY Ltd 1998).

7.4.2 Parameters

Cruciform joints with plates of 3mm thickness are modelled and analysed under cyclic tensile loading. An initial crack of 0.1 mm in depth was adopted as used by other researchers (Gurney 1979a; Maddox 1991; Ohta *et al* 1990; Nguyen and Wahab 1995,1996). Gurney (1979b) reported that, fatigue cracks in most welded joints initiate from the weld toe and that it is well established that the actual initiation point is formed by small, sharp slag intrusions, typically 0.1-0.4mm deep at the toe. The majority of service life is therefore occupied in propagating small cracks. It is therefore a reasonable approximation to assume crack depths of 0.1-0.4mm in determining fatigue crack propagation life. A crack depth of 0.1mm is therefore assumed as the initial crack size in all the 2-dimensional models analysed in this chapter. For weld profile models the initial crack is located at the weld toe. For the undercut models the initial crack is located at the base of the undercut profile, where cracks are likely to initiate because of the high notch stresses. The stress ratio, R used was 0.1. A stress ratio of 0.1 was chosen because this is the value normally used in fatigue tests of welded structures. However fatigue design guidelines show that the design of welded structures is independent of stress ratio but rather depended on the stress range applied. The yield stress of the plates is 350MPa, the same as the steel grade of the welded samples from which the weld profiles and undercut were measured. The values of n and C in equation (7.1) of 3 and 3×10^{-13} respectively have been adopted (Maddox 1991). The values of C and n are similar to the values in British Standards Published Document PD 6493 (BSI 1991). The value of exponents, p and q in equation (7.1) is 0.5 and the value of fracture toughness, K_C, of 52127N·mm$^{-3/2}$ is given for this steel in the BEASY database file (Computational Mechanics BEASY Ltd 1998). The value of ΔK_{th} used was 91.7N·mm$^{-3/2}$, as recommended by the Japanese Society of Steel Construction for mean propagation life (JSSC 1995). This value takes into account tensile residual stress conditions, and is recommended for welded structural steels. da/dN is calculated in mm/cycle.

7.4.3 Symmetry

If the loading and the cracks are not considered, the cruciform joint is symmetrical about both x- and y- axes. However this is not the case when the crack is taken into account. The model becomes unsymmetrical. The joint can be simplified from a full model shown in Figure 7-3 to a half model shown in Figure 7-4. The half model has about 165 elements and 1120 degrees of freedom (DOF). The percentage difference in the number of cycles for fatigue crack propagation life between the simplified half model and a full model is 0.3% (Mashiri *et al* 1997). The half models are therefore a reasonable approximation of the cruciform joints and can be used to estimate the fatigue crack propagation life of these joints.

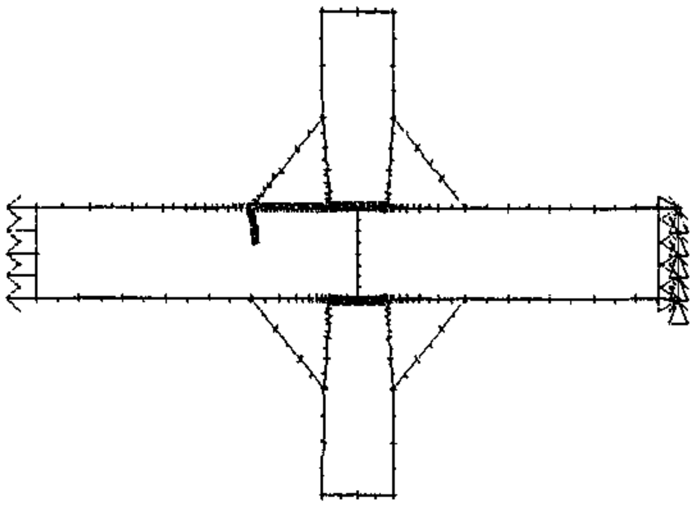

Figure 7-3: Full Model

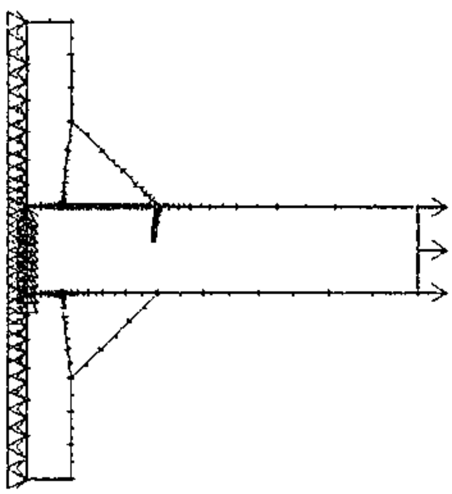

Figure 7-4: Half Model

7.4.4 Failure Mode

The half models were used to determine the fatigue propagation life under cyclic tensile loading. For all the models an initial crack depth of 0.1mm was used. Fatigue failure was assumed to occur when the depth of propagation was at 40% of the plate thickness. It has been shown that after this depth the increase in fatigue life is insignificant (Mori *et al*, 1997), although some researchers have used 50% of the plate thickness (Bell *et al* 1989; Swamidas *et al* 1989; Nguyen & Wahab 1995). Since Mori *et al* 1997 has shown that when the crack front reaches 40% of the plate thickness there is no longer any significant fatigue propagation life left in plated 2-dimensional cruciform joints, this mode of failure is comparable to fatigue crack propagation life at final fracture.

7.5 EFFECT OF WELD PROFILE

The mean values of the weld profile results of the MIG and TIG welds for C350LO steel shown in Tables 3-15 and 3-16 of Chapter 3 are modelled so that their effect on fatigue crack propagation life is determined. The shapes of the weld profiles are shown in Figures 7-5(a) and 7-5(b). The MIG weld profile is close to a convex shape while the TIG weld profile resembles a concave shape. It has also been decided to compare the fatigue crack propagation life of the measured profiles to the weld profiles that are normally assumed when no measurements of weld shape are available. This is the triangular shaped fillet weld of equal leg length shown in Figure 7-5(c) named the Triangular weld profile. The Triangular weld profile does not incorporate weld toe radius and has a size in throat thickness of 3mm. EC3 (1992) and AS 4100-1998 (SAA 1998a) recommend that the throat thickness of a fillet shall not be less than the wall thickness of the hollow section member which it connects, for welded tubular joints under fatigue load. The recommended throat-thickness of the weld is lower than the mean value in the measured profiles for fillet welds formed using the MIG welding method for C350LO steel, see Table 3-15 of Chapter 3. However the recommended throat-thickness of the weld is higher than the mean value of measured profiles for fillet welds formed using the TIG welding method for C350LO steel, see Table 3-16 of Chapter 3.

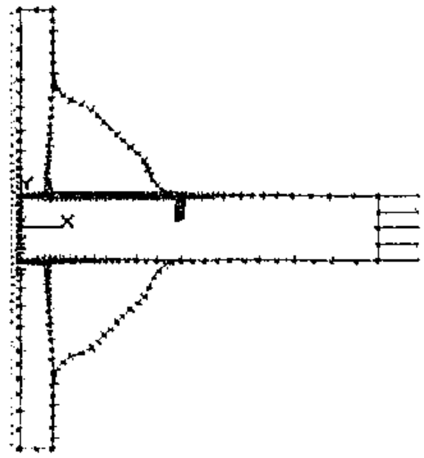

(a) *MIG weld profile*

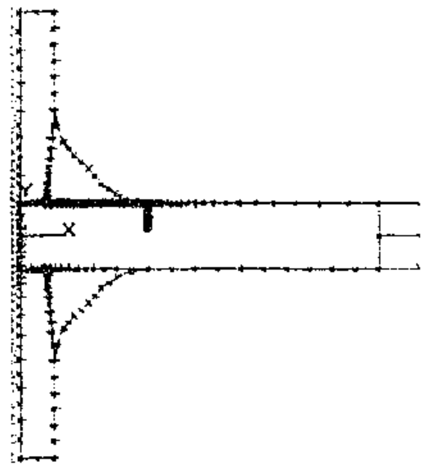

(b) *TIG weld profile*

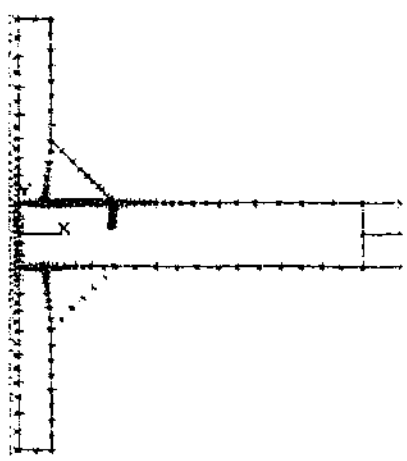

(c) *Triangular weld profile*

Figure 7-5: Half Models with different weld profiles, with 3mm thick plates.

Figure 7-6 shows the plot of normal stress at distances from the weld toe at an applied tensile stress of 150MPa, as an example for the MIG, TIG and Triangular weld profiles without undercut. It shows the differences in stress concentrations that occur from the different weld shapes. The ratio of peak stress at weld toe to the nominal stress applied gives an indication of the stress concentration. The ratios are 2.2, 1.4 and 1.2 respectively for the Triangular weld profile (which has no weld toe radius), MIG weld profile and TiG weld profile (which has the largest weld toe radius).

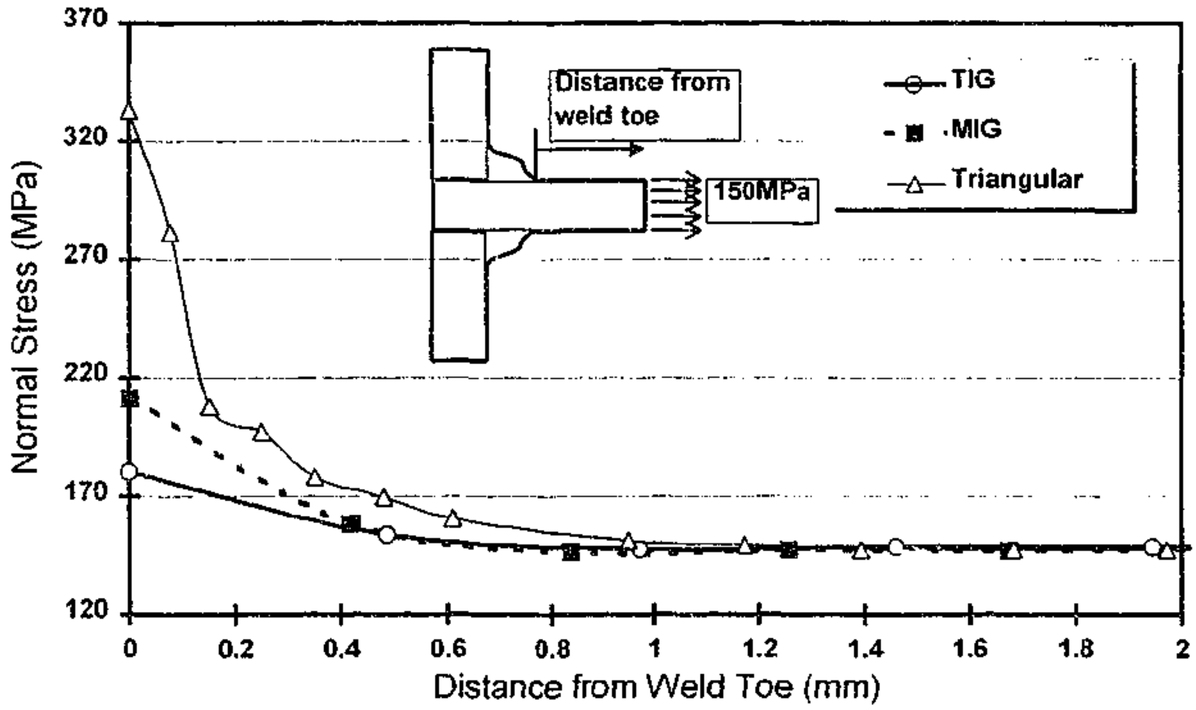

Figure 7-6: Normal stress (perpendicular to the weld toe) against distance from the weld toe for an applied tensile stress of 150MPa.

Figure 7-7 shows the plot of effective stress intensity factor against the crack depth for the three profiles without undercut, at an applied tensile cyclic stress of 150MPa. The effective stress intensity factor depends on crack depth and increases as the depth of crack increases. The effective stress intensity factor at a crack depth of 0.1mm and an applied tensile cyclic stress of 150MPa, decreases from 161$Nmm^{-3/2}$ for the Triangular weld profile to 119$Nmm^{-3/2}$ for the MIG weld profile and to 108$Nmm^{-3/2}$ for TIG weld profile. As the crack depth increases, the difference in effective stress intensity factor for the three weld profiles decreases. At depths greater than 0.8mm the effective stress intensity factor becomes almost equal for the three weld profiles. The difference in fatigue crack growth rate thus occurs at depth close to the surface where the stress raisers are situated. The effect of the stress concentration resulting from the stress raisers decreases as the depth of the crack increases.

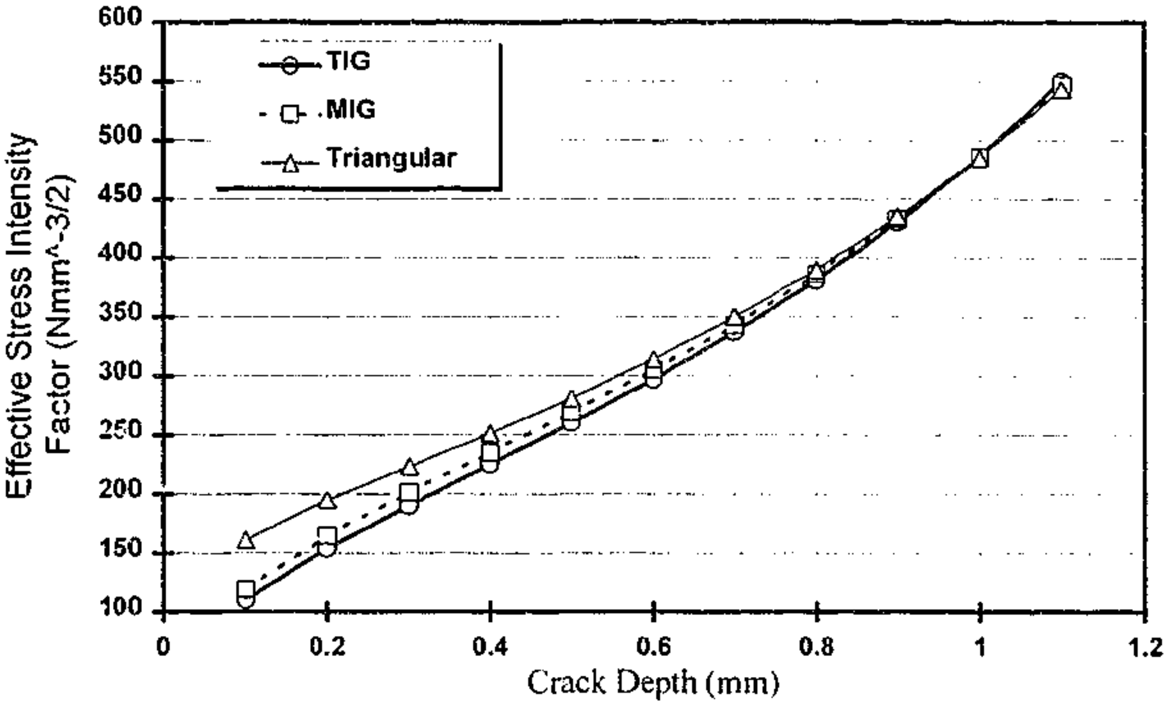

Figure 7-7: Effective stress intensity factor against crack depth for a cyclic tensile stress of 150MPa

Fatigue crack propagation analysis was performed at different values of stress range to obtain the S-N curves. The resultant S-N curves for the MIG, TIG and Triangular weld profiles without undercut are shown in Figure 7-8. For all the models an initial crack depth of 0.1mm, located at the weld toe was used. Fatigue failure was assumed to occur when the depth of propagation was at 40% of the plate thickness. The S-N curves produced relate stress range to fatigue crack propagation life under cyclic tensile loading. There is an increase in fatigue crack propagation life from the Triangular profile to the MIG profile and to the TIG profile. The fatigue crack propagation life of the MIG weld profile is about 2.3 times that of the Triangular weld profile at an applied tensile cyclic stress of 150MPa. The fatigue crack propagation life of the TIG weld profile is 3.3 times that of the Triangular weld profile and about 1.4 times that of the MIG weld profile at an applied tensile cyclic stress of 150MPa. The weld profile from

TIG welding method results in a joint that is more fatigue resistant if undercut is not considered. This is due to the fact that there is a reduction in stress concentration for the weld profile with a larger toe radius. The fact that the weld profile of the TIG weld is concave-like also contributes to form the smooth transition between the TIG weld and the welded plates. However care should be taken to make certain that the design throat thickness is achieved when a concave weld profile is achieved. The TIG weld profile has the same effect on fatigue as TIG arc remelting and plasma dressing. The convex-like shape of the MIG weld results in a more abrupt transition between the MIG weld and the welded plates, causing a higher stress concentration.

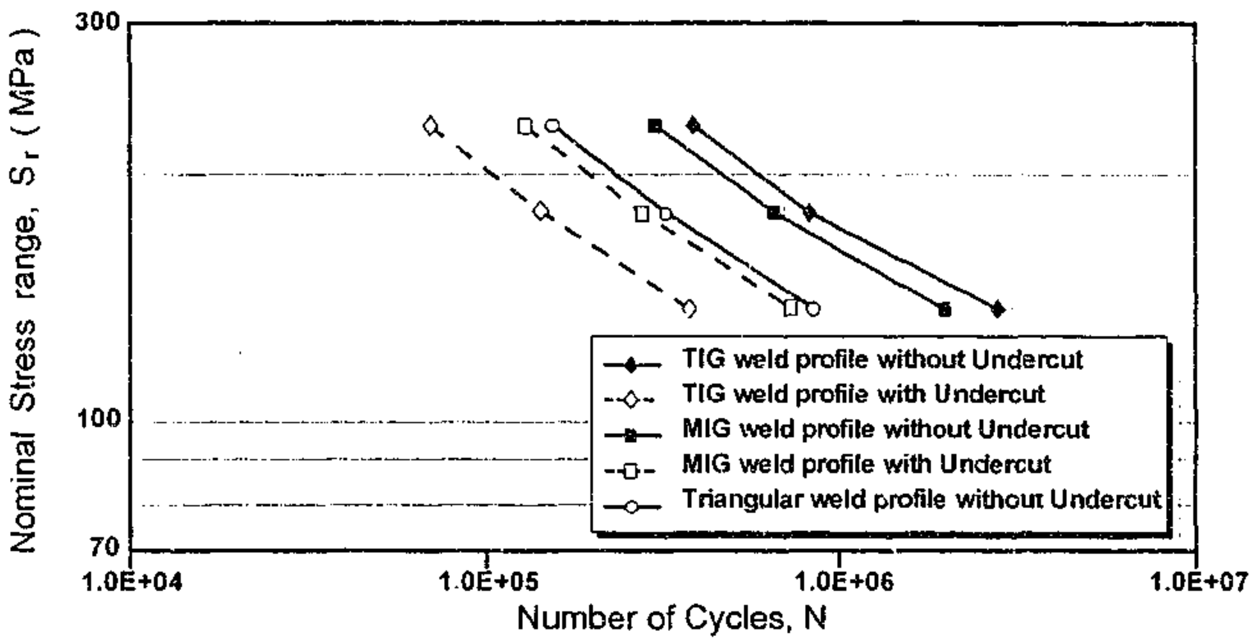

Figure 7-8: S-N curves (Weld profiles with maximum undercut depth and without undercut)

It can also be realised that there are more occurrences of undercut in the TIG welds than the MIG welds (Tables 3-19 and 3-20 of Chapter 3). This may be enough to eliminate the advantage that has been observed from the concavity of the TIG weld profile. Mashiri *et al* 1997 has shown that the fatigue crack propagation life of a thin-walled cold-formed cruciform joint decreases with the depth of undercut for the Triangular weld profile. The maximum value of undercut depth in the TIG weld profile was found to be 0.3mm compared to 0.16mm in the MIG weld profile, see Tables 3-19 and 3-20 of

Chapter 3. The larger value of undercut depth in the TIG weld profile means that there is a greater risk of reduction in fatigue crack propagation life in this profile. Figure 7-8 also shows the S-N curves of the MIG and TIG weld profiles with undercut of maximum depth, 0.16mm for MIG and 0.3mm for TIG, compared to the same profiles without undercut. There is a significant reduction in fatigue crack propagation life as a result of the introduction of undercut to each of the weld profiles. The reduction in fatigue crack propagation life is greater for the TIG weld profile with an undercut depth of 0.3mm compared to that of the MIG weld profile with an undercut depth of 0.16mm. It can be seen that the advantage of the TIG weld profile resulting from its concave-like shape and larger toe radius is eliminated by the existence of larger undercut depth in this welding method. This results in a lower fatigue crack propagation life for the TIG weld profile with undercut depth of 0.3mm compared to the MIG weld profile with undercut depth of 0.16mm, as shown in Figure 7-8.

7.6 EFFECT OF UNDERCUT

A range of undercut values which were measured from the TIG welded connections were used for determining the sensitivity of fatigue crack propagation life over a range of undercut depth, width and radius. This is because a significant number of undercuts were found from this type of welding. For all the models an initial crack depth of 0.1mm located at the base of the undercut profile was used. Fatigue failure was assumed to occur when the depth of propagation was at 40% of the plate thickness. The results from this analysis are compared with the results of a similar cruciform joint made from 20mm thick plates (Miki *et al* 1990). This will serve to demonstrate the effect of undercut on the reduction of fatigue crack propagation life in thin-walled structures compared to thick walled joints under cyclic tensile loading.

7.6.1 The effect of undercut depth, width and radius

The effect of undercut dimensions on the fatigue crack propagation life of thin-walled cruciform joints was obtained by analysing the modelled cruciform joints under cyclic tensile loading for the following cases:

1) <u>the effect of undercut depth</u> at constant radius and constant depth to width ratio of undercut.

2) the effect of undercut width at constant depth and radius of undercut, and

3) the effect of undercut radius at constant depth and width of undercut.

The nature of 2-dimensional models is that they assume that undercut is continuous throughout the whole length of the weld toe. This should give a conservative value of fatigue crack propagation life compared to real cruciform joints under tensile cyclic loading where cracks can initiate at multiple points along the weld toe of the cruciform joints and propagate before coalescence occurs (Booth 1987).

Figure 7-9 shows the S-N curves for different values of undercut depth at constant radius and constant depth to width ratio of undercut. It can be observed that the fatigue crack propagation life of the modelled joint decreases significantly with increase in undercut depth. The values of nominal stress range at 2 million cycles for different values of undercut depth are plotted graphically in Figure 7-10. It can be noted that the nominal stress range at 2 million cycles of the cruciform joint without undercut is 1.4 times that with an undercut of depth of 0.25mm.

S-N curves for increasing undercut width at constant radius and constant depth of undercut are shown in Figure 7-11. The S-N curves demonstrate that the fatigue crack propagation life of the modelled cruciform joint increases with increasing undercut width. The values of nominal stress range at 2 million cycles for the different values of undercut width are plotted graphically in Figure 7-12. The nominal stress range at 2 million cycles of the joint with an undercut width of 2.5mm is 1.2 times that with an undercut width of 1.0mm.

The effect of increasing undercut radius at constant depth and constant width of undercut on fatigue crack propagation life is demonstrated by the S-N curves shown in Figure 7-13. Like undercut width, the increase in undercut radius results in an increase in the fatigue crack propagation life. The values of nominal stress range at 2 million cycles at different values of undercut radius are represented graphically in Figure 7-14. The nominal stress range at 2 million cycles for a model with an undercut radius of 2mm is 1.4 times that with an undercut radius of 0.25mm.

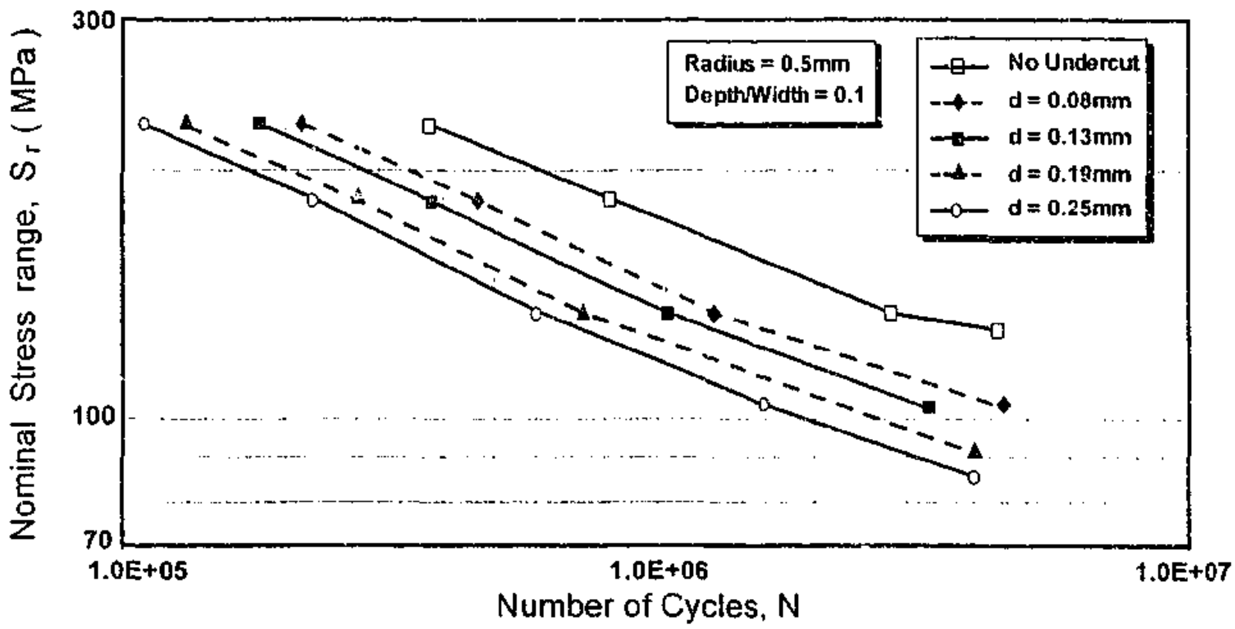

Figure 7-9: S-N curves (Effect of undercut depth).

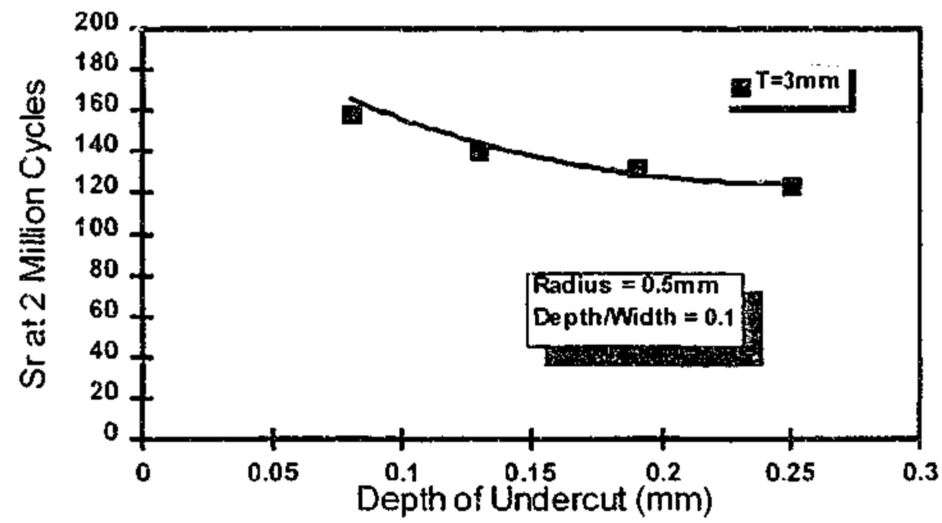

Figure 7-10: Nominal stress range at 2million cycles versus depth of undercut.

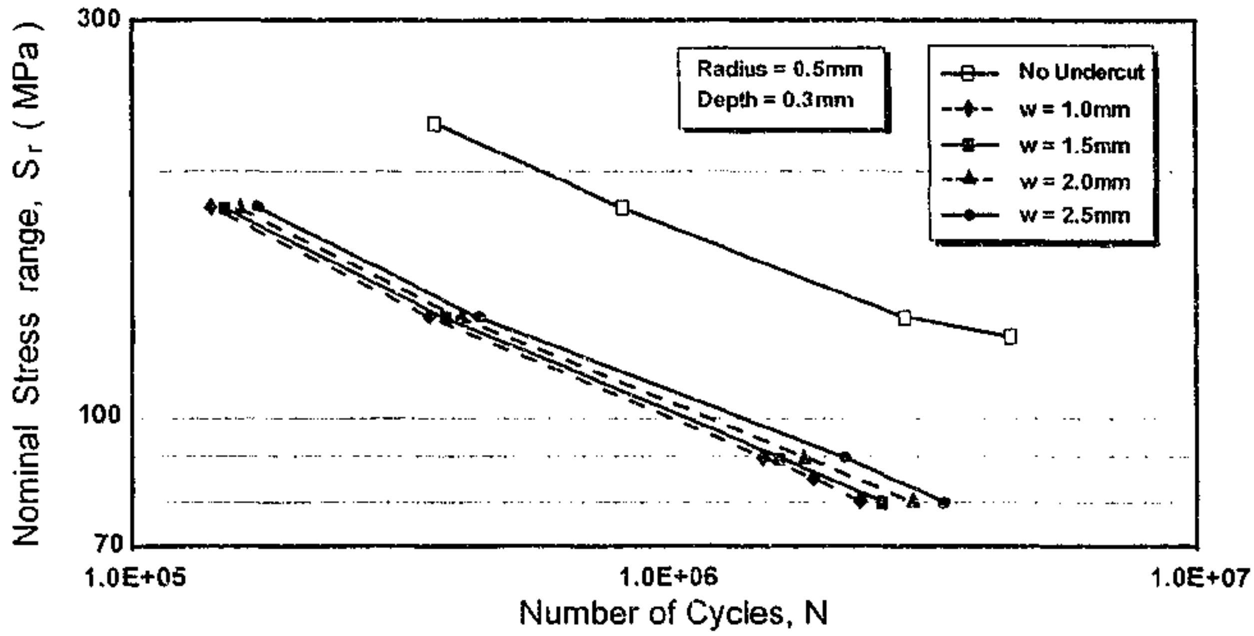

Figure 7-11: S-N curves (Effect of undercut width).

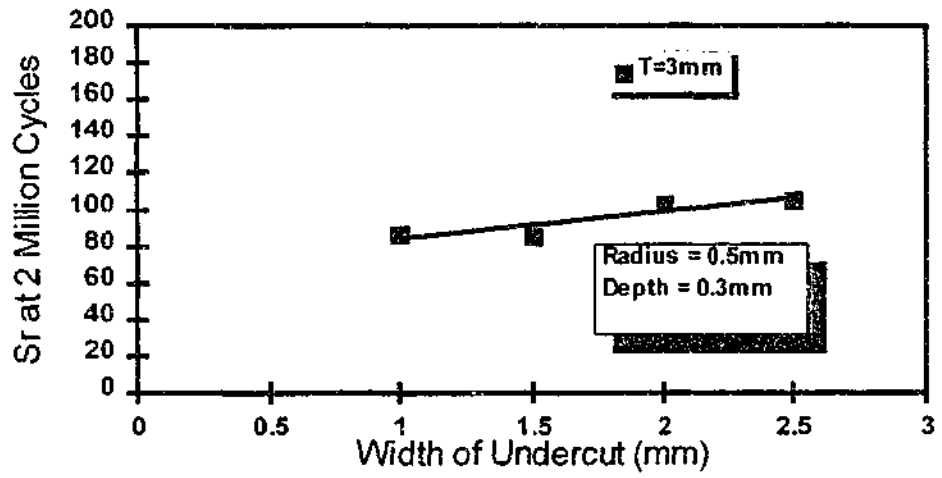

Figure 7-12: Nominal stress range at 2millon cycles versus width of undercut.

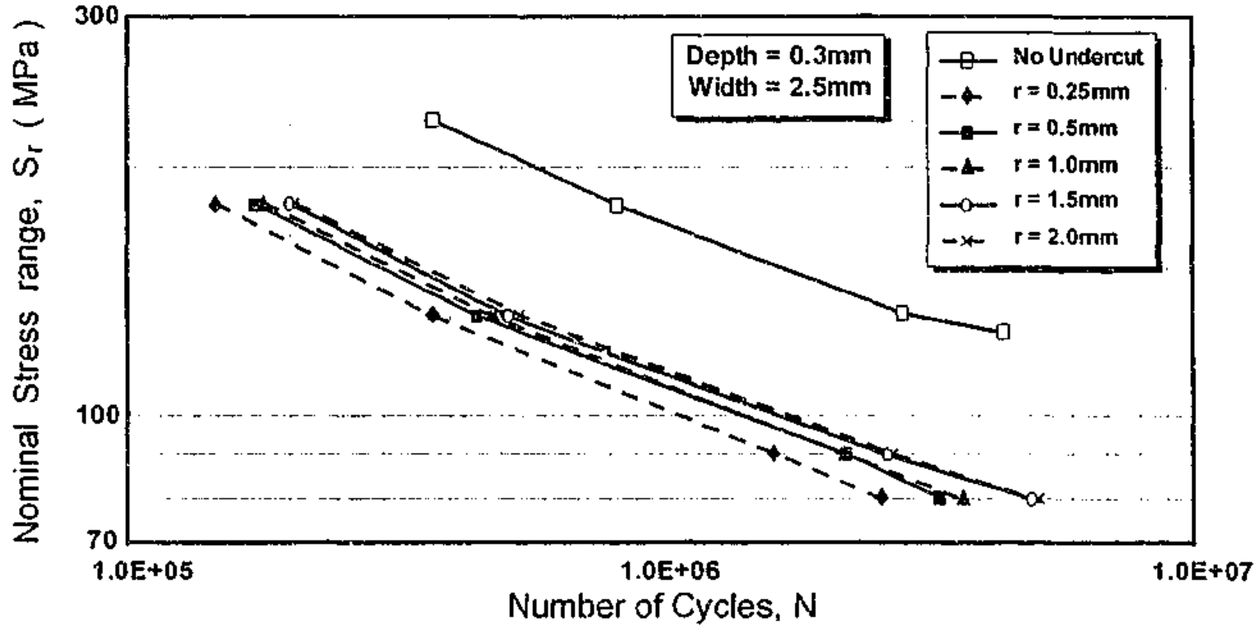

Figure 7-13: S-N curves (Effect of undercut radius).

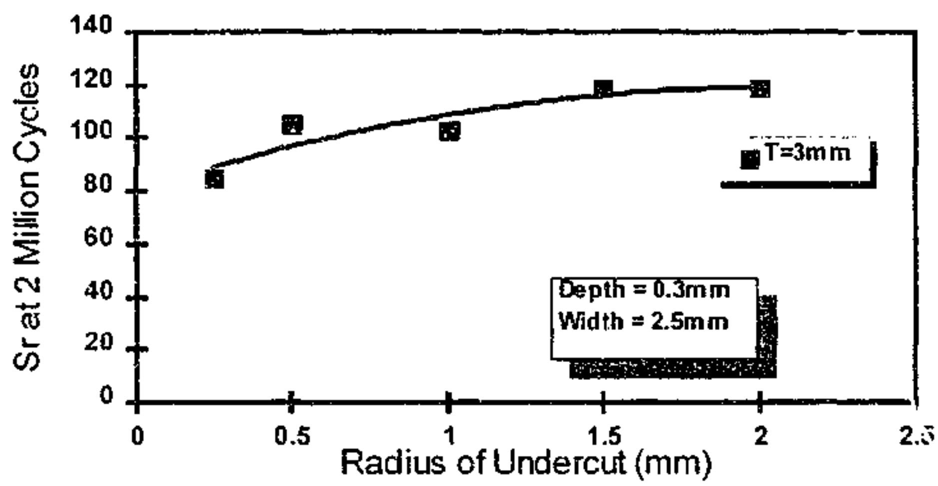

Figure 7-14: Nominal stress range at 2million cycles versus radius of undercut.

7.6.2 Comparison of thin-walled (3mm) and thick-walled joints (20mm)

Miki *et al* (1990) have carried out a similar analysis of the effect of different values of undercut depth, width and radius on fatigue crack propagation life of a cruciform joint. The cruciform joint consisted of 20mm thick plates under uniaxial tension. In order to be able to compare the relative changes in the fatigue crack propagation life which occur in the thin-walled and the thicker-plated joint, normalised values of nominal stress range and normalised depth, width and radius of undercut are calculated for the two joints.

The nominal stress range is normalised by dividing the nominal stress range at 2million cycles for given undercut dimensions by the nominal stress range at 2 million cycles for the joint without undercut. The undercut depth is normalised by obtaining the ratio of undercut depth to the plate thickness. The undercut width is normalised by dividing the undercut width by the undercut depth. The undercut radius is normalised by obtaining the ratio of undercut radius to undercut width.

Table 7-2 shows the values of undercut depth and stress range at 2 million cycles and their corresponding normalised values. Table 7-2 summarises the results of the models which were analysed at constant undercut radius and constant depth to width ratio of undercut, in order to determine the influence of undercut depth on fatigue crack propagation life.

Table 7-3 shows the values of undercut width and stress range at 2 million cycles and their corresponding normalised values. Table 7-3 summarises the results of the models which were analysed at constant undercut depth and constant undercut radius, in order to determine the influence of undercut width on fatigue crack propagation life.

Table 7-4 shows the values of undercut radius and stress range at 2 million cycles and their corresponding normalised values. Table 7-4 summarises the results of the models which were analysed at constant undercut depth and constant undercut width, in order to determine the influence of undercut radius on fatigue crack propagation life.

Table 7-2: Values of undercut depth and fatigue strength and corresponding normalised values

Undercut depth, d (mm)	Normalised Undercut Depth (=d/T)	Stress Range at 2 million cycles (S_{ri})	Normalised Fatigue Strength (=S_{ri}/S_{r0})
Thin-Walled Joint; Thickness of plates, T = 3mm ; Radius, ρ = 0.5mm; d/δ = 0.1 Fatigue Strength ($2x10^6$ cycles for d=0mm), S_{r0} = 174MPa			
0	0	174	1
0.08	0.027	158	0.91
0.13	0.043	141	0.81
0.19	0.063	132	0.76
0.25	0.080	123	0.71
Thick-Walled Joint; Thickness of plates, T = 20mm; Radius, ρ = 0.5mm; d/δ = 0.5 Fatigue Strength ($2x10^6$ cycles for d=0mm), S_{r0} = 97.5MPa			
0	0	97.5	1.00
0.2	0.010	86	0.88
0.5	0.025	86	0.88
1.0	0.050	81	0.83
1.5	0.075	84	0.86
2.0	0.100	80	0.82

Table 7-3: Values of undercut width and fatigue strength and corresponding normalised values

Undercut Width, δ (mm)	Normalised Undercut Width (=δ/d)	Stress Range at 2 million cycles (S_{ri})	Normalised Fatigue Strength (=S_{ri}/S_{r0})
Thin-Walled Joint; Thickness of plates, T = 3mm; d = 0.3mm, ρ = 0.5mm Fatigue Strength ($2x10^6$ cycles for d=0mm), S_{r0} = 174MPa			
0	0	174	1.00
1.0	3.3	86	0.50
1.5	5.0	85	0.50
2.0	6.7	103	0.59
2.5	8.3	105	0.60
Thick-Walled Joint; Thickness of plates, T = 20mm; d = 0.5mm, ρ = 0.5mm Fatigue Strength ($2x10^6$ cycles for d=0mm), S_{r0} = 97.5MPa			
0	0	97.5	1.00
1.0	2	87	0.89
1.5	3	87	0.89
2.0	4	95	0.97

Table 7-4: Values of undercut radius and fatigue strength and corresponding normalised values

Undercut Radius, ρ (mm)	**Normalised Undercut Radius (=ρ/δ)**	**Stress Range at 2 million cycles (S_{ri})**	**Normalised Fatigue Strength (=S_{ri}/S_{r0})**
Thin-Walled Joint; Thickness of plates, T = 3mm; d=0.3mm; δ = 2.5mm Fatigue Strength ($2x10^6$ cycles for d=0mm), S_{r0} = 174MPa			
0.25	0.1	85	0.49
0.50	0.2	105	0.60
1.00	0.4	103	0.59
1.5	0.6	119	0.68
2.0	0.8	119	0.68
Thick-Walled Joint; Thickness of plates, T = 20mm; d=0.5mm; δ = 1.0mm Fatigue Strength ($2x10^6$ cycles for d=0mm), S_{r0} = 97.5MPa			
0.1	0.1	77	0.79
0.5	0.5	86	0.78
1.3	1.3	96	0.98

A plot of the normalised values of undercut depth, versus the normalised values of nominal stress ranges at 2 million cycles for the 3mm and 20mm cruciform joints is shown in Figure 7-15. Similar comparison is performed for the undercut width and radius in Figures 7-16 and 7-17.

Figures 7-15, 7-16 and 7-17 show that the relative reduction in fatigue strength for the thin-walled joint is greater than that of the thicker walled joint analysed by Miki *et al* (1990).

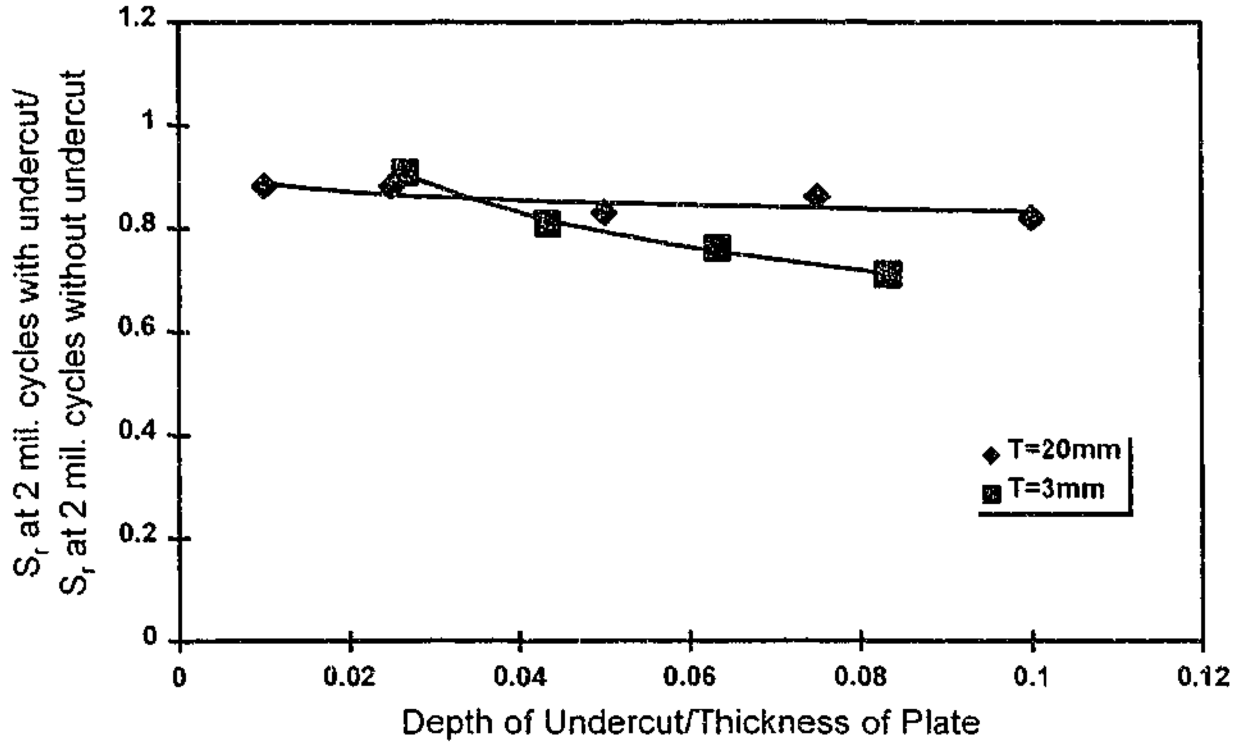

Figure 7-15: Comparison of the effect of undercut depth on welded cruciform joints of 3mm and 20mm.

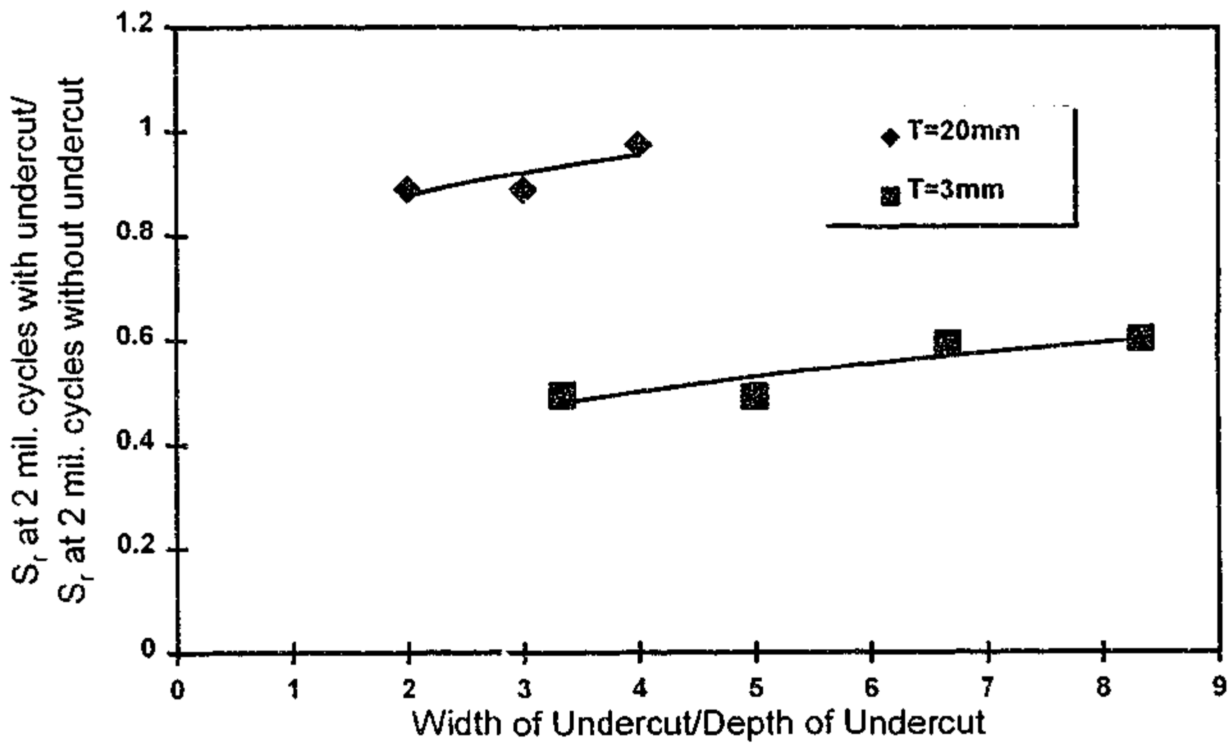

Figure 7-16: Comparison of the effect of undercut width on welded cruciform joints of 3mm and 20mm.

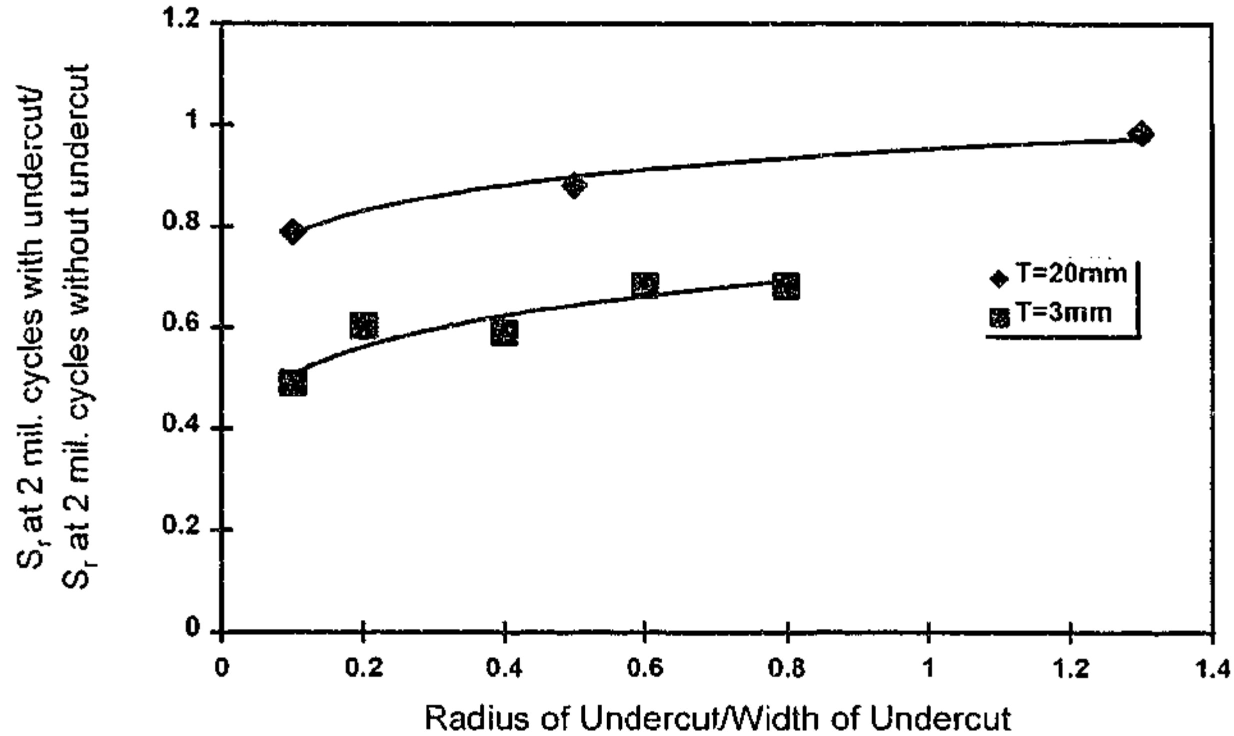

Figure 7-17: Comparison of the effect undercut radius on welded cruciform joints of 3mm and 20mm.

7.7 SUMMARY

The following are observations and conclusions which were made as a result of the analysis of 2 dimensional thin-walled cruciform joints (T=3mm), to determine the effect of weld profile and weld toe undercut on fatigue crack propagation life. The conclusions and observations relating to the subsequent comparison of the results with those from the analysis of a thicker-walled cruciform joint (T=20mm) are also included.

(a) The concave weld profile has a better fatigue resistance compared to the joints with a convex shaped weld profile. Another factor contributing to the better fatigue performance of the concave weld profile is the larger toe radius associated with this profile unlike the convex weld profile where a smaller toe radius is obtained. The concave weld profile and the larger toe radius results in lower stress concentration at weld toe. However care should be taken to ensure that the design throat thickness is achieved when concave shaped weld profiles are achieved for structures under fatigue loading.

(b) It has also been demonstrated that when larger undercut depth is present the benefits of the concave weld profile which cause a favourable fatigue crack propagation life can be outweighed by the high notch stresses resulting from the undercuts, resulting in a worse fatigue performance.

(c) The Boundary Element Analysis System Software (BEASY) has been used to determine differences in fatigue crack propagation life of a thin-walled cruciform joint with differences in undercut depth, width and radius of the order of a tenth of a millimetre. It has been observed that fatigue crack propagation life of the thin-walled cruciform joint decreases significantly with increase in undercut depth at constant radius and constant depth to width ratio of undercut. However fatigue crack propagation life of the thin-walled cruciform joint increases as the undercut width increases at constant depth and radius of undercut. Like undercut width, fatigue crack propagation life also increases as undercut radius increases at constant depth and width of undercut.

(d) The loss in fatigue crack propagation life of the thin-walled cruciform joint (T=3mm) is relatively more than the loss in fatigue crack propagation life of the thicker walled joint (T=20mm). Significant loss of fatigue crack propagation life occurs due to the presence of undercut in thin-walled structures. This suggests that care is needed to avoid undercut through experienced welders or suitable welding techniques when thin-walled welded joints are used in structures subjected to fatigue loading.

Chapter 8

DESIGN RULES FOR TUBE-TO-PLATE T-JOINTS

8.1 INTRODUCTION

Chapter 8 deals with the fatigue design of tube-to-plate moment connections. Some of the tube-to-plate T-joints used in the manufacture of road and agricultural industry equipment are made up of square hollow sections with thicknesses less than 4mm. In this investigation tube-to-plate T-joints made up of square hollow section tubes of wall thicknesses 1.6mm, 2mm and 3.0mm were tested and have been reported in Chapter 5. Fatigue tests of tube-to-plate connections under cyclic in-plane bending were carried out to check if the existing S-N curve is applicable to tube-to-plate T-joints made from thin-walled square hollow sections with thicknesses less than 4mm. Fatigue tests were carried out on tube-to-plate T-joints made from square hollow sections welded to a 10mm plate. The tubes are of three different steel grades, C350LO, C450LO and S355JOH. Grades C350LO and S355JOH tubes are non-galvanised cold-formed steel tubes. Grade C450LO tubes are in-line galvanised steel tubes. Full details of the tube-to-plate connections tested are given in Chapter 5.

The design of the tube-to-plate moment connection can currently be carried out using an existing S-N curve in the Canadian Standard CAN/CSA-S16.1-M89 (CSA 1989). The current fatigue design of the tube-to-plate moment connection (see Figure 8-1a) however, is based on an S-N curve derived from a longitudinally loaded plate with welded non-load carrying attachments (see Figure 8-1b). The tube-to-plate moment connection was assigned the S-N curve of the longitudinally loaded plate with fillet welded non-load carrying attachments by the S16 Technical Committee, see Figure 8-2. The category, which has been assigned to tube-to-plate joints under cyclic loading, is the lowest S-N curve determined for longitudinally loaded plate with welded non-load carrying attachments. The existing S-N curve from the Canadian Standard CAN/CSA-S16.1-M89 is given in terms of the classification method. In the classification method, the S-N curve relates the nominal stress range to the number of cycles to failure.

A design S-N curve also exists for tube-to-plate T-joints in the form of end-to-end connections (see Figure 8-3) and is given in AS4100-1998 (SAA 1998a) and EC3

(1992). The S-N curve for the end-to-end connections is shown in Figure 8-4. However the end-to-end connection detail is subjected to cyclic axial tension load, unlike the tube-to-plate T-joint under investigation which is subjected to cyclic in-plane bending.

Since the existing S-N curves are given in terms of the classification method, statistical analysis is used to determine S-N curves, for the classification method, from the resulting fatigue data, reported in Chapter 5. The least-squares method of analysis is used. Traditionally the S-N curves are determined from the assumption that the number of cycles is the dependent variable (Nakazawa & Kodama 1987; ASTM 1980). This is because most fatigue tests are controlled through the monitoring of stress or strain. Stress or strain is therefore considered to be the independent variable.

In this investigation however, the same basic equations of the least-squares method will also be used to determine the S-N curves but with the stress range as the dependent variable (Johnson 1999). The stress level and the number of cycles to failure of each specimen are interrelated. For application of data for the development of design rules the number of cycles (N) will be the dependent variable in order to be consistent with existing design procedures. The approach using the stress range (S) as the dependent variable is included to indicate the fact that an alternative design approach could result in a different assessment of risk.

Therefore, two cases of analyses using the least-squares method are going to be considered;

a) Determination of S-N curves assuming the number of cycles is the dependent variable and the stress is the independent variable and;
b) Determination of S-N curves assuming the stress is the dependent variable and the number of cycles is the independent variable.

These two cases are also considered under the following conditions:

i) The inverse of the slope of the S-N curve is assumed to be equal to -3. This is the slope adopted by design guidelines such as EC3 (1992), AS4100-1998 (SAA 1998a) and the Canadian Standard, CAN/CSA-S16.1-M89 (CSA 1989) and derives from the exponent m in the Paris equation, $da/dN = C\Delta K^m$, which has a value of 3 for ferritic steels with yield or 0.2% proof strength below 600N/mm^2 (BSI 1991) and,

ii) The slope of the S-N curve is determined by using the least-squares method. In this case the natural slope of the S-N fatigue data is derived.

There is a trend in current fatigue welding standards such as IIW (2000) and Zhao *et al* (1999a) to give fatigue design curves in terms of the hot spot stress approach. As such the S-N data from the tube-to-plate T-joints will also be analysed to determine fatigue design curves in terms of the hot spot stress approach. Stress concentration factors for the different tube-to-plate connections tested in this investigation have been determined and reported in Chapter 5. These stress concentration factors have been used to convert the nominal stress ranges, in the brace members where fatigue failure occurred, to hot spot stress ranges. The fatigue design of tube-to-plate T-joints can therefore be determined in terms of the hot spot stress method as well. Similar methods of analyses as that in the classification method will be used to determine design $S_{r,hs}$– N curves in the hot spot stress method.

8.2 EXISTING DESIGN S-N CURVES FOR TUBE-TO-PLATE CONNECTIONS

8.2.1 Tube-to-Plate Joints under Cyclic Bending Load

The Canadian Standard CAN/CSA-S16.1-M89 (CSA 1989) gives an S-N curve, in terms of nominal stress range for tube-to-plate connections under bending. The tube is fillet welded to the base plate. According to the classification method, the class or detail category of the tube-to-plate connection is 40. The class is the nominal stress range corresponding to a failure of 2 million cycles. The S-N curve has a single slope of 1:3. The constant amplitude threshold stress range or cut-off limit, below which no fatigue damage will occur is 18MPa. The existing S-N curve from the Canadian Standard is shown in Figure 8-2.

This category is obtained from the lowest S-N curve for longitudinally loaded plate with welded non-load carrying attachments. The detail is shown in Figure 8-1(b). The category for the longitudinally loaded plate containing the fillet-welded attachment depends on the length of the attachment, L (see Figure 8-1(b)). Category E1 occurs when the value of L is greater than 12 times the thickness or 100mm and when the detail thickness is greater than 25mm (Kulak *et al* 1995).

It can clearly be seen that the welds in detail category E1 are non-load carrying, whereas the fillet welds in the tube-to-plate connection are load carrying, subjected to shear, tensile and compressive stresses. On the other hand the thicknesses involved in determining the E1 curve are much larger than the thicknesses in the current tests.

The tube-to-plate connection, was assigned the lowest category, E1, of the longitudinally loaded plate with welded non-load carrying attachments, by the S16 Technical committee. The S-N curve may not be applicable to thin-walled tube-to-plate T-joints. Details of the longitudinally loaded plate with fillet welded attachments and the tube-to-plate connections are shown in Figure 8-1. Table 8-1 shows some of the differences of the two types of connections.

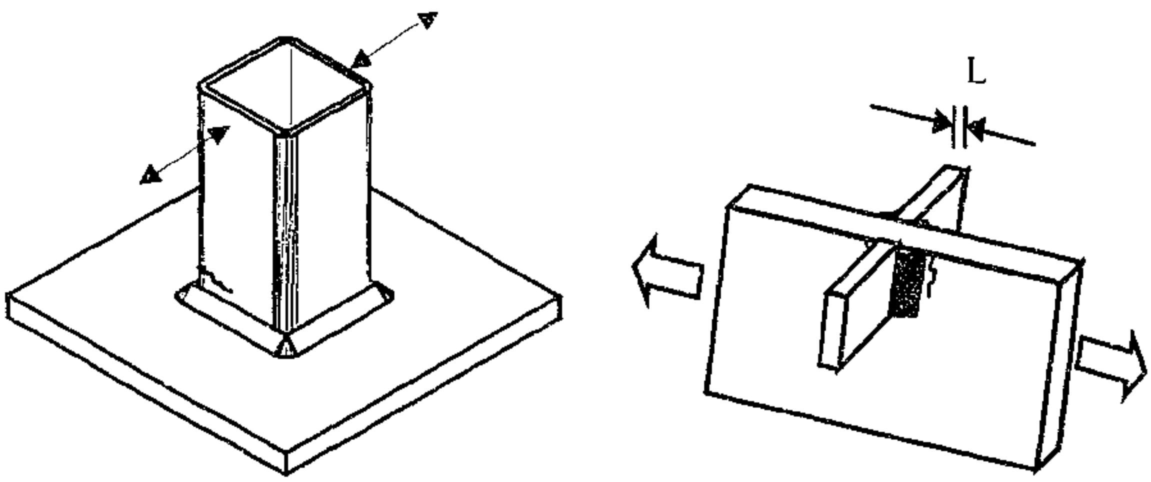

(a) **(b)**

Figure 8-1: (a) Tube-to-plate joint (b) Category E1 in CSA (1989) Longitudinally loaded plate with fillet welded attachments

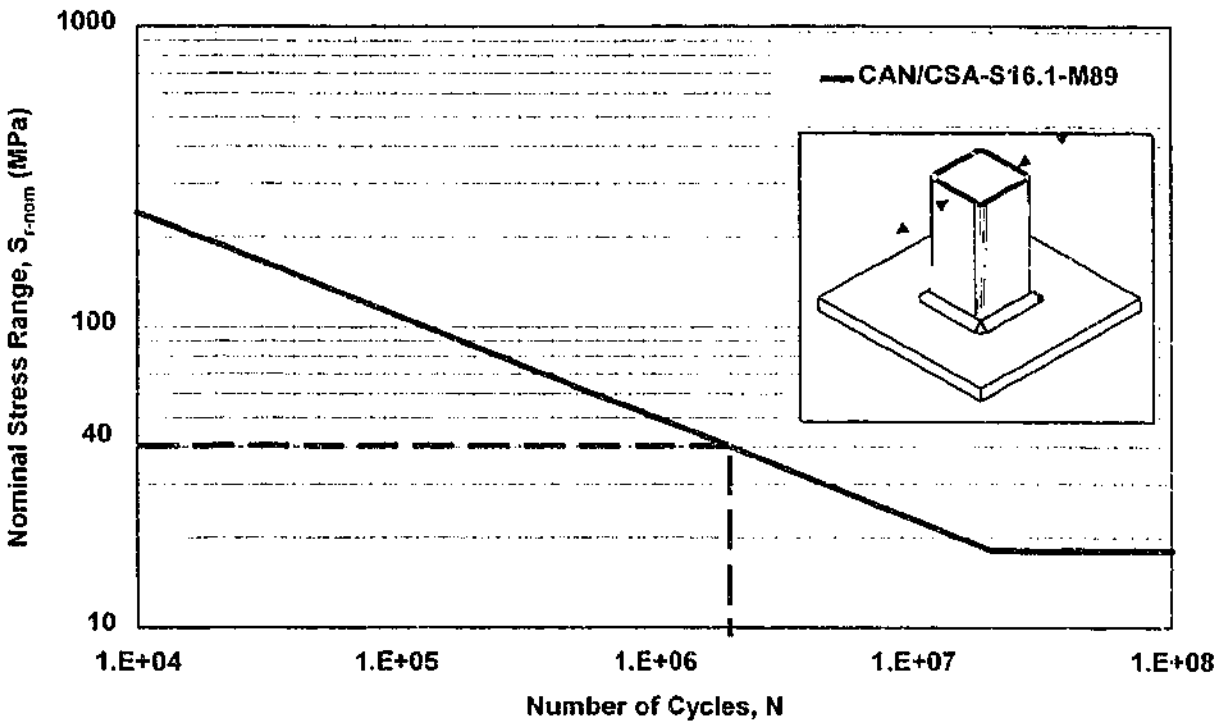

Figure 8-2: Design S-N curve for tube-to-plate moment connections, Figure 8-1(a), (CSA 1989)

Table 8-1: Differences between category E1 and tube-to-plate connection

Category E1, CAN/CSA-S16.1-M89	T-joint under Study
Plate-to-plate	Tube-to-plate
Non-load carrying fillet weld	Load carrying fillet welds
Non-load carrying attachment	Load carrying tube
Cyclic Tension	Cyclic Bending
$t \geq 25$mm	$t < 4$mm

8.2.2 Tube-to-Plate Joint under Cyclic Tension Load

The other existing curve for tube-to-plate T-joints is the end-to-end connection (EC3 1992, SAA 1998a). However, the end-to-end connection detail is subjected to axial loading unlike the tube-to-plate T-joint considered in this investigation which is under bending. The load path and plate stress in the end-to-end and the tube-to-plate connection details are different. The end-to-end connection consists of two square hollow sections fillet welded to an intermediate plate as shown in Figure 8-3. The end-to-end connection detail is valid for tubes of wall thicknesses less than 8mm (SAA

1998a). It has an S-N curve in the classification method with a detail category of 36. This S-N curve has a double slope, a slope of 1:3 between 10^3 cycles and $5x10^6$ cycles and a slope of 1:5 between $5x10^6$ cycles and $1x10^8$ cycles. The S-N curve for the axially loaded end-to-end connection is shown in Figure 8-4.

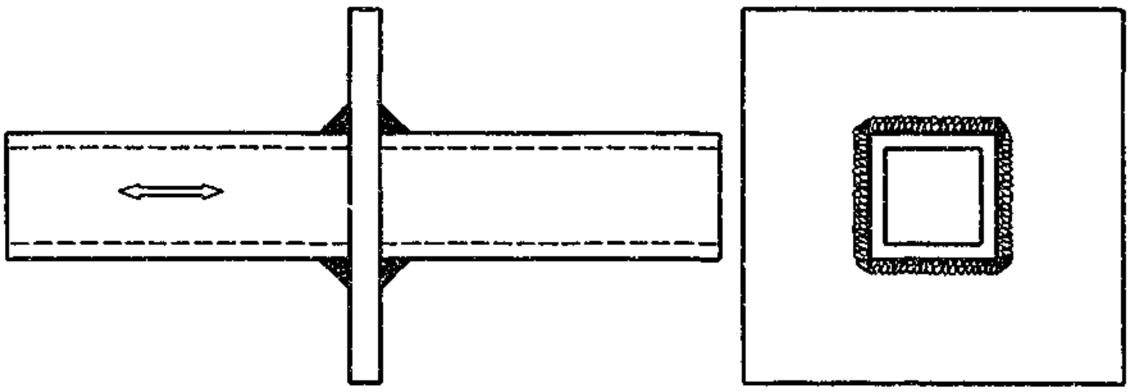

Figure 8-3: End-to-end connection under cyclic axial tension load

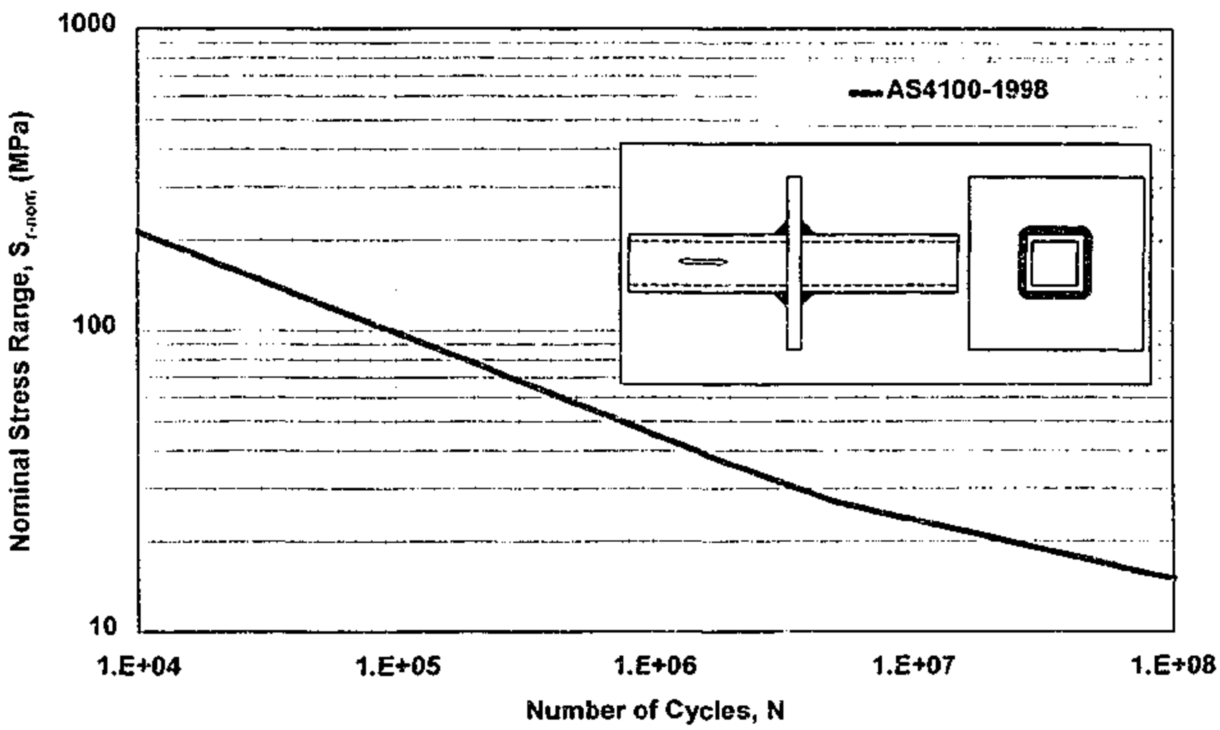

Figure 8-4: Design S-N curve for axially loaded end-to-end connection (EC3 1992; SAA 1998a)

8.3 DETERMINATION OF S-N CURVES FROM FATIGUE DATA

8.3.1 Methods of Analysis

Some of the methods that can be used in the determination of S-N curves are the deterministic analysis and least-squares method.

In deterministic analysis, a deterministic lower bound curve represents an eyeball fit through the lowest failure data. Run-outs are not taken into account in the analysis. The deficiency of a lower bound curve of this type is that it does not give any direct quantifiable statistical information about the data (Wallin 1999).

The common statistical method of analyzing S-N data is the least-squares method. Details of the least-squares method are given in Appendix G. Only failed data can be used. The method assumes implicitly that the data follows a constant lognormal distribution.

Only one run-out was obtained during fatigue testing of the tube-to-plate T-joints, see Table 5-5 of S-N data in Chapter 5. The least-squares method is therefore an appropriate method for use in this analysis. Neglecting a runout however produces a conservative result.

8.3.2 Definition of Design S-N Curve

The definition of design S-N curves given in the Department of Energy guidelines was adopted in this analysis. The Department of Energy Guidelines define the design S-N curve as the mean-minus-two-standard-deviation curve of the relevant experimental data (Department of Energy, 1990). For a normally distributed population of given mean, μ and standard deviation, σ, the $\mu \pm 2\sigma$ contains about 95% of the population (Little and Jebe, 1975). The design S-N curves for the two cases are therefore as follows;

(i) when *log N* is the dependent variable, $\log N = A + B \log S \pm 2\sigma_{\log N}$ and

(ii) when *log S* is the dependent variable, $\log S = a + b \log N \pm 2\sigma_{\log S}$.

8.4 DESIGN S-N CURVES: CLASSIFICATION METHOD

8.4.1 S-N Fatigue Data Set

All the S-N data from the failed specimens obtained from the experimental investigation (see Section 5.3 of Chapter 5) is analyzed using the statistical methods of least squares to determine the design S-N curves in terms of the classification method. The class or detail category is defined by the fatigue strength at 2 million cycles of the mean-minus-two-standard-deviation S-N curve.

It has been shown that galvanizing and steel grades do not have any noticeable influence on the fatigue strength of the tube-to-plate T-joints, see Sections 5.4.1 and 5.4.2. As such these factors do not warrant any separation and analysis of obtained data.

Stress ratio has been shown to have some influence on fatigue life of thin-walled tube-to-plate T-joints, when data is analyzed in terms of mean S-N curves, see Section 5.4.3 of Chapter 5. The fatigue life at a stress ratio of 0.1 was found to be longer than the life at a stress ratio of 0.5, showing that the damaging effect of a fully tensile cyclic stress range tends to increase as the mean stress or stress ratio increases (Maddox 1991). The determination of the influence of stress ratio is based on the mean S-N curves for the S-N data plots for the stress ratios of 0.1 and 0.5 as reported in Section 5.4.3 of Chapter 5. Fatigue design curves however are mean-minus-two-standard-deviation S-N curves, with a fixed inverse of the slope of –3 similar to the slope in the Canadian Standard, CAN/CSA-S16.1-M89 (CSA 1989). When the mean-minus-two-standard-deviation S-N curves are determined for the S-N data plots at the two stress ratios of 0.1 and 0.5, the effect of stress ratio shown in Section 5.4.3 of Chapter 5 is no longer apparent, see Figure 8-5. This is because the design S-N curves take into account the scatter of the fatigue test data. S-N data obtained at the two stress ratios can therefore be considered as a single entity in determining design S-N curves because of the inherent scatter associated with the data at the two stress ratios, found in this investigation.

The trend of fatigue life with tube wall thickness of welded thin-walled tube-to-plate T-joints described in Section 5.4.4 of Chapter 5, showed that for mean regression S-N curves, fatigue life decreases with a decrease in tube wall thickness of the member under failure. The design S-N curves however take into account the scatter, which is inherent in fatigue test data. The design S-N curves with a fixed inverse of the slope, *B* of –3 for the three different thicknesses of 3mm, 2mm and 1.6mm are shown in Figure 8-6. The effect of tube wall thickness on fatigue life, as described in Section 5.4.4 of Chapter 5, is no longer evident when scatter is taken into account. The design S-N curves for the 3mm and 2mm thick tubes are identical. The design S-N curve for the 1.6mm thick tubes is slightly higher than that of the 3mm and 2mm tubes showing an overlap in S-N data when scatter is taken into account. In this investigation, the scatter of the data for the three different wall thicknesses is such that design S-N curves cannot be evaluated for the different thicknesses below 4mm.

Therefore it has been decided to consider all the fatigue data from failed specimens obtained from the experimental investigation as a single group of results to obtain a design S-N curve for tube-to-plate T-joints made up of square hollow sections, where the thicknesses of the tubes are below 4mm. A plot of all the S-N data obtained from the tube-to-plate T-joints is shown in Figure 8-7, Section 8.4.2. The data consists of (a) 25 specimens made from 3mm thick tubes, (b) 13 specimens made from 2mm thick tubes and (c) 9 specimens made from 1.6mm thick tubes,which have failed under constant stress amplitude cyclic loading:

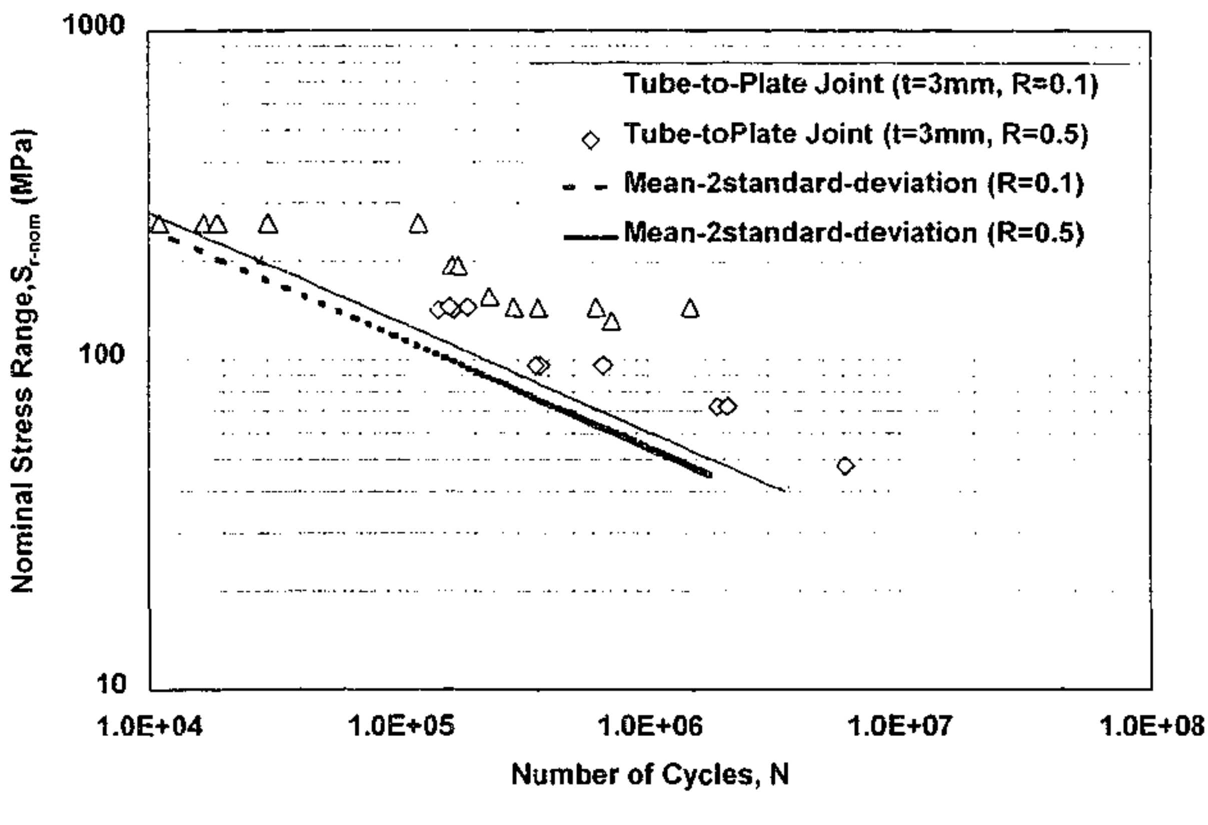

Figure 8-5: Design S-N curves for fatigue data at different stress ratios, B=-3

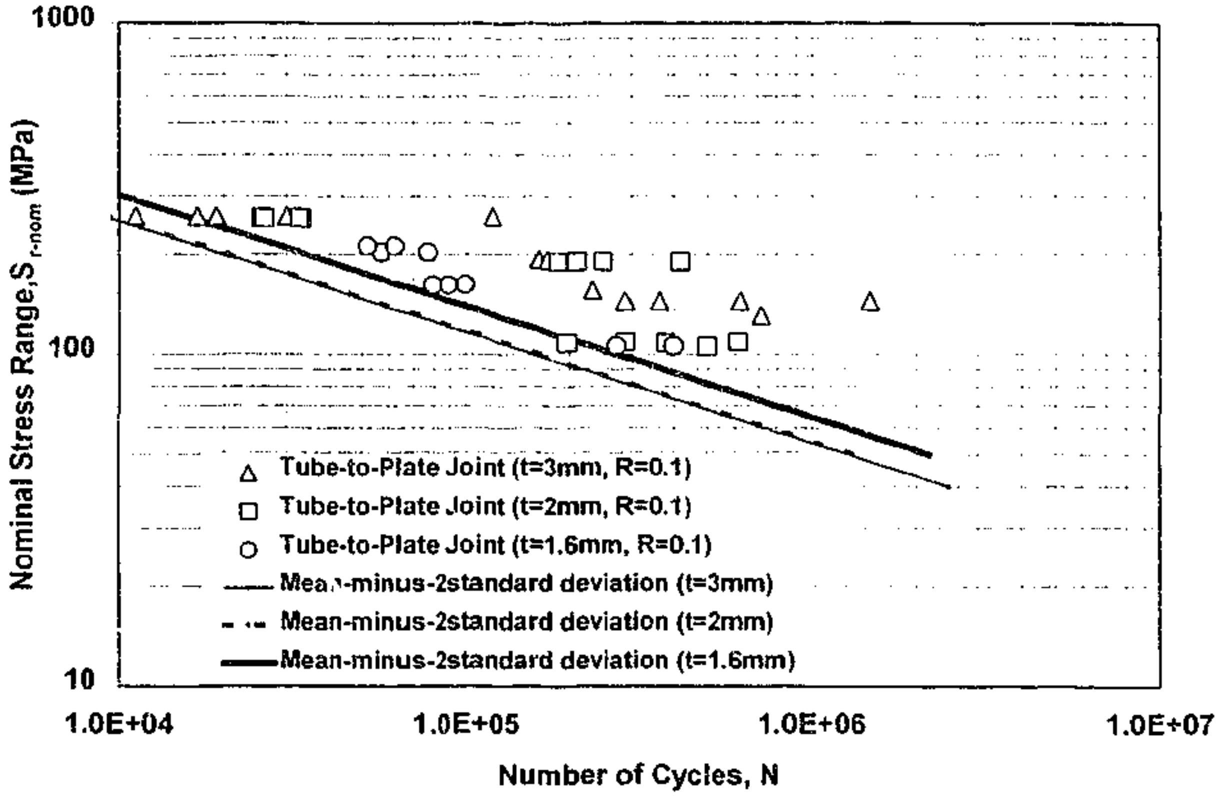

Figure 8-6: Design S-N curves for fatigue data with different thicknesses, B=-3

8.4.2 Analysis of Fatigue Data

Four sets of analysis are proposed using the least-squares method of analysis as follows;

(a) Assuming that *log N* is the dependent variable, such that the linear model, $\log N = A + B{\cdot}\log S$ is determined. This is the method recommended in guidelines such as those given by the American Society of Testing and Materials (ASTM 1980) and the Japan Society of Mechanical Engineers (Nakazawa & Kodama 1987). In this case the following two analyses are carried out;

(i) estimate both parameters A and B of the S-N curve, Figure 8-7 and

(ii) assume that the parameter B of the S-N curve is -3 and estimate parameter A, Figure 8-8.

(b) Assuming that *log S* is the dependent variable, such that the linear model, $\log S = a + b{\cdot}\log N$ is determined. In this case the following two analyses are carried out;

(iii) estimate both the parameters a and b of the S-N curve, Figure 8-9 and

(iv) assume that the parameter b of the S-N curve is -0.3333 and determine parameter a, Figure 8-10.

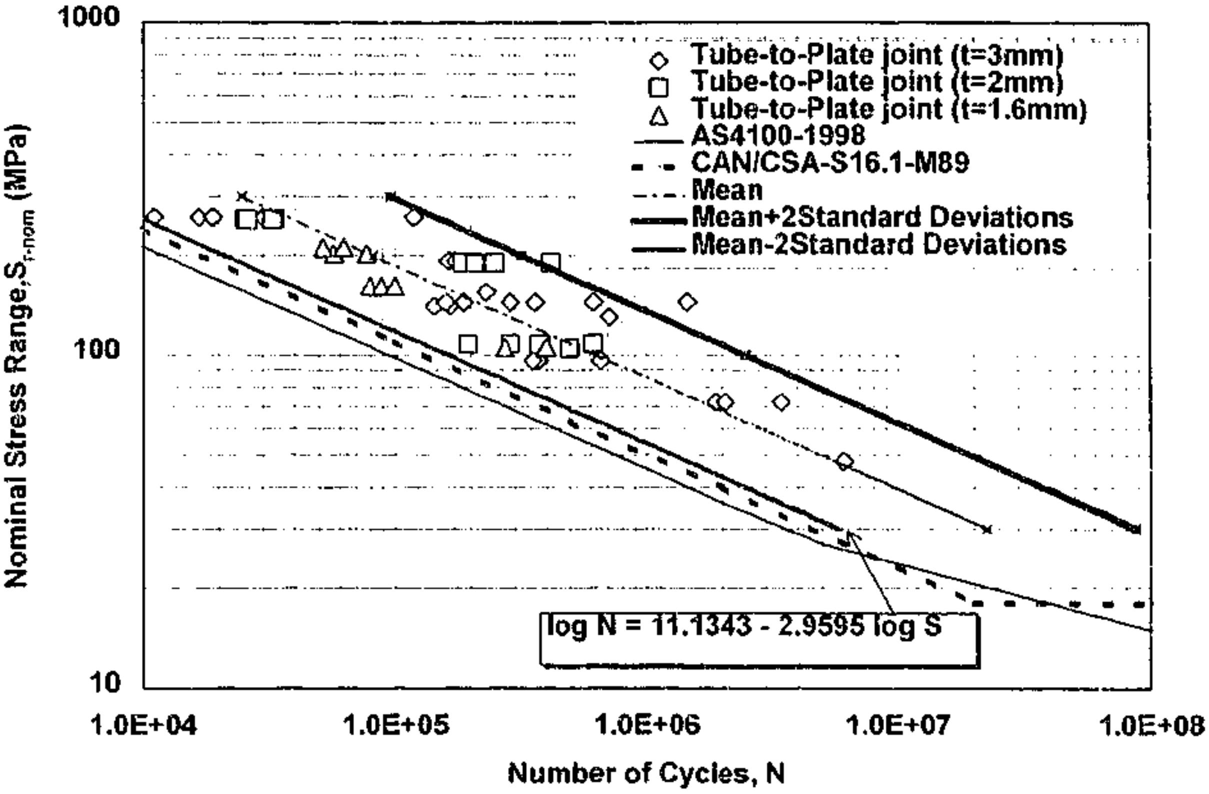

Figure 8-7: Data Analysis of tube-to-plate T-joints, log N dependent variable, A and B determined, Classification Method

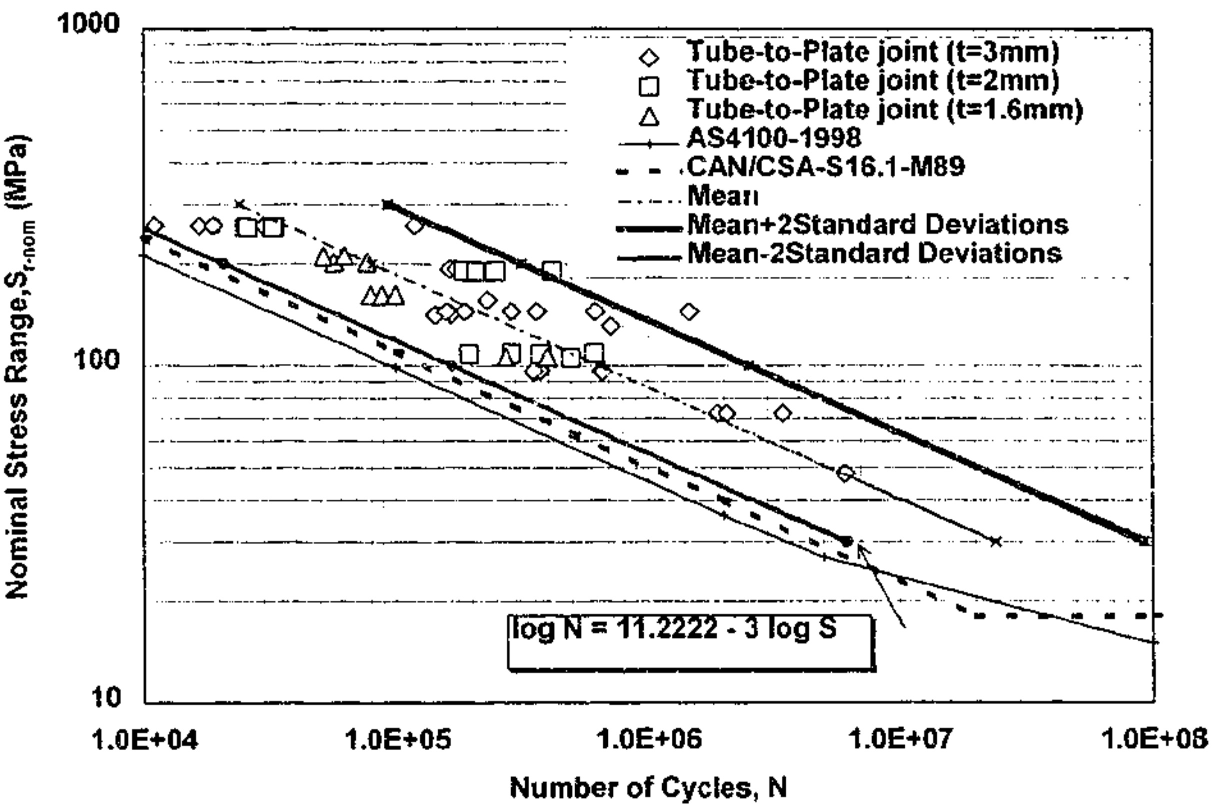

Figure 8-8: Data Analysis of tube-to-plate T-joints, log N dependent variable, B=-3 and A determined, Classification Method

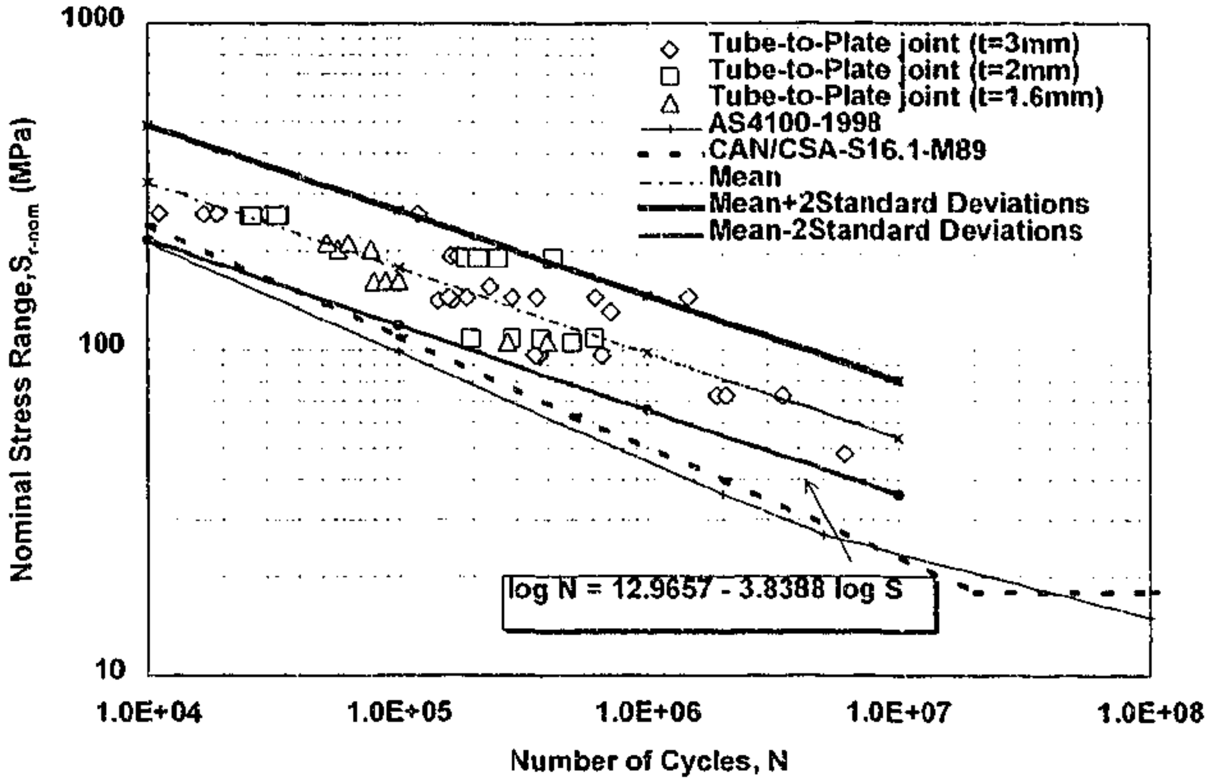

Figure 8-9: Data Analysis of tube-to-plate T-joints, log S dependent variable, a and b determined, Classification Method

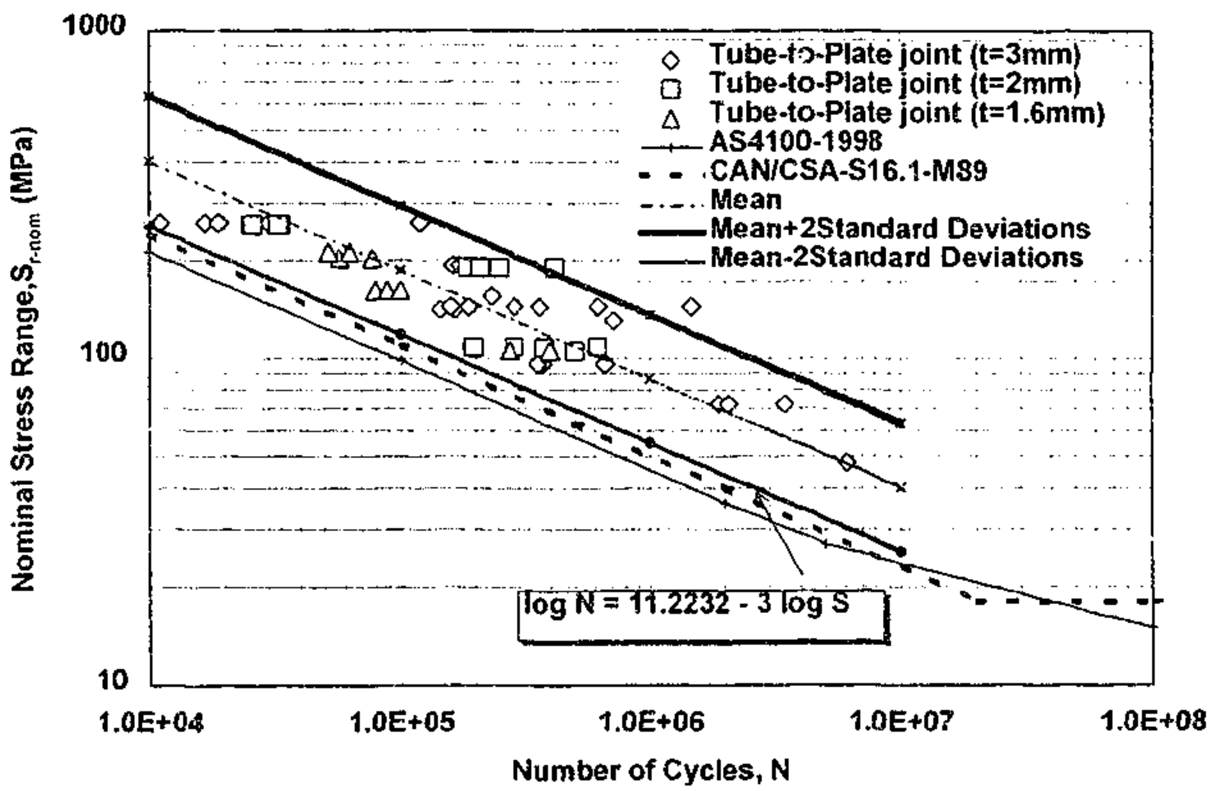

Figure 8-10: Data Analysis of tube-to-plate joints, log S dependent variable, b=-0.3333 and a determined, Classification Method

A summary of the results from the four analyses is shown in Table 8-2. Table 8-2 gives the parameters determined from the least-squares method, including the standard deviation and hence, the lower bound design S-N curve equation from each of the analyses considered.

The inverse of the slope of the S-N data when *log N* is the dependent variable and for the case when both *A* and *B* are determined is –2.9595. This is the natural slope of the S-N fatigue data obtained experimentally. This value is very close to –3 the value of the inverse of the slope of the S-N data adopted by AS4100-1998 (SAA 1998a) and EC3 (1992). The two cases considered when *log N* is the dependent variable therefore give fatigue design curves that are almost the same since their slopes are almost equal.

Table 8-2 shows that similar results are obtained from the two analyses when *log N* is assumed to be the dependent variable as well as when *log S* is assumed to be the dependent variable, when the inverse of the slope of the S-N curves is assumed to be –3.

The fatigue design S-N curves obtained when *log S* is the dependent variable are significantly different. This is because the natural slope of the S-N data when *log S* is the dependent variable is significantly different from the slope adopted in the design standards AS4100-1998 and EC3. The inverse of the natural slope of the S-N data when *log S* is the dependent variable is –3.8388 compared to a value of –3 adopted by the design standards.

The analysis when *log S* is the dependent variable and when *a* and *b* are determined, yields mean-minus-two-standard-deviation and mean-plus-two-standard deviation curves with a smaller scatter in terms of stress, compared to the analysis when *log N* is the dependent variable and when both *A* and *B* are determined. The scatter is a factor of 2.24 on stress measured on the EC3 class of the upper and lower bound S-N curves (see Figure 8-7) when *log S* is the dependant variable. A slightly larger scatter of 2.50 on stress measured on the EC3 class of the upper and lower S-N curves (see Figure 8-9) is obtained when *log N* is the dependent variable. This results in a design S-N curve with a less steep slope when *log S* is the dependent variable compared to that when *log N* is the dependent variable and when both *A* and *B* are determined, see Table 8-2. The analysis when *log S* is the dependent variable and when *a* and *b* are determined, therefore produces an S-N curve which is non-conservative at lower stress ranges and conservative at higher stress ranges compared to the corresponding analysis when *log N* is the dependent variable.

Table 8-2: Parameters, standard deviation and lower bound design S-N curve equations, Classification Method

Method	Parameters *A or a* and *B or b*	Standard Deviation, $\sigma_{log\,N}$ or $\sigma_{log\,S}$	Design S-N Curve Equation	Class (N=2E6 from mean-2SD curve) (MPa)
(a) *log N*, dependent variable				
(i) *A, B* determined	*A=11.7243* *B=-2.9595*	$\sigma_{log\,N}$=*0.2950*	*log N=11.1343–2.9595log S*	*43*
(ii) *A* determined, *B*=-3	*A=11.8124* *B=-3*	$\sigma_{log\,N}$=*0.2951*	*log N=11.2222 –3log S*	*44*
(b) *log S*, dependent variable				
(i) *a, b* determined	*a=3.5526* *b=-0.2605*	$\sigma_{log\,S}$=*0.08752*	*log N=12.9657–3.8388log S*	*54*
(ii) *a* determined, *b*=-1/3	*a=3.9375* *b=-1/3*	$\sigma_{log\,S}$=*0.0984*	*log N=11.2232 –3log S*	*44*

The equations derived for the case when the inverse of the slope of the S-N curve is assumed to be -3 should be adopted for fatigue design of tube-to-plate T-joints, where the tubes are square hollow sections of thicknesses less than 4mm. This is in order to be consistent with design guidelines such as EC3 (1992), AS4100-1998 (SAA 1998a) and CAN/CSA-S16.1-M89 (CSA 1989) where the inverse of the slopes of the S-N curves adopted is -3. Traditionally *log N* is regarded as the dependent variable (ASTM 1980; Nakazawa and Kodama 1987). Therefore the design S-N curve when the inverse of the slope of the S-N curve is assumed to be -3 and *log N* is the dependent variable is recommended for design. The design S-N curve in terms of the classification method for tube-to-plate T-joints, under in-plane bending, made from cold-formed square hollow sections of thicknesses less than 4mm, is given by the equation $log\ N = 11.2222 - 3log\ S$. This gives a class or detail category of 44.

8.5 DESIGN S_{r-hs}-N CURVES: HOT SPOT STRESS METHOD

The stress concentration factors of the different tube-to-plate T-joints connections under investigation were measured using strip strain gauges and reported in Section 5.5 of Chapter 5. The nominal stress ranges in the braces where fatigue failure occurred can therefore be converted to the corresponding hot spot stress ranges. This allows the fatigue data to be expressed in terms of the hot spot stress method. In the hot spot stress method the maximum structural stress concentration is taken into account but local stress concentrations due to the weld bead are not included, see Chapter 2, Section 2.3. The S-N data in Section 5.3 of Chapter 5 given in terms of the nominal stress approach is converted $S_{r.hs}$-N data in terms of the hot spot stress approach using the maximum stress concentration factors measured for each tube-to-plate T-joint.

8.5.1 $S_{r.hs}$-N Fatigue Data Set

The maximum stress concentration factors that have been obtained from experimental measurements, using the quadratic extrapolation method (see Section 5.5 of Chapter 5), for the different tube-to-plate T-joints are as follows;

(a) 1.775 for the connection series with a 50x50x3SHS brace (S1PL2R2B),

(b) 1.575 for the connection series with a 50x50x1.6SHS brace (S2PL3R2A), and

(c) 1.6 for the connection series with a 40x40x2SHS brace (D7PL2B).

This shows that the stress concentration factors in the tube-to-plate T-joints tested are almost the same. Since the conversion of the nominal stresses to the hot spot stresses in these joints involve SCF values that are almost equal it implies that the distribution of $S_{r.hs}$-N data plots remains the same, see Figure 8-11 (compared to Figure 8-7). Since the distribution of the $S_{r.hs}$-N data plots remains almost the same, the fatigue data has been considered as a single data set as in the classification method. The design $S_{r.hs}$-N curves are therefore determined for the tube-to-plate T-joints made up of square hollow section tubes of thicknesses less than 4mm.

There are no parametric equations for the determination of SCFs for tube-to-plate T-joints from current design standards. Therefore only the experimental SCFs are used to determine the design $S_{r.hs}$-N curves for the hot spot stress approach.

8.5.2 Analysis of Fatigue Data

Four different analyses have been considered similar to the cases considered in the classification method. Both *log N* and *log $S_{r.hs}$* were considered as dependent variables. For each of these cases, *log N* or *log $S_{r.hs}$* as the dependent variable, two different analyses are carried out, one when the natural slope of the $S_{r.hs}$-N is considered and the other when the inverse of the slope of the $S_{r.hs}$-N data is fixed to a value of -3. The inverse of the slope of the $S_{r.hs}$-N data for the hot spot stress method of –3 was also assumed following the slope adopted by EC3 (1992). All constructional details currently not included in EC3 (1992) are assumed to have a design $S_{r.hs}$-N curve with a double slope for fatigue assessments based on geometric stress ranges. A slope of 1:3 is adopted between 10^4 to $5x10^6$ cycles and a slope of 1:5 is adopted between $5x10^6$ and 10^8cycles.

The part of the $S_{r.hs}$-N curve between 10^4 to $5x10^6$ cycles defines the region for constant amplitude loading, while the part of the between $S_{r.hs}$-N curve $5x10^6$ and 10^8cycles defines the region for variable amplitude loading. The constant stress amplitude fatigue tests carried out in this investigation will therefore be used to determine the part of the $S_{r.hs}$-N curve between 10^4 to $5x10^6$ cycles. The region for variable amplitude loading is going to be defined using the constant amplitude curve at $5x10^6$ cycles and a negative slope of 1:5 thereafter up to 10^8 as given for design $S_{r.hs}$-N curves in EC3 (1992).

The results of the analyses when *log N* is the dependent variable are shown in Figures 8-11 and 8-12. The results of the analyses when *log $S_{r.hs}$* is the dependent variable are shown in Figures 8-13 and 8-14. Figures 8-11 to 8-14 show the mean, mean-minus-two-standard-deviation as well as the mean-plus-two-standard-deviation $S_{r.hs}$-N curves.

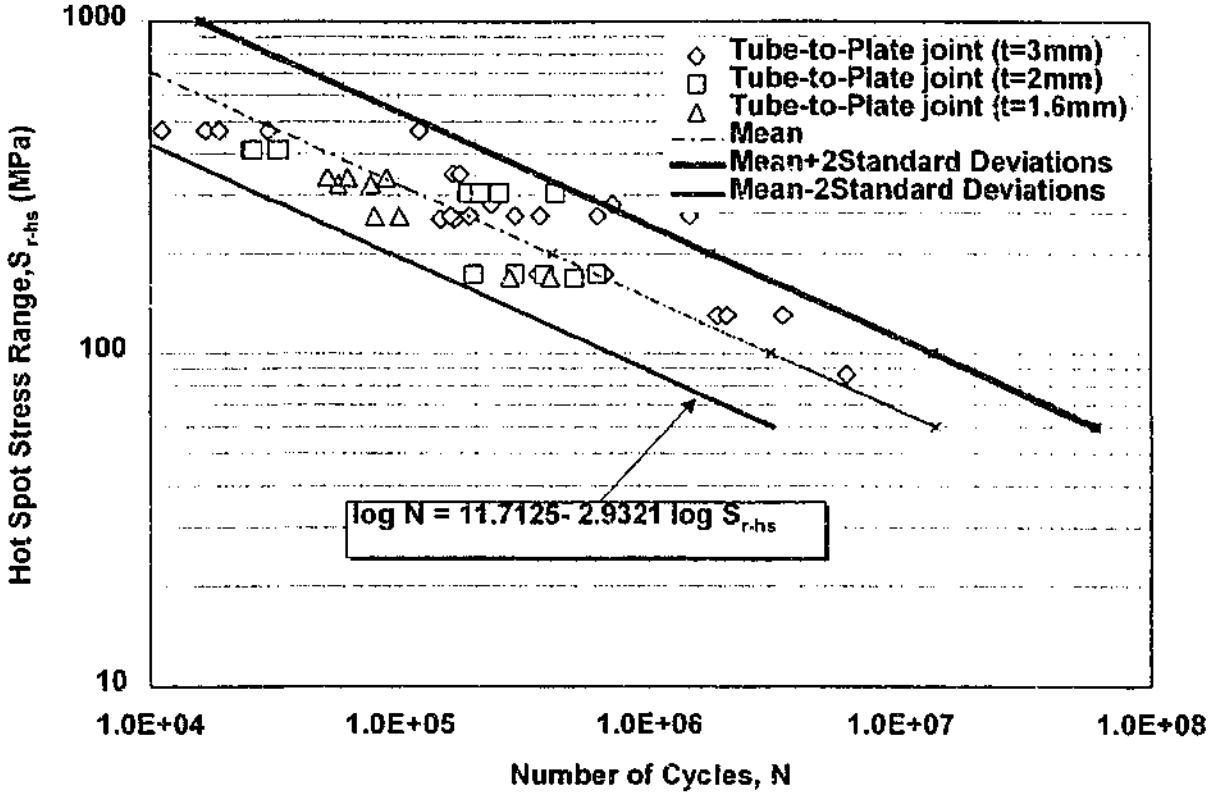

Figure 8-11: Data Analysis of tube-to-plate T-joints, log N dependent variable, A and B determined, Hot Spot Stress Method

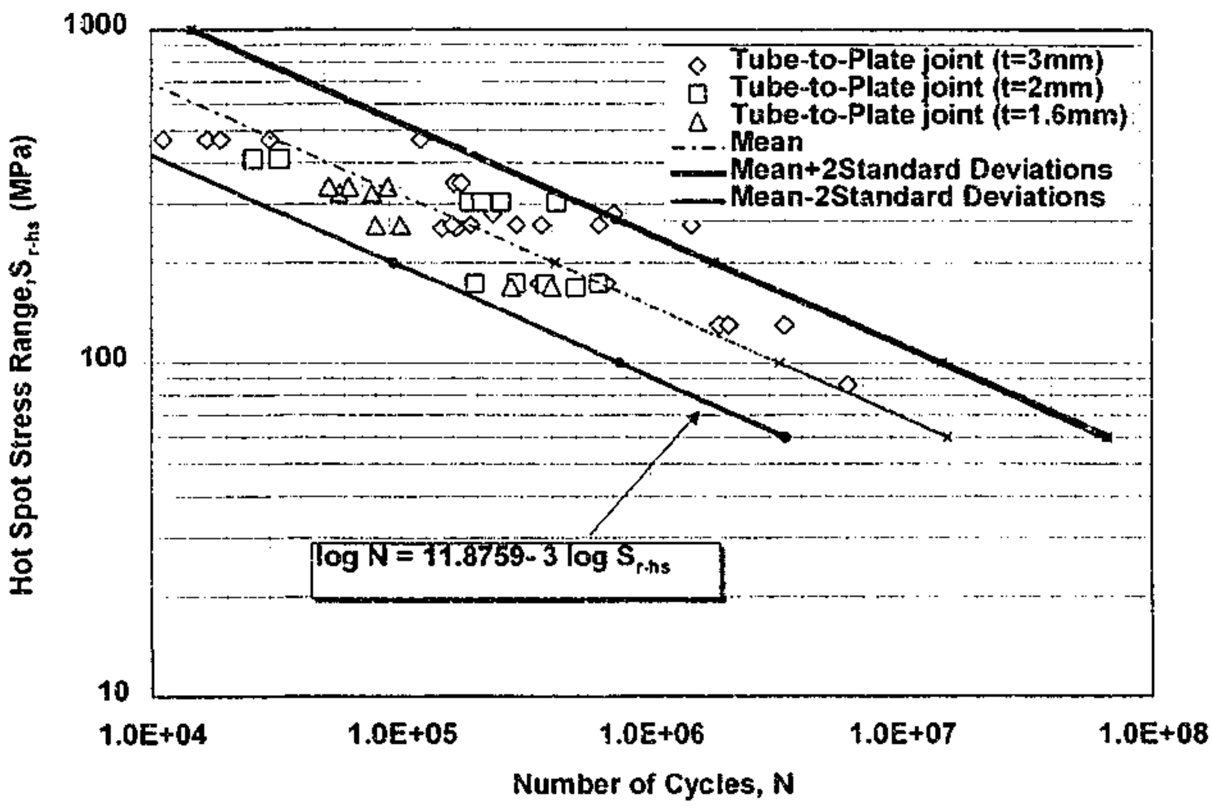

Figure 8-12: Data Analysis of tube-to-plate T-joints, log N dependent variable, B=-3 and A determined, Hot Spot Stress Method

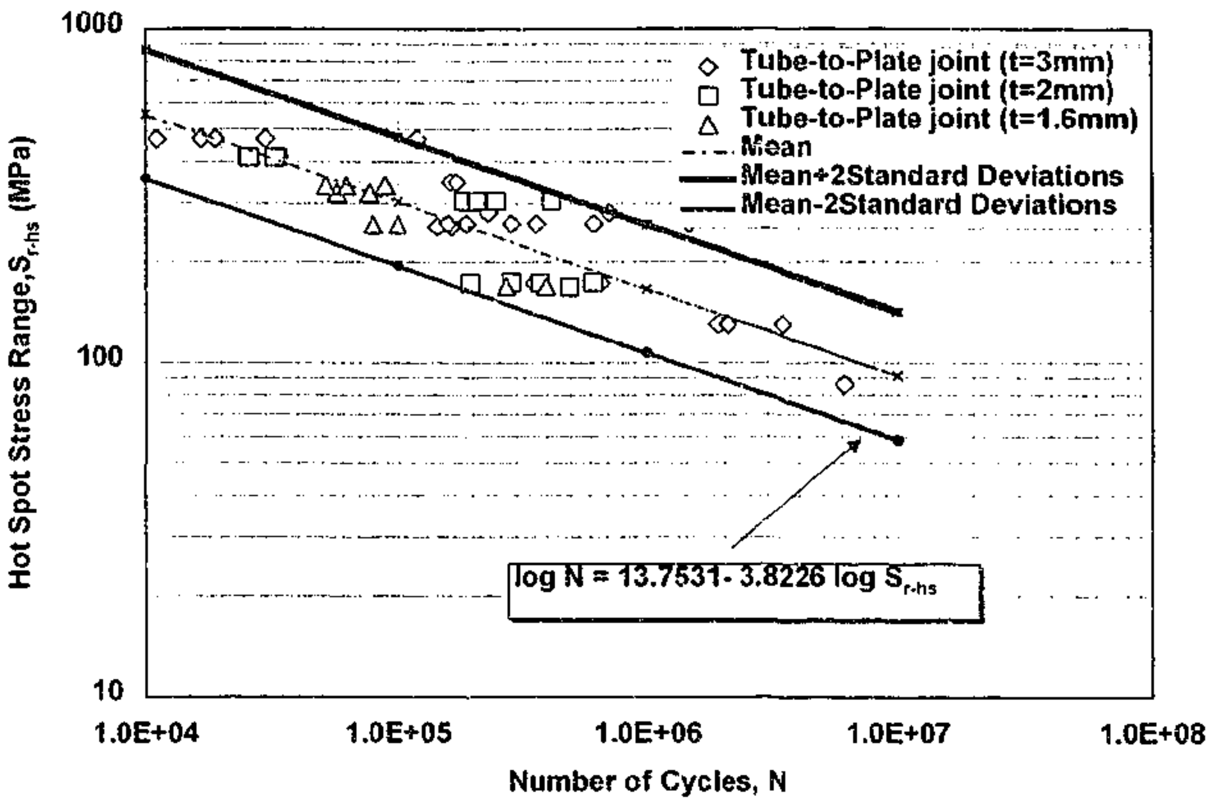

Figure 8-13: Data Analysis of tube-to-plate T-joints, log $S_{r.hs}$ dependent variable, a and b determined, Hot Spot Stress Method

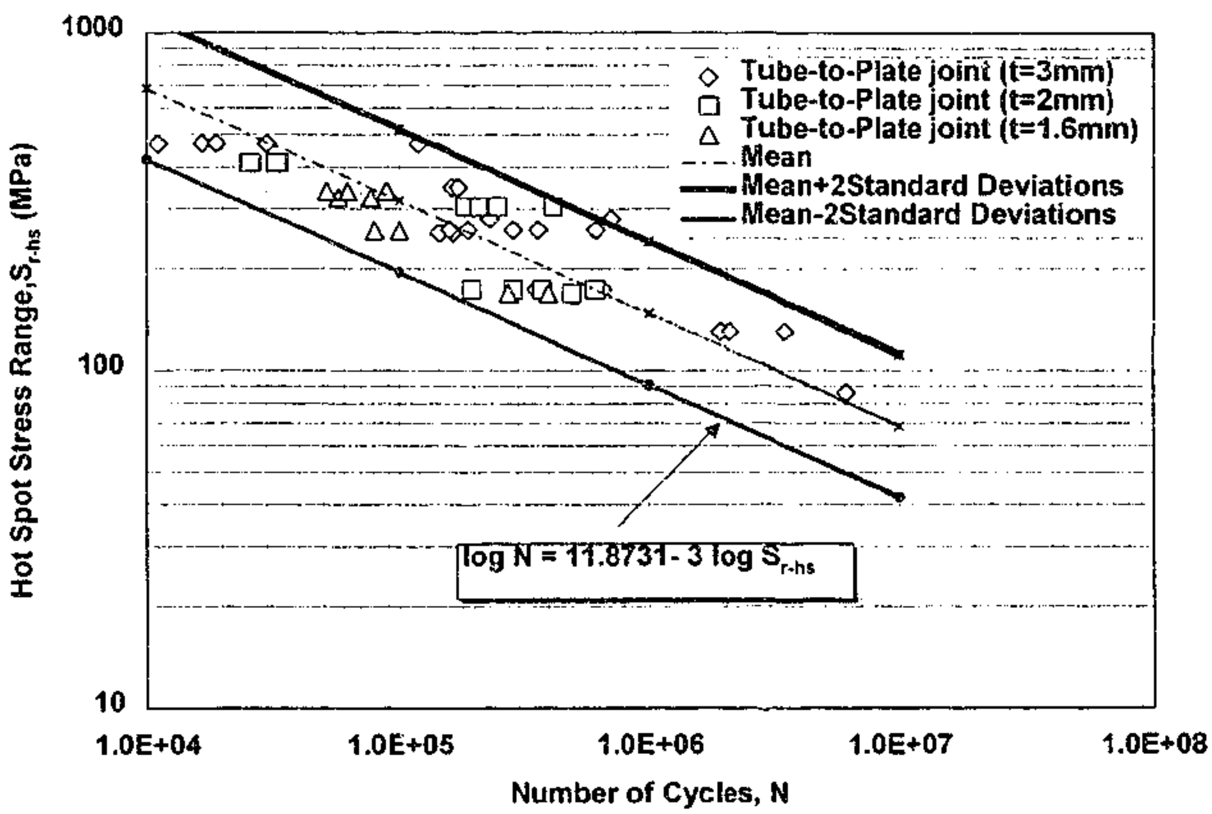

Figure 8-14: Data Analysis of tube-to-plate joints, log $S_{r.hs}$ dependent variable, b=-0.3333 and A determined, Hot Spot Stress Method

A summary of the parameters of the linear models and the resulting design $S_{r,hs}$-N equations for the four analyses are shown in Table 8-3. Similar observations to those obtained when the data was analysed in the classification method were realised.

The inverse of the slope of the $S_{r,hs}$-N data when *log N* is the dependent variable and for the case when both *A* and *B* are determined is –2.9321. This is the natural slope of the $S_{r,hs}$-N fatigue data obtained experimentally. This value is very close to –3 the value of the inverse of the slope of the S-N data adopted by EC3 (1992).

Table 8-3 shows that similar results are obtained from the two analyses when *log N* is assumed to be the dependent variable as well as when *log* $S_{r,hs}$ is assumed to be the dependent variable, when the inverse of the slope of the $S_{r,hs}$-N curves is assumed to be –3.

The fatigue design $S_{r,hs}$-N curves obtained when *log* $S_{r,hs}$ is the dependent variable are significantly different. This is because the natural slope of the $S_{r,hs}$-N data when *log* $S_{r,hs}$ is the dependent variable is significantly different from the slope adopted in the design standard EC3 (1992) for the hot spot stress method. The inverse of the natural slope of the S-N data when *log* $S_{r,hs}$ is the dependent variable is –3.8226 compared to a value of –3 adopted by the design standards.

Table 8-3: Parameters, standard deviation and lower bound design S-N curve equations, Hot Spot Stress Method

Method	**Parameters** *A or a* **and** *B or b*	**Standard Deviation,** $\sigma_{log N}$ **or** $\sigma_{log S}$	**Design $S_{r.hs}$-N Curve Equation**	**Hot Spot Stress range (N=2E6 from mean-2SD curve) (MPa)**
(c) ***log N*****, dependent variable**				
(i) *A, B* determined	*A=12.3549* *B=-2.9321*	$\sigma_{log N}$=0.3212	*log N=11.7125–2.9321log S*	70
(ii) *A* determined, *B*=-3	*A=12.5187* *B=-3*	$\sigma_{log N}$=0.3214	*log N=11.8759 –3log S*	72
(d) ***log S*****, dependent variable**				
(i) *a, b* determined	*a=3.7902* *b=-0.2616*	$\sigma_{log S}$=0.0962	*log N=13.7531–3.8226log S*	89
(ii) *a* determined, *b*=-1/3	*a=4.1691* *b=-1/3*	$\sigma_{log S}$=0.1059	*log N=11.8731 –3log S*	72

The equations derived for the case when the inverse of the slope of the $S_{r.hs}$ -N curve is assumed to be -3 should be adopted for design in order to be consistent with the design rules in EC3 (1992) for the geometric stress or hot spot stress method. The equation derived for the case when *log N* is the dependent variable is however recommended for fatigue design since *log N* is traditionally regarded as the dependent variable (ASTM 1980). The design $S_{r.hs}$-N curve in terms of the hot spot stress method for tube-to-plate T-joints, under in-plane bending, made from cold-formed square hollow sections of thicknesses less than 4mm, is given by the equation $log\ N = 11.8759 - 3log\ S_{r.hs}$. This gives a hot spot stress range of 72 at 2 million cycles. All the stress concentration factors determined experimentally for the tube-to-plate T-joints tested in this investigation have values less than 1.8. A stress concentration factor of 1.8 can therefore be used to convert the nominal stress ranges due to in-plane bending load in the tube to hot spot stress ranges. A minimum stress concentration factor (SCF) of 2.0 may conservatively be used as recommended in IIW (2000).

8.6 SUMMARY

8.6.1 Summary: Classification Method

Analysis of fatigue data to determine design S-N curves in terms of the classification method has been carried out using the least- squares method and assuming that *log N* or *log S* is the dependent variable. The following deductions were made from the analyzed results;

1. The whole database of results of tube-to-plate T-joints has been considered as a single group of results in determining the design S-N curve for tube-to-plate T-joints where the tubes are of wall thicknesses less than 4mm. Although the mean S-N curves of the S-N data show that there is an effect of both stress ratio and tube wall thickness on fatigue life, this is no longer the case when scatter of the S-N data is taken into account as is the case in the determination of design S-N curves.
2. When *log N* is the dependent variable and for the case when both parameters A and B are determined, the inverse of the slope of the S-N curve is -2.9595. This is the natural slope of the S-N data. This inverse of the slope is very close to -3 the value of the parameter B adopted for S-N curves in AS4100-1998 (SAA 1998a), EC3 (1992) and the Canadian Standard CAN/CSA-S16.1-M89 (CSA 1989). Since the value of the parameter B for the S-N curve where the natural slope of the data obtained is very close to –3, the design S-N curves obtained from the two methods of analysis, (i) when A and B are determined and (ii) when A is determined and B=-3, are almost the same.
3. The analysis of the data when *log N* is the dependent variable and considering the case when the inverse of the slope of the S-N curve is –3, gives a design S-N curve with a class of 44, see Table 8-2. This analysis produces the same design S-N curve as the analysis when *log S* is taken as the dependent variable and for the case when the inverse of the slope of the S-N curve is taken as –3.
4. The design S-N curves from the four different approaches both give lower bound design S-N curves which are above the existing design S-N curves from the Canadian Standard, CAN/CSA-S16.1-M89 and the Australian Standard, AS4100-

1998. The existing S-N curves are therefore conservative for tube-to-plate T-joints made up of square hollow sections of tube wall thicknesses less than 4mm.

5. The equation derived for the case when the inverse of the slope of the S-N curve is assumed to be -3 and when *log N* is the dependent variable is recommended for fatigue design of tube-to-plate T-joints, where the tubes are square hollow sections of thicknesses less than 4mm. This is in order to be consistent with design guidelines such as EC3 (1992), AS4100-1998 (SAA 1998a) and CAN/CSA-S16.1-M89 (CSA 1989) where the inverse of the slopes of the S-N curves adopted is -3. Traditionally *log N* is also regarded as the dependent variable (ASTM 1980; Nakazawa and Kodama 1987). The design S-N curve in terms of the classification method for tube-to-plate T-joints, made from cold-formed square hollow sections of thicknesses less than 4mm, is given by the equation $log\ N = 11.2222 - 3log\ S$. This gives a class of 44, see Figure 8-15.

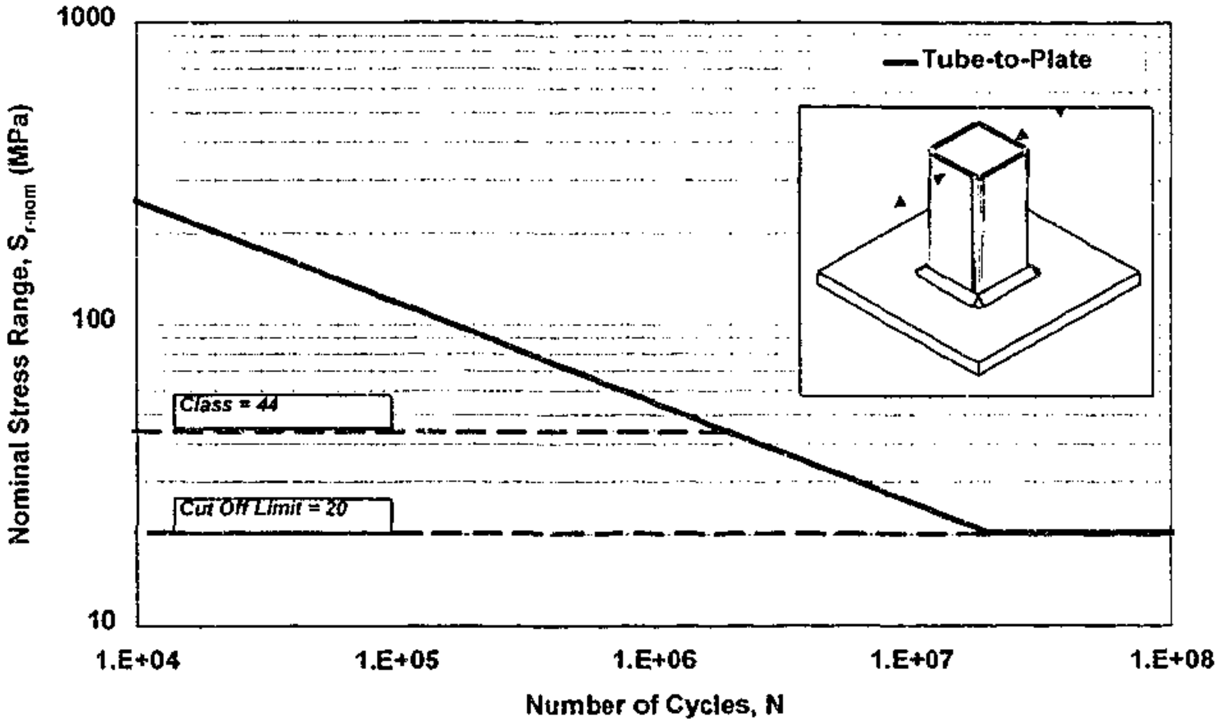

Figure 8-15: Design S-N curve for tube-to-plate T-joints, under in-plane bending, made up of SHS of thicknesses less than 4mm, Classification Method

8.6.2 Summary: Hot Spot Stress Method

Analysis of fatigue data to determine design $S_{r.hs}$-N curves in terms of the hot spot stress method has been carried out using the least- squares method and assuming that *log N* or $log\ S_{r.hs}$ is the dependent variable. Similar observations to those realised when the data was analysed in the classification method were obtained. The following deductions were made from the analyzed results;

1. The whole database of results of tube-to-plate T-joints has been considered as a single group of results in determining the design $S_{r,hs}$-N curve for tube-to-plate T-joints where the tubes are of wall thicknesses less than 4mm. Since the conversion of the nominal stresses to the hot spot stresses in these joints involve SCF values that are almost equal it implies that the relative distribution of $S_{r,hs}$-N data plots remains almost the same as that in the classification. Since the relative distribution of the $S_{r,hs}$-N data plots remains the same, the fatigue data has been considered as a single data set as in the classification method.
2. When $log\ N$ is the dependent variable and for the case when both parameters A and B are determined, the inverse of the slope of the $S_{r,hs}$-N curve is -2.9321. This is the natural slope of the $S_{r,hs}$-N data. This inverse of the natural slope is very close to -3 the value of the parameter B adopted for S-N curves in EC3 (1992).
3. The analysis of the data when $log\ N$ is the dependent variable and considering the case when the inverse of the slope of the $S_{r,hs}$-N curve is –3, gives a design $S_{r,hs}$-N curve with a hot spot stress range of 72 at 2 million cycles, see Table 8-3. This analysis produces the same design $S_{r,hs}$-N curve as the analysis when $log\ S_{r,hs}$ is taken as the dependent variable and for the case when the inverse of the slope of the $S_{r,hs}$ -N curve is taken as –3.
4. The equation derived for the case when the inverse of the slope of the $S_{r,hs}$ -N curve is assumed to be -3 and when $log\ N$ is the dependent variable is recommended for fatigue design of tube-to-plate T-joints in order to be consistent with the design rules in EC3 (1992) for the geometric stress or hot spot stress method. The equation derived for the case when $log\ N$ is the dependent variable is recommended for fatigue design since $log\ N$ is traditionally regarded as the dependent variable (ASTM 1980). The design $S_{r,hs}$-N curve in terms of the hot spot stress method for tube-to-plate T-joints, made from cold-formed square hollow sections of thicknesses less than 4mm, is given by the equation $log\ N = 11.8759 - 3log\ S_{r,hs}$ between 10^4 and $5x10^6$ cycles. It is also defined by the equation $log\ N = 15.3272 - 5log\ S_{r,hs}$ between $5x10^6$ and 10^8 cycles, see Figure 8-16. This gives a hot spot stress range of 72 at 2 million cycles. In design the SCF of 1.8 can be used or more conservatively a value of SCF of 2.0.

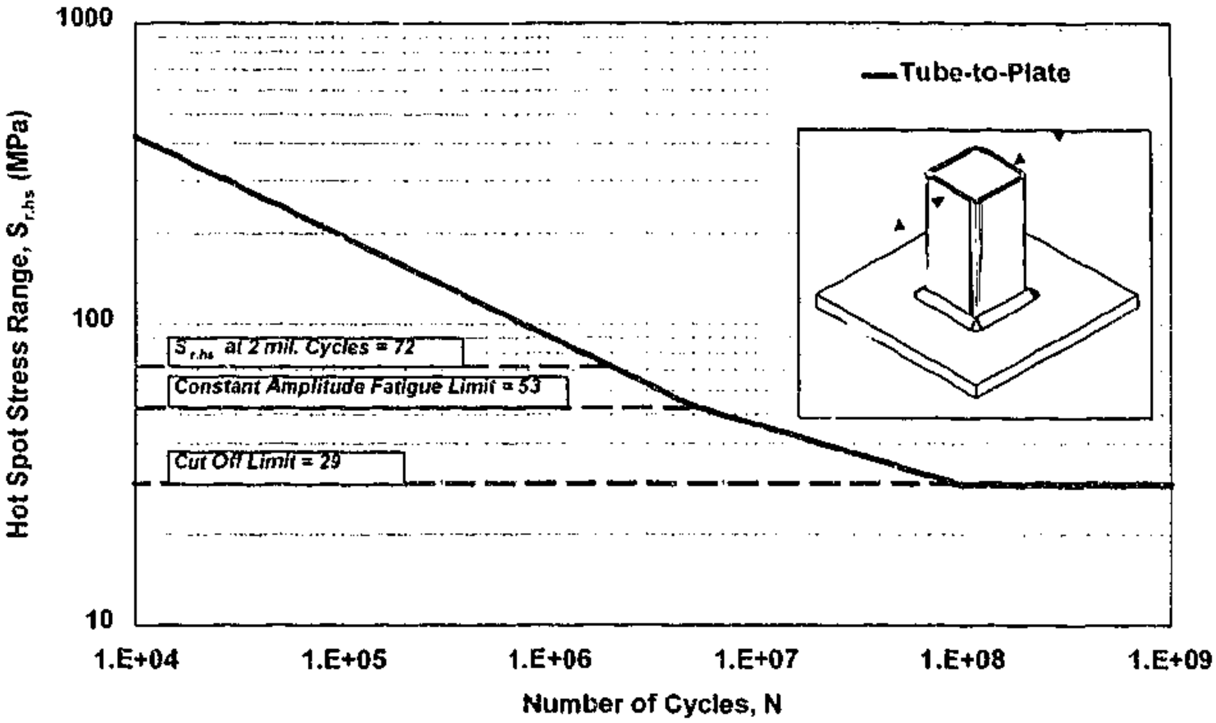

Figure 8-16: Design $S_{r\,hs}$-N curve for tube-to-plate T-joints, under in-plane bending, made up of SHS of thicknesses less than 4mm, Hot Spot Stress Method

Chapter 9

DESIGN RULES FOR TUBE-TO-TUBE T-JOINTS

9.1 INTRODUCTION

Tube-to-tube T-joints made up of square hollow section chords and braces were tested and reported in Chapter 6. The square hollow sections that make up the chords and braces are of thicknesses less than 4mm. These are the typical thicknesses currently being increasingly used in the manufacture of equipment in the road transport and agricultural industry as reported in Chapter 1.

The S-N data obtained in terms of nominal stress range will be converted into $S_{r,hs}$-N data in terms of hot spot stress range using stress concentration factors (SCFs). The SCFs used to convert the nominal stress ranges to hot spot stress ranges are those determined experimentally as detailed in Chapter 6. Stress concentration factors determined from existing parametric equations given in IIW (2000) and determined by van Wingerde (1992), will also be used to convert the nominal stress ranges into hot spot stress ranges. The SCFs from the existing parametric equations are used with the assumption that the trend in SCFs as determined by existing parametric equations remains the same for thin-walled joints and for values of β, 2γ and τ outside the current validity range. Design curves will thus be determined for $S_{r,hs}$-N data obtained from the use of stress concentration factors determined both experimentally and from existing parametric equations in IIW (2000).

The $S_{r,hs}$-N data is used to determine the design $S_{r,hs}$-N curves for tube-to-tube T-joints in the hot spot stress method. This is because current design standards such as IIW (2000), CIDECT Design Guide No. 8 (Zhao *et al* 1999a), Department of Energy (1990), EC3 (1992) and API (1991) give design curves for tubular nodal joints expressed in terms of the hot spot stress method. The design curves from the current fatigue design guidelines are reported in more detail in Chapter 2. The scatter of the $S_{r,hs}$-N data of the welded thin-walled tube-to-tube T-joints will be compared with the existing design curves from current design guidelines.

The least-squares method will be used to determine the mean-minus-two standards deviation curves, which define the design $S_{r.hs}$-N curves. Two set of analyses will be carried out with either *log N* or *log $S_{r.hs}$* as the dependent variable, for the two cases of $S_{r.hs}$-N data obtained from experimental SCFs and SCFs derived from existing parametric equations. A method of analysis similar to that used by Puthli *et al* (1989) will be used to determine the design $S_{r.hs}$-N curves.

9.2 $S_{r.hs}$-N FATIGUE DATA SET

Fatigue design of tube-to-tube nodal joints made up of hollow sections has been found to be dependent on the tube wall thickness in which fatigue cracks initiate and propagate to cause fatigue failure of the joint (van Delft *et al* 1985; van Wingerde *et al* 1997b). The tube wall thickness in which the fatigue cracks develop can be considered as the critical thickness in the joint, which determines the fatigue life of the joint. For all the tubes, some of the measured thicknesses are below the nominal thickness away from the corners of the tubes (Mang *et al* 1987) and slightly greater than but sometimes less than the nominal thickness at the corners. On average the actual thicknesses are close to the nominal thicknesses of the tubes, but within the tolerance limits allowed by the standards (Mashiri *et al* 2000c). The critical thicknesses used for design are therefore the nominal thicknesses of the tubes. Four different modes of failure where observed during the fatigue tests of welded thin-walled tube-to-tube T-joints as described in Section 6.3.2 of Chapter 6. The failure modes depend on whether the fatigue cracks develop in the brace member, the chord member or in both the chord and the brace.

The mode of failure in most of the tube-to-tube T-joints tested was the chord-tension-side failure, where failure occurs due to the development of fatigue cracks in the chord side which is under tension. Out of the 59 tests carried out 46 (78%) failed under the chord-tension-side failure mode. All the chord members were made up of square hollow sections of 3mm thickness. Therefore, the critical thickness of the joints where the chord-tension-side failure mode occurred is 3mm.

Tube-to-tube T-joints also failed in the chord-and-brace-tension-side failure mode. Out of the 59 specimens tested 11 (18.6%) failed under the chord-and-brace-tension-side failure mode. In this mode of failure, cracks first developed in the chord, where the maximum stress concentration factors occur. At a later stage the cracks then developed in the brace. In most of the joints that failed under the chord-and-brace-tension-side failure mode, the cracks developed in the chord member first and then into the brace member close to the failure of the joint. The chord wall thickness can thus be taken as the critical thickness in these joints because most of the fatigue life was spent in propagating the cracks in the chord. Therefore, the critical thickness of the joints where the chord-and-brace-tension-side failure mode occurred is 3mm, since all the chords used in this investigation had wall thicknesses of 3mm.

Brace-tension-side failure occurred in only one sample (1.7%) out of the 59 samples that were tested in this investigation. The critical thickness of this joint (S6S2L1A), is 1.6mm, the wall thickness of the brace in this joint, see Section 6.3.2.3 of Chapter 6.

Another mode of failure that was observed was the chord-compression-side failure. This mode of failure also occurred in just one specimen (1.7%) out of the 59 tests that were carried out. In chord-compression-side failure, cracks developed on the compression side of the chord, see Section 6.3.2.4 of Chapter 6. The critical thickness of the joint that failed under the chord-compression-side failure mode was 3mm. However this specimen was considered to be a runout since crack arrest occurred as the cracks grew away from the weld toes on the compressive side of the tube-to-tube interface.

A plot of the $S_{r,hs}$-N data, derived from experimental SCFs, showing the different modes of failure is shown in Figure 9-1. The $S_{r,hs}$-N data, is that shown in Tables 6-11 to 6-13 of Chapter 6 where the total hot spot stress has been determined using Equation 6.8. The tested samples and failure modes are shown in Tables 6-2 to 6-4 of Chapter 6. According to the scatter of this $S_{r,hs}$-N data, the mode of failure does not seem to affect the fatigue strength of the joint, especially for the 96.6% of the joints tested, which failed under both the chord-tension-side failure mode and the chord-and-brace-tension-side failure mode. As described above, the $S_{r,hs}$-N data of joints, that failed under both the chord-tension-side and chord-and-brace-tension-side failure modes, have a critical thickness of 3mm and are therefore expected to fall within the same scatter band, since they have the same critical thickness. The sample that failed under the chord-compression-side failure mode also had a critical thickness of 3mm. However the $S_{r,hs}$-N data plot of the specimen that failed under the chord-compression-side failure mode will not be included in the fatigue analysis since it is a runout. The $S_{r,hs}$-N data plot of the specimen that failed under the chord-compression-side failure mode can be seen to define the upper bound of the $S_{r.hs}$-N data. The single result obtained from the brace-tension-side failure mode also lies in this scatter band and will be included in the analysis, although this result has a critical thickness of 1.6mm.

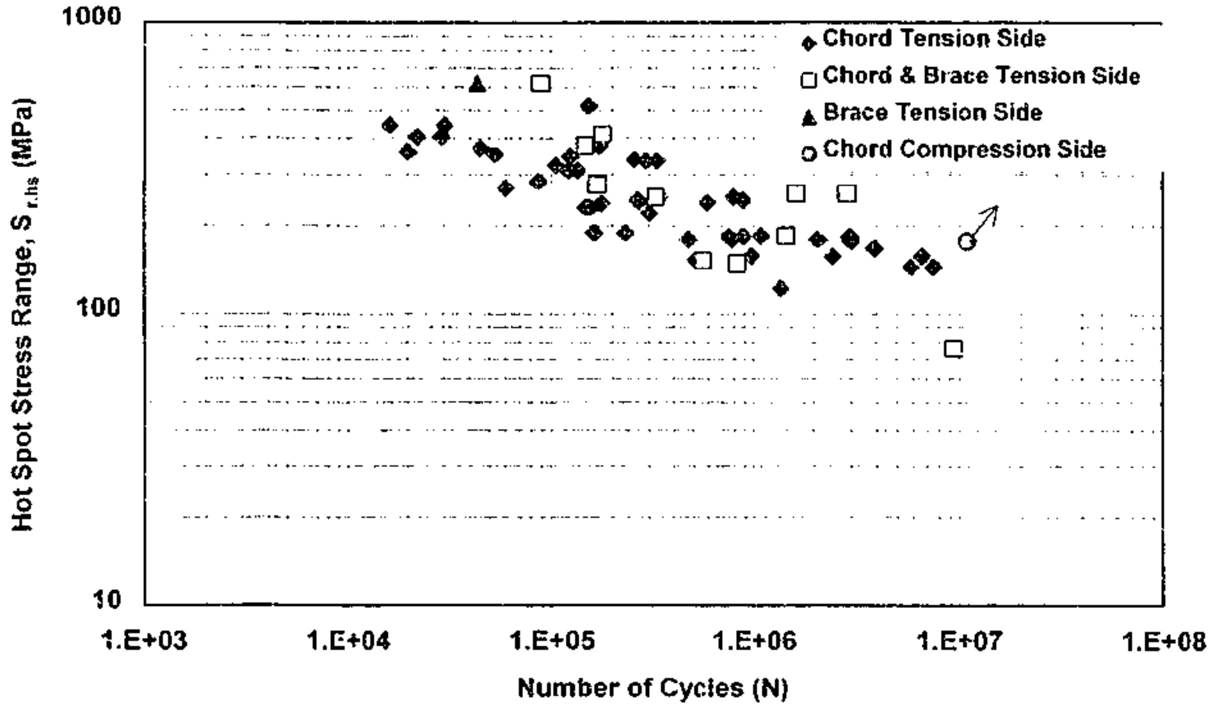

Figure 9-1: Plot of the $S_{r.hs}$-N data showing the different modes of failure

9.3 COMPARISON OF $S_{r.hs}$-N DATA WITH EXISTING DESIGN CURVES

The S-N data obtained from the fatigue tests of tube-to-tube T-joints is reported in detail in Chapter 6. All tests were carried out at a stress ratio of 0.1. The following tube-to-tube T-joints were tested under cyclic in-plane bending load; (a) 27 connections made from grade C450LO DuraGal steel, (b) 9 connections made from grade C350LO steel and, (c) 23 connections made from grade S355JOH steel. A total of 59 tube-to-tube T-joints made up of thin-walled ($t<4$mm) square hollow sections were tested.

9.3.1 $S_{r.hs}$-N Data based on Experimental SCFs

The stress concentration factors determined experimentally through the measurement of strain at predefined lines were used to convert the nominal stress ranges in Figure 6-10 (Chapter 6) into hot spot stress ranges, see Figure 9-2. This resulted in the $S_{r.hs}$-N plot expressed in terms of the hot spot stress method. The $S_{r.hs}$-N data is that shown in Tables 6-11 to 6-13 in Chapter 6 where the total hot spot stress has been determined using Equation 6.8. There is a considerable reduction in scatter of the $S_{r,hs}$-N data plots when the stress range is expressed in terms of hot spot stress (see Figure 9-2) compared to the scatter of the S-N data plots when the stress range is expressed in terms of nominal stress (see Figure 6-10, Chapter 6). The $S_{r,hs}$-N data expressed in the hot spot stress method can be compared to $S_{r,hs}$-N curves in some of the current design guides such as IIW (2000), CIDECT Design Guide No. 8 (Zhao *et al* 1999a), the Department of Energy (1990), EC3 (1992) and API (1991). The Department of Energy (1990) T Curve is a mean-minus-two-standard deviation $S_{r,hs}$-N curve. The IIW (2000), CIDECT Design Guide No. 8 (Zhao *et al* 1999a), EC3 (1992) and API (1991) $S_{r,hs}$-N curves are 95% confidence limits for survival curves.

The IIW 4mm $S_{r,hs}$-N curve shown in Figure 9-2, corresponds to the design curve for welded tubular joints where fatigue failure occurs due to fatigue cracks developing in tubes of wall thickness equal to 4mm. This is the same curve recommended by the CIDECT Design Guide No. 8 (Zhao *et al* 1999a). The IIW 4mm $S_{r,hs}$-N curve is derived from a thickness correction where the EC3 class 114 is used as a reference curve for a thickness of 16mm (van Wingerde *et al* 1997b). Classical fracture mechanics theory identifies a thickness effect, which in broad terms show that fatigue life is proportional to $t^{-3/4}$, where t is the thickness of the failed member. The hot spot stress $S_{r,hs}$-N curves in IIW (2000) and CIDECT Design Guide No. 8 (Zhao *et al* 1999a) show that the fatigue strength of nodal joints increase with a decrease in the thickness of the failed member down to 4mm. Using the classical fracture mechanics theory, the $S_{r,hs}$-N data plots for the tubes with wall thicknesses less than 4mm are expected to have a better fatigue strength than the 4mm $S_{r,hs}$-N curve from the CIDECT Design Guide No. 8. Although some of the tested joints have a better fatigue strength than the IIW 4mm $S_{r,hs}$-N curve, most of the $S_{r,hs}$-N data points lie below it, see Figure 9-2. Similar reduction in fatigue strength for thin-walled joints have been found by other researchers (Puthli *et al* 1989; Noordhoek *et al* 1980).

The Department of Energy (1990) T-curve is the basic $S_{r,hs}$-N curve for tubular nodal joints with a thickness of 32mm. The T-curve is equivalent to the EC3 Class 90 $S_{r,hs}$-N curve up to 5 million cycles. The EC3 Class 90 curve is recommended by EC3 for the fatigue assessment of non-classified details and of all hollow section members and tubular joints with wall thicknesses greater than 12.5mm based on geometric stress ranges. Category 90 however is recommended for fatigue assessment of joints with full penetration butt welds when both weld profile and permitted weld defects acceptance criteria are satisfied. The API X curve represents the $S_{r,hs}$-N curve for nodal joints where the weld profile merges smoothly with the welded tube walls. Most of the $S_{r,hs}$-N data points lie above the Department of Energy (1990) T-curve and the EC3 Class 90 $S_{r,hs}$-N curve. All of the tested joints have fatigue strength greater than the API X curve.

It is clear that the $S_{r,hs}$-N data of the welded thin-walled tube-to-tube T-joints whose critical thicknesses are less than 4mm, lie on the unsafe side of the IIW 4mm $S_{r,hs}$-N design curve. The lower than expected fatigue strength in welded thin-walled tubular joints when S-N data is terms of nominal stress is converted to $S_{r,hs}$-N data in terms of hot spot stress may be twofold. Firstly, the decrease in fatigue strength for welded joints with wall thicknesses less than 4mm is attributed to the greater impact of weld toe undercuts as shown in the analysis on thin-walled cruciform joints in Chapter 7 and Mashiri *et al* (1998b, 2000b). Another reason is that the experimental SCFs used to convert the nominal stress ranges to hot spot stress ranges are lower than those specified in IIW (2000). The low experimental estimate of SCF may be attributed to the fact that the positioning of strain gauges are limited to a distance of 4mm for welded thin-walled joints. The limiting of the first point of extrapolation for hot spot stresses to 4mm may result in the critical zone of stress amplification being missed. The lower stress concentration factors in welded thin-walled joints may also be associated with the oversized welds, which are obtained for these joints. The oversized welds push the hot spot stress locations, which occur at the toes of the welds in tube-to-tube welded joints, into lower stress regions (Maddox *et al* 1995).

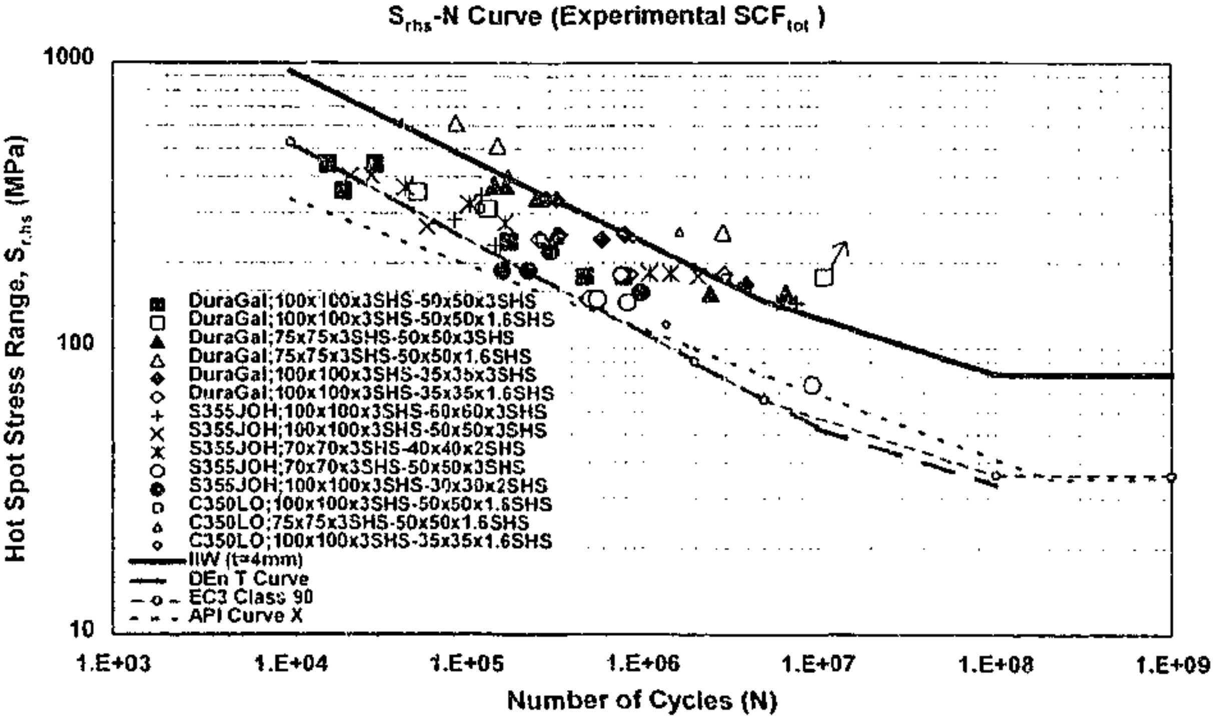

Figure 9-2: Hot Spot Stress $S_{r,hs}$-N data, based on Experimental SCF

9.3.2 $S_{r,hs}$-N Data based on SCFs derived using Existing Parametric Equations

In IIW (2000) and CIDECT Design Guide No. 8 (Zhao *et al* 1999a), the stress concentration factors of uniplanar square hollow section T-joints are determined using parametric equations as shown in Appendix F. The parametric equations for determining stress concentration factors (SCFs) of uniplanar square hollow section T-joints have a validity range within which they are applicable as follows;

$$0.35 \le \beta \le 1.0$$

$$12.5 \le 2\gamma \le 25.0$$

$$0.25 \le \tau \le 1.0$$

The tube-to-tube T-joints made up of thin-walled square hollow sections, which were tested in this investigation lie within the following parameter range;

$$0.30 \le \beta \le 0.71$$

$$23.3 \le 2\gamma \le 33.3$$

$$0.53 \le \tau \le 1.0$$

The tested specimens in which β = 0.30 or 2γ = 33.3 lie outside the validity range of the parametric equations given in IIW (2000).

However, although some of the tube-to-tube T-joints tested in this investigation have parameters which lie outside the validity range, the following assumptions can be adopted in order to incorporate the current test results into the IIW (2000) and CIDECT Design Guide No. 8 (Zhao *et al* 1999a):

(i) the sizes of welds for thin-walled joints are proportional to their thicknesses and the phenomena of oversized welds realized in thin-walled joints can be ignored, and

(ii) the trend in SCFs remains the same outside the validity ranges in IIW (2000) and Zhao *et al* (1999a).

These assumptions have the following advantages:

(i) they allow the existing parametric equations in IIW (2000) to be used in the design of thin-walled tube-to-tube T-joints , before extensive BEM or FEM analysis is carried out to determine the parametric equations for thin-walled joints and

(ii) the design $S_{r,hs}$-N curve derived from the use of the existing parametric equations in IIW (2000) can be incorporated directly into the IIW Fatigue Design Procedure without any further amendments to the existing parametric equations.

The existing parametric equations will therefore be used to determine the SCFs for the tube-to-tube specimen tested in this investigation. The SCFs from the existing parametric equations in IIW (2000) will be used to convert the nominal stress ranges to hot spot stress ranges. The maximum value of total hot spot stress range around the hot spot locations A to E, has been determined from a similar approach to that used for the experimentally determined SCFs, for each connection tested. Equation 6.8 (Chapter 6) has therefore, been used to determine the total hot spot stress ranges corresponding to the SCFs determined from parametric equations. The $S_{r,hs}$-N data determined using the SCFs from the parametric equations is shown in Tables 9-1 to 9-3 for the tube-to-tube T-joints made up from different grade tubes.

The $S_{r,hs}$-N data plots for welded thin-walled tube-to-tube T-joints from Tables 9-1 to 9-3 are compared to existing design $S_{r,hs}$-N curves in Figure 9-3. The $S_{r,hs}$-N data from this investigation is clearly above the Department of Energy T curve and API Curve X, which are fatigue design curves mainly used in the design of offshore structures where tubes of larger wall thickness are used. The $S_{r,hs}$-N data from the welded thin-walled tube-to-tube T-joints has a critical thickness of 3mm whereas for example, the Department of Energy T curve is the basic $S_{r,hs}$-N curve for tubular nodal joints with a thickness of 32mm. The $S_{r,hs}$-N data from the welded thin-walled tube-to-tube T-joints is therefore expected to have fatigue lives greater than that in the Department of Energy T curve and API Curve X, according to the classical fracture mechanics theory.

The trend for $S_{r,hs}$-N curves in the current standards for tubular nodal joint fatigue design (IIW 2000; Zhao *et al* 1999a) show an increase in fatigue life with a decrease in tube wall thickness up to 4mm. The $S_{r,hs}$-N data from this investigation which have a critical thickness of 3mm are therefore expected to be above the IIW 4mm $S_{r,hs}$-N curve according to the classical fracture mechanics theory. If the nominal stress ranges are converted to hot stress ranges using the SCFs from the parametric equations in IIW (2000) most of the $S_{r,hs}$-N data plots from the tested joints lie above the 4mm IIW $S_{r,hs}$-N curve, see Figure 9-3. The $S_{r,hs}$-N data plots in Figure 9-3 however, show that some of the tested joints have a lower fatigue life than the IIW 4mm curve, see Figure 9-3.

The reduced fatigue life in welded thin-walled tube-to-tube T-joints is still evident even when the nominal stress ranges are converted to hot spot stress ranges using SCFs from parametric equations, which have been shown to be considerably higher than experimental SCFs in Table 6-7 of Chapter 6. The reduced fatigue life of welded thin-walled specimens can be attributed to the greater negative impact of weld toe undercut on fatigue propagation life as reported in Mashiri *et al* (1998b, 2000b) and detailed in Chapter 7. Noordhoek *et al* (1980) also reported this phenomena and attributed it to the difficulty associated with welding smaller wall thickness sections.

Table 9-1: S-N data for tube-to-tube T-joints in terms of hot spot stress range using parametric stress concentration factors (Grade C450LO)

Connection Name	Fatigue Life, N (cycles)	P_{max} (N)	R	$\sigma_{r,m1}$ (MPa)	$\sigma_{r,a0}$ (MPa)	$\sigma_{r,m0}$ (MPa)	SCF_{m1}	SCF_{a0} or SCF_{m0}	$S_{r,hs}$ (Eqn. 6.8) (MPa)
D3D1L1A	16302	990	0.1	37.06	0.39	4.08	30.55	1.12	1137.13
D3D1L1B	30360	990	0.1	37.06	0.39	4.08	30.55	1.12	1137.13
D3D1L2A	783679	400	0.1	14.97	0.16	1.65	30.55	1.12	459.45
D3D1L3A	471200	400	0.1	14.97	0.16	1.65	30.55	1.12	459.45
D3D1L3B	175744	533	0.1	19.95	0.21	2.20	30.55	1.12	612.22
D3D1L3B	19937	800	0.1	29.95	0.32	3.29	30.55	1.12	918.90
D3D2L1A	133625	700	0.1	43.62	0.28	2.88	19.06	0.99	834.44
D3D2L2A	10969239	400	0.1	24.92	0.16	1.65	19.06	0.99	476.82
D3D2L3A	52829	800	0.1	49.85	0.32	3.29	19.06	0.99	953.64
D6D1L1A	170766	1200	0.1	44.92	0.64	9.16	18.95	1.23	863.27
D6D1L1B	145444	1200	0.1	44.92	0.64	9.16	18.95	1.23	863.27
D6D1L2A	2453350	500	0.1	18.72	0.27	3.82	18.95	1.23	359.70
D6D1L2B	6642981	500	0.1	18.72	0.27	3.82	18.95	1.23	359.70
D6D1L3B	324153	800	0.1	29.95	0.43	6.11	18.95	1.23	575.52
D6D1L3A	254276	1075	0.1	40.24	0.58	8.21	18.95	1.23	773.35
D6D2L1A	89294	1200	0.1	74.77	0.64	9.16	11.83	1.10	895.30
D6D2L2A	2885483	500	0.1	31.15	0.27	3.82	11.83	1.10	373.04
D6D2L3A	152682	1000	0.1	62.31	0.54	7.63	11.83	1.10	746.09
D3D4L1A	288292	400	0.1	26.36	0.16	1.27	15.54*	1.77*	412.23
D3D4L1B	328247	400	0.1	26.36	0.16	1.27	15.54*	1.77*	412.23
D3D4L2A	589163	288	0.1	19.01	0.11	0.91	15.54*	1.77*	297.22
D3D4L2B	340417	300	0.1	19.77	0.12	0.95	15.54*	1.77*	309.17
D3D4L3B	3925476	200	0.1	13.18	0.08	0.63	15.54*	1.77*	206.11
D3D4L3A	799808	300	0.1	19.77	0.12	0.95	15.54*	1.77*	309.17
D3D5L1A	264239	400	0.1	41.50	0.16	1.27	9.70*	1.52*	404.71
D3D5L2A	754797	300	0.1	31.13	0.12	0.95	9.70*	1.52*	303.54
D3D5L3A	2959837	300	0.1	31.13	0.12	0.95	9.70*	1.52*	303.54

* Most of the SCFs giving the highest total hot spot stress range occurred along line C except in the connection series D3D4 and D3D5 where the highest total hot spot stress range occurred along line D

Table 9-2: S-N data for tube-to-tube T-joints in terms of hot spot stress range using parametric stress concentration factors (Grade S355JOH)

Connection Name	Fatigue Life, N (cycles)	P_{max} (N)	R	$\sigma_{r,m1}$ (MPa)	$\sigma_{r,a0}$ (MPa)	$\sigma_{r,m0}$ (MPa)	SCF_{m1}	SCF_{a0} or SCF_{m0}	$S_{r,hs}$ (Equ. 6.8) (MPa)
V3V5L1A	124028	1200	0.1	29.88	0.47	4.94	36.36	1.22	1093.12
V3V5L1B	86947	985	0.1	24.53	0.39	4.06	36.36	1.22	897.27
V3V5L2A	5846429	500	0.1	12.45	0.20	2.06	36.36	1.22	455.47
V3V5L2B	155368	800	0.1	19.92	0.32	3.29	36.36	1.22	728.75
V3V5L3A	147376	800	0.1	19.92	0.32	3.29	36.36	1.22	728.75
V3V5L3B	7536844	500	0.1	12.45	0.20	2.06	36.36	1.22	455.47
V3V1L1A	29183	900	0.1	33.69	0.36	3.71	30.55	1.12	1033.76
V3V1L2B	22069	900	0.1	33.69	0.36	3.71	30.55	1.12	1033.76
V3V1L3A	60055	600	0.1	22.46	0.24	2.47	30.55	1.12	689.17
V3V1L3B	2093716	400	0.1	14.97	0.16	1.65	30.55	1.12	459.45
V6V2L1A	45365	800	0.1	67.23	0.46	7.11	12.24	1.05	830.82
V6V2L2A	1453800	400	0.1	33.61	0.23	3.56	12.24	1.05	415.41
V6V2L2B	105456	700	0.1	58.82	0.40	6.22	12.24	1.05	726.97
V6V2L3B	1095618	400	0.1	33.61	0.23	3.56	12.24	1.05	415.41
V6V2L3A	168446	600	0.1	50.42	0.35	5.33	12.24	1.05	623.11
V6V1L1A	513067	1200	0.1	44.92	0.69	10.67	15.15	1.27	693.60
V6V1L2B	560477	1200	0.1	44.92	0.69	10.67	15.15	1.27	693.60
V6V1L3B	9423530	600	0.1	22.46	0.35	5.33	15.15	1.27	346.80
V6V1L3A	825878	1169	0.1	43.76	0.67	10.39	15.15	1.27	675.69
V3V4L1A	162405	300	0.1	37.14	0.12	0.95	9.52*	1.55*	355.26
V3V4L2A	229799	300	0.1	37.14	0.12	0.95	9.52*	1.55*	355.26
V3V4L2B	303680	350	0.1	43.33	0.14	1.11	9.52*	1.55*	414.47
V3V4L3A	979654	250	0.1	30.95	0.10	0.79	9.52*	1.55*	296.05

* Most of the SCFs giving the highest total hot spot stress range occurred along line C except in the connection series V3V where the highest total hot spot stress range occurred along line D

Table 9-3: S-N data for tube-to-tube T-joints in terms of hot spot stress range using parametric stress concentration factors (Grade C350LO)

Connection Name	Fatigue Life, N (cycles)	P_{max} (N)	R	$\sigma_{r.m1}$ (MPa)	$\sigma_{r.a0}$ (MPa)	$\sigma_{r.m0}$ (MPa)	SCF_{m1}	SCF_{a0} or SCF_{m0}	$S_{r.hs}$ (Eqn. 6.8) (MPa)
S3S2L1A	121207	700	0.1	43.62	0.28	2.88	19.06	0.99	834.44
S3S2L2A	269341	550	0.1	34.27	0.22	2.27	19.06	0.99	655.63
S3S2L3A	3009445	400	0.1	24.92	0.16	1.65	19.06	0.99	476.82
S6S2L1A	43770	1200	0.1	74.77	0.64	9.16	11.83	1.10	895.30
S6S2L2A	1641907	500	0.1	31.15	0.27	3.82	11.83	1.10	373.04
S6S2L3A	177201	800	0.1	49.85	0.43	6.11	11.83	1.10	596.87
S3S5L1A	886078	400	0.1	41.50	0.16	1.27	9.70*	1.52*	404.71
S3S5L2A	886921	300	0.1	31.13	0.12	0.95	9.70*	1.52*	303.54
S3S5L3A	1371529	200	0.1	20.75	0.08	0.63	9.70*	1.52*	202.36

* Most of the SCFs giving the highest total hot spot stress range occurred along line C except in the connection series S3S5 where the highest total hot spot stress range occurred along line D

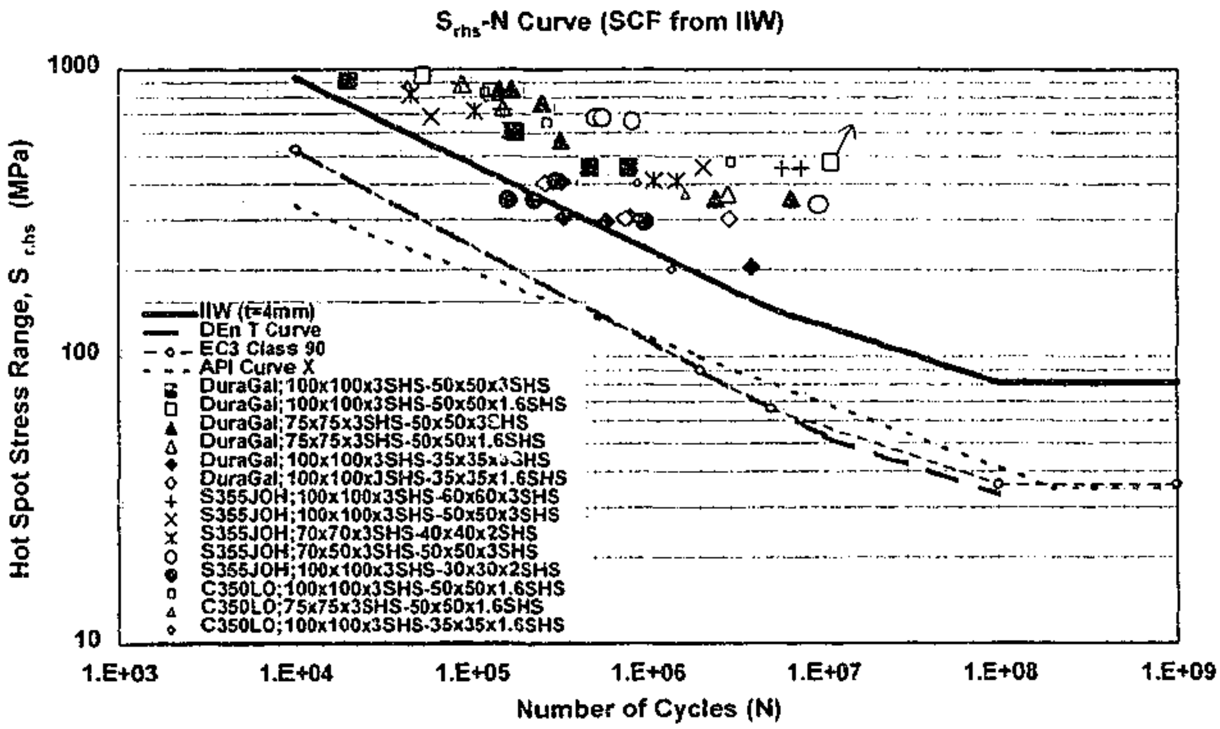

Figure 9-3: Hot Spot Stress $S_{r,hs}$-N data, based on IIW SCF

9.4 DETERMINATION OF $S_{r.hs}$-N DESIGN CURVES

The least-squares method of statistical analysis will be used to determine the mean $S_{r.hs}$-N curves, the mean-minus-two-standard deviation $S_{r.hs}$-N curves and the mean-plus-two-standard deviation $S_{r.hs}$-N curves. The least-squares method is described in Appendix G, where the equations used to calculate the parameters in the linear models relating stress range, S and number of cycles, N are also given. These equations can be used to estimate the parameters in the linear models relating S and N when either $log\ N$ or $log\ S$ is the dependent variable. The mean-minus-two-standard deviation $S_{r.hs}$-N curve defines the design curve for the experimental $S_{r.hs}$-N data (Department of Energy 1990).

A similar method to that used by Puthli *et al* (1989) will be used to determine the design $S_{r.hs}$-N curves for tube-to-tube T-joints as follows:

Determining $S_{r.hs}$-N Curves with Natural Slope of Data:

Step 1:

Statistical analysis carried out on data to determine the parameters in the linear model relating the number of cycles, N and the hot spot stress range, $S_{r.hs}$ when either $log\ N$ or $log\ S_{r.hs}$ is the dependent variable. This allows the mean $S_{r.hs}$-N curves and lines parallel to the mean line at plus and minus two-standard deviations to be defined.

Step 2:

The mean-minus-two-standard-deviation line equation determined from the values of the parameters in the linear model relating number of cycles and hot spot stress range as follows:

(i) when $log\ N$ is the dependent variable, $\log N = A + B\log S_{r.hs} - 2\sigma_{\log N}$ **(9.1)**

(ii) when $log\ S_{r.hs}$ is the dependent variable, $\log S_{r.hs} = a + b\log N - 2\sigma_{\log S_{r.hs}}$ **(9.2)**

The natural slope of the experimental $S_{r.hs}$-N data is determined.

Determining $S_{r.hs}$-N Curves with Forced Slope:

Step 1:

The equation used for determining design $S_{r.hs}$-N curves in IIW (2000) and CIDECT Design Guide No. 8 (Zhao *et al* 1999a) is used to evaluate the slope for the thickness under consideration. The equation used for determining the different $S_{r.hs}$-N curves for different thicknesses is (see Section 2.4.6 of Chapter 2 for more details):

$$\log(N)=\frac{12.476-3\cdot\log(S_{r.hs})}{1-0.18\cdot\log\left(\frac{16}{t}\right)} \tag{9.3}$$

Since all the tests except one had a critical thickness of 3mm, t is taken as 3mm. For t=3mm, equation 9.3 yields the $S_{r.hs}$-N design equation:

$$\log(N)=14.3544-3.4517\cdot\log(S_{r.hs}). \tag{9.4}$$

According to this equation the design $S_{r.hs}$-N curve for a thickness of 3mm has a negative slope of 1:3.4517.

Step 2:

By adopting the negative slope of 1:3.4517 for the $S_{r.hs}$-N curve as determined by step (1) for a thickness of 3mm, the parameter A or a as well as the corresponding standard deviation can be determined.

Step 3:

The design $S_{r.hs}$-N equation can then be defined as follows:

(i) when *log N* is the dependent variable, $\log N = A-3.4517\cdot\log S_{r.hs}-2\sigma_{\log N}$ **(9.5)**

(ii) when *log* $S_{r.hs}$ is the dependent variable, $\log S_{r.hs} = a-0.2897\cdot\log N-2\sigma_{\log S_{r.hs}}$ **(9.6)**

This procedure will be performed for both *log N* and *log* $S_{r.hs}$ as the dependent variable. Cases will also be considered for SCFs determined experimentally and SCFs derived using the existing parametric equations.

9.4.1 Analyses of $S_{r.hs}$-N Data based on Experimental SCFs

The $S_{r.hs}$-N data shown in Figure 9-2 has been derived from stress concentration factors determined experimentally as described in Chapter 6. The $S_{r.hs}$-N data is that shown in Tables 6-11 to 6-13 in Chapter 6 where the highest total hot spot stress around the hot spot locations A to E for each joint has been determined using Equation 6.8 of Chapter 6. The runout shown in Figure 9-2 will not be included in the analysis. This data will be analyzed using the steps given above to determine the design curves for $S_{r.hs}$-N data obtained by converting the nominal stress ranges into hot spot stress ranges using SCFs determined experimentally. The analysis details are shown in Table 9-4.

The analysis of the linear model relating the number of cycles to the hot spot stress range when *log N* is the dependent variable, yields the mean $S_{r,hs}$-N curves mean-minus and mean-plus two-standard deviation $S_{r,hs}$-N curves shown in Figure 9-4 when the natural slope of the $S_{r,hs}$-N data is determined, see corresponding analysis in Table 9-4. When the slope of the $S_{r,hs}$-N curve is forced to that expected from equation 9.3 for t=3mm, the mean $S_{r,hs}$-N curves, mean-minus and mean-plus two-standard deviation $S_{r,hs}$-N curves are those shown in Figure 9-5, see corresponding analysis in Table 9-4.

Mean $S_{r,hs}$-N curves, mean-minus and mean-plus two-standard deviation $S_{r,hs}$-N curves obtained when $log\ S_{r,hs}$ is the dependent variable are given in Figure 9-6 for the natural slope of the $S_{r,hs}$-N data and in Figure 9-7 when the slope of the $S_{r,hs}$-N data is forced to a negative slope of 1:3.4517.

The natural slope of the $S_{r,hs}$-N fatigue data when *log N* is the dependent variable is 1:3.0961. This slope is very close to the slope of 1:3 adopted in EC3 (1992) for the EC3 Class 90 curve and the Department of Energy (1990) for the T-curve.

The analysis, when either *log N* or $log\ S_{r,hs}$ is the dependent variable and when the slope of the $S_{r,hs}$-N curve is forced to 1:3.4517, yields similar design $S_{r,hs}$-N curve, which give the same hot spot stress range at 2 million cycles, see Table 9-4. The same observation was made for the analysis of tube-to-plate T-joints when the slope of the S-N was fixed to a given value for the two cases when *log N* or *log S* is the dependent variable, see Section 8.4 and 8.5, Chapter 8.

The analysis when $log\ S_{r,hs}$ is the dependent variable and when a and b are determined, yields mean-minus-two-standard-deviation and mean-plus-two-standard deviation curves with a smaller scatter in terms of stress to the analysis when *log N* is the dependent variable and when both A and B are determined. The scatter is a factor of 2.78 on stress measured on the EC3 class of the upper and lower bound $S_{r,hs}$-N curves (see Figure 9-4) when $log\ S_{r,hs}$ is the dependent variable. A considerably larger scatter with a factor of 3.61 on stress measured on the EC3 class of the upper and lower bound $S_{r,hs}$-N curves (see Figure 9-6) is obtained when *log N* is the dependent variable. This results in a design $S_{r,hs}$-N curve with a less steep slope compared to that when *log N* is the dependent variable and when both A and B are determined, see Table 9-4. The analysis when $log\ S_{r,hs}$ is the dependent variable and when a and b are determined, therefore produces an S-N curve which is non-conservative at lower stress ranges and conservative at higher stress ranges compared to the corresponding analysis when $log\ N$ is the dependent variable. A similar observation was also made in Section 8.4.2 of Chapter 8.

Table 9-4: Determination of design $S_{r,hs}$-N curves from data derived using experimental SCFs

Slope	Step	Dependent Variable	
		Log N	**Log $S_{r,hs}$**
Natural Slope	(1)	Linear Model: $\log N = A + B \cdot \log S_{r,hs}$ A = 12.7689 B = -3.0179 σ_{logN} = 0.4207	Linear Model: $\log S_{r,hs} = a + b \cdot \log N$ a = 3.5599 b = -0.2104 $\sigma_{logSr,hs}$ = 0.1111
	(2)	*(i)* $\log N = 12.7689 - 3.0179 \cdot \log S_{r,hs} - 2(0.4207)$ ***(ii)*** $\boldsymbol{\log N = 11.9275 - 3.0179 \cdot \log S_{r,hs}}$ Hot spot stress range at 2 million cycles = 73MPa	*(i)* $\log S_{r,hs} = 3.5599 - 0.2104 \cdot \log N - 2(0.1111)$ ***(ii)*** $\boldsymbol{\log N = 15.8636 - 4.7529 \cdot \log S_{r,hs}}$ Hot spot stress range at 2 million cycles = 103MPa
Forced Slope	(1)	B = -3.4517	b = -0.2897
	(2)	When B = -3.4517 A = 13.8066 and σ_{logN} = 0.4482	When b = -0.2897 a = 3.9999 and $\sigma_{logSr,hs}$ = 0.1240
	(3)	*(i)* $\log N = 13.8066 - 3.4517 \cdot \log S_{r,hs} - 2(0.4282)$ ***(ii)*** $\boldsymbol{\log N = 12.9502 - 3.4517 \cdot \log S_{r,hs}}$ Hot spot stress range at 2 million cycles = 84MPa	*(i)* $\log S_{r,hs} = 3.9999 - 0.2897 \cdot \log N - 2(0.1240)$ ***(ii)*** $\boldsymbol{\log N = 12.9510 - 3.4517 \cdot \log S_{r,hs}}$ Hot spot stress range at 2 million cycles = 84MPa

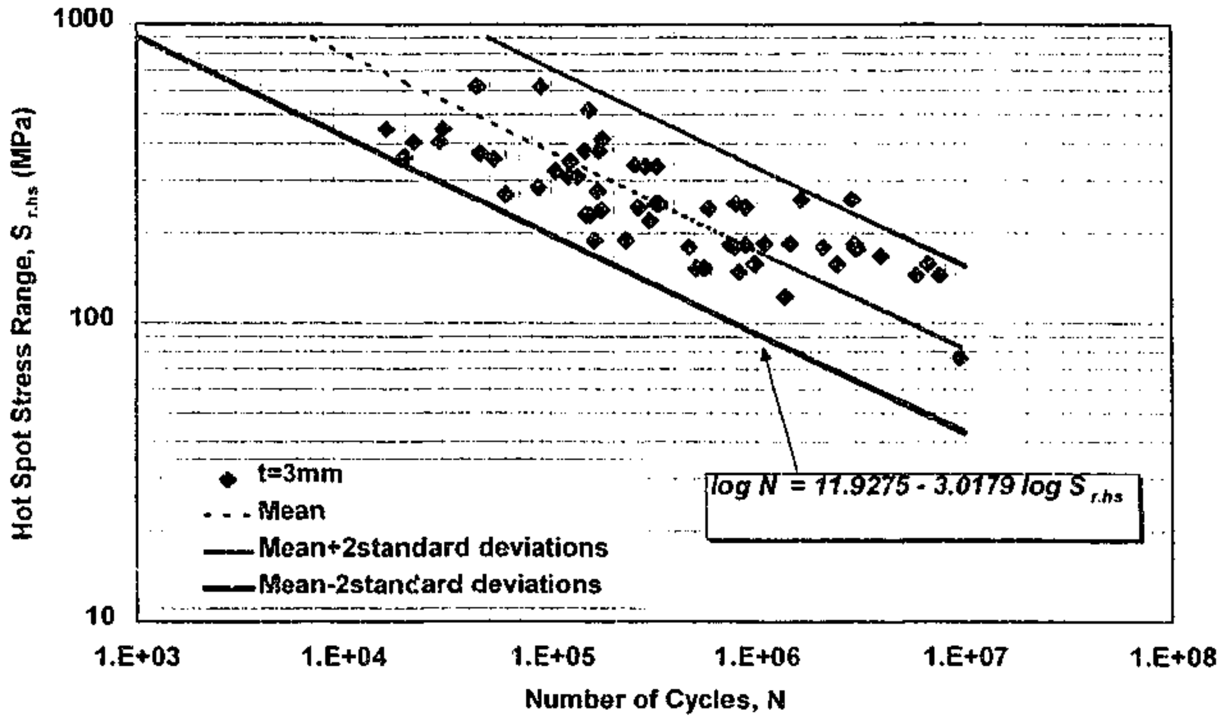

Figure 9-4: $S_{r.hs}$-N curves from Data Analysis, log N dependent variable, A and B determined, Hot Spot Stress Method, Experimental SCFs used

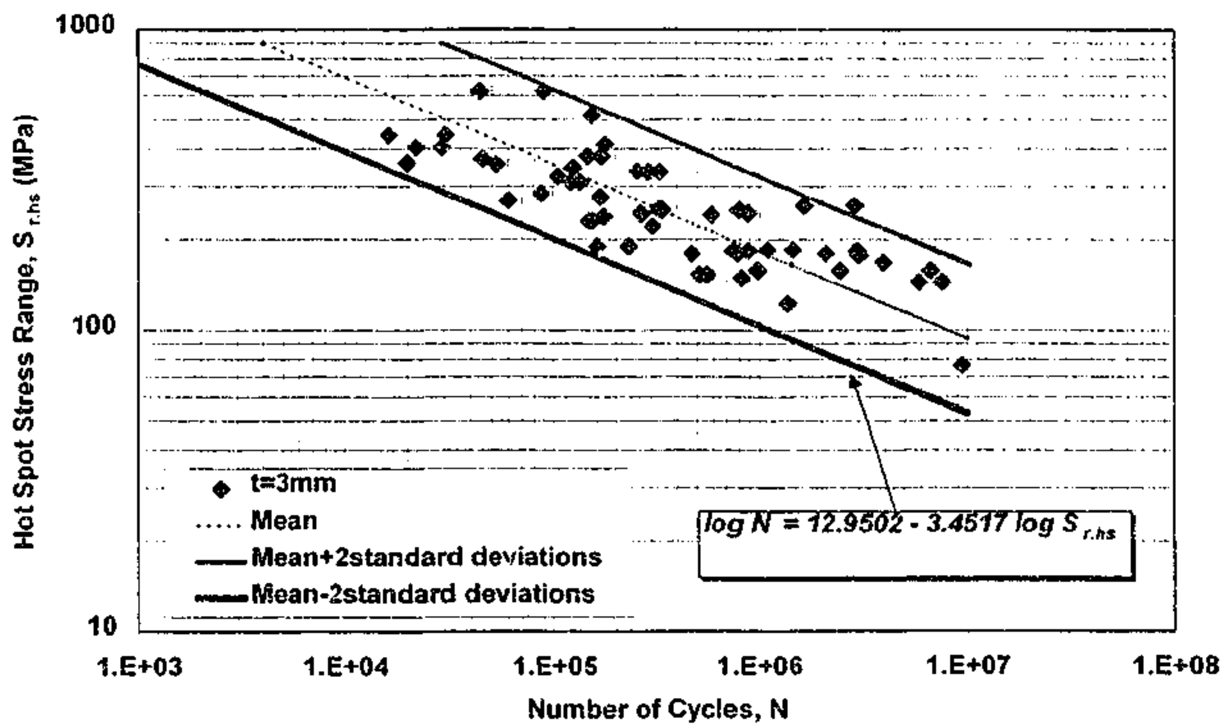

Figure 9-5: $S_{r.hs}$-N curves from Data Analysis, log N dependent variable, B=-3.4517, A determined, Hot Spot Stress Method, Experimental SCFs used

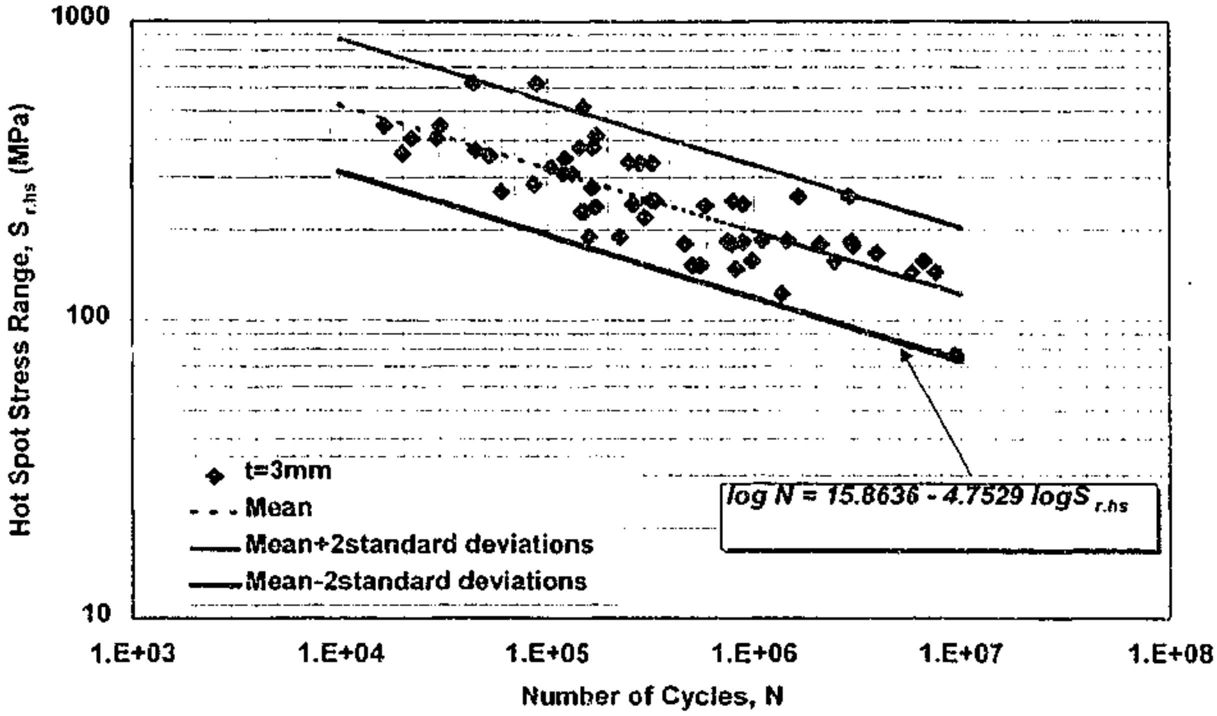

Figure 9-6: $S_{r,hs}$-N curves from Data Analysis, log $S_{r,hs}$ dependent variable, a and b determined, Hot Spot Stress Method, Experimental SCFs used

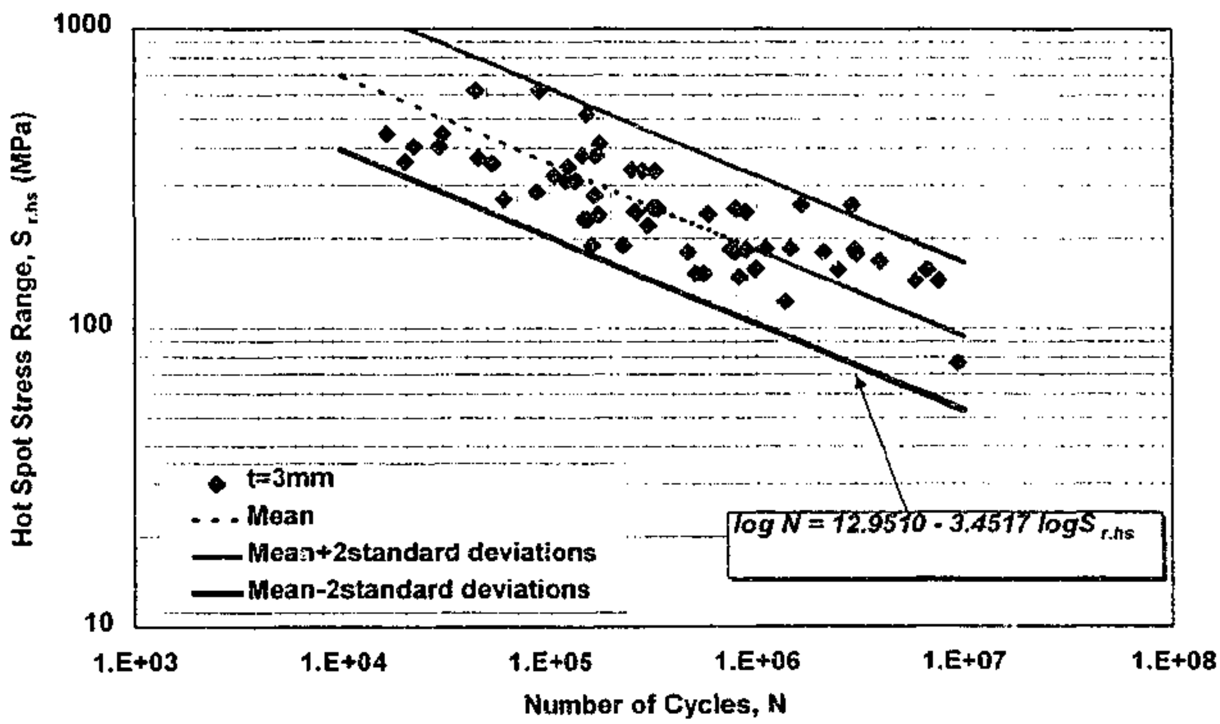

Figure 9-7: $S_{r,hs}$-N curves from Data Analysis, log $S_{r,hs}$ dependent variable, b=-0.2897, a determined, Hot Spot Stress Method, Experimental SCFs used

9.4.2 Analyses of $S_{r,hs}$-N Data based on Parametric Equation SCFs

The $S_{r,hs}$-N data shown in Figure 9-3 has been derived from stress concentration factors determined from existing parametric equations in IIW (2000). The $S_{r,hs}$-N data is that shown in Tables 9-1 to 9-3 where the highest total hot spot stress around the hot spot locations A to E for each joint has been determined using Equation 6.8 of Chapter 6. The runout shown in Figure 9-3 will not be included in the analysis. This data will be analyzed using the steps described at the beginning of Section 9.4 to determine the design curves for $S_{r,hs}$-N data obtained by converting the nominal stress ranges into hot spot stress ranges using SCFs derived from the existing parametric equations in IIW (2000). The analysis details are shown in Table 9-5.

The analysis of the linear model relating the number of cycles to the hot spot stress range when *log N* is the dependent variable yields the mean $S_{r,hs}$-N curves, mean-minus and mean-plus two-standard deviation $S_{r,hs}$-N curves shown in Figure 9-8 when the natural slope of the $S_{r,hs}$-N data is determined, see corresponding analysis in Table 9-5. When the slope of the $S_{r,hs}$-N curve is forced to that expected from equation 9.3 for t=3mm, the mean $S_{r,hs}$-N curves, mean-minus and mean-plus two-standard deviation $S_{r,hs}$-N curves are those shown in Figure 9-9, see corresponding analysis in Table 9-5.

Mean $S_{r,hs}$-N curves, mean-minus and mean-plus two-standard deviation $S_{r,hs}$-N curves obtained when $log\ S_{r,hs}$ is the dependent variable are given in Figure 9-10 for the natural slope of the $S_{r,hs}$-N data and in Figure 9-11 when the slope of the $S_{r,hs}$-N data is forced to a negative slope of 1:3.4517.

As in the previous analyses in Section 9.4.1, the analyses when either *log N* or $log\ S_{r,hs}$ is the dependent variable and when the slope of the $S_{r,hs}$-N is forced to 1:3.4517, yields similar design $S_{r,hs}$-N curve, giving the same hot spot stress range at 2 million cycles, see Table 9.5.

Table 9-5: Determination of design $S_{r,hs}$-N curves from data derived using parametric equation SCFs

Slope	**Step**	**Dependent Variable**	
		Log N	**Log $S_{r,hs}$**
Natural Slope	(1)	Linear Model: $\log N = A + B \cdot \log S_{r,hs}$ $A = 12.8837$ $B = -2.6851$ $\sigma_{\log N} = 0.4481$	Linear Model: $\log S_{r,hs} = a + b \cdot \log N$ $a = 3.9425$ $b = -0.2182$ $\sigma_{\log Sr,hs} = 0.1277$
	(2)	*(i)* $\log N = 12.8837 - 2.6851 \cdot \log S_{r,hs} - 2(0.4481)$ ***(ii)*** $\boldsymbol{\log N = 11.9875 - 2.6851 \cdot \log S_{r,hs}}$ Hot spot stress range at 2 million cycles = 131 MPa	*(i)* $\log S_{r,hs} = 3.9425 - 0.2182 \cdot \log N - 2(0.1277)$ ***(ii)*** $\boldsymbol{\log N = 16.8978 - 4.5829 \cdot \log S_{r,hs}}$ Hot spot stress range at 2 million cycles = 205 MPa
Forced Slope	(1)	$B = -3.4517$	$b = -0.2897$
	(2)	When $B = -3.4517$ $A = 14.9776$ and $\sigma_{\log N} = 0.4732$	When $b = -0.2897$ $a = 4.3391$ and $\sigma_{\log Sr,hs} = 0.1371$
	(3)	*(i)* $\log N = 14.9776 - 3.4517 \cdot \log S_{r,hs} - 2(0.4732)$ ***(ii)*** $\boldsymbol{\log N = 14.0312 - 3.4517 \cdot \log S_{r,hs}}$ Hot spot stress range at 2 million cycles = 174MPa	*(i)* $\log S_{r,hs} = 4.3391 - 0.2897 \cdot \log N - 2(0.1371)$ ***(ii)*** $\boldsymbol{\log N = 14.0314 - 3.4517 \cdot \log S_{r,hs}}$ Hot spot stress range at 2 million cycles = 174MPa

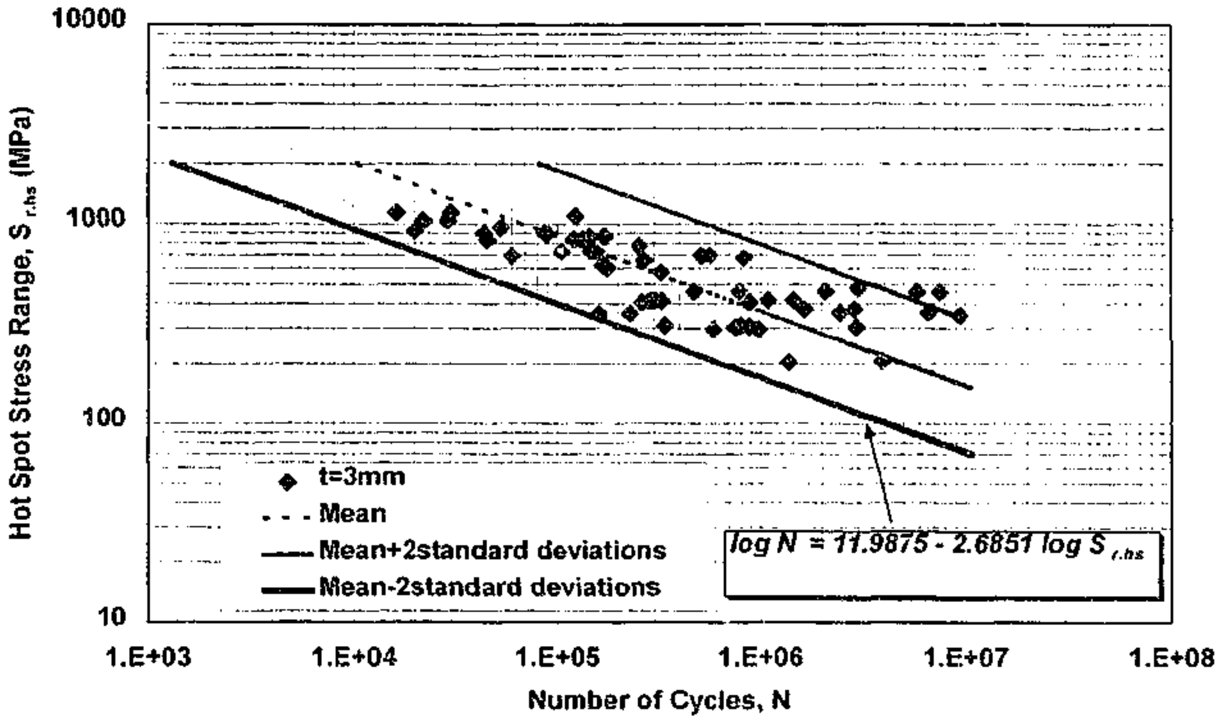

Figure 9-8: $S_{r,hs}$-N curves from Data Analysis, log N dependent variable, A and B determined, Hot Spot Stress Method, Parametric Equation SCFs used

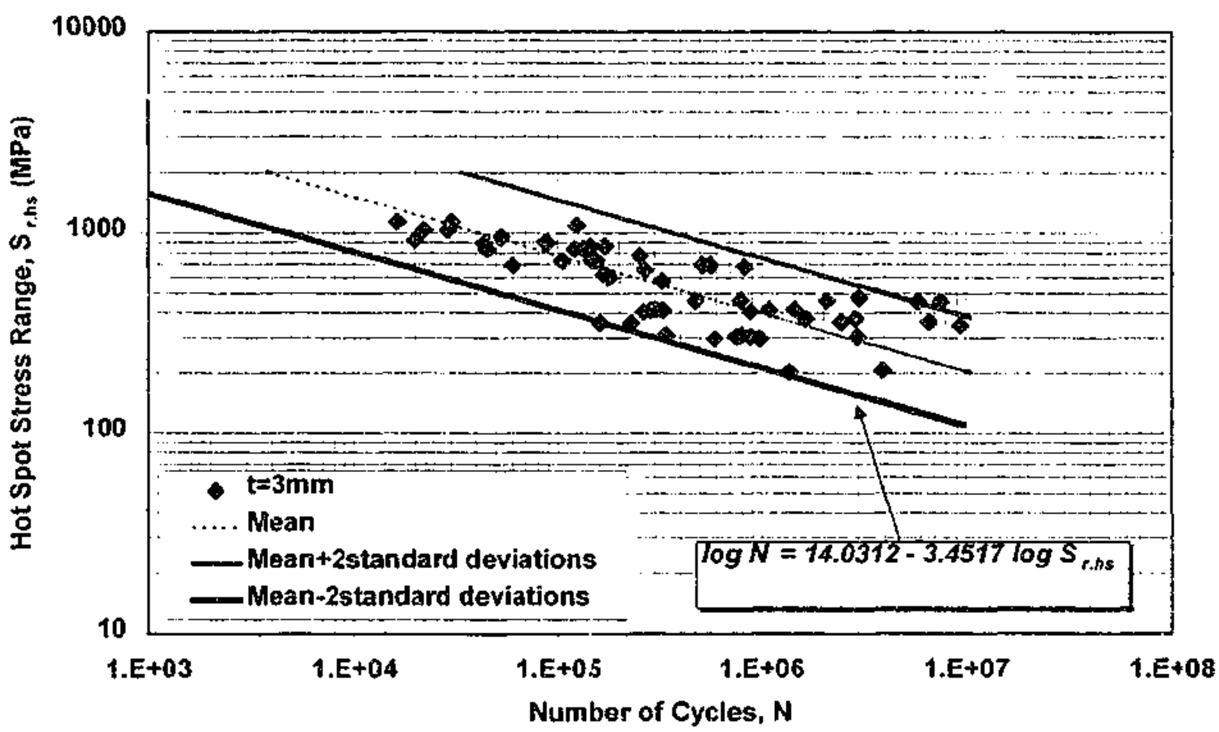

Figure 9-9: $S_{r,hs}$-N curves from Data Analysis, log N dependent variable, B=-3.4517, A determined, Hot Spot Stress Method, Parametric Equation SCFs used

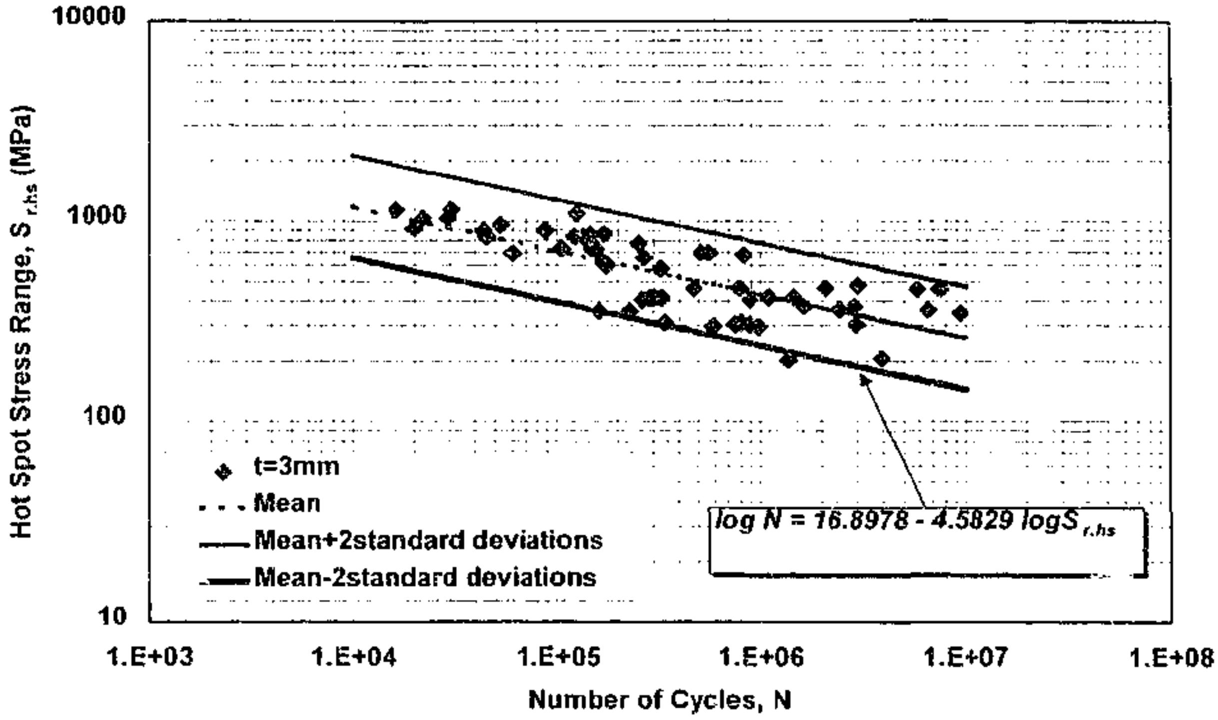

Figure 9-10: $S_{r,hs}$-N curves from Data Analysis, log $S_{r,hs}$ dependent variable, a and b determined, Hot Spot Stress Method, Parametric Equation SCFs used

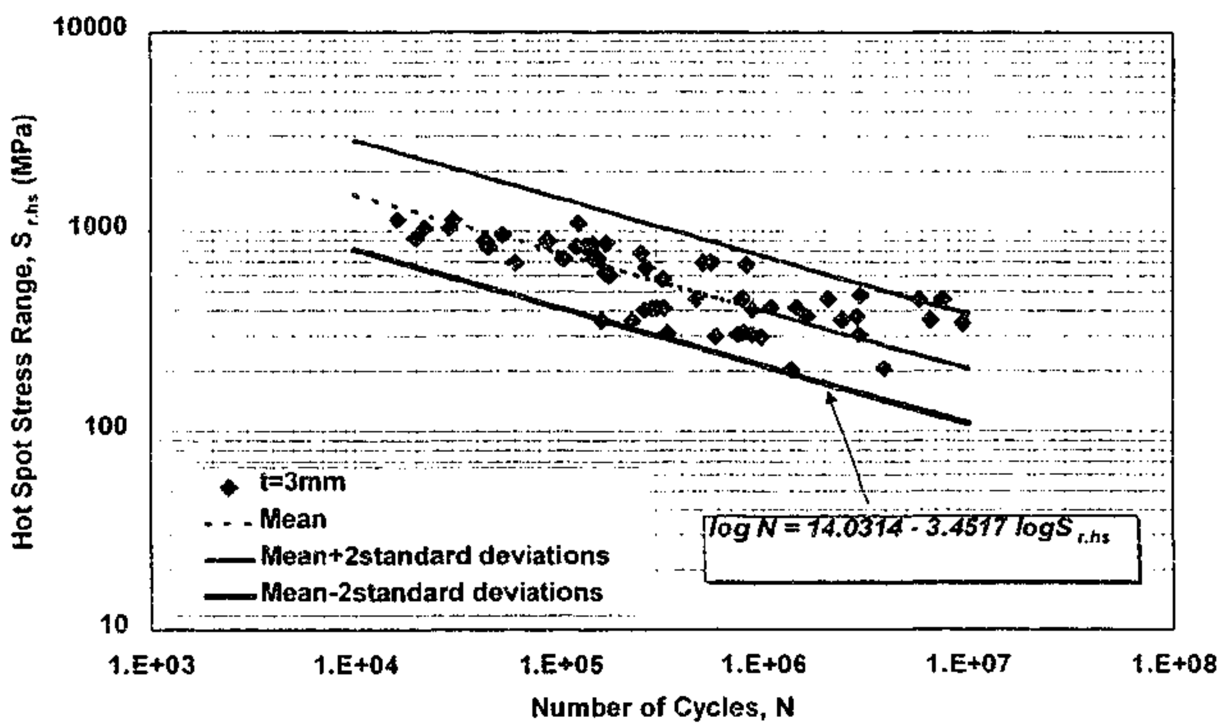

Figure 9-11: $S_{r,hs}$-N curves from Data Analysis, log $S_{r,hs}$ dependent variable, b=-0.2897, a determined, Hot Spot Stress Method, Parametric Equation SCFs used

9.5 EQUATIONS DEFINING DESIGN $S_{r,hs}$-N CURVES

Design $S_{r,hs}$-N curves have been determined for two different cases in Section 9.4 as follows;

(a) when the natural slope of the $S_{r,hs}$-N data is evaluated using the least-squares method, and

(b) when the slope of the $S_{r,hs}$-N data is forced to a predetermined value according to the existing trend of design $S_{r,hs}$-N curves for different thicknesses in IIW (2000).

In order to be consistent with the current design $S_{r,hs}$-N curves in IIW (2000) and the CIDECT Design Guide No. 8 (Zhao *et al* 1999a), the design $S_{r,hs}$-N curves determined using a forced slope will be adopted for the proposed design curves. Puthli *et al* (1989) adopted a similar approach for the design of K-joints with gap made up of square hollow sections of thicknesses equal to 2.9mm. The design $S_{r,hs}$-N curves which are adopted for design are those determined when *log N* is taken as the dependent variable. Traditionally *log N* is taken as the dependent variable in determining design S-N curves because the load applied and hence the applied stress range is the variable that is controlled during fatigue testing.

The design $S_{r,hs}$-N curves for tubular nodal joints in IIW (2000) and Zhao *et al* (1999a) have double slopes between 10^3 and 10^8 cycles. For the range of cycles between 10^3 and $5x10^6$ cycles, the slope of the design $S_{r,hs}$-N curves is defined by a varying slope for different thicknesses as determined by equation 9.3. For the range of cycles between $5x10^6$ and 10^8 cycles however, the slope of the design $S_{r,hs}$-N curves for different thicknesses is the same, see equation 9.7. The cut off limit is defined by the hot spot stress range at 10^8 cycles.

The part of the $S_{r,hs}$-N curve between 10^3 and $5x10^6$ cycles defines the region for constant amplitude loading, while the part of the $S_{r,hs}$-N curve between $5x10^6$ and 10^8 cycles, defines the region for variable amplitude loading. The constant stress amplitude fatigue tests carried out in this investigation will thus be used to define the region between 10^3 and $5x10^6$ cycles. The region for variable amplitude loading is going to be defined using the point defined by the constant amplitude curve at $5x10^6$ cycles and a negative slope of 1:5 thereafter up to 10^8 cycles as given for design $S_{r,hs}$-N curves in IIW (2000).

The equations derived in Tables 9-4 and 9-5 for the forced slope and when *log N* is the dependent will therefore be adopted to define the design $S_{r,hs}$-N curves between 10^3 and $5x10^6$ cycles. The negative slope of 1:3.4517 between 10^3 cycles and $5x10^6$ cycles, is the slope of the $S_{r,hs}$-N equation for a thickness of 3mm as derived from equation 9.3 and shown in equation 9.4. The negative slope of 1:5 between $5x10^6$ cycles and 10^8 cycles, is the slope of the $S_{r,hs}$-N equation for a thickness of 3mm as derived from equation 9.7 and shown in equation 9.8 below:

$$\log(N) = 16.327 - 5 \cdot \log(S_{r,hs}) + 2.01 \cdot \log\left(\frac{16}{t}\right), \text{ for } 5\times10^6 \le N \le 10^8 \qquad \textbf{(9.7)}$$

$$\log(N) = 17.7883 - 5 \cdot \log(S_{r,hs}), \text{ for } t\text{=3mm and } 5\times10^6 \le N \le 10^8 \qquad \textbf{(9.8)}$$

Equation 9.7 shows that the slope of the design $S_{r,hs}$-N curve in IIW (2000) is independent of tube wall thickness, t between $5x10^6$ cycles and 10^8 cycles as opposed to the slope between 10^3 cycles and $5x10^6$ cycles, which changes with tube wall thickness, see equation 9.3. The slope of the design curves between $5x10^6$ cycles and 10^8 cycles for all thicknesses is 1:5.

Equations 9.4 and 9.8 define the IIW (t=3mm) curve shown in Figure 9-12 from the current trend of $S_{r,hs}$-N curves for different thicknesses, where fatigue life increases as the thickness of the member which fails under fatigue decreases.

The design $S_{r,hs}$-N curve derived from $S_{r,hs}$-N data obtained from experimental SCFs in Section 9.4.1, when *log N* is the dependent variable and when B=-3.4517, is defined by the following equation, see Table 9-4:

$$\log(N) = 12.9502 - 3.4517 \cdot \log(S_{r,hs}), \qquad \text{for } 10^3 \le N \le 5\times10^6 \qquad \textbf{(9.9)}$$

The curve (t=3mm, Experimental SCFs) is shown in Figure 9-12. By defining the hot spot stress range at $5x10^6$ cycles using equation 9.9, the equation defining the curve (t=3mm, Experimental SCFs) between $5x10^6$ and 10^8 cycles can be determined since it has a negative slope of 1:5 according to equation 9.7, as follows;

$$\log(N) = 15.7543 - 5 \cdot \log(S_{r,hs}), \qquad \text{for } 5\times10^6 \le N \le 10^8 \qquad \textbf{(9.10)}$$

The design $S_{r.hs}$-N curve derived from $S_{r.hs}$-N data obtained from Parametric SCFs in Section 9.4.2, when *log N* is the dependent variable and when B=-3.4517, is defined by the following equation, see Table 9-5:

$$\log(N) = 14.0312 - 3.4517 \cdot \log(S_{r,hs}), \qquad \text{for } 10^3 \le N \le 5\times10^6 \qquad \textbf{(9.11)}$$

The curve (t=3mm, Parametric SCFs) is also shown in Figure 9-12. By defining the hot spot stress range at 5x10^6 cycles using equation 9.11, the equation defining the curve (t=3mm, Parametric SCFs) between 5x10^6 and 10^8 cycles can be determined since it has a negative slope of 1:5 according to equation 9.7, as follows;

$$\log(N) = 17.3202 - 5 \cdot \log(S_{r,hs}), \qquad \text{for } 5\times10^6 \le N \le 10^8 \qquad \textbf{(9.12)}$$

9.6 COMPARISON OF NEW AND EXISTING DESIGN $S_{r.hs}$-N CURVES

Figure 9-12 shows some of the existing $S_{r.hs}$-N design curves for tubular nodal joints from EC3 (1992), API (1991) and IIW (2000). Figure 9-12 also shows the two design $S_{r.hs}$-N curves determined in this investigation for tube-to-tube T-joints using experimental SCFs (t=3mm, Experimental SCFs) and SCFs determined from existing parametric equations (t=3mm, Parametric SCFs).

The $S_{r.hs}$-N curve determined from SCFs derived from existing parametric equations lie below the 4mm IIW curve, but is higher than EC3 Class 90 and API X curves.

The $S_{r.hs}$-N curve determined from experimental SCFs, lies below the EC3 Class 90 curve between 10^3 cycles and 5x10^6 cycles, but is very close to the EC3 Class 90 curve after 5x10^6 cycles. The API X curve lies below the t=3mm (Experimental SCFs) curve below 10^5 cycles but lies above the t=3mm (Experimental SCFs) curve between 10^5 cycles and 2x10^8 cycles.

The IIW (t=3mm) curve is parallel to the t=3mm (Experimental SCFs) curve, since both curves have the same slope of curve for a given range of number of cycles to failure. The ratio of the hot spot stress range at 2 million cycles for the t=3mm (Experimental SCFs) curve to the IIW (t=3mm) curve is:

$$\frac{S_{r,hs}(t = 3mm, ExperimentalSCFs)}{S_{r,hs}(IIW, t = 3mm)} = \frac{84}{215} = 0.39 \qquad \textbf{(9.13)}$$

In tests carried out on 5 specimens of K-joints with gap where failure occurred in square hollow sections of 2.9mm tube wall thicknesses, Puthli *et al* (1989) found the ratio of the hot spot stress range at 2 million cycles for the experimentally determined curve to the curve determined from a design equation for RHS incorporating thickness correction to be 0.44. The ratios of 0.39 in this investigation and 0.44 from Puthli *et al* (1989) show a reduction in fatigue strength in tubes of wall thicknesses less than 4mm.

The ratio of the hot spot stress range at 2 million cycles for the t=3mm (Parametric SCFs) curve to the IIW (t=3mm) curve is:

$$\frac{S_{r,hs}\left(t = 3mm, ParametricSCFs\right)}{S_{r,hs}(IIW, t = 3mm)} = \frac{174}{215} = 0.81 \tag{9.14}$$

The ratio of 0.81 also shows a reduction in fatigue strength for nodal joints made up of tubes of wall thicknesses less than 4mm. The reduced fatigue life of welded thin-walled specimens can be attributed to the greater negative impact of weld toe undercut on fatigue propagation life as reported in Mashiri *et al* (1998b, 2000b) and detailed in Chapter 7. Noordhoek *et al* (1980) also reported this phenomena and attributed it to the difficulty associated with welding smaller wall thickness sections.

The design $S_{r,hs}$-N curves based on both the parametric SCFs and the experimental SCFs are compared to the series of design $S_{r,hs}$-N curves for different thicknesses from IIW (2000) in Figure 9-13. The design $S_{r,hs}$-N curve based on parametric SCFs (t=3mm, Parametric SCFs) is very close to the t=5mm curve from the IIW (2000) after 5 million cycles. However, the t=3mm (Parametric SCFs) curve is conservative compared to the t=5mm curve below 5 million cycles, because it has the slope for a thickness of 3mm as determined by Equation 9.3.

Lower SCFs have been obtained through experimental measurements compared to those SCFs determined by the parametric equations. The low experimental SCFs coupled by the reduction in life for welded thin-walled joints are such that the design $S_{r,hs}$-N curve based on experimental SCFs is very close to the t=32mm curve after 5 million cycles. Below 5 million cycles however the t=3mm (Experimental SCFs) curve adopts the slope for a thickness of 3mm which is less steep than that for t=32mm. The t=3mm (Experimental SCFs) curve therefore gives conservative fatigue lives at higher stress ranges than the design $S_{r,hs}$-N curves for t=32mm and t=50mm from IIW (2000).

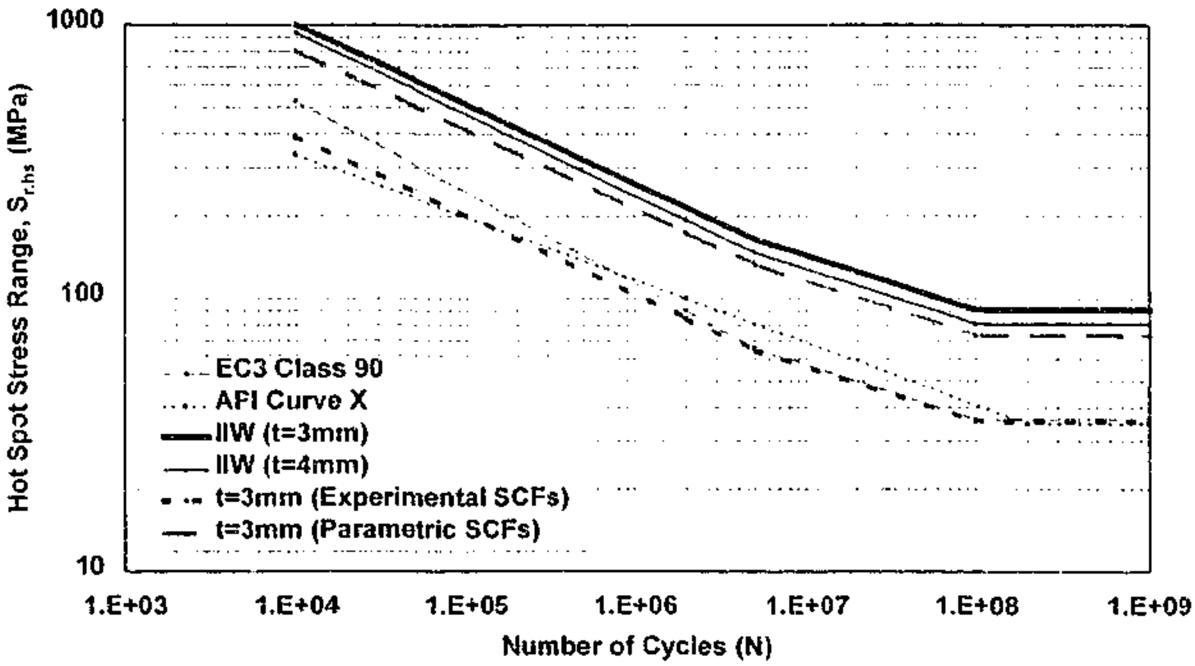

Figure 9-12: Existing Design $S_{r,hs}$-N curves and New Design $S_{r,hs}$-N curves for t<4mm

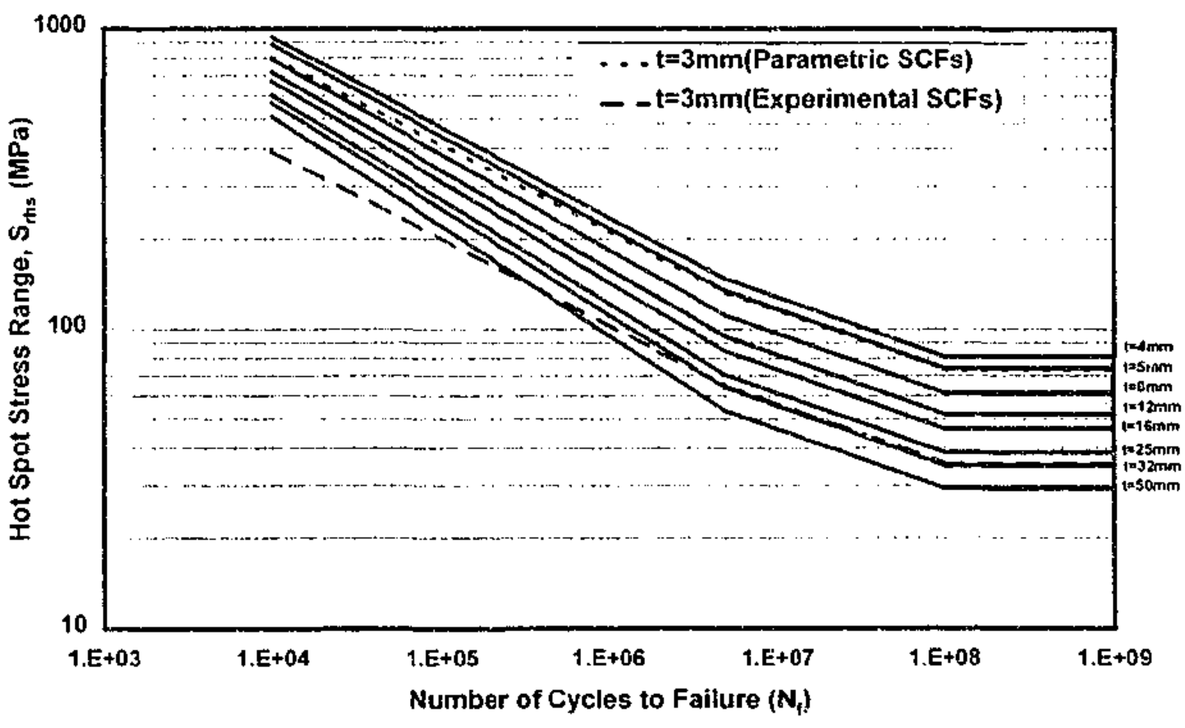

Figure 9-13: Existing Design $S_{r,hs}$-N curves from IIW (2000) and New Design $S_{r,hs}$-N curves for t<4mm

9.7 PROPOSED DESIGN METHODS

The design $S_{r.hs}$-N curve derived from $S_{r.hs}$-N data obtained from experimental SCFs (t=3mm, Experimental SCFs) and that from $S_{r.hs}$-N data obtained from the use of parametric equation SCFs (t=3mm, Parametric SCFs) have identical slopes in given ranges of number of cycles to failure, N and are therefore parallel. The ratio of the hot spot stress range at 2 million cycles for the t=3mm (Parametric SCFs) curve to the t=3mm (Experimental SCFs) curve is (see Figure 9-12):

$$\frac{S_{r.hs}(t = 3mm, ParametricSCFs)}{S_{r.hs}(t = 3mm, ExperimentalSCFs)} = \frac{174}{84} = 2.07 \approx 2.00 \qquad \textbf{(9.15)}$$

The total hot spot stress range in the design $S_{r.hs}$-N curve derived from SCFs obtained from existing parametric equations (t=3mm, Parametric SCFs) is therefore related to the total hot spot stress range in the design $S_{r.hs}$-N curve obtained from experimental SCFs (t=3mm, Experimental SCFs) by a factor of 2.0. The fatigue design of tube-to-tube T-joints made up of square hollow sections of thicknesses less than 4mm can thus be performed using the t=3mm (Experimental SCFs) design curve and taking into account the relationship between the total hot spot stress range in the t=3mm (Experimental SCFs) curve and the t=3mm (Parametric SCFs) curve as follows:

(i) Determine the maximum total hot spot stress range at the "hot spot" location for the T-joint made up of square hollow sections with thicknesses less than 4mm using existing parametric equations in IIW (2000) and equation 9.16:

$$S_{r.hs} = \sigma_{r.a1} \cdot SCF_{a1} + \sigma_{r.m1} \cdot SCF_{m1} + \sigma_{r.a0} \cdot SCF_{a0} + \sigma_{r.m0} \cdot SCF_{m0} \qquad \textbf{(9.16)}$$

(ii) Divide the total hot spot stress range determined by equation 9.16 by 2.0, the factor in equation 9.15 to obtain a factored total hot spot stress range related to the t=3mm (Experimental SCFs) design curve.

(iii) Use the t=3mm (Experimental SCFs) design curve to determine number of cycles corresponding to the factored total hot spot stress range from (ii).

The above design procedure can be used to determine fatigue life of tube-to-tube T-joints made up of tubes of wall thicknesses less than 4mm before detailed parametric studies are carried out to establish parametric equations for these joints. These parametric studies will determine the following:

(a) the influence of oversized welds on thin-walled tube-to-tube T-joints made up of square hollow sections and

(b) the stress distribution close to the toe of the weld in thin-walled tube-to-tube T-joints and hence determine if there is a need to introduce new rules for use in evaluating hot spot stresses using either the linear or quadratic extrapolation methods.

Alternatively, the t=3mm (Parametric SCFs) design curve can be used in the fatigue design of tube-to-tube T-joints made up of square hollow sections of thicknesses less than 4mm as follows:

(a) Determine the maximum total hot spot stress range at the "hot spot" location for the T-joint made up of square hollow sections with thicknesses less than 4mm using existing parametric equations in IIW (2000) and equation 9.16.
(b) Use the t=3mm (Parametric SCFs) design curve to 'etermine number of cycles corresponding to the maximum total hot spot stress range to determine the fatigue life of the T-joint.

This design procedure uses the assumptions detailed Section 9.3.2.

9.8 SUMMARY

Two different design $S_{r,hs}$-N curves have been derived for the fatigue design of tube-to-tube T-joints, under in-plane bending, made up of thin-walled square hollow sections of thicknesses less than 4mm. The design $S_{r,hs}$-N curves are based on hot spot stress ranges determined using experimental stress concentration factors (SCFs) and SCFs determined from existing parametric equations in IIW (2000). The design $S_{r,hs}$-N curves derived from the use of experimental SCFs and parametric equation SCFs are parallel and are assigned double slopes as predicted by the existing equations in IIW (2000) following an earlier procedure adopted by Puthli *et al* (1989). The design $S_{r,hs}$-N curves adopt negative slopes of 1:3.4517 between 10^3 cycles and $5x10^6$ cycles and a slope of 1:5 between $5x10^6$ cycles and 10^8 cycles.

The design $S_{r,hs}$-N curve based on hot spot stress ranges determined using experimental stress concentration factors (SCFs) is defined by the following equations between 10^3 and 10^8 cycles (see *t=3mm (Experimental SCFs)* curve in Figure 9-14):

$$\log(N) = 12.9502 - 3.4517 \cdot \log(S_{r,hs}), \qquad \text{for } 10^3 \leq N \leq 5 \times 10^6 \qquad \textbf{(9.9)}$$

$$\log(N) = 15.7543 - 5 \cdot \log(S_{r,hs}), \qquad \text{for } 5\times10^6 \le N \le 10^8 \qquad \textbf{(9.10)}$$

On the other hand, the design $S_{r,hs}$-N curve based on hot spot stress ranges determined using stress concentration factors (SCFs) determined from existing parametric equations in IIW (2000) is defined by the following equations between 10^3 and 10^8 cycles (see *t=3mm (Parametric SCFs)* curve in Figure 9-14):

$$\log(N) = 14.0312 - 3.4517 \cdot \log(S_{r,hs}), \qquad \text{for } 10^3 \le N \le 5\times10^6 \qquad \textbf{(9.11)}$$

$$\log(N) = 17.3202 - 5 \cdot \log(S_{r,hs}), \qquad \text{for } 5\times10^6 \le N \le 10^8 \qquad \textbf{(9.12)}$$

Two methods have been proposed for the fatigue design of tube-to-tube T-joints, under in-plane bending, made up of square hollow sections of thicknesses less than 4mm as follows:

Method 1: Using the t=3mm (Experimental SCFs) Curve in Figure 9-14

(a) Determine the maximum total hot spot stress range at the "hot spot" location for the T-joint made up of square hollow sections with thicknesses less than 4mm using existing parametric equations in IIW (2000) and equation 9.16:

$$S_{r,hs} = \sigma_{r,a1} \cdot SCF_{a1} + \sigma_{r,m1} \cdot SCF_{m1} + \sigma_{r,a0} \cdot SCF_{a0} + \sigma_{r,m0} \cdot SCF_{m0} \qquad \textbf{(9.16)}$$

(b) Divide the total hot spot stress range determined by equation 9.16 by 2.0, the factor in equation 9.15 to obtain a factored total hot spot stress range related to the t=3mm (Experimental SCFs) design curve.

(c) Use the t=3mm (Experimental SCFs) design curve to determine number of cycles corresponding to the factored total hot spot stress range from (b).

Method 2: Using the t=3mm (Parametric SCFs) Curve in Figure 9-14

(a) Determine the maximum total hot spot stress range at the "hot spot" location for the T-joint made up of square hollow sections with thicknesses less than 4mm using existing parametric equations in IIW (2000) and equation 9.16.

(b) Use the t=3mm (Parametric SCFs) design curve to determine number of cycles corresponding to the maximum total hot spot stress range to determine the fatigue life of the T-joint.

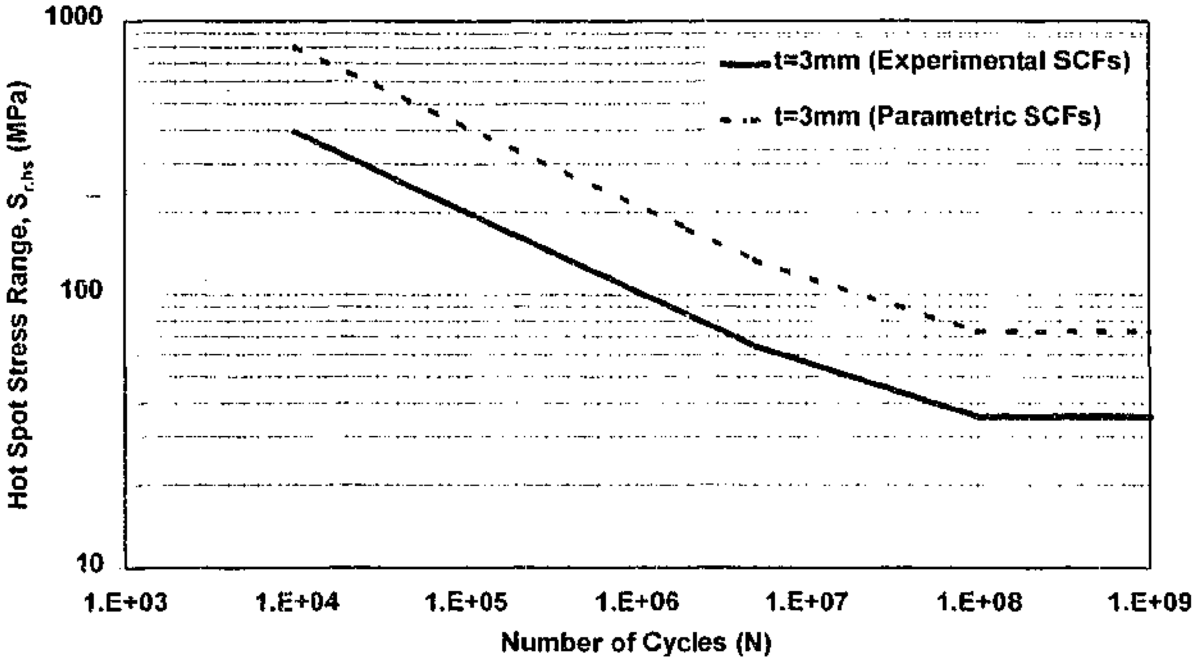

Figure 9-14: Proposed Design $S_{r,hs}$-N curves for tube-to-tube T-joints, under in-plane bending, made up of SHS of thicknesses less than 4mm

Chapter 10

3D CRACK PROPAGATION ANALYSIS OF TUBE-TO-PLATE T-JOINT USING BOUNDARY ELEMENT METHOD

10.1 INTRODUCTION

Fatigue tests of welded thin-walled ($t<4$mm) tube-to-plate T joints under in-plane bending have been carried to obtain S-N data as reported in Chapter 5. Subsequent analysis of the tube-to-plate fatigue data has been undertaken in Chapter 8, to determine design S-N curves. Although fatigue life can be determined experimentally, Chapter 10 will estimate the fatigue life of a welded thin-walled tube-to-plate T-joint under in-plane bending using the fracture mechanics method. The tube-to-plate joint analysed is made up of a square hollow section of size, 50x50x3SHS welded to a 10mm thick plate. This analysis is carried out to demonstrate the use of the fracture mechanics method in fatigue propagation life estimation.

Three-dimensional crack growth analysis of a tube-to-plate T-joint under cyclic in-plane bending is carried out to estimate fatigue crack propagation life using the boundary element method. The Boundary Element Analysis Sytem Software (BEASY) is used to carry out the 3D crack growth analysis. In order to perform a crack growth increment, BEASY has facilities to estimate the stress intensity factors, crack incremental sizes and crack incremental direction, thereby defining a new crack front from the points on the existing initial crack. In 3D analysis, the stress intensity factors are determined from the crack opening displacement method. The incremental size and direction are estimated using the minimum strain energy density criterion. The incremental size can also be determined using a criterion based on the Paris equation for fatigue crack growth.

This Chapter determines the stress concentration factors, stress intensity factors and the fatigue life of a tube-to-plate T-joint under cyclic in-plane bending. The 3D stress analysis for evaluating hot spot stresses required for determining stress concentration factors and the 3D crack propagation analysis for determining stress intensity factors and incremental sizes required for estimating fatigue crack propagation life is performed using BEASY. Three-dimensional models of the T-joint are created using the MIG weld profiles determined from the silicon-imprint technique and reported in Section 3.3 of Chapter 3 as well as nominal dimensions of the square hollow section, 50x50x3 SHS conforming to AS1163-1991 (SAA 1991a). The 50x50x3 SHS has a yield stress of 450MPa and is fillet welded to a 10mm thick plate with a yield stress of 350MPa.

The stress concentration factors (SCFs) determined from the boundary element analysis are compared to the stress concentration factors determined experimentally and reported in Section 5.5 of Chapter 5. The resultant S-N curve from the boundary element analysis is compared to the S-N curve obtained from experimentally determined fatigue data for welded thin-walled tube-to-plate T-joints, under in-plane bending. This is done to check the validity of the 3D models adopted and the reliability of the fatigue analysis obtained using the boundary element method.

Future work will be carried out to determine the fatigue life of the other tube-to-plate and tube-to-tube T-joints tested in this investigation, using the fracture mechanics method.

10.2 FATIGUE ASSESSMENT METHODS

Most of the current design codes such as AS4100-1998 (SAA 1998a), EC3 (1992), AWS (1998), IIW (2000) and the CIDECT design guide (Zhao *et al* 1999a) have fatigue design recommendations for steel hollow sections of thickness greater than or including 4mm only. The reason why most codes do not cover fatigue strength of thicknesses less than 4mm is because,

(i) the rules in these codes are derived mostly from research related to offshore structures where large section sizes and thicknesses are used,

(ii) thin-walled sections with thicknesses less than 4mm are relatively new and,

(iii) lack of research data on these sections.

There is therefore a need to undertake research for thin-walled cold-formed hollow sections with thicknesses below 4mm. Different fatigue assessment methods can be used to determine the fatigue life of the welded joints.

Some of the common methods used in fatigue assessment of welded tubular structures are the classification method, hot-spot stress method and the fracture mechanics method (Zhao *et al* 1999b). The classification method is based on structural details for different types of joints, which are classified into various detail categories (EC3 1992; SAA 1998; JSSC 1995; AISC 1993; CSA 1989). The hot-spot stress method relates fatigue life to the so-called hot-spot stress at the joint (IIW 2000; Zhao *et al* 1999a). The classification and hot-spot stress methods for fatigue design are established through laboratory fatigue tests of full-scale joints. This procedure for determining S-N curves is expensive and time consuming, especially for high cycle fatigue where the applied loads are within the elastic range of the load-displacement response of the connection.

The fracture mechanics method involves modelling of the welded joint and the application of the Paris equation for fatigue crack propagation (Atluri 1997). This method can be used to estimate the fatigue crack propagation life of a structural component with crack-like defects. For welded joints, it is often assumed that there is no initiation period due to the presence of weld defects. Small fatigue cracks actually initiate at an early stage of fatigue in the welded joints, where crack-like defects or high stress concentrations exist. These reduce the initiation stage of the fatigue and make it relatively less important than the propagation stage (Yamada and Kainuma 1996). The small crack-like discontinuities, termed intrusions, exist at the weld toe. They are a product of conditions during welding which arise with most of the arc processes (Maddox 1991).

Fatigue of welded structures can therefore be determined using the fracture mechanics method. This is especially true for thin-walled welded connections where the weld defects, especially undercut make up a significant percentage of the wall thickness. By assuming a small initial crack in the welded joint, crack propagation analysis can then be carried out to determine the fatigue crack propagation life of the connection. The other advantage of the fracture mechanics method is that the effects related to fabrication of welds such as weld profile, the weld toe radius and weld toe undercut can be studied relatively easily by varying these parameters in the models, see Chapter 7.

10.2.1 FEM and BEM

Although the finite element method (FEM) has been used previously to establish parametric equations used in the hot-spot stress method for determining stress concentration factors (van Wingerde 1992), establishing S-N curves using this method requires a high CPU-time especially in 3D FEM crack propagation analysis. This is because in FEM the problems with steep solution gradients in elastic bodies cannot be accurately approximated by the FEM unless extremely refined meshes are used (Mi 1996). The problem associated with CPU-time has been found to be relatively small while using the Boundary Element Analysis System (BEASY) software. The CPU-time for using BEASY depends on the complexity of the model (2D or 3D), number of elements, number of degrees of freedom (DOF); software version (DOS, Windows 95 or UNIX) and hardware (PC, Personal Workstation or Silicon Graphics High Performance Computer). Some examples are listed in Table 10-1.

Table 10-1: Examples on CPU-time

Problem	Model	Software	Hardware	CPU-time
Non-Load Carrying Cruciform Joint (Fatigue life propagation)	2D 160 elements 990 DOF	DOS Version	PC	12 hours
		Windows 95	PC	15 minutes
Tube to Plate T-joint (One crack extension)	3D 1135 elements 15717 DOF	Windows 95	PC	Insufficient Memory
		UNIX	Silicon Graphics High Performance Computer	5 hours
Tube to Plate T-joint (One crack extension)	3D 285 elements 6012 DOF	Windows 95	PC	45 minutes
		UNIX	Silicon Graphics High Performance Computer	30 minutes

10.2.2 Boundary Element Method

The finite element method (FEM) is the most widely used technique for the solution of general mechanics problems in structural mechanics. Based on an energy interpretation, it can be used to approximate many physical phenomena including crack problems (Mi 1996). However there are some drawbacks for using FEM as given below:

(a) Problems with steep solution gradients in elastic bodies cannot be accurately approximated by FEM, unless extremely refined meshes are used. This is the case with crack problems since stresses tend to infinity.

(b) The continuous re-meshing requirement for crack growth simulation.

The boundary element method (BEM) can be applied to fracture mechanics problems more efficiently compared to the finite element method:

(a) Problems with solution gradients varying rapidly in elastic bodies can be modelled accurately with reasonably fine meshes.

(b) Because only boundary discretization is required for the application of the boundary element method, re-meshing work for the simulation of the crack growth process is reduced dramatically compared to FEM. The advantage is more apparent in three-dimensional crack growth analysis.

(c) Integration is performed at the surface.

(d) Solutions (unknowns) are found at nodal points rather than Gauss points as FEM implement and solution obtained by extrapolation.

(e) Nodal displacements and stresses are computed at once not like FEM where the displacement solution is obtained first and then stresses.

There is fundamental difficulty in the direct application of BEM to fracture mechanics due to the modelling of two coplanar crack surfaces. Collocating the boundary integral equations on crack surfaces gives a system with fewer independent linear equations than unknowns obtained. One of the techniques used to overcome this problem is the dual boundary element method (Mi 1996). The dual boundary element method incorporates the displacement and traction boundary integral to solve the problem. The displacement boundary integral equation is applied on one of the crack surfaces and the traction boundary integral equation on the other. The general mixed mode crack problems can then be solved in a natural single region way. The dual boundary element method has been effectively used for both two-dimensional and three-dimensional problems (Portela and Aliabadi 1992; Portela *et al* 1993; Mi and Aliabadi 1993; Mi and Aliabadi 1994)

10.3 THREE-DIMENSIONAL CRACK GROWTH ANALYSIS IN BEASY

BEASY uses dual boundary elements for 3D crack growth analysis (Computational Mechanics BEASY Ltd 1998). The dual boundary element method incorporates two independent boundary integral equations, the displacement equation applied at the collocation point on one of the crack surfaces and the traction equation on the other surface (Mi and Aliabadi 1994; Mi 1996).

10.3.1 Fatigue Propagation Life Estimation used in BEASY

The boundary element analysis system software (BEASY), uses the NASGRO equation:

$$\frac{da}{dN}=\frac{C\cdot(1-f)^{n}\cdot\Delta K^{n}\cdot\left(1-\frac{\Delta K_{th}}{\Delta K}\right)^{p}}{(1-R)^{n}\cdot\left(1-\frac{\Delta K}{(1-R)K_{c}}\right)^{q}} \qquad \textbf{(10.1)}$$

where,

$$\Delta K=K_{\max}-K_{\min}=K_{\max}(1-R) \qquad \textbf{(10.2)}$$

and

$$R=\frac{K_{\min}}{K_{\max}} \qquad \textbf{(10.3)}$$

The crack only grows when ΔK, the stress intensity factor range is greater than ΔK_{th}, the threshold stress intensity factor range. For a 3D model which is subjected to mode I, mode II and mode III loading:

$$K_{\max}=K_{eff}=\sqrt{(K_{I}+|K_{III}|)^{2}+2K_{II}^{2}} \qquad \textbf{(10.4)}$$

where, a is the crack length in mm; ΔK is the stress intensity factor range; ΔK_{th} is the threshold stress intensity factor range; f is the crack opening function; K_c is the critical stress intensity factor; K_{max} is the maximum stress intensity factor; K_{min} is the minimum stress intensity factor; K_I, K_{II}, K_{III} are the stress intensity factors for mode I, II and III respectively. The unit of stress intensity factor is $N.mm^{-3/2}$; C is the crack growth rate coefficient; n, q and p are the exponents; N is the number of cycles to failure.

The BEASY program takes into account fatigue crack closure analysis in 2D models only, calculating the effect of the stress ratio on crack growth rate under constant amplitude fatigue loading as detailed in Section 2.5.3 of Chapter 2. For 3D modeling of the tube-to-plate T-joint it was therefore assumed that the effect of crack closure is negligible. The effect of crack closure is assumed to be negligible when $f=R$ (Computational Mechanics BEASY Ltd 1998). When $f=R$, Equation 10-1 becomes:

$$\frac{da}{dN}=\frac{C\cdot\Delta K^{n}\cdot\left(1-\frac{\Delta K_{th}}{\Delta K}\right)^{p}}{\left(1-\frac{\Delta K}{(1-R)K_{c}}\right)^{q}} \tag{10.5}$$

Equation 10-5 has been adopted for determining fatigue crack propagation life in the 3D tube-to-plate T-joint model.

10.3.2 Stress Intensity Factors

The stress intensity factors in BEASY are computed using the crack opening displacement method. When one point formulae are employed, the Mode I, II and III stress intensity factors are evaluated as (Mi 1996; Computational Mechanics BEASY Ltd 1998):

$$K_{I}^{P}=\frac{E}{4(1-\nu^{2})}\sqrt{\frac{\pi}{2r}}\left(u_{b}^{P}\big|_{\theta=\pi}-u_{b}^{P}\big|_{\theta=-\pi}\right) \tag{10.6}$$

$$K_{II}^{P}=\frac{E}{4(1-\nu^{2})}\sqrt{\frac{\pi}{2r}}\left(u_{n}^{P}\big|_{\theta=\pi}-u_{n}^{P}\big|_{\theta=-\pi}\right) \tag{10.7}$$

$$K_{III}^{P}=\frac{E}{4(1-\nu^{2})}\sqrt{\frac{\pi}{2r}}\left(u_{t}^{P}\big|_{\theta=\pi}-u_{t}^{P}\big|_{\theta=-\pi}\right) \tag{10.8}$$

where, the displacement $\boldsymbol{u}^P$ is evaluated at point P as shown in Figure 10-1; u_b^P, u_n^P and u_t^P are projections of $\boldsymbol{u}^P$ on the coordinate directions of the local crack front coordinate system (i.e $u_b^P = \boldsymbol{u}^P \cdot \boldsymbol{b}$, $u_n^P = \boldsymbol{u}^P \cdot \boldsymbol{n}$ and $u_t^P = \boldsymbol{u}^P \cdot \boldsymbol{t}$) and $\theta=\pi$ and $\theta=-\pi$ denote upper and lower crack surfaces respectively. $K_I^{P'}$, $K_{II}^{P'}$ and $K_{III}^{P'}$ are approximations of stress intensity factors corresponding to the point **P'** along the crack front and on a normal line to the front as shown in Figure 10-1.

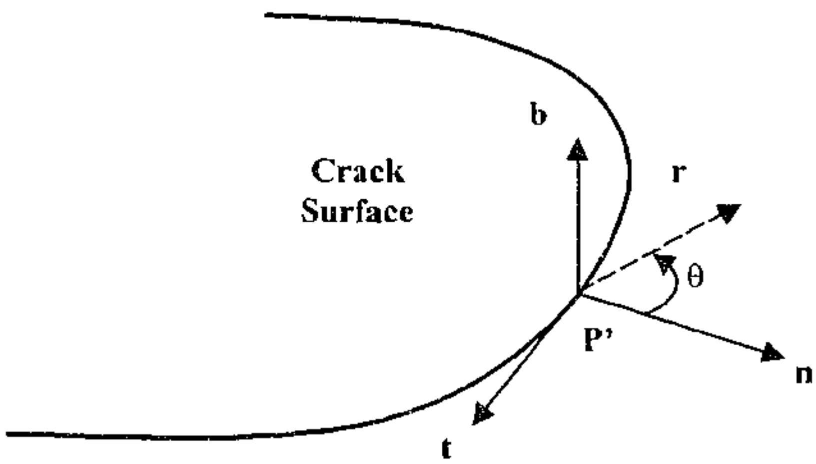

Figure 10-1: Calculation of SIF using crack opening displacement

10.3.3 Incremental Direction

The crack growth direction is computed by the minimum strain energy density criterion. The theory of minimum strain energy density is based on three hypotheses:

(1) The direction of the crack growth at any point along the crack front is toward the region with the minimum value of strain energy factor, S as compared with other regions on the same spherical surface surrounding the point.

(2) Crack extension occurs when the strain energy density factor in region determined by (1), $S = S_{min}$, reaches a critical value, S_{cr}.

(3) The length, r_o, of the initial crack extension is assumed to be proportional to S_{min} such that S_{min}/r_o remains constant along the new crack front.

The strain energy density factors S(θ), after each analysis along the crack front are evaluated by (Mi and Aliabadi 1994; Mi 1996; Computational Mechanics BEASY Ltd 1998):

$$S(\theta) = a_{11} \cdot K_I^2 + 2a_{12} \cdot K_I \cdot K_{II} + a_{22} \cdot K_{II}^2 + a_{33} \cdot K_{III}^2 \quad \textbf{(10.9)}$$

where, K_I, K_{II} and K_{III} are mode I, II and III stress intensity factors and

$$a_{11} = \frac{1}{16\pi\mu}(3 - 4\nu - \cos\theta)(1 + \cos\theta) \quad \textbf{(10.10)}$$

$$a_{12} = \frac{1}{8\pi\mu}\sin\theta(\cos\theta - 1 + 2\nu) \quad \textbf{(10.11)}$$

$$a_{22} = \frac{1}{16\pi\mu}\left[4(1-\nu)(1-\cos\theta) + (3\cos\theta - 1)(1+\cos\theta)\right] \quad \textbf{(10.12)}$$

$$a_{33} = \frac{1}{4\pi\mu} \quad \textbf{(10.13)}$$

where μ is the shear modulus of elasticity, ν is the Poisson's ratio and θ is the angle in the crack front coordinate system in Figure 10-1. S is the strain energy density factor, which plays a similar role to the stress intensity factor (SIF).

The minimum strain energy density criterion can be used in both the two and three dimensions. The direction evaluated by the criterion in three-dimensional cases in insensitive to K_{III}.

The crack growth direction angle θ is obtained by minimizing the strain energy density factor $S(\theta)$ of Equation 10.9 with respect to θ. The minimum strain energy density factor $S(\theta)$ is denoted by S_{min}.

Locating the minimum of $S(\theta)$ with respect to θ is carried out numerically using the bisection method by solving:

$$\frac{dS(\theta)}{d\theta} = 0 \qquad -\pi < \theta < \pi \quad \textbf{(10.14)}$$

10.3.4 Incremental Size

The determination of the crack incremental size must address the problems associated with the reference size as well as the relationship between the maximum incremental size and other incremental sizes along the crack front (Mi and Aliabadi 1994; Mi 1996; Computational Mechanics BEASY Ltd 1998). Two methods based on either the strain energy density criterion method or the Paris equation can be used as follows:

10.3.4.1 Incremental Size based on Strain Energy Density Criterion

Hypothesis (3) of the strain energy density criterion given in Section 10.3.3 states that the length, r_o, of the initial crack extension is assumed to be proportional to S_{min} such that S_{min}/r_o remains constant along the new crack front. Therefore, the incremental size along the crack front can be decided as follows. First, a $max\{S_{min}\}$ value is chosen among the values of S_{min} evaluated at a set of discrete points along the crack front. Then, the incremental size at the point corresponding to the $max\{S_{min}\}$ is defined as Δa_{max} which has been chosen beforehand (Mi and Aliabadi 1994; Mi 1996; Computational Mechanics BEASY Ltd 1998). The incremental size is evaluated by;

$$\Delta a = \Delta a_{\max}\left(\frac{S_{\min}}{\max\{S_{\min}\}}\right) \qquad \textbf{(10.15)}$$

along the crack front, where S_{min} is the minimum strain energy factor evaluated at a set of discrete points along the crack front and Δa_{max} is the incremental size at the point corresponding to the $max\{S_{min}\}$.

10.3.4.2 Incremental Size based on Paris Equation

The generalized relationship for crack growth rate calculations called the NASGRO 2.0 equation is given by (Computational Mechanics BEASY Ltd 1998):

$$\frac{da}{dN} = \frac{C\cdot(1-f)^n\cdot\Delta K^n\cdot\left(1-\frac{\Delta K_{th}}{\Delta K}\right)^p}{(1-R)^n\cdot\left(1-\frac{\Delta K}{(1-R)K_c}\right)^q} \qquad \textbf{(10.16)}$$

The NASGRO equation can be reduced to the Paris equation by setting the parameters p and q equal to zero. The Paris model is used to model fatigue crack propagation:

$$\frac{da}{dN} = C\cdot\Delta K_{eff}{}^n. \qquad \textbf{(10.17)}$$

where,

$$\Delta K_{eff} = K_{eff}{}^{\max} - K_{eff}{}^{\min} = K_{eff}{}^{\max}(1-R) \qquad \textbf{(10.18)}$$

in which K_{eff} is the effective stress intensity factor, i.e

$$K_{eff}{}^2 = \left(K_I + |K_{III}|\right)^2 + 2K_{II}{}^2 \qquad \textbf{(10.19)}$$

After each boundary element method analysis, the directions of the next increment of the crack growth are calculated by minimizing the strain energy density factor as described in Section 10.3.3. The maximum amount of Δa_{max} of the next increment is fixed, corresponding to the crack front point where the maximum effective stress intensity factor, ΔK_{eff}^{max} occurs (Mi and Aliabadi 1994; Mi 1996). From the Paris equation, Equation 10-17;

$$\Delta a \approx C\left(\Delta K_{eff}\right)^{n} \cdot \Delta N \tag{10.20}$$

Since ΔN is constant along the crack front:

$$\Delta a_{max} \approx C\left(\Delta K_{eff}^{\ max}\right)^{n} \cdot \Delta N \tag{10.21}$$

Therefore;

$$\frac{\Delta a}{\Delta a_{max}} = \left(\frac{\Delta K_{eff}}{\Delta K_{eff}^{\ max}}\right)^{n} \tag{10.22}$$

Thus the incremental size at any crack front is given by:

$$\Delta a = \Delta a_{max}\left(\frac{\Delta K_{eff}}{\Delta K_{eff}^{\ max}}\right)^{n} \tag{10.23}$$

10.4 BEM ANALYSIS OF TUBE-TO-PLATE T-JOINT

10.4.1 Three Dimensional Model of Tube-to-Plate T-Joint

The tube-to-plate T-joint was modelled in BEASY using quadrilateral and triangular elements. For 3D models, boundary elements are surfaces. The total number of elements in each model was 660 and the total number of degrees of freedom in each model was 10400. The mesh adopted for the tube-to-plate T-joint followed a convergence test in which the mesh was refined until further refining of the mesh produced no significant difference in stress distribution in the joint, especially the hot spot locations. The elements were of reduced quadratic type. BEASY version 7.0 has a discontinuous element type that is assigned automatically by the analysis module when a crack is defined. Although the model has two planes of symmetry, half instead of a quarter of the joint was modelled because the joint was under uniaxial bending. Fatigue crack initiation in the tube-to-plate fatigue experiments reported in Chapter 5, was also observed to occur on the two corners of the tube on the tube-plate welded interface, on the side under tension. This also shows that the joint has to be considered as having one plane of symmetry. The end of the brace has been modelled with a thick cover plate to avoid cross sectional warping at the points where the loads are applied (Sedlacek *et al* 1998; Morgan and Lee 1998b). The tube-to-plate T-joint made up by MIG welding a 50x50x3SHS tube to a 10mm plate is shown in Figure 10-2. One feature of these models is that the actual shape of the fillet weld is modelled using the MIG weld profile for grade C450LO steel obtained from the silicon imprint technique in Section 3.3 of Chapter 3. The shape of the weld can be easily incorporated into the model using surface boundary elements, see Figure 10-2.

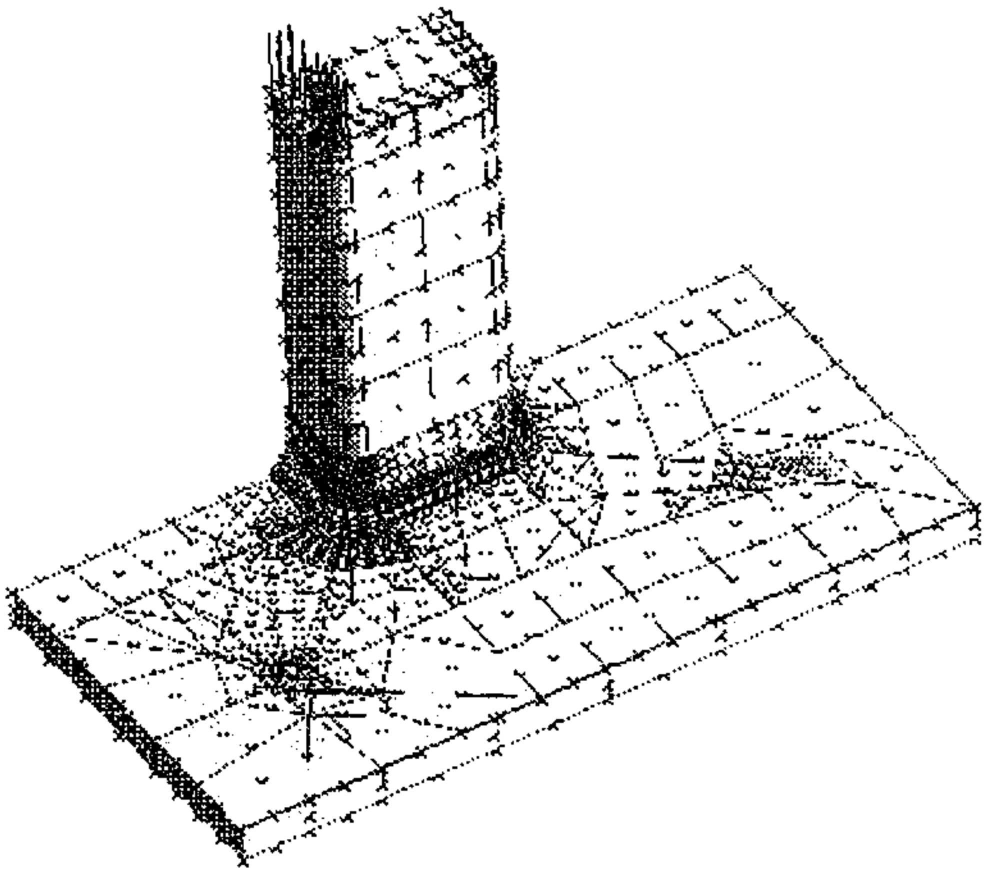

Figure 10-2: Half Model (3D)

10.4.2 Stress Analysis of Tube-to-Plate T-Joint

In order to predict the point along the weld toe where the crack is likely to initiate a stress analysis of the joint was carried out. Maximum principal stresses were found to occur at the corner of the square hollow section on the interface of the brace and the plate. This is consistent with the location of the hot spots found during the experimental determination of stress concentration factors (SCFs) in tube-to-plate T-joints, see

Section 5.5 of Chapter 5. For this reason it is highly recommended not to start and stop weld sequences at corners of square or rectangular hollow sections, as they are potential hot spot locations (Dutta *et al* 1998). During the determination of weld profiles, the authors have also realised that there is more likelihood of undercut occurring at the corners of welded square hollow section joints. This is due to the fact that the welder has to undertake a continuous change in direction during welding around the corners of square or rectangular hollow sections.

A plot of the principal stresses versus distance from the weld toe for specified lines A to E (Figure 10-3) are shown in Figure 10-4. The maximum principal stresses occur along lines A and E, which are located in the brace. The determination of hot spot stresses that are used in evaluating SCFs can be carried out through linear or quadratic extrapolation. For linear extrapolation, the first point is $0.4t$ or a minimum of 4mm away from the weld toe while the second point is $0.6t$ further away from the first point (van Wingerde 1992; Gurney 1979; van Delft 1981). For quadratic extrapolation, the first point is $0.4t$ or a minimum of 4mm away from the weld toe while the second point is $1.0t$ further away from the first point. All the stress distribution points between the above specified first and second points in quadratic extrapolation are used for determining the hot spot stress. The stress distribution was observed to be almost linear in the region recommended for extrapolation to determine hot spot stresses.

The applied nominal bending stress for the stress distribution shown in Figure 10-4 is 122.2MPa. The stress distribution used for determining hot spot stresses for the 50x50x3SHS-Plate joint model is shown in Figure 10-5 for line A and in Figure 10-6 for line E. The hot spot stresses, which were obtained using both the linear and quadratic methods of extrapolation are shown in Table 10-2. Since the stress distribution in the regions recommended for extrapolation by both the linear and quadratic methods is almost linear, the values of the hot spot stresses from both methods of extrapolation are almost the same for lines A and E, see Figures 10-5 and 10-6. The resultant stress concentration factors (SCFs) for lines A and E are shown in Table 10-2. Line E gave higher SCFs for both methods of extrapolation. In quadratic extrapolation, for example, a SCF of 1.67 was determined for line E compared to a SCF of 1.27 for line A.

The SCFs determined from the boundary element method are compared to the SCFs determined from experimental measurements in Table 10-3. There is a good agreement between the experimental SCFs and the numerically determined SCFs. Percentage differences between the experimental and the numerical SCFs ranges between 2.4 and 11.2.

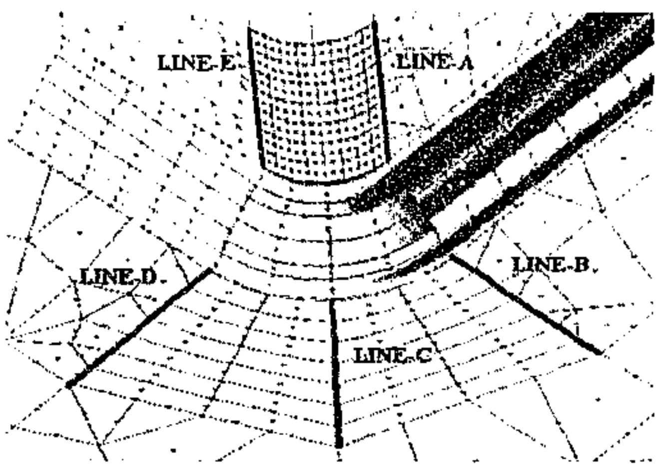

Figure 10-3: Lines A-E on brace-plate interface

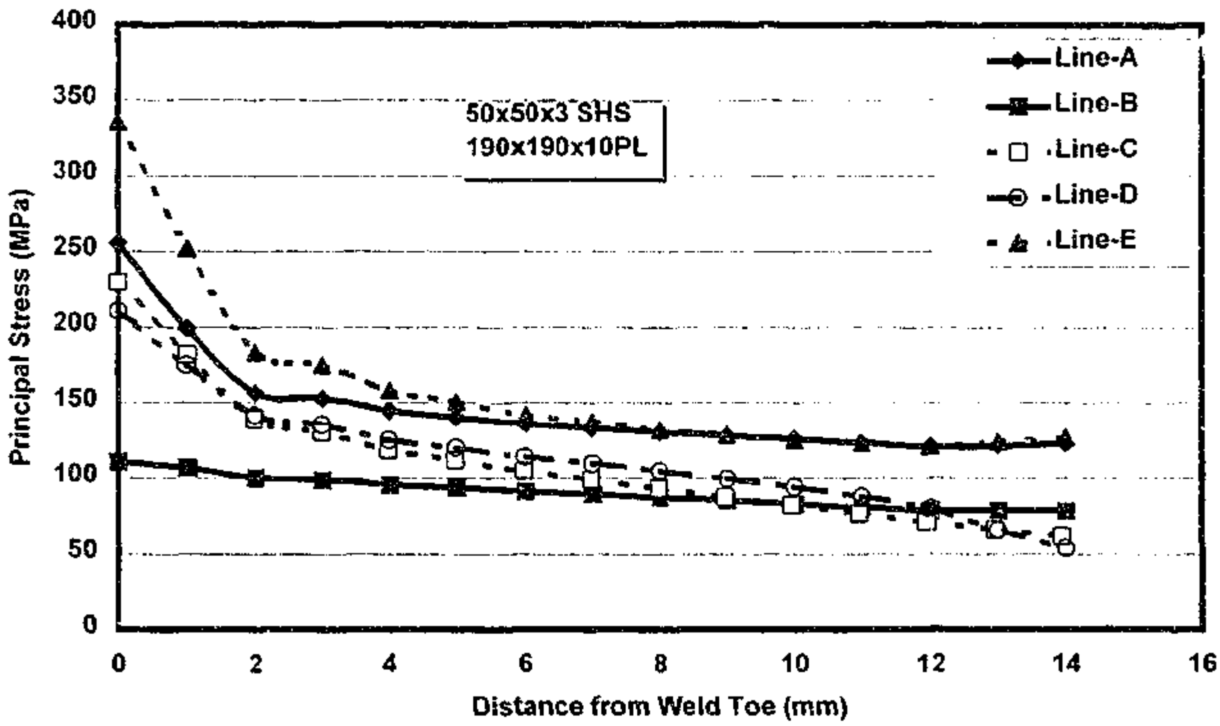

Figure 10-4: Plot of maximum principal stresses

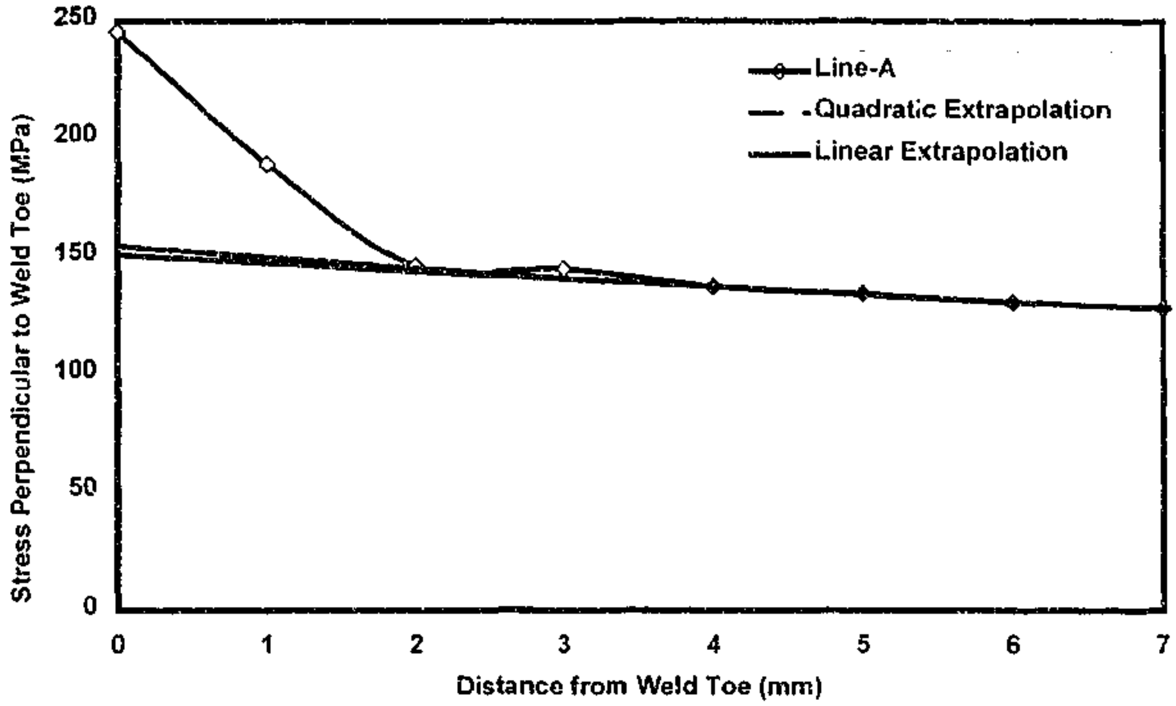

Figure 10-5: Extrapolation for Hot Spot Stresses Line A.

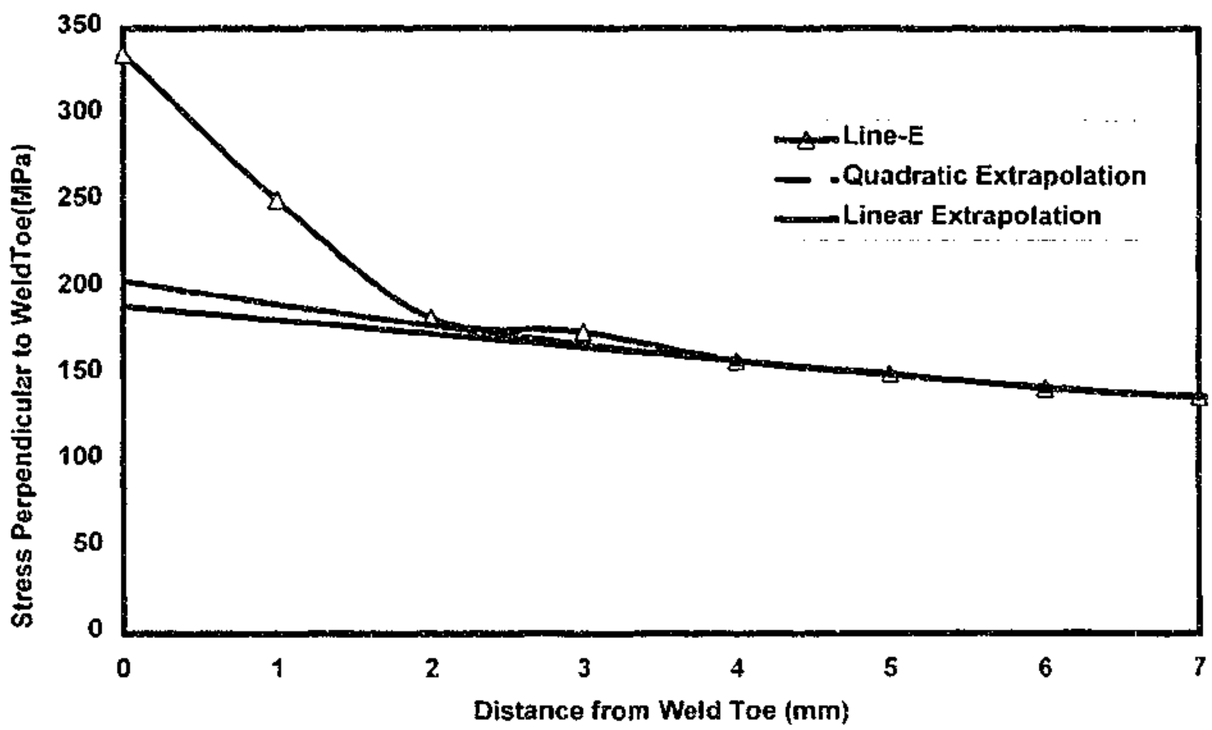

Figure 10-6: Extrapolation for Hot Spot Stresses Line E.

Table 10-2: SCF for 50x50x3SHS-Plate Joint from BEM Analysis

Connection	Position	Nominal Stress, σ_{nom} (MPa)	Linear Extrapolation		Quadratic Extrapolation		$\frac{SCF_q}{SCF_l}$
			σ_{hs} (MPa)	SCF_l	σ_{hs} (MPa)	SCF_q	
50x50x3SHS-Plate	Line E	122.2	189.5	1.55	204.41	1.67	1.06
	Line A	122.2	150.7	1.23	154.65	1.27	1.08

Table 10-3: Comparison of SCF for 50x50x3SHS-Plate Joint from BEM and Experiments

Connection	Position	Linear Extrapolation SCF_l			Quadratic Extrapolation SCF_q		
		BEASY	Experiment	% Difference	BEASY	Experiment	% Difference
50x50x3SHS -Plate	Line E	1.55	1.625	4.6	1.67	1.775	5.9
	Line A	1.23	1.1	-11.8	1.27	1.3	2.4

10.4.3 Fatigue Crack Propagation Life of Tube-to-Plate T-joint

In the 3D crack growth analysis of a joint, the following modeling strategy is adopted in BEASY (Mi and Aliabadi 1994):

(i) crack surfaces are modeled with discontinuous quadratic elements,

(ii) surfaces intersecting a crack surface are modeled with edge-discontinuous elements,

(iii) all other surfaces are modeled with continuous elements,

(iv) the displacement integral equation is applied for collocation on one of the crack surfaces (say the upper surface),

(v) the traction integral equation is applied on the opposite crack surface (say the lower surface), and

(vi) the displacement integral equation is used for collocation on all other surfaces.

Fatigue analysis was carried out by introducing a semi-elliptical initial crack of depth 0.2mm, and a/c ratio of 0.08 (a and c are the minor and major axis dimensions respectively). An initial crack depth of 0.2mm was used because this is the maximum depth of undercut which was found during the measurements of undercut depth in MIG weld profiles, see Table 3-15 of Chapter 3. An initial crack with the same depth as the maximum depth of undercut observed in the MIG weld profiles, means that the fatigue crack propagation life obtained from the cracked model is that corresponding to the lower bound of the life obtained from the real welded joints. The fatigue crack propagation life obtained from this model should therefore be comparable to the design S-N curves obtained from the tube-to-plate T-joints. Undercuts have been found to exhibit crack-like flaws at the base of the notch (Smith and Hirt 1993). Therefore, in real structures the initiation of cracks at the weld toe can be from the base of the notch forming the undercut. An initial crack depth of 0.2mm for the 3D model was also chosen as this was still below the maximum allowable depth of undercut recommended for tubular welded joints in AWS D1.1-1998: Structural Steel Welding Code. The AWS regulations state that the maximum depth of undercut should not exceed 0.25mm. The initial crack depth is also smaller than the maximum permissible depth for intermittent undercut in the Australian welding standards. For intermittent undercut, the maximum allowable undercut depth should be $t/10$ but not greater than 1.5mm (SAA 1995a).

Using the Boundary Element Analysis System Software BEASY, the effective stress intensity factors along the crack front of each crack growth increment were determined. Crack growth increments were carried out for three nominal stress ranges, of 40MPa, 50MPa and 110MPa. Plots of effective stress intensity factors along the crack fronts are shown in Figures 10-7 to 10-9. There is an increase in effective stress intensity factor as the crack grows. Figure 10-7 also shows the resultant beach marks as projected onto the horizontal plane. Fatigue life was defined as the propagation to a through-thickness crack of the initial semi-elliptical crack located in the brace at the corner of the brace/plate interface. This is one of the failure modes recommended by the European Offshore Programme (van Wingerde 1992).

The following steps are undertaken during the 3D crack growth analysis:

a) Automatically using the BEASY program

(i) carry out a dual boundary element method stress analysis of the cracked structure,

(ii) compute the stress intensity factors along the crack front,

(iii) compute the direction of crack extension increment using the minimum strain energy density criterion and,

(iv) compute the amount of increment along the crack front using the minimum strain energy criterion or the Paris equation for fatigue crack growth (Mi 1996; Mi and Aliabadi 1994).

b) Manually by user using the BEASY Post-processing facilities

(v) using the post-processing features, instruct BEASY to automatically create new crack front points from data obtained in (a)

(vi) using the new crack front points created in (v) and the crack front points from the initial crack, to define an extension of the crack surface,

(vii) repeat all the above steps until a through-thickness crack is obtained.

The crack growth cycles for each increment were determined using the effective stress intensity factor (K_{eff}) and the crack growth increment (da) obtained from the boundary element analysis. The parameters used were: the crack growth coefficient, (C) of 3×10^{-13} and an exponent, (n) of 3 recommended in PD6493 (BSI 1991) and a threshold stress intensity factor range of 91.7Nmm$^{-3/2}$ for mean S-N curve recommended by the Japanese Society of Steel Construction (JSSC 1995). The value of exponents p and q in Equation 10.24 is 0.5 and the value of fracture toughness, K_c is 5212N.mm$^{-3/2}$ is given for ASTM steel with the same mechanical properties as grade 450 steel used in this investigation. A value of stress ratio R, of 0.1 similar to that used in the tube-to-plate fatigue tests was adopted for this analysis. Using the aforementioned values for each crack growth increment and the NASGRO equation, the crack growth cycles were estimated as follows:

$$dN = \frac{da \cdot \left(1 - \frac{\Delta K}{(1-R)K_c}\right)^q}{C \cdot \Delta K^n \left(1 - \frac{\Delta K_{th}}{\Delta K}\right)^p} \qquad \textbf{(10.24)}$$

The fatigue crack propagation life is the sum of the respective crack growth cycles for each crack growth increment.

The S-N data obtained from the boundary element method is plotted in Figure 10-10 and compared to the design S-N curve for the welded thin-walled (t<4mm) tube-to-plate T-joints under in-plane bending from Figure 8-15 of Chapter 8. Regression of the S-N data from the boundary element method gives a fatigue design S-N curve defined by the equation $\log N = 11.1521 - 2.9815 \cdot \log S$, which gives a class of 42. The design S-N curve from the experimental data is given by the equation $\log N = 11.2222 - 3 \cdot \log S$ which gives a class of 44. A ratio of the class of the S-N curve from experimental data to the class of the S-N curve from the boundary element method is:

$$\frac{Class_{experimental}}{Class_{BEM}} = \frac{44}{42} = 1.05 \quad \textbf{(10.25)}$$

This shows that there is a good agreement between the S-N data from the boundary element method and the experimental S-N data.

There are still a few issues that need to be addressed in BEM analysis. The definition of fatigue failure used for the boundary element analysis was the through-thickness fatigue life. The definition of failure used in the experimental tests was a crack length equal to the entire width of the tube in the tube-to-plate T-joint. Another issue is the modelling the real life weld toe conditions. Undercut has not been included in these 3D crack growth models. Undercuts, which are an inherent feature of real welded joints, are difficult to model since their distribution and shape around a welded joint is hard to document. The notch stresses at the bottom of an undercut, where cracks are likely to initiate may also affect the stress field on the crack surfaces and hence the stress intensity factors at the crack front. Further research is needed in this area.

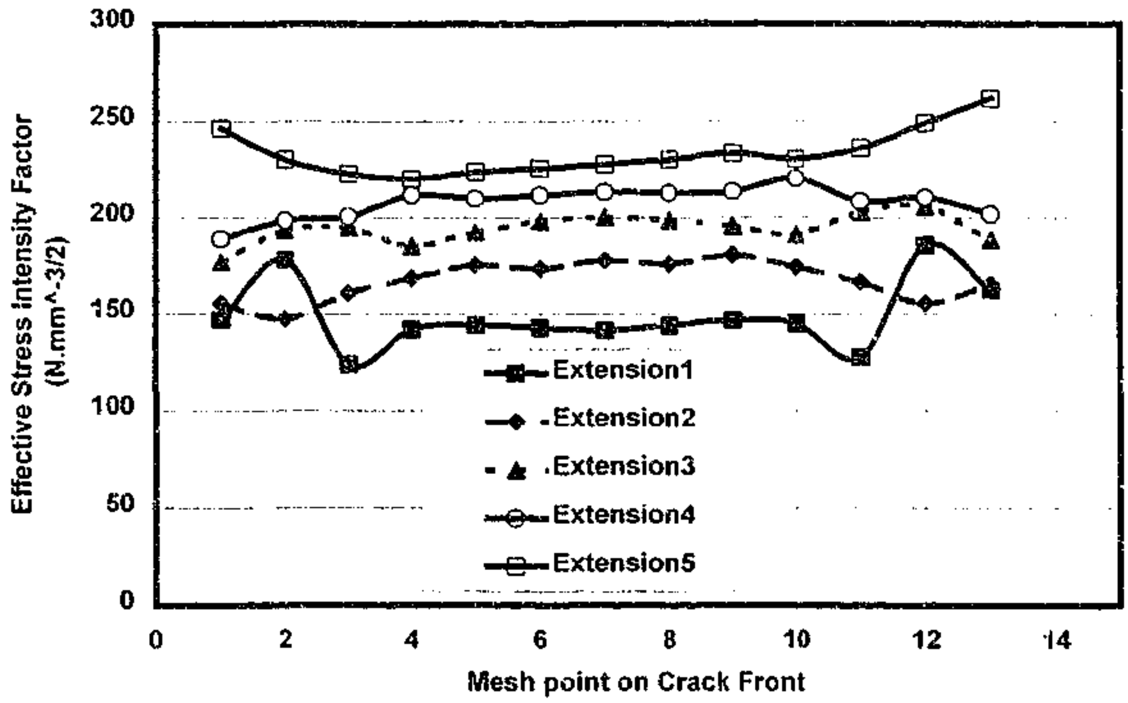

(a)

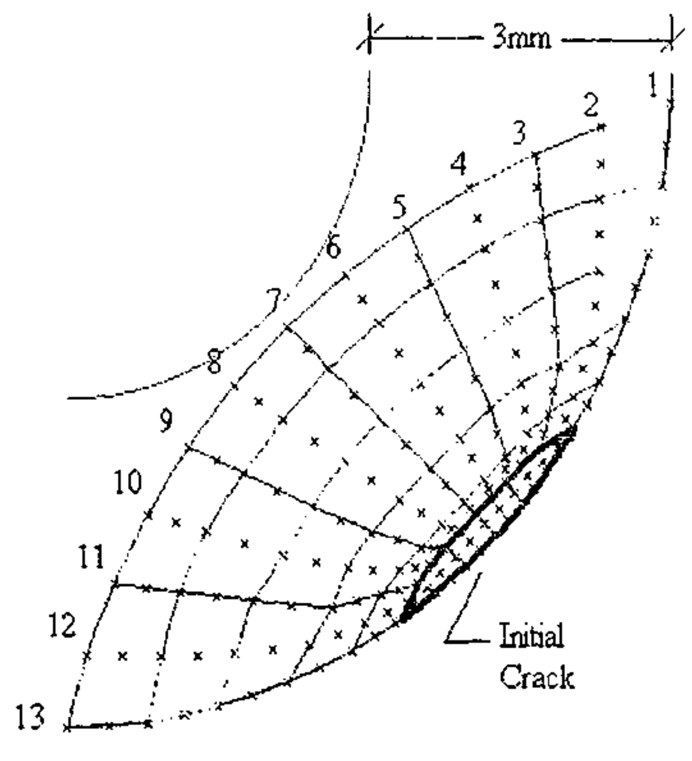

(b)

Figure 10-7: (a) Graph of effective stress intensity factor versus mesh point on crack front for $S_{r\text{-}nom}$ of 40MPa, and (b) the diagram of the corner of the SHS showing the resultant beach marks from successive crack growth increments.

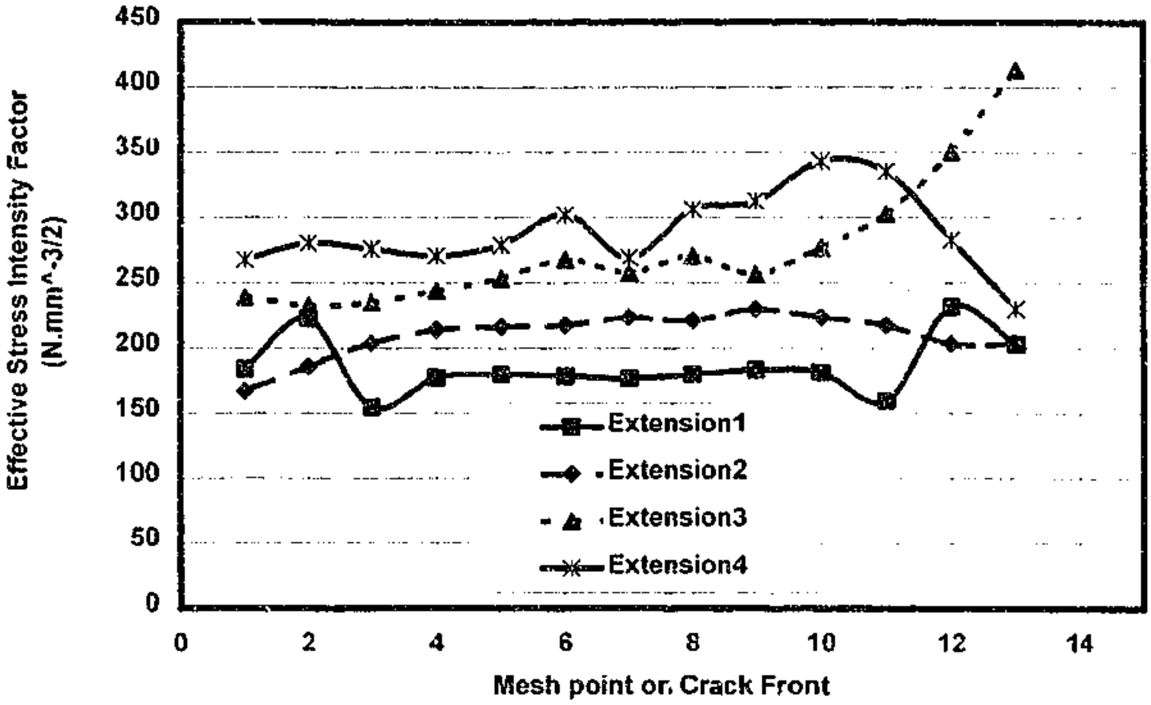

Figure 10-8: Graph of effective stress intensity factor versus mesh point on crack front for $S_{r\text{-}nom}$ of 50MPa.

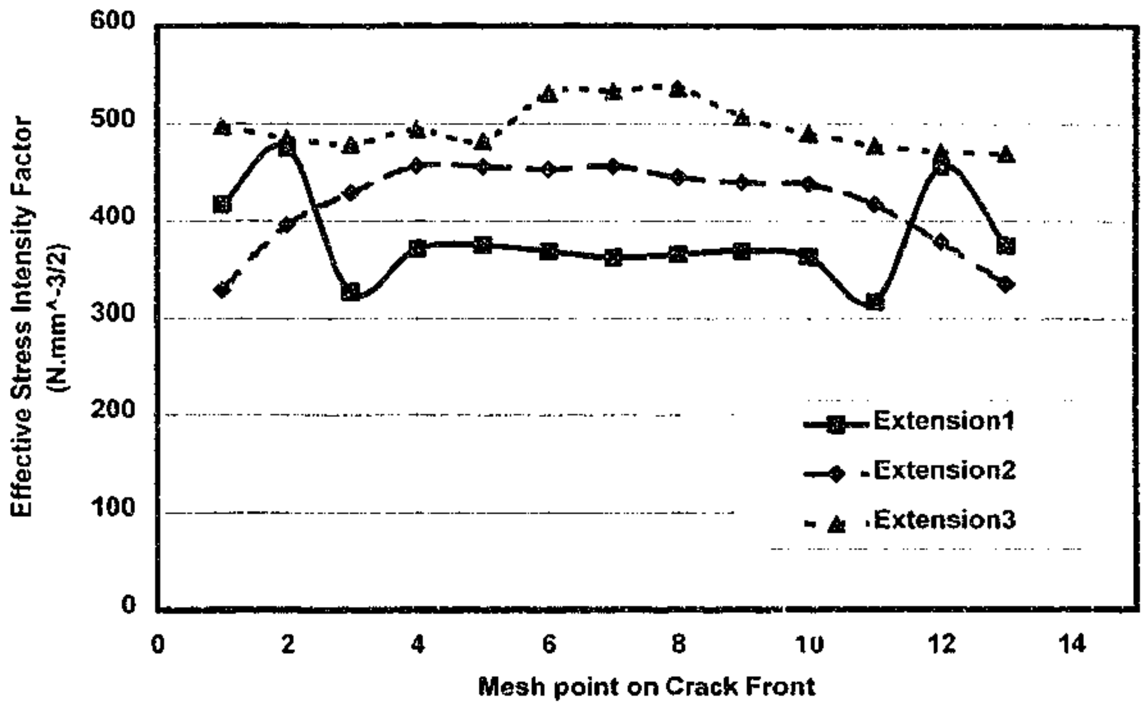

Figure 10-9: Graph of effective stress intensity factor versus mesh point on crack front for $S_{r\text{-}nom}$ of 110MPa.

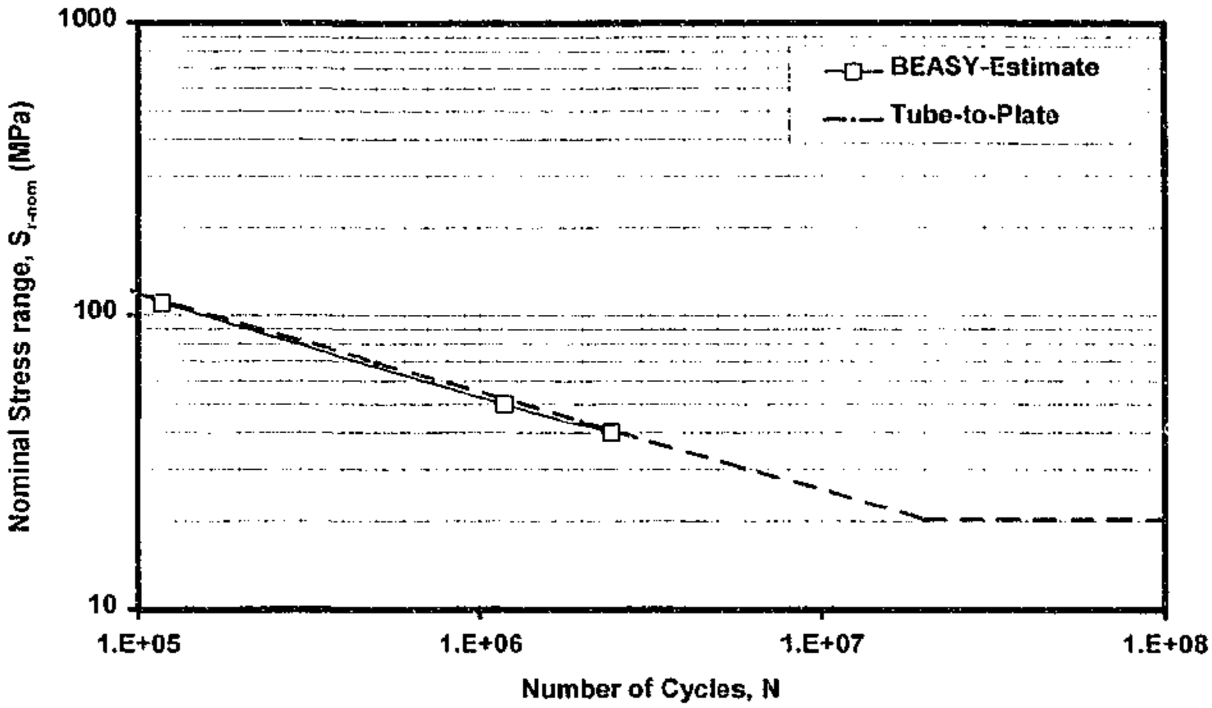

Figure 10-10: Comparison of fatigue life estimates from BEASY and tube-to-plate T-joint S-N curve determined from experimental results

10.5 SUMMARY

(a) Three-dimensional crack growth analysis of a tube-to-plate T-joint under in-plane bending has been undertaken using the boundary element method. The tube-to-plate T-joint is made up of a square hollow section of size, 50x50x3SHS, welded to a 10mm plate, which is one the tube-to-plate connection series tested in this investigation. The methods that are used for 3D crack growth analysis in BEASY have been described. They include the crack opening displacement method for determining stress intensity factors and the minimum strain energy density criterion for determining both the incremental size and direction. The Paris law for crack growth can also be used for determining the incremental size.

(b) A stress analysis of the uncracked tube-to-plate T-joint has been performed to determine the stress concentration factors (SCFs). The linear and the quadratic methods of extrapolation, for hot spot stresses have been used. The SCFs evaluated from the boundary element method are in good agreement with the SCFs determined experimentally through strain gauge measurements. Percentage differences ranging from 2.4 to 11.8 have been found between the experimentally determined SCFs and the SCFs from the boundary element method.

(c) Fatigue crack propagation life was estimated using the dual boundary element method. The fatigue crack propagation life of the welded thin-walled tube-to-plate T-joint was compared to the design S-N curve from experimentally determined fatigue data. The ratio of the class of the S-N curve determined from the experimental fatigue data to that derived from crack growth analysis is 1.05. This shows that there is good agreement between the fatigue life estimated by the dual boundary element method and the fatigue life determined experimentally.

(d) Future work will be carried out to estimate fatigue crack propagation life of the other tube-to-plate and tube-to-tube T-joints tested in this investigation.

Chapter 11
CONCLUSIONS

11.1 GENERAL

Different design standards have been reviewed and it has been shown that there is a lack of fatigue design rules for welded thin-walled tubular joints where the tube wall thickness is less than 4mm. This thesis has therefore focussed on the determination of fatigue design curves for tube-to-plate and tube-to-tube T-joints made up of square hollow sections of wall thicknesses less than 4mm under cyclic in-plane bending.

The need for fatigue design rules of welded thin-walled joints derives from the fact that thin-walled tubes are increasingly being used for the manufacture of equipment and structural systems in the road transport and agricultural industry as reported in Chapter 1. The thin-walled tubes are cold-formed.

Extensive welding procedure qualifications have been carried out to check the compliance of welded thin-walled tubular joints with Australian welding standards. Emphasis was also made on the determination of weld profiles and the measurement of weld toe undercut.

A detailed numerical analysis has been carried out on two-dimensional cruciform joints to determine the major factors influencing fatigue life in welded thin-walled cruciform joints. These analyses have been carried out using weld profiles and weld toe undercuts that were measured from thin-walled tubular T-joints using the silicon imprint technique. This part of the research aimed at determining the major factors affecting fatigue crack propagation life of thin-walled joints.

Extensive fatigue tests have been carried out for both the tube-to-plate and tube-to-tube T-joints under cyclic in-plane bending. Cold-formed square hollow sections with thicknesses of 3mm, 2mm and 1.6mm have been used in the manufacture of the test specimens. The cold-formed tubes used are of three different steel grades. Some of the cold-formed tubes were in-line galvanised while the tubes were non-galvanised. The fatigue test data from the specimens has been used to determine the design S-N curves using the least-squares method of analysis.

11.2 WELDING PROCEDURE AND WELD DEFECTS IN WELDED THIN-WALLED TUBULAR JOINTS

- Welded thin-walled tubular T-joints were joined using the MIG and TIG welding methods. The welded thin-walled tubular T-joints tested in this investigation satisfied the macro-cross section examination tests in the Australian welding standards AS1554.1-1995 (SAA 1995a) and AS1554.5-1995 (SAA 1995b), for penetration, fusion and freedom from significant defects. The tests were carried out on welded non-galvanised and in-line galvanised sections of thicknesses 1.6mm, 2mm and 3mm. The hardnesses in the heat-affected zone (HAZ), weld metal and parent metal of the welded thin-walled joints also satisfied the recommended values in the standards. The hardness tests include a test on the maximum value of Vickers hardness for the heat-affected zone and a test on the difference in hardnesses between the weld metal and the parent metal. The details of the macro-cross section examination tests and the hardness tests are given in Chapter 3.

- An extensive program was undertaken to measure weld profiles and weld toe undercuts for the MIG and TIG welded connections using the silicon imprint technique. The MIG welding method was found to give convex-like weld profiles. The TIG welding method was found to produce concave-like weld profiles. The undercut depths, found in the MIG welded connections satisfied the maximum permissible depth of intermittent undercut recommended in Australian standards and the maximum permissible depth of undercut recommended by the AWS regulations. However, some of the undercut depths found from the TIG welded connections were found to be above the maximum permissible depth of intermittent undercut recommended by Australian standards and the maximum permissible depth of undercut recommended by the AWS regulations. More occurrences of undercut were also found for the TIG welded connections in an equal number of silicon imprint samples that were prepared from both the MIG and TIG welded connections. The MIG welding method was therefore chosen as the method of welding in this investigation, although it is believed that the undercut which were obtained from the TIG welded connections can be eliminated through the use of a favourable combination of voltage and current.

- Prior to fatigue or static testing the specimens, magnetic particle testing was performed on all the welded connections. Magnetic particle testing showed that there are no inherent surface cracks on the welded thin-walled tubular joints, although one blow hole occurred in only one tube-to-plate specimen made up from a 1.6mm thick tube. The occurrence of the blow-hole in one of the welded connections, shows that the 100% visual scanning of the structural purpose (SP) welds recommended in AS1554.1-1995 (SAA 1995a) should be strictly adhered to for welded thin-walled tubular joints where the tube wall thickness is less than 4mm.

11.3 STATIC BEHAVIOUR IN RELATION TO HIGH CYCLE FATIGUE

- Static tests carried out on tube-to-plate and tube-to-tube T-joints showed that part of the load versus deformation curve gives a linear response. The maximum elastic moment corresponding to the highest load on the linear part of the load-deformation response was used to define the maximum allowable applied moment in the fatigue tests under cyclic in-plane bending. Loads corresponding to the maximum elastic moment and below were applied to obtain a high-cycle fatigue response.

- A comparison of the maximum elastic moment to the static strength for in-plane bending of the T-joints showed that the maximum elastic moment for each joint is always less than 60% of the static strength. This is in agreement with the Department of Energy (1990) guidelines, which states that the calculated tensile stress in a member under fatigue loading conditions should not exceed 60% of yield stress.

- For the tube-to-tube T-joints the ratio of maximum elastic moment to static strength depends on chord slenderness ratio (b_0/t_0) and on the bracing to chord width ratio (b_1/b_0). The ratio of maximum elastic moment to static strength increases as the strength and flexural rigidity of an unstiffened vierendeel connection increases. Packer *et al* (1992) showed that the strength and flexural rigidity of an unstiffened vierendeel connection decreases as the chord slenderness ratio increases and as the bracing to chord width ratio decreases.

11.4 FATIGUE BEHAVIOUR OF THIN-WALLED TUBE-TO-PLATE T-JOINTS

- Failure of tube-to-plate T-joints under cyclic in-plane bending occurred due to the initiation and propagation of cracks on the weld toe on the brace on the brace-plate interface in all the tube-to-plate T-joints tested. This is because the maximum SCF occurs at the weld toe on the corners of the brace. The measured SCF around the corners of the brace-plate interface showed that the maximum SCF occurred on the hot spot locations in the brace and is in agreement with the numerical analysis on tube-to-plate T-joints reported in Mashiri *et al* (1999a).

- Welded tube-to-plate connections were made up from tubes which were either "in-line" galvanised or non-galvanised. Fatigue tests on welded "in-line" galvanised and non-galvanised T-joints showed that "in-line" galvanising of cold-formed tubes does not have any noticeable influence on fatigue life.

- Stress grade, was found not to influence the fatigue life of welded tube-to-plate T-joints. Noordhoek *et al* (1980), also found that steel grade does not have an influence on fatigue life of welded end-to-end connections made up of square hollow sections. The effect of steel grade on fatigue life can be explained from the fact that macro-cracks are inherent in welded connections and that the crack growth rate coefficient in steel grades of yield strength less than 600MPa is very similar (BSI 1991).

- Stress ratio has been found to have an influence on the fatigue strength of tube-to-plate T-joints when S-N data is analyzed in terms of mean S-N curves. Stress ratio normally does not influence the fatigue life of welded structures because they have residual stresses of yield stress value, which result in the onset of fatigue cracking at any level of applied stress. The influence of stress ratio on fatigue life of tube-to-plate T-joints may be explained in terms of the damaging effect of a fully-tensile cyclic stress range which tends to increase as the mean stress or stress ratio increases (Maddox 1991). Further research needs to be undertaken to study the distribution of residual stresses in tube-to-plate T-joints to develop an understanding of the effects of stress ratio on fatigue life of tube-to-plate T-joints.

- The fatigue life of tube-to-plate T-joints has been found to decrease with a decrease in the tube wall thickness of the failed member, contrary to the classical fracture mechanics theory where fatigue strength is proportional to $t^{-1/4}$. This phenomenon of fatigue strength in welded thin-walled tubular joints is due to the greater negative impact of undercut depth on thin-walled joints compared to thicker walled joints as demonstrated by numerical analysis of two dimensional cruciform joints in Chapter 7.

- Stress concentration factors along the lines A and E where the highest stress concentrations occurred as revealed by the initiation of cracks in the fatigue tests were measured experimentally using strain gauges, as detailed in Section 5.5 of Chapter 5. All the stress concentration factors on the hot spot locations A and E where found to be less than 2.0. It was demonstrated that the stress gradients at the hot spot locations in the tube-to-plate T-joints were not as highly non-linear as those in tube-to-plate T-joints by comparing SCFs determined using the quadratic extrapolation method to those obtained using the linear extrapolation method.

11.5 FATIGUE BEHAVIOUR OF THIN-WALLED TUBE-TO-TUBE T-JOINTS

- The fatigue testing of welded thin-walled tube-to-tube T-joints revealed different modes of failure. The modes of failure were classified into different groups depending on the initiation and propagation of cracks in either the brace or the chord or both as explained in Section 6.3 of Chapter 6. Fatigue failure was defined as the length of a through thickness crack extending along the whole length of the brace width on the tension side resulting in the separation of the brace from the chord.

- The nominal stresses in the brace from strain gauge measurements were found to be comparable to the nominal stresses obtained from the simple beam theory.

- The stress concentration factors were measured along some of the hot spot locations A to E using both the quadratic and the linear extrapolation methods. The stress gradients at the hot spot locations in the tube-to-tube T-joints were found to be highly non-linear compared to the stress gradients at the hot spot locations in the tube-to-plate T-joints. This was demonstrated by the magnitude of the ratio of stress concentration factors (SCFs) obtained from the quadratic extrapolation method to the SCFs from the linear extrapolation method.

- The stress concentration factors determined experimentally from the measurement of strains have been found to be lower than the SCFs determined from the existing parametric equations by van Wingerde (1992) and Soh and Soh (1990). This is likely to be due to the oversized welds associated with thin-walled joints, which move the toe of the weld into a lower stress region as reported by Maddox *et al* (1995). Another reason for the discrepancy between the experimental and the parametric SCFs is likely to be due to the restriction of the first extrapolation point for hot spot stresses in thin-walled joints. The first point of extrapolation for hot spot stresses is given as $0.4t$ but restricted to 4mm for joints less than 10mm. Further research needs to be carried out to determine the influence of oversized welds and the effect of restricting the first point of extrapolation for hot spot stresses to 4mm on the magnitude of the stress concentration factors.

- The influence of the induced axial load and bending moment in the chord in tube-to-tube T-joints under in-plane bending has been shown to be negligible using the trends in existing parametric equations given in IIW (2000).

11.6 EFFECT OF WELD PROFILE AND WELD UNDERCUT ON FATIGUE CRACK PROPAGATION LIFE OF THIN-WALLED CRUCIFORM JOINTS

- The two-dimensional thin-walled cruciform joints modeled with the concave-like weld profile obtained from TIG welded connections produced a better fatigue performance compared to those models incorporating the convex-like weld profile obtained from the MIG welded connections. The better fatigue performance in the models with concave-like weld profile can be attributed to the larger toe radius associated with this profile and hence a smoother merge between the weld and the plate resulting in lower stress concentration.

- The larger sizes of undercut depth measured from the TIG welded connections have however been shown to introduce high notch stresses that result in a reduction in the fatigue crack propagation life of two-dimensional cruciform joints to levels lower than that for the models with a convex-like weld profile where smaller undercut depths have been found.

- Fatigue crack propagation life of welded thin-walled cruciform joints was found to decrease significantly with an increase in undercut depth at constant radius and constant depth to width ratio.

- Fatigue crack propagation life of welded thin-walled cruciform joints increases as the undercut width increases at constant depth and constant radius of undercut.

- Fatigue crack propagation life of welded thin-walled cruciform joints also increases as the radius of undercut increases at constant depth and constant width of undercut.

- The loss in fatigue crack propagation life in thin-walled cruciform joints (T=3mm) with undercut is relatively more than the loss in fatigue crack propagation life of thicker walled cruciform joints (T=20mm).

11.7 DESIGN RULES OF WELDED THIN-WALLED TUBE-TO-PLATE T-JOINTS

- The least-squares method of analysis was used to determine the design S-N curves of welded thin-walled tube-to-plate T-joints under in-plane bending.

- The analysis of the S-N data of welded thin-walled tube-to-plate T-joints, taking *log N* as the dependent variable and for the case when *A* and *B* are determined, yields a design S-N curve with a negative slope 1:2.9595. This natural slope of the experimental S-N data is very close to the slope adopted by the Canadian standard (CSA 1989), the Australian standard (SAA 1998a) and EC3 (1992) for design S-N curves of tube-to-plate T-joints.

- When the natural slope of the S-N data is determined, the analysis where *log S* is the dependent variable, yields a design S-N curve with a less steep slope to the analysis when *log N* is taken as the dependent variable. This analysis, when *log S* is taken as the dependent variable, produces mean-plus-two-standard-deviation and mean-minus-two-standard-deviation curves with less scatter in terms of stress range compared to the analysis when *log N* is taken as the dependent variable. This analysis, when *log S* is taken as the dependent variable, results in a design S-N curve that is non-conservative at lower stress ranges but conservative at higher stress ranges compared to the corresponding analysis when *log N* is the dependent variable.

- When the slope of the S-N data is forced to a predetermined value (to maintain consistency with current design rules), both the analyses when *log S* and when *log N* is a dependent variable yield similar results. The analysis for either *log N* or *log S* as a dependent variable and when the slope of the data is forced to a predetermined value, produces fatigue design equations which define S-N curves with the same class or detail category.

- The results of the analysis when *log N* is the dependent variable and for the case when the slope of the S-N curve is forced to a predetermined value equal to that in the current standards should be adopted for design to maintain consistency with these existing fatigue design standards. Traditionally, *log N* is taken as the dependent variable because the load applied and hence the applied stress range is the controlled variable in fatigue testing.

- For the classification method, the design S-N curve adopted for the fatigue design of welded thin-walled tube-to-plate T-joints under in-plane bending, where the tube wall thickness is less than 4mm was found to be higher than the existing S-N curves for tube-to-plate T-joints. This means that the existing design S-N curves for tube-to-plate T-joints are conservative for the fatigue design of welded thin-walled tube-to-plate T-joints under in-plane bending. The design S-N curves adopted for the welded thin-walled tube-to-plate T-joints, with tube wall thicknesses less than 4mm, under in-plane bending has a class of 44 and is given by the equation $\log N = 11.2222 - 3 \cdot \log S$.

- For the hot spot stress method, a stress concentration factor of 2.0 may be adopted for converting nominal stress ranges for welded thin-walled tube-to-plate T-joints under in-plane bending, to hot spot stress ranges. Note that the nominal stress used in calculating the hot spot stress is the maximum flexural stress in the tube by conventional theory of bending. The design $S_{r.hs}$-N curve has a hot spot stress range at 2 million cycles of 72 and is given by the equation $\log N = 11.8759 - 3 \cdot \log S$.

11.8 DESIGN RULES OF WELDED THIN-WALLED TUBE-TO-TUBE T-JOINTS

- Welded thin-walled tube-to-tube T-joints made up of square hollow sections of wall thicknesses less than 4mm were fatigue tested under in-plane bending. 96.6% of the welded thin-walled tube-to-tube T-joints failed in either the chord-tension-side failure mode or the chord-and-brace-tension-side failure mode. A plot of the $S_{r.hs}$-N data showing the different modes of failure revealed that the data of the specimens with the chord-tension-side failure mode or the chord-and-brace-tension-side failure mode lie within the same scatterband. This is because the cracks in these two modes of failures both initiated and propagated in the chord member where the thickness was 3mm in all cases. In the chord-and-brace-tension side failure mode the cracks initiate and propagate in the chord member and then develop in the brace at a later stage. Since there is no significant difference in fatigue life between the two modes of failure (chord-tension-side and chord-and-brace-tension-side) in terms of scatter, the cracks in the chord-and-brace-tension-side failure mode developed in the brace close to failure. The propagation of cracks in the brace wall tube therefore, does not constitute a significant part of the fatigue life in those connections where chord-and-brace-tension-side failure occurs. The critical thickness of the two different modes of failure is therefore the chord wall thickness.

- Most $S_{r,hs}$-N data based on experimental SCFs lie below the IIW 4mm design $S_{r,hs}$-N curve. The $S_{r,hs}$-N data has a critical thickness of 3mm and is therefore expected to have higher fatigue strength than the IIW 4mm design $S_{r,hs}$-N curve according to the classical fracture mechanics theory. The lower fatigue life in the welded thin-walled tube-to-tube T-joints is attributed to the greater negative impact of weld toe undercut on thin-walled joints compared to thick-walled joints as demonstrated by the numerical analysis of thin-walled cruciform joints in Chapter 7. The experimental SCFs were also found to be lower than SCFs from the parametric equations.

- Most of the $S_{r,hs}$-N data based on parametric equation SCFs lie above the IIW 4mm curve. However, some of the $S_{r,hs}$-N data lie below the IIW 4mm curve. The fact that in both the $S_{r,hs}$-N data based on experimental SCFs and parametric equation SCFs, some of the data lies below the IIW 4mm curve, shows that the increase in fatigue life with a decrease in tube wall thickness that is evident in IIW fatigue design $S_{r,hs}$-N curves for different thicknesses, is no longer true for tube wall thicknesses less than 4mm.

- Analysis of $S_{r,hs}$-N data to determine fatigue design curves has been carried out for the hot spot stress approach based on both experimental SCFs and parametric equation SCFs, using the least squares method.

- The slope adopted for the design $S_{r,hs}$-N curves between 10^3 and $5x10^6$ cycles is that given by equation 9.3 of Chapter 9. Equation 9.3 is from IIW (2000) and is used for determining the different design equations for different tube wall thicknesses for the constant amplitude region.

- Two analyses, involving hot spot stress fatigue data based on experimental SCFs and parametric equation SCFs, result in two different fatigue design $S_{r,hs}$-N curves. Two different design methods are thus proposed as detailed in Section 9.7 of Chapter 9.

- The design $S_{r,hs}$-N curve derived from the least squares method is used for defining the constant amplitude region between 10^3 to $5x10^6$ cycles. The variable amplitude region between $5x10^6$ to 10^8 cycles is defined using the point at $5x10^6$ from the constant amplitude region and a negative slope of 1:5 up to 10^8 cycles. The negative slope of 1:5 is derived from equation 9.7, which is from IIW (2000).

- The two analyses involving, $S_{r,hs}$-N data based on both the experimental, SCFs and the parametric equation SCFs, produce design $S_{r,hs}$-N curves which are lower than the expected design curve from the IIW (2000) trend of increase in fatigue life with a decrease in tube wall thickness. This shows that for tube wall thicknesses less than 4 mm the classical fracture mechanics theory that states that fatigue strength is proportional to $t^{-1/4}$, no longer applies. This can be explained from the fact that weld toe undercuts present in welded thin-walled joints have a greater negative impact on fatigue crack propagation life as shown in Chapter 7.

11.9 3D CRACK PROPAGATION ANALYSIS OF TUBE-TO-PLATE T-JOINT USING BOUNDARY ELEMENT METHOD

- Three-dimensional crack growth analysis of a tube-to-plate T-joint under in-plane bending has been undertaken using the boundary element method. The tube-to-plate T-joint is made up of a square hollow section of size, 50x50x3SHS, welded to a 10mm plate, which is one the tube-to-plate connection series tested in this investigation. The methods that are used for 3D crack growth analysis in BEASY have been described. They include the crack opening displacement method for determining stress intensity factors and the minimum strain energy density criterion for determining both the incremental size and direction. The Paris law for crack growth can also be used for determining the incremental size.

- A stress analysis of the uncracked tube-to-plate T-joint has been performed to determine the stress concentration factors (SCFs). The linear and the quadratic methods of extrapolation, for hot spot stresses have been used. The SCFs evaluated from the boundary element method are in good agreement with the SCFs determined experimentally through strain gauge measurements. Percentage differences ranging from 2.4 to 11.8 have been found between the experimentally determined SCFs and the SCFs from the boundary element method.

- Fatigue crack propagation life was estimated using the dual boundary element method. The fatigue crack propagation life of the welded thin-walled tube-to-plate T-joint was compared to the design S-N curve from experimentally determined fatigue data. The ratio of the class of the S-N curve determined from the experimental fatigue data to that derived from crack growth analysis is 1.05. This shows that there is good agreement between the fatigue life estimated by the dual boundary element method and the fatigue life determined experimentally.

- Future work will be carried out to estimate fatigue crack propagation life of the other tube-to-plate and tube-to-tube T-joints tested in this investigation.

11.10 RECOMMENDATIONS

1. Method of Welding for Thin-Walled Tubular Joints

From the results of the weld toe undercut depth sizes and the frequency of occurrence of undercuts in both the MIG and TIG welded connections reported in Section 3.3 of Chapter 3, the gas metal-arc welding method (MIG) is recommended for the joining of welded thin-walled joints. This is due to the fact that there is a greater negative impact of weld toe undercut depth on fatigue crack propagation life of welded thin-walled joints as reported in Chapter 7.

2. *Visual Scanning of Welded Thin-Walled Tubular Joints*

Although there was only one occurrence of a blow-hole in all the welded joints tested, it is recommended that the 100% visual scanning of the structural purpose (SP) welds recommended in AS1554.1-1995 (SAA 1995a) be strictly adhered to for thin-walled tubular joints with a thickness less than 4mm.

3. *Loading for High Cycle Fatigue Response*

It is recommended that the load applied to a thin-walled welded T- joint under in-plane bending, should not be greater than that corresponding to the highest point on the linear part of the moment versus angle-of-inclination graph in order to obtain a high cycle fatigue response. The ratio of maximum elastic moment to static strength as reported in Chapter 4 was found to be less than 0.6 for both the tube-to-plate and the tube-to-tube T-joints tested. This ratio was found to be close to 0.6 for the tube-to-plate T-joints tested. For the tube-to-tube T-joints tested the ratio was found to vary from 0.6 to 0.2 depending on the chord slenderness ratio (b_o/t_o) and the bracing to chord width ratio (b_1/b_o).

4. *Fatigue design of Tube-to-Plate T-joints using the Classification Method*

The following S-N curve is recommended for the fatigue design of welded thin-walled tube-to-plate T-joints under in-plane bending, where the tubes are SHS of wall thicknesses less than 4mm, using the classification method:

Equation defining S-N curve: $\log N = 11.2222 - 3 \cdot \log S$ **(11.1)**

Class or Detail Category: 44

5. *Fatigue design of Tube-to-Plate T-joints using the Hot Spot Method*

The following $S_{r,hs}$-N curve is recommended for the fatigue design of welded thin-walled tube-to-plate T-joints under in-plane bending, where the tubes are SHS of wall thicknesses less than 4mm, using the hot spot stress method:

Equation defining S-N curve: $\log N = 11.8759 - 3 \cdot \log S_{r,hs}$ **(11.2)**

Hot Spot Stress Range at 2 million cycles: 72

SCF for converting nominal stresses to hot spot stresses: 2.0

6. ***Fatigue design of Tube-to-Tube T-joints using the Hot Spot Method***

Either of the following design $S_{r,hs}$-N curves are recommended for the fatigue design of welded thin-walled tube-to-tube T-joints under in-plane bending, where the tubes are SHS of wall thicknesses less than 4mm, using the hot spot stress method:

Method 1: Equations defining $S_{r,hs}$-N curve:

$$\log N = 12.9502 - 3.4517 \cdot \log S_{r,hs} \qquad \text{for } 10^3 \le N \le 5\times10^6 \qquad \textbf{(11.3)}$$

$$\log N = 15.7543 - 5 \cdot \log S_{r,hs} \qquad \text{for } 5\times10^6 \le N \le 10^8 \qquad \textbf{(11.4)}$$

Hot spot stress range at 2 million cycles: 84

The method for fatigue design using the $S_{r,hs}$-N curve defined by the equations 11.3 and 11.4 is detailed in Section 9.8 of Chapter 9.

Method 2: Equations defining $S_{r,hs}$-N curve:

$$\log N = 14.0312 - 3.4517 \cdot \log S_{r,hs} \qquad \text{for } 10^3 \le N \le 5\times10^6 \qquad \textbf{(11.5)}$$

$$\log N = 17.3202 - 5 \cdot \log S_{r,hs} \qquad \text{for } 5\times10^6 \le N \le 10^8 \qquad \textbf{(11.6)}$$

Hot spot stress range at 2 million cycles: 174

The method for fatigue design using the $S_{r,hs}$-N curve defined by the equations 11.5 and 11.6 is detailed in Section 9.8 of Chapter 9.

11.11 FUTURE RESEARCH

The following research will be carried out at Monash University, Australia in the near future:

1. Maximum Permissible Depth of Undercut in Welded Thin-Walled Joints

It has been demonstrated that there is a greater negative impact of weld toe undercut on the fatigue crack propagation life of thin-walled cruciform joints compared to thick walled joints in Chapter 7. The negative impact of weld toe undercut can also be attributed to the phenomenon of decrease in fatigue life with a decrease in tube wall thickness which has been observed for tube-to-plate T-joints reported in Chapter 5. The greater negative impact of weld toe undercut on the fatigue life of welded thin-walled joints means that research needs to be undertaken to determine the maximum permissible depth of undercut for thin-walled joints. The maximum permissible depth of undercut given by the Australian welding standards and AWS regulations need to be reviewed to ascertain their applicability to thin-walled joints.

2. Fatigue Behaviour of TIG Welded Thin-Walled Joints

Some of the undercut depths in TIG welded thin-walled joints have been found to be larger than the maximum permissible depth of undercut recommended by Australian welding standards and the AWS regulations. More occurrences of undercut have also been observed in TIG welded thin-walled connections, compared to MIG welded thin-walled connections. However, there is a possibility that the depth and occurrences of undercut observed in the TIG welded thin-walled T-joints might be due to an unfavourable combination of current and voltage used in this investigation. By improving the TIG welds it is believed that the welded thin-walled connections joined by the TIG welding method might offer a higher resistance to fatigue loading because of the inherent concave-like weld profile of the TIG welds. The improvement of the TIG welds and subsequent testing of the TIG welded thin-walled joints needs to be carried out to determine the fatigue behaviour of TIG welded thin-walled joints.

3. Fatigue Behaviour of Welded Thin-Walled Tubular Joints

There is a general lack of fatigue design rules for thin-walled tubular joints where the tube thickness is less than 4mm. Research therefore, needs to be undertaken to determine the fatigue design rules of welded thin-walled K, X and Y joints. Different actions such as cyclic axial loading and in- and out-of-plane bending should be investigated. Connections made up of both square and circular hollow sections should be fatigue tested.

4. Parametric Equations for SCFs in Welded Thin-Walled Joints

The parametric equations in current fatigue design standards such as IIW (2000) and Zhao *et al* (1999a) have a validity range, which does not cover some of the 2γ and β values characteristic of welded thin-walled tubular joints such as those tested in this investigation. A detailed numerical analysis needs to be undertaken to determine parametric equations that cover the typical parameters in welded thin-walled tubular joints.

5. Effect of Current Extrapolation Rules for Hot Spot Stresses on the Magnitude of Hot Spot Stresses Determined in Welded Thin-Walled Joints

Current extrapolation rules used for determining hot spot stresses limit the first point of extrapolation to 4mm in thin-walled joints of thicknesses less than 10mm. This might have an effect on the hot spot stresses determined and hence the SCFs evaluated especially for thin-walled joints of thicknesses less than 4mm. A detailed analysis needs to be carried out to determine the effect of the current extrapolation rules on the magnitude of the hot spot stresses determined in welded thin-walled joints.

6. Effect of Oversized Welds on Hot Spot Stresses in Welded Thin-Walled Joints

Measurement of weld profiles in Chapter 3 has shown that the welds in thin-walled joints are oversized. Oversized welds move the toe of the weld away from the regions of higher stress. This results in the hot spot stresses determined in thin-walled joints being lower than expected. An analysis needs to be undertaken to determine the influence of oversized welds on the hot spot stresses determined in thin-walled joints.

7. Residual Stresses in Tube-to-Plate T-joints

The residual stress distribution in thin-walled tube-to-plate T-joints needs to be determined to explain the effect of stress ratio on fatigue life of tube-to-plate T-joints which has been observed in Section 5.4 of Chapter 5.

8. Concrete Filled Chord Members in Nodal Joints

The filling of chord members with concrete in tube-to-tube T-joints can result in a change in stress distribution on the tube-to-tube welded interface. Since the chord becomes more rigid when concrete filled, this may result in fatigue failure occurring more in the braces of the nodal joints compared to failure in the chords as concrete filling is likely to reduce chord face yielding. The behaviour of the tube-to-tube T-joints where the chord is concrete filled is therefore likely to resemble fatigue failure in tube-to-plate T-joints. The advantage of increasing the rigidity of the chord and increasing the chances of failure in the brace means that the tube-to-tube T-joints are likely to have a greater static strength and hence able to withstand cyclic loads of larger stress ranges. Therefore the behaviour of tube-to-tube T-joints where the chords are concrete filled needs to be investigated.

9. Thickness Effect for Thin Plates

Most of the research projects on thickness effect summarised in Section 2.6 of Chapter 2, cover plates with thicknesses larger than 15mm. Research is needed to investigate the thickness effect for thin plates.

10. 3D BEM Analysis of Tube-to-tube T-joints

Three dimensional crack propagation analysis has been carried out on a tube-to-plate T-joint made up of a square hollow section of size 50x50x3SHS welded to a 10mm plate. The tube-to-plate T-joint analysed represents one of the connection series of tube-to-plate T-joints tested in this investigation. Future work will be carried out to estimate fatigue crack propagation life of the other tube-to-plate and tube-to-tube T-joints tested in this investigation.

REFERENCES

AISC 1993: Load and resistance factor design specification for structural steel buildings, American Institute of Steel Construction, Chicago, USA.

American Petroleum Institute (API) 1991, "Recommended practice for planning, designing and constructing fixed offshore platforms", API Recommended Practice 2A (RP 2A), Nineteenth Edition, August 1991, Washington, USA

ASTM 1980, "Standard Practice for Statistical Analysis of Linear or Linearized Stress-Life (S-N) and Strain-Life (-N) Fatigue Data" ASTM Designation E739-80, ASTM Committee E-9 on Fatigue, *Statistical Analysis of Fatigue Data*, ASTM STP 744, American Society for Testing and Materials, 1980

Atluri S.N. "Structural Integrity and Durability", Tech Science Press, Forsyth, Georgia, USA, 1997

AWS 1998, Structural Welding Code-Steel, ANSI/AWS D1.1-98, American Welding Society, Miami, USA.

Bell R, O. Vosikovsky O. & S.A. Bain 1989. The significance of weld toe undercuts in the fatigue of steel plate T-joints. *International Journal of Fatigue*, Vol. 11, No. 1, pp. 3-11

Berge S. 1985, "On the effect of plate thickness in fatigue of welds", *Engineering Fracture Mechanics*, **21**, pp. 423-435

Berge S. 1989, "The plate thickness effect in fatigue-predictions and results (A review of Norwegian work)", Proceedings of the Eighth International Conference on Offshore Mechanics and Arctic Engineering, Vol. III, The Hague, The Netherlands, March 19-23, 1989, pp 21-30

Berge S. and Webster S.E. 1987, "The size effect on the fatigue behaviour of welded joints", Paper PS 8, Developments in Marine Technology 3, *Steel in Marine Structures*, Proceedings of the 3rd International Conference on Steel in Marine Structures, SIMS'87, Delft, The Netherlands, 15-18 June 1987, Eds. C. Noordhoek and J. de Back, Elsevier Science Publishers, pp 179-203

Berge S., Eide O.I., Astrup O.C., Palm S., Wastberg S., Gunleiksrud A and Lian B. 1987, "Effect of plate thickness in fatigue of welded joints in air and in seawater", Paper TS 45, Developments in Marine Technology 3, *Steel in Marine Structures*, Proceedings of the 3rd International Conference on Steel in Marine Structures, SIMS'87, Delft, The Netherlands, 15-18 June 1987, Eds. C. Noordhoek and J. de Back, Elsevier Science Publishers, pp 799-810

BHP 1995: *Spanning History in Walhalla*. Steel Structures, Issue No. 8, BHP Structural Steel Development Group, Melbourne, Australia.

Booth G.S. 1987, "The effect of thickness on the fatigue strength of plate welded joints ", Paper TS 2, Developments in Marine Technology 3, *Steel in Marine Structures*, Proceedings of the 3rd International Conference on Steel in Marine Structures, SIMS'87, Delft, The Netherlands, 15-18 June 1987, Eds. C. Noordhoek and J. de Back, Elsevier Science Publishers, pp 259-268

BSI 1991: *Guidance on methods for assessing acceptability of flaws in fusion welded structures*, British Standards Published Document PD 6493: 1991, British Standards Institute, London, UK

CEN 1997, "Cold formed welded structural hollow sections of non-alloy and fine grain steels-Part 2: Tolerances, dimensions and sectional properties", EN10219-2: 1997, Committee for European Standardization (CEN), Brussels

Chang E. and Dover W.D. 1999, "Prediction of stress distributions along the intersection of tubular Y- and T-joints", *International Journal of Fatigue*, 21, 1999, pp. 361-381

Computational Mechanics BEASY limited 1998: BEASY User Guide, Volumes 1 & 2, England

Connolly M.P., Hellier A.K., Dover W.D. and Sutomo J. 1990, "A parametric study of the ratio of bending to membrane stress in tubular Y- and T-joints", *International Journal of Fatigue*, Vol. 12, No. 1, 1990, pp. 3-11

CSA 1989: Limit State Design of Steel Structures, CAN/CSA-S16.1-M89, Canadian Standards Association, Rexdale, Ontario, Canada.

de Back J., van Delft D.R.V., and Noordhoek C. 1989, "The effect of plate thickness on fatigue life of welded tubular joints and flat specimens", Proceedings of the Eighth International Conference on Offshore Mechanics and Arctic Engineering, Vol. III, The Hague, The Netherlands, March 19-23, 1989, pp 31-37

Dean, B.K. and Bennett, J.D. (1994), "Roof Top Communication Towers", in *Tubular Structures VI*, Grundy, P et al (eds), Balkema, Rotterdam, pp 41-44

Department of Energy, 1990, " Offshore Installations: Guidance on design, construction and certification", Fourth Edition, London, HMSO, UK.

Det Norske Veritas, 1981, " Rules for the Design, Construction and Inspection of Offshore Structures", Det Norske Veritas 1977, Reprint with Corrections 1981, Oslo, Norway

Dijkstra O.D. and de Back J. 1980, "Fatigue Strength of Welded Tubular T- and X-Joints", *Proc. Offshore Technology Conference*, OTC 3639, May 1980, Houston, Texas, USA.

Dutta, D., Wardenier, J., Yeomans, N., Sakae, K., Bucak, Ö and Packer, J.A. (1998): Design guide for fabrication, assembly and erection of hollow section structures, CIDECT series "Construction with hollow steel sections", Serial No. 7, TÜV-Verlag GmbH, Köln, Germany

EC3 1992, Eurocode 3: Design of Steel Structures-Part 1.1: General Rules and Rules for Buildings, ENV 1993-1-1, European Committee for Standardisation.

Efthymiou M. and Durkin S. 1985, "Stress concentrations in T/Y and gap overlap K-joints", *Proceedings of the International Conference on Behaviour of Offshore Structures*, Elsevier Science Publishers, pp. 429-441

Eide O.I. and Berge S. 1987, "Fatigue of large scale plate girders with plate thicknesses 20, 40 and 60 mm", Paper TS 7, Developments in Marine Technology 3, *Steel in Marine Structures*, Proceedings of the 3rd International Conference on Steel in Marine Structures, SIMS'87, Delft, The Netherlands, 15-18 June 1987, Eds. C. Noordhoek and J. de Back, Elsevier Science Publishers, pp 337-347

Finch D.M. and Burdekin F.M. 1992, "Effects of welding residual stresses on significance of defects in various types of welded joint", *Engineering Fracture Mechanics*, Vol. 41, No. 5, pp. 721-735

Finch D.M. 1992, "Effects of welding residual stresses on significance of defects in various types of welded joint-II", *Engineering Fracture Mechanics*, Vol. 42, No. 3, pp. 479-500

Forman R.G., Shivakumar V. and Newman J.C. 1993, "Fatigue Crack Growth Computer Program "NASA/FLAGRO" Version 2.0", National Aeronautics and Space Administration, Lyndon B. Johnson Space Center, Houston, Texas, USA.

Gibstein M.G. 1981, "Stress Concentration in Tubular Joints, it's Definition Determination and Applications", Proc. International Conference, *Steel in Marine Structures*, Paris, October 1981

Grover J.L. 1989: Thickness, weld profile and initial flaw considerations for tubular joints. *Presented at the Eighth International Conference on Offshore Mechanics and Arctic Engineering*, The Hague, March 19-23, pp. 39-47

Gurney T.R. 1977a, "Theoretical analysis of the influence of toe defects on the fatigue strength of fillet welded joints", Welding Institute Research Report 32/1977/E

Gurney T.R. 1977b, "Some recent work relating to the influence of residual stresses on fatigue strength", Paper 23, In: *Residual Stresses in Welded Construction and their Effects*, An International Conference, Vol. 1-Papers, The Welding Institute, London 15-17 November 1977, pp. 151-163

Gurney T.R. 1979a, "Fatigue of Welded Structures", 2nd Edition, Cambridge University Press, Cambridge, UK.

Gurney T.R. 1979b, "The influence of thickness on the fatigue strength of welded joints", Paper 41, Second International Conference on Behaviour of Offshore Structures, BOSS'79, Imperia College, London, England, 28-31 August 1979, pp. 523-534

Gurney T.R. 1981, "Some comments on fatigue design rules for offshore structures", Proc. Second International Symposium on Intergrity of Offshore Structures, Eds. D. Faulkner, M.J. Cowling and P.A. Frieze, pp. 219-234, Applied Science Publishers, Barking, Essex, England, 1981

Gurney T.R. 1989, "The influence of thickness on fatigue of welded joints-10 years on (a review of British work)", Proceedings of the Eighth International Conference on Offshore Mechanics and Arctic Engineering, Vol. III, The Hague, The Netherlands, March 19-23, 1989, pp 1-8

Haagensen P.J. 1989, "Improvement Techniques", Proceedings, International Symposium on the Occasion of the Retirement of Prof. J. de Back, Delft, The Netherlands, pp. 77-89

Hancock, G.J. 1994, "Design of Cold-formed Steel Structures" – To Australian Standards AS1538-1988, 2nd edition, The Australian Institute of Steel Structures, Sydney, Australia

Hancock G.J. 1999, "Recent research and design developments in cold-formed open section and tubular members", *Advances in Steel Structures Vol. I*, Proceedings of The Second International Conference on Advances in Steel Structures, ICASS'99, Editors Chan S.L. and Teng G.J., Elsevier Science Ltd, Hong Kong, 15-17 December 1999, pp. 25-37

Harrison J.D. 1981, "The effect of residual stresses on fatigue behaviour", In: *Residual Stresses and their Effect*, The Welding Institute, Abington Hall, Abington, Cambridge, UK, pp. 9-16

Heemskerk 2000: Stress concentration factors in square hollow section T-joints-A finite element analysis, MSc. Thesis, Norwegian Institute of Science and Delft University of Technology, The Netherlands, January 2000

Hellier A.K., Connolly M.P. and Dover W.D. 1990a, "Stress concentration factors for tubular Y- and T-joints", *International Journal of Fatigue*, Vol. 12, No. 1, 1990, pp. 13-23

Hellier A.K., Connolly M.P. and Dover W.D. 1990b, "Prediction of stress distribution in tubular Y- and T-joints", *International Journal of Fatigue*, Vol. 12, No. 1, 1990, pp. 25-33

Hertogs A.A., Puthli R.S. and Wardenier J. 1989, "Stress concentration factors in plate-tube connections", Proceedings, 8th International Conference on Offshore and Arctic Engineering, The Hague, March 19-23, 1989, pp. 719-727

Hilton G.A. and Webster S.E. 1989, "The effect of plate and attachment thickness on the fatigue life of welded joints", Proceedings of the Eighth International Conference on Offshore Mechanics and Arctic Engineering, Vol. III, The Hague, The Netherlands, March 19-23, 1989, pp 49-56

IIW 2000: Fatigue Design Procedures for Welded Hollow Section Joints, IIW Doc. XIII-1804-99, IIW Doc. XV-1035-99, Recommendations for IIW Subcommission XV-E, Edited by X.L. Zhao and J.A. Packer, Abington Publishing, Cambridge, UK

Japanese Society of Steel Construction (JSSC) 1995: *Fatigue Design Recommendations for Steel Structures*. English Version, Tokyo, Japan

Johnson R.P. 1999, "Resistance of stud shear connectors to fatigue", The University of Warwick, School of Engineering, Research Report CE62, March 1999.

Key P.W. Hasan S.W. and Hancock G.J. 1988, "Column Behaviour of Cold-Formed Hollow Sections", *Journal of Structural Engineering*, ASCE, 114(2), pp. 390-407

Kuang J.G., Potvin A.B., Leick R.D. and Kahlich J.L. 1977, "Stress concentrations in tubular joints", *Journal of the Society of Petroleum Engineers*, August, pp. 287-299

Kulak G.L., Adams P.F. and Gilmor M.J. 1995, "Limit States Design in Structural Steel", Canadian Institute of Steel Construction, Ontario, 1995

Kurobane Y. 1989, "Recent Development in the Fatigue Design Rules in Japan", Proceedings, International Symposium on the Occasion of the Retirement of Prof. J. de Back, Delft University Press, Delft, 173-187

Lind, N.C. 1974, "Strength, Deformation and Design of Cold Formed Steel Structures", Design of Cold Formed Steel, Edited by R.M. Schuster, Solid Mechanics Division, University of Waterloo Press, Ontario Canada, 1974.

Little R.E. and Jebe E.H. 1975, "Statistical Design of Fatigue Experiments", Applied Science Publishers Ltd., Essex, England, 1975.

Louthan Jr., M.R. 1992, "Tensile Testing of Metals and Alloys" in Tensile Testing, edited by Patricia Han, ASM International, USA, June 1992.

Maddox S.J. 1991: *Fatigue strength of welded structures*. Second Edition, 1991, Abington Publishing, Cambridge, England.

Maddox S.J. Wylde J.G. and Yamamoto N. 1995, "Significance of weld profile on fatigue lives of tubular joints", International Conference on Offshore Mechanics and Arctic Engineering, OMAE-Vol. III, Material Engineering, American Society of Mechanical Engineers (ASME 1995), pp. 127-134

Mang F. and Bucak Ö. 1982, "Fatigue Behaviour of Welded Joints in Trusses of Steel Hollow Sections", IABSE Colloqium on Fatigue of Steel and Concrete Structures, Lausanne

Mang F. and Bucak Ö. 1996: Tauglichkeit und Lebensdauer von bestehenden Stahlbauwerken, Stahlbau Handbuch, Band 1 Teil B, Stahlbau, Verlagsgesellschaft mbH, Köln, Germany

Mang F., Herion S., Klingler J. and Bucak Ö. 1987, "Zeit- und Dauerfestigkeit von geschweiβten unversteiften Rechteck-Hohlprofilverbindungen von Fachwerken und Vierendeel trägern", Experimentelle Untersuchugen und Dauerfestigkeit unter Momentenbelastunf der Diagonalen, Vertrag: 7210-SA/111, Versuchsanstalt Für Stahl, Holz and Steine, Amtliche Materialprüfungsanstalt, Universität Karlsruhe (TH), Germany, November 1987.

Marshall P.W. 1992, "Design of Welded Tubular Connections, Basis and Use of AWS Code Provisions", Shell Oil Company, Houston, Texas, USA, Elsevier Science Publishers B.V. 1992

Mashiri F.R., Zhao X.L., Grundy P. 1997, "Crack Propagation Analysis of Welded Thin-Walled Cruciform Joint using the Boundary Element Method", Materials Research Forum '97 Conference Proceedings, Institute of Metals and Materials Australasia Ltd (IMMA '97), Melbourne, 20-21 November 1997, Australia, pp. 109-112

Mashiri F.R., Zhao X.L., Grundy P. 1998a, "Effects of Weld Profile on the Fatigue Life of Thin-walled Cruciform Joint", *Tubular Structures VIII*, Proceedings of the 8th Symposium on Tubular Structures, ISTS8, Editors, Choo Y.S. and van Der Vegte G.J., 26-28 August 1998, pp. 331-340

Mashiri F.R., Zhao X.L., Grundy P. 1998b, "Effects of Weld Undercut on the Fatigue Life of Welded Connections in Thin-Walled Structures" Structural Integrity and Fracture Proceedings, Australian Fracture Group Inc., 21-22 September 1998, pp. 81-91

Mashiri F.R., Zhao X.L., Grundy P. 1999a, "3D BEM Analysis of Thin-walled Tube-to-tube T-joints under Fatigue Loading", Paper U-072, The Second Australasian Congress on Applied Mechanics (ACAM99), CD-ROM, 10-12 February 1999, Canberra, Australia

Mashiri F.R., Zhao X.L., Grundy P. 1999b, "Fatigue Strength of Thin-Walled Tube-to-Tube T-joints under In-Plane Bending" *Advances in Steel Structures Vol. II*, Proceedings of The Second International Conference on Advances in Steel Structures, ICASS'99, Editors Chan S.L. and Teng G.J., Elsevier Science Ltd, Hong Kong, 15-17 December 1999, pp. 983-990

Mashiri F.R., Zhao X.L., Grundy P. 1999c, "Fatigue Analysis of Welded Connections in High Strength Cold-Formed SHS (t<4mm)" CIDECT Project No. 7T, Interim Report No. 2, Department of Civil Engineering, Monash University, Australia, June 1999.

Mashiri F.R., Zhao X.L., Grundy P. 2000a, "Fatigue Design of Welded Very Thin-walled Tube-to-Plate Joints using the Classification Method" *Structural Failure and Plasticity*, Proceedings of The 7th International Symposium on Structural Failure and Plasticity, IMPLAST2000, Melbourne, Australia, 4-6 October 2000, pp.735-740

Mashiri F.R., Zhao X.L., Grundy P. 2000b, "Crack Propagation Analysis of Welded Thin-Walled Joints using Boundary Element Method" *Computational Mechanics*, Vol. 26, No. 2, Springer-Verlag 2000, pp. 157-165

Mashiri F.R., Zhao X.L., Grundy P. 2000c, "Fatigue Analysis of Welded Connections in High Strength Cold-Formed SHS (t<4mm)" CIDECT Project No. 7T, Interim Report No. 3, Department of Civil Engineering, Monash University, Australia, May 2000.

Mashiri F.R., Zhao X.L., Grundy P. 2001, "Fatigue behaviour of thin-walled tube-to-tube T-joints under in-plane bending", *Tubular Structures IX*, Proceedings of the 9th International Symposium on Tubular Structures, ISTS9, Editors Puthli R. and Herion S., 3-5 April 2001

Mi Y. 1996, "Three-dimensional Analysis of Crack Growth", Topics in Engineering Vol. 28, Computational Mechanics Publications, Editors C.A. Brebbia and J.J. Connor, Southampton, U.K.

Mi Y. and Aliabadi M.H., 1993, "Dual boundary element method for three-dimensional crack growth analysis", Boundary Elements XV, Vol. II, Editors C.A. Brebbia and J.J. Rencis, Computational Mechanics Publications and Elsevier Science Publishers

Mi Y. and Aliabadi M.H. 1994," Three-dimensional crack growth simulation using BEM", *Computers and Structures*, Vol 52, No. 5, pp 871-878, 1994

Miki T, Mori T. and Masuhara Y. 1990: Influence of undercut on fatigue strength of transverse fillet welded joints, Reports on remaining life and evaluation of steel bridges. Supported by Japanese Ministry of Education 1990, (In Japanese).

Morgan M.R. and Lee M.M.K. 1998a, "Stress concentration factors in tubular K-joints under in-plane moment loading", *Journal of Structural Engineering*, Vol. 124, No. 4, April 1998, pp. 382-390

Morgan M.R. and Lee M.M.K. 1998b, "Prediction of stress concentrations and degrees of bending in axially loaded tubular K-joints", *Journal of Constructional Steel Research*, Vol. 45, No. 1, pp. 67-97.

Morgan M.R. and Lee M.M.K. 1998c, "Parametric equations for distributions of stress concentration factors in tubular K-joints under out-of-plane moment loading", *International Journal of Fatigue*, Vol. 20, No. 6, pp. 449-461.

Mohaupt U.H., Burns D.J., Kalbfleisch J.G., Vosikovsky O. and Bell R. 1987, "Fatigue crack development, thickness and corrosion effects in welded plate to plate joints", Paper TS 3, Developments in Marine Technology 3, *Steel in Marine Structures*, Proceedings of the 3rd International Conference on Steel in Marine Structures, SIMS'87, Delft, The Netherlands, 15-18 June 1987, Eds. C. Noordhoek and J. de Back, Elsevier Science Publishers, pp 269-280

Monahan C.C. 1999: Early Fatigue Crack Growth at Welds. Topics in Engineering, Vol. 26, Edited by Brebbia C.A. and Connor J.J. Wessex Institute of Technology (WIT) Press, Southampton, UK

Mori T., Zhao X.L. and Grundy P. 1997, "Fatigue strength of transverse single sided fillet welded joints", *Australian Civil/Structural transactions*, Vol. C39, No. 23, 1997, pp 95-105.

Nakazawa H. and Kodama S. 1987, "Statistical S-N Testing Method with 14 Specimens: JSME Standard Method for Determination of S-N Curves" in Current Japanese Materials Research, Vol. 2, *Statistical Research on Fatigue and Fracture*, Editors: Tanaka T., Nishijima S. and Ichikawa M., Elsevier Applied Science, 1987

Newman Jr J.U.C. 1984: A crack opening stress equation for fatigue crack growth. *International Journal of Fracture*, Vol. 24, No. 3, pp. 131-135.

Nguyen T.N. and Wahab M.A. 1995, "A Theoretical Study of the Effect of Weld Geometry Parameters on Fatigue Crack Propagation Life", *Engineering Fracture Mechanics*, 51(1), 1-18

Nguyen T.N. and Wahab M.A. 1996, "The Effect of Undercut and Residual Stresses on Fatigue Behaviour of Misaligned Butt Joints", *Engineering Fracture Mechanics*, 55(3), 453-469

Niemi E.J. 1995, "A Novel Fatigue Analysis Approach for Tubular Welded Joints", Proceedings, Fatigue Design '95, Helsinki, Finland, 189-201

Nihei K, Inamura F, & Koe S. 1997, "Study on Hot Spot Stress for Fatigue Strength Assessment of Fillet Welded Structure" Proceedings of the Seventh International Offshore and Polar Engineering Conference, Vol. IV, Honolulu, USA, May 25-30, 1997

Noordhoek C., Wardenier J. and Dutta D. 1980, "The fatigue behaviour of welded joints in square hollow sections-Part 2, Analysis", Stevin Report 6-80-4, TNO-IBBC Report BI-80-10/0063.4.3821, Department of Civil Engineering, Delft University of Technology, Delft, The Netherlands

Noordhoek C., van Delft D.R.V. and Verheul A. 1987, "The influence of plate thicknesses on the fatigue behaviour of welded plates up to 160mm with an attachment or butt weld", Paper TS 4, Developments in Marine Technology 3, *Steel in Marine Structures*, Proceedings of the 3rd International Conference on Steel in Marine Structures, SIMS'87, Delft, The Netherlands, 15-18 June 1987, Eds. C. Noordhoek and J. de Back, Elsevier Science Publishers, pp. 281-301

Ohta A., Mawari T. and Suzuki N. 1990, "Evaluation of Effect of Plate Thickness on Fatigue Strength of Butt Welded Joints by a Test Maintaining Maximum Stress at Yield Strength", *Engineering Fracture Mechanics*, 37, 987-993

Örjasaeter O., Drågen A., Haagensen P.J., Lian B and Gunleiksrud Å. 1987, "Effect of plate thickness on the fatigue properties of low carbon-micro-alloyed steel", Paper TS 6, Developments in Marine Technology 3, *Steel in Marine Structures*, Proceedings of the 3rd International Conference on Steel in Marine Structures, SIMS'87, Delft, The Netherlands, 15-18 June 1987, Eds. C. Noordhoek and J. de Back, Elsevier Science Publishers, pp 315-335

Overbeeke J.L. and Wildschut H. 1987, "The influence of plate thickness on the endurance of welded joints", Paper TS 1, Developments in Marine Technology 3, *Steel in Marine Structures*, Proceedings of the 3rd International Conference on Steel in Marine Structures, SIMS'87, Delft, The Netherlands, 15-18 June 1987, Eds. C. Noordhoek and J. de Back, Elsevier Science Publishers, pp 247-257

Packer J.A. and Henderson J.E. 1997, "Design Guide for Hollow Structural Section Connections", 2nd Edition Canadian Institute of Steel Construction, Ontario, Canada

Packer J.A., Wardenier J., Kurobane Y., Dutta D. and Yeomans N. 1992, "Design Guide for Rectangular Hollow Section (RHS) Joints under Predominantly Static Loading" CIDECT Construction with Hollow Steel Sections, Verlag TUV Rheinland, Cologne, Germany.

Petershagen H. 1985, "Influence of undercuts on the fatigue strength of welded joints-a review", Welding and Cutting 6, 1985, pp E90-E91

Phillips C.E. and Heywood R.B. 1951, "The size effect in fatigue of plain and notched specimens loaded under reversed direct stress", *Proceedings, Institution of Mechanical Engineers*, Vol. 165, pp. 113-124

Portela A. and Aliabadi M.H. 1992, "The dual boundary element method: effective implementation for crack problems" *International Journal of Numerical Methods in Engineering*, Vol. 33, pp. 1269-1287, 1992.

Portela, A., Aliabadi, M.H. and Rooke, D.P. 1993, "Dual boundary element incremental analysis of crack propagation", *Computers and Structures*, Vol. 46, No. 2, 237-247

Puthli R.S., de Koning C.H.M., van Wingerde A.M., Wardenier J. and Dutta, D. (1989): Fatigue strength of welded unstiffened RHS joints in lattice structures and vierendeel girders, Final Report Part III: Evaluation for Design Rules, TNO-IBBC Report No. BI-89-097/63.5.3800, Stevin Report No. 25-6-89-36/A1, June, Delft, The Netherlands

Puthli R.S., Wardenier J., Mang F. and Dutta D. 1992: Fatigue behaviour of multiplanar welded hollow section joints and reinforcement measures for repair, Final report Part V-Evaluation and design recommendation, TNO-Bouw Report No. BI-92-0079/21.4.6394, Stevin Report No. 6.92.17/A1/12.06, Sept., Delft, The Netherlands

Romeyn A., Puthli R.S., de Koning C.H.M. and Wardenier J. 1992: Stress and strain concentration factors of multiplanar joints made of circular hollow sections, Proceedings of the Second International Offshore and Polar Engineering Conference, San Francisco, USA, 14-19 June 1992, Vol. IV, pp. 384-393

Romeijn A. 1994: Stress and strain concentration factors of welded multiplanar tubular joints, PhD Thesis, Delft University Press, Delft, The Netherlands.

Romeijn A., Wardenier J., de Koning C.H.M., Puthli R.S. and Dutta D. 1993: Fatigue behaviour and influence of repair on multi planar K-joints made of circular hollow sections, The Third International Offshore and Polar Engineering Conference, Singapore, Vol. IV, 1993, pp. 27-36

SAA 1988a, *Methods of Destructive Testing of Welds in Metal, Part 5: Metallographic Tests, Method 5.1: Macro Test-Cross-Section Examination*, Australian Standard AS 2205.5.1-1988, Standards Association of Australia, Sydney, Australia.

SAA 1988b: *Methods of Destructive Testing of Welds in Metal, Part 6: Hardness Tests, Method 6.1: Weld Joint Hardness Test, Australian Standard AS 2205.6.1-1988*, Standards Association of Australia, Sydney, Australia.

SAA 1991a, Structural Steel Hollow Sections, Australian Standard AS1163-1991, Standards Association of Australia, Sydney, Australia

SAA 1991b, *Metallic materials-Vickers hardness test*, Australian Standard AS 1817-1991, Standards Association of Australia, Sydney, Australia

SAA 1995a, *Structural Steel Welding, Part 1: Welding of Steel Structures*, Australian Standard AS/NZS 1554.1-1995, Standards Association of Australia, Sydney, Australia.

SAA 1995b, *Structural Steel Welding, Part 5: Welding of Steel Structures subject to High Levels of Fatigue Loading*, Australian Standard AS/NZS 1554.5-1995, Standards Association of Australia, Sydney, Australia.

SAA 1998a, *Steel Structures, Australian Standard AS 4100-1998*, Standards Association of Australia, Sydney, Australia.

SAA 1998b, *Methods for Magnetic Particle Testing of Ferromagnetic Products and Components*, Australian Standard AS 1171-1998, Standards Association of Australia, Sydney, Australia.

Sedlacek G., Grotmann D, Jo J.B., and Dutta D. 1992, "The Determination of the Fatigue Resistance of Steel Structures on the Basis of the Combined Method", ISOPE '92 Conference, San Fransisco, USA, Vol. IV, 296-300

Sedlacek G., Grotmann D, Schafer M. and Zhao X.L. 1998, "Fatigue behaviour of Hollow Section Joints, CIDECT Report 7N, RWTH, Aachen, Germany

Shi Y.W., Chen B.Y. and Zhang J.X. 1990, "Effects of welding residual stresses on fatigue crack growth behaviour in butt wlds of a pipeline steel", *Engineering Fracture Mechanics*, Vol. 36, No. 6, pp. 893-902

Sih G.C. and Cha B.C.K. 1974, "A fracture criterion for three dimensional crack problems", *Journal of Engineering Fracture Mechanics*, Vol. 6, pp. 699-732.

Smedley P. and Fisher P. 1991, "Stress concentration factors for simple tubular joints", *Proceedings of the first International Offshore and Polar Engineering Conference*, International Sociaty of Offshore and Polar Engineers, Edinburgh, U.K., pp. 475-483

Smith I. F. C. and Hirt M.A. 1983, "Fatigue Crack Growth in a Fillet Welded Joint", *Engineering Fracture Mechanics*, 18, 861-869

Smith I. F. C. and Hirt M.A. 1985, "A review of fatigue strength improvement methods", *Canadian Journal of Civil Engineering*, 12, 166-183

Snedden N.W. 1981, "Background to Proposed New Fatigue Design Rules for Steel Welded Joints in Offshore Structures", Report of the Department of Energy Guidance Notes Revisions Drafting Panel, May 1981

Soh A.K. and Soh C.K. 1990, "A parametric stress analysis of T/Y and K square-to-square tubular joints", *Journal of Constructional Steel Research*, No. 15, pp. 173-190

Swamidas A.S.J., Cheema P.J. and Muggeridge D.B. 1989: Fatigue strength of fillet welded cruciform joints. *Canadian Journal of Civil Engineering*, Vol. 16, No. 2, pp 162-171

Trevelyan J. 1994, "Boundary Elements for Engineers, Theory and Application", Computational Mechanics Publications, Southampton, UK

Tubemakers of Australia Ltd 1994, "The DuraGal and Galtube Plus Easy Welding Guide", The Welding Guide No. 1, Produced by Tubemakers Structural and Engineering Products, a Division of Tubemakers of Australia Ltd, April 1994

Underwater Engineering Group (UEG) 1985: Design of tubular joints for offshore structures, UEG Publication UR-33, Vol. 2, 1985

van Delft D.R.V. 1981, "A two dimensional analyses of stress at the vicinity of weld toes of tubular structures" Stevin Report 6-81-8, Stevin Laboratory, delft University of Technology, Delft, The Netherlands.

van Delft D.R.V., Noordhoek C. and de Back J. 1985, "Evaluation of the European fatigue test data on large size welded tubular joints for offshore structures", 17th Annual Offshore Technology Conference, Houston, Texas, OTC 4999, pp. 351-356

van der Vegte G.J. 1988, "Low cycle fatigue of welded structures-Part C: Tubular T- and X-joints", Report Stevin Laboratory, Delft University of Technology.

van Wingerde A.M. 1992: The fatigue behaviour of T- and X-joints made of SHS, *Heron*, Vol. 37, No. 2, pp. 1-180

van Wingerde A.M., Puthli R.S., Wardenier J., Dutta D. and Packer J.A. 1992: Design recommendations and commentary regarding the fatigue behaviour of hollow section joints", Proceeding os the Second International Offshore and Polar Engineering Conference, San Francisco, USA, 14-19 June 1992, Vol. IV, pp. 288-295 van Wingerde A.M., Packer J.A. & Wardenier J. 1996a: New guidelines for Fatigue Design of HSS Connections. *Journal of Structural Engineering*, ASCE, Vol. 122, No. 2, pp 125-132

van Wingerde A.M., Packer J.A., Wardenier J. and Dutta, D. 1996b: The fatigue behaviour of K-joints made of square hollow sections, CIDECT Report 7P-19/96, University of Toronto, Canada

van Wingerde A.M., Packer J.A., Wardenier J. and Dutta, D. 1997a: Simplified design graphs for the fatigue design of multiplanar K-joints with gap, CIDECT Report 7R-01/97, January, University of Toronto, Canada

van Wingerde A.M., van Delft D.R.V., Wardenier J. & Packer J.P., 1997b: Scale Effects on the Fatigue Behaviour of Tubular Structures. *IIW International Conference on Performance of Dynamically Loaded Welded Structures*, July 14-15, San Francisco, U.S.A, pp. 123-135

van Wingerde A.M., Packer J.A. and Wardenier J. 1997c. "IIW fatigue rules for tubular joints", IIW International Conference on Performance of Dynamically Loaded Welded Structures, July 1997, San Francisco, USA, pp. 98-107

Verheul A. & Noordhoek C. 1987: *Fatigue behaviour of joints between rectangular hollow sections, T-joints Part 1*, TNO-IBBC Report BI-87-118/63.5.3.820, Delft, Netherlands.

Vosikovsky O., Bell R., Burns D.J., and Mohaupt U.H. 1989, "Thickness effect on fatigue of welded joints-review of the Canadian Program", Proceedings of the Eighth International Conference on Offshore Mechanics and Arctic Engineering, Vol. III, The Hague, The Netherlands, March 19-23, 1989, pp 9-19

Walker A.C. 1975, "Design and Analysis of Cold-Formed Sections", John Wiley and Sons, New York, USA

Wallin K. 1999, "The probability of success using deterministic reliability", *Fatigue Design and Reliability*, Editors: G. Marquis and J. Solin, ESIS Publication 23, Elsevier Science Ltd., 1999

Wardenier, J. 1982: *Hollow Section Joints*, Delft University Press, Delft, The Netherlands.

Wardenier J. 1999: Hollow Sections in Structural Applications, International Committee for the Study of Tubular Structures (CIDECT), Verlag TUV Rheinland, Koln, Germany.

Wilkinson T. and Hancock G.J. 1998a, "Tests on stiffened and unstiffened welded knee connections in cold-formed RHS", *Tubular Structures VIII*, Proceedings of the 8th International Symposium on Tubular Structures, ISTS8, Editors, Choo Y.S. and van Der Vegte G.J., 26-28 August 1998, pp. 177-186

Wilkinson T. and Hancock G.J. 1998b, "Tests of bolted and internal sleeve knee connections in cold-formed RHS", *Tubular Structures VIII*, Proceedings of the 8th International Symposium on Tubular Structures, ISTS8, Editors, Choo Y.S. and van Der Vegte G.J., 26-28 August 1998, pp. 187-195

Wilkinson T. and Hancock G.J. 1998c, "Compact or Class 1 limits for rectangular hollow sections in bending", *Tubular Structures VIII*, Proceedings of the 8th International Symposium on Tubular Structures, ISTS8, Editors, Choo Y.S. and van Der Vegte G.J., 26-28 August 1998, pp. 409-416

Wilkinson T. and Hancock G.J. 1998d, "Tests of portal frames in cold-formed RHS", *Tubular Structures VIII*, Proceedings of the 8th International Symposium on Tubular Structures, ISTS8, Editors, Choo Y.S. and van Der Vegte G.J., 26-28 August 1998, pp. 521-529

Wilkinson T. and Hancock G.J. 2000a, "Tests to examine plastic behaviour of knee joints in cold-formed RHS", *Journal of Structural Engineering*, ASCE, Vol. 126, No. 3, March 2000, pp. 297-305

Wilkinson T. and Hancock G.J. 2000b, "Effect of GMAW on the Mechanical Properties of In-Line Galvanised Cold-Formed Steel", Proceedings, IIW Asian Pacific International Congress, Melbourne, Australia, November 2000

Woordsworth A.C. and Smedley G.P. 1978, "Stress concentrations at unstiffened tubular joints', *Proceedings of the European Offshore Steel Research Seminar*, Paper 31, The Welding Institute, Cambridge, U.K., pp. 719-740

WTIA 1996, "The Weldability of Steels", TN 1-96, WTIA Technical Note No. 1, Welding Technology Institute of Australia, NSW, Australia

WTIA 1998, "Commentary on the Structural Steel Welding Standard AS/NZS 1554", TN 11-98, WTIA Technical Note No. 11, Published jointly by the Welding Technology Institute of Australia and the Australian Institute of Steel Construction, NSW, Australia.

Yamada K & S. Kainuma 1996: Practical aspects of fracture mechanics applied to fatigue. Key note Paper, *The Fourth International Symposium on Structural Engineering for Young Experts*, Tsinghua University, Beijing, China, 1996

Yu W.W. 1991, "Cold-Formed Steel Design", 2nd Edition, John Wiley and Sons, New York, USA

Zhao X.L and Hancock G.J. 1991: T-joints in Rectangular Hollow Sections subject to Combined Actions, *Journal of Structural Engineering*, ASCE, 117 (8), pp. 2258-2277

Zhao X.L and Hancock G.J. 1992: Square and Rectangular Hollow Sections subject to Combined Actions, *Journal of Structural Engineering*, ASCE, 118 (3), pp. 648-668

Zhao X.L. and G.J. Hancock 1993: *Tests and Design of Butt Welds and Transverse Fillet Welds in Thin Cold-formed RHS Members*, Research Report No. R681, The University of Sydney, NSW 2006, Australia.

Zhao X.L and Hancock G.J. 1995a: Square and Rectangular Hollow Sections under Transverse End Bearing Force, *Journal of Structural Engineering*, ASCE, 121 (11), pp. 1565-1573

Zhao X.L and Hancock G.J. 1995b: Butt Welds and Transverse Fillet Welds in Thin Cold-Formed RHS Members, *Journal of Structural Engineering*, ASCE, 121 (11), pp. 1674-1682

Zhao X.L and Hancock G.J. 1995c: Longitudinal Fillet Welds in Thin Cold-Formed RHS Members, *Journal of Structural Engineering*, ASCE, 121 (11), pp. 1683-1690

Zhao X.L and Hancock G.J. and Trahair N.S. 1995: Lateral Buckling Tests of Cold-Formed RHS Beams, *Journal of Structural Engineering*, ASCE, 121 (9), pp. 1323-1329

Zhao X.L. and Hancock G.J. 1996: Welded connections in Thin Cold-Formed RHS, Connections in Steel Structures III, Bjorhovde, Colson and Zandonini (eds), pp. 89-98

Zhao X.L., Hancock G.J. & Sully R. 1996: Design of Tubular Members and Connections using Amendment Number 3 to AS4100. *Journal of the Australian Institute of Steel Construction*, Vol. 30, No. 4, pp 2-15

Zhao X.L. and Hancock G.J. 1998, "Recent research on cold-formed tubular structures", *Journal of Constructional Steel Research*, Vol. 40, No. 1-3, April-June 1998, Paper 229

Zhao X.L. and Mahendran M. 1998, "Recent innovations in cold-formed tubular sections", *Journal of Constructional Steel Research*, Vol. 46, Nos. 1-3, April-June 1998, Paper 228

Zhao X.L., Mashiri F.R., Grundy P. 1998, "Fatigue Analysis of Welded Connections in High Strength Cold-Formed SHS (t<4mm)" CIDECT Project No. 7T, Interim Report No. 1, Department of Civil Engineering, Monash University, Australia, July 1998, 23 pages

Zhao X.L., Herion S., Packer J.A., Puthli R., Sedlacek G., Wardenier J., Weynand K., Wingerde A., and Yeomans N. 1999a, "Design Guide for Circular and Rectangular Hollow Section Joints under Fatigue Loading", Verlag TUV Rheinland, Koln, Germany.

Zhao X.L., Sedlacek G., Schafers M. and Mori T. 1999b, "Fatigue resistance of welded tubular joints using fracture mechanics approach", Paper R-064, The Second Australasian Congress on Applied Mechanics (ACAM '99), CD-ROM, 10-12 February 1999, Canberra, Australia

Zhao X.L., Al-Mahaidi R. and Kiew K.P. 1999c: Longitudinal Fillet Welds in Thin-Walled C450 RHS members, *Journal of Structural Engineering*, ASCE, 125 (8), pp. 821-828

Appendix A:

MACRO-CROSS SECTION EXAMINATION MICROGRAPHS

A.1 C350LO TUBE-TO-TUBE

Figure A1: 50x50x3SHS-100x100x3SHS; Side Position; TIG

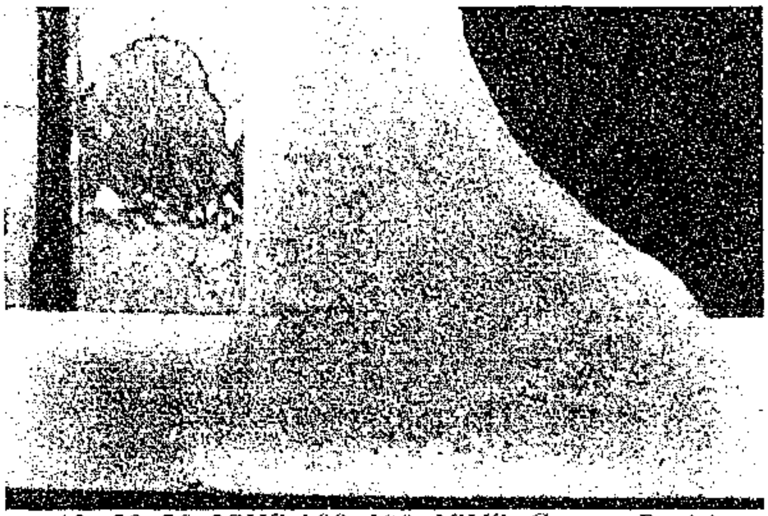

Figure A2: 50x50x3SHS-100x100x3SHS; Corner Position; TIG

Figure A3: 50x50x3SHS-100x100x3SHS; Side Position; MIG

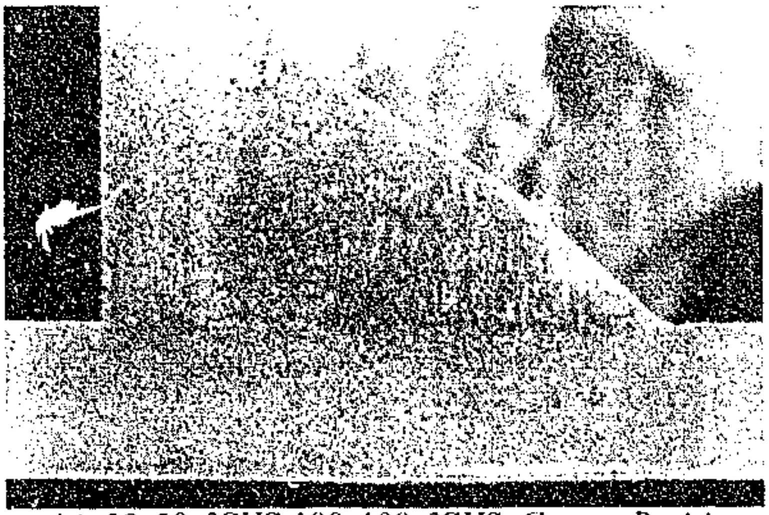

Figure A4: 50x50x3SHS-100x100x3SHS; Corner Position; MIG

A.2 DURAGAL C450LO TUBE-TO-TUBE

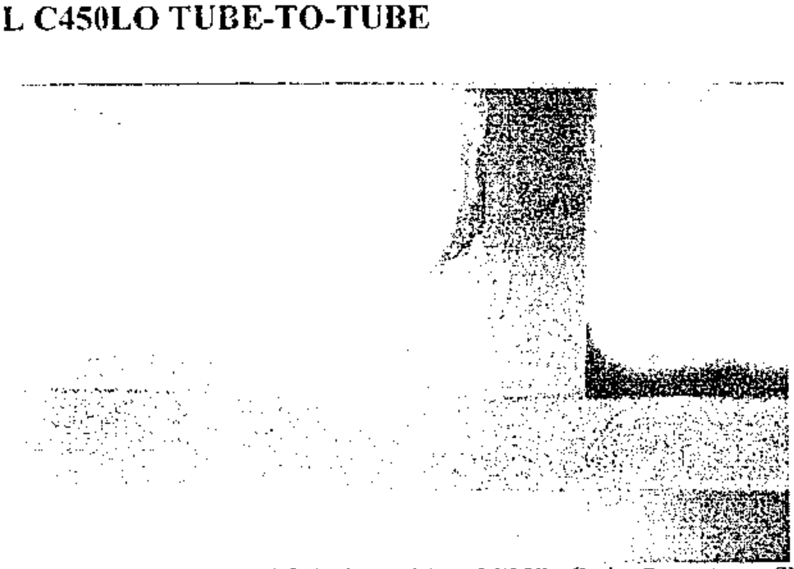

Figure A5: 50x50x3SHS-100x100x3SHS; Side Position; TIG

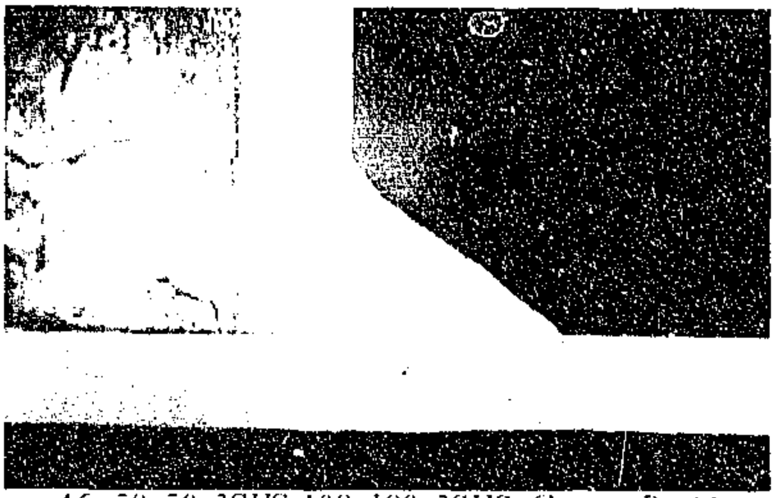

Figure A6: 50x50x3SHS-100x100x3SHS; Corner Position; TIG

Figure A7: 50x50x1.6SHS-100x100x3SHS; Side Position; TIG

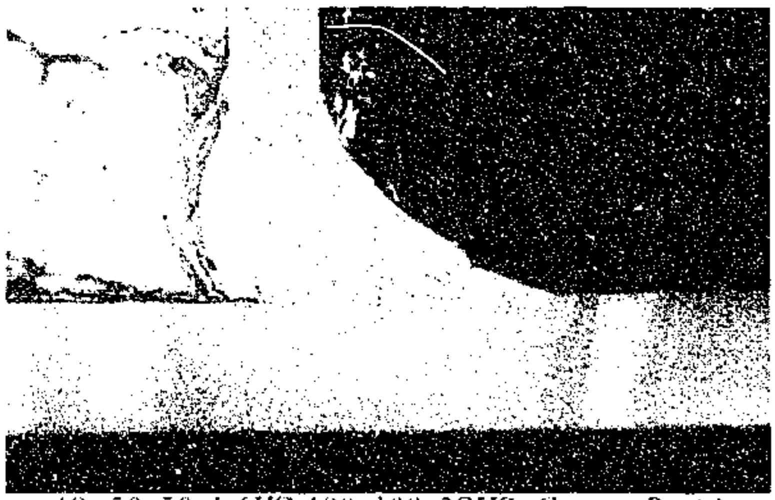

Figure A8: 50x50x1.6HS-100x100x3SHS; Corner Position; TIG

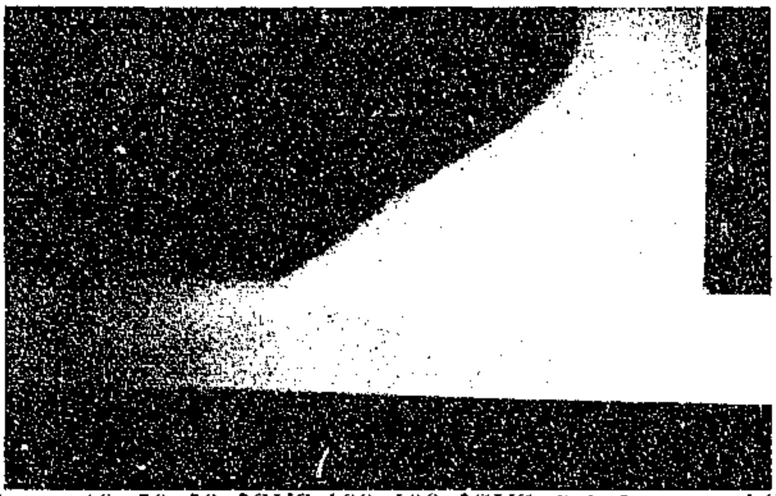

Figure A9: 50x50x3SHS-100x100x3SHS; Side Position; MIG

Figure A10: 50x50x3SHS-100x100x3SHS; Corner Position; MIG

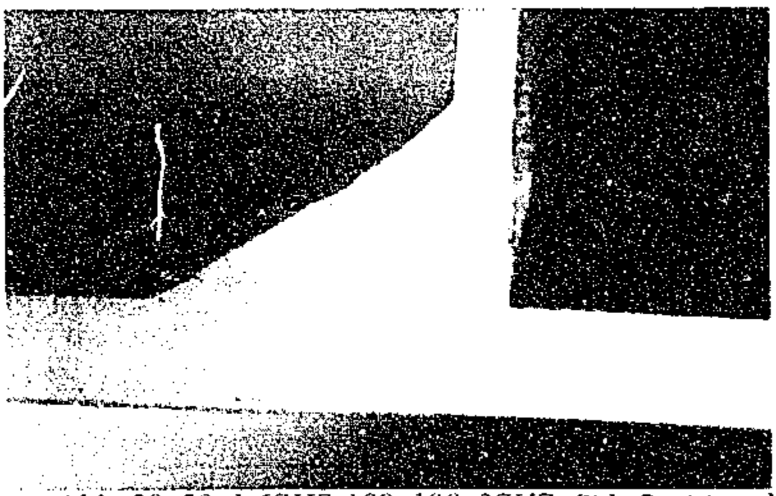

Figure A11: 50x50x1.6SHS-100x100x3SHS; Side Position; MIG

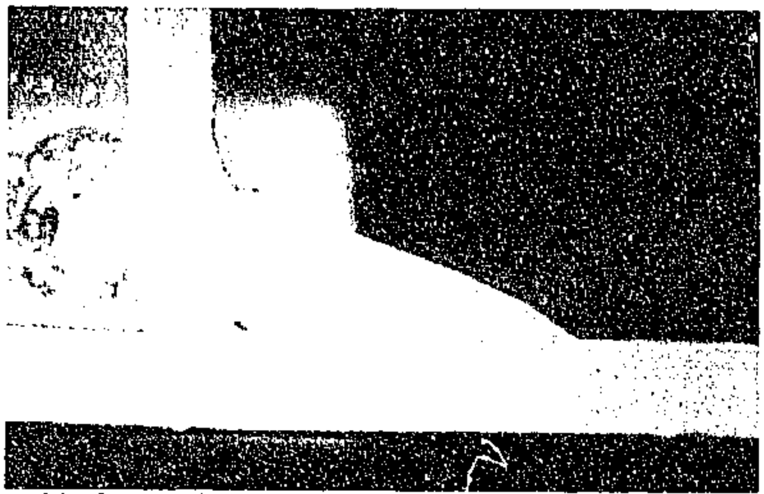
Figure A12: 50x50x1.6SHS-100x100x3SHS; Corner Position; MIG

A.3 DURAGAL C450LO TUBE-TO-PLATE

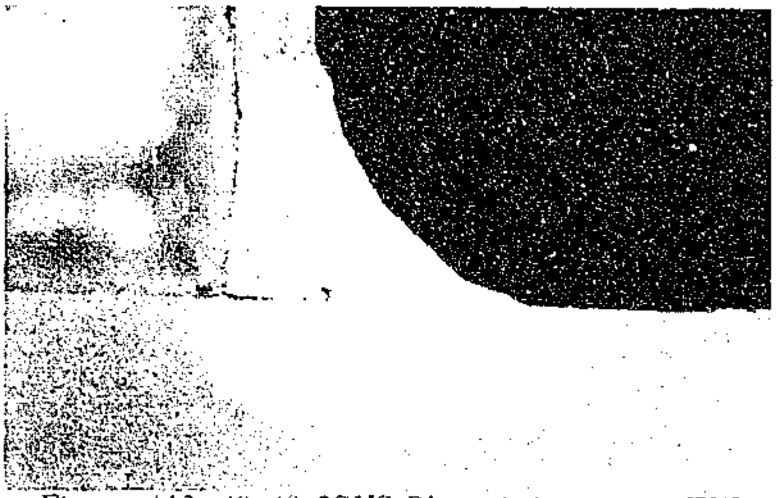
Figure A13: 40x40x2SHS-Plate; Side Position; TIG


Figure A14: 40x40x2SHS-Plate; Corner Position; TIG

Figure A15: 50x50x3SHS-Plate; Side Position; TIG

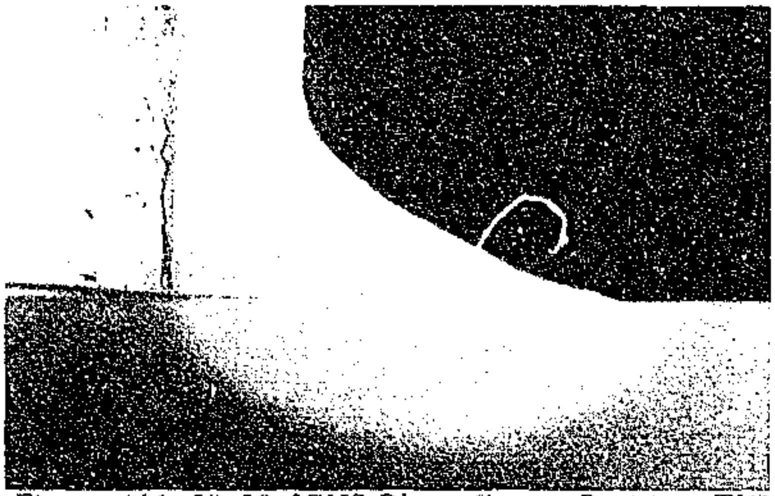

Figure A16: 50x50x3SHS-Plate; Corner Position; TIG

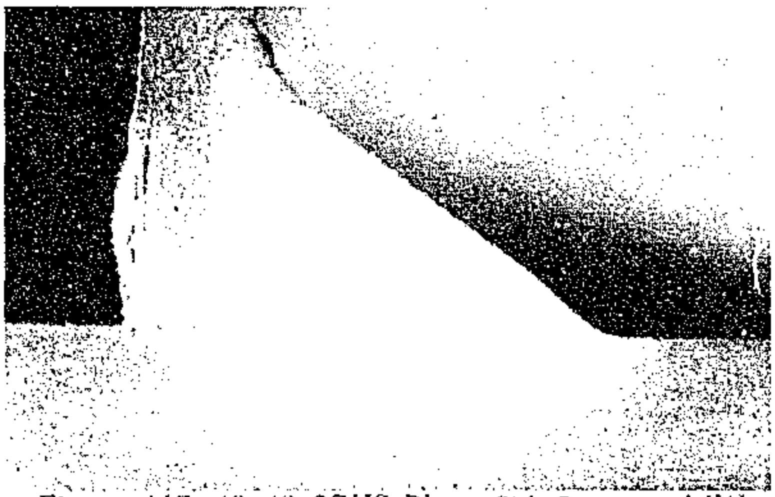

Figure A17: 40x40x2SHS-Plate; Side Position; MIG

Figure A18: 40x40x2SHS-Plate; Corner Position; MIG

Figure A19: 50x50x3SHS-Plate; Side Position; MIG

Figure A20: 50x50x3SHS-Plate; Corner Position; MIG

A.4 GRADE S355JOH TUBE-TO-TUBE

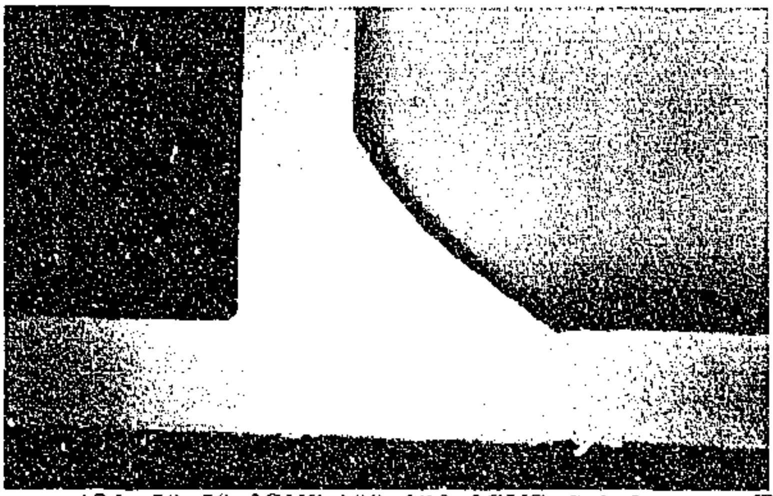

Figure A21: 50x50x3SHS-100x100x3SHS; Side Position; TIG

Figure A22: 50x50x3SHS-100x100x3SHS; Corner Position; TIG

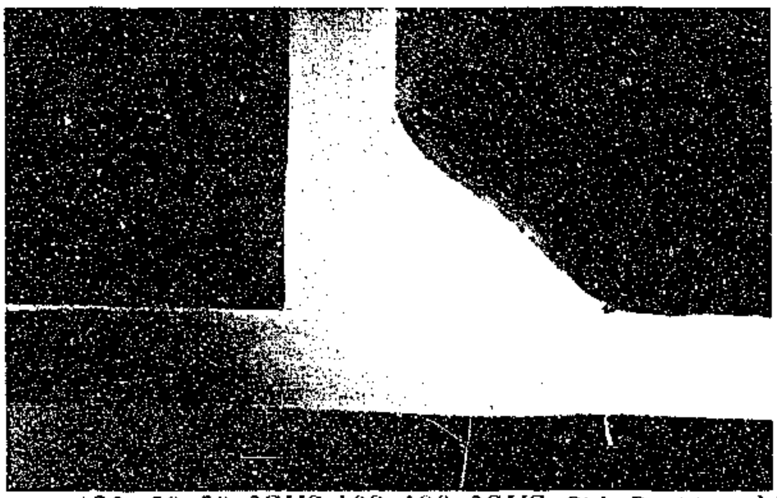

Figure A23: 50x50x3SHS-100x100x3SHS; Side Position; MIG

Figure A24: 50x50x3SHS-100x100x3SHS; Corner Position; MIG

A.5 GRADE S355JOH TUBE-TO-PLATE

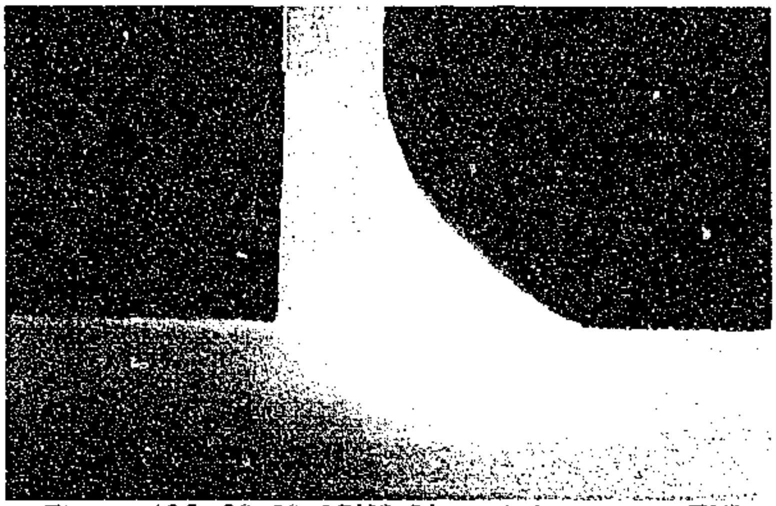

Figure A25: 50x50x3SHS-Plate; Side Position; TIG

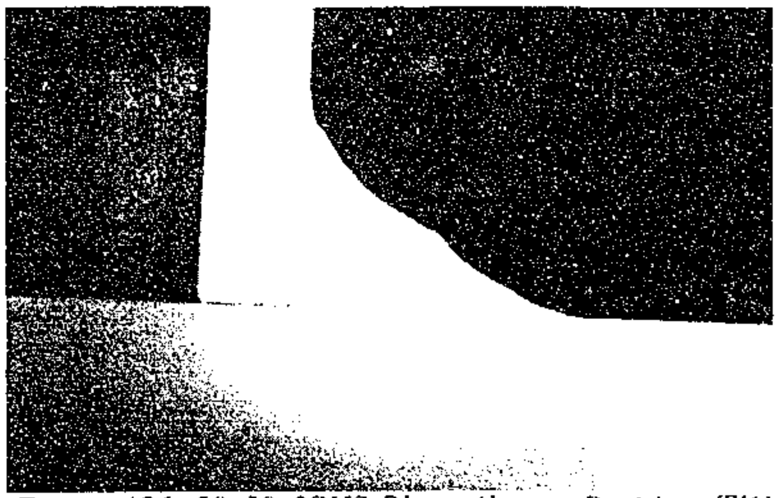

Figure A26: 50x50x3SHS-Plate; Corner Position; TIG

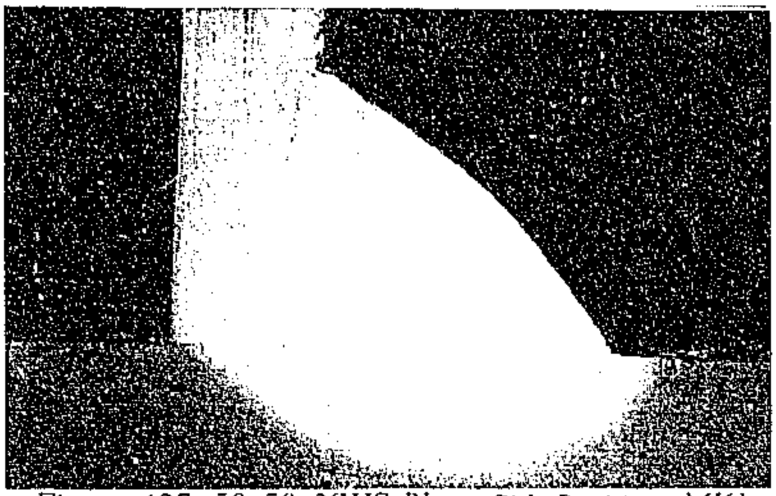

Figure A27: 50x50x3SHS-Plate; Side Position; MIG

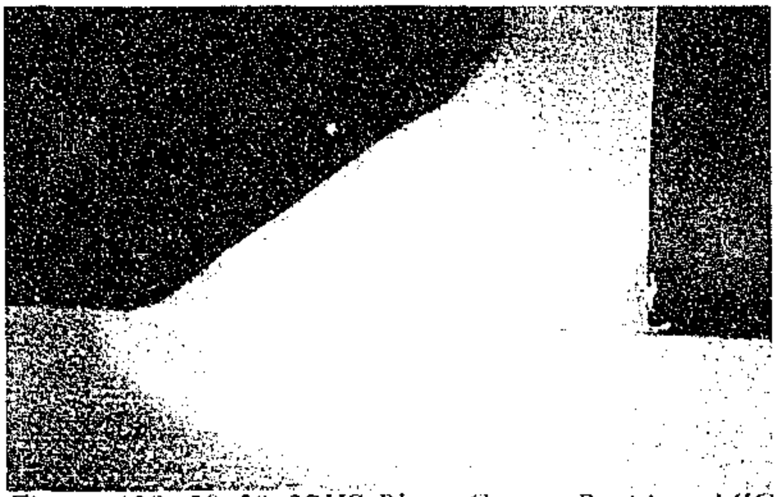

Figure A28: 50x50x3SHS-Plate; Corner Position; MIG

Appendix B

WELD JOINT HARDNESS PLOTS

B.1 DURAGAL C450LO TUBE-TO-PLATE

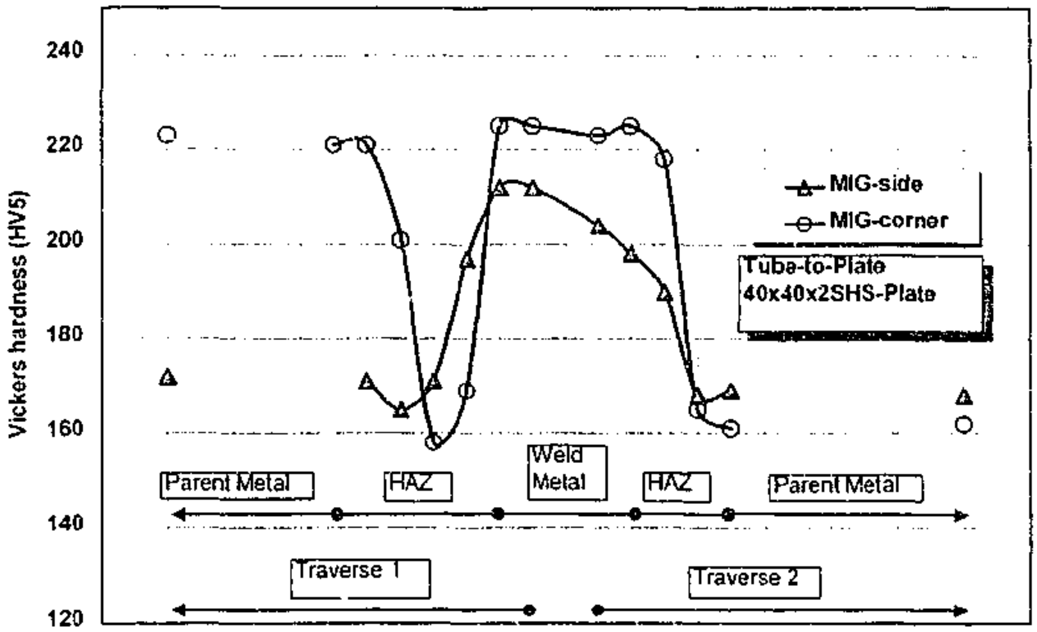

Figure B1: *Plot of hardness traverse values (40x40x2SHS-Plate: MIG welding) DuraGal Steel C450LO*

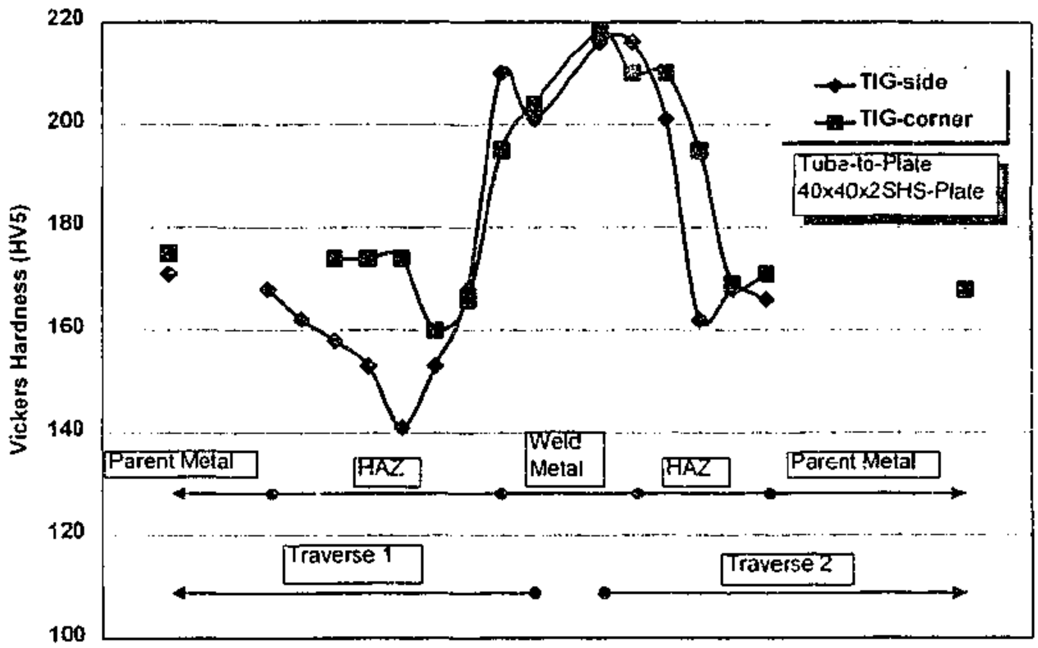

Figure B2: *Plot of hardness traverse values (40x40x2SHS-Plate: TIG welding) DuraGal Steel C450LO*

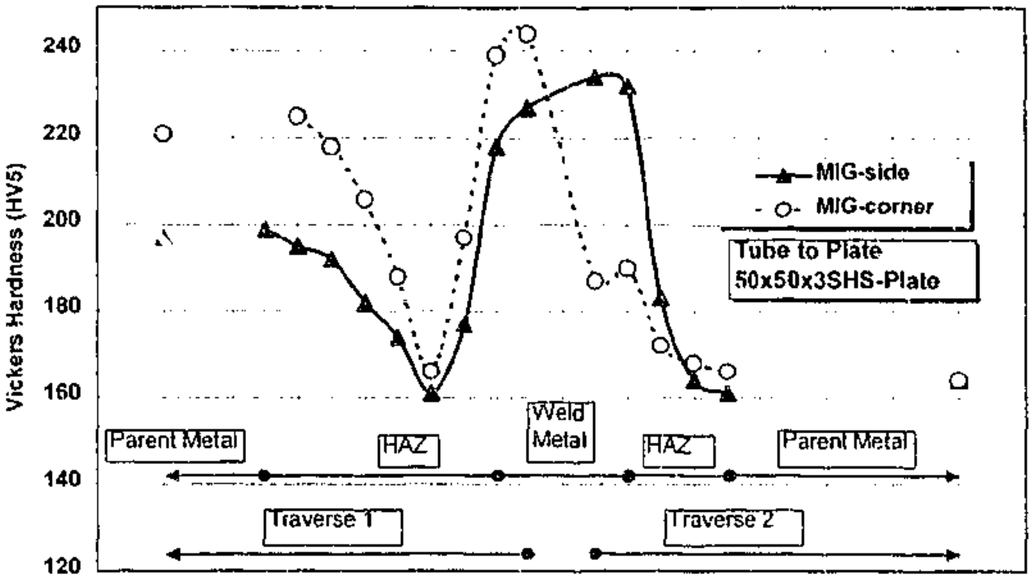

Figure B3: Plot of hardness traverse values (50x50x3SHS-Plate; MIG welding) DuraGal Steel C450LO

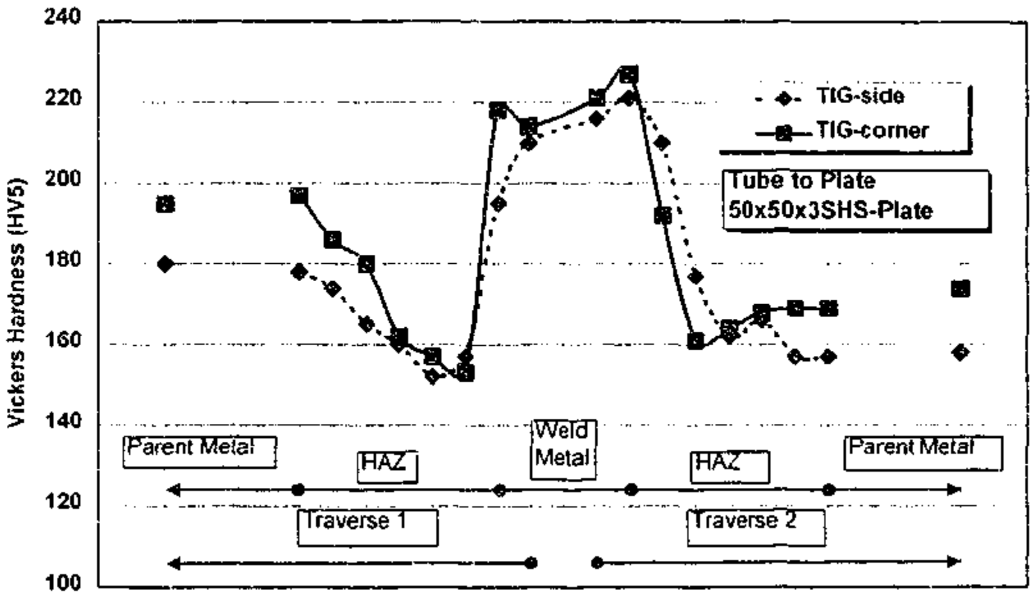

Figure B4: Plot of hardness traverse values (50x50x3HS-Plate; TIG welding) DuraGal Steel C450LO

B.2 DURAGAL C450LO TUBE-TO-TUBE

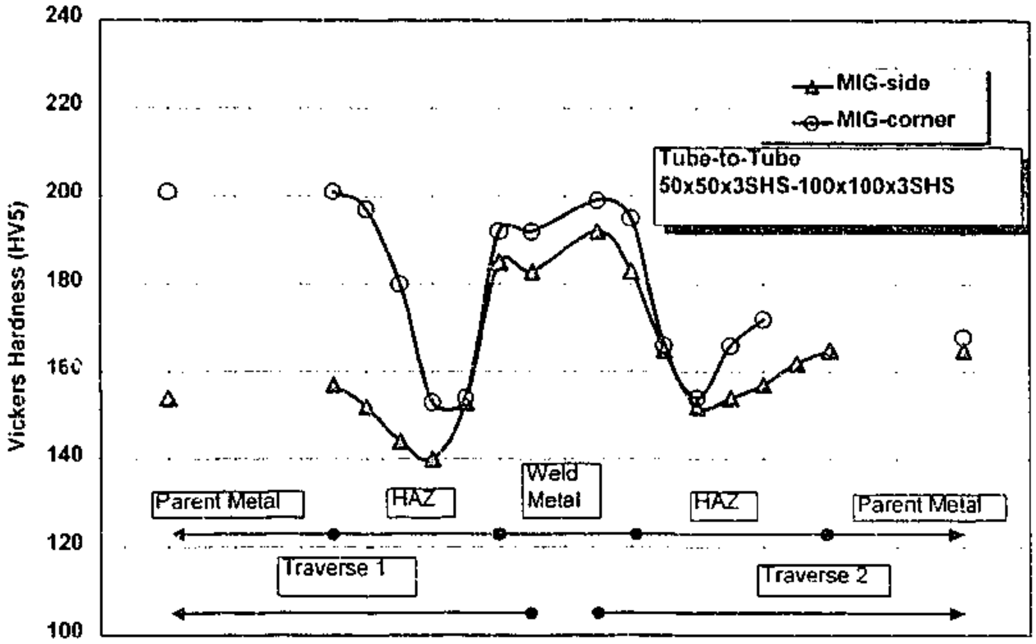

Figure B5: Plot of hardness traverse values (50x50x3SHS-100x100x3SHS; MIG welding) DuraGal Steel C450LO

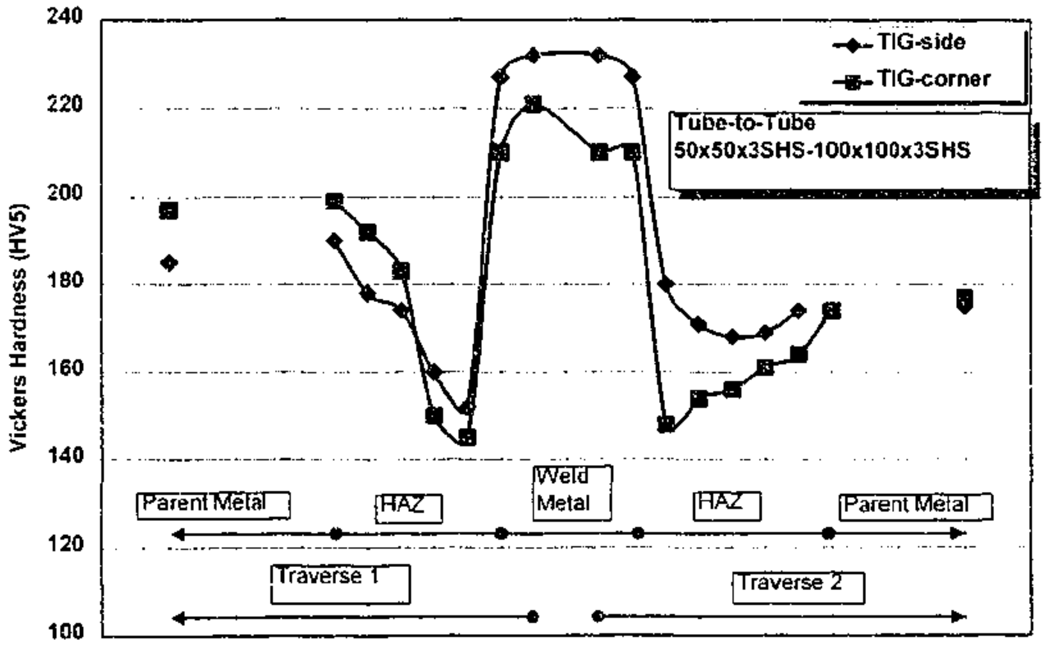

Figure B6: Plot of hardness traverse values (50x50x3SHS-100x100x3SHS; TIG welding) DuraGal Steel C450LO

B.2 DURAGAL C450LO TUBE-TO-TUBE

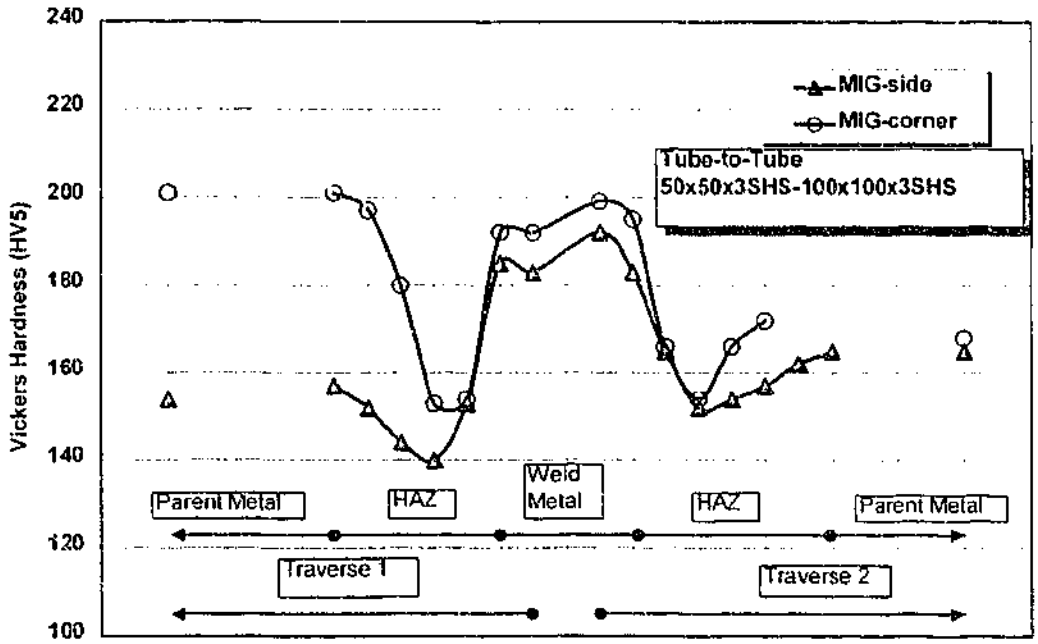

Figure B5: Plot of hardness traverse values (50x50x3SHS-100x100x3SHS; MIG welding) DuraGal Steel C450LO

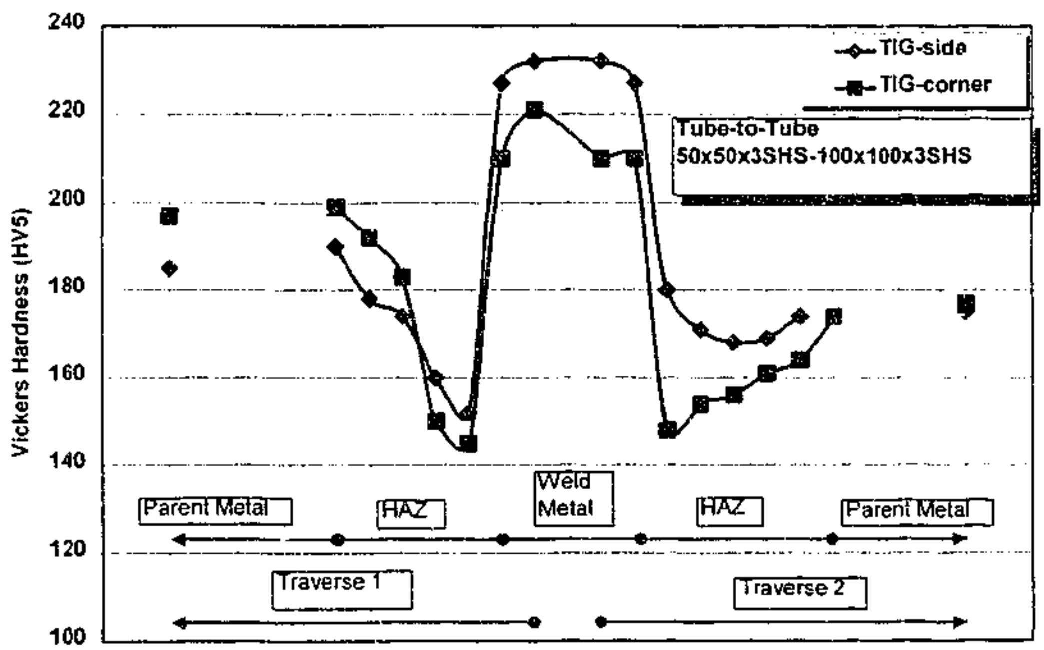

Figure B6: Plot of hardness traverse values (50x50x3SHS-100x100x3SHS; TIG welding) DuraGal Steel C450LO

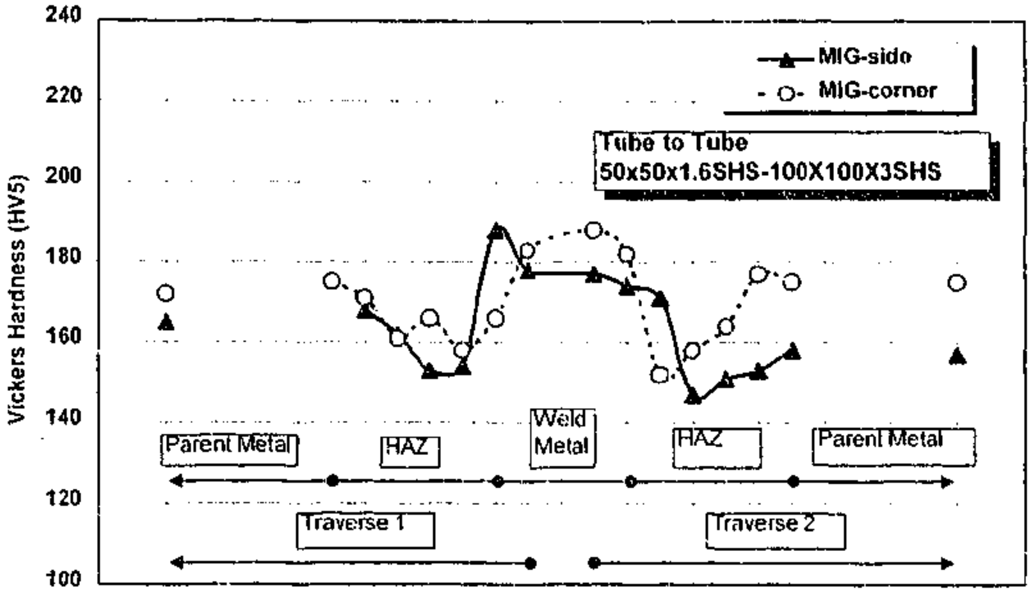

Figure B7: Plot of hardness traverse values (50x50x1.6SHS-100x100x3SHS; MIG welding) DuraGal Steel C450LO

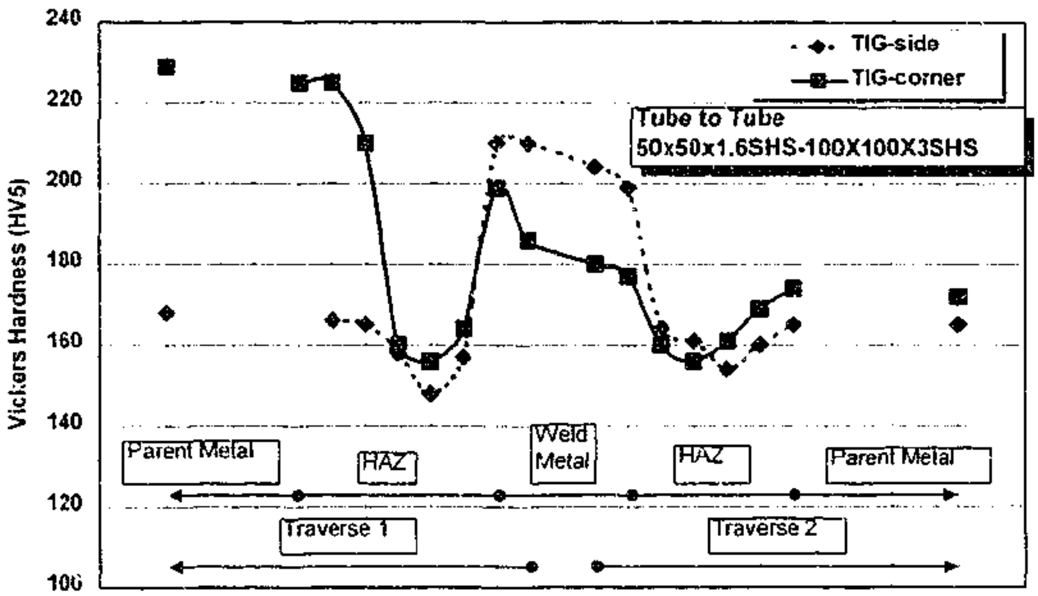

Figure B8: Plot of hardness traverse values (50x50x1.6SHS-100x100x3SHS; TIG welding) DuraGal Steel C450LO

B.3 S355JOH TUBE-TO-PLATE

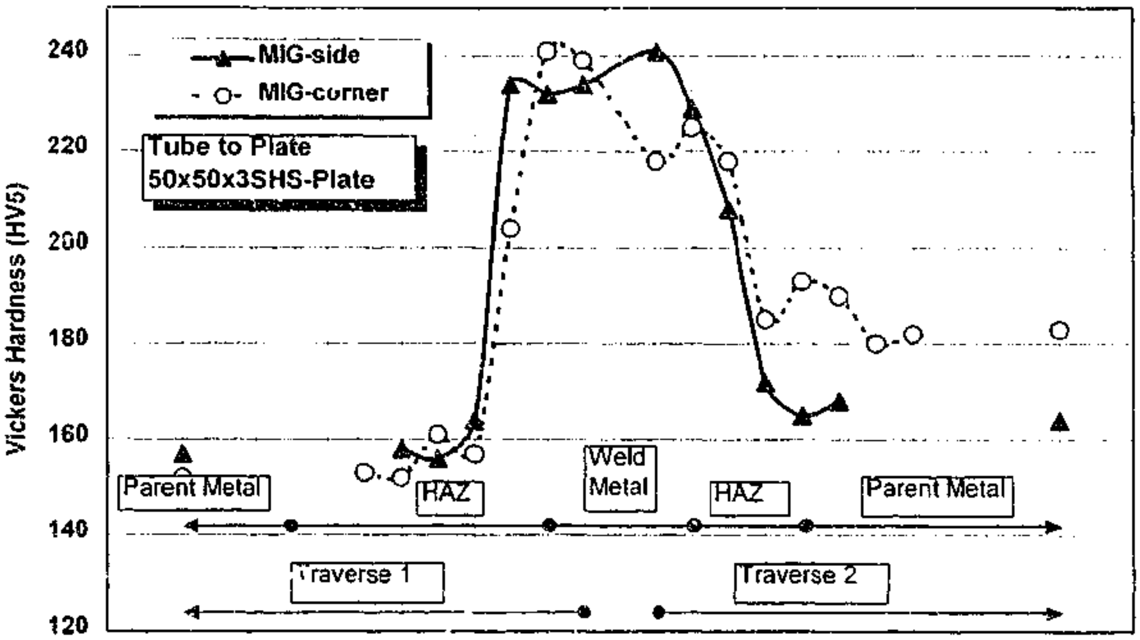

Figure B9: Plot of hardness traverse values (50x50x3SHS-Plate; S355JOH; MIG welding)

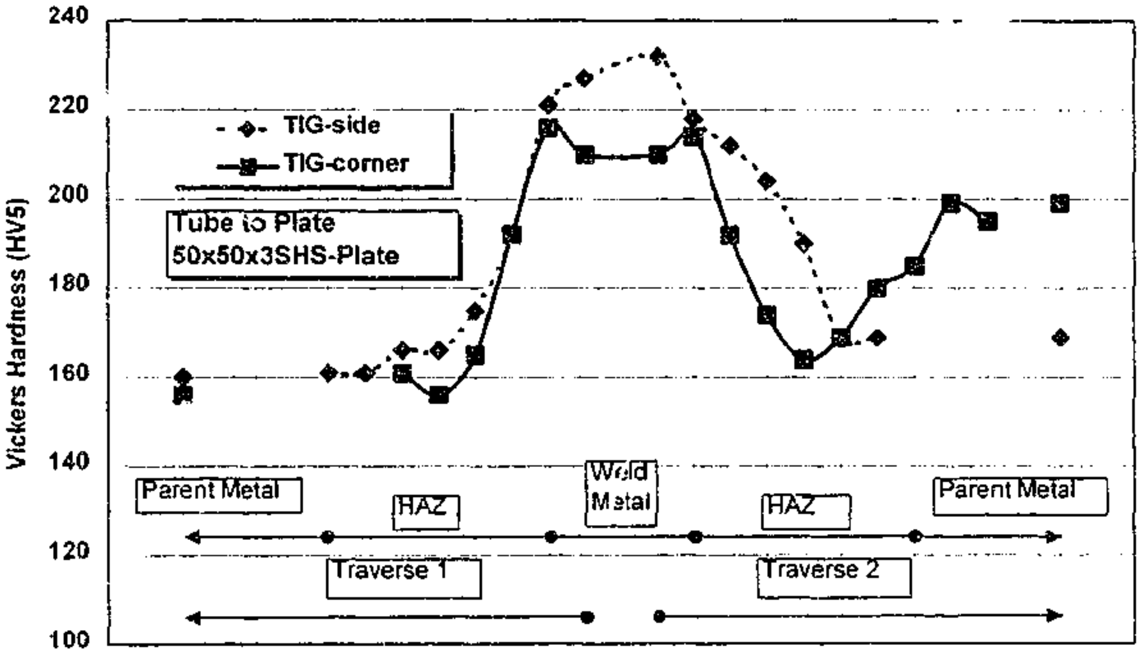

Figure B10: Plot of hardness traverse values (50x50x3SHS-Plate; S355JOH; TIG welding)

B.4 S355JOH TUBE-TO-TUBE

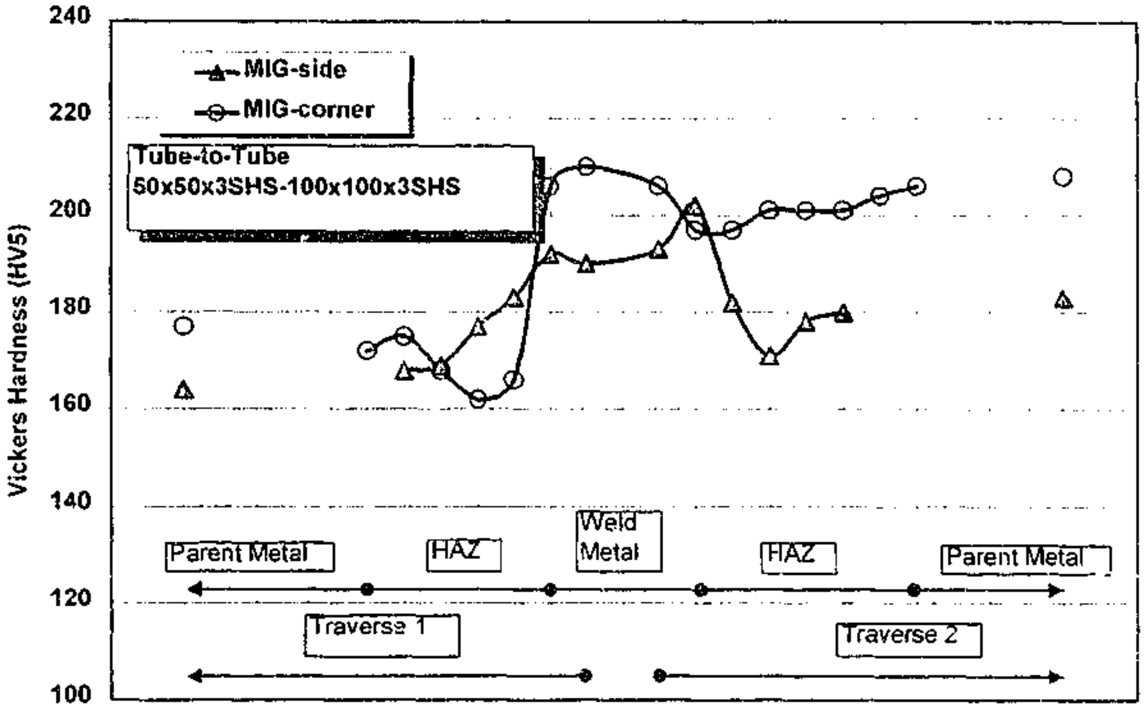

Figure B11: Plot of hardness traverse values (50x50x3SHS-100x100x3SHS; S355JOH; MIG welding)

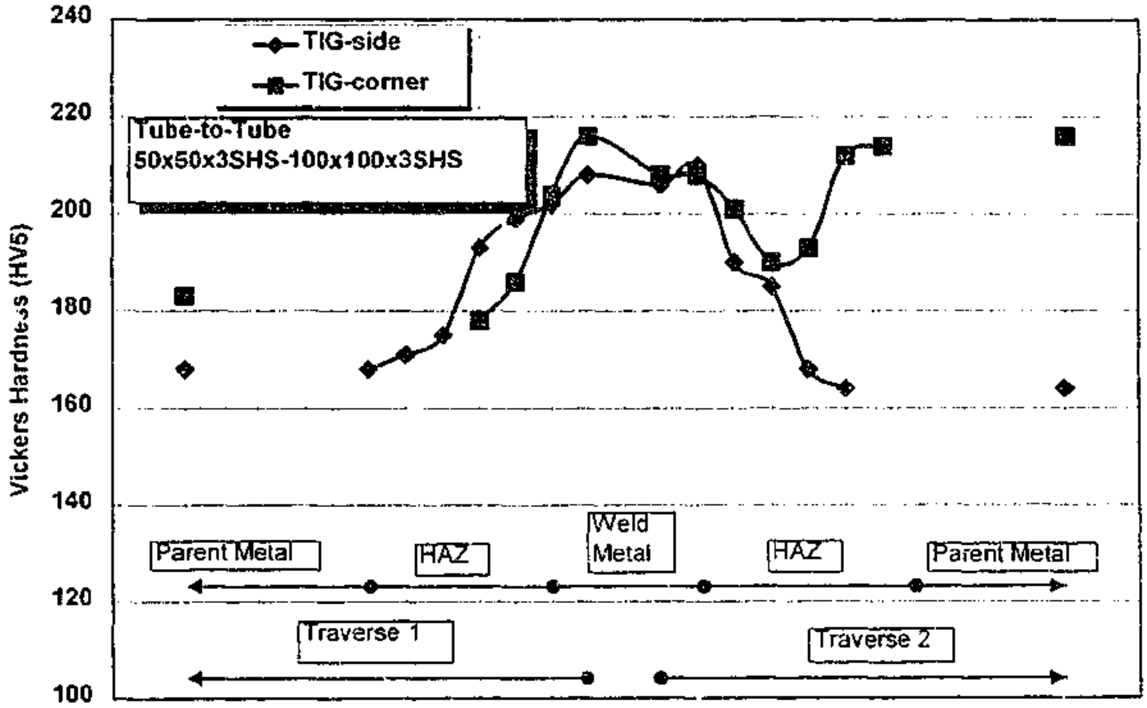

Figure B12: Plot of hardness traverse values (50x50x3SHS-100x100x3SHS; S355JOH; TIG welding)

Appendix C:
MOMENT-DEFLECTION AND MOMENT-ANGLE OF INCLINATION GRAPHS

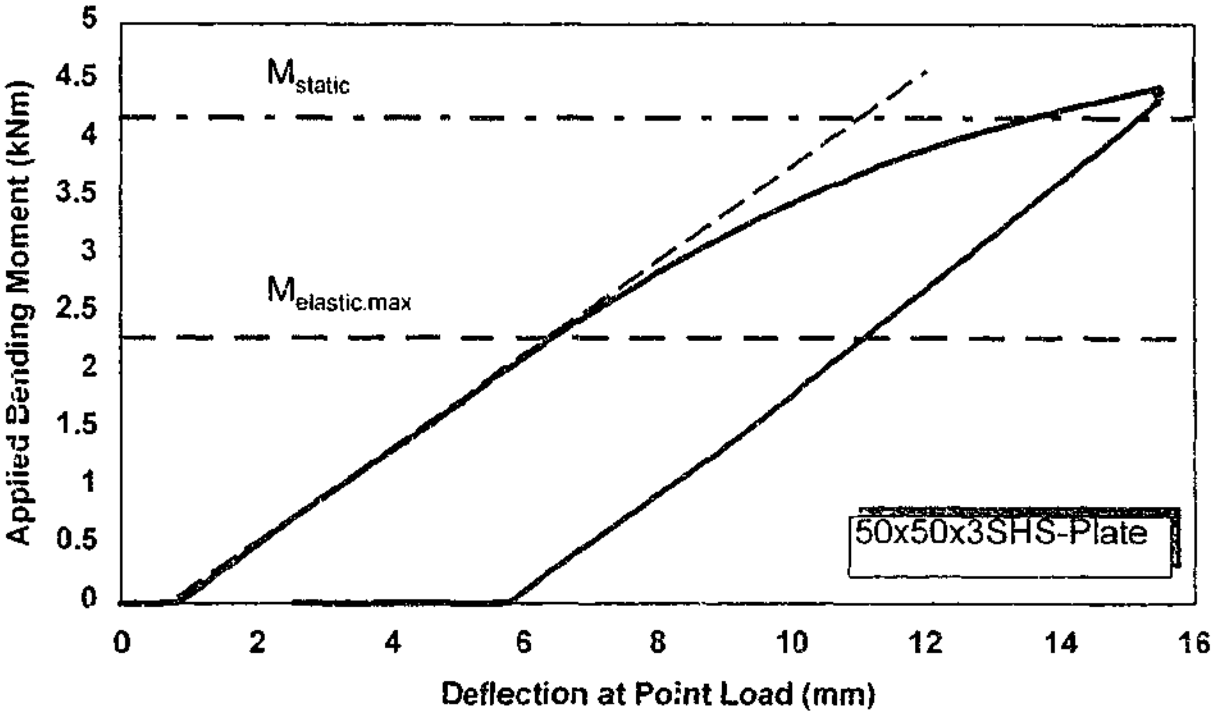

Figure C1: Moment-deflection graph, tube-to-plate joint, 50x50x3SHS-Plate

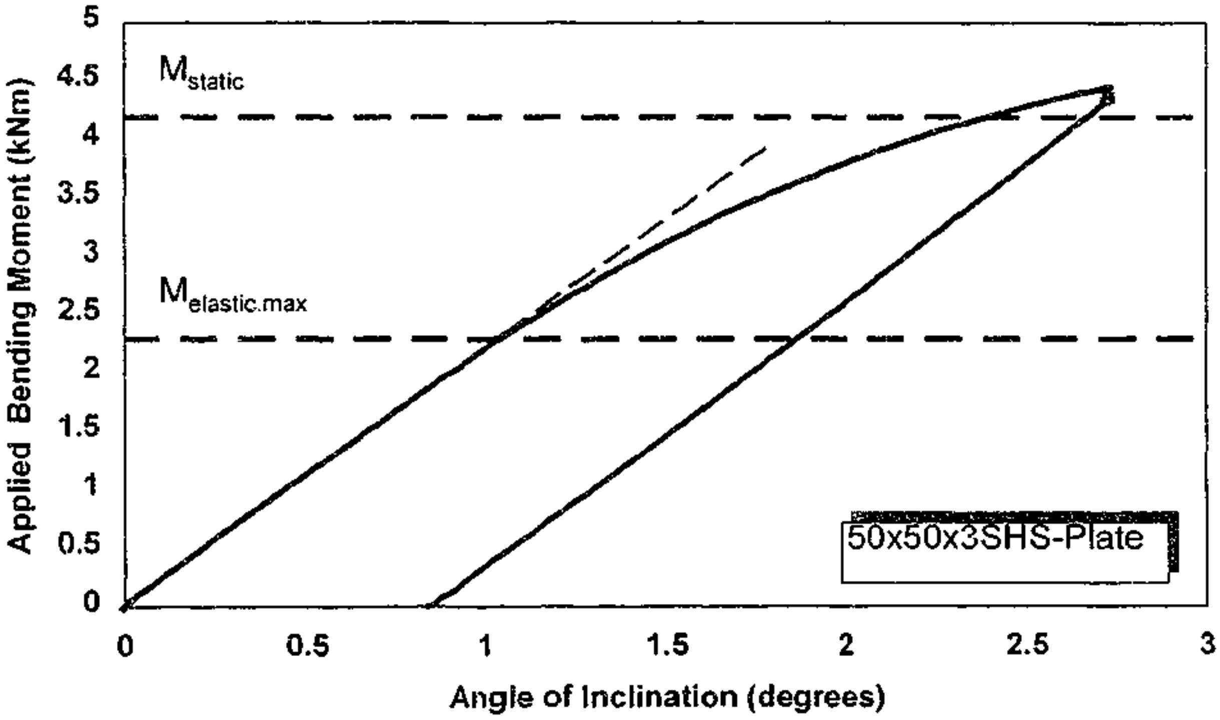

Figure C2: Moment-angle of inclination graph, tube-to-plate joint, 50x50x3SHS-Plate

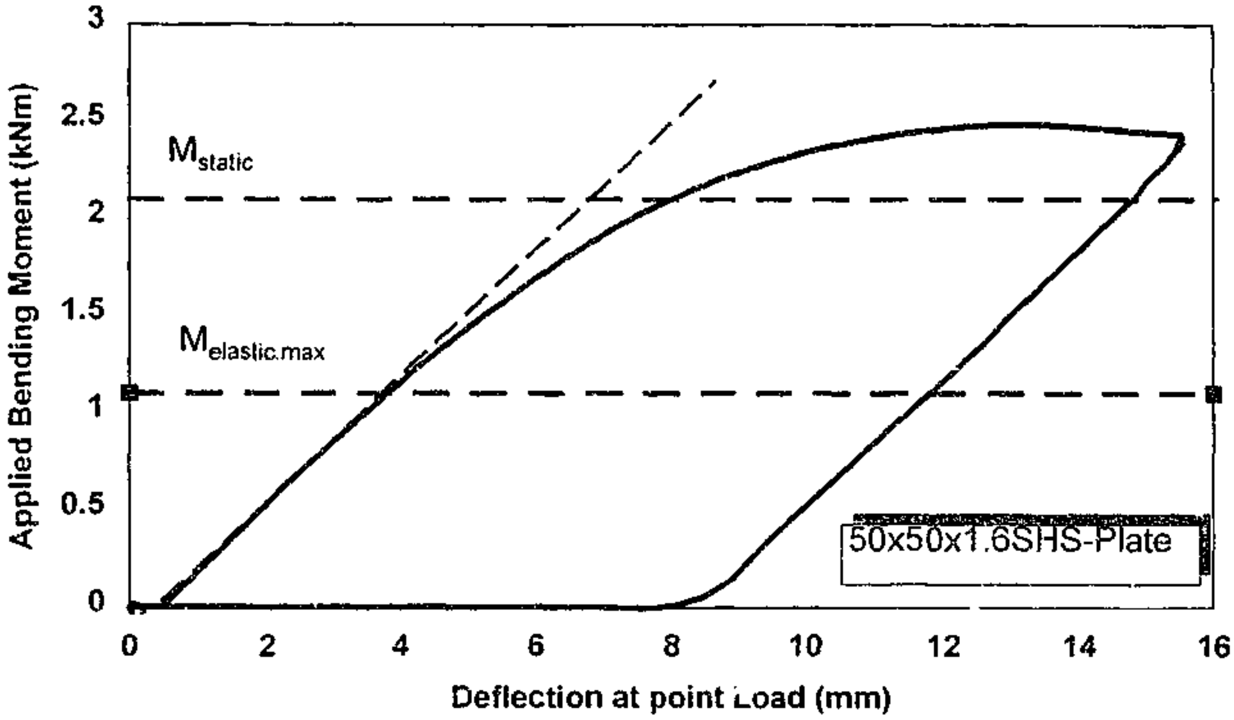

Figure C3: Moment-deflection graph, tube-to-plate joint, 50x50x1.6SHS-Plate

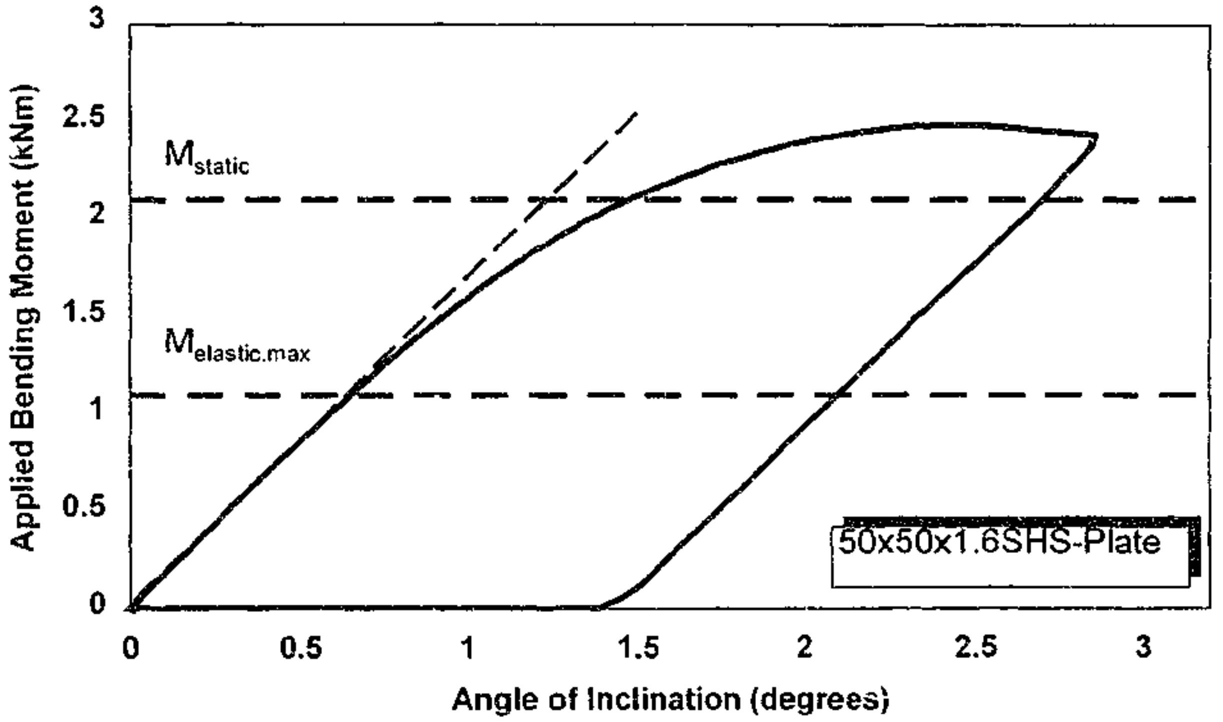

Figure C4: Moment-angle of inclination graph, tube-to-plate joint, 50x50x1.6SHS-Plate

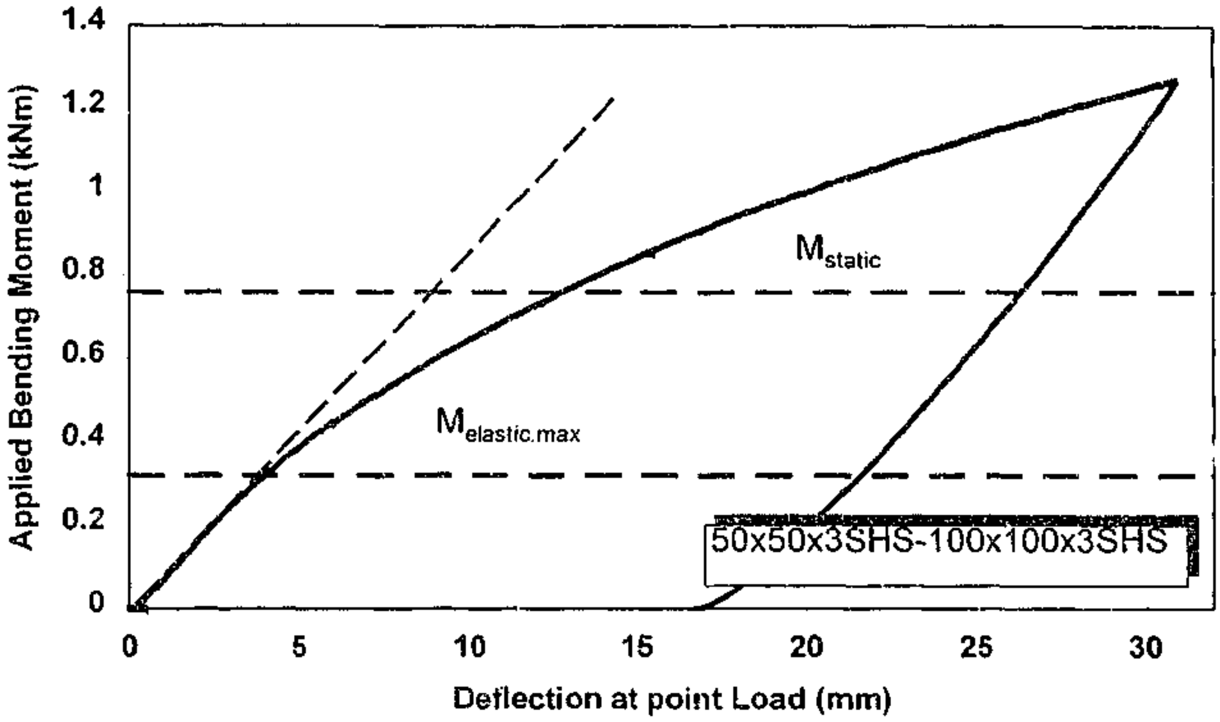

Figure C5: Moment-deflection graph, tube-to-tube joint, 50x50x3SHS-100x100x3SHS

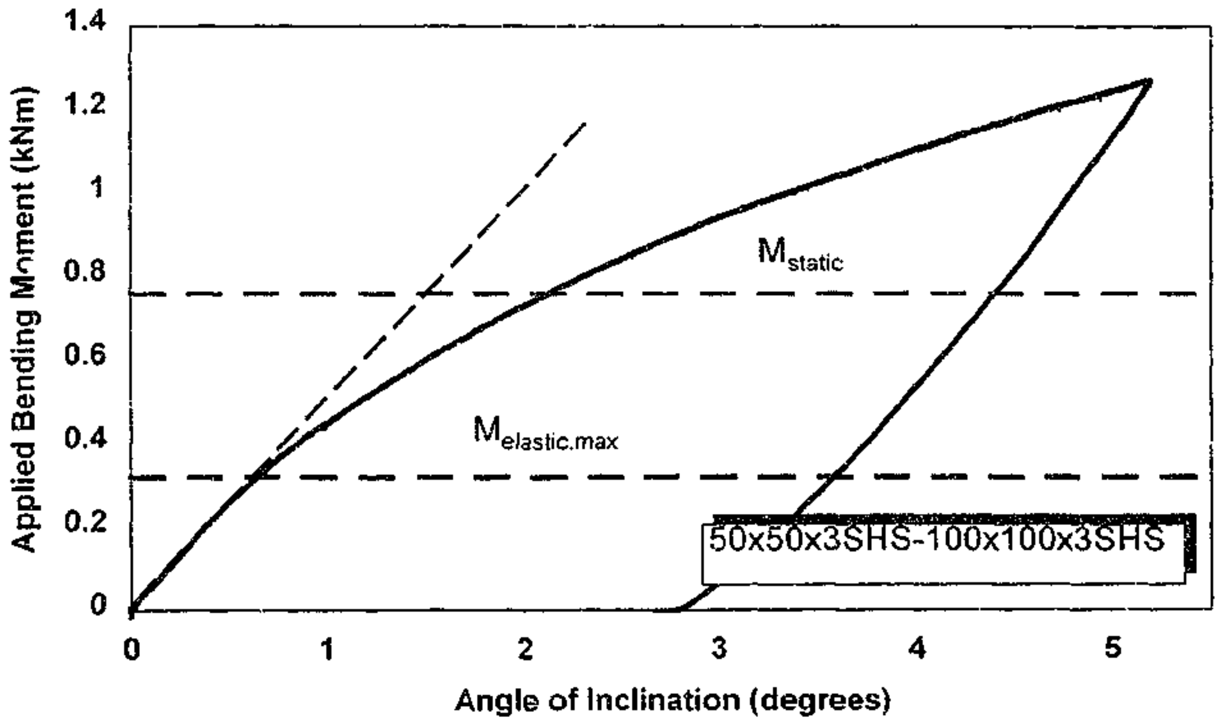

Figure C6: Moment-angle of inclination graph, tube-to-tube joint, 50x50x3SHS-100x100x3SHS

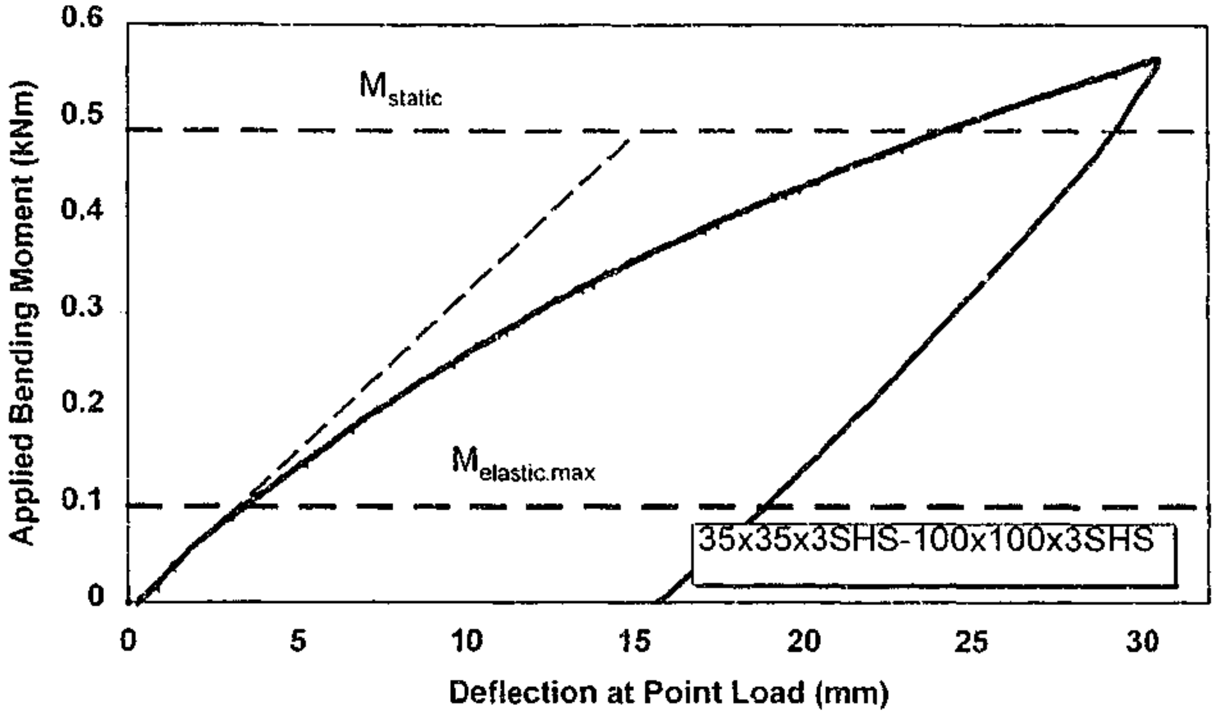

Figure C7: Moment-deflection graph, tube-to-tube joint, 35x35x3SHS-100x100x3SHS

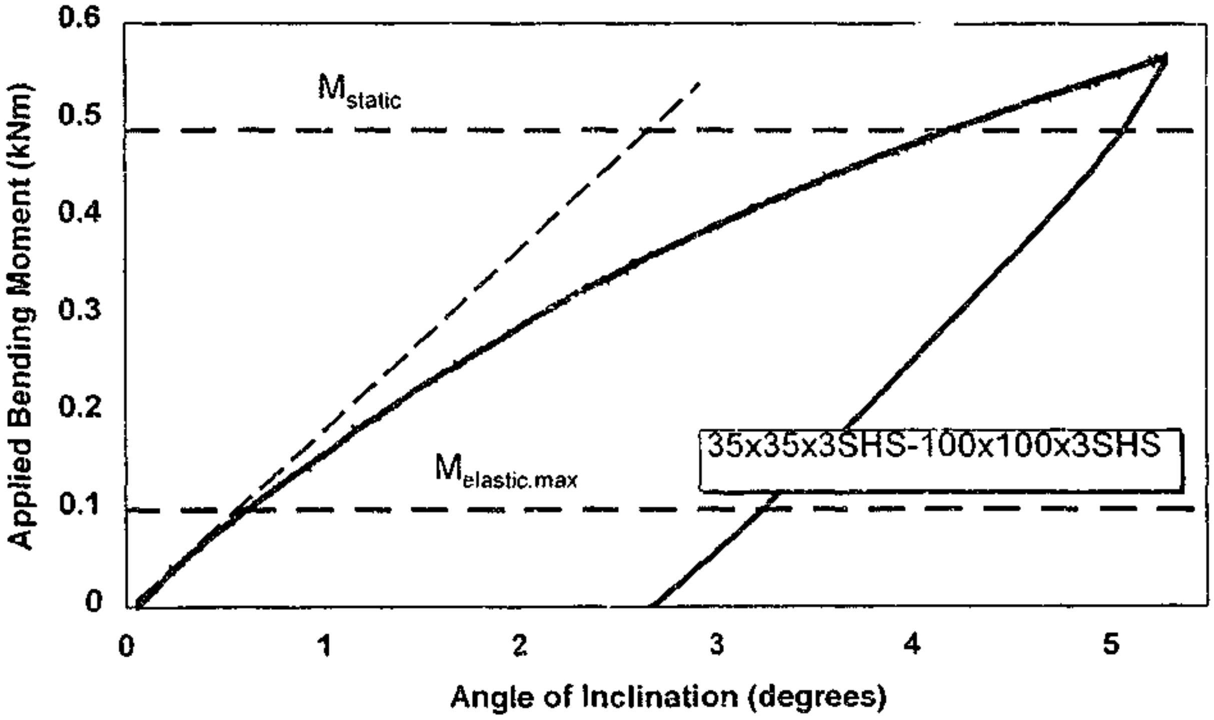

Figure C8: Moment-angle of inclination graph, tube-to-tube joint, 35x35x3SHS-100x100x3SHS

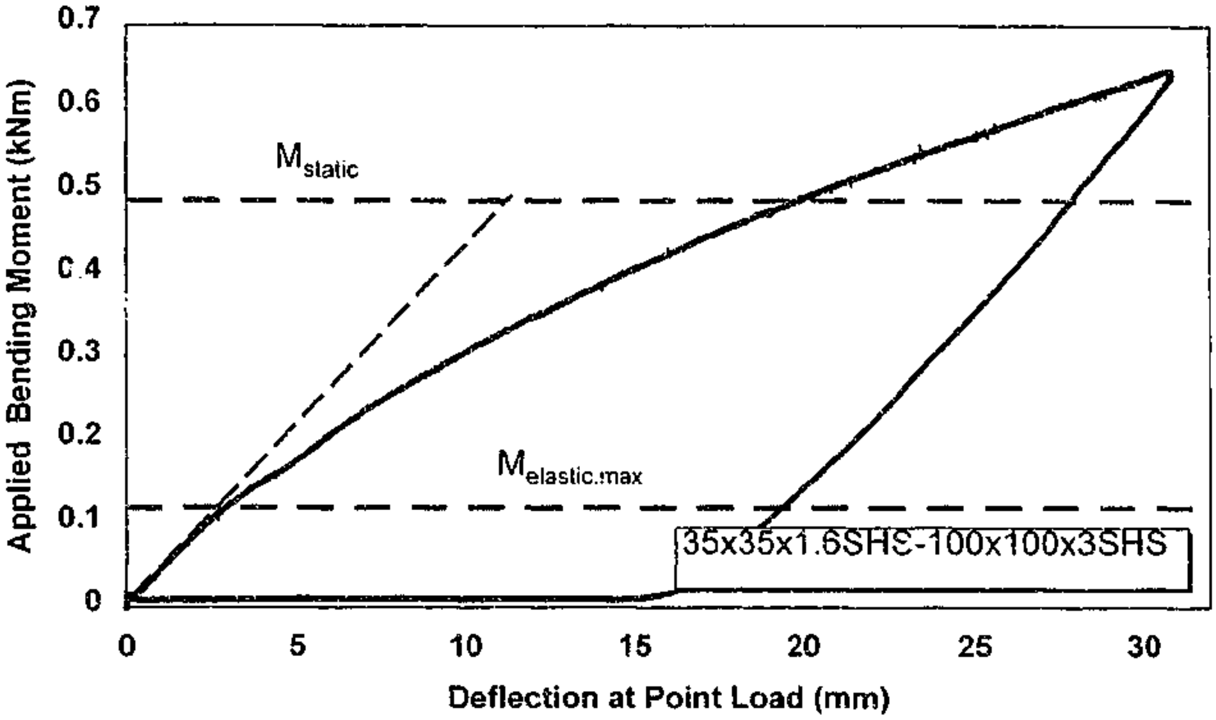

Figure C9: Moment-deflection graph, tube-to-tube joint, 35x35x1.6SHS-100x100x3SHS

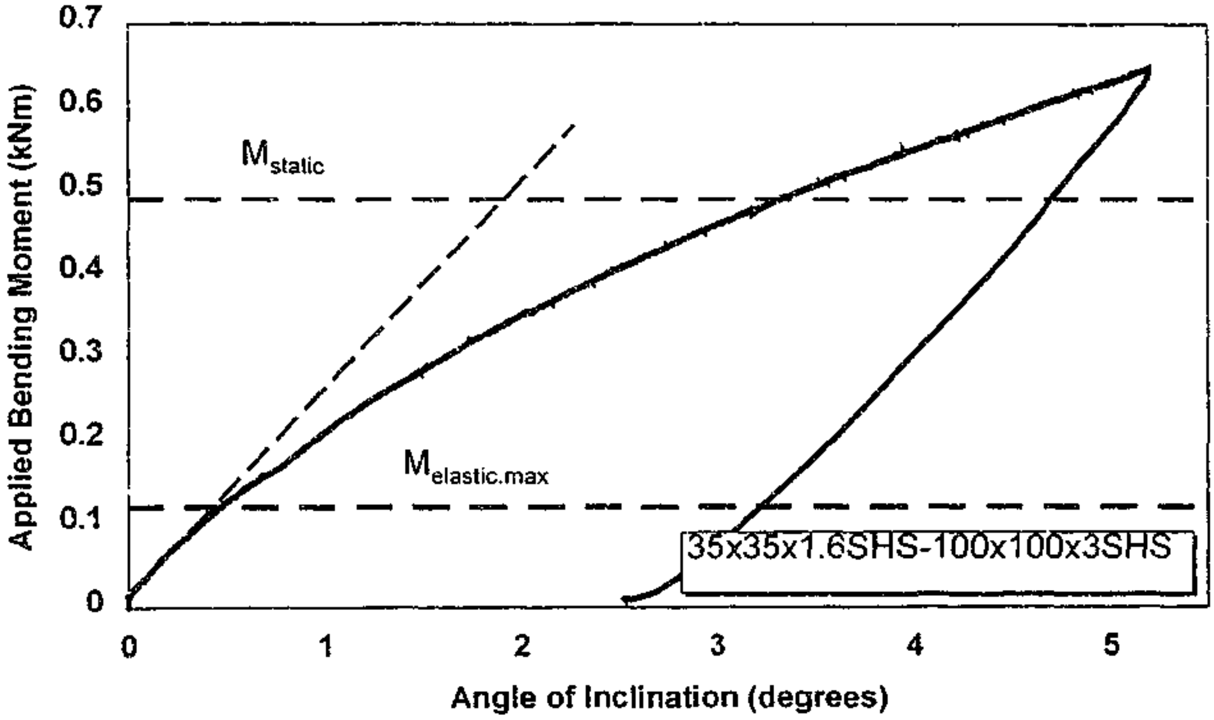

Figure C10: Moment-angle of inclination graph, tube-to-tube joint, 35x35x1.6SHS-100x100x3SHS

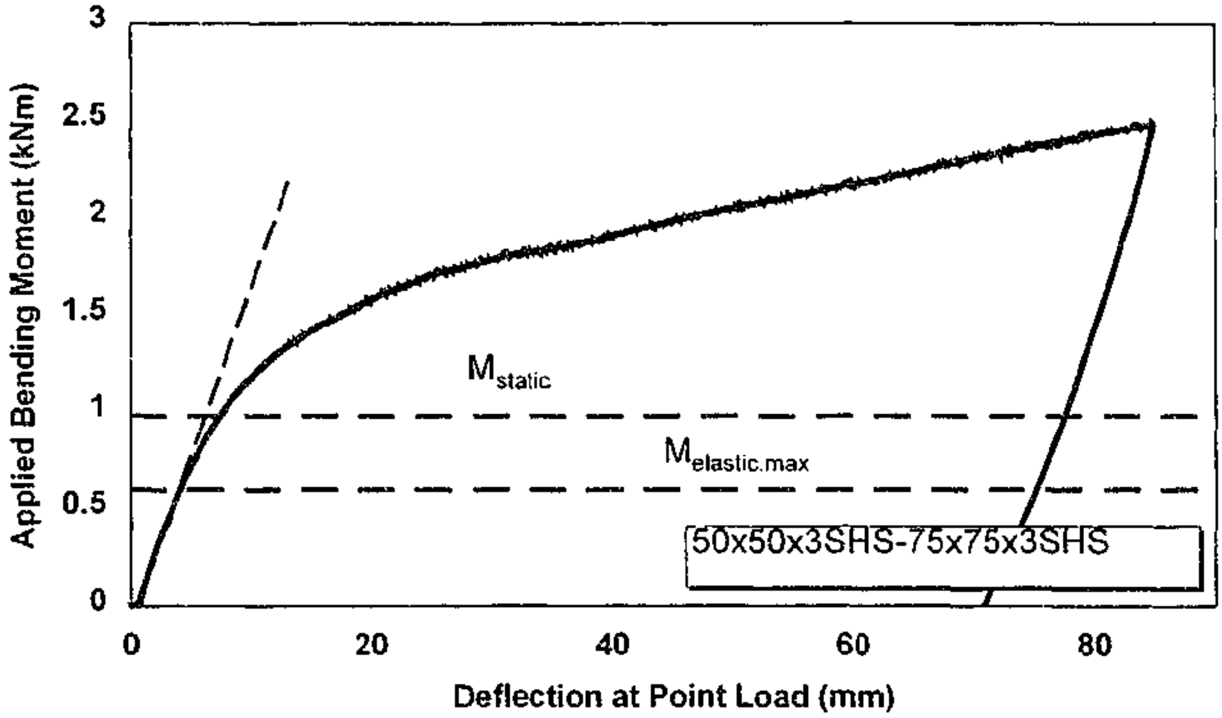

Figure C11: Moment-deflection graph, tube-to-tube joint, 50x50x3SHS-75x75x3SHS

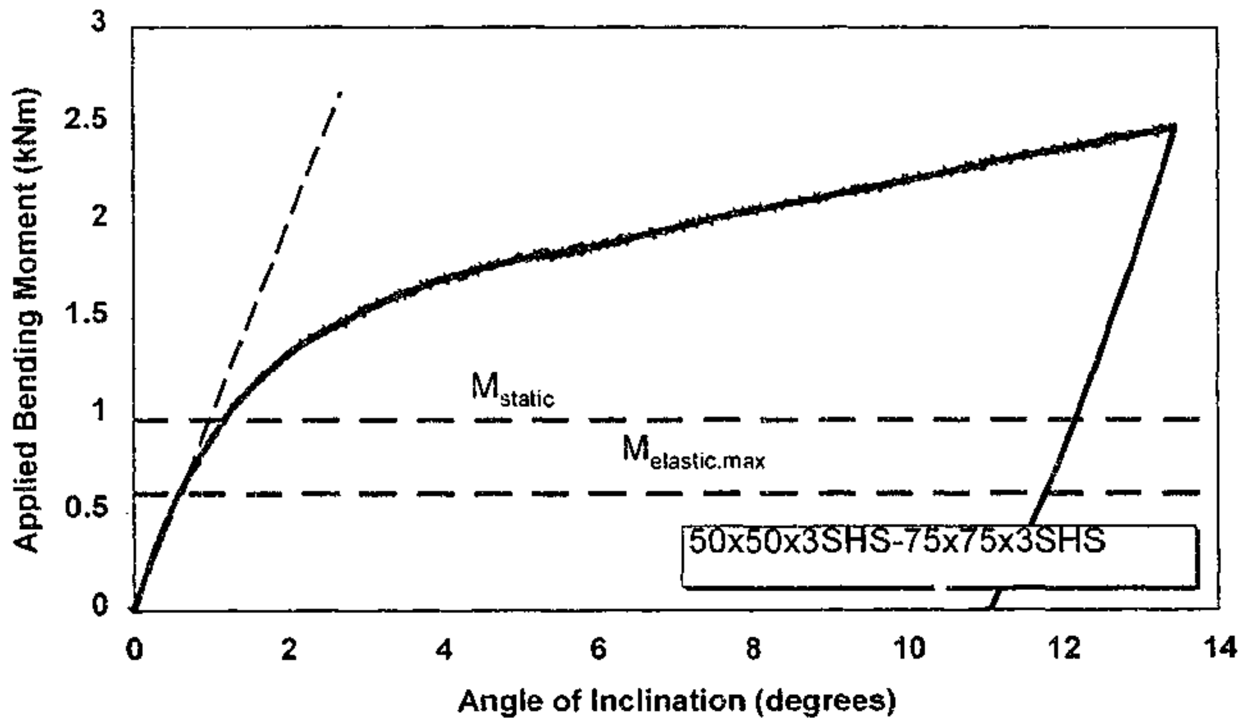

Figure C12: Moment-angle of inclination graph, tube-to-tube joint, 50x50x3SHS-75x75x3SHS

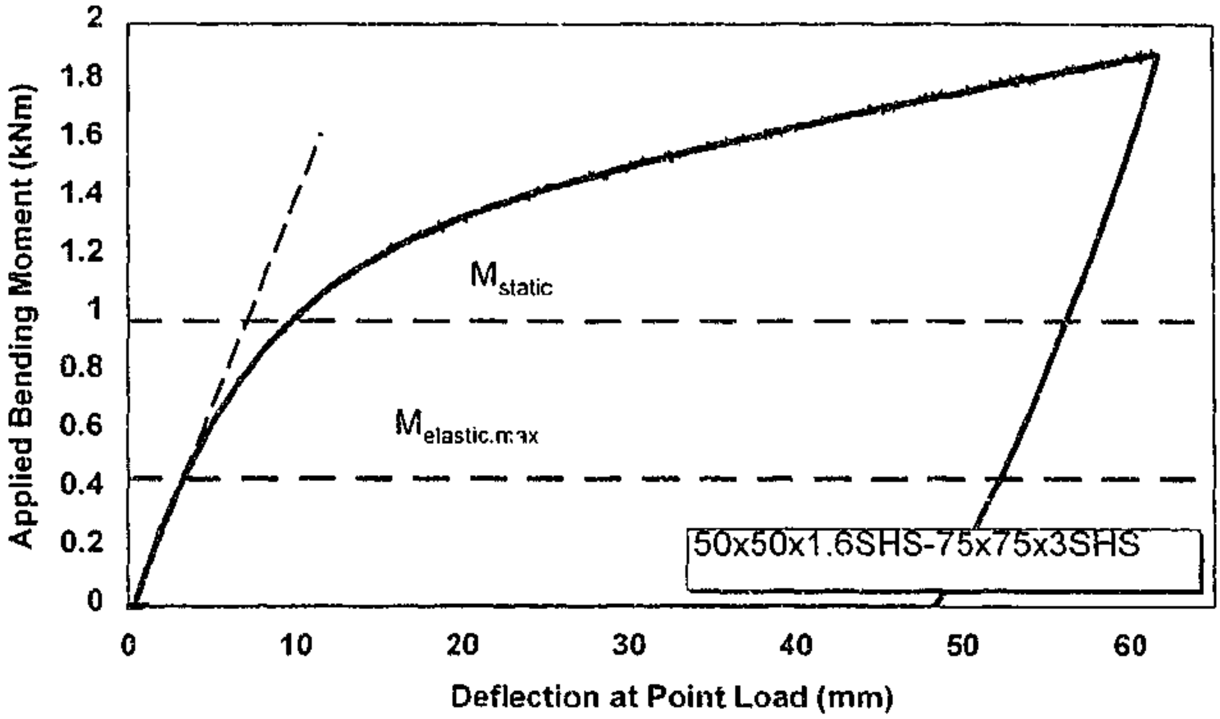

Figure C13: Moment-deflection graph, tube-to-tube joint, 50x50x1.6SHS-75x75x3SHS

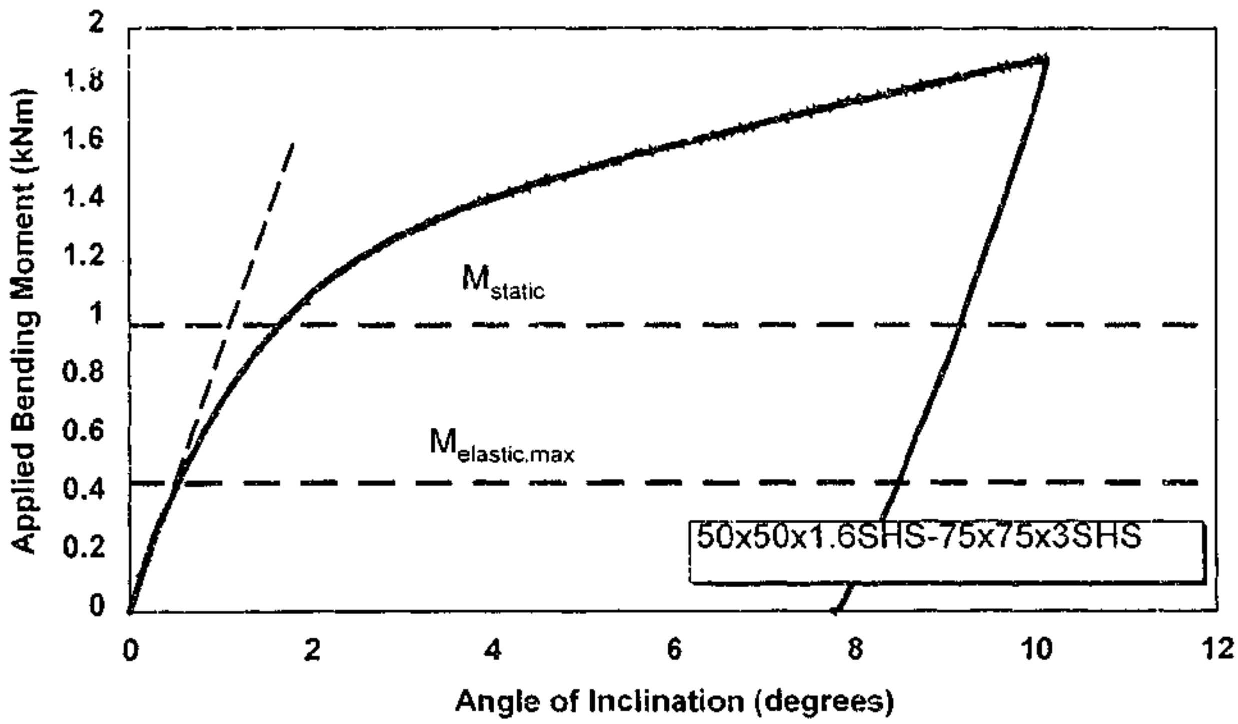

Figure C14: Moment-angle of inclination graph, tube-to-tube joint, 50x50x1.6SHS-75x75x3SHS

Appendix D
POSITIONS OF STRAIN GAUGES FOR SCF

D1: TUBE-TO-PLATE JOINTS

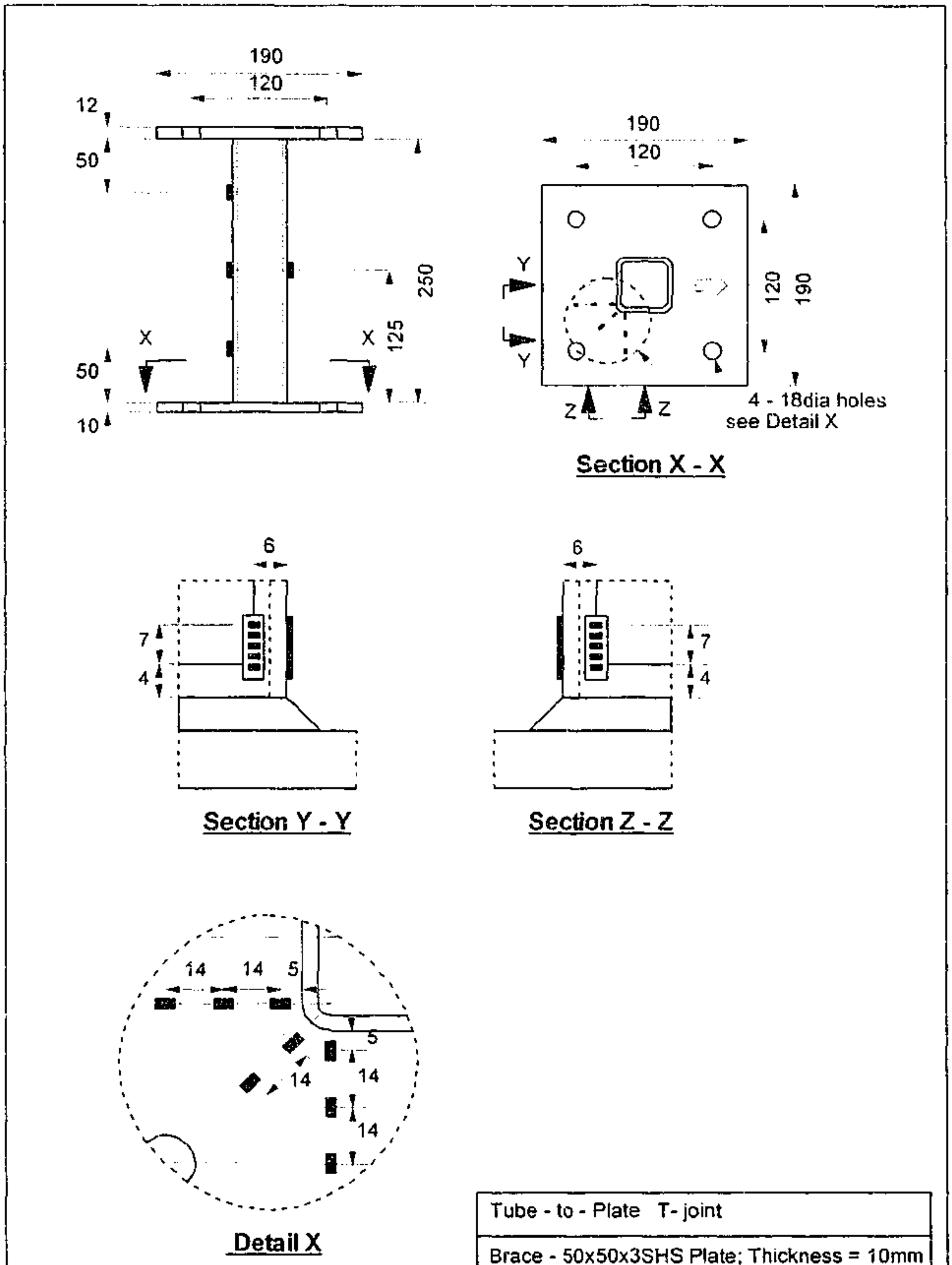

Tube - to - Plate T- joint	
Brace - 50x50x3SHS Plate; Thickness = 10mm	

Figure D1: Positions of Strain Gauges; 50x50x3SHS-Plate, S1PL2R2B

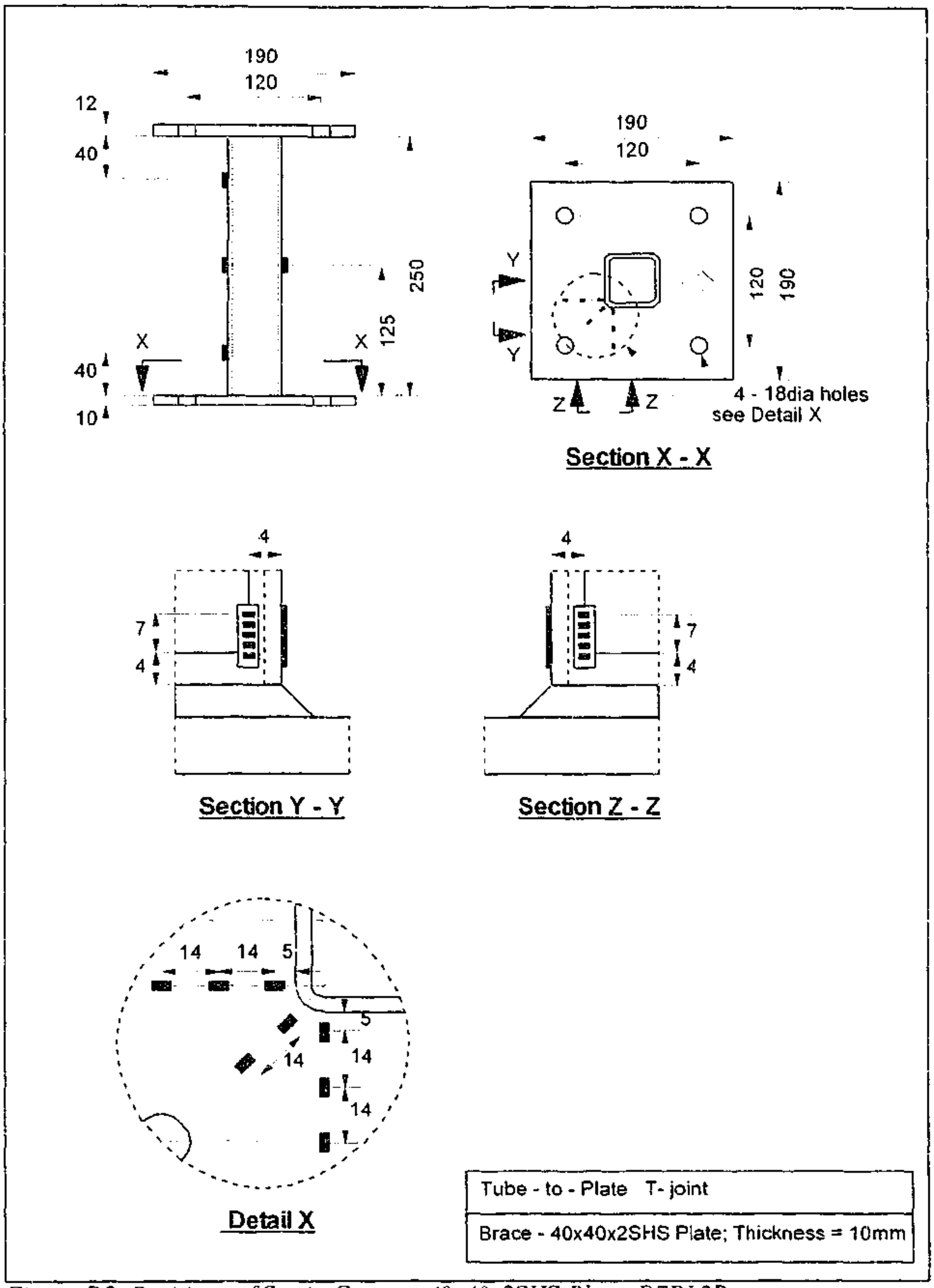

Figure D2: Positions of Strain Gauges; 40x40x2SHS-Plate, D7PL2B

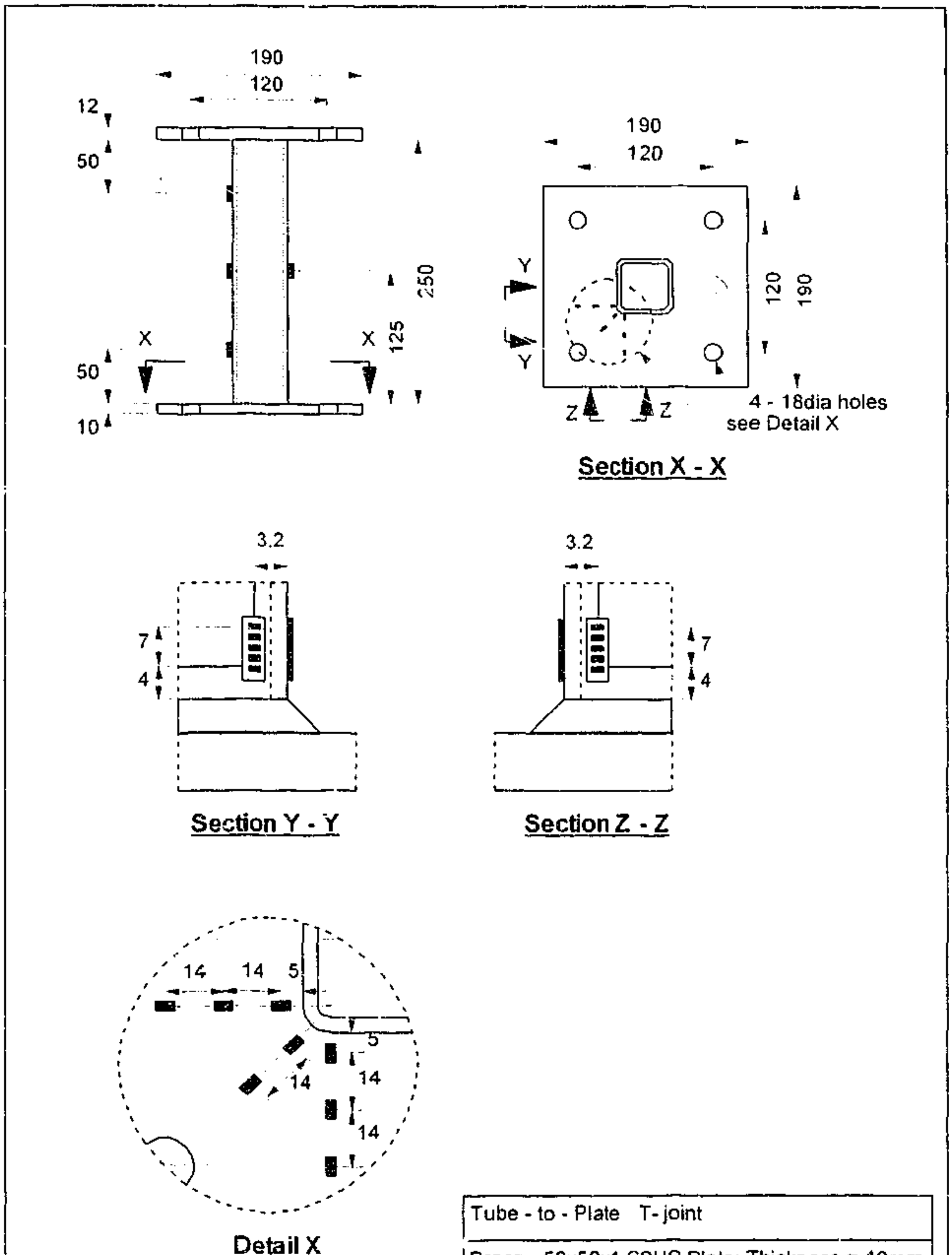

Tube - to - Plate T-joint
Brace - 50x50x1.6SHS Plate; Thickness = 10mm

Figure D3: Positions of Strain Gauges; 50x50x1.6SHS-Plate, S2PL3R2A

D2: TUBE-TO-TUBE T-JOINTS

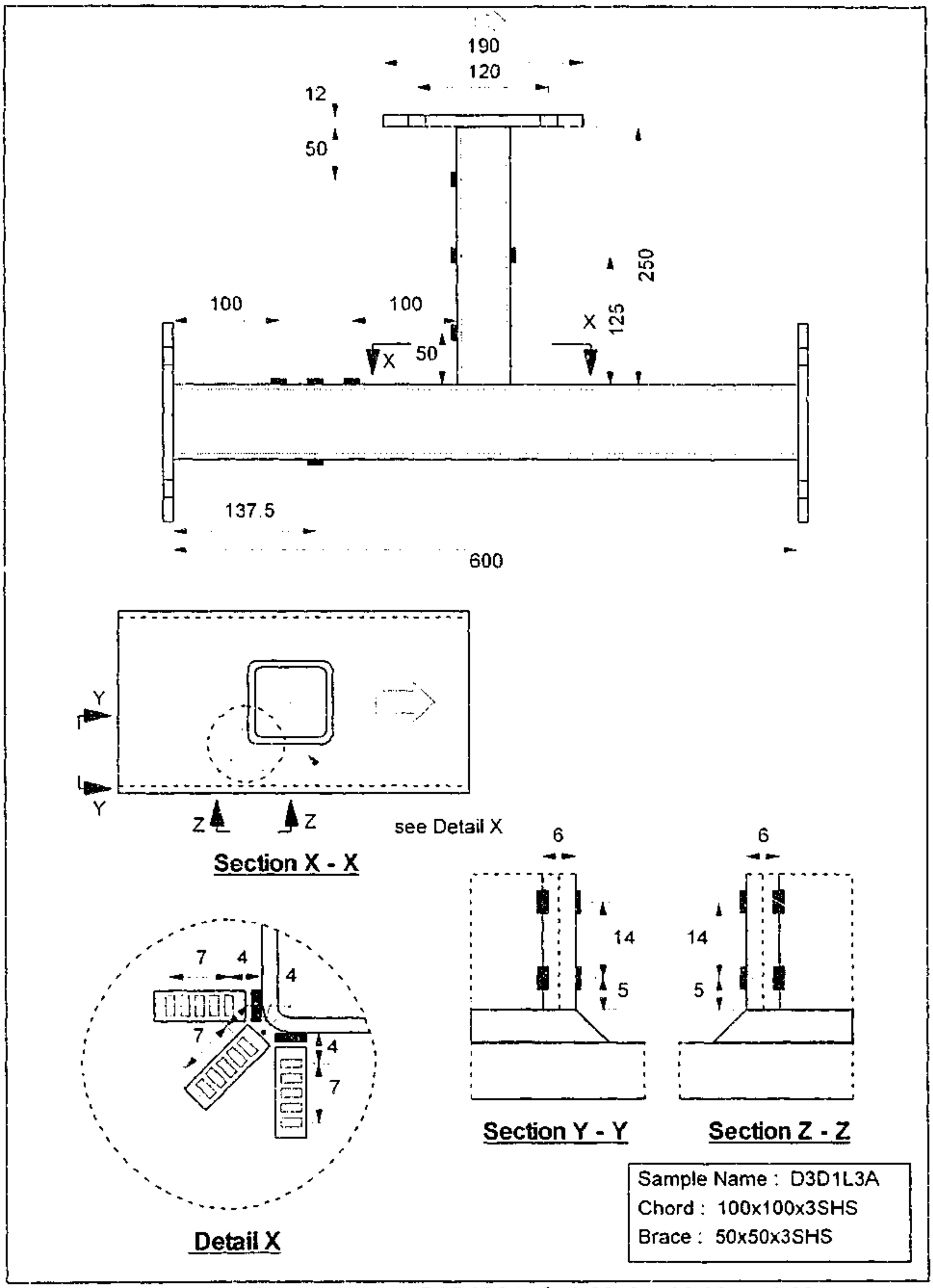

Figure D4: Positions of strain gauges, D3D1L3A, β=0.50, 2γ=33.33, τ=1.00

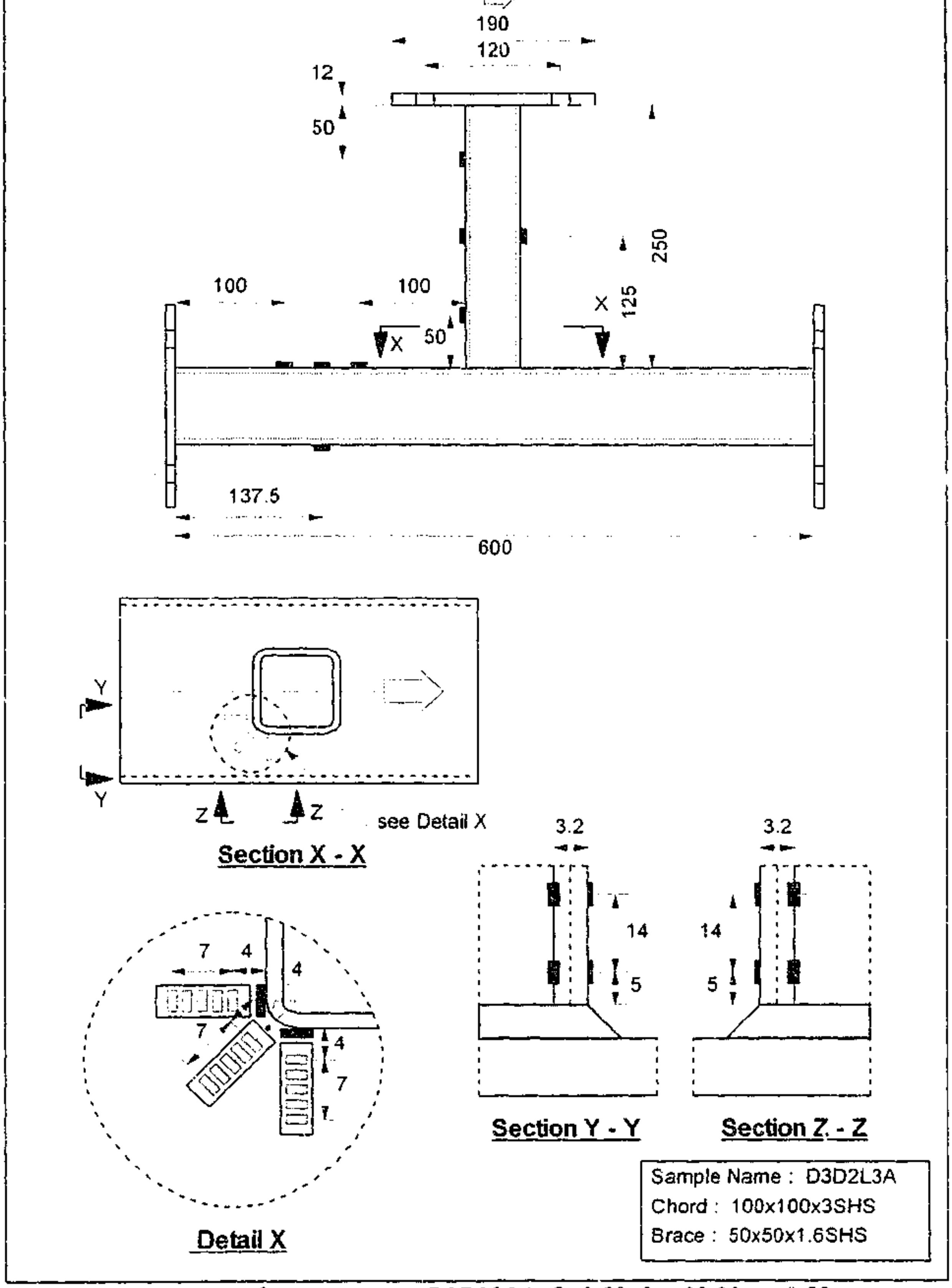

Figure D5: Positions of strain gauges, D3D2L3A, β=0.50, 2γ=33.33, τ=0.53

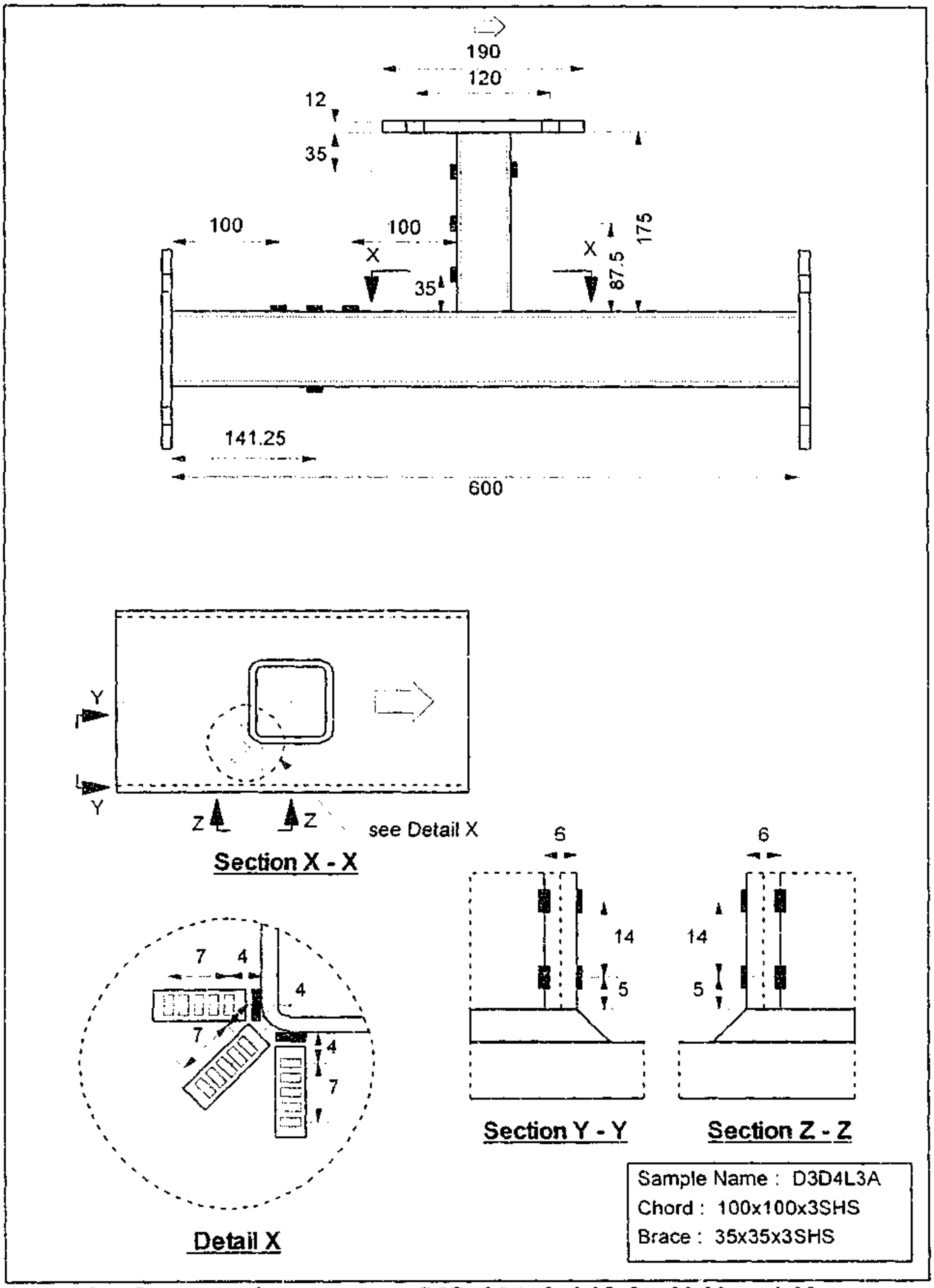

Figure D6: Positions of strain gauges, D3D4L3A, β=0.35, 2γ=33.33, τ=1.00

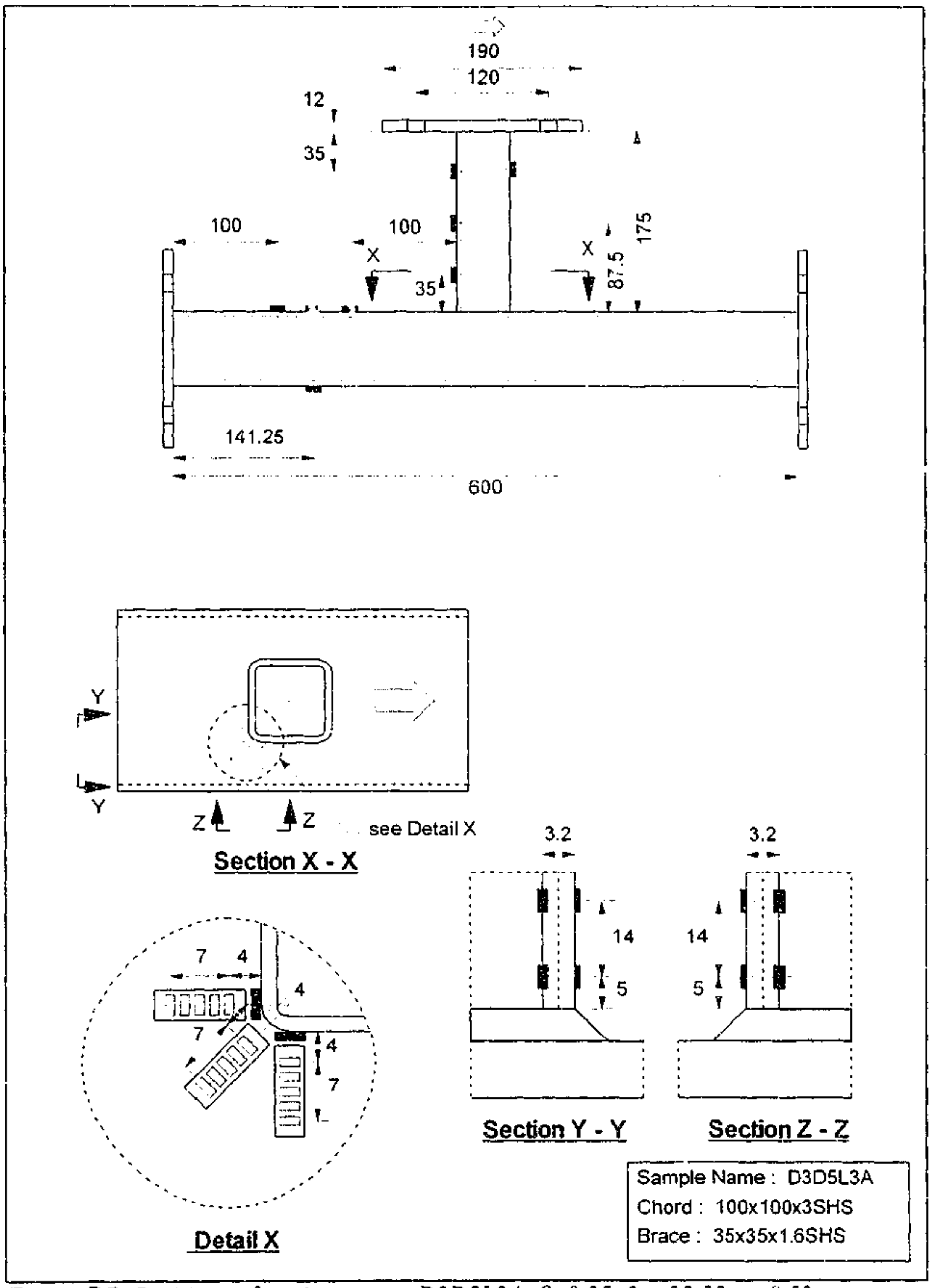

Figure D7: Positions of strain gauges, D3D5L3A, β=0.35, 2γ=33.33, τ=0.53

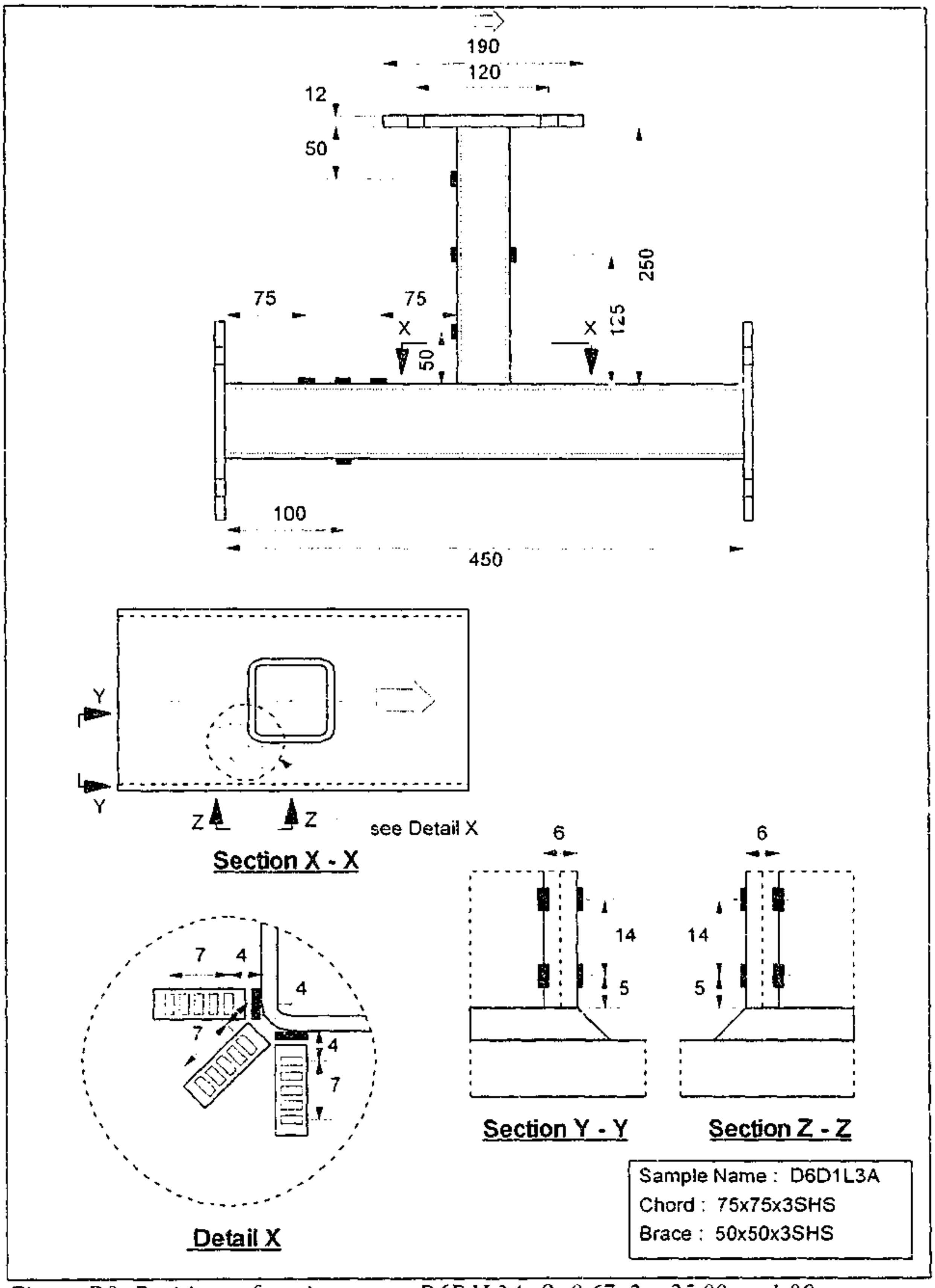

Figure D8: Positions of strain gauges, D6D1L3A, β=0.67, 2γ=25.00, τ=1.00

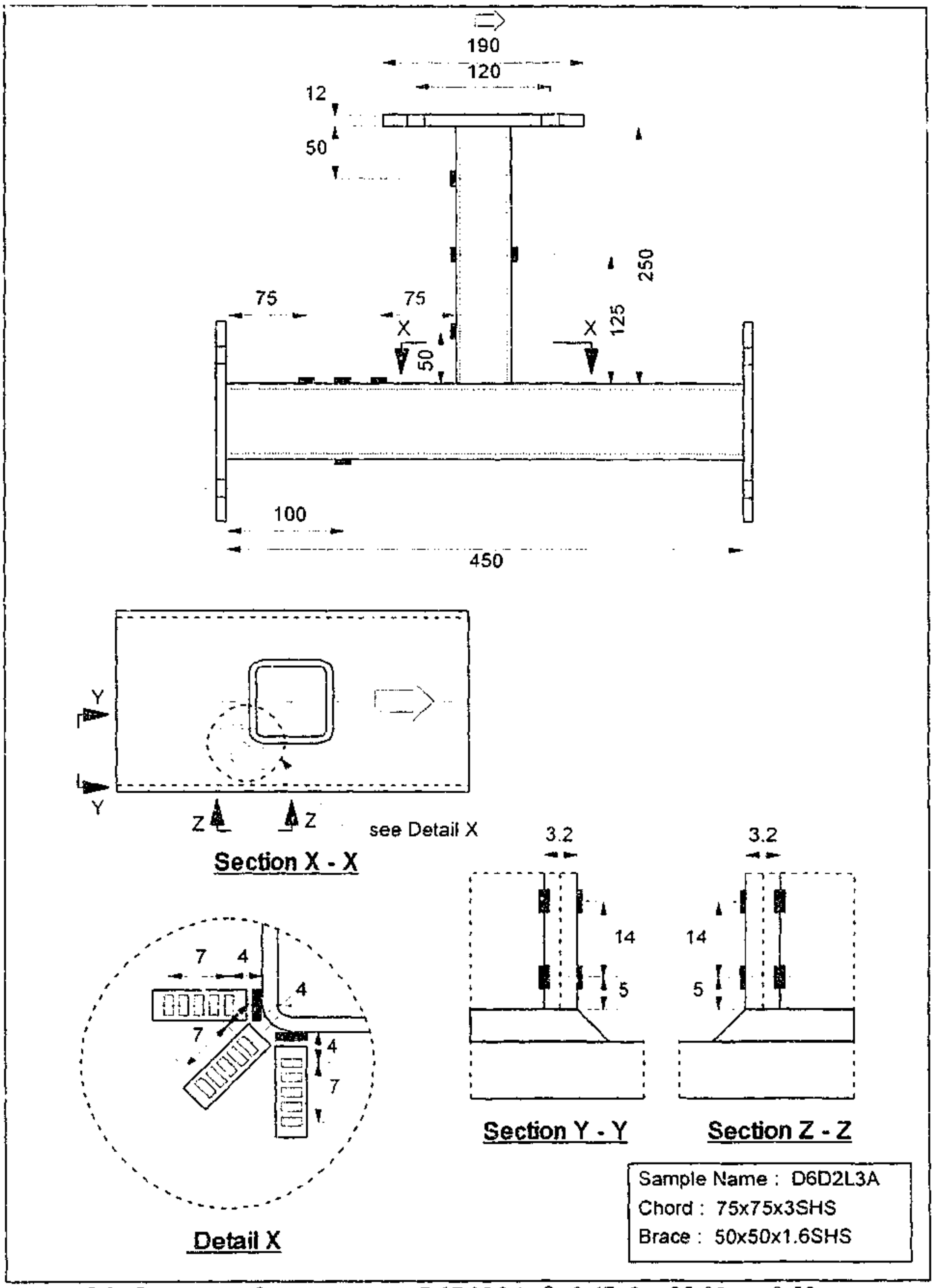

Figure D9: Positions of strain gauges, D6D2L3A, β=0.67, 2γ=25.00, τ=0.53

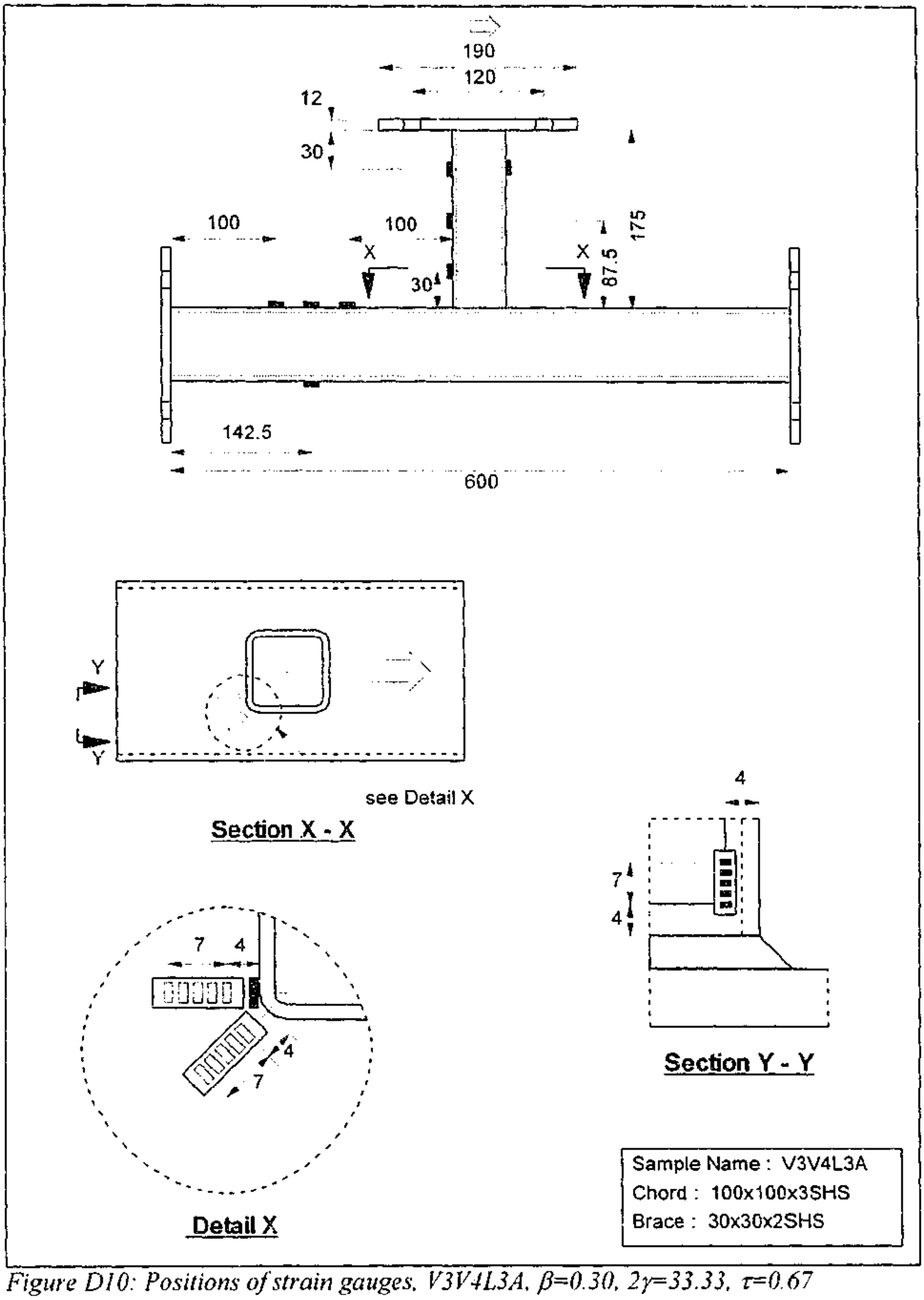

Figure D10: Positions of strain gauges, V3V4L3A, β=0.30, 2γ=33.33, τ=0.67

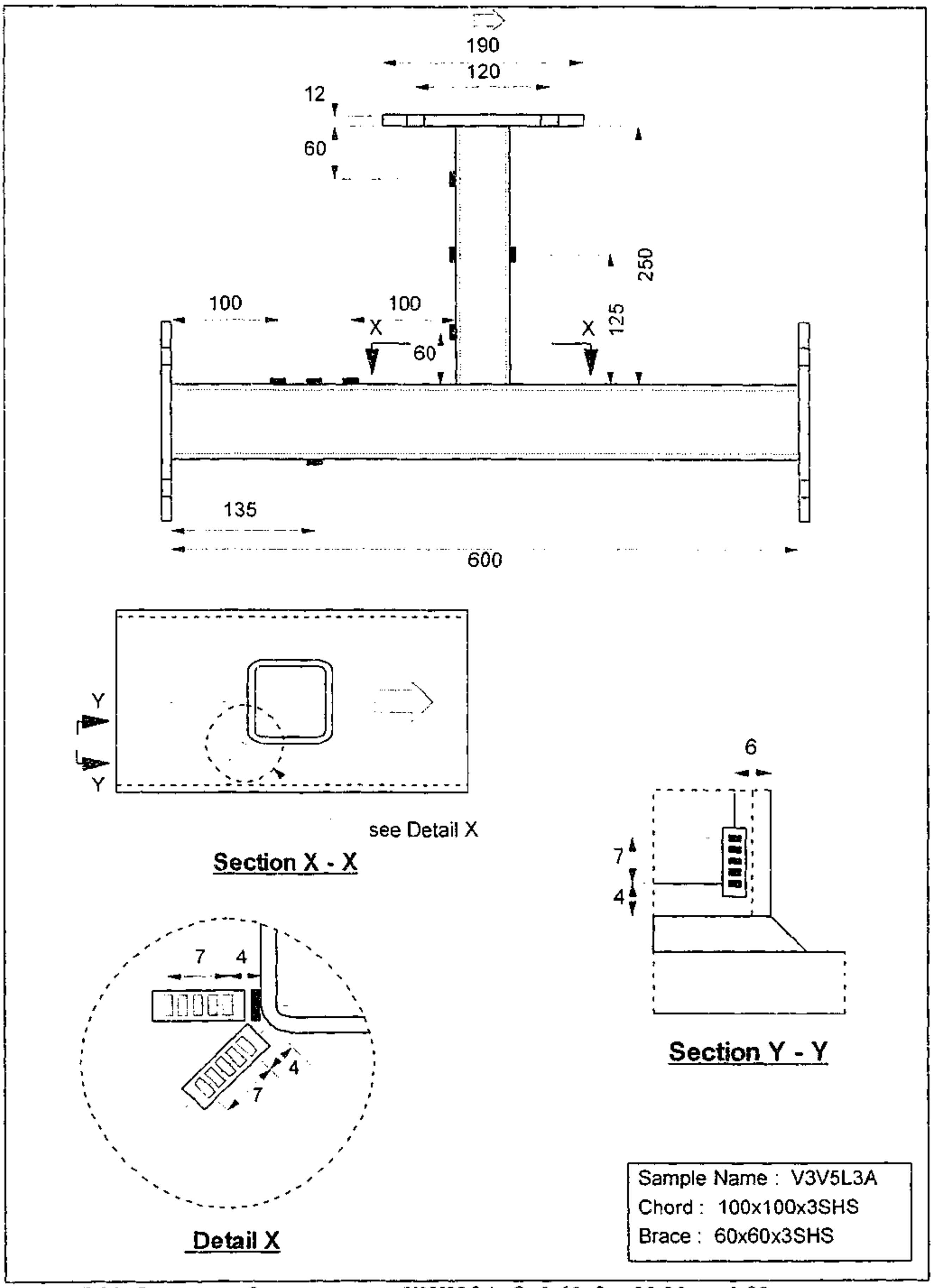

Figure D11: Positions of strain gauges, V3V5L3A, β=0.60, 2γ=33.33, τ=1.00

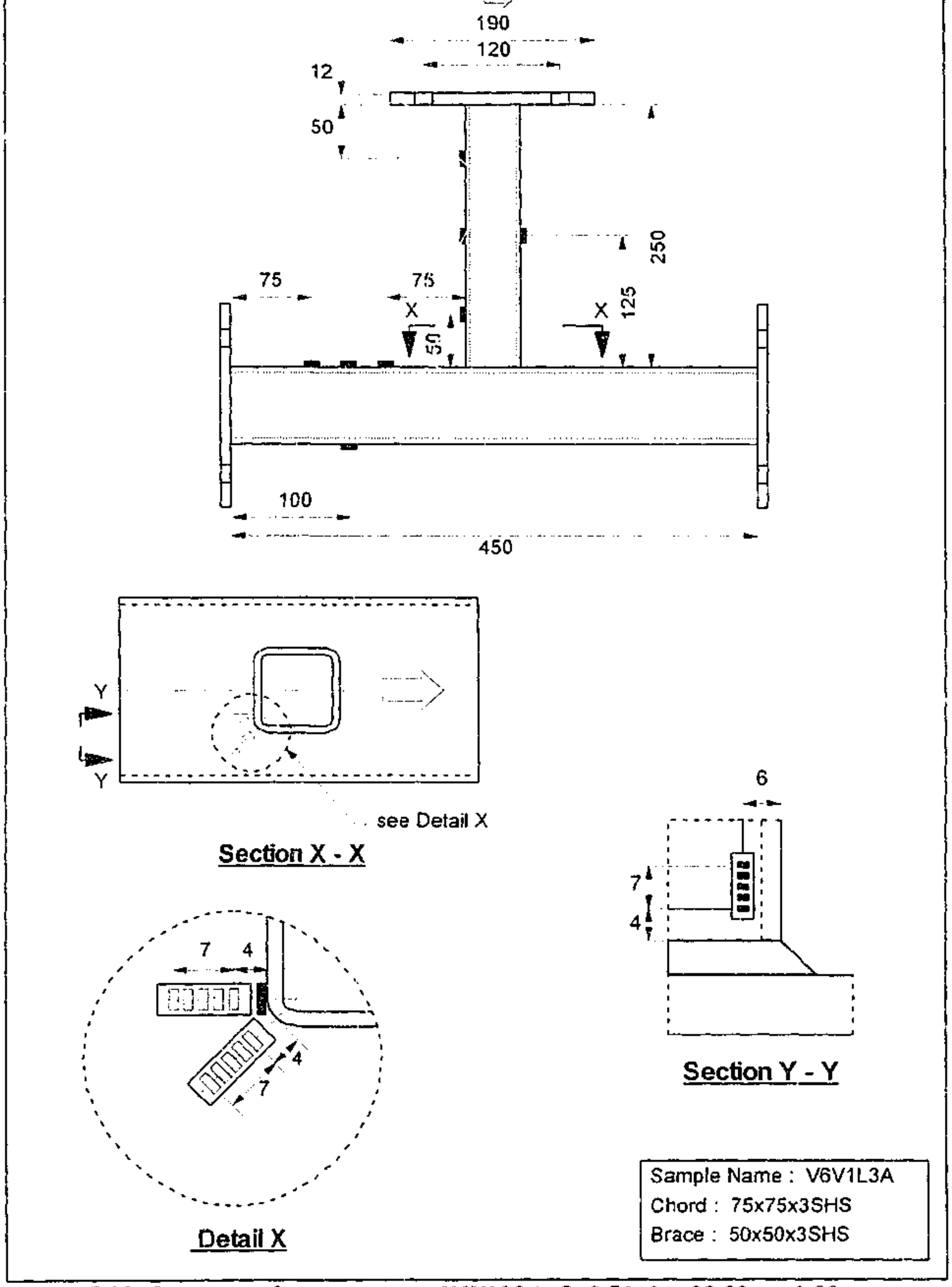

Figure D12: Positions of strain gauges, V6V1L3A, β=0.71, 2γ=23.33, τ=1.00

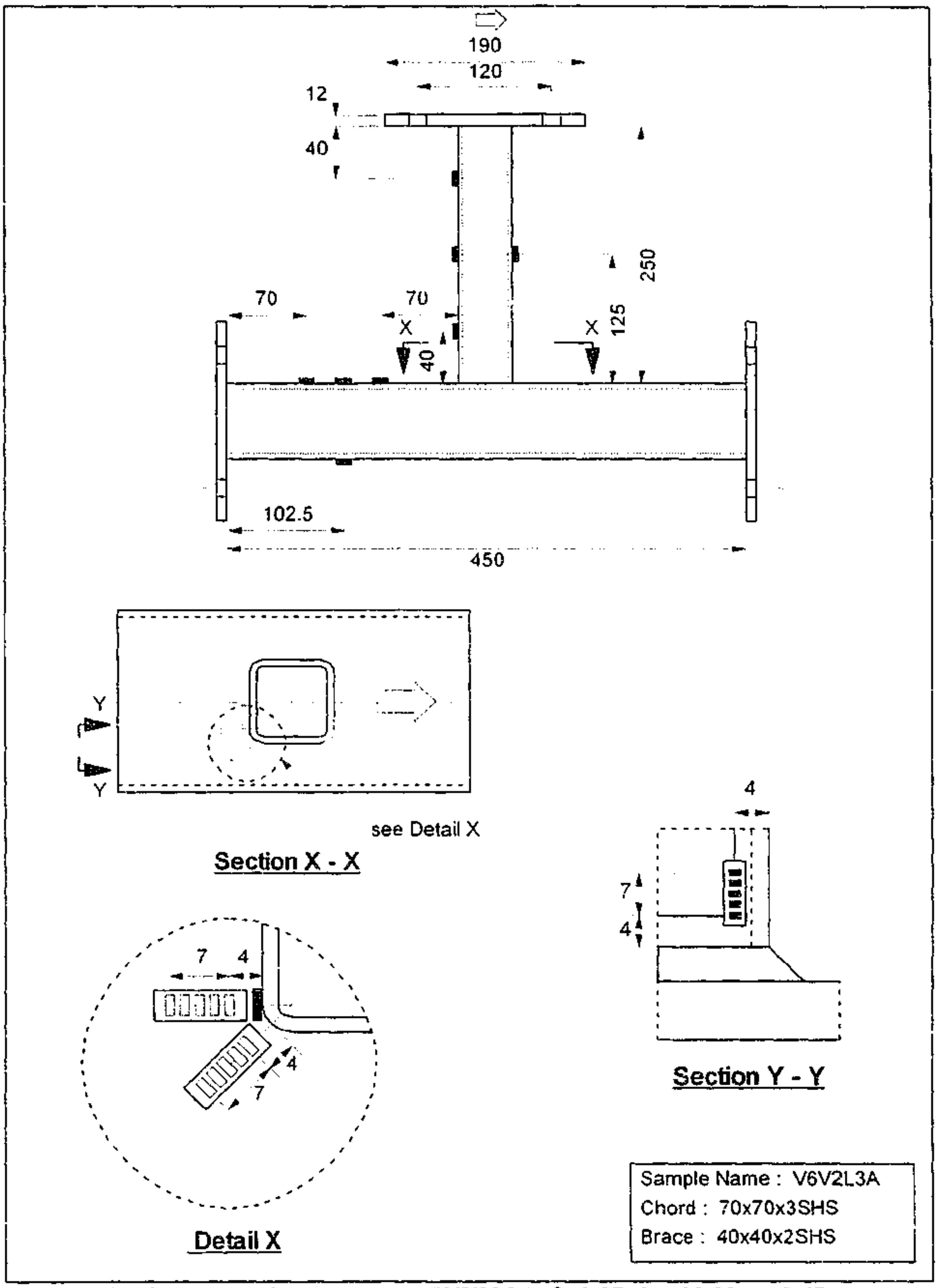

Figure D13: Positions of strain gauges, V6V2L3A, β=0.57, 2γ=23.33, τ=0.67

Appendix E
EXTRAPOLATION FOR EXPERIMENTAL SCF

E1: TUBE-TO-PLATE T-JOINTS

Extrapolation Curves : S1PL2R2B

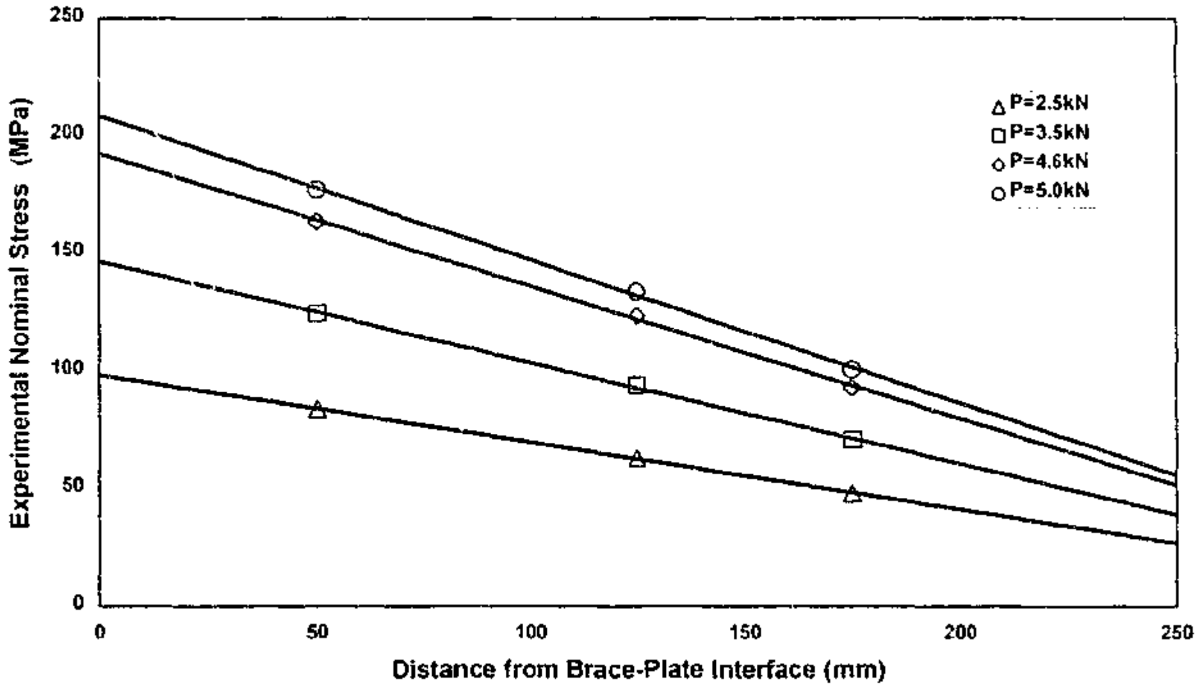

Figure E1: Plot of stresses on tension side of brace for estimation nominal stress: 50x50x3SHS-Plate

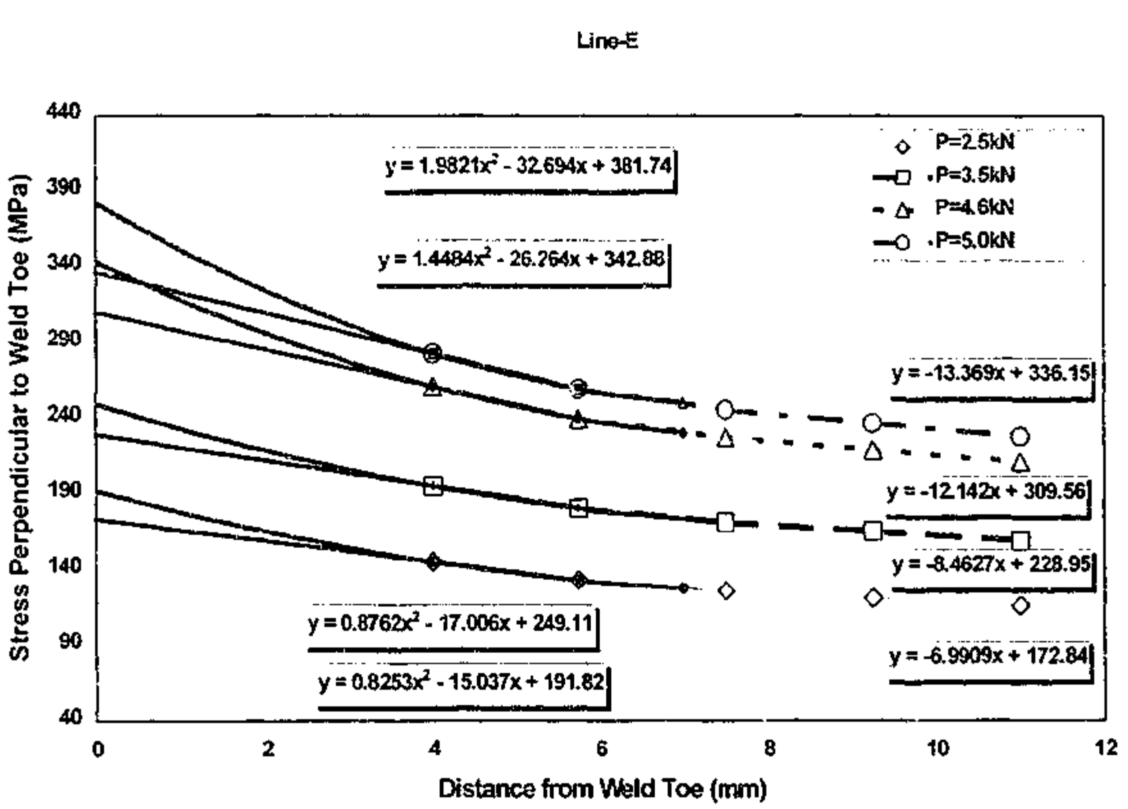

Figure E2: Determinat'on of hot-spot stresses, Line E, Tube-to-plate joint, 50x50x3SHS-Plate

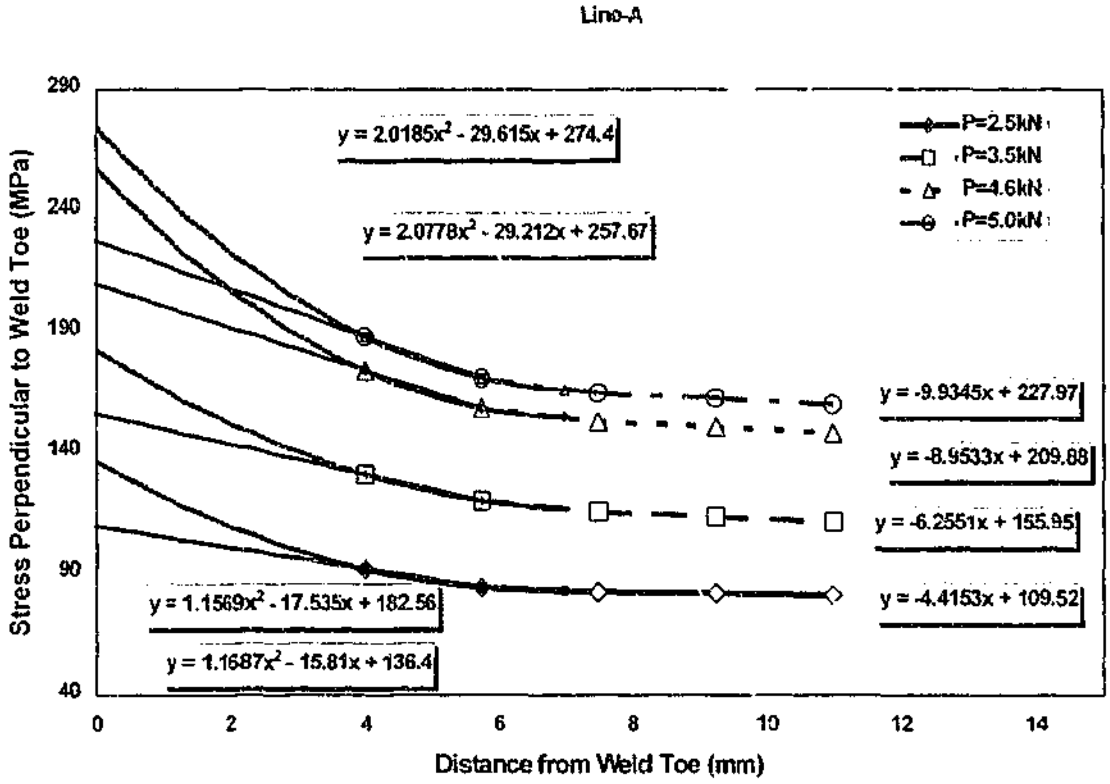

Figure E3: Determination of hot-spot stresses, Line A, Tube-to-plate joint. 50x50x3SHS-Plate

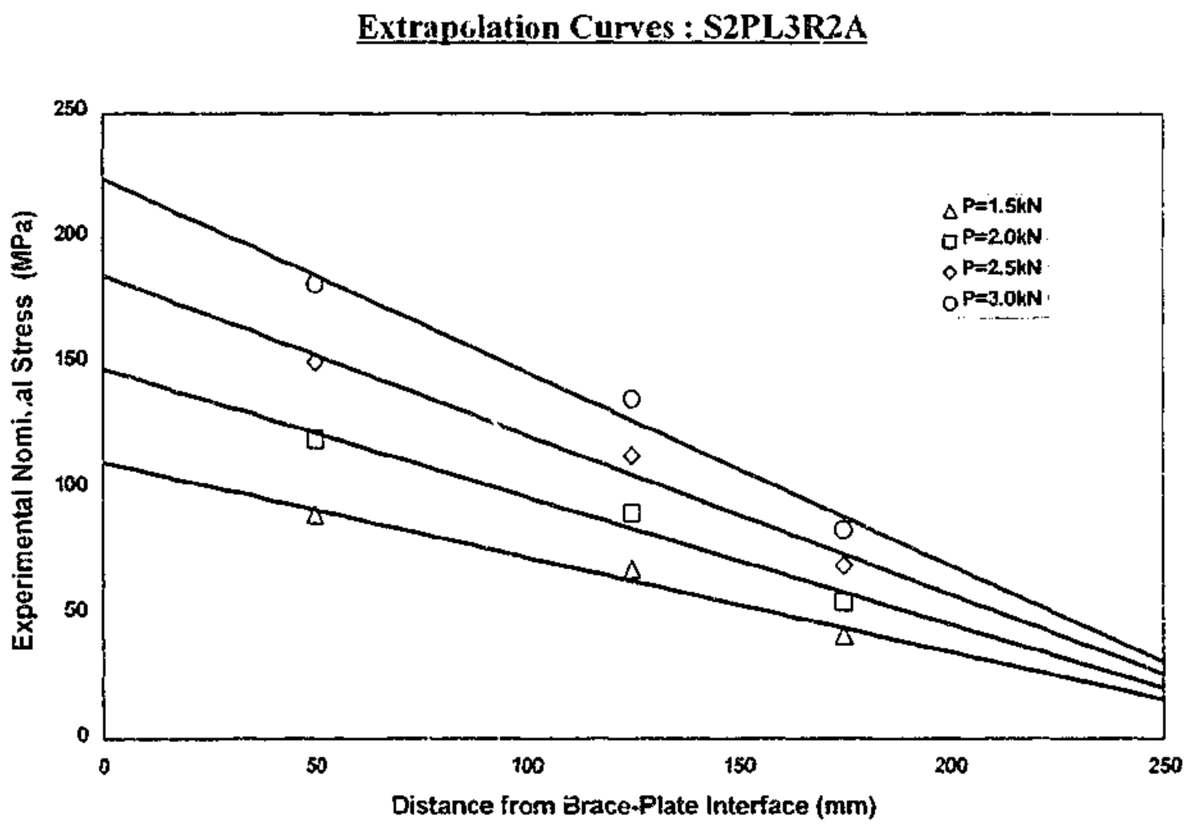

Figure E4: Plot of stresses on tension side of brace for estimation nominal stress: 50x50x1.6SHS-Plate.

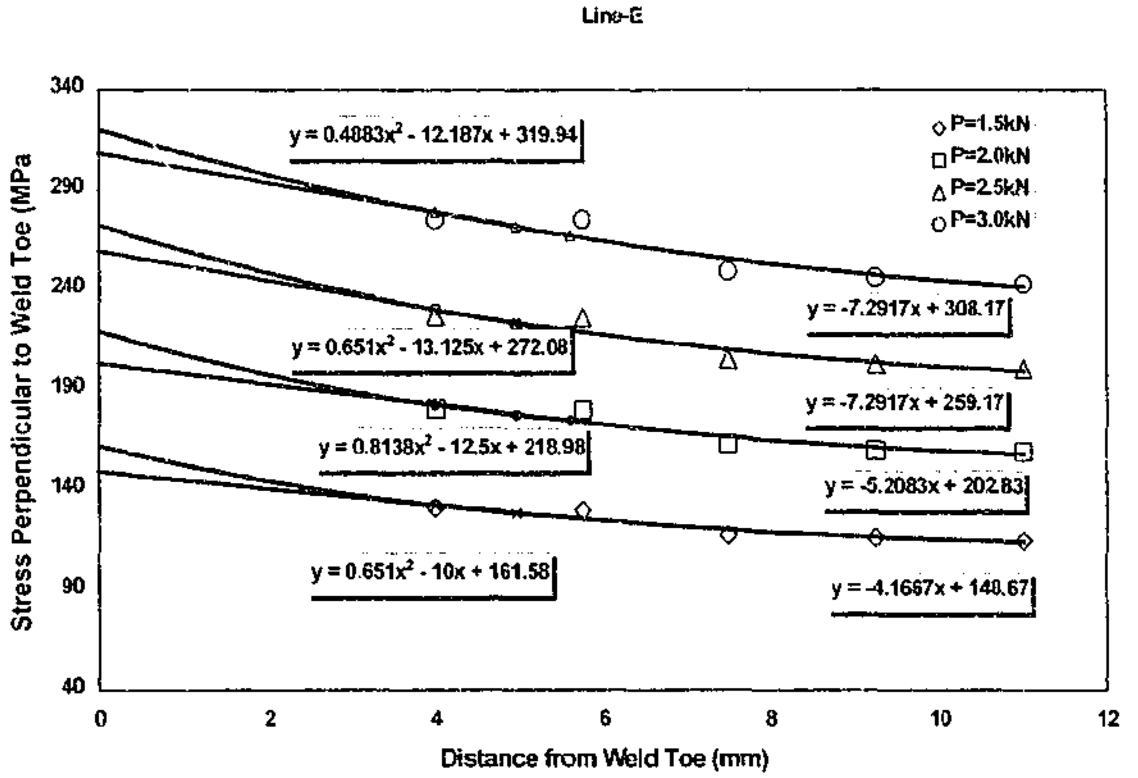

Figure E5: Determination of hot-spot stresses, Line E, Tube-to-plate joint, 50x50x1.6SHS-Plate

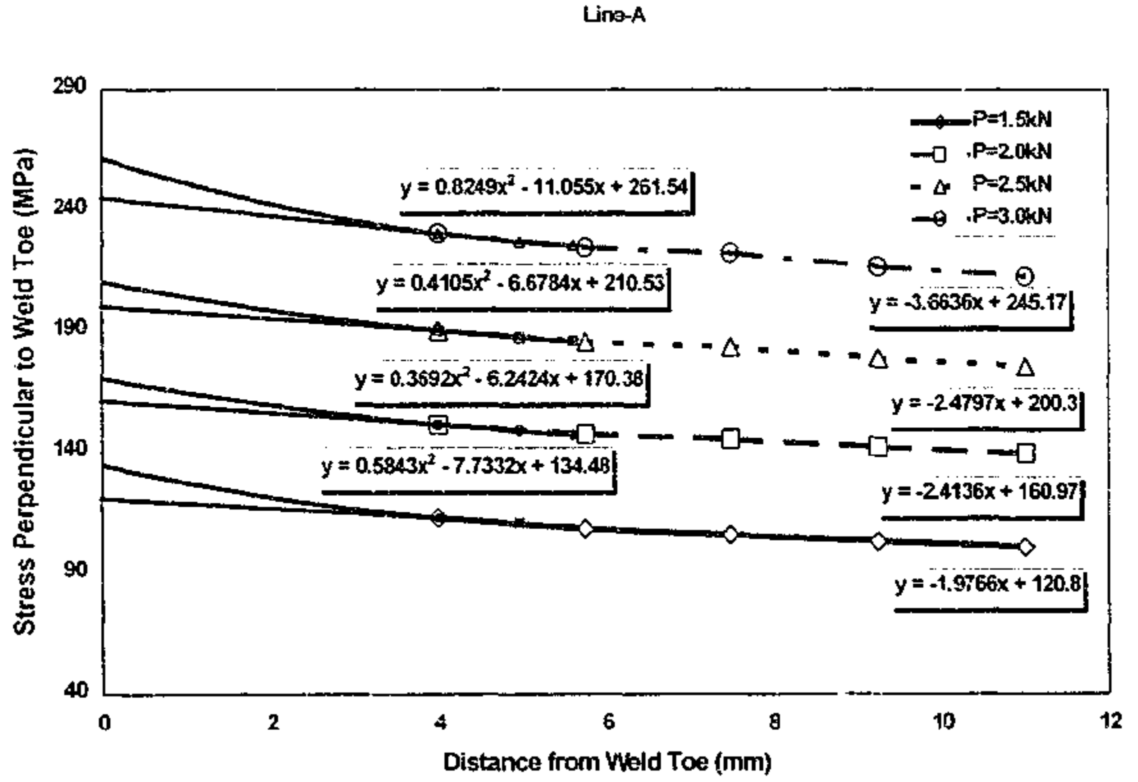

Figure E6: Determination of hot-spot stresses, Line A, Tube-to-plate joint, 50x50x1.6SHS-Plate

Extrapolation Curves : D7PL2B

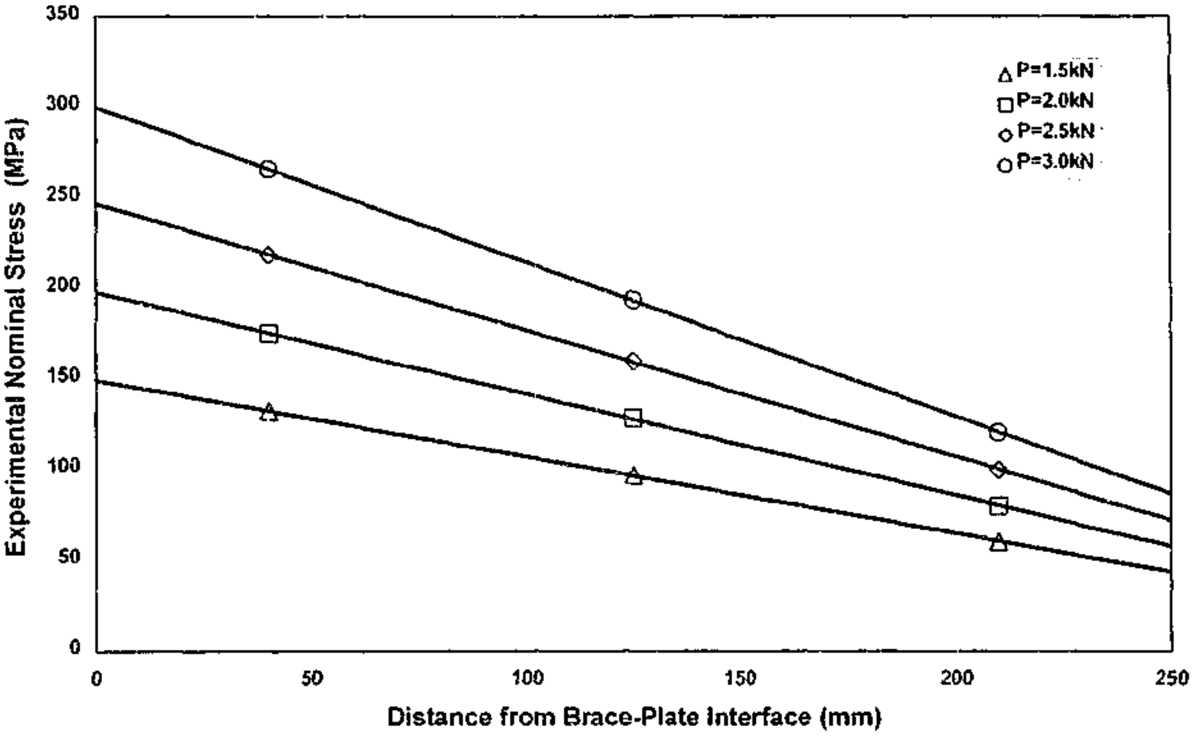

Figure E7: Plot of stresses on tension side of brace for estimation nominal stress; 40x40x2SHS-Plate

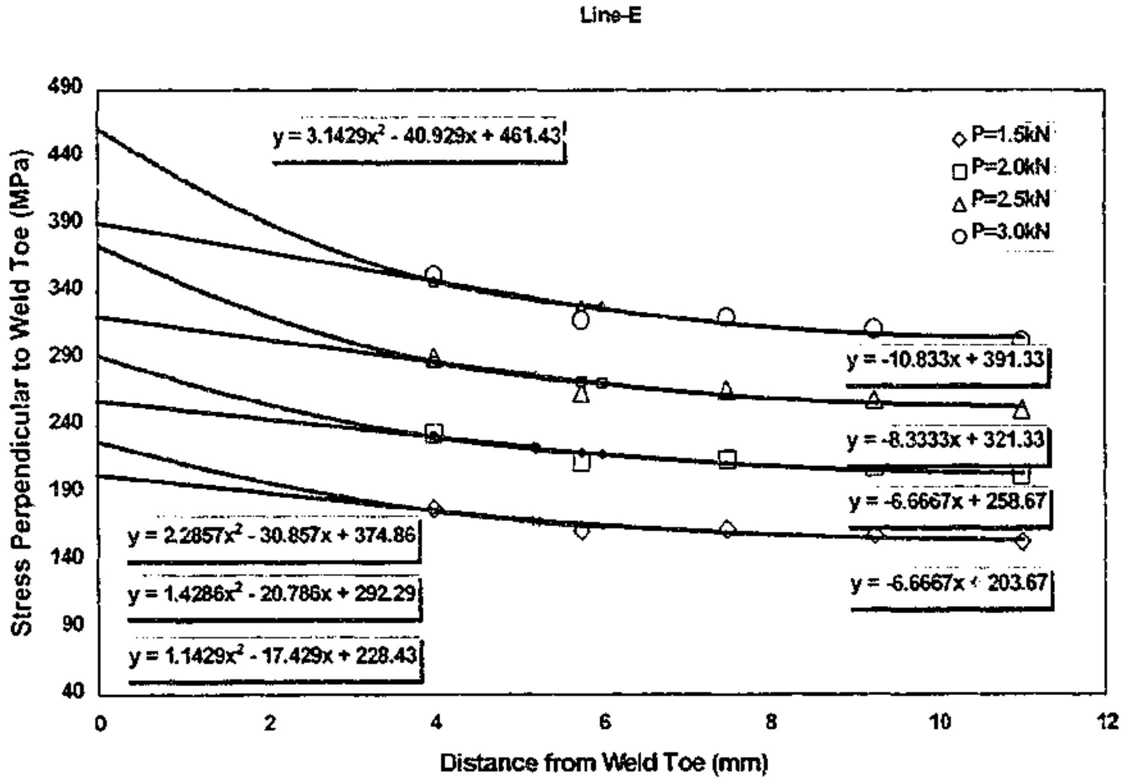

Figure E8: Determination of hot-spot stresses, Line E, Tube-to-plate joint, 40x40x2SHS-Plate

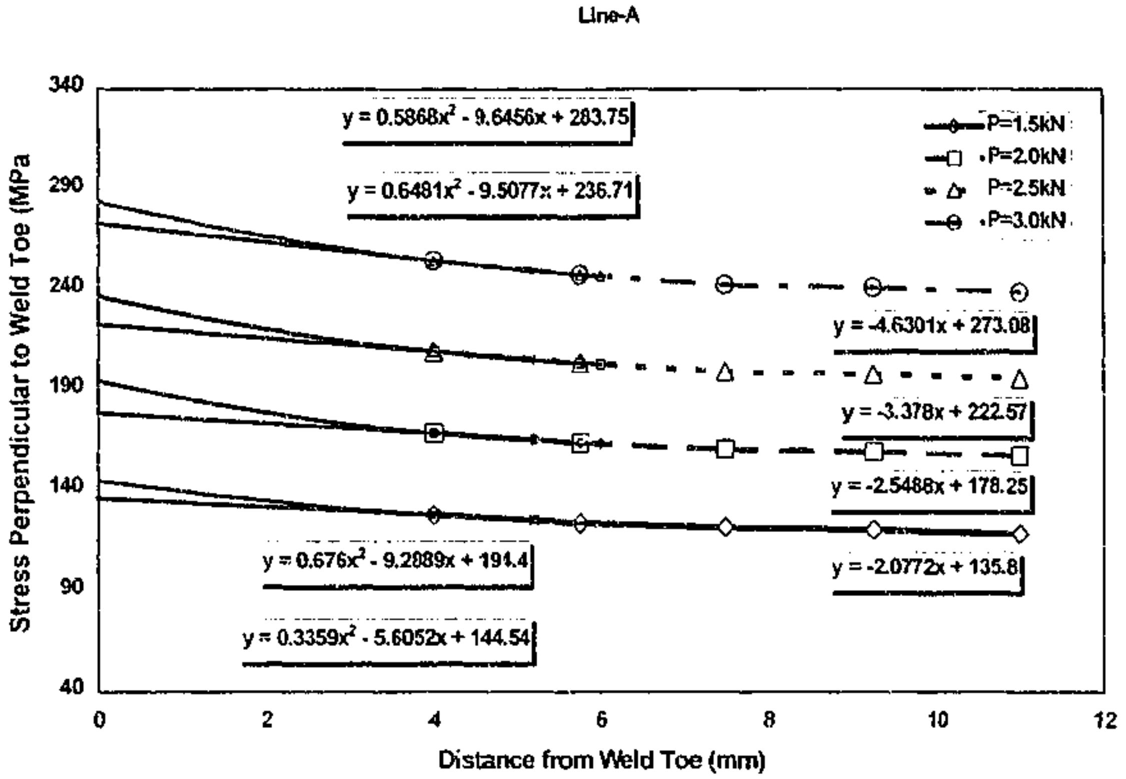

Figure E9: Determination of hot-spot stresses, Line A. Tube-to-plate joint, 40x40x2SHS-Plate

E2: TUBE-TO-TUBE T-JOINTS

Extrapolation Curves : D3D1L3A

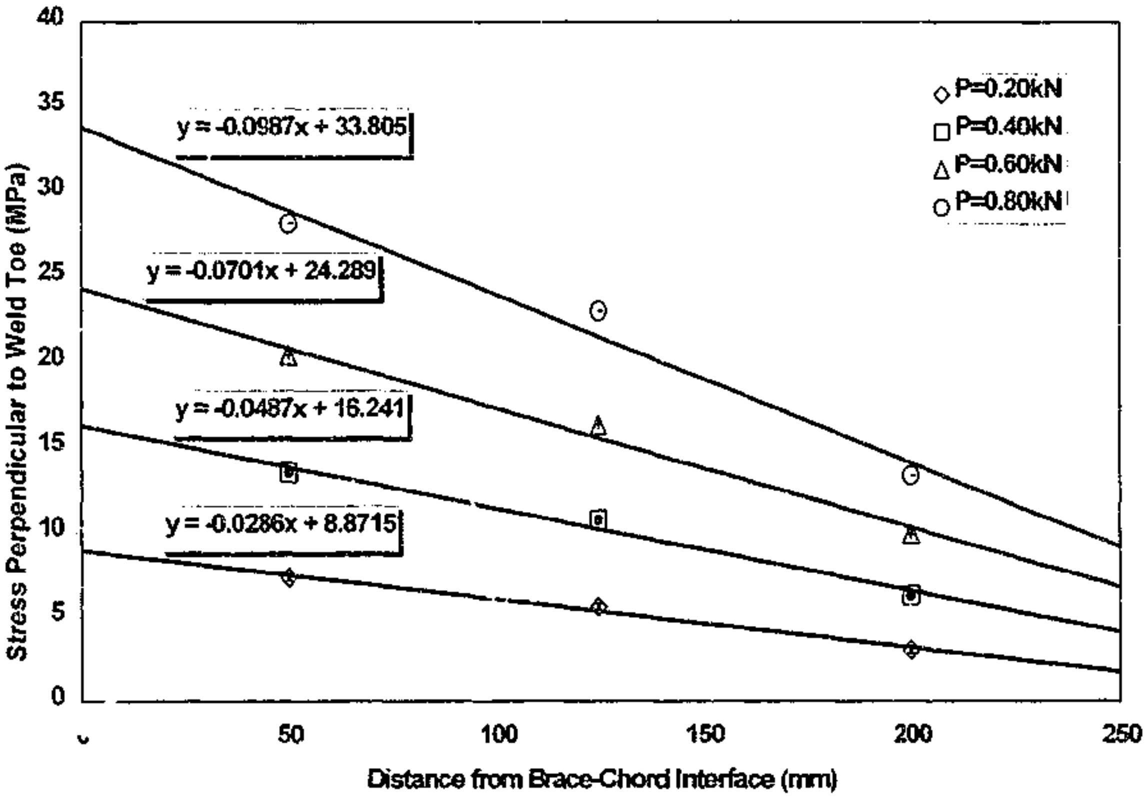

Figure E10: Nominal stress in brace, D3D1L3A

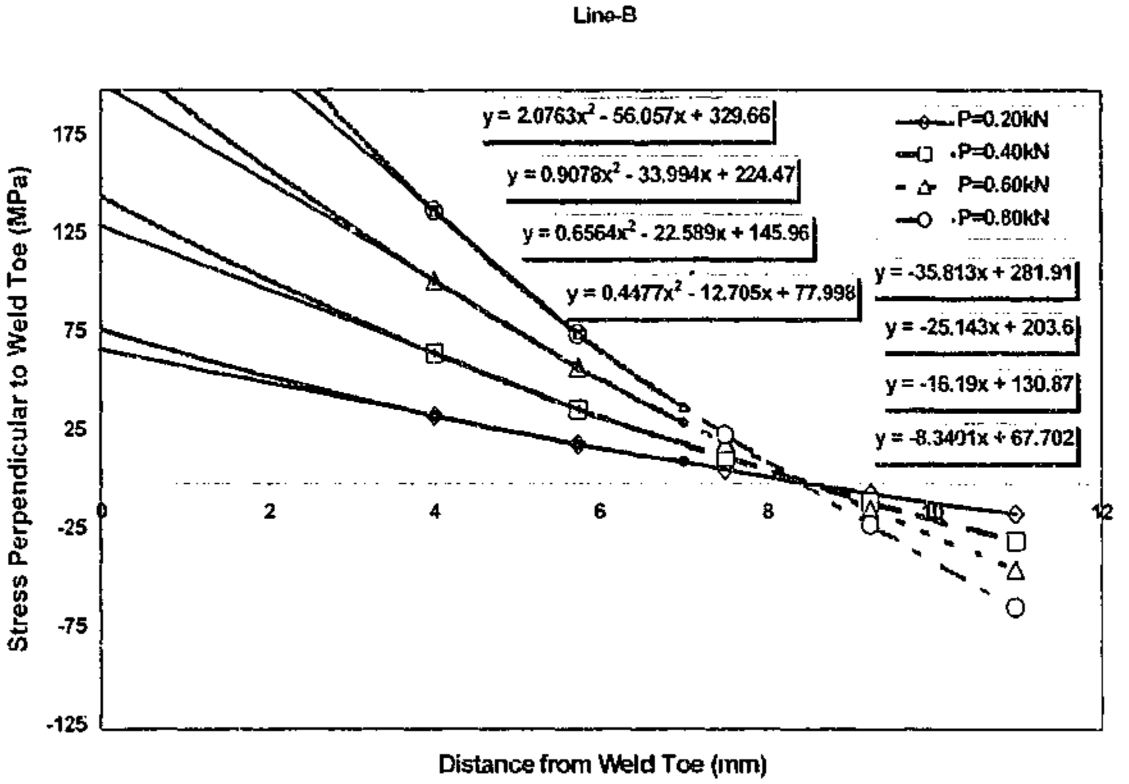

Figure E11: Line B , D3D1L3A

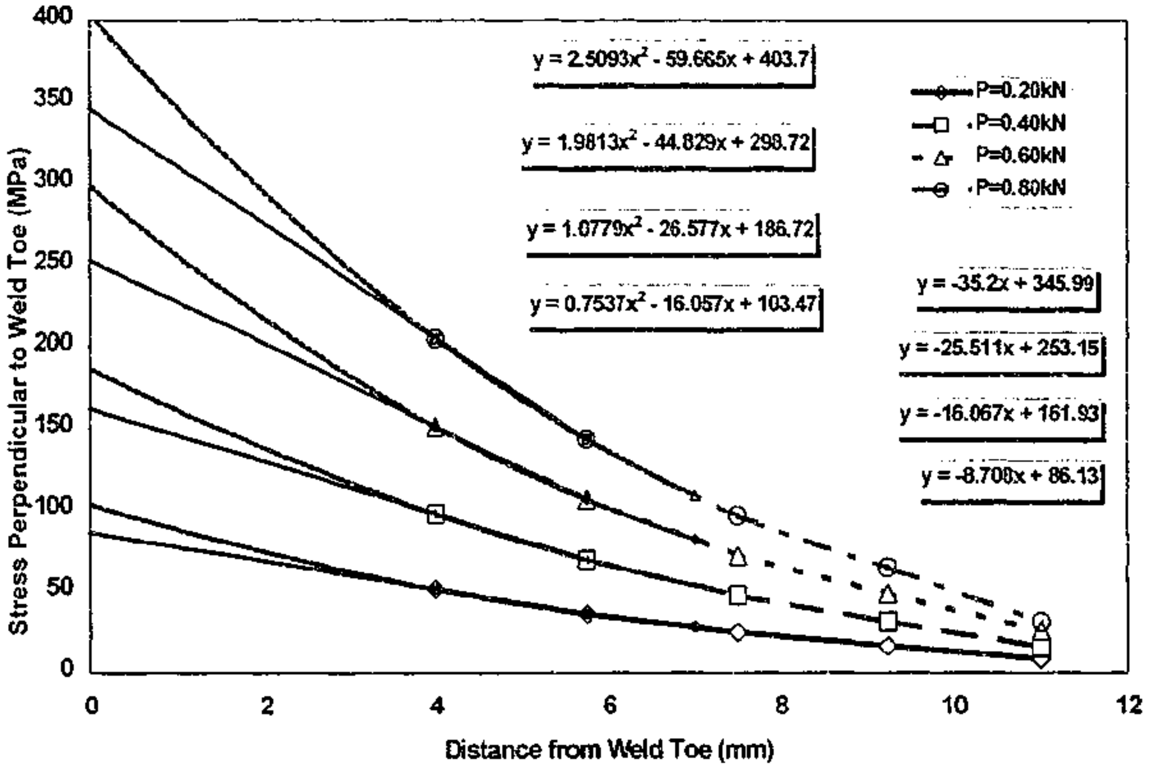

Figure E12: Line C, D3D1L3A

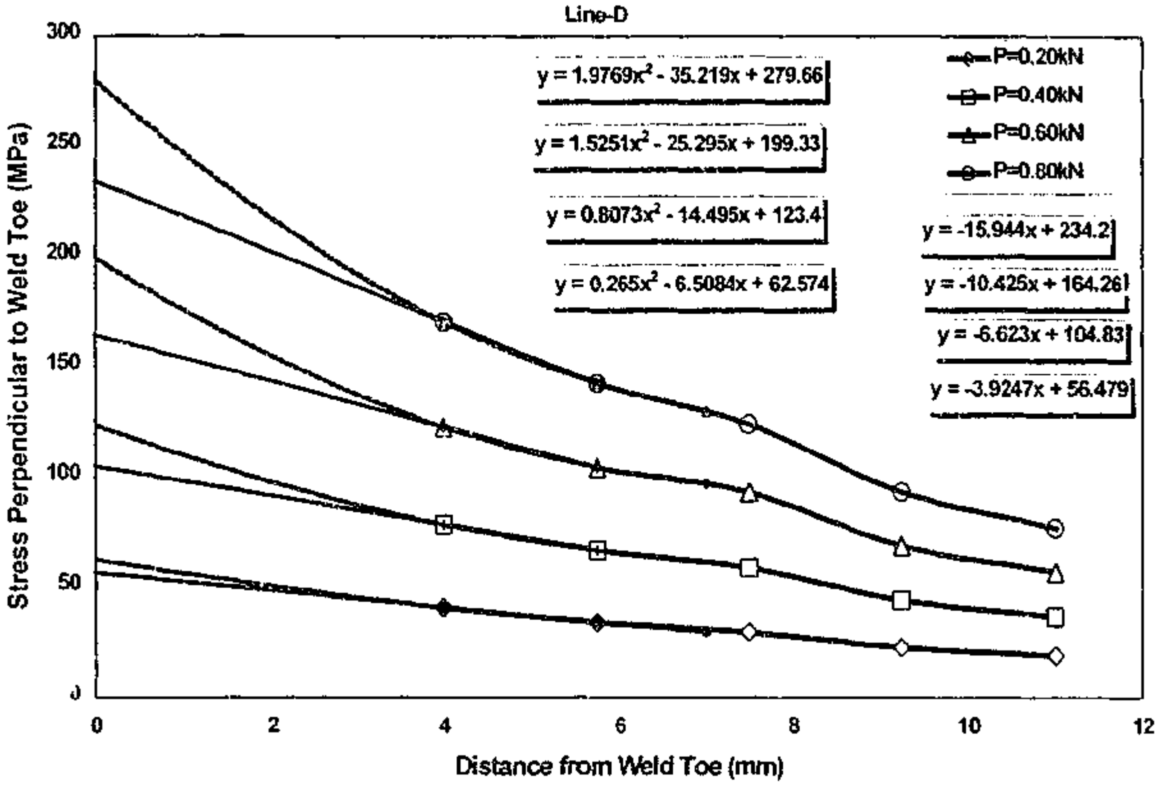

Figure E13: Line D, D3D1L3A

Extrapolation Curves : D3D2L3A

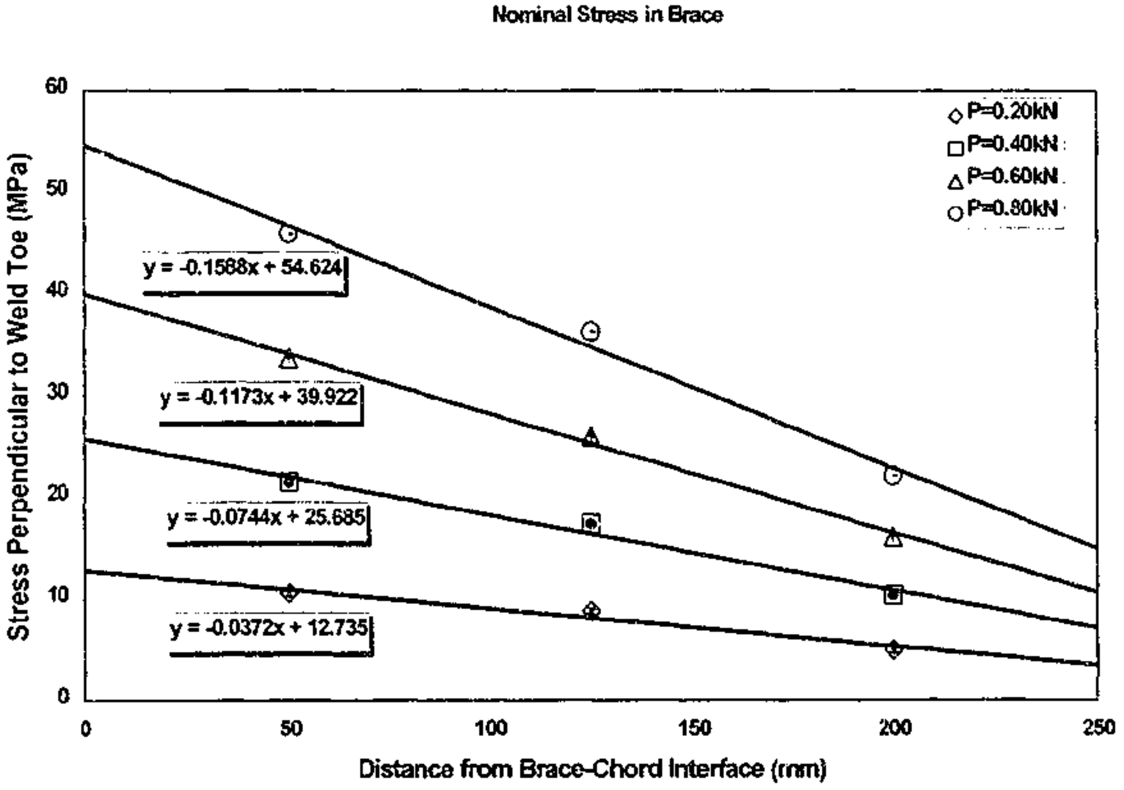

Figure E14: Nominal stress in brace, D3D2L3A

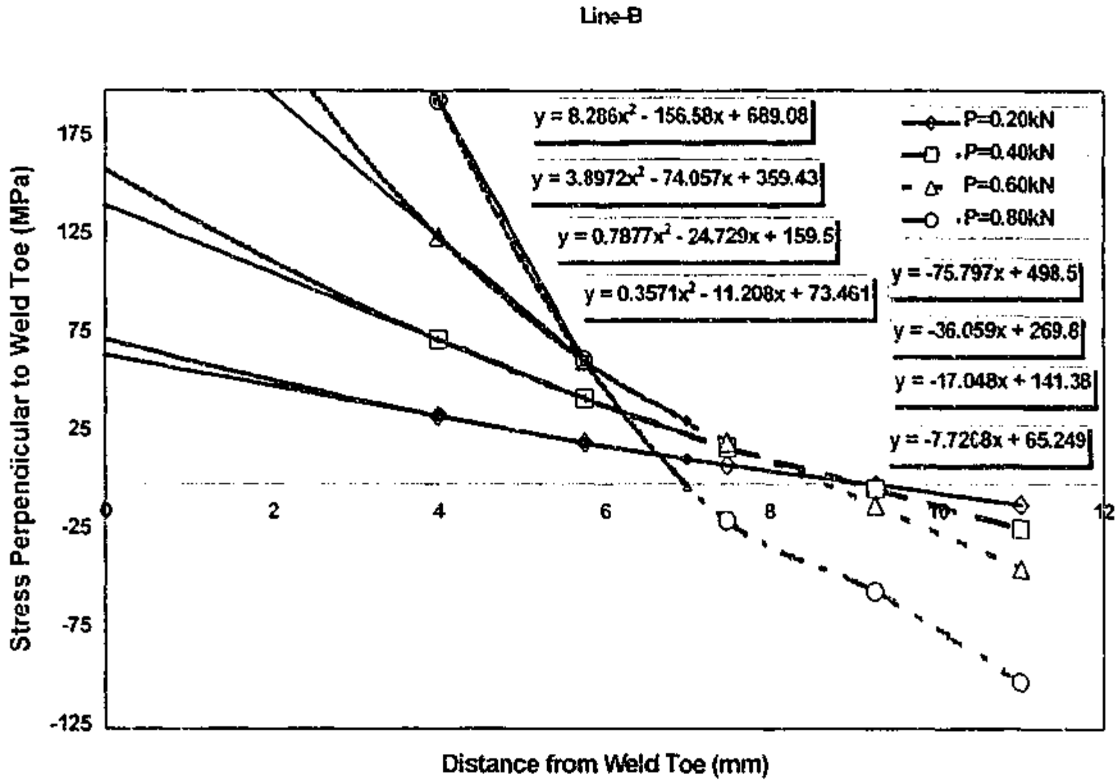

Figure E15: Line B, D3D2L3A

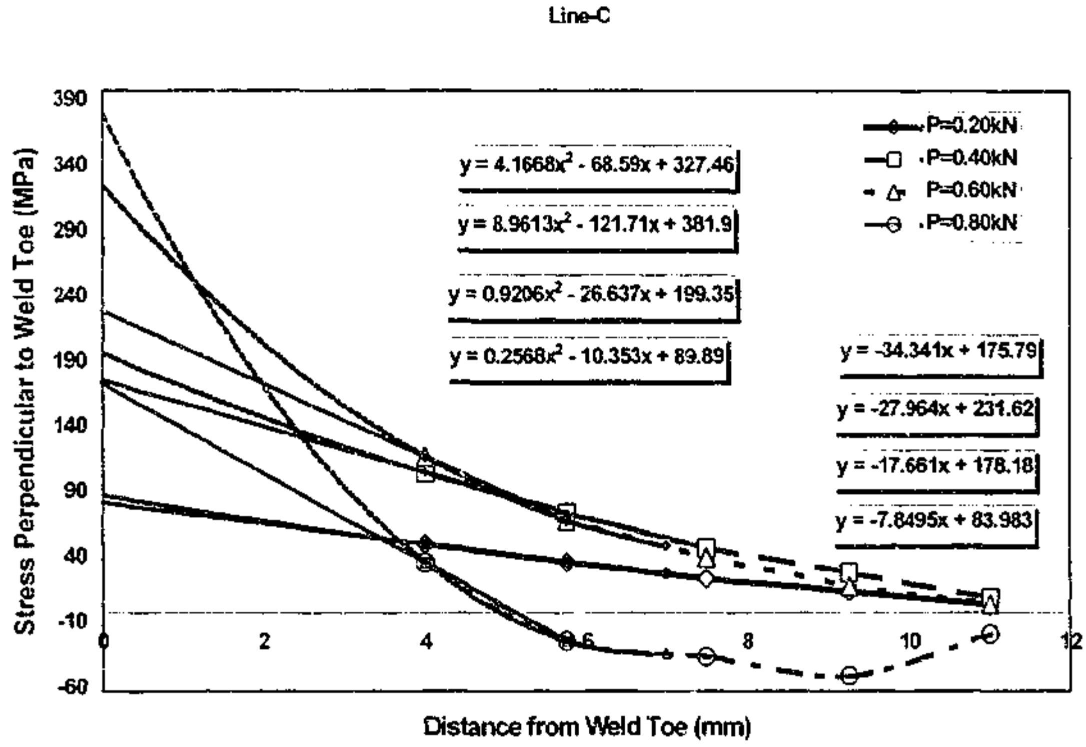

Figure E16: Line C, D3D2L3A

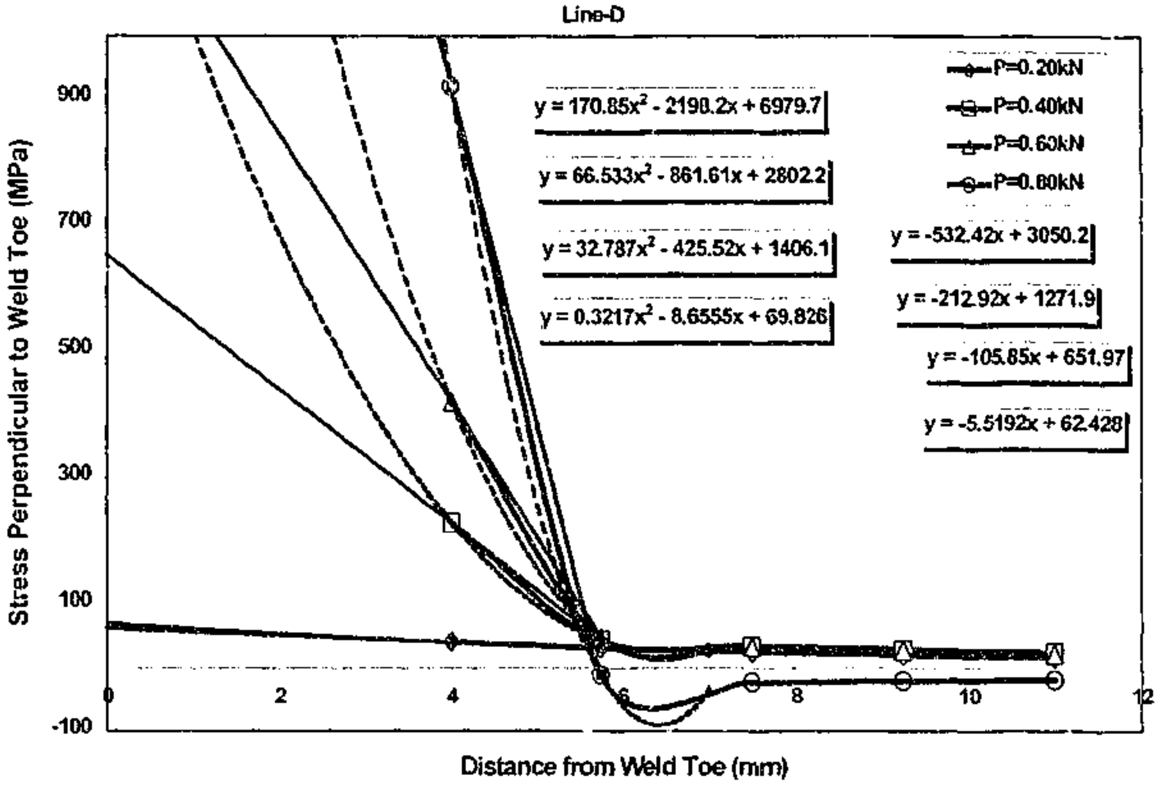

Figure E17: Line D, D3D2L3A

Extrapolation Curves : D3D4L3A

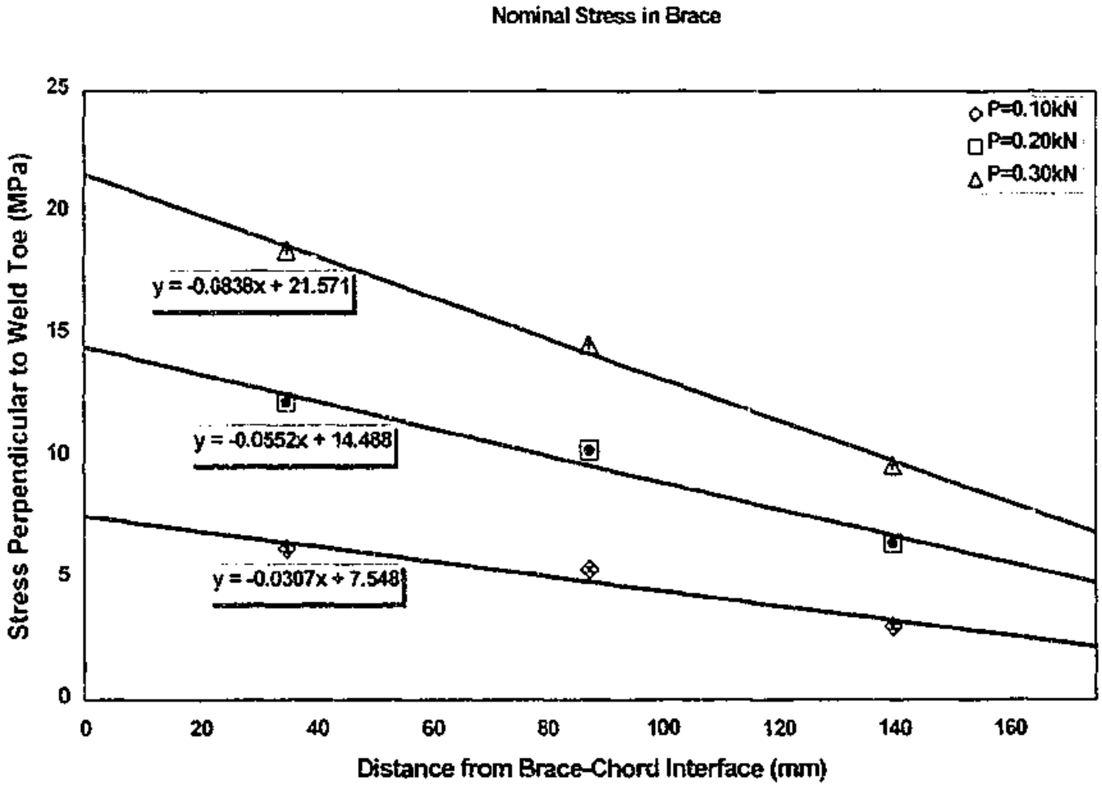

Figure E18: Nominal stress in brace, D3D4L3A

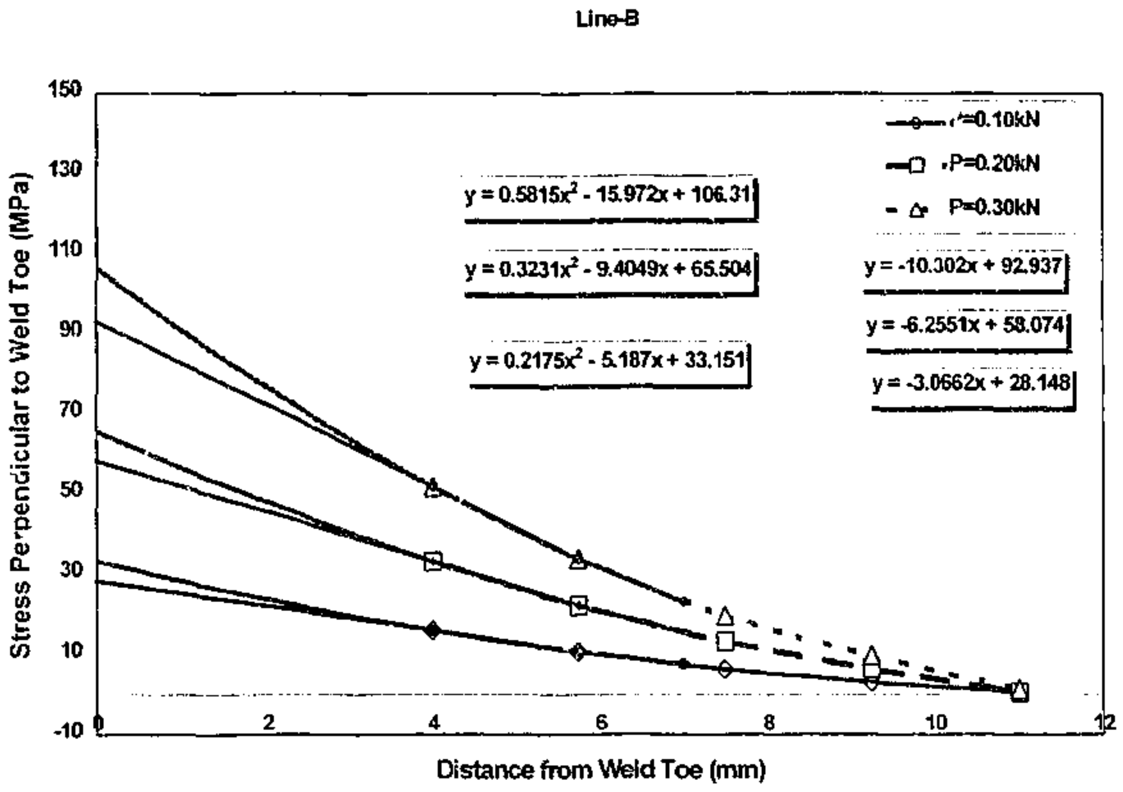

Figure E19: Line B, D3D4L3A

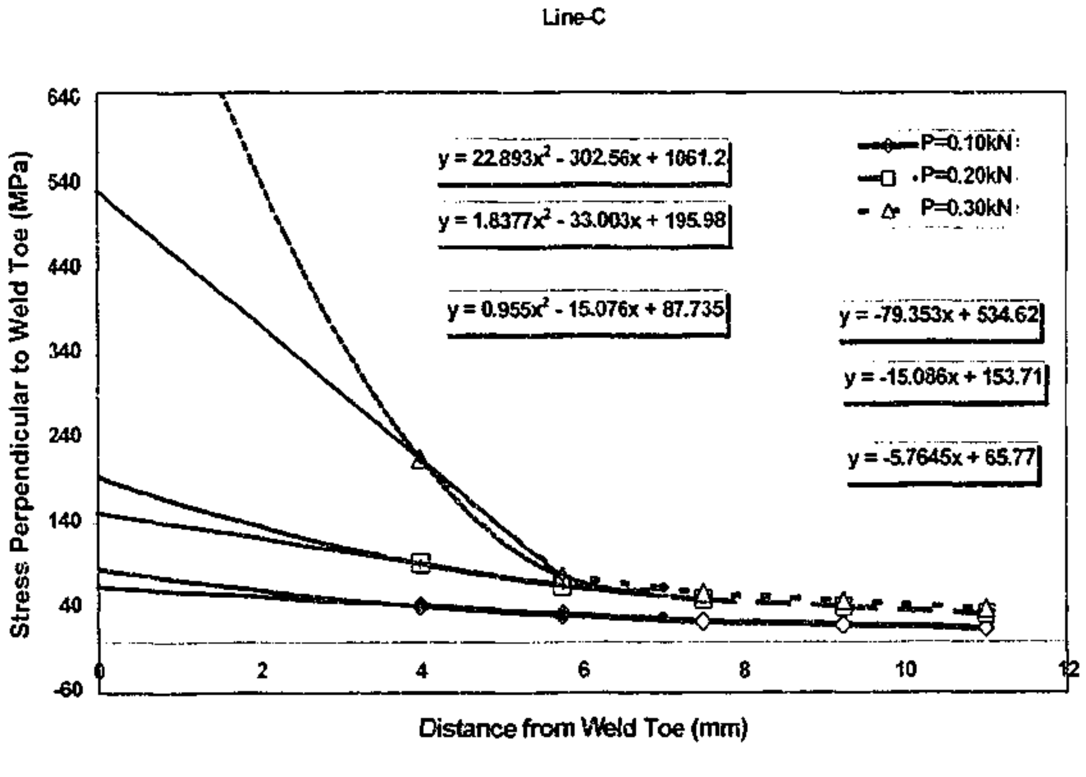

Figure E20: Line C, D3D4L3A

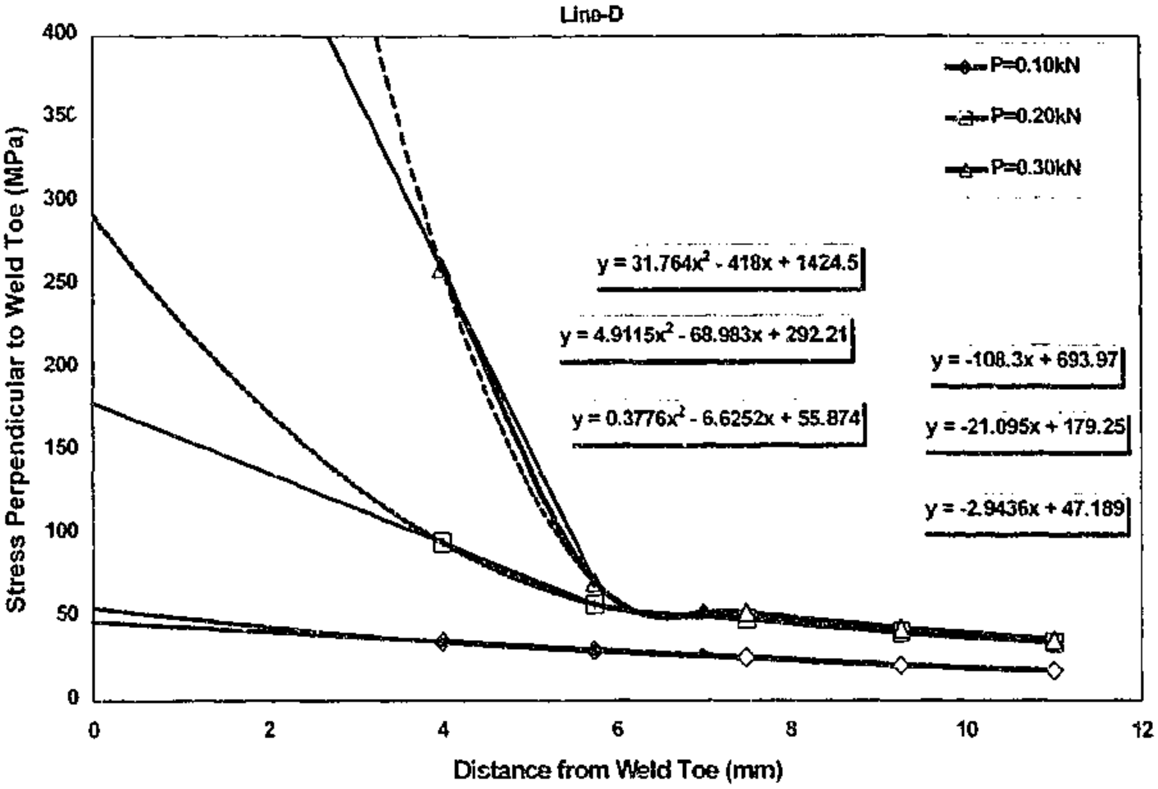

Figure E21: Line D, D3D4L3A

Extrapolation Curves : D3D5L3A

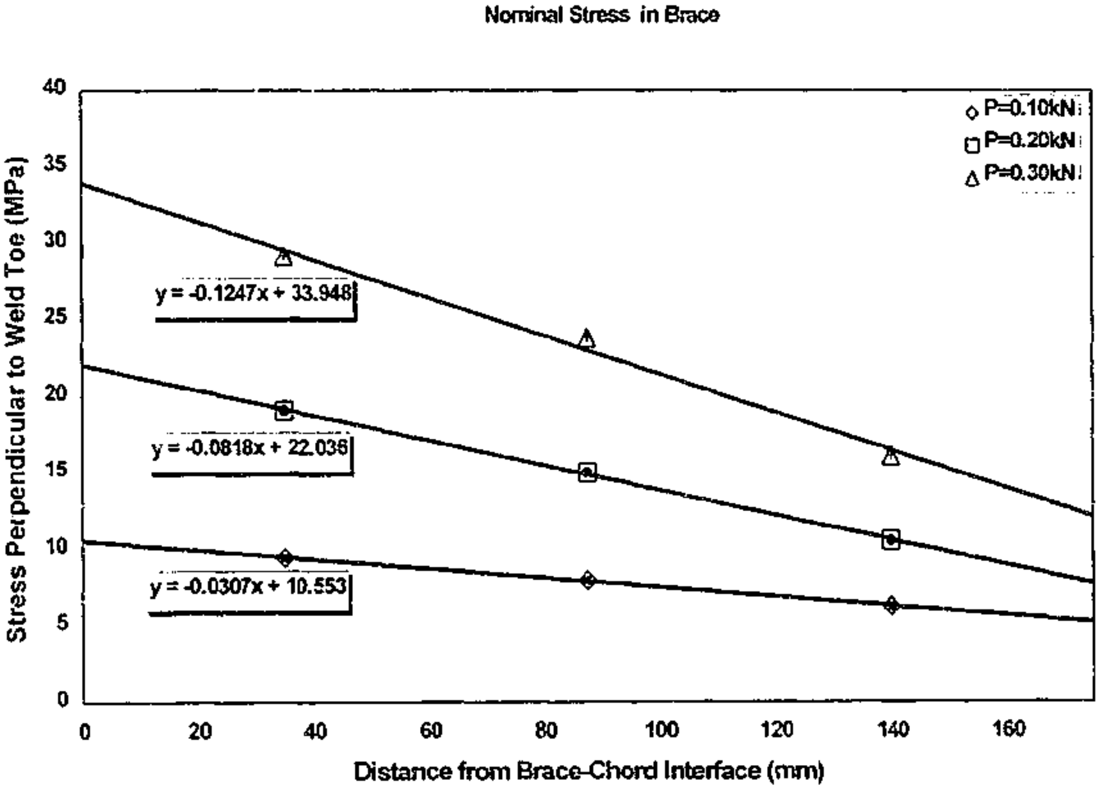

Figure E22: Nominal stress in brace, D3D5L3A

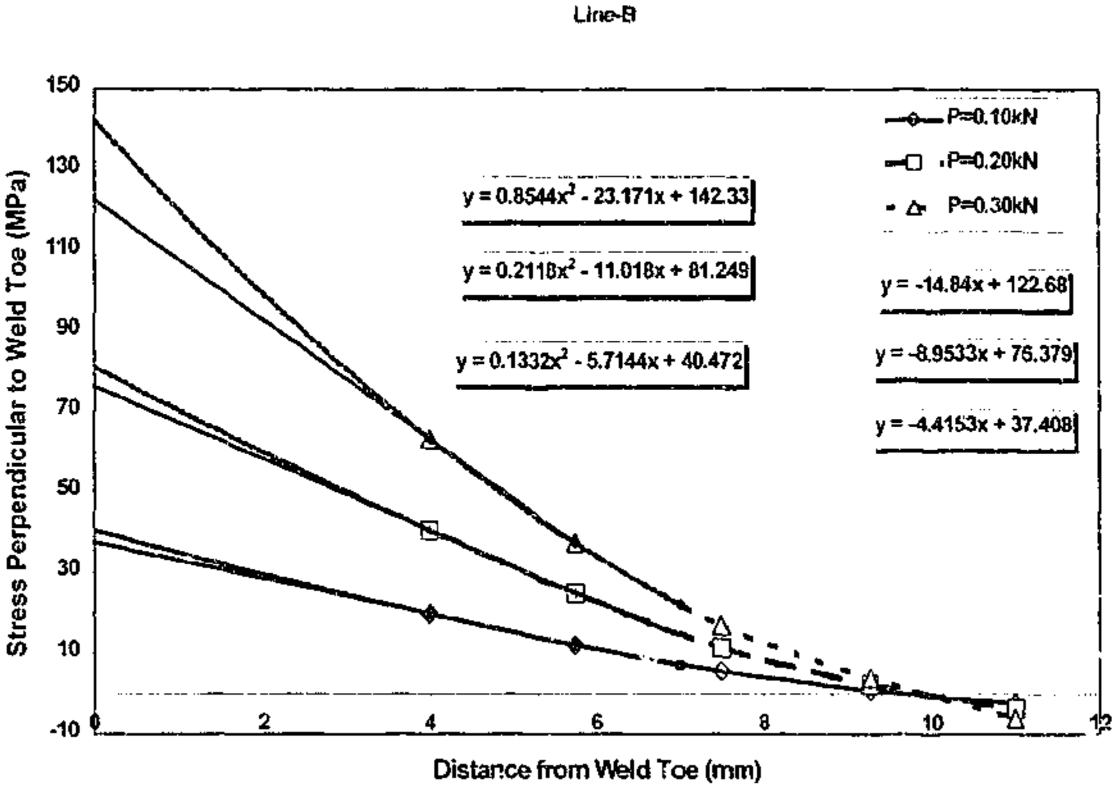

Figure E23: Line B, D3D5L3A

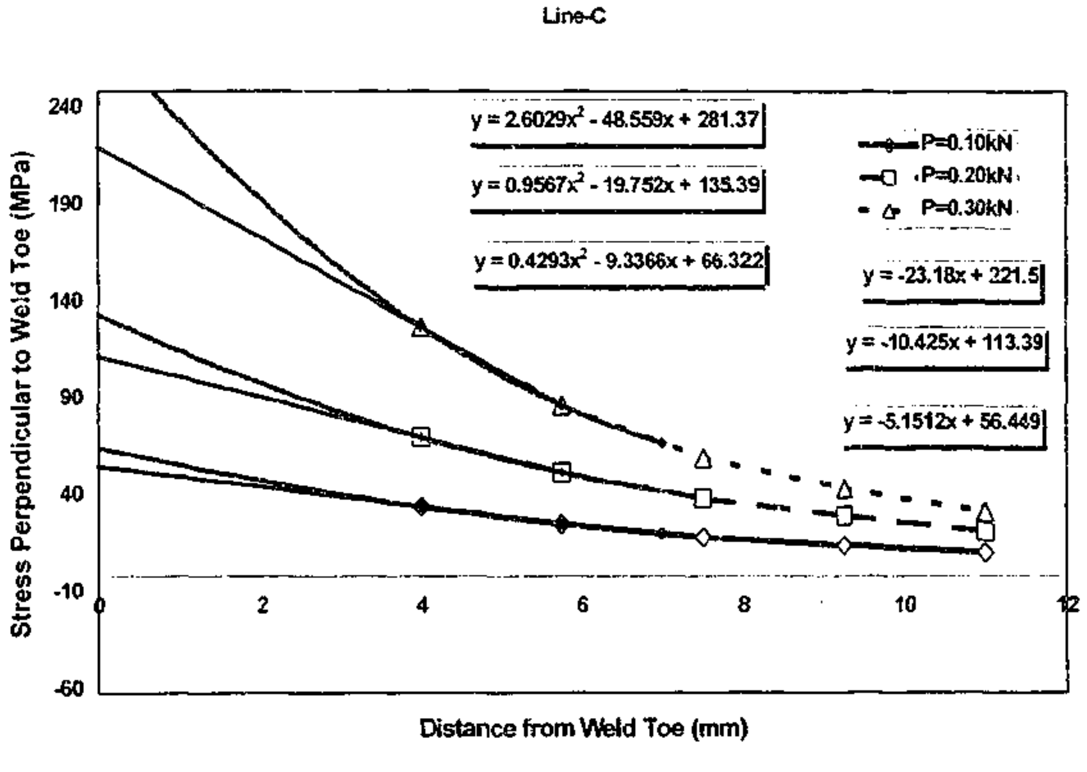

Figure E24: Line C, D3D5L3A

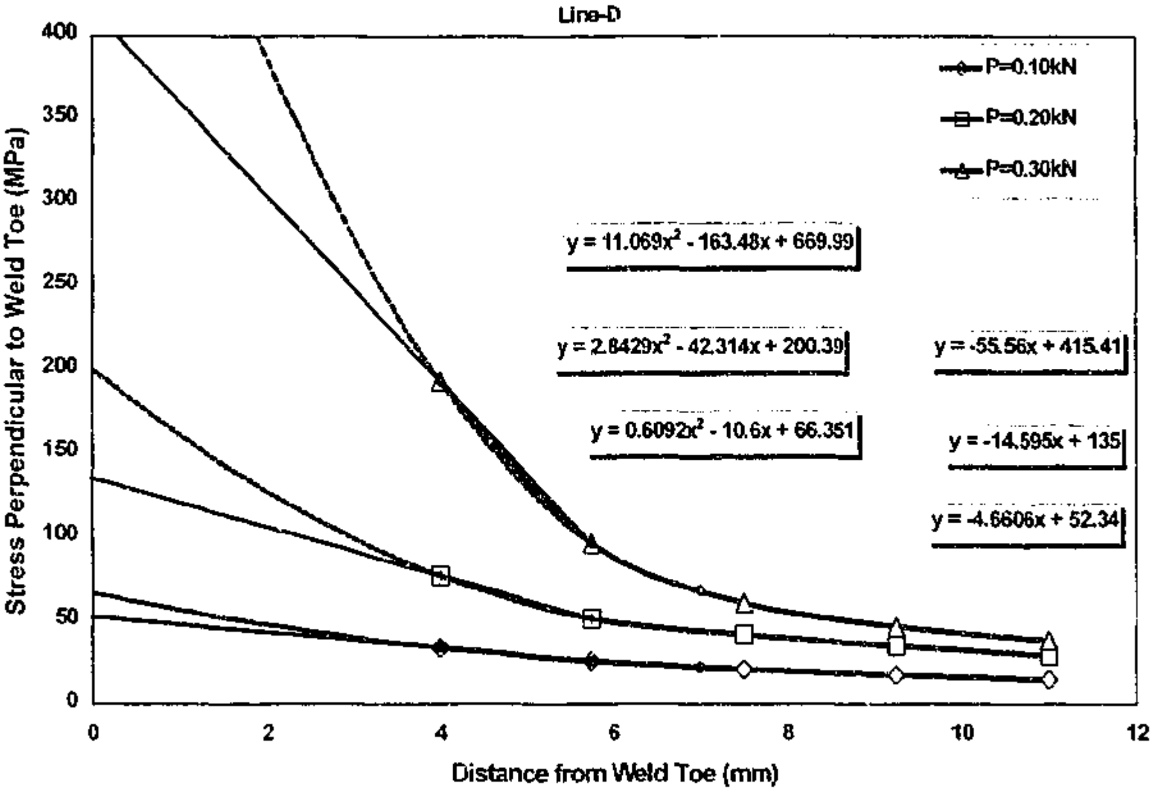

Figure E25: Line D, D3D5L3A

Extrapolation Curves : D6D1L3A

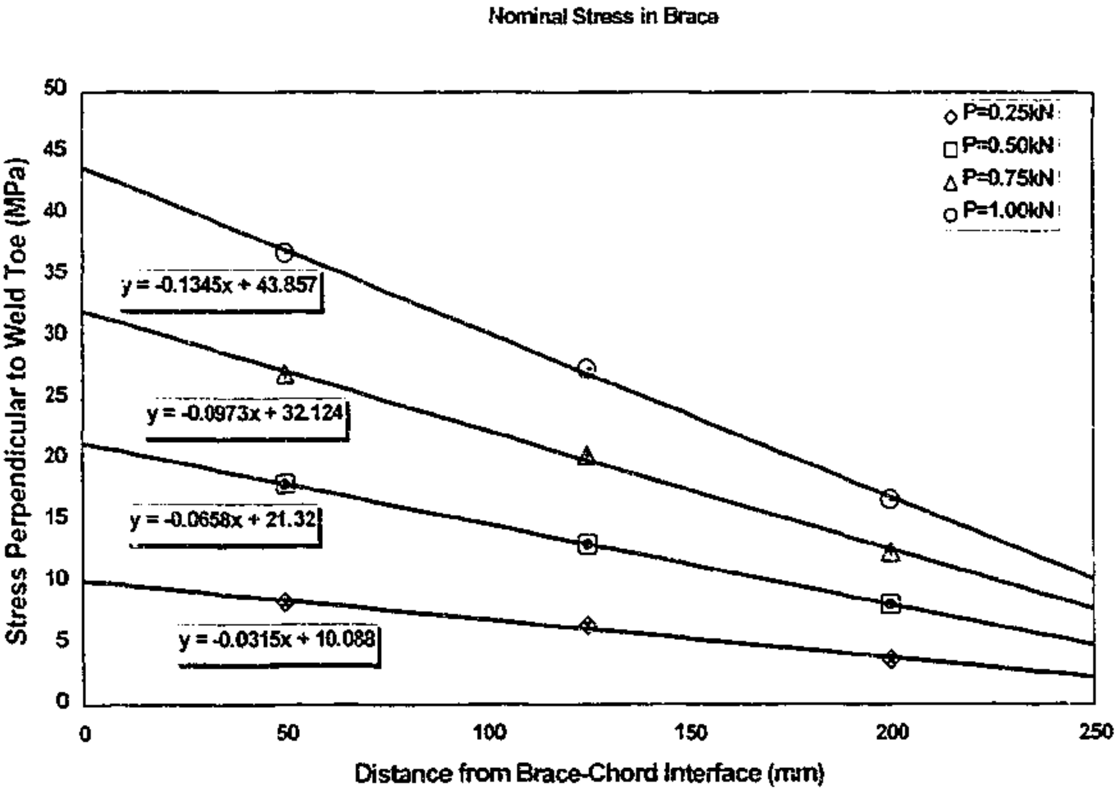

Figure E26: Nominal stress in brace, D6D1L3A

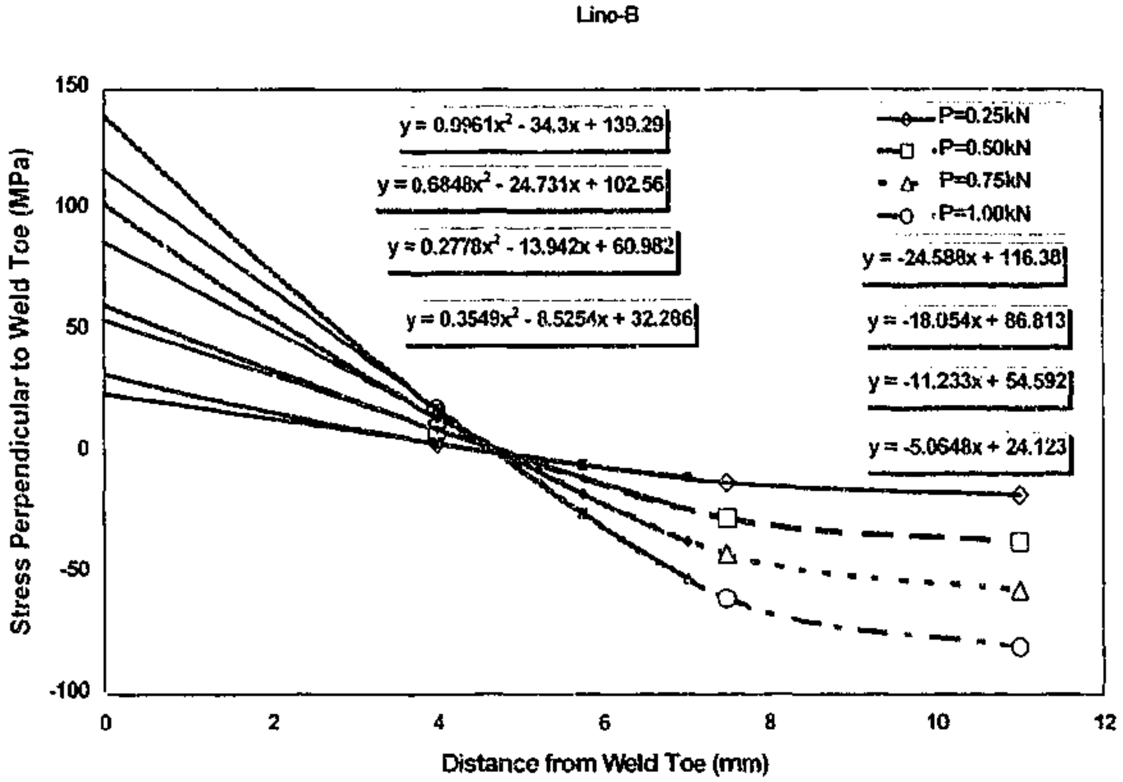

Figure E27: Line B, D6D1L3A

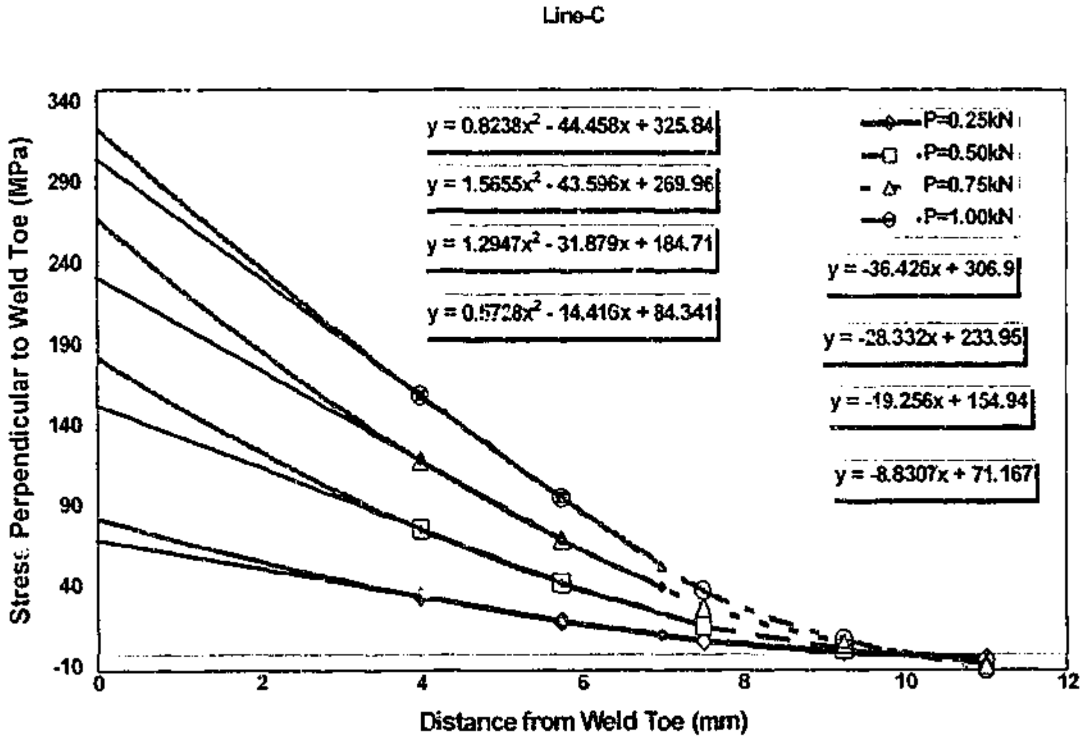

Figure E28: Line C, D6D1L3A

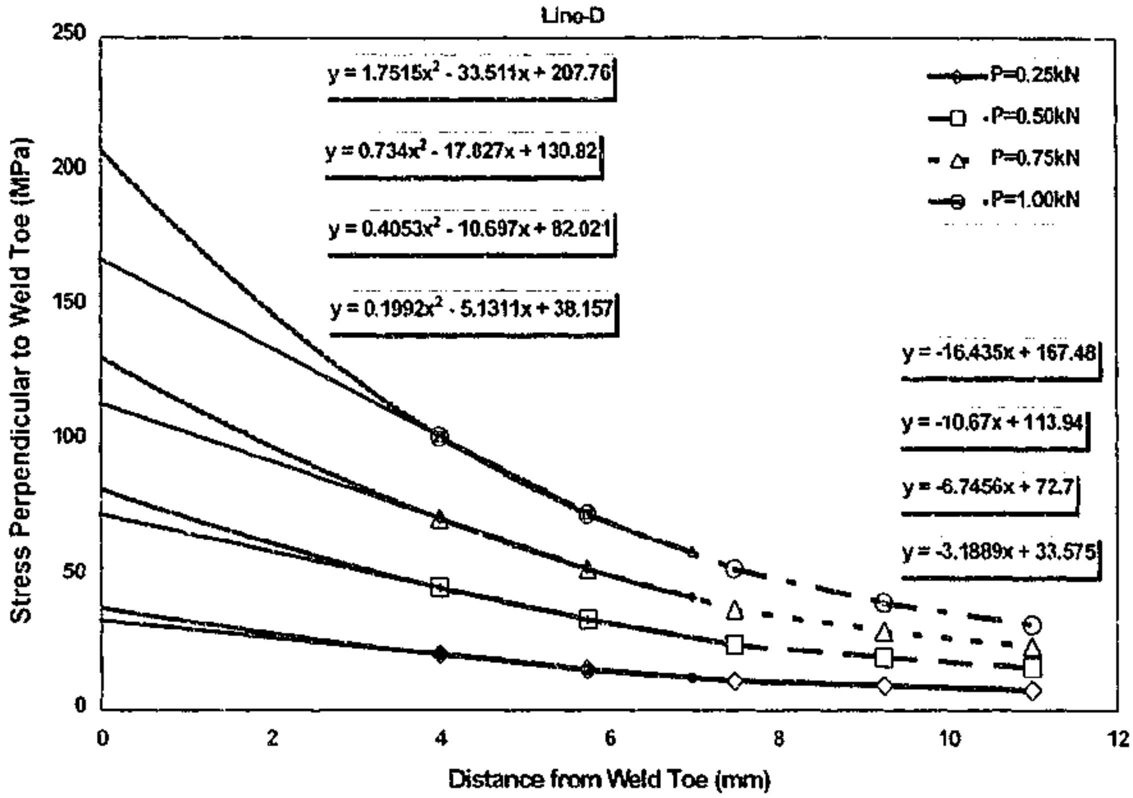

Figure E29: Line D, D6D1L3A

Extrapolation Curves : D6D2L3A

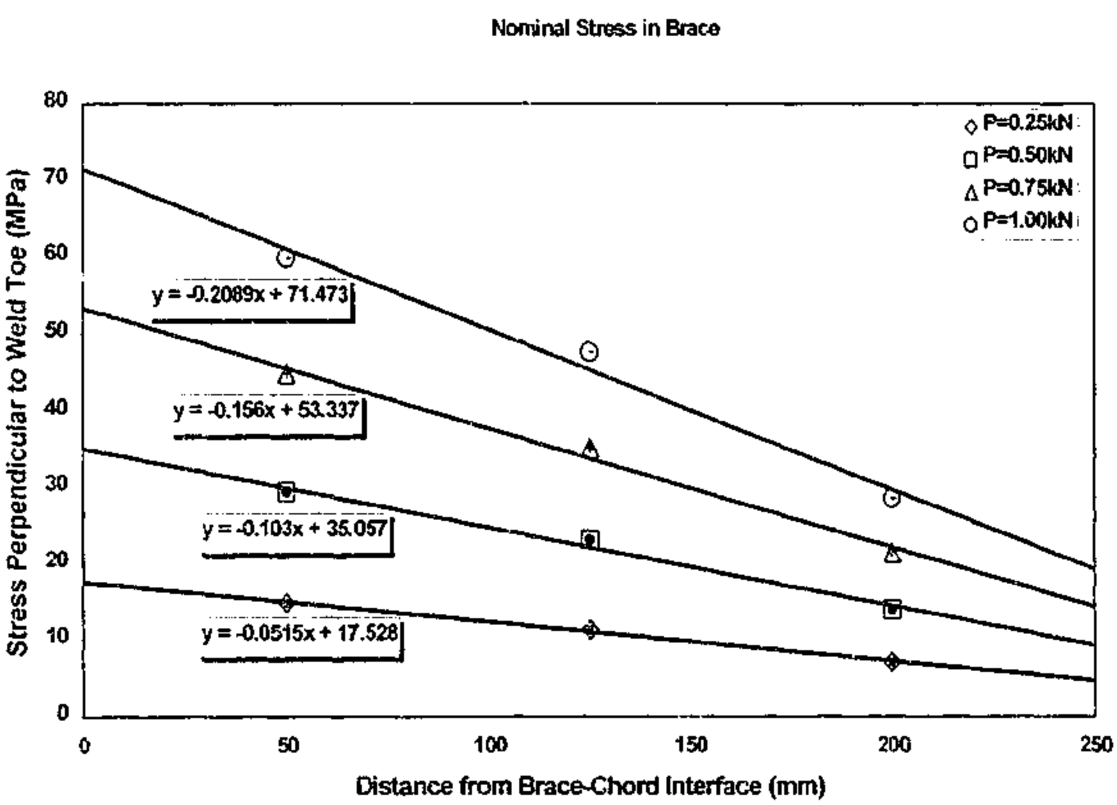

Figure E30: Nominal stress in brace, D6D2L3A

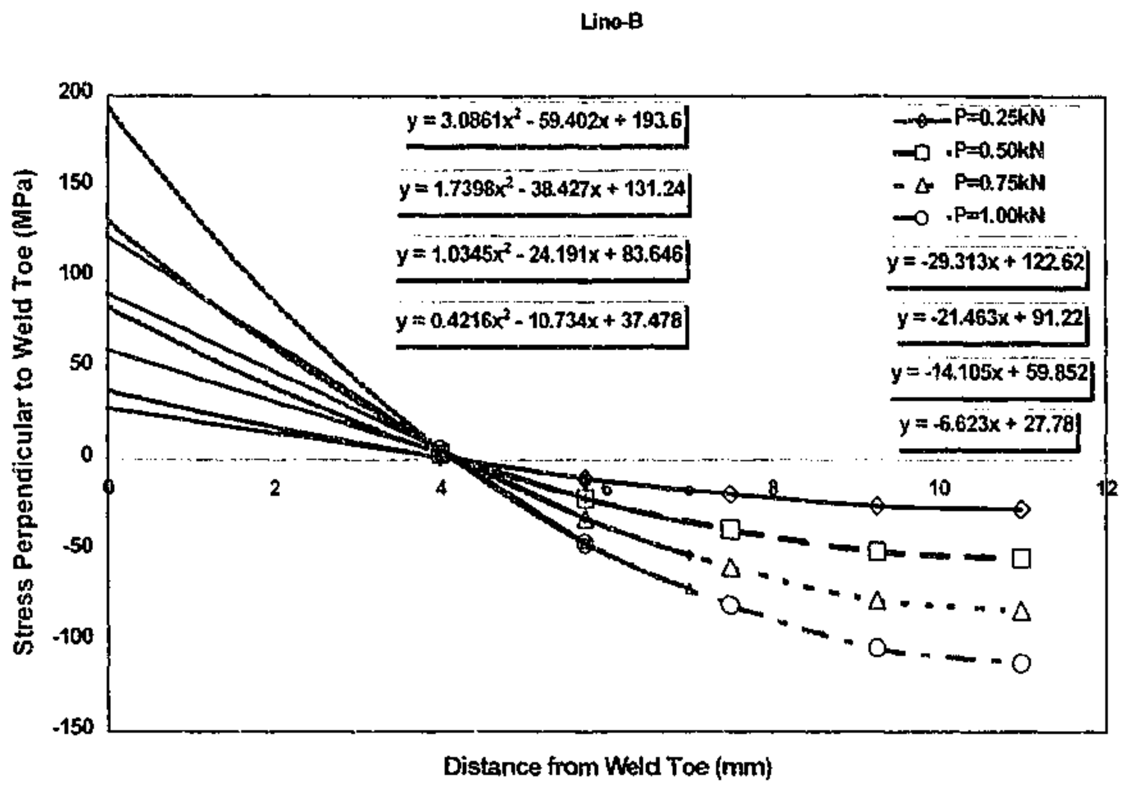

Figure E31: Line B, D6D2L3A

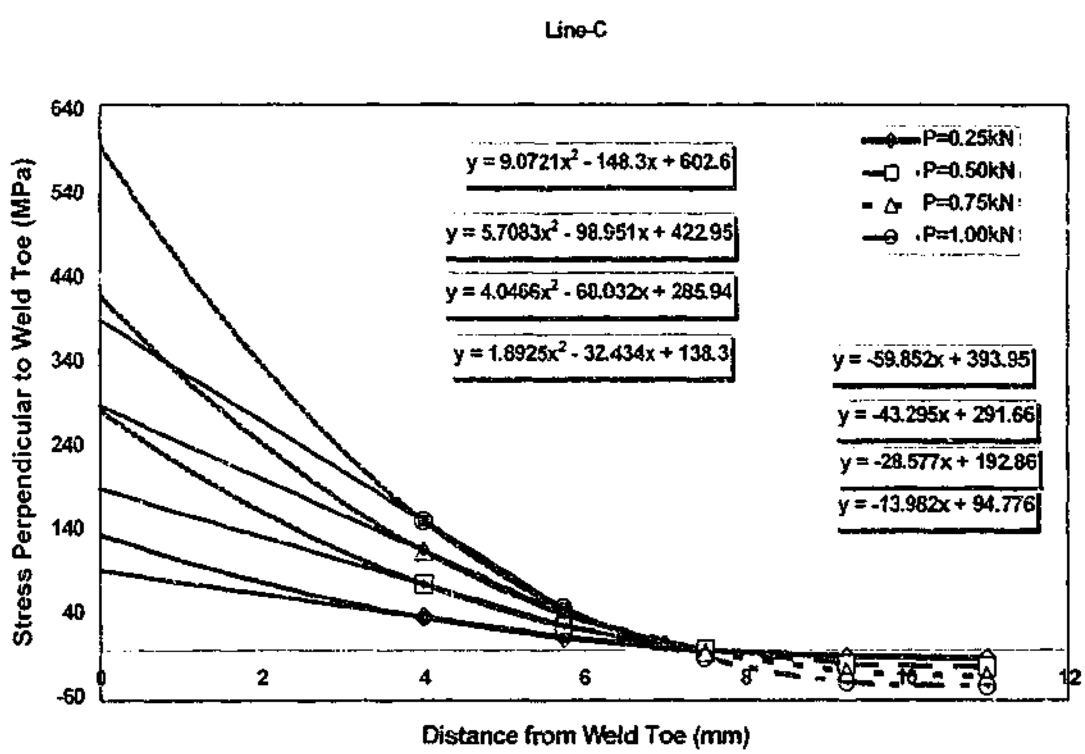

Figure E32: Line C, D6D2L3A

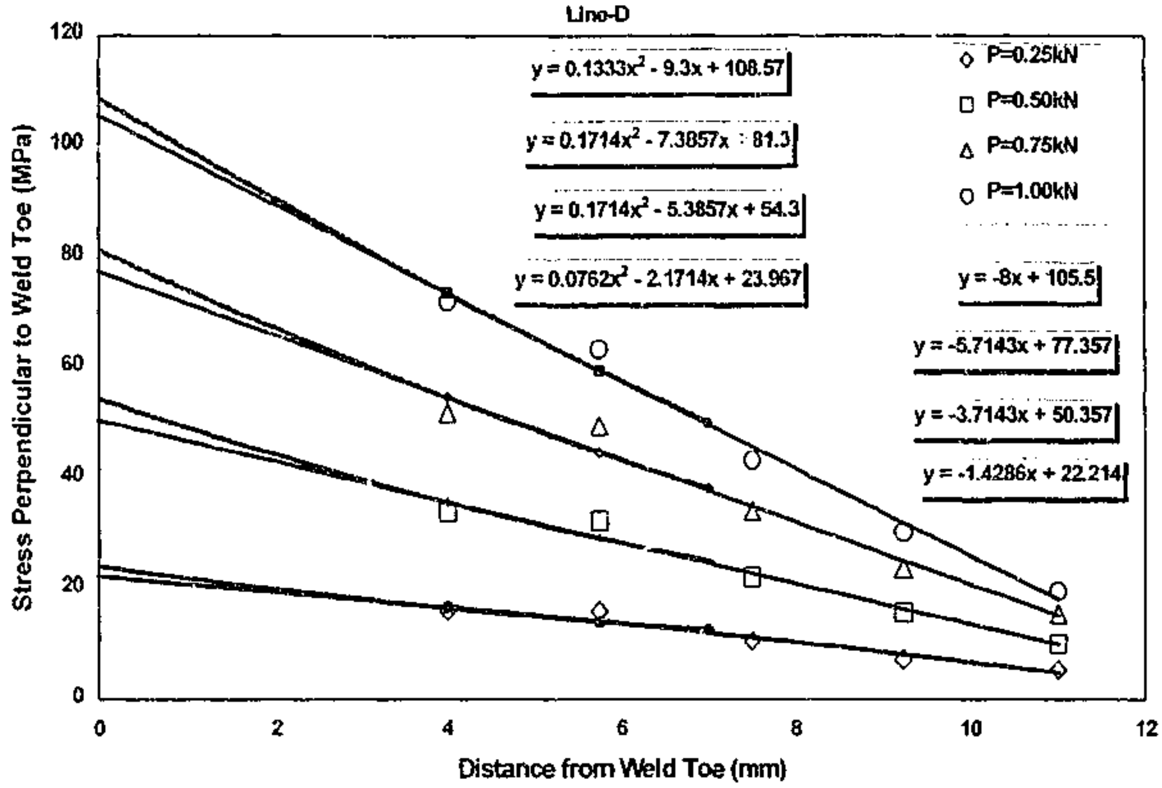

Figure E33: Line D. D6D2L3A

Extrapolation Curves : V3V5L3A

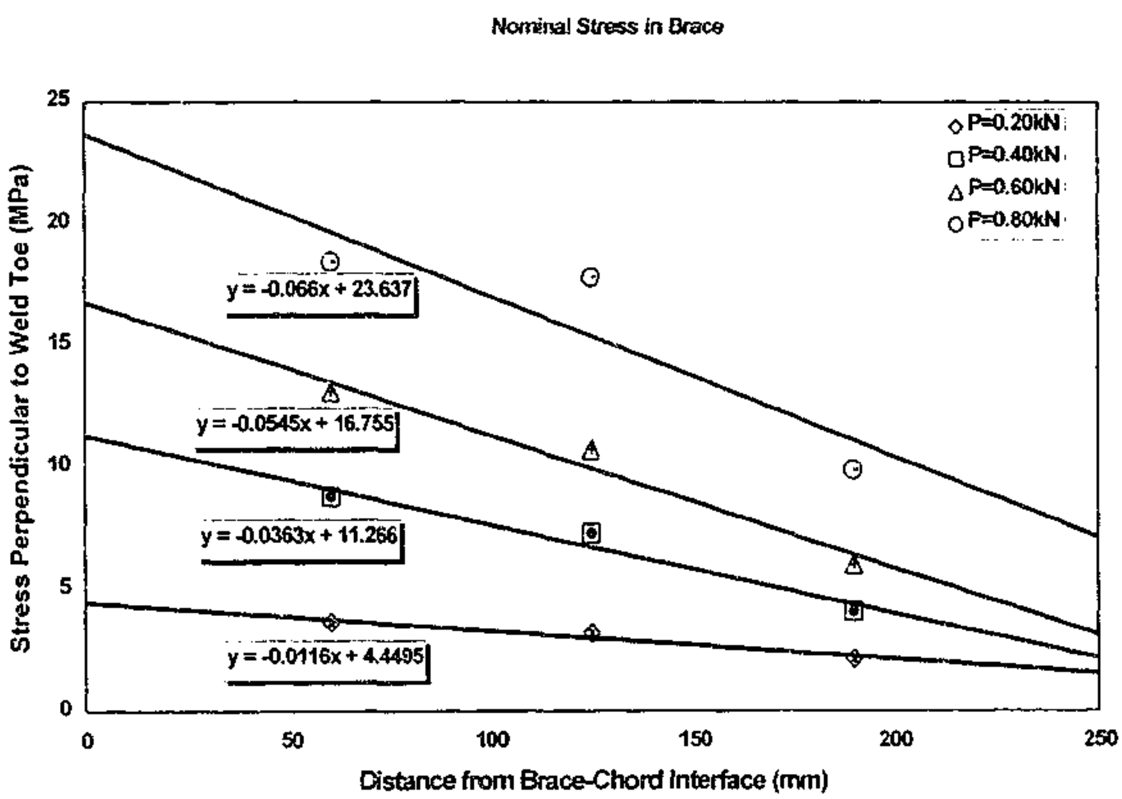

Figure E34: Nominal stress in brace, V3V5L3A

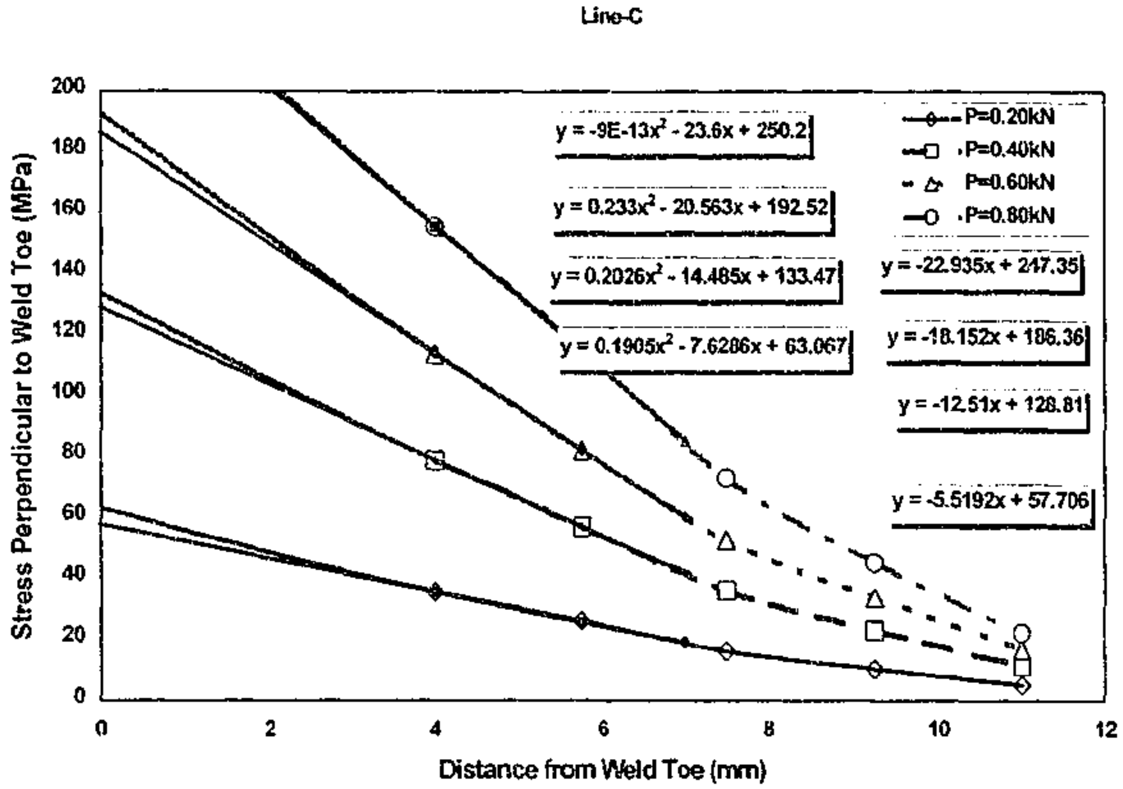

Figure E35: Line C, V3V5L3A

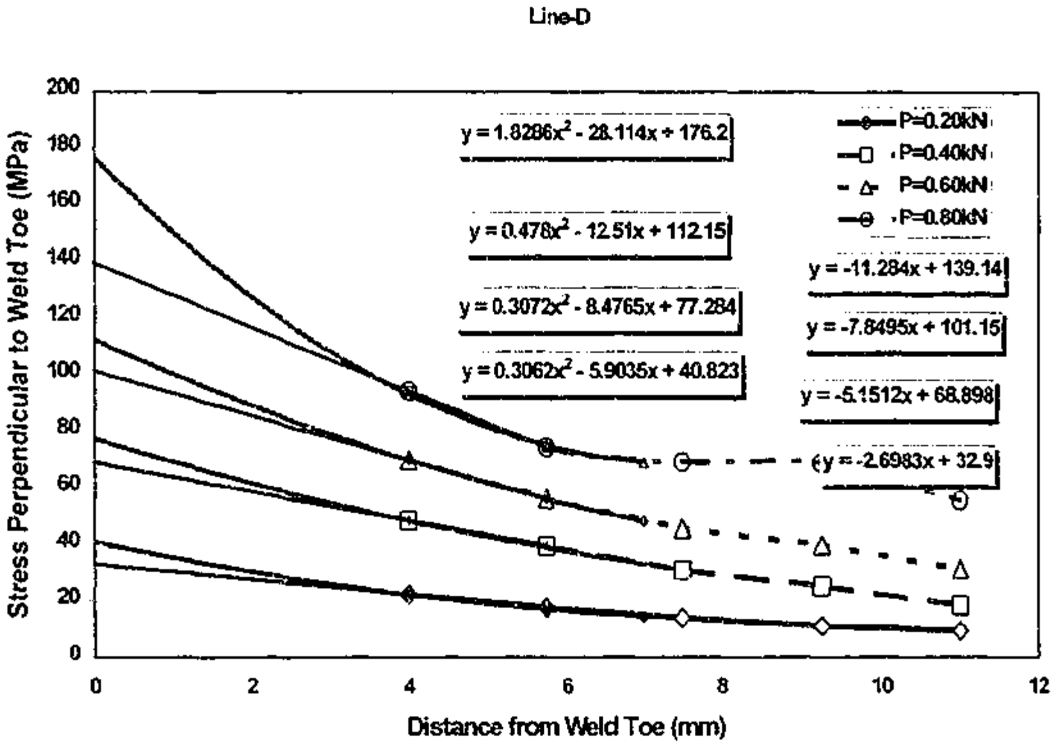

Figure E36: Line D, V3V5L3A

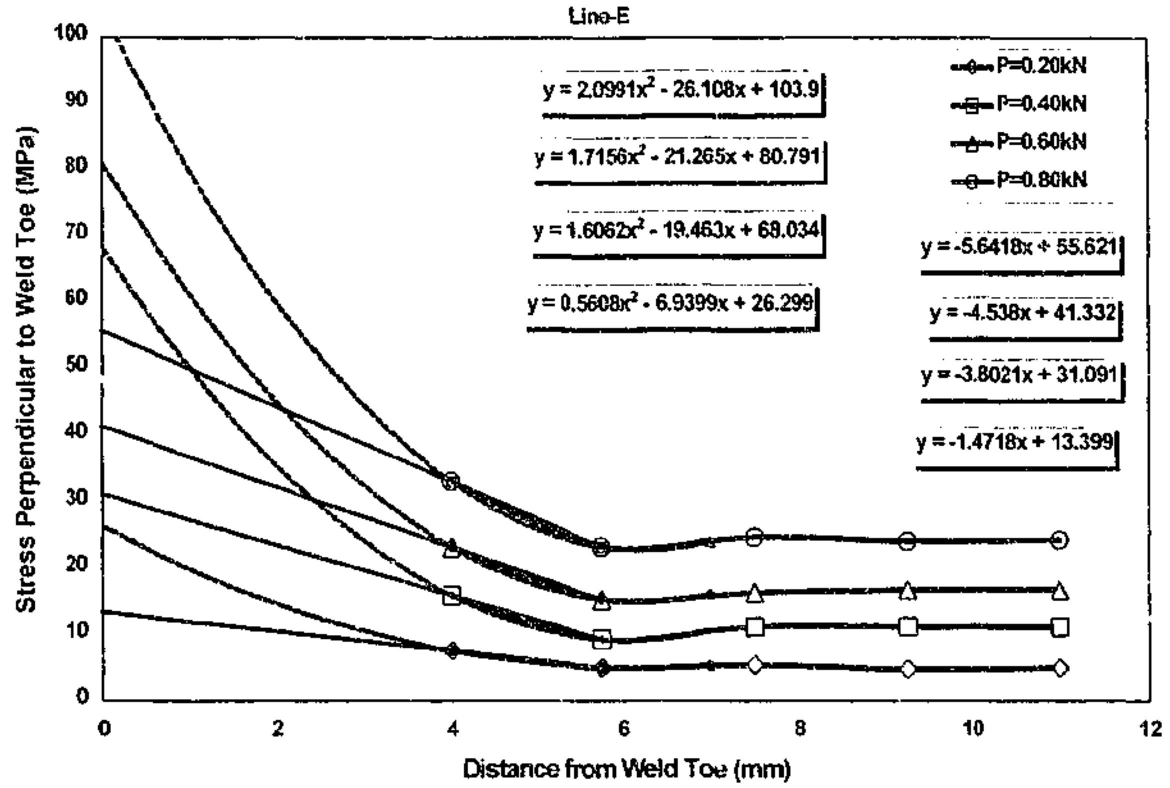

Figure E37: Line E, V3V5L3A

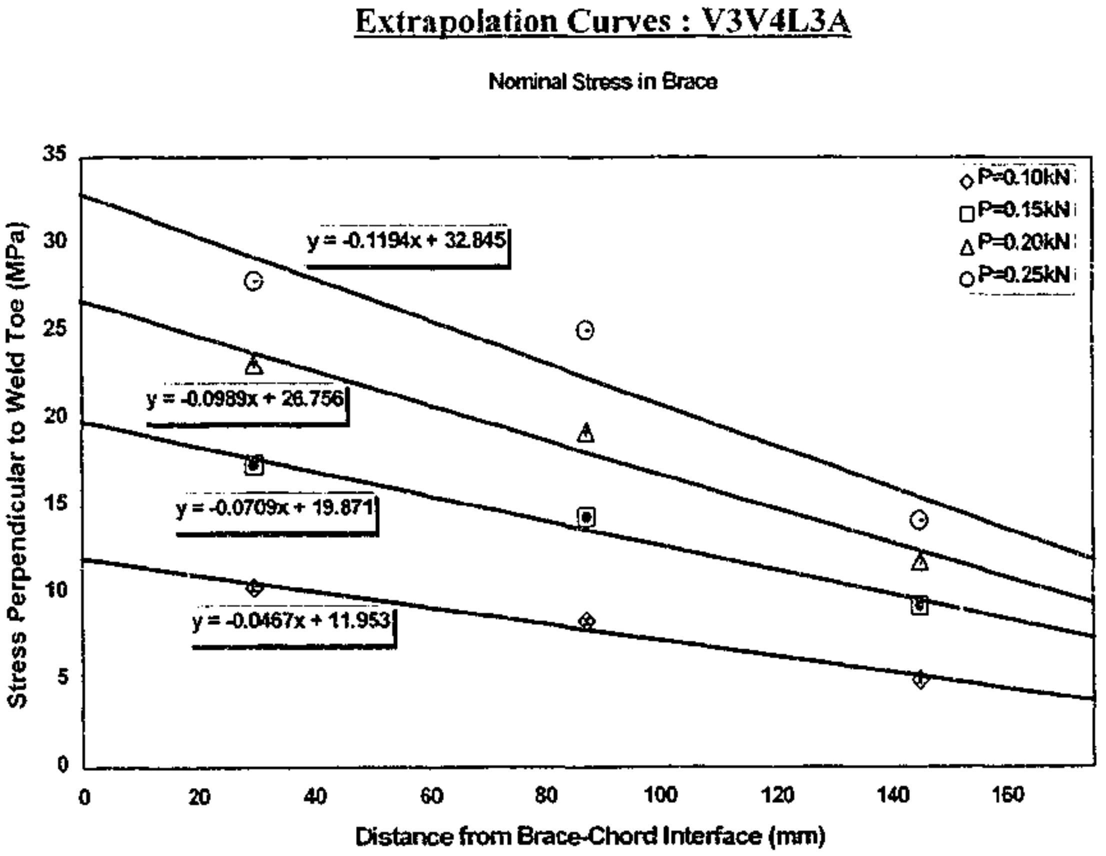

Figure E38: Nominal stress in brace, V3V4L3A

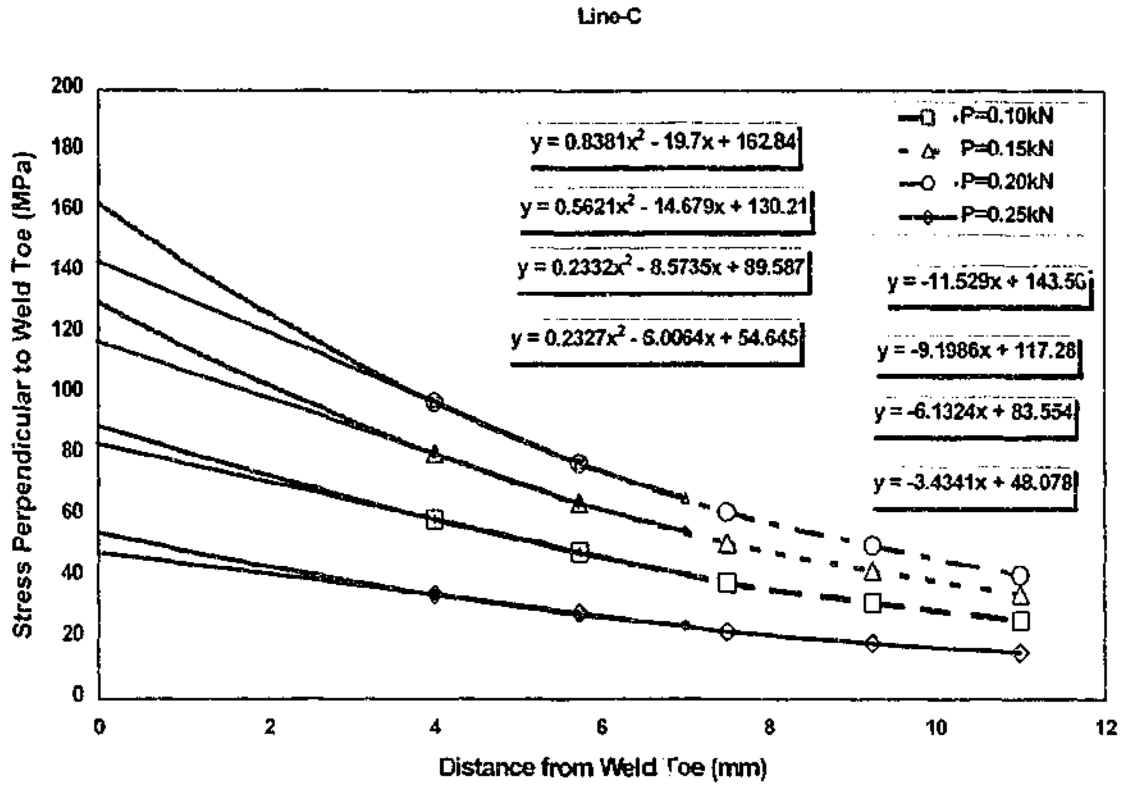

Figure E39: Line C, V3V4L3A

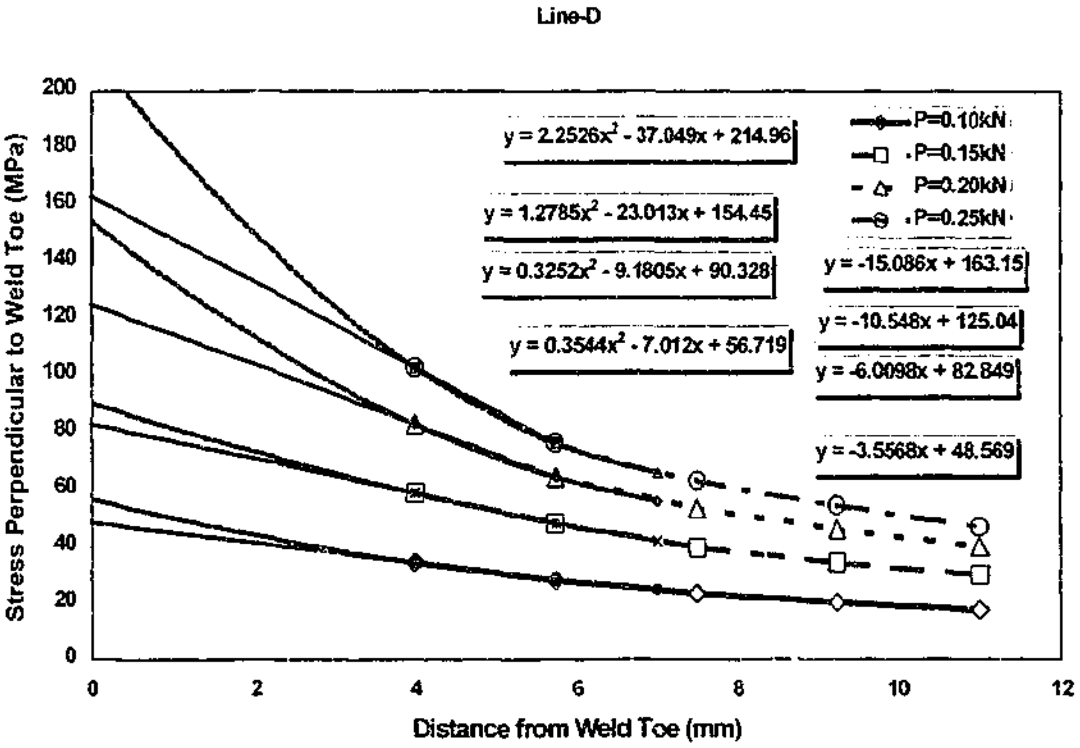

Figure E40: Line D, V3V4L3A

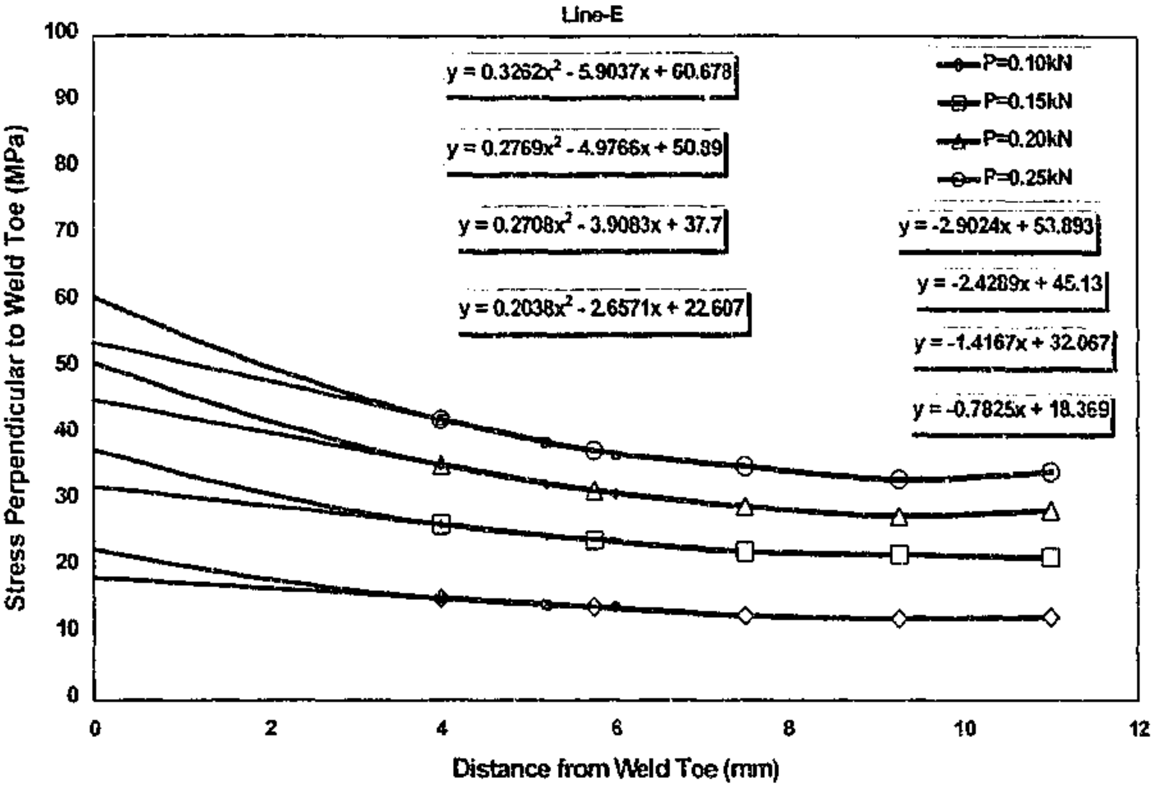

Figure E41: Line E, V3V4L3A

Extrapolation Curves : V6V1L3A

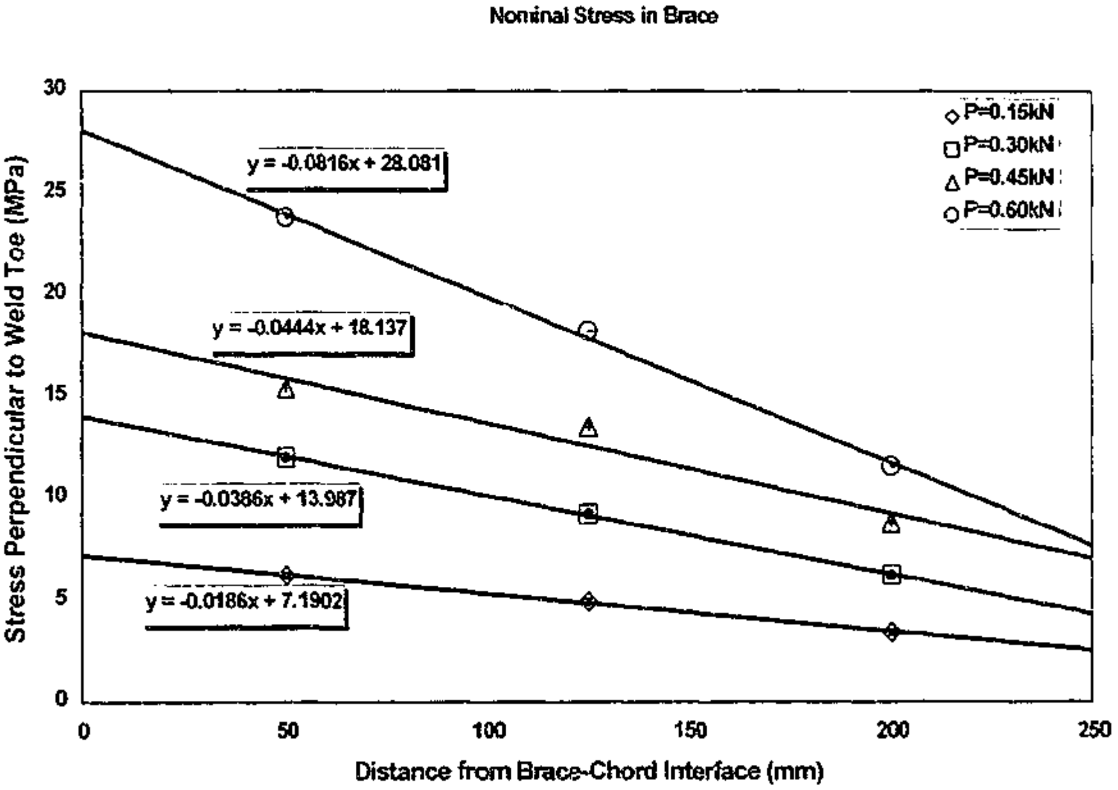

Figure E42: Nominal stress in brace, V6V1L3A

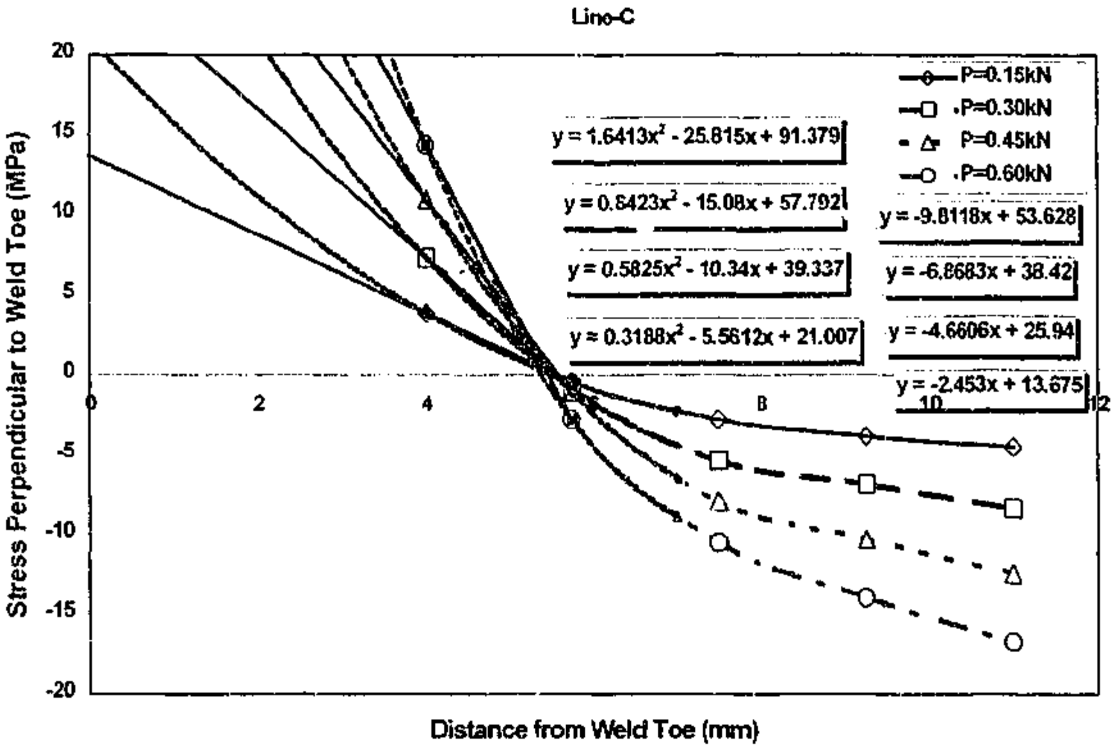

Figure E43: Line C, V6V1L3A

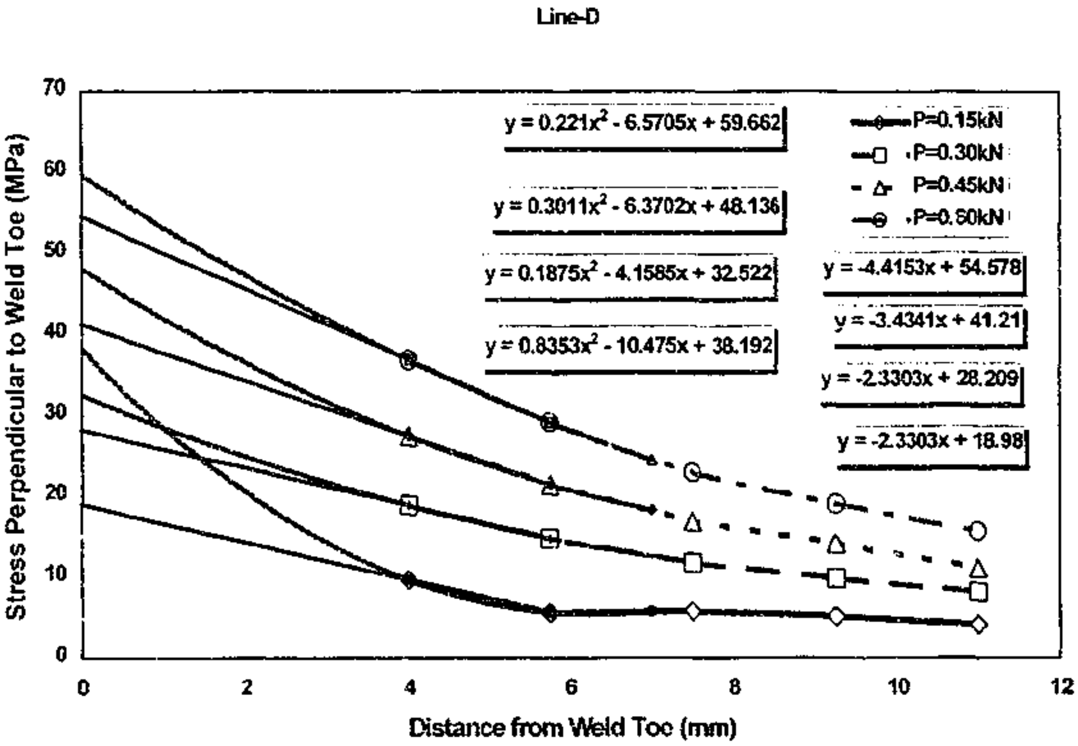

Figure E44: Line D, V6V1L3A

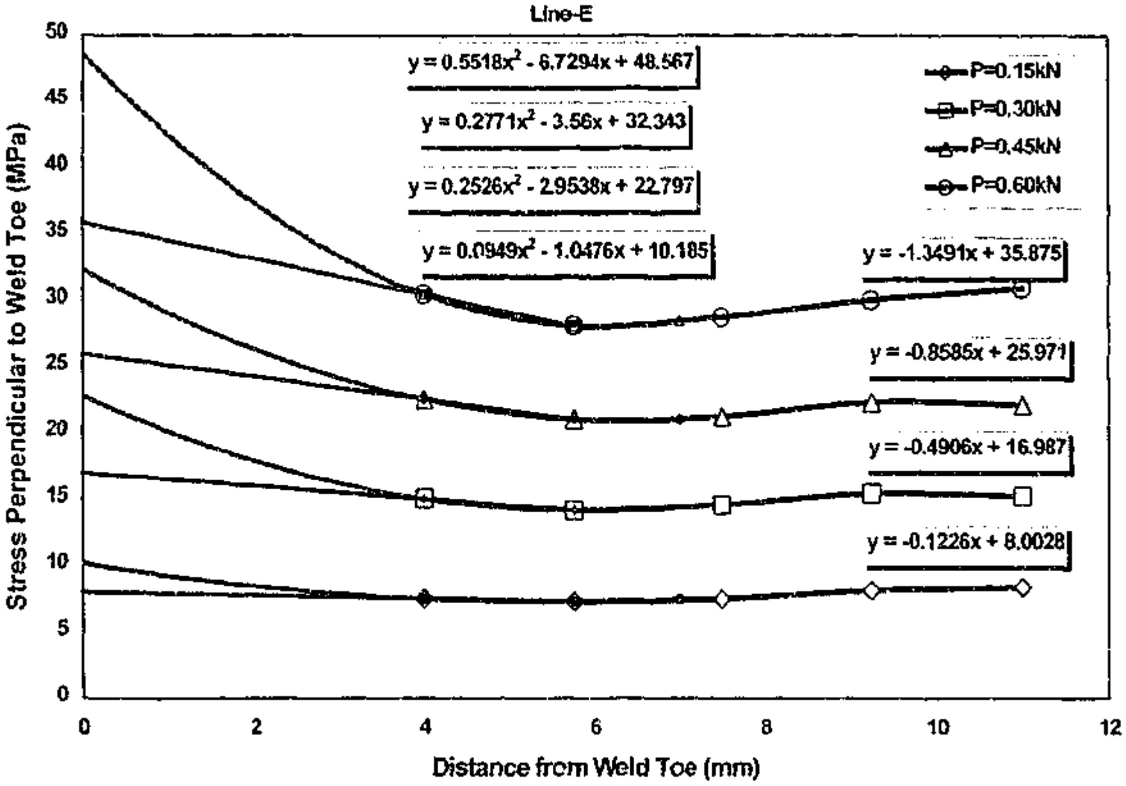

Figure E45: Line E, V6V1L3A

Extrapolation Curves : V6V2L3A

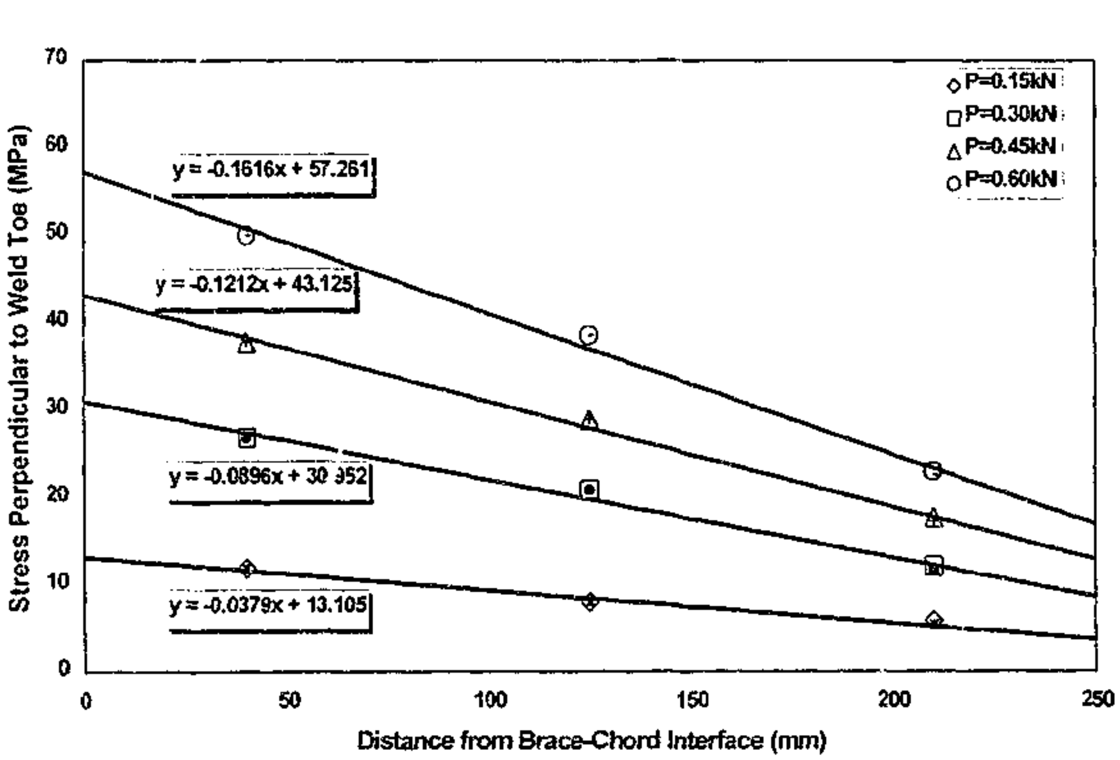

Figure E46: Nominal stress in brace, V6V2L3A

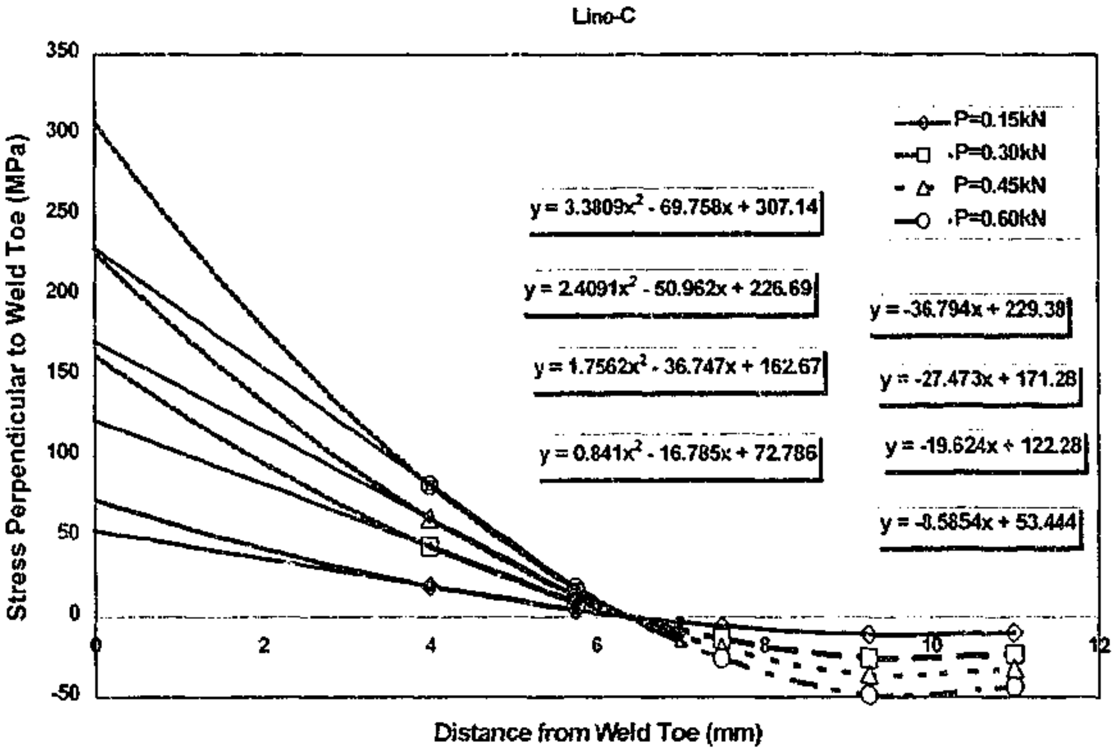

Figure E47: Line C, V6V2L3A

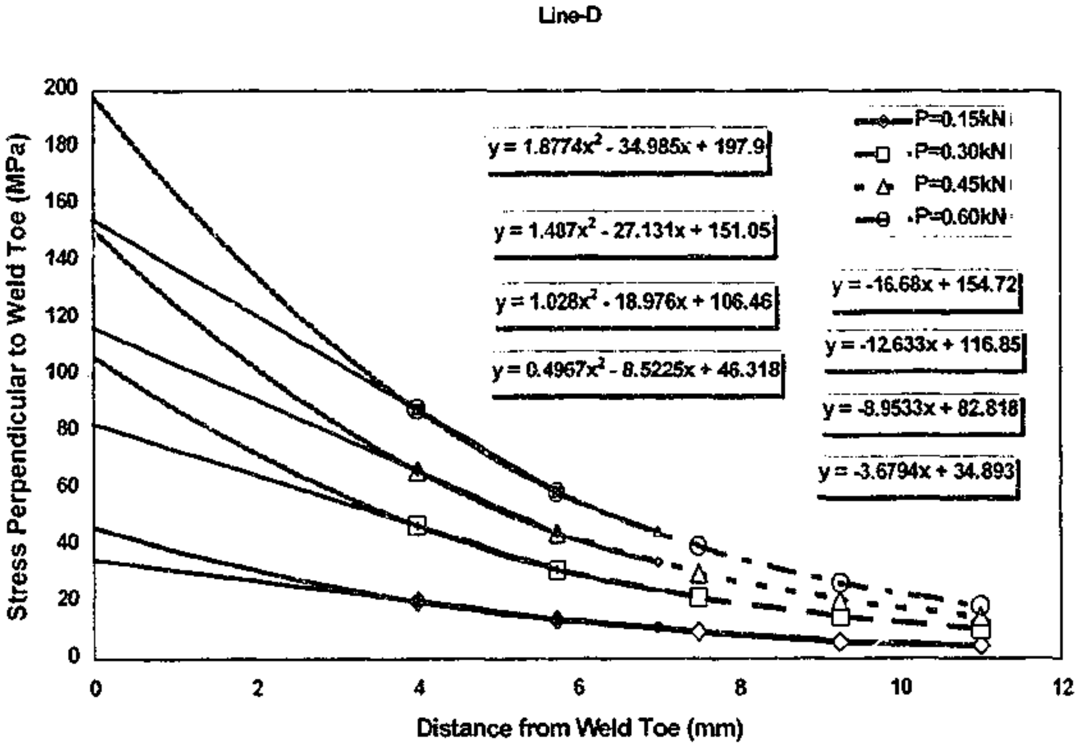

Figure E48: Line D, V6V2L3A

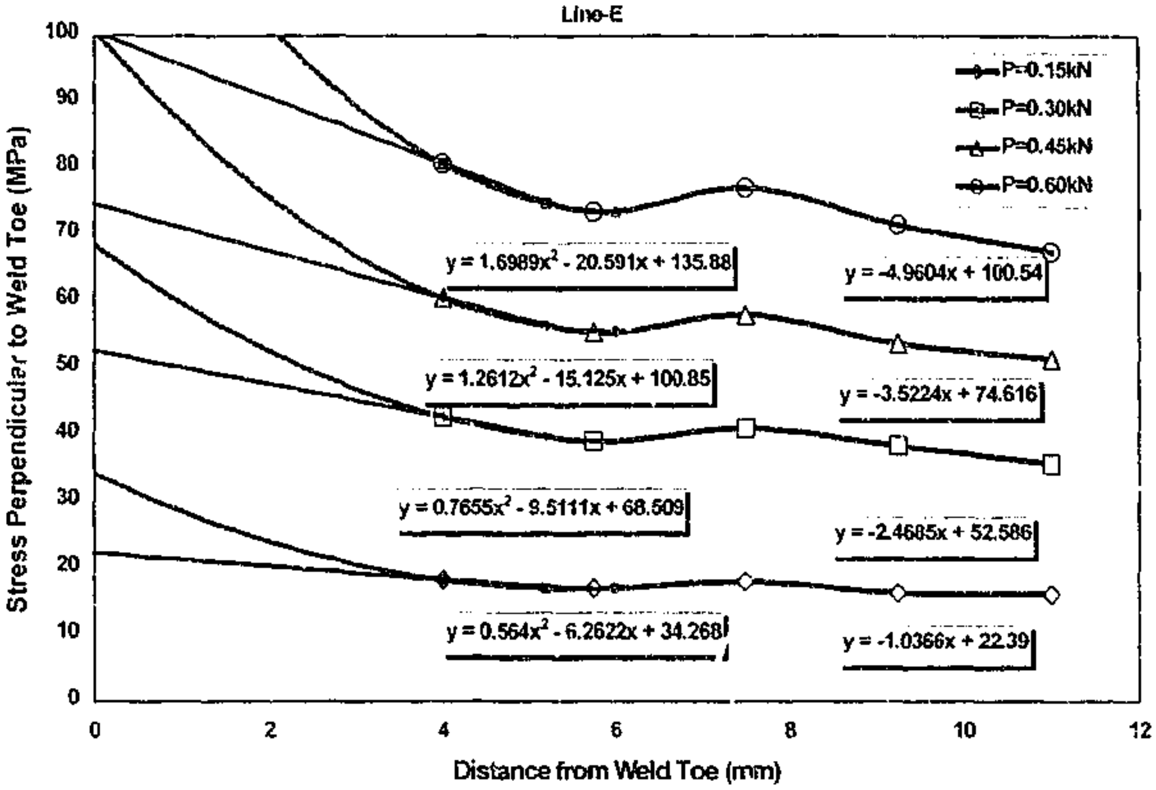

Figure E49: Line E, V6V2L3A

Appendix F

EXISTING SCF PARAMETRIC EQUATIONS FOR T-JOINTS MADE OF RECTANGULAR OR SQUARE HOLLOW SECTIONS

F.1: van Wingerde (1992)

Current design guidelines (IIW 2000, Zhao *et al* 1999a) adopted parametric equations derived by van Wingerde (1992). These equations are produced from regression analysis of results of SCF obtained from numerical analysis using finite element methods. Depending on the connections analysed the parametric equations are capable of estimating SCF for joints with non-dimensional parameters (β, 2γ, τ) lying within the range of validity.

The parametric equations given by (van Wingerde 1992, IIW 2000, Zhao *et al* 1999a) for uniplanar rectangular hollow section T- and X-joints have a range of validity as follows:

$$0.35 \le \beta \le 1.0$$

$$12.5 \le 2\gamma \le 25.0$$

$$0.25 \le \tau \le 1.0$$

The SCF's for uniplanar RHS T- and X-joints under in-plane bending on the brace, are given by the following equations for the hot spot locations, lines A to E;

(i) Chord (lines B,C,D)

$$SCF_{B,ipb} = \left(-0.011 + 0.085 \cdot \beta - 0.073 \cdot \beta^2\right) \cdot (2\gamma)^{\left(1.722 + 1.151 \cdot \beta - 0.697 \cdot \beta^2\right)} \cdot \tau^{0.75} \qquad \textbf{(F.1)}$$

$$SCF_{C,ipb} = \left(0.952 - 3.062 \cdot \beta + 2.382\beta^2 + 0.0228 \cdot 2\tau\right) \cdot (2\gamma)^{\left(-0.690 + 5.817 \cdot \beta - 4.685 \cdot \beta^2\right)} \cdot \tau^{0.75} \qquad \textbf{(F.2)}$$

$$SCF_{D,ipb} = \left(-0.054 + 0.332 \cdot \beta - 0.258 \cdot \beta^2\right) \cdot (2\gamma)^{\left(2.084 - 1.062 \cdot \beta + 0.527 \cdot \beta^2\right)} \cdot \tau^{0.75} \qquad \textbf{(F.3)}$$

(ii) Brace (line A & E)

$$SCF_{A,ipb} = SCF_{E,ipb} = \left(0.390 - 1.054 \cdot \beta + 1.115 \cdot \beta^2\right) \cdot (2\gamma)^{\left(-0.154 + 4.555 \cdot \beta - 3.8097 \cdot \beta^2\right)} \quad \textbf{(F.4)}$$

(for joints with fillet welds, $SCF_{A,ipb}$ and $SCF_{E,ipb}$ are multiplied by a factor of 1.40)

The SCF's for uniplanar RHS T- and X-joints under chord loading (axial or bending), are given by the following equations for the hot spot locations, lines A to E;

(i) Chord (lines B,C,D)

$$SCF_{B,ch} = 0 \quad \textbf{(F.5)}$$

$$SCF_{C,ch} = 0.725 \cdot (2\gamma)^{0.248 \cdot \beta} \cdot \tau^{0.19} \quad \textbf{(F.6)}$$

$$SCF_{D,ch} = 1.373 \cdot (2\gamma)^{0.205 \cdot \beta} \cdot \tau^{0.24} \quad \textbf{(F.7)}$$

(ii) Brace (line A & E)

$$SCF_{A,ch} = SCF_{E,ch} = 0 (negligible) \quad \textbf{(F.8)}$$

F2: Soh and Soh (1990)

The other parametric equations used for determining SCF for tube-to-tube T-joints made of square hollow sections were determined by Soh and Soh (1990).

The welds of tubular joints could not be included in the finite element models due to the use of facet shell elements. This ommission of welds should give rise to higher stresses at brace-to-chord intersections and therefore the stress concentration factors obtained should be conservative.

The stress concentration factor for a joint was obtained by taking the ratio of the absolute maximum principal stress, which occurs at the brace-to-chord intersection, to the nominal stress of the brace.

The parametric study for T/Y joints was carried out within the following geometrical bounds;

$$0.40 \le t_1/t_0 \le 1.00$$

$$7.89 \le d_0/2t_0 \le 23.81$$

$$0.20 \le d_1/d_0 \le 0.75$$

$$3.33 \le l_0/d_0 \le 18.33$$

$$30^{\circ} \le \theta \le 90^{\circ}$$

The formulae for estimating SCF's in T/Y joints for in-plane bending in the brace are as follows;

$$SCF_{brace} = 1.4088 \cdot (t_1/t_0)^{0.748} \cdot (d_0/2t_0)^{0.952} \cdot (d_1/d_0)^{0.880} \cdot (l_0/d_0)^{0.045} \cdot (\sin\theta)^{0.812} \qquad \textbf{(F.9)}$$

$$SCF_{chord} = 1.3586 \cdot (t_1/t_0)^{1.134} \cdot (d_0/2t_0)^{1.347} \cdot (d_1/d_0)^{1.173} \cdot (l_0/d_0)^{-0.248} \cdot (\sin\theta)^{0.502} \qquad \textbf{(F.10)}$$

The above equations can be expressed using the non-dimensional parameters $\beta(d_1/d_0)$,$\tau(t_1/t_0)$,$2\gamma(d_0/t_0)$ and $\alpha(2l_0/d_0)$. For the T-joints tested in this research $\theta = 90^{\circ}$. The range of validity is therefore;

$$0.40 \le \tau \le 1.00$$

$$15.78 \le 2\gamma \le 47.62$$

$$0.20 \le \beta \le 0.75$$

$$6.66 \le \alpha \le 36.66$$

The formulae for estimating SCF's in T/Y joints for in-plane bending in the brace, expressed in terms of the non-dimensional parameters, are therefore as follows;

$$SCF_{brace} = 0.7059 \cdot \tau^{0.748} \cdot 2\gamma^{0.952} \cdot \beta^{0.880} \cdot \alpha^{0.045} \qquad \textbf{(F.11)}$$

$$SCF_{brace} = 0.6342 \cdot \tau^{1.134} \cdot 2\gamma^{1.347} \cdot \beta^{1.173} \cdot \alpha^{-0.248} \qquad \textbf{(F.12)}$$

Appendix G
LEAST SQUARES METHOD FOR DETERMINING DESIGN S-N CURVES

G.1. Least-Squares Method

Fitting a straight line S-N curve through fatigue data requires the use of the regression analysis. The method of estimation almost universally applied in regression analysis is least- squares. When the experimental error can be assumed to be normally distributed, the least- squares and maximum likelihood estimation methods give identical parameter estimates. Details and explanation of a model for simple linear regression with one independent variable are given in (Little & Jebe 1975). Little & Jebe (1975) derive the equations used in estimating the slope, intercept and random measurement error by the least-squares method and also give the properties of the least-squares solution obtained. Similar equations for calculating the slope and intercept of a straight line S-N curve passing through fatigue data are given in guidelines for statistical analysis of fatigue data by the Japan Society of Mechanical Engineers, JSME (Nakazawa & Kodama 1987) and the American Society for Testing and Materials (ASTM 1980).

The Japan Society of Mechanical Engineers and the American Society for Testing and Materials give formulas for the case where the number of cycles is the dependent variable and the stress is the independent variable.

An analysis where the stress is the dependent variable and the number of cycles the independent variable will also be considered in this paper. The equations for the two cases are given below.

E.2 Determination of S-N curves assuming the number of cycles is the dependent variable and the stress is the independent variable (ASTM 1980).

Statistical Analysis for a linear model, *log N = A + B.log S*

For the case where

(a) fatigue life data pertain to a random sample, i.e where all $\log N_i$ are independent,

(b) there are neither run-outs nor suspended tests and where for the entire interval of testing,

(c) the S-N and ε-N relationship is described by the linear model: $\log N = A + B.\log S$

(d) the two parameter log-normal distribution describes the fatigue life N, and

(e) the variance of the log-normal distribution is constant, the maximum likelihood estimators of A and B are as follows

The super-hat symbol "^" used in the following equations denotes the estimate, and the super-bar symbol "–"denotes the average.

$$\hat{A} = \overline{\log N} - \hat{B}\,\overline{\log S} \qquad \textbf{(G.1)}$$

$$\hat{B} = \frac{\sum_{i=1}^{k}\left(\log S_i - \overline{\log S}\right)\left(\log N_i - \overline{\log N}\right)}{\sum_{i=1}^{k}\left(\log S_i - \overline{\log S}\right)^2} \qquad \textbf{(G.2)}$$

$$\overline{\log N} = \frac{1}{k}\sum_{i=1}^{k}\log N_i \qquad \textbf{(G.3)}$$

$$\overline{\log S} = \frac{1}{k}\sum_{i=1}^{k}\log S_i \qquad \textbf{(G.4)}$$

where k is the total number of specimens.

The recommended expression for estimating the standard deviation of the normal distribution for *log N* is:

$$\hat{\sigma}_{\log N} = \left[\frac{\sum_{i=1}^{k} \left\{ \log N_i - \left(\hat{A} + \hat{B} \log S_i \right) \right\}^2}{k-2} \right]^{1/2} \quad \textbf{(G.5)}$$

The term *(k-2)* in the denominator is used instead of k to make $\hat{\sigma}$ an unbiased estimator of the normal population standard deviation σ.

E.3 Determination of S-N curves assuming the stress is the dependent variable and the number of cycles is the independent variable.

<u>Statistical Analysis for a linear model, *log S = a + blog N*</u>

Similar equations are used except that a stress is now defined as a function of the number of cycles.

$$\hat{a} = \overline{\log S} - \hat{B}\, \overline{\log N} \quad \textbf{(G.6)}$$

$$\hat{b} = \frac{\sum_{i=1}^{k} \left(\log S_i - \overline{\log S} \right)\left(\log N_i - \overline{\log N} \right)}{\sum_{i=1}^{k} \left(\log N_i - \overline{\log N} \right)^2} \quad \textbf{(G.7)}$$

$$\overline{\log N} = \frac{1}{k} \sum_{i=1}^{k} \log N_i \quad \textbf{(G.8)}$$

$$\overline{\log S} = \frac{1}{k} \sum_{i=1}^{k} \log S_i \quad \textbf{(G.9)}$$

where k is the total number of specimens.

The recommended expression for estimating the standard deviation of the normal distribution for *log S* is:

$$\hat{\sigma}_{\log S} = \left[\frac{\sum_{i=1}^{k} \left\{ \log S_i - \left(\hat{a} + \hat{b} \log N_i \right) \right\}^2}{k-2} \right]^{1/2} \qquad \textbf{(G.10)}$$